Towards the development of a liver *in vitro* system that recapitulates Wnt-driven zonation

Eider Valle-Encinas

A thesis presented for the award of Doctor of *Philosophy* (*Ph. D*)

Cardiff School of Biosciences

Sep 2016 – April 2020

Acknowledgements

I would like to thank my supervisor Trevor Dale for giving me the opportunity to initiate and lead my own research. I would also like to thank my second supervisor, Matt Smalley, for his valued scientific input throughout the years. This work couldn't have been completed without the constant support of my PhD assessor, Catherine Hogan, who I admire personally and scientifically and has become a mentor role model for me.

I am also very grateful to our fantastic collaborator Tom Bird from whom I learnt so much in such little time, as well as to his lab members, Dr Miryam Mueller and Christos Kiourtis, who made me feel part of the team during my visit to the Beatson Institute. I am also grateful to our collaborator Stuart Forbes and the current and past members of his laboratory, Niya Aleksieva and Alex Raven, whom have offered excellent work and advice during this project.

I am grateful to Dr Roel Nusse, who by sharing the protocols of his laboratory enabled the work presented in Chapter 5 of this thesis, and to Dr Jeremy Nathans, who donated the HEK293T TCF-Luc cell line that has been used in numerous important experiments. My gratitude and admiration also goes to Alexandra Elbakyan, the funder of 'Sci-hub', for the unlimited access to papers during my PhD. Thank you for breaking the frontiers of human knowledge.

My gratitude is extended to all members of Dale's lab and everyone at ECSCRI that I have worked with. Thanks specially to Anika Offergeld and Nuria Abajo Lima for being a constant source of advice all along. I have also been fortunate to supervise a great number of students -Sonia Muñoz, Beth Bradford, Maria del Carmen Velasco Martinez, Michael Dawes and Kate McSweeney- who not only did great scientific contributions to the project but also (hope) made me a better mentor. Thank you especially to Carmen who stayed in our lab and became a friend.

I also feel very fortunate to have been a Marie Sklodowska-Curie Fellow and a member of the ITN programme PolarNet. I gather great gratitude for our coordinator, Mike Boxem, who put together the proposal of this program and minded for our

scientific development all along. I am also thankful for the friendship of Amalia, Yamini, Philippos, Sarah, Janine and Victoria(s) and the rest of my PolarNet peers for making this experience so valuable.

Used to rapidly and successfully adapt to new environments across countries and continents, adaptation to Cardiff was unexpectedly challenging. I feel really privileged to have counted with a supportive network of wonderful friends distributed across the globe. To my 'Amsterdamer' family Dila, Caye, Manu, Periklis, Cristina and Dimitris, thank you for always making room in your lives to share a laugh and a glass of wine with me. I am also grateful for my biotechnologist friends from Universidad de Leon- Patri, Paloma, Lorena, Natalia and Bea- for the many reunions and adventures lived all along. Thanks also to my always inspiring friend Juncal who from Boston has navigated with me through all the PhD challenges encountered and to my long-lasting friends Paloma and Andrea who always make Leon feel like home. I could not forget either the numerous post card and emails exchanged with my 'secret PI' Julian that has enlighten my day in so many occasions. Last, but not least, I want to thank my very especial and supportive friends Thania, Riccardos, Marta and Mark who are my family in Cardiff and changed my life in Wales. This work couldn't have been done without you and I could never thank you enough for all the joy you bring to my life.

I am also very lucky to have a biological family that has always believed in my potential and encouraged me to pursue my dreams. My dad, who together with my mom shaped my core values, challenged my understanding of the world from very early stages and awakened my curiosity for science. Despite not being present today, your memory, which I deeply treasure, will always be. My extraordinary mom who is a constant model of resilience. Thank you for your unconditional love and support in my numerous endeavours. I am also grateful to my truly amazing brother Oscar and his girlfriend Ana, who brings him love and balance. Finally, and taking the risk of stepping out from an orthodox PhD acknowledgment section, I feel the necessity to also mention and name my grandparents- Jacoba, Marti, Maximino and Fernando-, aunts and uncles- Begoña, Toño, Flory, Cris and Goyo-, cousins –Rubén, María, David, Eri, Dani, Cesar y Mayte- as well as the newbies of the family -Marta, Desire and Izan-, as they make my family as unique and united as any. There is nothing that can break our bond.

Abstract

A local Wnt niche sustained by the hepatic central vein shape the transcriptional program of pericentral hepatocytes. The Wnt pathway additionally orchestrates liver regeneration following injury. In the recent years, protocols for the growth of two types of hepatic organoids (bile duct(BD)-derived and primary hepatocyte (PH)-derived organoids) have been developed. However, these *in vitro* systems do not capture aspects of metabolic zonation in a continuous and thereby fail to fully replicate the organ biology. In this thesis, I aimed to make significant advances in the development of a zonated liver *in vitro* system by developing the molecular tools to recreate the Wnt microenvironment of the hepatic central vein i*n vitro* and assessing the cellular responses of the current hepatic organoid systems to Wnt activation. Using covalently immobilized Wnt and Rspo ligands, the local presentation of Rspo3 and addition of soluble Wnt9b was found an attractive strategy to recreate the central vein microenvironment *in vitro*. Activation of the Wnt pathway in PH organoids resulted in an increased expression of Wnt-driven metabolic pericentral genes. By contrast, activation of the Wnt pathway in BD organoids resulted in an enhanced expression of hepatocyte progenitor cell markers rather than pericentral metabolic genes. Using bile BD organoids in combination with different genetic mouse models, we uncovered a potential role for the Wnt pathway in BEC plasticity. Together, this study suggests that PH organoids but not BD organoids mirror the behaviour of homeostatic hepatocytes and thereby may serve as cellular platform to recapitulate the biology of the resting liver. The adaptation and controlled presentation of biological and physicochemical cues in hepatocyte culture systems may help us to better understand the mechanisms that govern zonation and develop therapies for pathological conditions where zonation is perturbed.

List of abbreviations

A

2-AAF, 2-acetylaminofluorene
AFP, α-fetoprotein
AJs, adherens junctions
ALP, alkaline phosphatase
AO, acridine orange

B

BD, bile duct
BDL, bile duct ligation
BDorg-EM, BD organoid expansion medium
BDorg-DM, BD organoid differentiation medium
BDorg-IM, BD organoid isolation medium
BECs, Bile duct epithelial cells
BSA, bovine serum albumin

C

CCl_4, carbon tetrachloride
CDE, choline-deficient, ethionine-supplemented
CHIR, CHIR99021
CM, conditioned medium
CPM, Counts per million
CRD, Cysteine Rich Domain
CV, Central vein

D

DAG, diacylglycerol
DDC, 3, 5-diethoxycarbonyl-1,4-dihydrocollidine
Dkk, Dickkopf
Dox, Doxycycline
DR, ductal reactions
Dvl, Dishvelled

E

ECM, extracellular matrix
EDC, 1-ethyl-3-(-3-dimethylaminopropyl)
EMT, epithelial-to-mesenchymal transition
ER, endoplasmic reticulum

F

FAA, fumarylacetoacetate
FBS, foetal bovine serum
FDR, false discovery rate
FPMK, Fragments per kilobase per million
FW, Forward
Fzd, Frizzled

G

GSH, glutathione

H

HCC, hepatocellular carcinoma
HPCs, hepatic progenitor cells
HSPGs, heparin sulphate proteoglycans

I

IF, immunofluorescence
iPSCs, induced pluripotent stem cells
ISH, in situ hybridization

J

JNK, JUN N-terminal kinase

L

LCM, laser capture microdissection
LEF, Lymphoid Enhancing Factor
LRP, Lipoprotein Receptor-related Protein

LSECs, liver sinusoidal endothelial cells

M

MCD, methionine and choline-deficient
mES cells, mouse embryonic stem cells
MRP, multidrug resistance protein
mTORC1, mTOR complex 1

N

NASH, non-alcoholic steatohepatitis
NAFLD, non-alcoholic fatty liver disease
NHS, *N*-hydroxysuccinimide
NTBC, 2-(2-nitro-4-trifluoro-methylbenzoyl)-1,3 cyclohexanedione

O

4-OHT, (Z)-4-hHydroxytamoxifen
O/n, overnight

P

PCA, Principal component analysis
PCP, planar cell polarity
pcRNAseq, paired-single cell RNA sequencing
PEMT, phosphatidylethanolamine N-methyltransferase
PH, primary hepatocytes
PHorg-DM, PH organoid differentiation medium
PHorg-EM, PH organoid expansion medium
PHorg-IM, PH organoid isolation medium
PI, propidium iodide
PIP_2, phosphatidylinositol 4,5-biphosphate
PIP_3, 1,4,5-triphosphate
PKC, protein kinase C
PLC, phospholipase C
PXR, pregnane X receptor

R

RIP, regulated intramembrane proteolysis
Rnf43, Ring Finger 43
Rock, Rho kinase
Rspo, R-spondin
RT, room temperature
RV, reverse

S

SAM, S-adenosylmethionine
scRNAseq, single-cell RNA sequencing
sFRP, secreted Fzd-related proteins
SSEA-1, stage-specific embryonic antigen 1

T

TAA, thioacetamide
TCF, T-Cell Factor
tdTom, tdTomato

W

WRE, Wnt responsive element
WT, wild type

Z

Znrf3, Zinc and Ring Finger 3

Table of Contents

Chapter 1. INTRODUCTION

1.1 Significance of this research

With an estimated development cost of $2.6 billion per drug that reaches the clinic, there is a strong desire in the pharmacological industry to the decrease the dependence on animal models, speed up the time to market and reduce the high attrition rate of candidate drugs [1]. The detoxification of xenobiotics is mainly carried out by the hepatocytes in the liver. Hence, the development of *in vitro* models that better recapitulate the toxicology response of this organ is an attractive strategy to cover these needs.

Liver *in vitro* systems have been traditionally limited by the difficulty of expanding and maintaining functional adult hepatocytes in culture [2]. Recent advances in the liver organoid technology claim, however, to have improved both these aspects [3,4]. Now, a second great challenge in the extracorporeal recapitulation of liver function derives from the fact that the metabolic functions of this organ are distributed amongst different pools of hepatocytes. To date, no available liver *in vitro* system retains hepatocyte cellular heterogeneity and thereby this second challenge persists unsolved.

The ability to control the hepatocellular heterogeneity *in vitro* will not only have a great impact in the drug development pipeline and the pharma industry but also, in gaining understanding in the regulatory mechanisms that govern hepatocyte functional specification and spatial separation of physiological tasks amongst cells of the same apparent cell type. Furthermore, bioartificial liver devices have additionally other potential applications including the stabilization of patients undergoing acute liver failure, the support of liver functions to aid organ restoration alone or in combination with cell-based therapies and/or as 'bridge' treatment strategy during organ transplantation.

1.2 Adult mammalian liver architecture

The mammalian liver is organized into polygonal structural units, the hepatic lobules, that resembles the structure of a filter. Each hepatic lobule is centered on a branch of the hepatic vein (central vein, CV) and surrounded by multiple peripheral structures, portal triads, which are composed by bile ducts, the hepatic artery and the portal vein (Figure1.1). In the portal fields, blood rich in nutrients from the intestine transported by

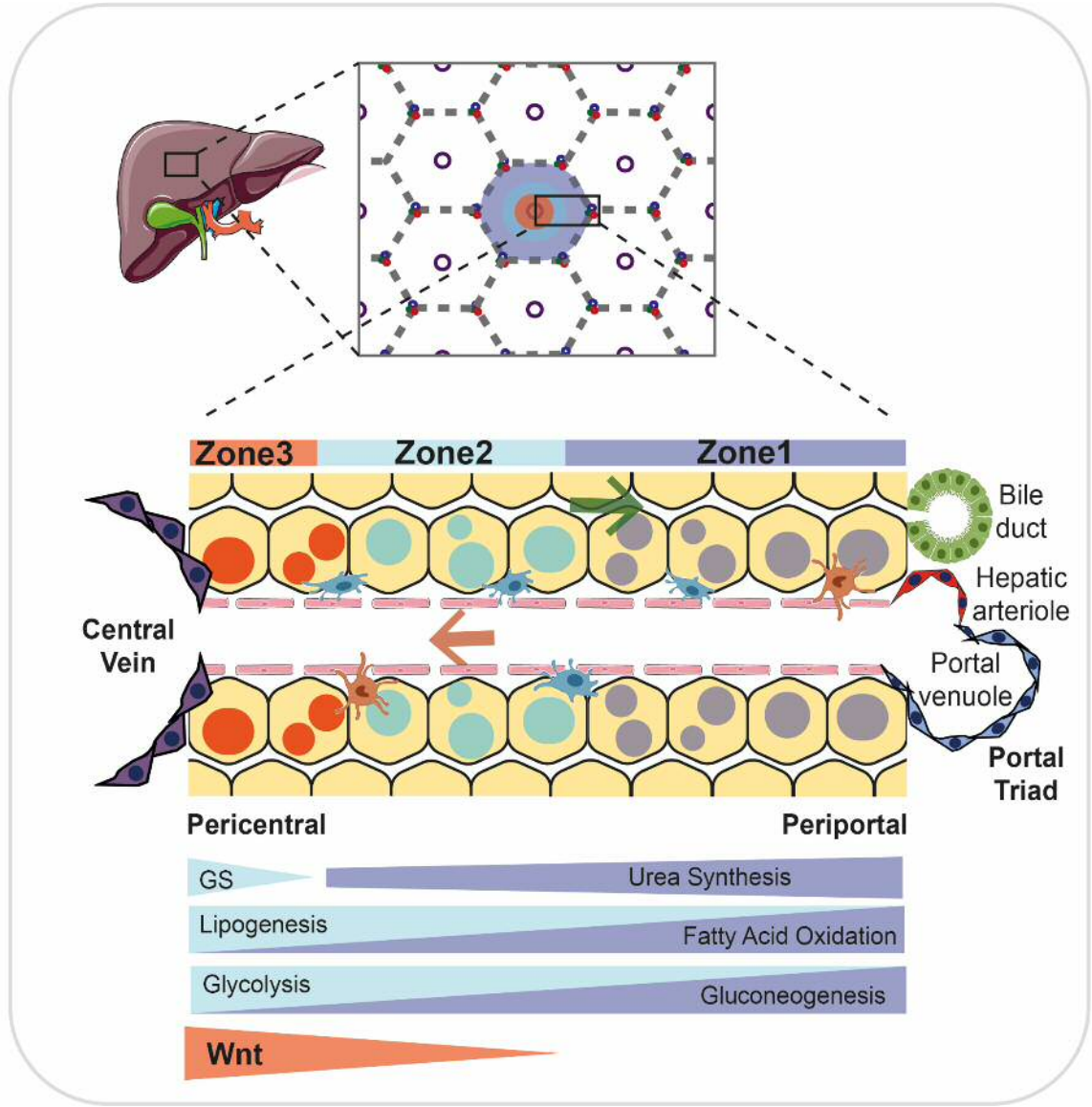

Figure1.1 Structure of the zonated liver lobule. The liver is organized in polygonal lobules. Blood flows from the portal venuole and hepatic arteriole through sinusoids to the central vein (CV). 14 to 25 hepatocytes escorted by liver sinusoidal endothelial cells (LSECs) are arranged in branching cords. Between the sinusoidal endothelial cells and the hepatocytes, a space (space of Disse) host other specialized cell types including phagocytic cells (Kupffer cells), stellate cells and occasionally, myofibroblasts. Bile produced by the hepatocytes is secreted into bile canaliculi and transported to bile ducts formed by BECs. Green and red arrows indicate the direction of the bile and blood, respectively. Hepatocytes have traditionally been described as having three different metabolic zones (zone1-3).

the portal vein mixes with oxygenated blood transported by the hepatic artery and flows through a network of heavily fenestrated liver sinusoidal endothelial cells (LSECs) that line up the hepatocytes, until it reaches the draining CV. Between the sinusoidal endothelial cells and the hepatocytes, a space (space of Disse), that contains components of the extracellular matrix (ECM), is created to host many other

specialized cell types including phagocytic cells (Kupffer cells), stellate cells and occasionally, myofibroblasts.

The liver harbors two epithelial cell types that share a common developmental progenitor (the hepatoblast): the hepatocytes and the bile duct epithelial cells (BECs) [5]. BECs are columnar epithelial cells that constitute the bile ducts and are polarized presenting one apical and one basal domain [6]. The apical domain faces the lumen of the bile duct and is covered by microvilli whereas the basal domain is in contact with the stroma and basal membrane and extracellular matrix.

The hepatocytes constitute around 60% of the cells of the liver and carry on most part of the metabolic functions of the organ [7]. The hepatocytes are epithelial cells 'atypically' polarized as they harbor more than one apical and basal domain [6]. The basal domains of the hepatocytes are 'smooth' cell surfaces that face the Space of Disse. By contrast, the apical surfaces of the hepatocytes are covered by cell microvilli and form an intricate network known as bile canaliculi, that collect the bile salts as well as other waste products that result from the metabolism of the hepatocytes. The diameter of the bile canaliculi is enlarged towards the portal fields and connect to the bile ducts through the canals of Hering, which are thought to be composed by cells with hybrid features between hepatocytes and BECs [8,9]. These 'hybrid' cells have been hypothesized to act as facultative hepatic progenitor cells (HPCs) in response to different injury stimuli (see section 1.8) [9,10]. The bile ducts connect with the gallbladder, where the bile stored for further release in the duodenum to assist in the digestion of lipids. Thus, the bile produced by the hepatocytes is drained out of the liver in the opposite direction to the blood.

1.3 Homeostatic turnover and regeneration of epithelial cells in the adult liver

The liver is an organ with extraordinary regenerative capacity. Upon surgical resection, it can grow and compensate for the loss of up to 70% of its mass [11]. In the adult organ, the homeostatic renewal of both hepatocytes and BECs is sustained by independent pools of epithelial cells.

Slow-dividing hepatocytes account for the cellular turnover of the hepatocellular compartment [12] [13]. Results from fate mapping of the hepatocyte population lining the central, described as positive for Axin2 expression, have suggested that pericentral ('high-Wnt') hepatocytes self-renew to replace more distally-located hepatocytes [12]. Axin2 positive hepatocytes, however, only replaced up to 30% of the liver parenchyma following a 'chase' period of 365 days, suggesting the presence of other hepatocyte pools accountable for the maintenance of the 70% of the remaining liver [12,14]. This is consistent with previous studies that showed slow-dividing hepatocytes positive for the expression of ki67 or PCNA are not restricted to pericentral hepatocytes but rather distributed along the lobule parenchyma with no preferential location [13,15]. Studies conducted by Lin et al. (2018) have also demonstrated that hepatocyte pools outside of the pericentral domain that express high levels of telomerase (Tert-CreERT2; R26-LSL-tdTom) also have the ability to self-renew and replace hepatocytes with lower levels of telomerase expression [13]. These observations, therefore, support the hypothesis that several pools of hepatocytes distributed along the parenchyma contribute to the homeostatic turnover of the hepatocellular compartment.

The biliary epithelium is renewed by cells committed to the BEC lineage (CK19 and HNF1β positive cells) [16,17]. Several studies have proposed the existence of a quiescent BEC progenitor population with inherent regenerative properties expressing genes such as Prom1, Foxj1, Sox9 and St14 [18-21]. Whilst recent studies conducted by Pepe-Mooney et al. (2019) using high-throughput single-cell RNAseq (scRNAseq) have failed to identify homeostatic BEC subpopulations enriched for traditional HPCs genes, Pepe-Mooney and colleagues have instead identified YAP signalling as the main driver of the transcriptional heterogeneity of amongst the different BECs subpopulations [22]. It remains currently unknown whether a defined pool of cells or all BECs account for the homeostatic turnover of the biliary epithelium.

Upon injury, the repair strategy of both epithelial cell types greatly depends on the type and extent of the damage. When the damage does not affect the proliferative capacity of BECs such as is the case following partial hepatectomy (the consequences of the different liver injuries strategies is explained in section 1.8), regeneration of the biliary

epithelium is fuelled by CK19-positive BECs. Similarly, self-replication of healthy or non-severely injured hepatocytes drives the regeneration of the hepatocellular compartment following administration of CCl_4, methionine and choline-deficient (MCD)/ choline-deficient, ethionine-supplemented
(CDE) diet, thioacetamide (TAA) or short-term exposure to 3, 5-diethoxycarbonyl-1,4-dihydrocollidine (DDC) (see section 1.8) [16,17,23,24].

By contrast, hepatocytes and BECs are able to transdifferentiate into each other's lineages to aid hepatobiliary repair when damage is prolonged or when the proliferation of the initial cell type is compromised. Hepatocyte-to-BEC transdifferentation has been described to occur following either bile duct ligation (BDL) or 18-week exposure to DDC, two injury regimes that induce damage of the biliary epithelium (see section 1.8) [25]. BEC-to-hepatocyte transdifferentation is has been exclusively reported when the proliferation of the pre-existing hepatocytes is impaired [17,23,24]. In mouse, there are at least three liver injuries strategies in which BECs escape their ductal committed state to give rise to mature and fully-functional hepatocytes: (1) administration of DDC diet for over 24 weeks, (2) depletion of β1-Integrin in the hepatocellular compartment in combination with DDC, MCD or TAA injury regime, (3) overexpression of p21 in the hepatocytes in combination with 2 weeks of CDE, MCD or DDC diet [17,23]. These mouse models will be explained in more detail in section 1.8.

Hepatocyte-to-BEC transdifferentation, and vice versa, is a liver regeneration strategy that may be of particular clinical relevance following long-term and repeated liver injury such as occurs during alcohol abuse, in response to an unbalanced diet or following virus infection. Progression of chronic liver disease, both in human and liver injury mouse models, is characterised by the formation of histologically defined ductal reactions (DR) [26-28]. DR are heterogeneous cellular systems originated in the vicinities of the portal triad tracks (canal of Hering, see section 1.2), which are composed by reactive HPCs, hyper-proliferative BECs, small hepatocytes with intermediate features as well as activated stellate cells and macrophages that infiltrate into the parenchyma. Although the dynamics of DR initiation are still unclear, it has been hypothesised that they act as HPCs amplifying niche. It remains also unclear

whether all BECs or only a subpopulation of BECs with HPC features can drive BEC-to-hepatocyte transdifferentation. It is also unknown whether these hypothetical BECs with HPC features reside in the vicinities of the canal of Hering.

1.4 The complexity of liver metabolic zonation

The liver is a secretory organ that carries out over 500 physiological tasks, including processes with biosynthetic and catabolic antagonistic roles such as gluconeogenesis/glycolysis or lipogenesis/fatty acid β-oxidation [7,14]. The fine-coupling of these processes is critical for the maintenance of the overall homeostasis of the body and is accomplished by the distribution of the liver labour in different subsets of hepatocytes. Thereby, the hepatocytes, rather than being a homogenous cell type, display a remarkable functional heterogeneity. In the current section, the complexity of such hepatocellular heterogeneity is reviewed. Later sections will discuss the physiological importance of this spatial division of liver's task in the metabolism of xenobiotics (section 1.6) and liver pathological states (section 1.7).

Hepatocyte functional heterogeneity is closely linked to the architecture of the liver. Based on their relative position in the porto/venous axis of the hepatic lobule, hepatocytes have been traditionally clustered in three metabolic groups (zone1 to 3) (Figure1.1) [29-31]. This first zonal classification was based on the patterns of expression of a defined set of markers (<10) using techniques such as immunohistochemistry or in situ hybridization (ISH) [29,31]. More recently, studies performed by Brosch et al. (2018), using RNAseq coupled to laser capture microdissection (LCM) to characterise the transcriptome landscape of pericentral, mid-lobular and periportal hepatocytes, have extended the panel of genes that are differentially expressed by periportal and perivenous hepatocytes to a total of 805 genes [32]. The authors of this study additionally concluded that mid-lobule hepatocytes constitute a 'transition zone' between periportal and pericentral hepatocytes rather than a zone with its own identity (Figure1.2) [32].

The studies conducted by Brosch and colleagues had a zonal resolution restricted by the number of areas dissected with LCM. To identify spatial patterns of gene expression with a higher resolution, Bahar Halpern et al. (2017) used a panel of 6 well-

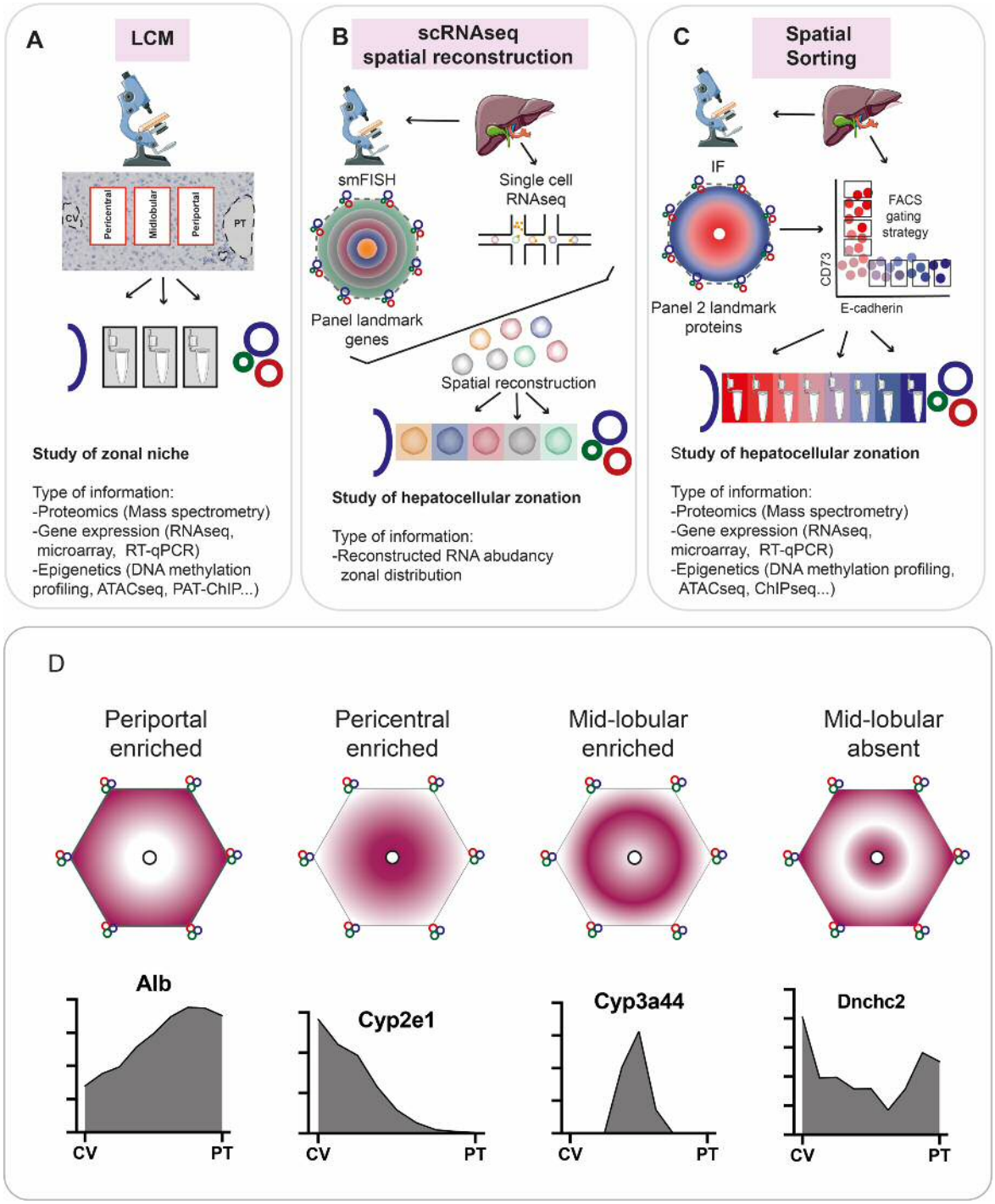

Figure1.2. The complexity of liver zonation (A) Laser capture microdissection (LCM) allowed the molecular profiling of small liver tissue areas from pericentral, mid-lobular and perivenous areas that aimed to exclude portal triad, connective tissue and central vein cells {Brosch:2018bi}. **(B)** Single cell RNAseq Spatial (scRNAseq) Reconstruction approach of Bahar Halpern et al. (2017) {Halpern:2017fm}. A panel of 6 landmark genes (Glul, Cyp2e1, Ass1, Asl, Alb and Cyp2f2) with differential zonal mRNA expression validated by smFISH was used to infer the location of individual hepatocytes in 9-zones in the lobule. **(C)** Spatial Sorting strategy from Ben-Moshe et al. (2019) based on the differential surface expression of two landmark proteins (periportal E-cadherin and pericentral CD73) for the 8-way zonal separation of hepatocytes by FACS {BenMoshe:2019ee}. (D) Gene expression patterns identified by Bahar Halpern et al (2017). On the bottom, representative examples of genes following such patters obtained by plotting Bahar Halpern et al (2017) data {Halpern:2017fm}.

characterized 'landmark' zonated genes characterised by FISH to infer the zonal

location of individually-isolated hepatocytes which had been subjected to scRNAseq (Figure1.2) [33]. Using this technique, termed scRNAseq spatial reconstruction, Bahar Halpern and colleagues generated a map of transcript abundance across the liver lobule with a near single-cell resolution (layers 1-9). According to this study, half of the genes expressed by the hepatocytes (~3500 out of 7000 genes) are not homogenously expressed across the liver lobule and these also include genes not directly involved in the cell metabolism such are E-cadherin. With this approach, Bahar Halpern and colleagues also identified a subset of genes that are specifically enriched in mid-lobular hepatocytes, arguing against the view that this region is a mere 'transition zone' (Figure1.2) [7,32,33].

A later study by Ben-Moshe et al. (2019) have also uncovered a transcriptomic and proteomic hepatocellular map using a technical approach termed 'spatial sorting'. Spatial sorting uses the surface expression of perivenous (CD73) and periportal markers (E-cadherin) to separate and isolate of hepatocytes into 8 spatially overlapping compartments by flow-cytometry (Figure1.2) [34]. Furthermore, it should be added that the phenomenon of asymmetric gene expression patterning in the liver is not restricted to hepatocytes but also present in LSEC, which can be clustered in at least two functional classes (pericentral and periportal) [35-37].

Taken together, the mammalian hepatocytes display complex gene expression patterns across the liver lobule. However, and for simplicity, a binary 'periportal' and 'pericentral' nomenclature will be generally used in this thesis when describing hepatocyte transcriptome and functional heterogeneity. Importantly, the term of 'liver zonation' in this thesis will be reserved to refer to the phenomenon of 'hepatocyte zonal specification'.

1.5 **Establishment of zonation in the developing liver**

Data about the onset of zonation in the developing liver remain limited to a few studies. Notenboom et al (1997) and Burke et al (2018) described expression of CPS1 and GS in hepatocytes as early as ~E15 and ~E13, respectively, although clear spatial segregation of hepatocytes expressing these markers into the periportal (CPS1) and pericentral (GS) areas did occur until ~E.18.5 [38] [39]. Burke et al (2018) further

reported that expression of both CPS1 and GS was highly increased after birth and that some CPS1 and GS double-positive cells were detectable in the 2-3 layers of hepatocytes surrounding the central vein form day P1 to P5. These results thereby suggest that, despite that segregation of these metabolic markers beings in the embryonic liver, maturation into the CPS1/GS mutually exclusive pattern observed in the juvenile (P15) and adult (> P30) liver occurs postnatally.

The onset and developmental pattern of expression for two zonated non-metabolic markers, E-cadherin and Claudin-2, have been also described. Ma et al (2020) reported that while E-cadherin protein is virtually present in all the hepatocytes of the foetal (E18.5) and new-born (P2) livers, expression of this protein is restricted to periportal hepatocytes in the juvenile liver (P15) [40]. In the same study, using a Cldn2-eGFP transgenic mouse model where presence of eGFP protein is used as a proxy for Claudin-2 expression, Claudin-2 expression was completely absent in the foetal liver (E18.5E) and ubiquitously expressed amongst new-born hepatocytes (P2) with no-zonal preference. Expression of Cldn2-eGFP was however found restricted to pericentral cells at P15, indicating that zonation of Claudin-2 is completely initiated postnatally. Furthermore, Ma et al (2020) further described that periportal and pericentral expression of E-cadherin and Claudin-2, respectively, was further accentuated from the juvenile (P15) to the adult (P30) liver, suggesting that complete zonal specification for these non-metabolic markers occurs during adulthood.

Taken together, it seems that while some zonation features are acquired prenatally, the full acquisition of a hepatocyte functional identity occurs after birth.

1.6 **Molecular determinants of hepatocyte functional specification**

The fact that hepatocyte functional specification is not fully-established prior to birth suggests that important molecular determinants of zonation enter in association with the hepatocytes postnatally. Some of these factors might be linked to the changes in the circulation and blood flow that occur in the neonate just after birth. During gestation, mammalian foetuses receive nutrients and oxygen necessary for their development through the umbilical vein that connects with the placenta. Around two-thirds of the blood supplied by the umbilical vein meets the embryo vascular system through the hepatic portal vein and one-third bypass the liver and reaches circulation

through a shunt (the ductus venosus) that connects the umbilical vein with the foetus inferior vena cava (IVC). After birth, the umbilical cordon is clamped and the ductus venosus closes (normally within the first week after birth), establishing the blood circulation through the liver as it will be maintained throughout adulthood.

Jungermann and Katz in 1989 introduced for the first time the idea that factors carried by the blood might be key for the maintenance of zonation in adulthood. They observed that the architecture of the liver lobule gives rise to polarized blood flow and proposed that depletion of morphogens together with the secretion of biological cues into the bloodstream generate complex microenvironments that might shape the transcriptional program of the hepatocytes (Figure1.3, A) [41]. This model was termed the 'upstream-downstream' hypothesis as the metabolism of periportal hepatocytes would affect the behaviour of pericentral hepatocytes.

In the adult liver, the oxygen tension drops ~30 mmHg (~42 μmol/L) from the periportal to the pericentral sinusoids and thereby this morphogen has been traditionally view as a key determinant of zonation [42]. According to this notion, transcriptome profiling studies have recently revealed that the transcriptome of the hepatocytes of the hepatocytes matches the patterns of availability of oxygen as periportal hepatocytes are overall more invested in energetically-demanding tasks such as synthesis of albumin, gluconeogenesis or ureagenesis [7] [33]. Mitochondria content and morphology have also been shown to variate along the porto/venous axis [7,43]. Furthermore, electron microscopy studies have also shown that periportal hepatocytes contain increased numbers of free lysosomes and autophagosomes when compared to their pericentral counterparts [43]. Direct evidence that oxygen modulates hepatocyte gene expression comes from *in vitro* studies that showed that oxygen levels in primary hepatocytes cultured in conventional monolayers or in a bioreactor influences the expression levels of pericentral markers members of the cytochrome

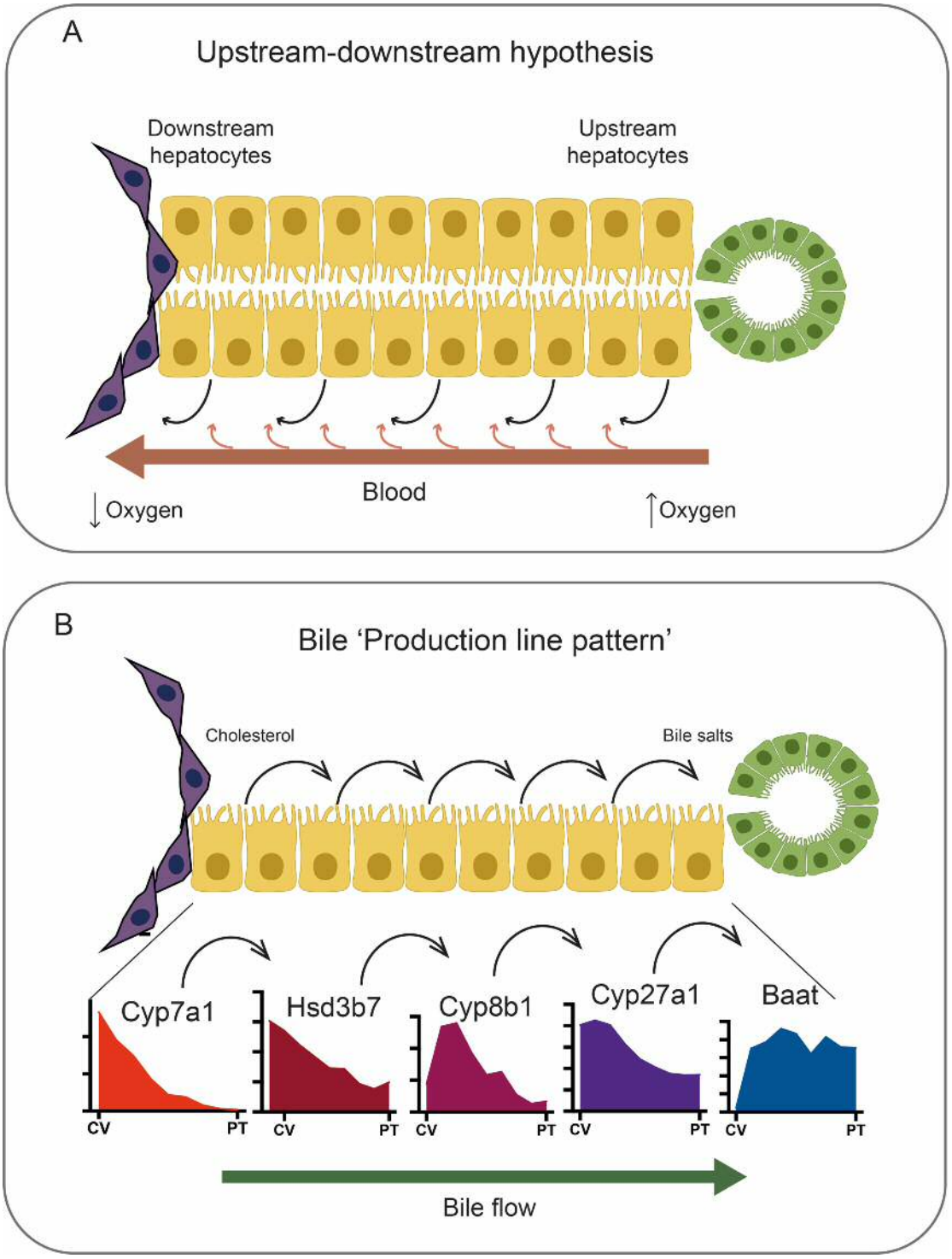

Figure1.3 Complex microenvironments are created along the CV-PT axis. (A) The upstream-downstream hypothesis sustains that polarization of liver metabolic functions arise as a consequence of the polarized bloodstream. According to this hypothesis, the metabolic activity of periportal (upstream) hepatocytes influences the genetic patterning of pericentral (downstream) hepatocytes. **(B)** The expression of enzymes 'production line pattern' of the bile argues against the unidirectionality of the original 'downstream-upstream' hypothesis as pericentral hepatocytes might also affect the microenvironment of periportal hepatocytes by controlling the production of rate limiting metabolites that are transported through the bile.

P450 family [44,45]. Despite this, none of the three-mammalian hypoxia-inducible

transcription factors (HIF1α, HIF2α, HIF3α) that commonly mediate oxygen responses are found transcriptionally zonated in the murine liver [33]. A direct for oxygen as a determinant morphogen in the establishment of zonation is yet to be determined *in vivo*.

Diverse hormones including glucagon, insulin, glucocorticoids, growth factors or thyroid hormones have also been proposed to control the expression patterns of enzymes involved in the biosynthesis of bile acids and cholesterol, ketogenesis, fatty acid β-oxidation and lipogenesis among others [46,47]. 9% (298 genes out of 3,496 genes) of all zonated genes appeared to be modulated by Ras-dependent mechanisms and expression of EGF receptor (*Egfr*) highly increases towards the portal region [33,48]. Accordingly, periportal hepatocytes cultured *in vitro* respond to lower concentrations of EGF than pericentral hepatocytes [49]. While no genetic model has yet proven that manipulations in *Egfr* expression affects the gene expression patterns of the hepatocellular compartment, the organoid protocol of Peng et al. (2018) showed that an EGF-based medium induces the mRNA levels of periportal genes in primary hepatocyte-derived organoids, implying an active role of this mitogen in the modulation of the gene signature of periportal hepatocytes [3].

The 'upstream-downstream' hypothesis is also extended to the establishment of metabolite gradients as the metabolic activity of the hepatocytes will impact the concentration of these in the blood stream upon consumption/production [47]. Interestingly, in a recent review, Ben-Moshe have pointed out to the presence of potential metabolite 'production line patterns' which are sustained by the sequential expression in adjacent hepatocyte layers of enzymes involved in the same metabolic pathway [7]. The 'production line pattern' hypothesis argues that intermediate metabolites are transferred from layer to layer of hepatocytes (Figure1.3, B). This is the case of the enzymes involved in the bioconversion of cholesterol to bile acids: pericentral hepatocytes highly express Cyp7a1 and Hsd3B7, which convert cholesterol to the first two bile acid metabolites intermediate (7α-hydroxylcholesterol and 7a-hydroxy-4 cholesten-3-one) [50]. These metabolites are then transferred to mid-lobular and periportal hepatocytes which are enriched for the expression of the enzymes (Cyp8b1, Cyp27a1 and Baat) that catalyse later reactions of the bile

synthesis pathway (Figure1.3, B). Importantly, the bile acid production line pattern is not only an illustration of the fine coupling of liver metabolic processes but also an example of how the metabolism of pericentral hepatocytes may also shape the microenvironment of periportal cells as the bile flows from pericentral to periportal hepatocytes. This particular 'line production pattern' argues therefore against the unidirectionality of the original 'downstream-upstream' hypothesis which only considered the transport of morphogens through the bloodstream and gives a flavour of the complexity of the hepatocyte-to-hepatocyte cell communication events that contribute to the establishment of zonation.

Other molecular determinants of liver zonation that are not initiated as a direct consequence of the bloodstream include a pericentral Wnt activation gradient that spreads out from the central vein to the mid-lobule and it is estimated that ~30 % of the zonated genes are under the transcriptional control of β-catenin, the main downstream effector of the canonical pathway [14] [33,51]. As the molecular mechanisms underpinning Wnt-driven zonation are of special interest in this thesis, a detailed introduction to the Wnt signalling pathway and its role in modulation of hepatocyte functional specification both in the developing liver and in adulthood will be elaborated in more detail in section 1.10 and 1.15.

1.7 Implications of liver zonation in the metabolism of xenobiotics

The clearance of xenobiotics in the liver can occur in three different phases. First, reactive groups are introduced into the xenobiotics by phase I reactions, which include chemical reactions such as oxidation, reduction, hydrolysis and acetylation [52]. In occasions, these reactions may lead to the biotransformation of inactive compounds to a pharmacologically active form. Enzymes involved in the catalysis of phase I reactions include members of the cytochrome P450 oxidase family and their expression is generally enriched in pericentral hepatocytes, although some members can also been found preferentially expressed in periportal hepatocytes or mid-lobule hepatocytes [52]. Drugs that are metabolized by phase I reactions are steroids, paracetamol and phenothiazines amongst others.

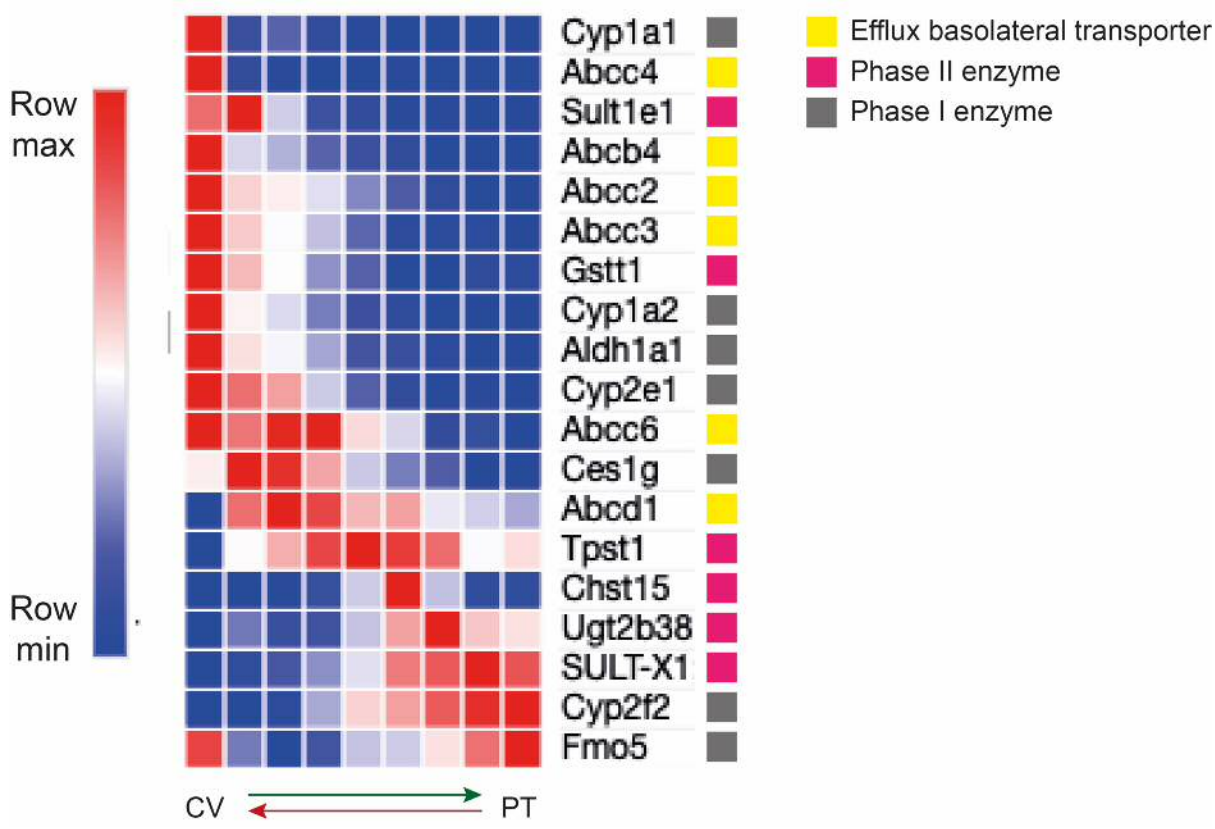

Figure1.4 Gene expression patterns of efflux basolateral transporters and Phase I and Phase II enzymes across the liver lobule obtained from Bahar Halpern et al (2017) scRNAseq data. Green and read arrows indicate the direction of the bile and blood flow, respectively.

Phase II reactions involve the chemical conjugation of polar or 'activated' xenobiotics to other polar molecules including gluthathione (GSH), glucuronide, sulfate and amino acids such as glycine [52]. The resulting product of these reactions is generally a more hydrophilic compound that can be either further modified, recycled or excreted into the bile by efflux pumps by the cell. Enzymes involved in the catalysis of phase II reactions include transferase enzymes such as glutathione S-transferase (GSTs proteins), methyltransferases, sulfotransferases, N-acetyltransferases and amino acid N-transferases (acetylation), XM-ligase and glycine N-acyltransferase (two step conjugation of glycine) or UPD-glucuronosyltransferases [52]. The expression of Phase II enzymes is generally enriched in, but not restricted to, periportal hepatocytes. Importantly, not all Phase II conjugates are 'activated' products derived from Phase I reactions. Instead, some xenobiotics containing polar groups may be direct substrates for these reactions. Phase II reactions may also lead to the pharmacological activation and increase toxicity of certain metabolites.

After phase II reactions, certain compounds may be further processed by phase III enzymes. Phase III reactions generally introduce modifications that facilitates the excretion of the metabolized compounds through a member of the multidrug resistance protein (MRP) family [52].

The expression of Phase I, Phase II and Phase III enzymes is zonated, meaning that coupling of these reactions may be subjected to the directionality of the blood/bile flow and/or transmission of metabolites between adjacent hepatocytes [34] (Figure 1.4). This, together with the fact that the catalysis of xenobiotics by Phase I and II reactions may result in the formation of activated metabolites with enhanced toxicity and thereby causing the zone-specific necrosis of the hepatocytes that metabolized them, makes the study of liver zonation necessary for a better prediction of potential drug-drug interactions and understanding of the putative mechanisms of toxicity as well as the overall impact of these in liver pathophysiology.

1.8 Metabolic zonation in liver pathological states

The boundaries of the liver metabolic zones are dynamic and subjected to changes in the hepatocellular microenvironment. As an example, mice deficient for glucagon expression, a peptide hormone that modulates the body energy metabolism by increasing the systemic levels of glucose and fatty acids and thereby with opposing effects to insulin, from developmental stages ($Gcg^{-/-}$) have altered protein and gene expression patterns in the liver lobule as they present enlargement of the areas covered by pericentral GS protein [48].

As result of this plasticity amongst the metabolic zones, disturbances in the liver zonation patterning are common in a plethora of liver pathologies, including fatty liver disease, cirrhosis, hepatitis and hepatocellular carcinoma. As a particular example, the expression of the pericentral enzyme phosphatidylethanolamine N-methyltransferase (PEMT) becomes progressively pan-lobular in patients undergoing simple steatosis and non-alcoholic steatohepatitis (NASH) [53]. Hence, the understanding of the basic principles of homeostatic liver zonation is therefore also at the heart of the understanding of the changes underlying different liver pathological states and is necessary for the development of potential therapies that alleviate their symptoms. Furthermore, the fact that the boundaries of zonation are dynamic

implicate that to accurately predict drug-liver induced toxicity in hepatocyte cultures, *in vitro* systems must permit hepatocyte-to-hepatocyte communication and the maintenance of hepatocyte cellular heterogeneity in a continuous.

1.9 Animal models/liver injury strategies to study hepatic regeneration

Upon injury, the repair strategy of the liver greatly depends on the type and extent of the damage. In the current section a brief summary of the most widely used liver injury strategies for the study hepatobiliary regeneration in animal models is provided.

1.9.1 Partial hepatectomy

Partial hepatectomy involves the surgical removal of a proportion of the adult liver. Normally a whole liver lobule is resected and, depending on the size of this lobule it is considered that either 30 or 70% of the liver mass has been removed. The remaining liver grows back and compensate for the loss of organ function by increasing the number of cells and/or hepatocyte size [54]. Regeneration in this model is driven by healthy cells.

1.9.2 Chemical injury

This type of injury strategy involves the administration of a toxic compound intraperitoneally, intravenously or by oral administration. Among the most common used compounds are TAA, 2-acetylaminofluorene (2-AAF), CCl_4 and DDC. Chemical agents can also be administrated in combination with partial hepatectomy.

TAA

Hepatocytes from zone 1 and zone 3 metabolize TAA into hepatotoxic TAA sulfine, causing an increase of reactive oxygen species (ROS). Exposure to TAA promotes necrosis of the hepatocytes leading to fibrosis. Long-term exposure to TAA induces cirrhosis and can lead to cholangiocarcinoma and HCC [55].

2-AAF

Administration of 2-AAF alone does not induce itself expansion of HPCs, however, this chemical injury in combination with partial hepatectomy induces prominent HPC regenerative response as early as 3-days after the surgery [56]. Prolonged exposure to 2-AAF causes malignant transformation in the liver, kidney and bladder.

CCl_4

CCl_4 administration is metabolised by Cyp2e1, an enzyme expressed by pericentral hepatocytes, leading to the production of unstable metabolites (trichloromethyl, CCl^*_3, and trichloromethyl per-oxyl, CCl_3OO^*) with free radicals. This leads to ROS-mediated cellular stress and finally cell apoptosis. Administration of CCl_4 induces prominent necrosis of pericentral hepatocytes, causes fibrosis and a modest HPC response [55].

DDC

DDC is a chemical compound that when is metabolized by enzymes members of the Cyp3a P450 cytochrome subfamily leads to the accumulation of protoporphyrin within the biliary epithelium [57]. Protophorphyrin accumulation leads to cholangitis, BEC proliferation, biliary fibrosis and leads to a decrease in bile flow and, therefore, DDC diet is used as a model for cholestatic liver disease [58] [59]. This type of injury regime is characterized for the formation of a prominent ductular reaction in the portal tract region and composed of HPCs with bipotent properties. Prolonged exposure to DDC ends causing additional damage in the hepatocytes, and has been previously used to model chronic human biliary disorders where hepatocellular necrosis is common.

1.9.3 Dietary interventions

Dietary interventions can vary from changes to diets with high content of fat such as high fat diet use to model non-alcoholic fatty liver disease or DDC or MCD injury regime. The most commonly used are the MCD and CDE diets.

CDE

Choline is a precursor of cell membrane phospholipids (phosphatidylcholine and sphingomyelin) and is required for the assembly and release of very low-density lipoproteins. Ethionine is a non-proteinogenic amino acid that structurally resembles the essential amino acid methionine, therefore acting as methionine antagonist and thereby preventing the incorporation of this amino acid into proteins. CDE diet leads to steatosis, hepatocellular hyper-proliferation, inflammation and fibrosis [59]. When administrated for long periods, CDE injury regime can lead to hepatocellular carcinoma (HCC) [60]. This injury regime also leads to the formation of DR although

these are less pronounced than in other injury regimes such as DDC [59]. When administrated for long periods, CDE injury regime can lead to HCC.

MCD

The MCD injury regime consists of methionine and choline-deficient diet. Methionine is an essential amino acid required for the synthesis of S-adenosylmethionine (SAM) and GSH whereas choline is a precursor of cell membrane phospholipids (phosphatidylcholine and sphingomyelin) and is required for the release of triglycerides. The MCD diet leads to lipid accumulation in the hepatocytes, hepatocellular hyper-proliferation, inflammation and fibrosis and, similarly to the CDE injury regime, is used as a model for NAFLD and NASH [55,61] [62]. Prolonged administration of MCD diet can result in the development of HCC in mouse [61].

1.9.4 Strategies for the impairment of hepatocyte proliferation

Depletion of β1-Integrin

β1-Integrin is expressed in various liver cell types including hepatocytes, BECs, hepatic stellate cells and sinusoidal cells. Loss of β1-Integrin in the hepatocytes results in inhibition of hepatocyte growth signaling and thereby impairing hepatocyte proliferation during liver regeneration [17]. Specific deletion of β1-Integrin in the hepatocytes can be achieved by the tail injection of AAV8 adenoviral particles carrying the sequence for Cre recombinase (AAV8.Cre) in animals in which *Igtbl,* the gene coding for β1-Integrin is flanked by two loxP sites (β1-Integrin$^{fl/fl}$). β1-Integrin deletion in combination with DDC, MCD or TAA injury regime has been shown to promote repopulation of the hepatocellular compartment with cells derived from the biliary epithelium [17].

Overexpression of p21

Senescence a state of permanent cell cycle arrest state initiates by various stress-inducing factors such as DNA damage, shortening of the telomers, autophagy, oxidative stress, etc. The senescence program can be initiated through p53-mediated activation of p21, which causes the inhibition of cyclin-dependent kinase2 (CDK2) [63]. In the absence of CDK2, Rb remains hypophosphorilated and promotes cell cycle exit. Overexpression of p21 in the hepatocytes by the tail injection delivery of AAV8

adenoviral particles containing p21 coding sequence (AAV8.p21) has been shown to be sufficient to inhibit hepatocyte proliferation in response to CCl4 acute liver injury [17]. Raven et al (2017) showed that overexpression of p21 in the hepatocytes in combination with MCD or DDC injury regime promotes BEC-to-hepatocyte transdifferentation [17].

1.10 The Wnt signalling pathway

The Wnt pathway plays a central role in the development, homeostasis and regeneration of the liver (see section 1.10 to 1.14). This pathway is activated through the binding of Wnt-secreted proteins to membrane receptors of the Frizzled (Fzd) family, which triggers an intracellular signalling that breaks in three major cascades: (1) the canonical or Wnt/β-catenin pathway, (2) the Wnt/Planar Cell Polarity (PCP) pathway and (3) the Wnt/Ca2+ pathway [64]. The Wnt intracellular cascades (2) and (3) are independent on β-catenin transcriptional activity and thereby, are also commonly referred as non-canonical Wnt cascades. In this section, the main branches of the Wnt signalling cascade together with the different Wnt ligands and their cognate receptors will be discussed (Figure 1.5).

1.10.1 The Wnt/β-catenin signalling cascade

Activation of the Wnt/β-catenin, also known as 'canonical Wnt signalling', requires the presence of at least two types of receptors: a receptor from the Fzd family and a receptor from the low-density Lipoprotein Receptor-Related Protein (Lrp5 or Lrp6) family [65]. Among the receptors Lrp5 and Lrp6, the member Lrp6 has been more studied in more detail. In the absence of Wnt proteins, β-catenin protein is actively targeted for β-Trcp mediated degradation by a complex comprising the Axin1, APC, PP2A, GSK3 and CK1γ proteins [66]. Lrp5 and 6 have five PPPSPxS motifs susceptible to phosphorylation [66]. Binding of Wnt proteins to Fzd and Lrp receptors induces the recruitment of Dishevelled scaffold protein (Dvl), which polymerizes though its DIX domain and enables the association of various Wnt ligand-receptor units known as the 'Wnt signalosome' at the cell surface [67]. Recruitment of Dvl, causes the binding of GSK3, which phosphorylates the intracellular PPPSPxS motif of Lrp6 priming the receptor for a second phosphorylation by CK1γ. Axin also engage and is incorporated in the Wnt signalosome through DIX-DIX interactions established

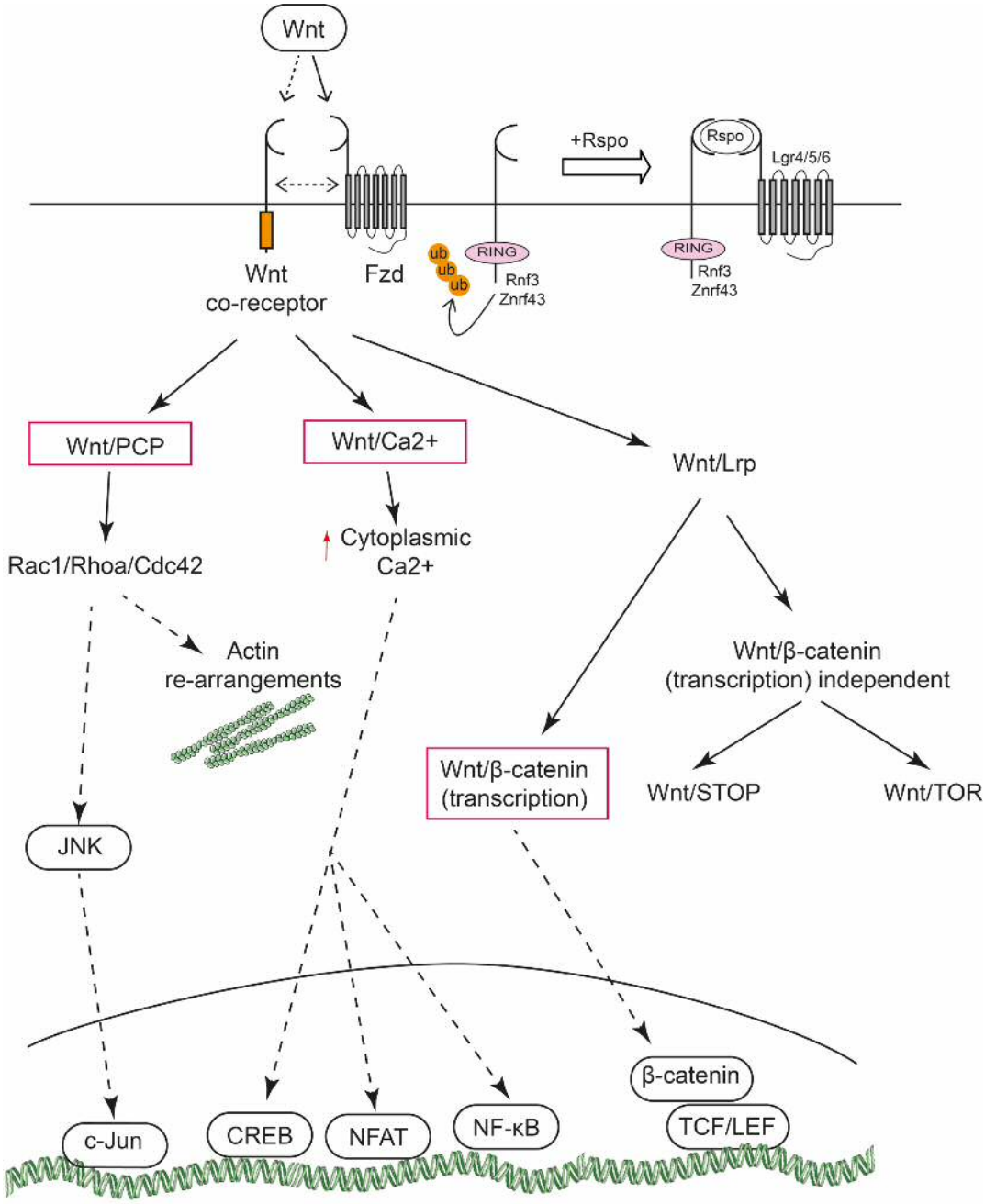

Figure1.5 The Wnt signaling pathway. The Wnt signaling pathway brakes in three major cascades: (1) the canonical or Wnt/β-catenin pathway, (2) the Wnt/Planar Cell Polarity (PCP) pathway and (3) the Wnt/Ca2+ pathway.

with Dvl. Upon formation, the signalosome is internalized via a Clathrin- or Caveolin-dependent mechanism [68]. These molecular events lead to the sequestration of other members of the recruitment of the β-catenin destruction complex (APC) and culminate with β-catenin protein stabilization and translocation to the cell nucleus where this protein modulates gene expression.

β-catenin (coded by the gene Ctnnb1) is a transcription factor co-activator as it does not contain itself a DNA binding domain. To regulate gene expression, β-catenin associates primarily with members of the T-Cell Factors (TCF)/ Lymphoid Enhancing Factors (LEF) family. DNA binding sites for TCF/LEF factors are found in the Wnt responsive element (WRE) sequences that regulate the expression of many canonical Wnt target genes. Generally, TCF/LEF factors are bond to WRE sequences prior to the arrival of β-catenin and may act as transcriptional repressors by associating with other proteins such as Groucho. When β-catenin is absent, however, DNA bound TCF/LEF factors are unable to drive gene expression and may act as transcriptional repressors. Thus, expression of a reporter gene such as firefly luciferase or eGFP under the control of several TCF/LEF binding motifs is commonly used as a proxy for Wnt pathway activation. Importantly, the genetic program elicited by β-catenin is cell-context dependent, Axin2 being one of the few common target genes amongst the different β-catenin-driven genetic programs.

To date, there is a growing body of the literature that recognises the importance of cell membrane scission and internalization of the Wnt signalosome for the activation of the Wnt/β-catenin signalling cascade. Importantly, the intracellular assembly of the Wnt

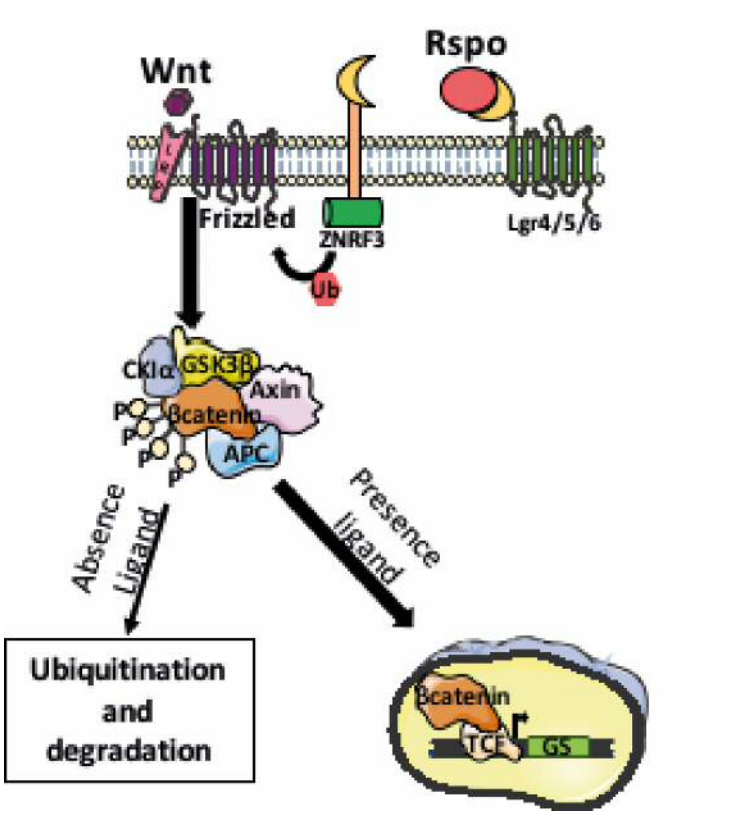

Figure1.6 The canonical Wnt pathway

signalosome, which is driven by the polymerization of Axin and Dvl and that causes the stable sequestration of the proteins of the β-catenin destruction complex and activation of the Wnt signalling cascade, should be distinguished from its subsequent internalization and the cellular process of endocytosis.

1.10.2 **The Wnt/PCP and the Wnt/Ca^{2+} signalling cascades**

In vertebrates, the Wnt/PCP and the Wnt/Ca^{2+} considerably overlap. As previously mentioned, both the Wnt/PCP and the Wnt/Ca^{2+} pathways are initiated with the binding of Wnt ligands to a Fzd receptor, which triggers the recruitment of Dvl at the cell surface [69].

The Wnt/Ca^{2+} pathway causes the activation of heterotrimeric G proteins, which mediate the activation phospholipase C (PLC) [69]. PCL catalyses then the hydrolysis of phosphatidylinositol 4,5-biphosphate (PIP_2), producing two secondary messengers, diacylglycerol (DAG) and 1,4,5-triphosphate (PIP_3). The hydrophobic DAG diffuses through the plasma membrane where, in the presence of Ca^{2+}, activates protein kinase C (PKC) whereas the soluble PIP_3 diffuses in the cytoplasm and binds to its receptor (InsP3R), which is a ER-bound Ca^{2+} channel that leads to the release of Ca^{2+} [70]. The increase of Ca^{2+} cytoplasmic levels then activates the Ca2+-responsive kinases PKC and CamKII as well as the phosphatase calcineurin, which modulate NFκB nuclear translocation. PKC additionally controls the nuclear shuttle of CREB whereas calcineurin and CamKII modulate the activity of the transcription factor NFAT [70].

In the Wnt/PCP (also referred as Wnt/JNK signalling cascade), recruitment of Dvl results in the activation of the small GTPases Rac1, Cdc42 and RhoA. This results in the activation of JUN N-terminal kinase (JNK) and Rho kinase (Rock) [71]. Activation of Rac1 is also mediated by PI3-kinase. These molecular events elicit remodelling of the cytoskeleton, changes in cell polarity and mobility. Activation of JNK can result in the activation of various transcription factors including c-Jun, ATF2, Sp1 and c-Myc (Figure1.5) [72].

1.10.3 **Other Wnt/Lrp6-dependent signalling cascades**

In addition to the Wnt/β-catenin cascade, phosphorylation of Lrp6 can activate a number of cellular processes independently β-catenin transcriptional activity. For instance, Lrp6 modulates the cellular localization of Axin1, APC and Dvl, proteins that also associate with the cytoskeleton and centrosome and participate in cell division, cell migration and cellular polarity [73]. Furthermore, Lrp6 modulate the activity of GSK3, which in turn regulates many other intracellular cascades including regulation of mTOR complex 1 (mTORC1) activity [73,74]. Lrp6 phosphorylation also mediates a recently described Wnt cascade known as the Wnt/STOP pathway that regulates cellular protein levels and cell size (Figure1.5) [75].

1.10.4 **Non-transcriptional roles of β-catenin**

In addition to its role as a transcription factor, β-catenin is also a structural component of adherens junctions (AJs) and mediates the association of cadherins (E-cadherin) with other catenins (α-catenin) thereby connecting the cell cytoskeleton to AJs. Adequate β-catenin/E-cadherin associations are required for the maintenance of cell polarity and adhesion and are often altered in pathologies such as cancer disease.

1.10.5 **Receptors of the Wnt signalling pathway**

The Fzd receptors are a family of seven transmembrane receptors composed by 10 members (Fzd1-10) [65]. The Fzd receptors participate in the signal transduction of both canonical and non-canonical cascades. These receptors display a high degree of homology and differences in their sequence are mostly related with modifications in their Cysteine Rich Domains (CRDs), which corresponds to the extracellular domain of the protein that binds to Wnt proteins. The CRD domain of each Fzd receptor have distinct predicted affinities for each ligand of the Wnt protein family. Thus, research efforts are currently being paid to link specific Wnt-Fzd interactions with the preferential activation of one or another branch of the signalling cascade.

Wnt proteins also bind to other Wnt co-receptors that are involved in the signal transduction of β-catenin dependent (Lrp5/6, Reck, Grpc124) and independent (Ror1/2, Vangl1/2, Ryk, PTK7, MUSK) branches of the Wnt signalling pathway [69,76,77].

1.10.6 Wnt ligands

In humans and mice, the family of Wnt proteins comprise 19 members that regulate a plethora of cellular processes based on the receptors and co-receptors they bind at the cell surface together with the intracellular state [78]. The Wnt proteins are secreted Cys-rich ligands highly conserved thorough evolution. For their secretion, Wnt ligands need to be palmitoleated in the endoplasmic reticulum (ER) by the acetyltransferase Porcupine. This modification of Wnt proteins is necessary for their transport through the Golgi and subsequent secretion. Thereby, inhibitors for Porcupine activity such as LGK974 are used to pharmacologically block Wnt secretion. Genetically, secretion of Wnt proteins can be disrupted by the deletion of Evi (the mammalian homologue of *Wls* in *Drosophila*), a carrier protein necessary for the transport of Wnt ligands from the ER/Golgi to the plasma membrane [79].

Wnt proteins contain hydrophobic modifications and therefore they usually work as short-range secreted signals. How long-range Wnt patternings are maintained in different tissues is a current topic of investigation. In the mammalian intestine, Wnt morphogen gradients have been proposed to arise as a result of the transmission of membrane-bound Wnt proteins following cell division [80]. Transport of membrane-bound Wnt ligands may occur by the association of Wnt proteins to cell surface heparin sulphate proteoglycans (HSPGs) such as Dally and Dlp (Drosophila glypican homologues for the mammalian GPCs) [81]. Wnt proteins may alternatively travel extracellularly accompanied by protein chaperones such as secreted Fzd-related proteins (sFRP) that hide their hydrophobic sequences or bound to exosomes.

Historically, Wnt proteins have been divided into canonical and non-canonical Wnt ligands based on their ability to activate the Wnt/β-catenin signalling cascade. However, such classification has come to question in the recent years as many of the Wnt proteins have been shown to be able to activate both branches of the Wnt cascade depending on the cellular context and array of Wnt receptors and co-receptors available at the time of the signalling [78]. Thence, it seems currently more adequate to refer as Wnt ligands that preferentially activate the canonical Wnt signalling pathway (eg. Wnt1, Wnt3a and Wnt8) or the non-canonical Wnt cascade (eg. Wnt5a, Wnt11, Wnt7b and Wnt7a).

1.10.7 **Wnt agonists and antagonists**

The Wnt signalling pathway is also modulated at the receptor level by the presence of agonists, such as R-spondin (Rspo) proteins. There are four members (Rspo1 to 4) in the Rspo family. Rspo proteins interact with seven-transmembrane Lgr4/5/6 receptors. This causes the inhibition of the Zinc and Ring Finger 3 (Znrf3) and Ring Finger 43 (Rnf43) E3-ubiquitin ligases which otherwise would degrade the Wnt receptors [77,82]. Out of the four members of the Rspo family, Rspo2 and Rspo3 have the ability of binding directly to Znrf3 and Rnf43 E3-ubiquitin ligases and therefore, do not require of the presence of Lgr receptors to potentiate Wnt signalling. Other proteins with Wnt agonistic activity include Norrin [69,82].

The Wnt signalling pathway is additionally modulated by proteins with antagonistic activity, such as members of the protein families of Dickkopf (Dkk1-3), secreted Fzd-related proteins (sFRP1-5, WIF1 and Cerberus) and Sclerostin (and its homologue Wise). Dkk proteins bind to Lrp receptors and compete for the same binding sites than Wnt proteins [69]. By contrast, sFRP proteins contain an extracellular domain structurally similar to the Fzd CRD and sequester and therefore prevents activation of the pathway by sequestering Wnt proteins [65].

1.11 Wnt signalling in BEC and hepatocyte lineage specification

The Wnt signalling pathway plays a pivotal role during liver foetal development. Firstly, Wnt and BMP signals orchestrate gastrulation in mammals. Then, inhibition of Wnt signalling in the foregut endoderm through the secretion of sFRP factors is required to permit the expression of Hhex, a transcription factor that promotes hepatic specification [8,83]. After foregut specification (~E9.5), initiation of the liver but is directed by TGF-β and Notch signals. The liver bud is comprised of bi-potent hepatoblasts, common developmental progenitors of both BEC and hepatocytes, that express markers such as Tbx3, Cebpa, Hnf4a, Albumin, Sox9, Hnf6, Hnf1b, Prox1 and α-fetoprotein (AFP). After initiation of the liver bud, the Wnt/β-catenin pathway is reactivated and, together with HGF, BMP and FGF factors, promotes hepatoblast proliferation and survival. A subpopulation of the hepatoblast pool (~2% of the bulk) placed at the apex of the bi-potent hierarchy, is positive for the expression of the β-

catenin target gene Lgr5, which is also the receptor mediating potentiation of Wnt signalling by Rspo ligands [84]. Stabilization of β-catenin by APC deletion in hepatoblasts promotes biliary fate specification [85]. Upon BEC maturation, the Wnt/β-catenin signalling pathway is, however, inhibited by Sox17 [83]. β-catenin seems also necessary for the commitment of hepatocytes as deletion of this in the mouse embryos also resulted in defects in hepatocyte maturation [83].

Altogether, tight spatiotemporal control of the Wnt/β-catenin pathway is required for hepatic development and adequate BEC/hepatocyte lineage specification and maturation.

1.12 Wnt signalling during homeostatic hepatocyte turnover and regeneration

In the adult liver, the Wnt/β-catenin pathway orchestrates hepatocyte homeostatic turnover as stabilization or loss of the transcription factor β-catenin increases or reduces, respectively, the rate of hepatocyte proliferation [86] [15,87,88]. There is also strong evidence that the canonical pathway modulates hepatocyte-driven regeneration. First, regenerative hepatocytes respond to Wnt injury cues as they upregulate Axin2 in response to CCl_4 liver damage [89]. Second, hepatocyte proliferation hepatectomy is delayed following partial hepatectomy when Wnt secretion is impaired in cells of the myeloid lineage (Lyz2-$Cre^{+/-}$; $Wls^{fl/fl}$), including Kupffer cells, or in liver endothelial cells (Lyve1-$Cre^{+/-}$; $Wls^{fl/fl}$), indicating that various cellular sources supply hepatocellular regenerative Wnt cues [90,91]. And lastly, a similar delay in hepatocyte proliferation occurs after partial hepatectomy in hepatocytes deficient for β-catenin, Wnt receptors (Lrp5/6) or Rspo receptors (Lgr4/5) from developmental stages [90,92].

1.13 Wnt in homeostatic BEC turnover and regeneration

To date, no study has assessed the effects in the proliferation baseline levels of the biliary epithelium upon genetic manipulation of the Wnt signalling pathway *in vivo* and the relative importance of the Wnt signaling pathway in BEC regeneration following injury is a subject of current debate.

Studies conducted by Huch et al. (2013) using an Lgr5-ires-CreERT2:R26LacZ reporter mouse model concluded that BECs activated the canonical branch of the Wnt cascade in response to acute liver damage caused by CCl_4, DDC or MCD injury regimes [89]. These observations however contrast with the latest studies of Planas-Paz et al. (2019) and Pepe-Mooney et al. (2019) who, when using scRNAseq to study single cell responses failed to identify a population of BECs positive for the expression of Lgr5 or Axin2 following DDC injury [22,93]. Studies from Planas-Paz et al. (2019) showed additionally that Rspo injury signals do not modulate the regenerative program of BECs following injury as genetic loss of the Rspo receptors Lgr4 and Lgr5 in the biliary epithelium in developmental stages using a $Lgr4/5^{fl/fl}$ Alb-Cre mouse model did not decrease the number of proliferative BECs nor affected the total number of BECs upon 2 weeks DDC administration [93].

More recently, Wilson et al. (2020) confirmed that the canonical branch of the pathway is not activated in this injury regime as the levels of Axin2 mRNA in BECs were not significantly altered following 2 weeks DDC administration [94]. However, in the same study, Wilson and colleagues also showed that, following TAA (12 weeks) or DDC (2 weeks) injury regime, BECs responded to non-canonical Wnt injury cues and provided evidence that loss of Vangl2 receptor in the biliary epithelium promoted resolution of the DR and decreased fibrotic scarring, suggesting a role for the Wnt/PCP pathway in chronic liver disease.

1.14 Wnt in HPC mediated regeneration

The Wnt pathway has additionally been proposed to modulate the biology of transient amplifying HPCs. Experiments conducted by Hu et al. (2007) reported that murine HPC that were positive for A6 expression responded to Wnt activating injury cues as they presented nuclear β-catenin and activated the TOPGAL Wnt reporter (TCF/LEF-LacZ) in response to 3-week DDC treatment [95]. Huch et al. (2013) also concluded that quiescent HPC activated canonical Wnt signaling in response to liver damage using an Axin2-LacZ reporter mouse model [89]. In the same study, it was also shown that these HPC-Wnt responsive cells labelled as Lgr5 positive cells can be isolated and expanded *in vitro* in the form of organoids when cultured in the presence of Rspo signals [89].

Additional *in vivo* experiments showing that Wnt signaling modulates HPC injury response came from the studies conducted by Apte et al. (2007) that showed that depletion of β-catenin (Ctnnb1$^{fl/fl}$ Alb-Cre) caused a significant reduction in the number of A6-positive ductal structures formed in response to a DDC diet [96]. Similarly, activation of Wnt pathway via pharmacological inhibition of GSK3β (SB216763), increased the number of HPC positive for A6 expression in livers of rats exposed to 2AA in combination with 70% partial hepatectomy [97]. All these studies, however, contrast with the recent observations of Okabe et al. (2016), who has showed that loss of the canonical Lrp5/6 receptors in the biliary epithelium (Lrp5/6fl/fl:Alb-Cre mouse model) did not have a detrimental effect in the formation of A6-positive ductular structures in response to BDL, a model of cholestasis and BEC hyper-proliferation [98]. It is therefore yet to be determined whether discrepancies between these studies are product of the different strategies used to genetically manipulate Wnt activation levels in HPCs and or a consequence of the different liver injury regime or experimental conditions used.

1.15 β-catenin modulates hepatocyte zonal specification in the adult liver

Experiments conducted by Benhamouche et al (2006) showed for the first time that, in the hepatic lobule, a gradient of Wnt/β-catenin pathway activation spreads out from the CV to the mid-lobule [87]. Prior to this, Cadoret et al. (2002) and Ovejero et al. (2004) had provided evidence that a panel of pericentral genes (Glul, Glt1, Oat and Lect2) were under the control of β-catenin as aberrant activation of β-catenin in the liver parenchyma was sufficient to cause ectopic expression of these in periportal areas of the lobule [99,100].

To further investigate the extent at which β-catenin defined hepatocyte zonal specification, Gougelet et al. (2014) combined ChIP-seq and RNAseq experiments in murine livers deficient for β-catenin or APC, a negative regulator of canonical Wnt signalling. In this study, a total of 7898 and 477 binding peaks were identified for TCF4 and β-catenin, respectively, in the hepatocytes upon loss of APC [51]. Many of these peaks were located in putative promoters of pericentrally expressed genes including Axin2, Glul and Cyp1a2. Additionally, loss of β-catenin caused a significant decline in the expression of 180 genes involved in functions associated with pericentral

hepatocytes including drug metabolism (Cyp2e1, Cyp1a2 and AhR), aminoacid metabolism (Slc1a2 and Glul), liver mass (Socs3 and Tgfa) and bile acid synthesis/cholesterol degradation (Cyp27a1) [51].

Interestingly, in the studies conducted by Gougelet and colleages, hepatocyte-specific deletion of the downstream Wnt negative regulator APC (TTR-CreERT2; APCfl/fl) did not cause the immediate ectopic expression of pericentral markers in periportal areas. Instead, histological spreading of pericentral markers (Axin2, GS, Rnase4, RhBg, Glt1 and Lect2) occurred in a step-wise manner across the lobule from the CV to the portal triad, which suggest that hepatocytes are not simply poised to respond to instructive Wnt signals but are instead subjected to spatial-temporal inhibitory mechanisms that actively repress Wnt propagation [87]. A range of potential Wnt inhibitors and pathways have been implicated in dampening Wnt signalling. Most directly, it has been shown that Wnt pathway inhibitors such as DKK3 and sFRP5 are expressed periportally [14] [33].

β-catenin also controls the biology and microenvironment to which periportal hepatocytes are exposed. For instance, it has been shown that loss of β-catenin (Alb-Cre Ctnnb1$^{fl/fl}$) reduces the number of microvilli in the apical domain of hepatocytes and promotes the enlargement of the bile canaliculi villi, which in turn causes a reduction of the bile flow rate by 50% [101]. β-catenin additionally modulates the composition of the bile as depletion of β-catenin lowered the levels of glutathione, bile duct acids, cholesterol, phospholipids, which are the major 4 components of the bile [101].

In section 1.5 it was introduced the concept developed by Ben-Moshe et al. (2019) of 'production line patterns' in the zonated liver and, to illustrate this concept, an example based on cholesterol-to-bile biotransformation was presented [34]. Interestingly, experiments performed by Yeh et al. (2010) showed that β-catenin controls the expression of Cyp7a1 and Cyp27, the rate limiting enzymes in the classic and alternate, respectively, pathways of bile acid synthesis [101]. Thence, it is possible, which in turn might affect the gene expression of downstream periportal hepatocytes [101]. Finally, Wnt signalling appears to also actively antagonize the expansion of the

periportal signature as abolition as inhibition of the Wnt/β-catenin pathway by the delivery of an adenovirus encoding for DKK1 causes the progressive histological expansion or suppression of periportal markers such as Arg1, Cps1 and Glutaminase2 [87].

1.15.1 Angiocrine signals are required for the establishment and maintenance of liver zonation

To uncover the cellular source responsible for the asymmetrical Wnt activation gradient of in the adult hepatic lobule, different research groups have systematically abolished Wnt ligands secretion in different liver resident cell types and evaluated the zonal expression of pericentral and periportal genes.

Deletion of Wls, a membrane protein dedicated to the secretion of Wnt proteins, from hepatocytes and cholangiocytes (Alb-Cre; $Wls^{fl/fl}$), liver-resident Kupffer (Lyz2-Cre; $Wls^{fl/fl}$) and stellate cells (Lrat-Cre; $Wls^{fl/fl}$) in the developing liver did not alter liver zonation [90,102,103]. By contrast, Wnt cues of angiocrine origin were found to be essential for zonation to occur as depletion of Wls in the endothelial compartment during embryogenesis (Lyve1-Cre; $Wls^{fl/fl}$ and Stab2-Cre; $Wls^{fl/fl}$) or adulthood (VE-Cadherin-CreERT2; $Wls^{fl/fl}$) prevents the establishment and maintenance of metabolic (RhBg, Cyp2e1, Cyp1a2, and GS) and non-metabolic (E-cadherin, Claudin-2 and Axin2) zonation markers [12,35,40,91]..

Endothelial cells in the hepatic lobule include (1) LSECs that line the sinusoids and (2) vascular endothelial cells comprising endothelial cells from the CV, the hepatic artery and the portal vein (see section 1.2). Of those, the centrolobular location of the central vein placed these endothelial cells as the putative source of the Wnt/β-catenin pathway activation gradient that spreads out from the centre of the lobule. ISH and RT-qPCR experiments confirmed that the endothelial cells of the central vein express Wnt2, Wnt9b [12,104].

Experiments conducted by Rocha et al., (2015) showed that CV endothelial cells additionally express Rspo3 and that loss of this gene in embryos (from E16.5) or in the adult mouse, using a tamoxifen-inducible pan cre- recombinase (cCAG-CreERT2:

Rspo3$^{fl/fl}$), abolished pericentral GS protein levels without altering Wnt2 and Wnt9b gene expression [104]. These data suggest that angiocrine expression of both Wnt and Rspo ligands is critical for zonation. Finally, recent studies performed by Ma et al (2020) have shown that shown that expression of Wnt9b, Wnt2 and Rspo3 in newborn mice (P2) was not restricted to the CV endothelium but also extended to pericentral LSECs, thereby the partial contribution the CV and pericentral LSECs is yet to be determined.

1.16 Study of localized Wnt and Rspo signals *in vitro*

The recreation and control of specialized cellular 'niche' *in vitro* microenvironments is an attractive strategy to gain insight in the molecular mechanisms that govern cell-fate designations during development and/or in established adult tissues. With the aim of understanding how spatially localized Wnt signals direct cell fate specification during embryogenesis, Habib et al. (2013) recreated for the first time a local Wnt and Rspo microenvironment *in vitro* by covalently immobilizing Wnt3a and Rspo1 ligands onto carboxylic acid-coated beads [105]. This was done by following a two-step coupling procedure with EDC (1-ethyl-3-(-3-dimethylaminopropyl)) and NHS (*N*-hydroxysuccinimide).

EDC is a carbodiimide broadly used as "zero-length" crosslinker (crosslinking without the induction of a spacer molecule) as is soluble in aqueous buffer solutions which are generally compatible with organic molecules such as proteins [106]. In the NHS/EDC two-step coupling procedure, EDC reacts with the carboxylic acid groups that cover the surface of the bead to give place an active *O*-acylisourea intermediate that reacts with primary amine groups present in the protein [106]. Thus, proteins result covalently immobilized onto the beads via the N-terminus and/or side chain of lysine residues present and accessible in the protein.

Using this strategy, Habib and colleagues showed that immobilized Wnt3a and Rspo1 ligands maintain their ability of activate or potentiate, respectively, canonical Wnt signalling *in vitro* [105]. Furthermore, it was shown that spatially localized Wnt3a but not Rspo1 signals orientate the plane of the mitotic spindle in mouse embryonic stem (mES) cells and that once the cell division is completed, the daughter cell proximal to the Wnt3a-bead expressed higher levels of nuclear β-catenin and various pluripotency

markers than the distal cell. This study therefore demonstrated that the covalent immobilization of upstream components of the Wnt signalling pathway may serve as a strategy to recreate local Wnt/Rspo microenvironments *in vitro*.

1.17 Bioartificial liver devices and current hepatocellular in vitro sources

Bioartificial livers are devices that aim to recapitulate liver function extracorporeally and that may serve as platforms for drug testing, to support liver functions during organ transplantation and/or to aid recovery from acute liver failure [107]. These devices are bio-reactors that accommodate hepatocyte cultures and, based on the conformation of their design, these can be classified in four major categories: (1) hollow fiber devices, (2) packed beads, (3) flat plate monolayer systems and (4) encapsulation-based reactors [108] Of these, most of the bioartificial liver devices currently in clinical trials belong to the category of hollow fiber devices, which are based in the grow of hepatic cells within inside or outside of the lumen of a porous fiber and where the patient's blood or culture medium is perfused on the other side.

Despite that many bioartificial liver systems have been tested in preclinical studies to date, their performance remains rather limited due to inherent disadvantages of adult hepatocyte cultures (eg. limited expansion capacity *in vitro*, see section 1.18) and the inability of these devices to accurately replicate the microenvironment of the liver lobule [108]. Hepatocyte physiology heavily relies on the establishment of adequate cell-cell and cell-ECM interactions and maintenance of cellular polarity and therefore research efforts have been made in the development of scaffold biomaterials and systems that support co-culture configurations of hepatocytes and non-parenchymal cells. Furthermore, for the accurate recapitulation of liver functions, the design of devices must integrate features of periportal and pericentral hepatocytes simultaneously and, therefore, these devices must enable the establishment oxygen, metabolite and hormone gradients. In this end, the liver bioreactors developed in recent years have paid special attention to the scale-up adaptations for the controlled presentation in this devices of environmental cues such is the oxygen gradient established along the porto/venous axis of the liver lobule [109]. Importantly, no bioartifical device has yet attempted to replicate the Wnt activation gradient that spreads for the hepatic CV.

1.18 Cell systems to predict drug-induced liver toxicity *in vitro*

The expansion and maintenance of hepatocyte cultures have been an important limitation for the evaluation of hepatocellular toxicity *in vitro* and the bottleneck for the use of primary hepatocytes (PH) as cell-base therapy for liver disease. To date, there are various cell sources can be used to feed bioartifical liver devices and/or serve as an *in vitro* platform to test drug hepatotoxicity in static conditions. These include PH cultured in conventional monolayers or embedded in hydrogels as '2D collagen sandwich cultures' or PH spheroids, induced pluripotent stem cells (iPSCs)-derived hepatocytes and liver organoids. In the current section a brief summary of these in vitro cellular platforms with their main limitations and advantages is provided.

PH cultured in 2D monolayers remain as the 'gold standard' for the prediction of drug-liver induced toxicity in the pharmacological industry [110]. However, when removed from their physiological environment and plated in 2D, hepatocytes undergo major changes in the cell architecture and rapidly losing the expression of hepatocyte-specific genes. Thereby, their use as a cellular platform to predict the drug hepatotoxicity is limited by (1) their short lifespan in culture, (2) their reduced ability to be expanded *in vitro* and subsequent constant dependency on primary tissue and (3) their high phenotypic instability product of the inter-donor variability.

The establishment of HCC-derived cell lines such as HepG2, Huh7 or HepRG cells overcome the limitation associated with the expansion and experiment-to-experiment reproducibility of PH 2D cultures [111,112]. However, the metabolic activity of hepatocyte cell lines highly differs from *in vivo* hepatocytes and therefore their hepatotoxicity prediction power and their ability to recapitulate hepatocellular function is rather limited [112].

As mentioned earlier, cell-cell and cell-ECM interactions are critical for the normal physiology of the hepatocytes. The culture of PH between two layers of collagen ('collagen sandwich culture') has been proven to enable the formation of tight junctions and functional bile canaliculi between hepatocytes and is a successful strategy to delay the loss of hepatocyte-specific functions upon PH culture [113]. Similarly, the culture of PH in hydrogels as hepatocyte spheroids enables the acquisition of adequate hepatocyte polarity and significantly improved the lifespan and power of

prediction of PH cultures [114]. Despite these significant improvements, PH collagen sandwich cultures and PH spheroids culture strategies retain the limitations of (1) the dependency of primary tissue as the cell expansion is also limited in these two culture platforms and (2) they retain high phenotypic instability product of the inter-donor variability.

The field of iPSCs have also attempted to solve both the limitations of the expansion and maintenance of hepatocyte-function *in vitro*. While the use of iPSC cultures definitively overcome the problem of the expansion of the biological material for an indefinite period of time, the currently available differentiation protocols do not yet produce cells similar to adult mature hepatocytes [112,115]. Instead, iPSC-derived hepatocytes are cells that rather resemble foetal or new-born hepatocytes as they retain expression of markers such as AFP [112].

Recent advances in 3D cultures techniques have allowed the development of various liver organoid protocols from adult tissue. The first of these protocols was introduced in 2013 by Meritxel Huch from the Clever's laboratory [89]. Huch's protocol used HPCs labelled as Lgr5 positive cells derived from the liver's biliary epithelium as a cell source to initiate the system [89]. As described earlier, HPCs are bi-potent cells that arise in response to liver damage. When cultured in 3D hydrogels, Huch and colleagues showed that Lgr5+ bile duct (BD)-derived cells gave rise to hollow and spherical 'organoids' that could be indefinitely expanded in Rspo1-containing medium and differentiated towards hepatocyte fate through the inhibition of Notch and TGFβ pathways [89]. Differentiated BD organoids were shown to express hepatocyte lineage markers (Alb and Hnf4a) as well as mature hepatocyte genes involved in lipid and cholesterol metabolism (Acox3, Acss2 or Apoa4) as well as members of the cytochrome P450 family (Cyp3a11, Cyp2c66 or Cyp4f18).

Fah is a gene coding for fumarylacetoacetate hydrolase (FAH), which is an enzyme involved in the metabolism of tyrosine. Genetic loss of Fah leads to the accumulation of hepatotoxic fumarylacetoacetate (FAA) unless that 2-(2-nitro-4-trifluoro-methylbenzoyl)-1,3 cyclohexanedione (NTBC) is administrated [116] [117]. Huch and colleagues also showed that $Fah^{+/+}$ differentiated BD-derived organoids were

successfully engrafted in $Fah^{-/-}$ mouse upon removal of NTCB in drinking water and generated fully functional hepatocytes upon transplantation, showing that these structures might serve as a potential therapeutic avenue toward liver regenerative therapy [89]. Despite that these structures were also introduced as a possible *in vitro* platform for drug testing, to date only a few studies have used differentiated BD-derived organoids for drug-screen proposes and comparative *in vivo* and *in vitro* studies showing competency of these structures to predict drug hepatotoxicity is currently lacking [118,119].

By the end of my second year of PhD, two new protocols from different laboratories described the generation of liver organoids using PH as the initiating cell type [3,4]. Both protocols used a medium composition that allows the long-term expansion (> 6 months) of the cells, therefore, potentially overcoming the limitation of previous PH spheroid culture protocols. Hu et al. (2018) protocol, from Dr Hans Clevers' laboratory, was based in a single medium in which cells are maintained into a highly proliferative state [4]. By contrast, Peng et al. (2018) protocol from Dr Roel Nusse's laboratory relied on the sequential culture of hepatocytes in two media compositions: a medium that promoted organoid formation and cell expansion and a second differentiation medium that enhanced the expression of metabolic enzymes including pericentral (Cyp1a2, Cyp3a11 and Fah) and periportal (Cyp2f2, Cps1 and Alb) markers to comparable levels to primary tissue [3]. Thereby, the protocol of Hu et al. (2018) was argue to resemble hyperproliferative hepatocytes after partial hepatectomy whereas Peng et al. (2018) potentially give rise to hepatocytes more close to the resting liver [3,4]. As yet, the ability of PH-derived organoids as an *in vitro* model to predict drug hepatotoxicity in culture has not been explored.

Altogether, hepatocyte *in vitro* cultures have been historically limited by deficiencies in (1) the expansion of the biological material for an indefinite period of time and (2) the maintenance of hepatocyte cell identity and function in culture. Recent advances in the organoid technology claim, however, to have improved both these aspects and therefore appear, currently, as the most attractive cellular source to feed bioartificial liver devices. Full-phenotypic characterization studies of BD- and PH-derived liver organoid cultures as well as information of their competency of as an *in vitro* platform

for drug testing is currently lacking. For simplicity, BD- and PH-derived organoids will be referred in this thesis as 'BD organoids' and 'PH organoids', respectively.

1.19 **Aim and objectives of this thesis**

The segregation of processes in different zones and metabolic coupling between hepatocytes is critical for the liver to integrate and carry out its diverse functions. Therefore, one of the great challenges in the modelling of liver responses *in vitro* is the recapitulation of metabolic zonation in a continuous, for which liver *in vitro* systems should integrate the signals responsible for hepatocyte functional specification. While previous research has focused in the integration of oxygen and metabolite gradients, no-work has yet done in the recreation of the Wnt niche of the hepatic central vein in liver *in vitro* systems. This thesis thereby aimed to make significant advances in the development of a Wnt-driven liver zonated *in vitro* system, for which the following specific objectives were established:

First, the establishment of the molecular tools for the recreation of a local Wnt microenvironment that resembles the hepatic CV *in vitro*. The experimental approach set to achieve this was the covalent immobilization of the CV ligands Wnt9b and Rspo3 onto beads following the studies of Habib et al. (2013) as a reference (Figure1.8) [105].

Second, the evaluation of the competency of the current hepatic organoid platforms (BD and PH organoids) as cell source to study and replicate Wnt-driven liver zonation *in vitro*. To achieve this aim, the expression of metabolic pericentral genes in response to Wnt activation was studied in these two platforms. As Wnt signalling additionally orchestrates the liver regeneration, the possibility that activation of the Wnt signalling pathway in these structures might elicit a cellular program related with the renewal of liver epithelial cells or BEC/hepatocyte plasticity was also explored.

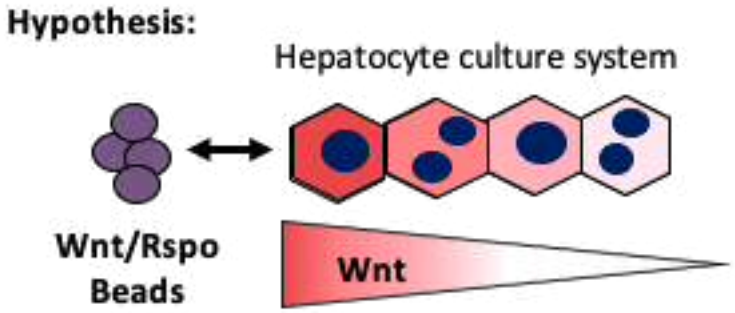

Figure1.8 The work presented in this thesis is sustained by the hypothesis that the immobilization of Wnt/Rspo ligands onto beads may recreate *in vitro* a local Wnt microenvironment similar to the CV.

Chapter 2. MATERIALS AND METHODS

2.1 Animal work

2.1.1 Animal Husbandry

Wild type (WT) C57BL/6J mice were supplied by Charles River Laboratory or by the T2 of Cardiff University. Axin2-CreERT2 mice were a gift from Chambon laboratory and were crossed with R26-LSL-tdTom mice (The Jackson Laboratory). R26-LSL-tdTom mice were also crossed with *Igtb1*$^{fl/fl}$ and Krt19-Cre animals (The Jackson laboratory). Tet-O-ΔN89β-catenin animals were generated in house [120]. Animals were housed at Cardiff University, the Beatson Institute or the MCR Center for Regenerative Medicine as indicated in a 12h light/dark cycle with free access to standard chow and water. All animal work was carried out under UK Home Office project and personal licenses following local ethical approval and in accordance with local and national guidelines.

2.1.2 Identification and ear clipping

At weaning age (4 weeks aprox.), mice were marked by ear clipping for identification proposes and the subsequent biopsies were stored at -20°C for further genotyping processing. Ear clipping services were provided by Cardiff University staff of the T2 and Heath Park facilities.

2.1.3 Genotyping

Genotyping of the colonies housed at Cardiff University was performed using a PCR approach that involved (1) extraction of DNA from ear biopsies, (2) a genotyping PCR reaction and (3) visualization of the PCR products by electrophoresis.

To extract the DNA from the collected ear clip biopsies, samples were defrosted at room temperature (RT) and digested overnight (o/n) in a shaking incubator at 37°C using a mixture of 250 μl of lysis buffer (Qiagen) and 5 μl of proteinase K (Sigma). When digestion was completed, samples were cool down at RT, mixed vigorously with 100 μl of protein precipitation solution (Qiagen) and centrifuged for 10 min at 13K rpm. The DNA present in the resulting aqueous supernatant was then transferred into a new tube, mixed with 250 μl of isopropanol and precipitated at 13K rpm for 15 min. Once the centrifugation was completed, the supernatant was discarded and the tubes

containing the pelleted DNA air-dried at RT for 1-2 h. DNA was then resuspended in 250 μl of RNase-free water (Thermofisher).

Genotyping PCR reaction was then carried out using GoTaq Hot Polymerase (Promega) in a Thermal Cycler T3000 (Biometra) 8-well PCR SnapStrip tubes (Anachem). The exact composition of the genotyping reaction, genotyping primers and the genotyping PCR programs are specified in Table2.1 and AppendixA Table1.

	Volume (μl)
DNA	3
Buffer 5x Promega	10
Mg (25 mM)	5
dNTP(25 mM)	0.4
Primers (100 μM)	0.1
Taq polymerase	0.2
Water	50

Table2.1 Genotyping reaction

The resulting PCR products were 5:6 mixed with 6x DNA loading dye (Promega), loaded into 1.5% agarose gels containing SafeView (5:100.000) prepared with TAE buffer and run at 80-120 V. Genotyping PCR products were then visualized under UV light. Expected genotyping bands are in (Appendix A, Table1).

Importantly, the Axin2-CreERT2 allele was always maintained in Het due to the impossibility of distinguishing between the PCR products generated by Hom and Het animals.

2.1.4 **Experimental Procedures**

The following experimental procedures were carried out at the MCR Center for Regenerative Medicine at Edinburgh by members of Dr Stuart Forbes laboratory [17]. To induce recombination of CK19+ BEC cells in vivo, Krt19-Cre R26-LSL-tdTom mice were exposed to 3 individual IP injections (20 mg/ml, Sigma) at a dose of 4 mg. To induce liver damage, normal chow was replaced by 0.1% DDC mixed with Rat &

Mouse No1 Maintenance diet (Special Diet Services) or MCD diet. AAV8.TBG.Cre (CS0644) and AAV8.TBG.null (CS0255) were from Penn vector core. To impair hepatocellular proliferation, AAV8 viral particles containing the coding sequence for p21 (AAV8.TBG.p21 plasmid) were generated by packing a pGEM p21 plasmid (Addgene plasmid # 8443) into a AAV8.TBG.Control plasmid (AV-8-PV0148) [17]. Viral particles were reconstituted at $7.5x10^{13}$ particles/μl in PBS and delivered by tail injection as previously described [17]. To inhibit Wnt secretion in vivo, animals were administrated twice per day by oral gavage with either LGK974 or an equivalent volume of its solvent (vehicle).

2.1.5 Tissue sampling and processing for histology

Tissue was sampled, processed and sectioned by Niya Aleksieva and Dr Alex Raven and Janet Man, members of the Forbes laboratory. Prior to dissection, the liver was perfused (see section 2.2.1) with PBS to clear the organ from circulating highly auto-fluorescent red blood cells. Samples from intestine, spleen and pancreas were also routinely collected. Once dissected, samples were immediately fixed for 8h at RT in 10% formalin and subsequently dehydrated using increasing concentrations of alcohols, xylene and paraffin following the standardized routine protocol of the MCR Centre for Regenerative Medicine in Edinburgh. Resulting paraffin blocks were stored at RT and cold down to 4°C prior to sectioning.

2.2 Isolation of PH

PHs were isolated following a classical two-step collagenase perfusion method with modifications using two aquarium pumps (EHEIM, Typ 1000.340, Serie 14042) connected to a home-made silicone tubing system. 1ml and 5ml syringes were cut and used as connectors between the different tubing sections. 1 to 3 filters of 0.22 μm were inserted in the circuit with the purpose of (1) regulating the speed of the flow to an optimal rate of 5-10 ml/min and (2) providing sterility to the perfused solution (Figure2.1).

2.2.1 Starting the aquarium perfusion pump system

Pumps were connected to the silicon tubes (without the 0.22 μm filters), immersed in a beaker containing 800 ml of 70% ethanol solution and switched on at full speed.

A

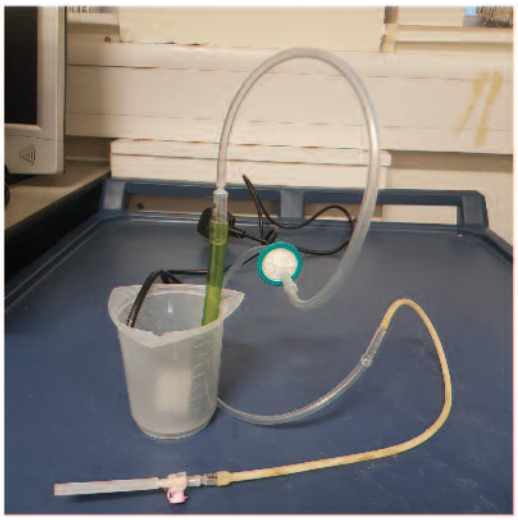

B

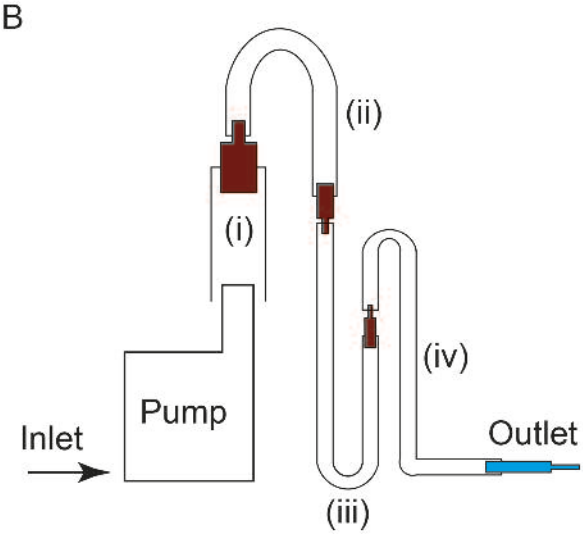

Figure2.1 (A) Image from aquarium perfusion pump system. (B) Aquarium perfusion pump system scheme. Four (i-iv) tubing section were connected using home-made connectors (red) made from 1ml and 5ml syringes. In blue, the catheter inserted in the animal has been highlighted in blue.

After 30 min, ethanol from the system was removed by transferring the pumps to a clean beaker containing milliQ water and washed for other 15 to 20 min. Each of the pumps was then immersed in different beaker containing either perfusion solution I and II (Table2.2). Pumps were then switch and bubbles from the system were removed by flicking the silicone tubes. Once the flow was stable, silicone tubing section (ii) and (iii) were disconnected and 2 filters of 0.22 μm pore size were inserted in between (Figure2.1). Once the flow was stabilized, the perfusion rate was determined by timing how long takes to fill a 15 ml falcon tube. 22 μm filters were inserted or removed between tubing section (ii) and (iii) to achieve an optimal perfusion speed of 5 to 10 ml/min. Once this was achieved, beakers containing the pumps were transferred to a 40°C water bath.

SOLUTION	COMPONENTS	AMOUNT (ml)	FINAL CONCENTRATION	STORAGE
Solution I				4°C
	Gibco EBSS (w/o calcium, w/o magnesium, w/o phenol red)	494.5		
	Gibco HEPES 1M solution	5	10 mM	
	EGTA 0.5M	10	EGTA 0.5 mM	
Solution II				
	DMEM/F12 no phenol red (Invitrogen)	495		
	Gibco HEPES 1M solution	5	10 mM	**4°C**
	Collagenase Type I		0.6-0.8 mg/ml	Use immediately

Table 2.2 Two-step EGTA/collagenase perfusion buffers.

2.2.2 Venepuncture and cannulation

Once the perfusion system was set up, mice were euthanized by cervical dislocation or CO_2 suffocation and immediately processed following a contention-based protocol. Firstly, livers were perfused through the portal vein (see section 2.2.3) (Figure2.2). If cannulation of the portal vein failed, livers were then perfused through the IVC in anterograde (see section 2.2.3) or retrograde (see section 2.2.4) manner (Figure2.2).

2.2.3 Portal vein cannulation

A media incision was performed from the pelvis to the sternum and then prolonged through the rib cage across the diaphragm to expose the heart and the abdominal viscera. Using flat square tip forceps, the intestine was gently removed to the left exposing the portal vein and a thread was passed carefully underneath it. Two additional threads were passed underneath the inferior vena cava (before and after the liver) as contention method (section 2.2.4 and 2.2.5) (Figure2.2). A catheter was inserted into the portal vein (Figure2.2). In this stage blood black flow in the catheter can be used as indicator of successful cannulation although the formation of blood

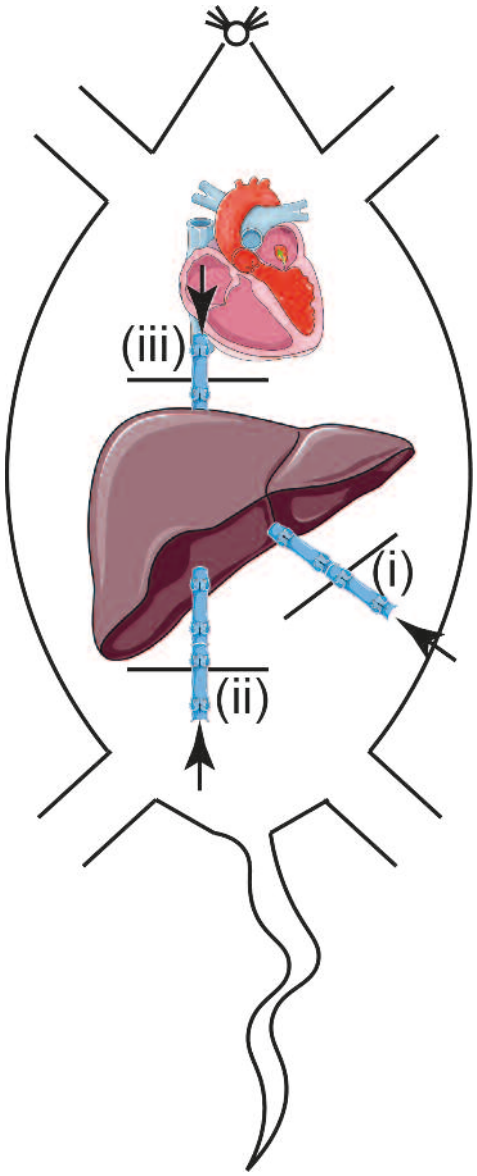

Figure2.2 Scheme representing the cannulations methods employed in this project to perfuse the murine liver. Three different threats were passed underneath the portal vein (i) and the IVC (ii and iii) after exposure of the viscera. Arrows indicate the direction of the flow during the perfusion. (i) Portal vein cannulation, section 2.2.3 (ii) IVC cannulation for anterograde perfusion, section 2.2.4 (iii) IVC cannulation for retrograde perfusion, section 2.2.5

clots might prevent this to occur. The silicone tubing pumping Solution I was then connected and the IVC was subsequently cut to reduce the likelihood of catheter expulsion due to negative pressure. Acquisition of liver pale appearance and immediate loss of liver blood through the served IVC served as indicators of successful portal vein cannulation. If successful cannulation was reported, the catheter was secured using the thread placed underneath the portal vein. If cannulation resulted unsuccessful, perfusion of the liver was continued as indicated in section 2.2.4.

2.2.4 IVC cannulation for anterograde perfusion

If portal vein cannulation failed, a catheter was then inserted through the IVC underneath the liver. This was done above the incision previously performed to cut the IVC. If cannulation through this method was successful, the catheter was secured

using the threat placed underneath the IVC (Figure2.2). If cannulation was unsuccessful, perfusion of the liver was continued as indicated in section 2.2.4.

2.2.5 IVC cannulation for retrograde perfusion

IVC cannulation for retrograde perfusion was used as an alternative method in case of section 2.2.4 failure. While holding the heart with flat forceps, a small incision was performed in the right atrium and the catheter lacking the inner needle was carefully inserted until the tip was noticeable in the IVC. Once this occurred, the catheter was secured using the thread placed underneath the IVC below the heart (Figure2.2).

2.2.6 Liver perfusion and two-step collagenase digestion

Upon successful cannulation of the portal vein or the IVC (see section 2.2.2 to 2.2.4), livers were perfused at 5-10 ml/min with Solution I (Table2.2) for 8-15 min. Solution I contains EGTA, a chelating agent that scavenges for trace amounts of Ca^{2+}, Mg^{2+} and Fe^{2+} and is perfused with the aim of (1) removing circulating blood and facilitate the penetrance of perfusion Solution II and (2) soften cell-cell tight junctions (Table2.2).

Once the liver was pale in appearance, the catheter was disconnected from the tubing pumping Solution I and subsequently connected to Solution II pumping system and the liver was monitored for signs of sufficient digestion (Table2.2). When digestion was sufficient, the liver was carefully removed from the animal and transferred to a petri dish containing Solution III (Table2.2).

2.2.7 Purification of hepatocyte cell population

After liver digestion (section 2.2.6) hepatocytes were released by dissociating the liver with the help of scissors and forceps and transferred to a 50 ml conical tube by passing them first through a 100 μm cell strainer followed by a 70 μm cell strainer. Hepatocytes were pelleted by centrifuging for 3 min at 30 g and washed three times (3 min, 30 g) with hepatocyte washing media (DMEM/F12 no phenol red (Invitrogen)) supplemented with 10mM HEPES (Invitrogen), 1:1000 ITS and 1% Pen/Strep) (Figure2.3). Abrupt or aggressive pipetting was avoided at every stage of the isolation as hepatocytes are extremely sensitive to shear stress. Supernatant from the washing steps from each

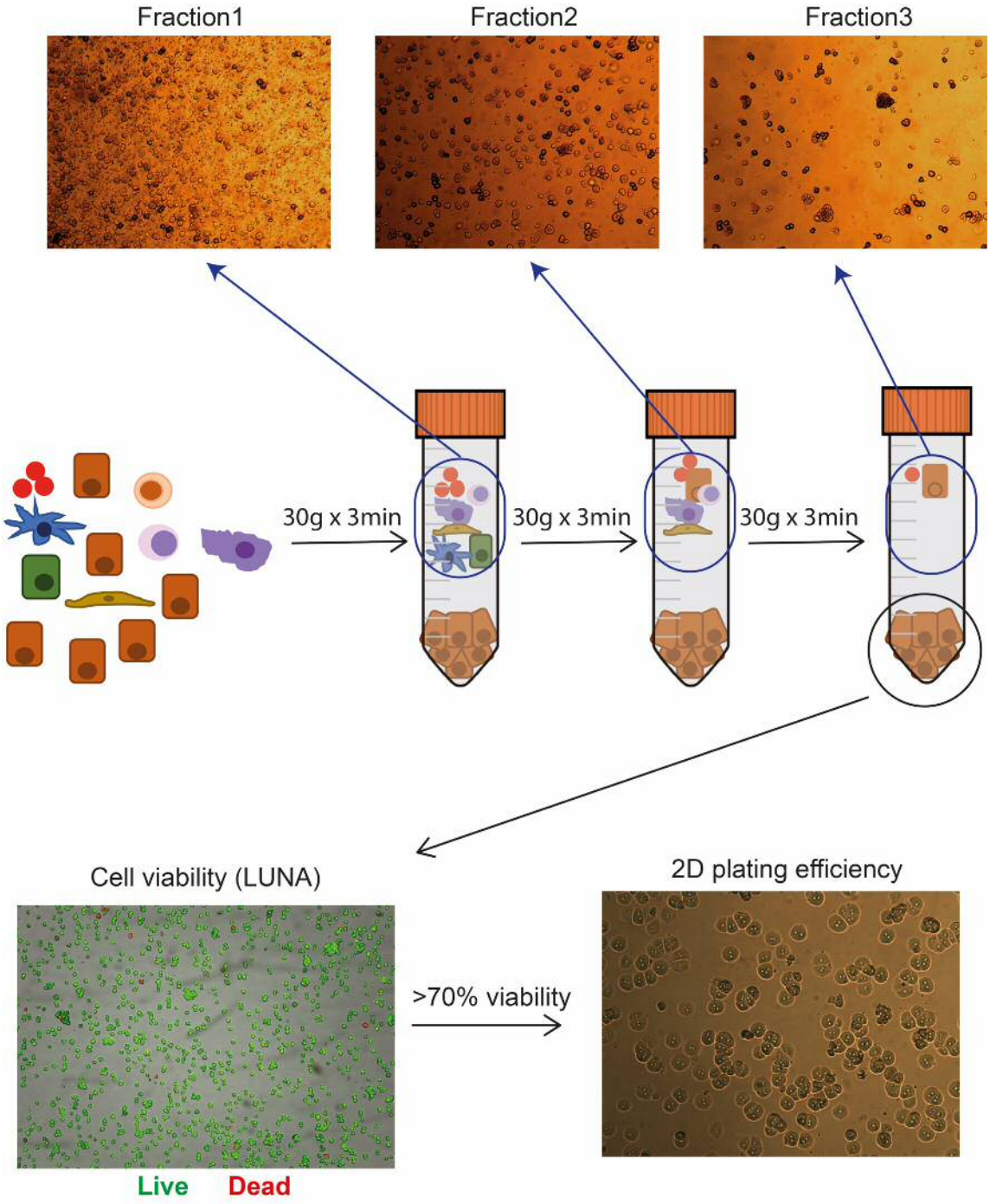

Figure2.3 Hepatocytes were purified by slow centrifugation (3 x 30g x 3min). Supernatant fractions, enriched for blood cells, non-parenchymal cells and dead hepatocytes, were discarded. Cell viability was assessed by LUNA and plated onto collagen-coated plates to assess their overall fitness. Dead cells are shown in red whereas green cells correspond to alive cells. Selected LUNA image shows a 99.9% cell viability.

fraction was collected and monitored for the presence of non-hepatocyte cells under the microscope (Figure2.3).

2.2.8 Determination of hepatocyte cell viability and concentration by acridine orange (AO) and propidium iodide (PI) staining.

Cell viability of the last hepatocyte enriched fraction was determined by AO/PI staining method. AO (green fluorescence) is an intercalating dye that can permeate both live and dead cells whereas PI (red fluorescence) can only enter and bind to the DNA of cells with compromised membrane integrity. When co-stained with both dyes, all live nucleated cells will be labelled by green fluorescence while dead cells will appear labelled as red. To determine cell viability, 18 μl of cells in suspension were mixed with 2 μl of AO/PI dual-staining (Thermofisher). 10 μl of mixture was then loaded onto a LUNA cell counting slide and concentration, viability and average size of the cells was calculated by fluorescence automated cell counter (LabTech) assuming a 1:20 sample dilution. Two readings per sample were performed and only samples with a viability higher than 70% were used for downstream proposes (Figure2.3).

2.2.9 Aquarium pump system cleaning procedure

After the perfusion was completed, pumps were immersed and washed in 70% ethanol for 30 min, air dried and stored at RT.

2.3 Isolation of primary BDs

Isolation of BDs was either (1) coupled after PHs isolation or (2) initiated with whole livers as starting material.

2.3.1 Isolation of BD after two-step EGTA/collagenase liver digestion

After PHs isolation and if liver digestion was complete, the fraction retained on top of the 100 μm cell strainer was collected, washed two times with Advanced DMEM/F12 media (100 g, 5 min), and screened for the presence of BDs. BDs were then hand-picked under the microscope and further processed for the establishment of organoid cultures (section 2.4.4). If liver digestion was not complete and large tissue pieces remained intact, these were chopped using a sterilized steel scalpel in smaller fragments (2-5 mm^2 aprox.) and subsequently processed as indicated in section 2.3.2. BDs isolated from this procedure were exclusively used to generate BD organoids.

2.3.2 Isolation of BD from whole livers

Mice were culled by cervical dislocation or CO_2 suffocation and livers were dissected and immediately placed on a petri dish containing ice-cold Advanced DMEM/F12 media. The diaphragm and gallbladder were removed using sterile scissors and forceps under a tissue culture hood and the livers were chopped into approximately 2-5 mm^2 pieces using a sterilized steel scalpel. At this point, liver fragments could be frozen in Advanced DMEM/F12 containing 40% FBS and 10% DMSO or immediately processed.

2-5 mm^2 were transferred into a 15 ml conical tube containing Advanced DMEM/F12 media and washed two times by letting the fragments to settle and replacing the media. After the second wash, media was replaced with 5-10 ml of collagenase/dispase digestion media (125 μg/ml collagenase type XI, 125 μg/ml dispase, 1:100 GlutaMAX, 1% Pen/Strep, 5%FBS in DMEM) and incubated at 37°C in a water bath for 1-3 h. Fragments were agitated in rotary motion every 5-10 min and up/down pipetted every 20-30 min. After each up/down pipetting step, collagenase/dispase digestion media was replaced and supernatants were collected, transferred to a petri dish and screened under the microscope for the presence of BDs. Upon digestion, BDs were hand-picked and used for gene expression profiling purposes or to generate of BD organoids (section 2.4.4). BD were always obtained from fresh tissue without any freezing/thaw intermediate cycle.

2.4 Cell culture

2.4.1 Culture of PHs in 2D monolayers

For PHs monolayer 2D culture, plates were first coated with collagen type I from rat tail (Thermofisher) following the indications of thin coating procedure of the manufacturer. Briefly, the volume of collagen needed for a final concentration of 50 μg/ml of collagen was calculated using the equation bellow and subsequently diluted in 20 mM acetic acid.

$$Volumen\ of\ collagen\ (V1) = \frac{\left(\frac{50\mu g}{ml}of\ collagen\right)x\ (Final\ Volume)}{(Initial\ concentration\ of\ collagen\ (\frac{3\mu g}{ml}))}$$

Plates were incubated with the collagen solution for 1 to 2 h at RT, rinsed three times with PBS and air dried. Plates were immediately used or stored at 4°C for further use.

PHs (see section 2.2 for isolation procedure) were seeded onto collagen-coated plates and cultured for 4-16 h in hepatocyte attachment media (1:1000 ITS, 5% ES qualified FBS, 1% Pen/Strep, 15mM HEPES DMEM/F12). Once cells were attached, dead cells were washed one time with pre-warmed (37°C) PBS and media was replaced with PHs 2D culture media (1:1000 ITS, 0.5% ES qualified FBS, 1% Pen/Strep, 15 mM HEPES DMEM/F12). Media was replaced every day of culture always using 37°C pre-warmed media. When indicated, PHs 2D culture media was supplemented with 100 ng/ml Wnt3a, 100 ng/ml of Wnt9b or 50 ng/ml of Rspo3.

2.4.2 Generation of PHs organoids

PHS organoids were generated as following Peng et al. (2018) protocol with minor modifications [3]. Briefly, PHs were resuspended in ice-cold Matrigel at a concentration of 50 to 100 cells/μl and distributed in 10-20x 25μl hydrogel drops on 6-well plates pre-warmed at 37°C. A maximum 1:5 ratio of hepatocyte suspension:Matrigel was used. After seeding, plates were incubated to 2-3min at 37°C, flipped upside/down and incubated for other 10-12 min at 37°C. PHs organoid expansion media (PHorg-EM) was subsequently added (Table2.3). Media was replaced every 2-3 days.

2.4.3 Passage and expansion of PHs organoids

After 14 to 20 days, organoids reached an average size of 300-1000 μm and were ready for passage. For organoid passage, media was removed from the well and Matrigel dissociated and collected using ice-cold PBS. Organoids were pelleted at 300 g for 5 min, re-suspended in TrypLE (Gibco) and incubated in a water bath at 37°C for 5-10 min. Organoids were gently resuspended using a p200 every 3 min during this incubation time and organoid cell dissociation was monitored under the microscope. Single cell dissociation was avoided. Upon organoid breakage onto clusters of 5 to 10 cell clusters, TrypLE digestion was interrupted by adding 10 ml of ice-cold William's E media, organoids pelleted at 300 g, 5 min, and resuspended in Matrigel. Organoids

were routinely maintained at a split rate of 1:2. During expansion, organoids were cultured in PHorg-EM (Table2.3) and this was replaced every 2-3 days.

PHs organoid basic medium

William's E media (no phenol red)
1% GlutaMAX
10nM HEPES
1% Pen/Strep
2% B27 Supplement
1% N2 Supplement
10mM Nicotidamide
1.25mM N-acetylcysteine
10μM Y-27632
1μM A83-01
1% (v/v) Non-Essential Amino Acids
10mM nicotidamide

PHorg-EM

PHs organoid basic medium
3μM CHIR99021
25ng/ml EGF
50ng/ml HGF
100ng/ml of TNFα
*50 ng/ml Noggin

Neutral PHorg-DM

PHs organoid basic medium
3 μM Dexamethasone

EGF/HGF PHorg-DM

PHs organoid basic medium
3 μM Dexamethasone
25ng/ml EGF
50ng/ml HGF

CHIR PHorg-DM

PHs organoid basic medium

3 μM Dexamethasone

3μM CHIR99021

Table 2.3 Composition of PHs organoids culture media used in this study. *Added after the second passage for the first 7 days of culture.

2.4.4 Differentiation of PHs organoids

For differentiation, PHs organoids were split, grown for 7 days in PHorg-EM (Table2.3) containing 50 ng/ml Noggin, grown 3 to 7 days in expansion media without Noggin and then switched to differentiation media (PHorg-DM). The composition of the three main PHorg-DM used in this project is shown in Table2.3. When indicated, CHIR from Wnt differentiation media was substituted for 50ng/ml Rspo3, 100ng/ml Wnt9b, 100ng/ml Wnt3a or a combination of 50ng/ml Rspo3 and 100ng/ml Wnt9b. Only organoids from passage P3 onwards were subjected to differentiation.

2.4.5 Cryopreservation of PHs organoids

For long term storage, PHs organoids were harvested with ice-cold PBS, pelleted by a 5min 300g centrifugation and resuspended in ice-cold serum-free Bambanker cell freezing media (Wako). PHs organoids were then distributed in 1.5-2ml cryovials and placed in a Mr. Frosty freezing container (Thermofisher) in a -80°C freezer. Mr. Frosty are freezing devices that use a foam layer embedded into 100% isopropanol as temperature isolation buffer to achieve a cooling rate of the vials very close to the optimal -1°C/min.

2.4.6 Generation of BD organoids

BD organoids were generated as previously described by Huch et *al.* (2013) protocol with minor modifications [89]. Briefly, BDs were isolated and hand-picked as described in section 2.3. When collection was completed, BDs were pelleted at 100 g for 5 min, resuspended in ice-cold Matrigel, distributed onto 50 μl Matrigel drops on 6-well plates pre-warmed at 37°C. A maximum 1:4 ratio of BD suspension:Matrigel was used. After seeding, Matrigel drops were gellified by incubating the plates for 15min at 37°C. BD organoid isolation medium (BDorg-IM) (Table2.4) was subsequently added. After 1 week of culture liver organoids were formed and ready to be passaged.

BDorg basic medium
Advanced DMEM/F-12
1% Pen/Strep
1% GlutaMAX
10 mM HEPES 10
1 mM *N*-acetylcysteine
1% N2 Supplement
2% B27 supplement (without vitamin A)
BDorg-EM
BDorg basic medium
10±2% (v/v) Rspo1-conditioned media (CM) or 300 ng/ml purified Rspo1
10 mM nicotinamide
10 nM recombinant human [Leu^{15}]-gastrin
50ng/ml recombinant mouse EGF
50ng/ml recombinant human HGF
100ng/ml recombinant human FGF-10
BDorg-IM
BDorg-EM
100ng/ml Noggin
10% (v/v) Wnt3a-conditioned media
BDorg-DM
BDorg basic medium
100ng/ml recombinant human FGF-10
50 ng/ml EGF (Peprotech)
100ng/ml FGF10 (Peprotech)
50 nM A-8301 (Prepotech)
10 μM DAPT (Sigma)
*30 μM dexamethasone

Table2.4 BD organoid medium composition. *Added during the last three days of differentiation.

2.4.7 Passage and expansion of BD organoids

For routine maintenance, organoids cultured in BD organoid expansion medium (BDorg-EM) (Table2.4) were passaged into 1:3 to 1:6 ratio by mechanical disruption every 7 to 10 days and cultured in 50 μl Matrigel drops. When plated for experiment (gene expression profiling, FACS analysis, immunostaining or microinjection), organoids were dissociated for 5 min at 37°C with TryplE into single cells and seeded at a density of 200-400 cells/μl Matrigel.

2.4.8 Differentiation of BD organoids

For differentiation, organoids were expanded for 2 to 4 days, and switched to BD organoid differentiation medium (BDorg-DM) (Table2.4) and cultured for 13 days. Differentiation media was changed every day. When indicated, differentiated organoids were treated with 100 ng/ml Rspo1 in 0.1% bovine serum albumin (BSA) PBS or Doxycycline (Dox) (0.1 mg/ml or 2 mg/ml in PBS). Organoids differentiated in this study were between passage 4 and 15.

2.4.9 Cryopreservation of BD organoids

For long term storage, BD organoids were harvested with ice-cold PBS, pelleted by a 5 min 300 g centrifugation and resuspended in a mixture of ice-cold 40% FBS, 10% DMSO and 50% BDorg-EM. BD organoids were then distributed in 1.5-2 ml cryovials and placed in a Mr. Frosty freezing container (Thermofisher) in a -80°C freezer.

2.4.10 BD organoid forming capacity assay

To assess organoid forming capacity, organoids were expanded for 2 to 4 days, and differentiated for 11 days. Media was supplemented with 30 μM dexamethasone for the last 24 h of culture. On the last day of culture, organoids were treated concurrently with 500 nM 4-OHT (Sigma) and 100 ng/ml Rspo1 (Prepotech) for 20 h. 4-OHT and Rspo1 were then withdrawn from the media for 4 h to both allow the recovery and reduce the levels of delayed Cre recombination. Organoids were subsequently collected, incubated for 7 min at 37°C with TriplE and dissociated into single cells and re-suspended in AdDMEM/F12 containing 2 mM EDTA for sorting. 1000 cells of either tdTom positive or negative cells were isolated by flow cytometry, centrifuged 5 min at

300 g, re-suspended in 150 µl of Matrigel (Corning) and distributed into 3 wells in a 24-well plate format. Cells were cultured in expansion media containing 25 ng/ml noggin (Peprotech) and where 10% Rspo1 CM was substituted by 300 ng/ml of purified Human Rspondin1 (Peprotech). 10 µM Y27632 (Prepotech) was added for the 3 first days of culture. At day 7, images were acquired using a GelCount instrument (Oxford Optronix) and organoid diameter was quantified by ImageJ. Structures with a diameter >100 µm were considered as organoids for the analysis.

2.4.11 Assessment of Dox effects on the BD organoid viability

To determine whether the addition of Dox affected organoid growth/viability, 200-400 cells/µl matrigel from WT bile duct organoids were seeded in 96-well plates compatible for bioluminescence and/or fluorescence reading. Organoids were cultured in expansion media for 2 to 4 days and were differentiated where indicated for 13 days. For the last 3 days of culture, differentiation media was supplemented with 30 µM dexamethasone and, when indicated, 0.1 mg/ml of Dox. Organoid viability was determined by CellTiter-Glo (Promega) and CellTox (Promega) following the manufacturer's instructions. Briefly, for CellTiter-Glo assay 100 µl of CellTiter-Glo reagent was added to each well containing the organoids grown in 100 µl of medium. Plates were then incubated for 5 min protected from the light on an orbital shaker at RT to assist cell lysis. After this, plates were left at RT for another 10min for the luminescence signal to stabilize and the signal was subsequently measured in a BMG-luminometer. For CellTox assays, 100 µl of 2x CellTox reagent was added per well containing the organoids and 100 µl of medium and the solution was incubated for 20 min at RT protected from the light. After incubation, the intensity of resulting green signal, which is proportional to the amount of late apoptosis events in culture, was measured using a BMG-luminometer.

2.4.12 mES cells culture

mES cells were a gift from Dr. Anika Offergeld. mES cells were unfrozen in FBS 2i medium (Figure2.4) and culture onto 0.1% gelating-coated plates at 37°C for 1h. For passage, mES cells were grown to 50-70% confluency, harvested using an enzyme-free cell dissociation buffer (Gibco) and enriched for pluripotent cells by premature detachment of the undifferentiated colonies. After the second passage, cells were

A

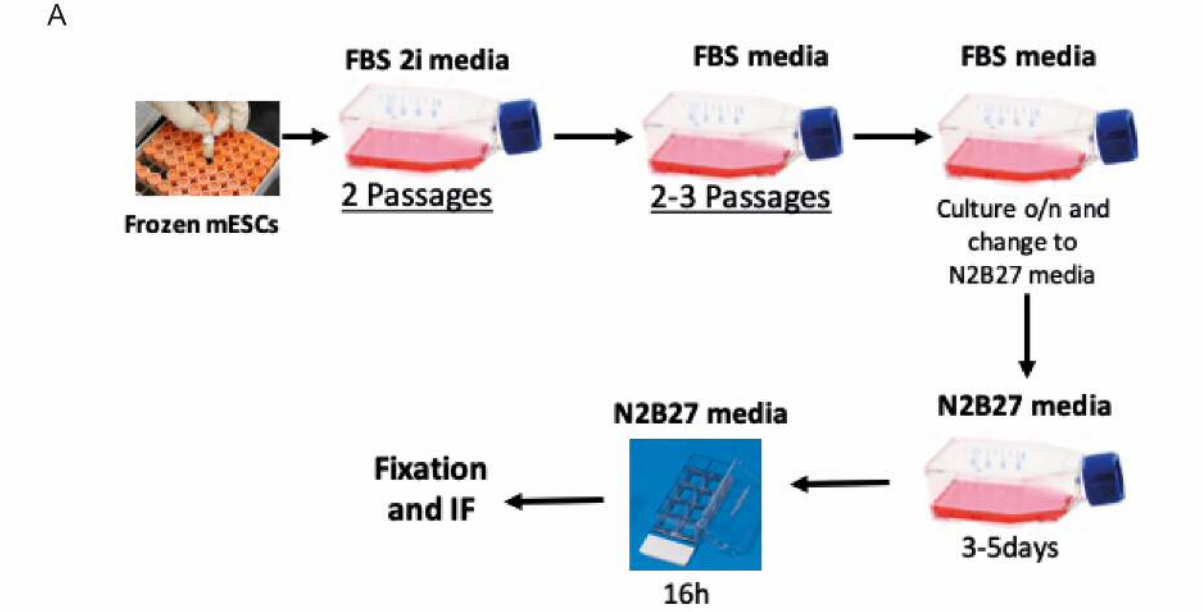

B

FBS 2i media	FBS media	N2B27 media
DMEM/F12 +Glutamax-1 +pyruvate (0.5mM)	DMEM High glucose	DMEM/F12 (50% v/v) +Glutamax-1 +pyruvate (0.5mM)
FBS (10%)	FBS (15%)	Neurobasal medium (50% v/v) 1% B27 Supplement 0.5% N2 Supplement 0.0025% BSA
PD0325901 (MEKi) (0.5uM) CHIR99021 (GSK3i) (3uM)		
B-ME (0.11mM)	B-ME (0.11mM)	B-ME (0.055mM)
LIF (10^6U/ml)	LIF (10^6U/ml)	LIF (10^6U/ml)
	Glutamax-1 Sodium pyruvate (1mM) Non-essential amino acids	100ng/ml Wnt3a

Figure2.4 mES cell culture (A) Scheme representing the mES cells culture steps followed in this study. Medium used in each passage has been indicated. (B) Comparative table indicating the medium composition used in the culture of mES cells.

switch to FBS medium (Figure2.4) and passaged 2 to 3 times in that medium composition. For experiment, cells grown in FBS medium were passaged, cultured o/n in FBS medium, switched to N2B27 medium (Figure2.4) and cultured for 3 to 5 days following Habib et *al.* (2013) recommendations [105]. When colonies were formed,

cells were passaged onto black clear bottom 96-well plates or 8-well ibidi μ-Slides coated with 0.1% gelatin at 37°C for 1h and cultured using N2B27 medium.

2.4.13 Cryopreservation of mES cells

For the propose of freezing, mES cells were incubated with enzyme-free cell dissociation buffer (Gibco) for 3-10min at 37°C, resuspended in a mixture of 40% FBS, 10% DMSO and 50% of the medium in which the mES cells were cultured at the moment of the split.

2.4.14 Culture of HEK293T cells

HEK293T cells were routinely cultured in HEK293T culture media (DMEM High Glucose supplemented with 10% FBS and 1%Pen/Strep). For passage cells in exponential growth phase at a 50-80% confluency were rinsed with 37°C pre-warmed PBS, incubated with 0.025% Trypsin (Gibco) for 2 to 4 min and harvested into 15ml conical tubes. Trypsin digestion was quenched with HEK293T culture media. Cells were then pelleted at 250 g for 5 min, resuspended in HEK293T culture media and seeded at a 1:5 – 1:8 split ratio.

2.4.15 Culture of HEK293T cells in a collagen sandwich platform

The solution for the first (1.5 mg/ml) and second (0.9 mg/ml) layer of rat tail collagen type I (Thermofisher) was prepared following the gelling procedure instructions of the manufacturer. Briefly, the volume of collagen, 10xPBS, NaOH and water for each of the layers was determined using the following equations:

$$Volumen\ of\ collagen\ (V1) = \frac{(Final\ concentration\ of\ collagen)x\ (Final\ Volume)}{(Initial\ concentration\ of\ collagen\ (\frac{3\mu g}{ml}))}$$

$$Volumen\ of\ 10xPBS\ (V2) = \frac{Final\ Volume}{10}$$

$$Volumen\ of\ NaOH\ (V3) = \mathrm{V1\ x\ 0.025}$$

$$Volumen\ of\ water\ (V4) = Final\ Volume - (V1 + V2 + V3)$$

The resulting volumes of water, NaOH, 10xPBS and collagen were gently mixed and kept on ice as gelling of the mixture rapidly occurs at RT.

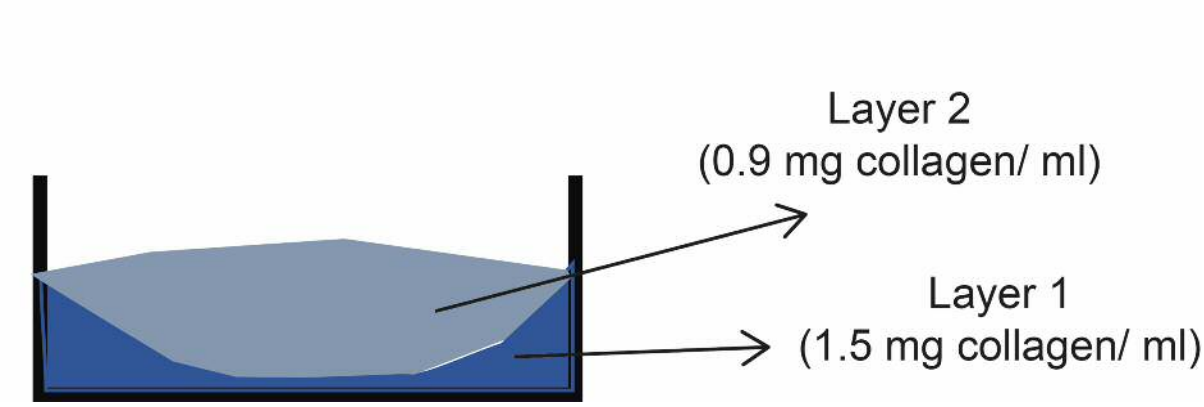

Figure 2.5 Collagen Sandwich scheme. First layer of collagen was spread with the help of a pipette tip. The first layer of collagen forms a very pronounced concave meniscus as the adhesive forced between the collagen solution and the culture plate are much higher than those between the collagen molecules of the solution. The second layer of collagen is then placed, generating a collagen sandwich of uneven thickness.

100 μl of collagen layer1 mixture were pipetted per well of an 8-well ibidi chamber slide and distributed using a p200 tip as indicated in Figure2.5 and plates were incubated for 30-45 min at 37°C. After a firm layer1 gel was formed, HEK297T cells were seeded on top of it. 12-16h later, dead cells and non-attached cells were washed one time with 37°C pre-warmed PBS, the second layer of collagen with the beads embedded was placed on top of them. Beads were attracted to the bottom of the plates with magnets and the collagen was for 30-45min at 37°C. After the second collagen layer was solidified, culture medium was pipetted on top.

2.4.16 Generation of HEK293T TCF-eGFP cell line

To generate TCF-eGFP reporter cells, HEK293T cells were transduced with p7TGC plasmid (Appendix A, Figure1) by exposing HEK293T cells in exponential growth phase and at 50% confluency to 25% lentivirus-containing medium (see section) diluted into DMEM High Glucose medium at 37°C. After o/n incubation, cells were rinsed 3 times with PBS, harvested with 0.025% Trypsin, washed two times with HEK293T culture media (250 g, 5 min) and resuspended at $1x10^6$ cells/ml in DMEM High Glucose supplemented with 2.5 mM EDTA for subsequent FACS sorting. The p7TGC plasmid carries a SV40-mCherry reporter cassette (Appendix A, Figure1).

Thus, to select successfully p7TGC transduced, cells expressing mCherry while lacking expression of GFP were isolated by FACS.

2.4.17 HEK293T TCF-Luc cell line

HEK293T cells stably transduced with the SuperTOPFlash-luciferase reporter (HEK293T-Luc cell line) were kindly provided by Prof. Nathan (Johns Hopkins University). For routine maintenance, HEK293T cells were cultured in HEK293T culture media supplemented with 100 μg/ml of G418 to prevent the silencing of the transgene [121]. When plated for experiment, G418 was removed from the media composition.

2.4.18 TCF-Luc reporter assay

To measure the response to soluble and immobilized Wnt/Rspo ligands, 5000 cells/well were plated onto clear-bottom 96-well plates white plates (Thermofisher), cultured for two days and then treated for 24 h with different concentrations and combinations of soluble Wnt/Rspo ligands as indicated. To study the synergistic effects of Wnt9b and Rspo3 in absence of endogenous Wnt production, cells were exposed for 24h to 500 nM LGK974 24h and then treated with Wnt9b (100 ng/ml) or Rspo3 (10 ng/ml) for another 24h. The porcupine inhibitor was maintained during the whole length of the experiment. To measure the response to immobilized ligands, Wnt/Rspo beads were washed 3 with PBS, 3 times with HEK293T media (10% FBS DMEM High Glucose) and re-suspended HEK293T media supplemented with 10 ng/ml Rspo3 when indicated. Cell media was then replaced for Wnt/Rspo beads containing media and cultured for 24h. The volume of media per well used in all the treatments was 100 μl.

After the treatments were completed, media was aspirated, cells washed with 37°C pre-warmed PBS and a combination of 50 μl PBS and 50 μl Blight-Glo (Promega) was added per well. Plates were incubated in a shaking incubator at RT for 5min and luminescence was subsequently measured using a BMG-luminometer.

2.4.19 HEK293T-HA-Rspo1-Fc cell line

HEK293T-HA-Rspo1-Fc cell line was a gift from Calvin Kuo [122]. This line over-express Rspo1 protein and was used to produce Rspo1 CM. For routine maintenance and to avoid the silencing of the transgene, HEK293T cells were cultured in HEK293T culture media supplemented with 300 ng/ml of Zeocin (Invitrogen).

2.4.20 Production of Rspo1 CM

Zeocin was removed from the HEK293T-HA-Rspo1-Fc culture media composition one passage prior to cell seeding for Rspo1 conditioning media production. To produce Rspo1 CM, cells in exponential growth rate were seeded at 30% confluency in T75 tissue culture flasks and grown in HEK293T culture media. After 4 days, supernatant was collected and media was replaced for fresh HEK293T culture media. 3 days later, a second supernatant fraction was harvested and mixed with the previous one. Cell debris from the mixture of both fractions were pelleted at 250g for 5min. Rspo1 CM was filtered through a 0.22μm low-protein-binding filter (Millipore), distributed into 10ml aliquots and stored at -20°C. The activity of each batch of Rspo1 CM after one freezing/thawing cycle was assessed by the TCF-Luc assay and compared to the activity of purified Rspo1 ligand (see section 2.3.4.2.1). The concentration of Rspo1 used for biliary duct liver organoid culture corresponded to the saturating concentration of the CM in this assay (usually 10±2%) and was equivalent to the activity of 300 ng/ml or purified Rspo1.

2.4.21 Cryopreservation of HEK293T cells

To freeze HEK293T, cells were harvested, resuspended in 40% FBS, 10% DMSO and 50% DMEM High Glucose, distributed in cryovials and immediately placed in Mr. Frosty freezing containers at -80C.

2.4.22 LWnt3a cells

LWnt3a cells express non-tagged Wnt3a protein under the control of a PGK promoter and were used to produce Wnt3a CM [123]. For routine culture, LWnt3a cells were cultured in L cells media (DMEM media containing GlutaMAX, 10% FBS, 1%Pen/Strep) supplemented with 100 μg/ml of G418 to prevent the silencing of the transgene.

2.4.23 Production of Wnt3a CM

G418 was removed from the media composition one passage prior to cell seeding for Wnt3a CM production. To produce Wnt3a CM, cells in exponential growth rate were seeded at 30% confluency in T75 tissue culture flasks and grown in L cells media. L cell media was harvested at day 4 and 7. Both conditioning media fractions were mixed, centrifuged at 250g 5min to pellet possible cell debris and filtered through a 0.22 μm low-protein-binding filter (Millipore). The resulting Wnt3a CM was distributed into 10ml aliquots and stored at -20°C. The activity of each batch of Wnt3a CM was tested after one freezing/thawing cycle by the TCF-Luc assay and compared to the activity of Wnt3a purified ligand.

2.5 Immobilization of proteins onto magnetic beads

Carrier free recombinant mouse Wnt3a (>95% purity, carrier free), Rspo1, Rspo3 and Wnt9b were purchased from R&D systems. Purified GFP was a gift from Dr Harley Worthy. GFP, Wnt3a, Wnt9b, Rspo1 or Rspo3 were immobilized onto 0.5 mg of 2.8 μm Dynabeads M-270 Carboxylic acid (Invitrogen) by using a two-step coating procedure with EDC and NHS as indicated by the manufacturer (Figure2.6). Briefly, beads were washed twice for 10 min with ice cold 25 mM MES buffer (pH 5) at a concentration of 10 mg beads/ml. Beads were pulled with a magnet for 4min between washes. Immediately before use, EDC and NHS were respectively dissolved at 50 mg/ml in ice cold 25 mM MES buffer (pH 5). Beads were then resuspended in EDC and NHS was subsequently added. Note that EDC is stored at -20°C. As this compound is highly hydrophilic at low temperatures, to preserve the purity of the compound over time is critical that EDC is equilibrated at RT before opening the lid of the container.

Beads were then incubated at RT with slow tilt rotation for 30 min and washed 1x with 25 mM MES buffer (pH 5). After this step, the beads were activated and open to form covalent bounds with the primary amines of the ligand. The lyophilized ligands of interest were reconstituted in PBS immediately prior to use and added directly to the activated beads. 25 mM MES buffer (pH 5) was added in 4:5 ratio and the protein-bead mixture was incubated for 1h at RT with slow tilt rotation. To assess the immobilization efficiency, the protein supernatant was collected after the incubation

and diluted to 100 μg/ml (based on the protein initial concentration) in PBS containing a final concentration of 0.1% BSA. The amount of ligand per mass (mg) of beads used during the crosslink was optimized in such a way that the remaining supernatant after the cross-link would retain at least 10% of its initial activity (Figure2.6). A table with the peptide concentrations and volumes per ligand used is provided (Table2.5). Beads containing the immobilised ligands were then washed 3x with PBS and quenched and

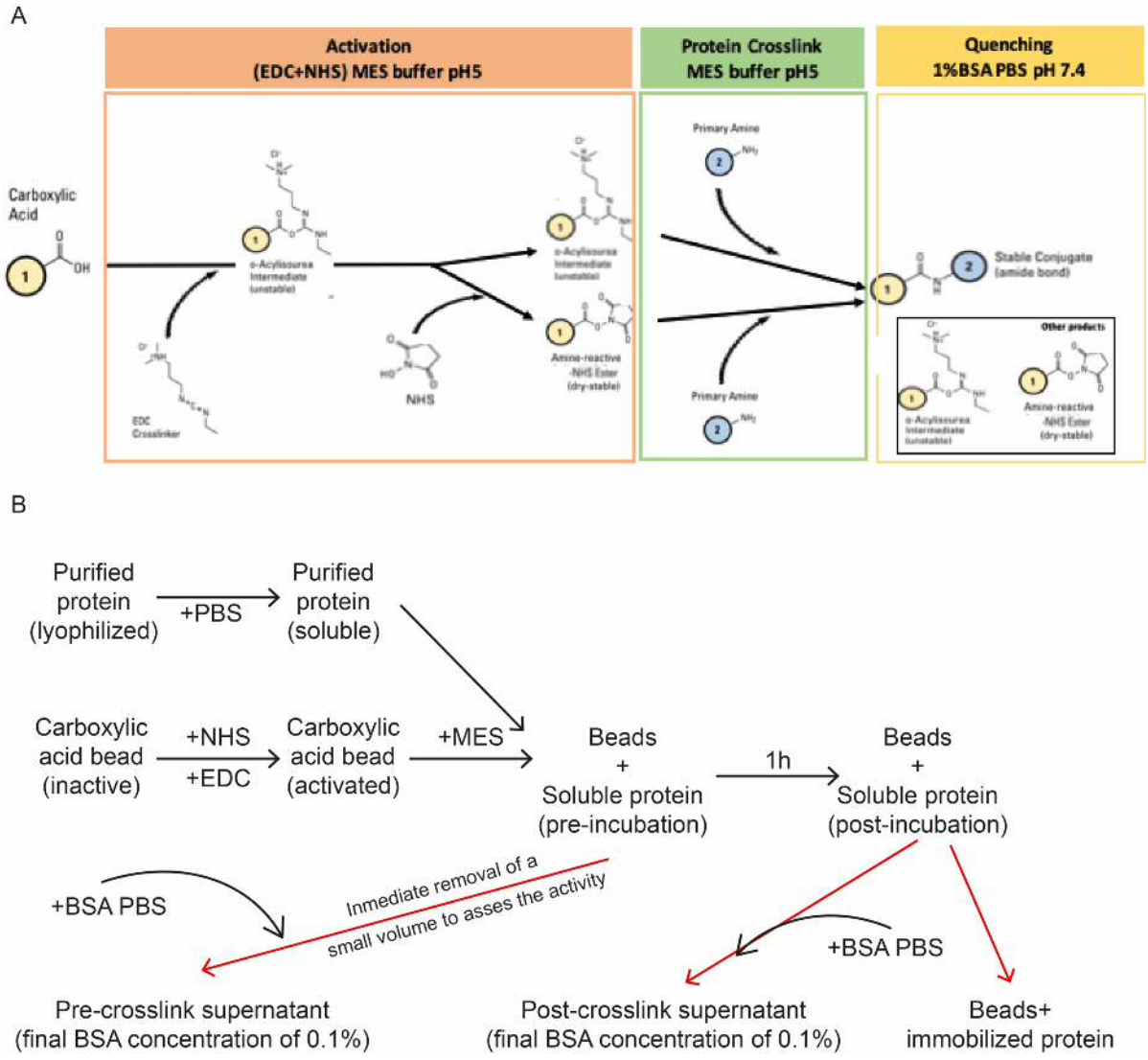

Figure2.6 (A) Two-step chemical crosslink reaction scheme. EDC carbodiimide crosslinker reacts with the carboxylic acid groups that cover the surface of the bead to give place an active O-acylisourea intermediate able to react with primary amino groups. The addition of NHS increases the efficiency of the activation. Once activated, beads are washed in MES buffer and subsequently incubated with the protein of interest. As a result, the primary amino groups (-NH2) present in the side chain of lysines and N-terminus part of the protein form a covalent bound with the beads giving rise to a stable conjugated. (B) Scheme summarizing protocol for bead immobilization. Red arrows point to the resulting products of the reaction. Pre- and post-crosslink supernatant were immediately stored at -80C. Immobilized ligands onto beads were stored at 4°C in 0.1% BSA.

stored in 1% BSA PBS. As a control, vehicle-beads that have undergo activation and 1% BSA quenching were used.

2.6 Flow cytometry analysis of BD organoids

2.6.1 Preparation of single cell suspension

Organoids were harvested with ice cold PBS, pelleted at 300g for 5min and incubated for 7 min at 37°C with TriplE and dissociated into single cells by gentle pipetting. Cells were washed one time (300 g, 5 min) with AdDMEM/F12, resuspended in 2mM EDTA AdDMEM/F12 and filtered through 40 μm FACS tube caps.

2.6.2 Live cells staining

For live/dead cell discrimination, 0.2 μg/ml DAPI was added to the single cell suspension prepared in section 2.6.1.

2.6.3 Fixed cells staining

Cells prepared as indicated in section 2.6.1 were incubated with 1:500 Zombie NIR fixable viability dye (Biolegend) on ice for 15min, washed one time with PBS (300 g, 5min) and resuspended in 100-200 μl of PBS. 16% of PFA was added at a ratio of 1:4 and cells were fixed on ice for 30 min. Cells were then permeabilized and stained using reagents from Click-iT Edu Flow Cytometry Assay Kit from ThermoFisher following the instructions of the manufacturer with modifications. Briefly, cells were washed one time with PBS and one time with 1X Click-iT saponin-based permeabilization buffer, permeabilized and blocked for 20 min with 1% BSA 1X Click-iT saponin-based permeabilization buffer at RT, and incubated with primary antibody in 1% BSA 1X Click-iT saponin-based permeabilization buffer for 1h. Cells were subsequently washed one time with 1X Click-iT saponin-based permeabilization buffer, incubated with secondary antibody in 1X Click-iT saponin-based permeabilization buffer for 45 min at RT. Cells were subsequently washed one time in PBS, incubated with 5 μg/ml DAPI in PBS for 15 min to counterstain the nuclei, washed one time in PBS and re-suspended in PBS for FACS analysis.

Ligand	Lyophilised amount protein (μg)	Amount of beads (mg)	Concentration Beads during incubation (mg/ml)	Volume EDC (μl)	Volume NHS (μl)	Volume PBS ligand resuspension (μl)	Volume MES buffer during crosslink (μl)	$[Protein]_{crosslink}$ (μg/ml)
Wnt3a	10	1.42	10	73	73	29 *(-3.73μl)	116	67
Wnt9b	25	2.49	10	125	125	50	200	100
Rspo1	25		10					
Rspo3	25	1	10	85	85	34 *(-1 μl)	136	147

Table2.5 Volume and protein concentrations used per ligand. NA (no applied). * Amount of protein removed to evaluate the activity of the supernatant before the crosslink. This volume was immediately mixed with BSA in PBS to a final concentration of 0.1% BSA.

2.7 RNAseq

For RNAseq of data presented in Chapter 6, total RNA from 2,000 to 100,000 tdTom positive, tdTom negative or untreated cells from differentiated BD organoids were isolated and sorted by flow cytometry as indicated in Appendix C, Figure2. RNA concentrations were determined by a Hi-sensitivity Qubic kit. Hi-sensitivity Qubic results. Single-end 75bp sequencing was performed with 100 ng of total RNA input. Library preparation ad sequencing was performed by Angela M. Marchbank and Georgina E. Smethurst on a NextSeq-500 sequencer and involved the pooling of equi-molar libraries from samples under comparison (Genomic Hub, School of Biosciences, Cardiff University, Cardiff, CF10 3AX, UK). Sequences were trimmed with Trimmomatic 0.35 and assessed for quality using FastQC 0.11.2, using the default parameters [124]. On average, 99% of the total reads were mapped to the mouse GRCm38 reference genome using STAR 2.5.1b. and counts were assigned to transcripts using featureCounts with the GRCm38.84 Ensembl gene build GTF [125,126]. Counts per million (CPM) and fragments per kilobase per million (FPKM) were calculated for each gene. Both the reference genome and GTF were downloaded from the Ensembl FTP site. Trimming, mapping and CPM and FPKM normalizations were performed by Dr Robert Andrews and Dr Sumukh Despande from the Data Hub at Cardiff University. Genes with <0.5 average FPKM in all biological groups were considered as not expressed and discarded from the analysis (see Appendix D). Differential gene expression was performed using DESeq2 R package, with default 0.1 false discovery rate (FDR), controlling for biological replicates differences [127]. The normalised gene expression values (default DESeq2 scaling-factor normalisation) of significantly expressed genes were subject to Principal Component Analysis (PCA) using in R using prcomp(). Normalized expression mRNA values in FPKM as well as padj values that had been assigned per two-by-two comparison can be found in Appendix E, Table 1 provided on the associated USB. Genes with adjusted P value (padj) $\leq$0.01 were considered as differentially expressed. Heat map generation and hierarchical clustering with CPM values were performed applying one minus Pearson correlation clustering method using the Broad Institute online tool Morpheus (https://software.broadinstitute.org/morpheus/). Gene set enrichment analysis was either performed using the Gene Ontology online tool AmiGO

(http://amigo.geneontology.org/amigo) or the Broad Institute GSEA desktop app using the molecular signature data base (MSigDB) v7.0 updated in August 2019. AmiGO Go-Term results were represented using the online tool REVIGO (http://revigo.irb.hr/) combined with R. Ax2pos/Ax2neg gene set enrichment and clustering analysis was restricted to differentially expressed genes displaying a 2-fold change (a total of 1341 genes).

2.8 RT-qPCR

2.8.1 RNA isolation

Total RNA was isolated from BDs, PHS or organoids following Trizol Reagent (Life Technologies) RNA extraction method coupled with RNaesy minElute columns (Qiagen). For that propose, samples were homogenized using 0.5 ml Trizol Reagent (Life Technologies) and chloroform was added into a 1:4 ratio. The aqueous containing RNA was separated by 13000 g, 4°C, 15 min centrifugation, mixed 1:1 with 70% ethanol and subsequently loaded into RNaesy minElute columns equilibrated at RT. RNA was then purified following the RNesy plus kit manufacturer instructions, which involved washing the column with 700 μl of RW1 buffer, followed by a 500 μl wash with RPE buffer and a 500 μl wash with 80% ethanol. After the last wash, columns were transferred to a clean tube and centrifuged at 15K rpm to further eliminate ethanol traces. Columns were then transferred to a clean collection tube and the RNA was eluted with 17 μl of RNAse-free water pre-warmed at 55°C to increase the RNA recovery yield.

2.8.2 cDNA synthesis

cDNA was synthetized using 100-500 ng starting RNA using iScript cDNA Synthesis Kit from Bio-Rad. For RT-qPCR gene expression analysis, cDNA was subsequently 1:4 diluted in water and stored at -80°C for further use as indicated in section 2.8.4. For the propose of primer *in vitro* testing (see section 2.8.3), undiluted cDNA was stored at -80°C.

2.8.3 RT-qPCR primer design

Primers sequences were obtained from the primer bank data base, members of Trevor Dale laboratory, published papers or designed using the primer design online tool from

NCBI (https://www.ncbi.nlm.nih.gov/nuccore). When primers were designed using the NCBI online tool the following designing and met two criteria: (i) PCR product with a length of 70-200bp and (ii) primer must span an exon-exon junction. In this project, amplification of all splicing variants was always desired and the pair of primers with the lowest self-complementary score was selected. Primer specificity was validated first *in silico* and then *in vitro*.

2.8.3.1 *In silico* testing

In silico analysis of primer specificity was run using UCSC Genome Browser online tool (https://genome.ucsc.edu/). Non-specific primers giving rise to PCR products from more than one gene were discarded.

2.8.3.2 *In vitro* testing

Primers that successfully passed *in silico* testing were reconstituted at 100 μM using nuclease free water (stock solution) and subjected to *in vitro* testing. Forward (FW) and reverse (RV) primers were 1:5 mixed in water to make a FW/RV mix working solution with a final concentration of 10 μM FW and 10 μM RV primer. For each primer pair a positive control sample that expressed the gene of interest was selected (usually BD organoids or PH) and RNA and cDNA were isolated and synthesised following the indications of sections 2.8.1 and section 2.8.2, respectively. Four 1:10 serial dilutions were generated with the resulting cDNA and a quantitative PCR (qPCR) and run as independent samples (see section 2.8.4). The qPCR reaction was carried out on a LightCycler 480 Real-Time PCR system (Roche). After the run, the relationship between the amount of cDNA and the Ct value was calculated by plotting the number of the dilution (1 to 4) against its mean Ct value and the R^2 linear regression coefficient was determined in Excel. qPCR products were also collected and evaluated in a 1.5% electrophoresis agarose gel. Primers with more of one melt-curve peak, an R^2 coefficient value below 0.9 or with more than one PCR product were discarded. The gene-specific primer pairs used in this study are in Appendix A, Table2 and the *in silico* testing results of all primers used in this thesis can be found in Appendix A, Figure1 to 7.

2.8.4 Quantitative PCR

Primers were reconstituted at 100 uM using nuclease free water to make stock primer solution. Three technical replicates were performed per condition. qRT-PCR reaction was carried out on a LightCycler 480 Real-Time PCR system (Roche) by mixing 5.5 µl of 'Primer mix' and 4.5 µl of 'cDNA mix' (see Table2.6 and 2.7). Quantified expression values for individual genes were normalized to B2M. The gene-specific primer pairs used in this study are in Appendix A, Table2.

	Primer mix
SensiFast Hi-Rox SYBR Green (Roche)	5 µl
milliQ water	0.1 µl
Primer mix (10 µM FW+ 10 µM RV)	0.4 µl

Table2.6 Primer mix

	cDNA mix
cDNA	0.5 µl
milliQ water	5 µl

Table2.7 cDNA mix

2.9 Immunofluorescence (IF)

IF buffers used in this thesis are indicated in Table2.8.

3D cultures IF buffer

PBS

0.1% Triton X-100

0.05% Tween-20

0.1% BSA

mES IF buffer

PBS

0.001% Tween-20

0.1% BSA
PH 2D cultures IF buffer
PBS
0.05% Tween-20
0.1% BSA

Table2.8 IF buffers used in this study.

2.9.1 Organoid preparation for light-sheet microscopy

Plates containing the organoids were placed on ice and Cell Recovery Solution (Corning) was pipetted in each well and incubated for 15 to 20 min, which caused the gentle dissociation of the organoids from the Matrigel droplets. Organoids were then harvested and transferred on top of a 40 μm pluriStrainer placed in a 6-well plate (Figure2.7, A). Alternatively, organoids were collected with cold PBS and placed directly on top of the 40 μm pluriStrainer. Once in the pluriStrainer, organoids were washed 2 times with PBS, fixed for 30 min with 4% PFA at RT and washed 3 times with PBS. Organoids were then carefully collected under the microscope with a p200 pipette and transferred on top of 40 μm FACS tube caps in a 24-well plate, permeabilized/blocked for 1h at RT with 10% donkey serum (Abcam) in IF buffer (Table2.8). After o/n primary antibody incubation in IF buffer at 4°C, cells were washed 3 times with IF buffer for 10min, incubated with secondary antibody in IF buffer for 1-2 h at RT, washed 2 times with IF buffer and counterstained with 4 mg/ml DAPI in PBS for 15 min. Stained organoids were hand-picked under the microscope, embedded in 1% low melting point agarose pre-warmed at 60°C and loaded into glass capillaries (Zeiss) (Figure7, B). Samples were imaged in PBS in a commercial Z.1 Zeiss light-sheet microscope (Figure2.8, C).

2.9.2 Organoid preparation for confocal microscopy

For confocal imaging, organoids were either cultured in black clear bottom 96-well plates or ibidi μ-Slides of 2, 4 or 8 wells, fixed either with 4% PFA for 1h at RT or with ice-cold 100% methanol for 30min at -20°C, washed 3 times with PBS for 10min and

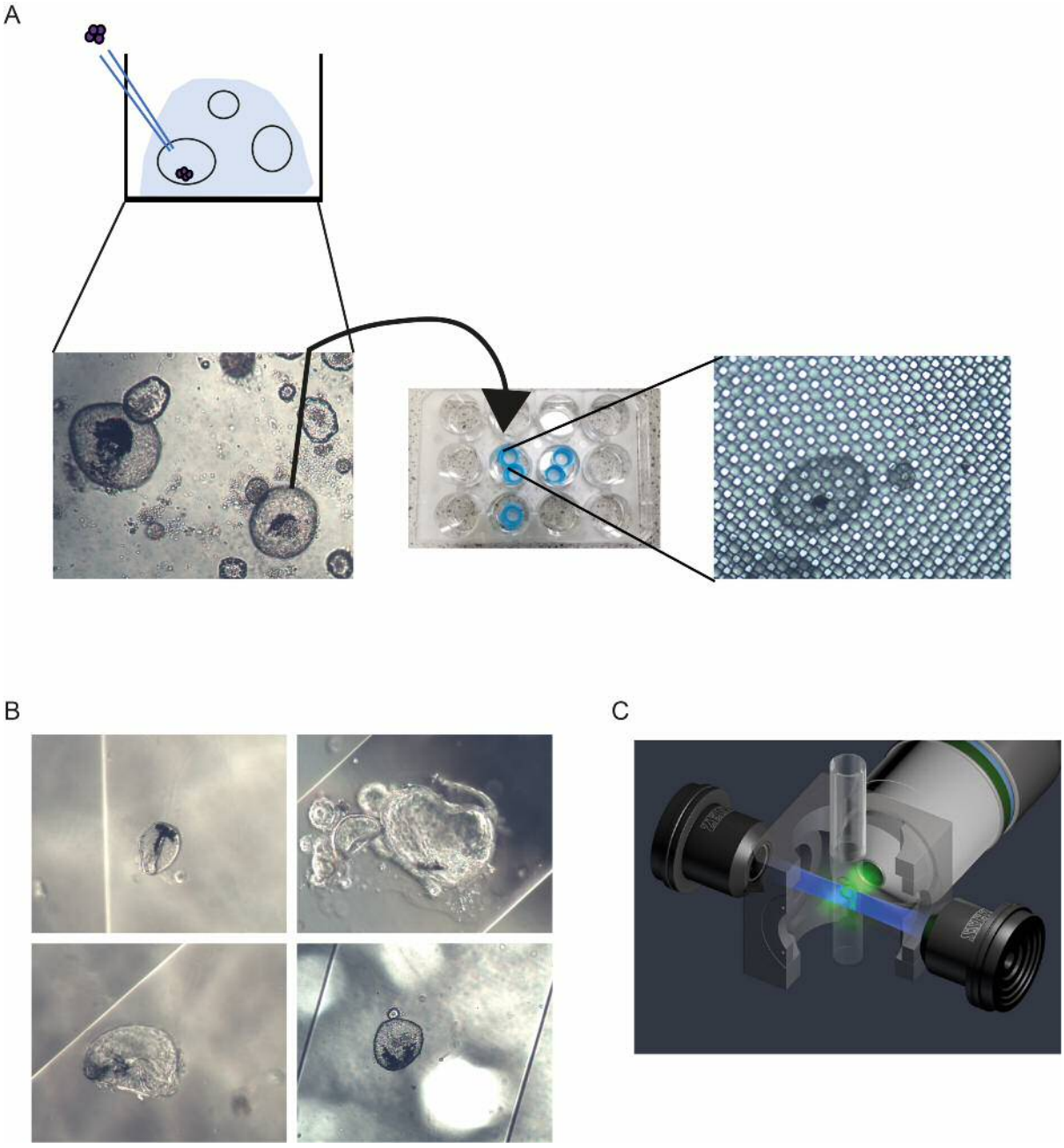

Figure2.7 Light-sheet imaging sample preparation (A) Scheme showing the collection and transfer of microinjected BD organoids for IF staining. Organoids were dissociated from the matrigel. Filters of 40 µm (pluriStrainer or FACS caps) were used to retain the organoids, wash and stain them without the need of centrifugation intermediated steps. This was critical to prevent the displacement of the beads once the microinjected organoid was fixed. (B) Images showing BD organoids microinjected with carboxylic acid beads and embedded into 1% agarose using Zeiss glass capillaries. (C) Image from Zeiss website showing Z.1 light-sheet microscope set up. Samples embedded in 1% agarose capillary are loaded into chambers filled with PBS. The objective is placed at 90° from the two illumination sources.

permeabilized/blocked for 3-5 h at RT with 10% donkey serum (Abcam) in IF buffer (Table2.8). Primary antibody incubation was performed o/n at 4°C in IF buffer. Thereafter cells were washed 3 times with IF buffer for 10min, incubated with

secondary antibody in IF buffer for 3-5 h at RT, washed 2 times with IF buffer and counterstained with 4 mg/ml DAPI in PBS for 15min. Samples were subsequently imaged in PBS.

2.9.3 mES cells immunostaining and validation of Wnt3a beads

After two passages in FBS mES medium, cells were cultured overnight, switched to N2B27 supplemented with 100 ng/ml Wnt3a and cultured for 3-5 days until colonies were formed and ready to proceed with the immunofluorescence imaging of single cells in presence of beads. For that purpose, 5000 mES in N2B27 media were mixed with 2.25μg of either Vehicle- or Wnt3a-beads and pleated onto 8-well ibidi chambered cover-glass slides previously coated with 10 μg/ml of human fibronectin for 1h at 37°C. After 16h, cells were washed with PBS and fixed with 4% PFA for 30min at 4°C. Cells were washed one time with PBS and other two times with mES IF buffer. Cells were then blocked with mES IF buffer containing 10% donkey serum for 30 min and subsequently incubated with primary antibodies in mES IF buffer o/n at 4°C. Samples were then washed three times with mES IF buffer and incubated in secondary antibody for 2 h. Cell nuclei was stained with 2 mg/ml of DAPI in PBS for 15min, washed one time with PBS. Samples cultured in clear bottom 96-well plates were imaged in PBS whereas cells grown in ibidi μ-Slides were mounted using Vectashield (Vector Laboratories). All washing steps were performed under the microscope to control for bead movement.

2.9.4 Characterization of 2D PH cultures by immunofluorescence

To characterise the dynamics of expression of Wnt pathway receptors upon 2D culture, fresh isolated murine PH were cultured onto three different collagen-coated black clear bottom 96-well plates, in hepatocyte attachment media (1:1000 ITS, 5% ES qualified FBS, 1% Pen/Strep, 15mM HEPES DMEM/F12). 4 h after seeding, plates containing the hepatocytes corresponding to a 4 h fixation time point were washed with PBS pre-warmed at 37°C, fixed with 4% PFA for 15min, washed 3 times with PBS, permeabilized for 15-20 min at RT with 0.1% Triton X-100 (Sigma) PBS and blocked for 1h in 10% donkey serum 2D IF buffer (Table2.6). Samples were then incubated in primary antibody o/n at 4°C, washed three times with 2D IF buffer and incubated in secondary antibody for 2 h. Cell nuclei was stained with 2 mg/ml of DAPI

in PBS for 15min, washed one time with PBS. Samples cultured in clear bottom 96-well plates were imaged in PBS whereas cells grown in ibidi μ-Slides were mounted using Vectashield (Vector Laboratories).

Plates containing hepatocytes corresponding to the fixation points of 16 h and 24 h were switched to PH 2D culture media (1:1000 ITS, 0.5% ES qualified FBS, 1% Pen/Strep, 15 mM HEPES DMEM/F12) 4 h after plating and cultured for another 12 and 20 h, respectively. After that time, cells were washed with PBS pre-warmed at 37°C, fixed with 4% PFA for 15 min and processed for IF as indicated for the hepatocytes corresponding to a 4 h fixation time point.

2.10 Lentivirus production

2.10.1 Plasmid preparation

The TCF-eGFP reporter plasmid (p7TGC) was a gift from Dr Roel Nusse (Addgene, #24304). The envelop plasmid VSV-G and the packing plasmid psPAX2 for lentivirus production were a gift from Dr Juan Bautista Menendez-Gonzalez from Neil Rodrigues laboratory.

VSV-G and psPAX2 plasmids were supplied as purified plasmids and amplified in One Shot Stbl3 Chemically Competent *E. coli* (Thermofisher) following the instructions of the manufacturer. Briefly, 100 ng of plasmid were gently added into a vial of Stbl3, incubated on ice for 30 min, transferred into a 42°C water bath for 45 s and incubated for 2 min on ice. Transformed bacteria were then mixed with 250 μl of S.O.C. medium, incubated at 37°C for 1 h in a shaking incubator and a volume of 50 μl was spread into LB broth agar plates supplemented with 100 μg/ml ampicillin. Plates were inverted, incubated at 37°C overnight and subsequent colonies hand-picked and used to inoculate 5 ml LB broth medium supplemented with 100 μg/ml ampicillin. Cultures were grown o/n at 37°C in a shaking incubator.

The p7TGC plasmid was supplied as transformed bacteria in stab culture format and therefore liquid bacterial cultures were generated by direct inoculation of 5 ml LB broth supplemented with 100 μg/ml ampicillin. Cultures were grown o/n at 37°C in a shaking incubator.

2.10.2 Plasmid purification

Plasmids present in bacteria liquid cultures were purified using a Midiprep Kit (Invitrogen) following the instructions of the manufacturer and stored at -80C.

2.10.3 Transfection of HEK293T cells and lentivirus collection

Lentivirus were generated by triple transfection of HEK293T cells with the envelop plasmid VSV-G, the packing plasmid psPAX2 and the TCF-eGFP reporter plasmid (p7TGC) by calcium-phosphate method. For this aim, $3x10^6$ HEK293T cells were seeded into a 10cm dish. 8h post seeding, 3 μg of VSV-G plasmid, 10 μg of pTGC plasmid and 6.5 μg of psPAX2 vector were diluted in water (up to 437.5 μl) and subsequently mixed with 62.5 μl of 2M $CaCl_2$ solution. 500 μl of 2x HBS solution (16 g/l NaCl, 10 g/l HEPES, 0.74 g/l KCl, 0.27g/l Na_2HPO_4 $2H_2O$ and 2 g/l dextrose in H_2O) PHs 7.05-7.1 were transferred into a 15 ml conical tube. The DNA/$CaCl_2$ mixture was added in a drop-wise manner to the 2x HBS solution while this was being vortexed and incubated for 20 min at RT. Medium from the HEK293T cells was replaced by HEK293T media supplemented with 25 μM of chloroquine and the DNA/$CaCl_2$/ 2xHBS solution was added in a drop-wise manner onto the cells. After o/n culture, media was replaced with conventional HEK293T culture media. Media containing p7TGC lentivirus was harvested 12h later, passed through a 45 μm syringe-filter and immediately stored at -80C for further use.

2.10.4 Lentivirus titration

HEK293T cells were seeded (50.000 cells/well) into 24-well plates, cultured for 24 h, exposed to different amounts (0, 1, 10, 50, 100 or 200 μl media per well) of lentivirus-containing medium (section 2.10.3) for 24 h, washed two times with PBS and cultured in HEK293T media for other 24 h. Cells were then collected using Trypsin, washed 3 times with PBS and re-suspended in 2.5 mM EDTA DMEM/High glucose and subsequently assessed for mCherry (lentivirus expression) production levels by flow-cytometry. As expected, number of successfully transduced cells (mCherry positive) was proportional to the amount of lentivirus to which cells were exposed (Figure2.8, A).

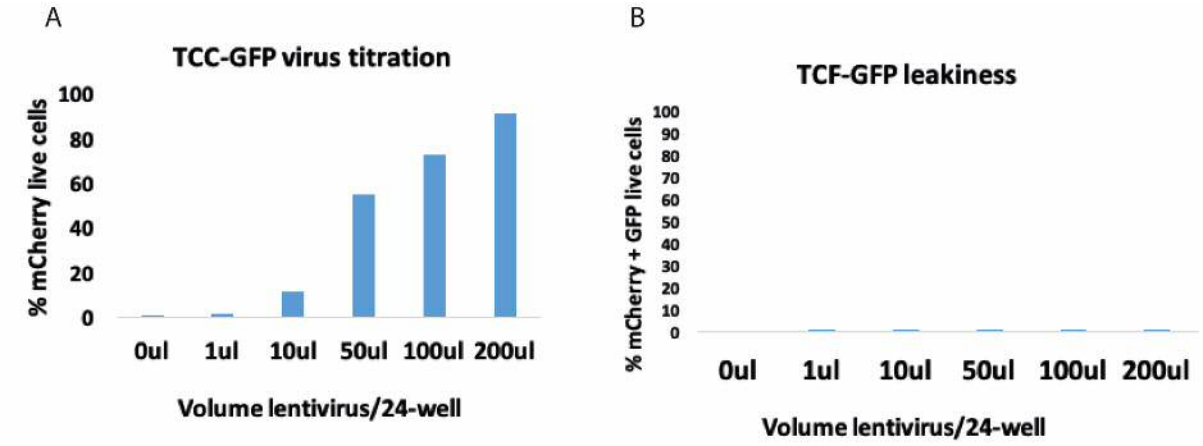

Figure2.8 HEK293T cells were transduced with different amounts of 7pTGC lentivirus. (A) Bar graph shows that proportion of successfully transduced cells (mCherry positive) is proportional to the amount of lentivirus used. (B) Proportion of eGFP positive cells remained constant and close to zero in all the treatments, indicating that the leakiness of the TCF-eGFP reporter is close to zero.

2.10.5 Transduction of HEK293T cells

To generate TCF-eGFP reporter cells, HEK293T cells were transduced with p7TGC plasmid by exposing HEK293T cells in exponential growth phase and at 50% confluency to 25% lentivirus-containing media diluted into DMEM High Glucose media at 37°C. After O/N incubation, cells were rinsed 3 times with PBS, harvested with 0.025% Trypsin, washed two times with HEK293T culture media (250g, 5min) and resuspended at $1x10^6$ cells/ml in DMEM High Glucose supplemented with 2.5mM EDTA for subsequent FACS sorting.

2.10.6 Assessment of the response of TCF-eGFP HEK297T cells to Wnt activation by flow cytometry

HEK293T TCF-eGFP reporter cells in exponential growth rate were plated at a 30% confluency in 12-well plates, grown for 2 days and exposed for 24 h to different concentrations of soluble or immobilized Wnt/Rspo ligands as indicated. When treated with immobilized ligands, Wnt/Rspo beads were washed 3 with PBS, 3 times with HEK293T media prior to the addition to the cells. After treatment was completed, cells were washed with 37°C pre-warmed PBS, harvested with 0.025% Trypsin, washed one time with 10% FBS DMEM High Glucose medium and re-suspended in DMEM

High Glucose medium supplemented with 2.5 mM EDTA. To distinguish between live/dead cells, DAPI was added to a final concentration of 0.4 μg/ml.

2.11 Semi-automatic IF quantifications

2.11.1 Quantification tdTom positive cells lineage tracing experiment in differentiated BD organoids (Chapter 6)

To obtain the percentage of tdTom positive cells, the number of tdTom positive cells divided by the number of nuclei per image field was quantified in a semi-automatic manner using FIJI. For semi-automatic nuclei quantification, nuclear masks were obtained using as an input a 10x confocal image were the nuclei has been counter-stained with DAPI and the different Z-planes have been projected using the maximum intensity of each plane (*Image>Stack>Z projection> Max Intensity*) (Figure2.9). A threshold range was then set up manually per picture to distinguish the nuclei apart from the background (*Image>Adjust>Threshold*). Images were subsequently converted into a binary image and nuclei were segmented from overlapping objects using a watershed function (*Process> Binary> Watershed*) (Figure2.9). Nuclei objects were counted using a minimum size cut-off criteria of 15^2 microns (Figure2.9). The output image with resulting outlines of counted nuclei was finally compared with the input image and thresholding parameters or nuclei size cut-off criteria were adjusted when required (Figure2.9).

2.11.2 Quantification of immunofluorescence images using Harmony Software

Samples stained for tdTom (Rabbit anti-RFP, Rockland), HNF4a (Rabbit anti-HNF4a, Santa Cruz), CK19 (Rat anti-CK19, TROMA-III, DSHB) and GS (Mouse anti-GS, Sigma) were quantified in a semi-automatic manner using the software Harmony. A total of 20 view fields at 20x magnification were quantified per animal and staining. View field analysed were from at least two different hepatic lobes. The pipeline of analysis and mask used for the quantifications of samples stained for GS can be found in Figure2.10. The masks used for the quantifications of samples stained for tdTom and HNF4a have been detailed in Figure2.11. Samples stained for tdTom and CK19 were quantified as indicated in Figure2.12.

2.12 Statistical methods

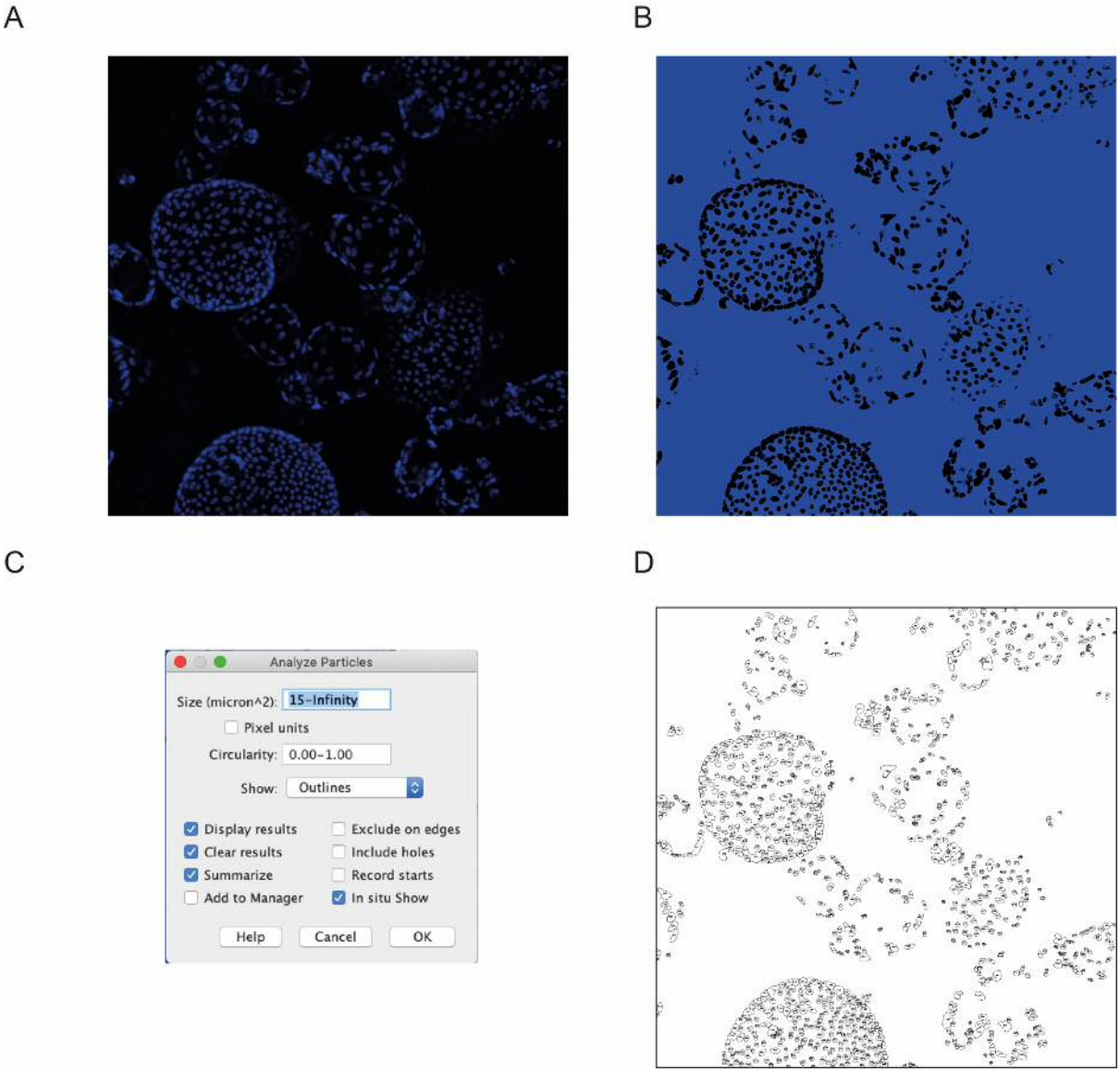

Figure2.9 Screen shoots of image analysis for nuclear segmentation and semi-automatic quantification using FIJI. (A) 10x input a confocal image where the cell nuclei has been counterstained with DAPI and the different Z-planes have been projected using the maximum intensity of each plane. (B) Corresponding binary image where threshold has been adjusted for the identification of the nuclei (objects of interest) over the image background. Watershed separation was applied for the segmentation of overlapping nuclei. (C) Panel with FUJI settings employed for the quantification of nuclei particles. (D) Output image were the outlines of the counted particles have been highlighted.

GraphPad Prism 7.0 Software was used for all statistical analysis and graphs representation. Statistical test used are indicated in each individual figure.

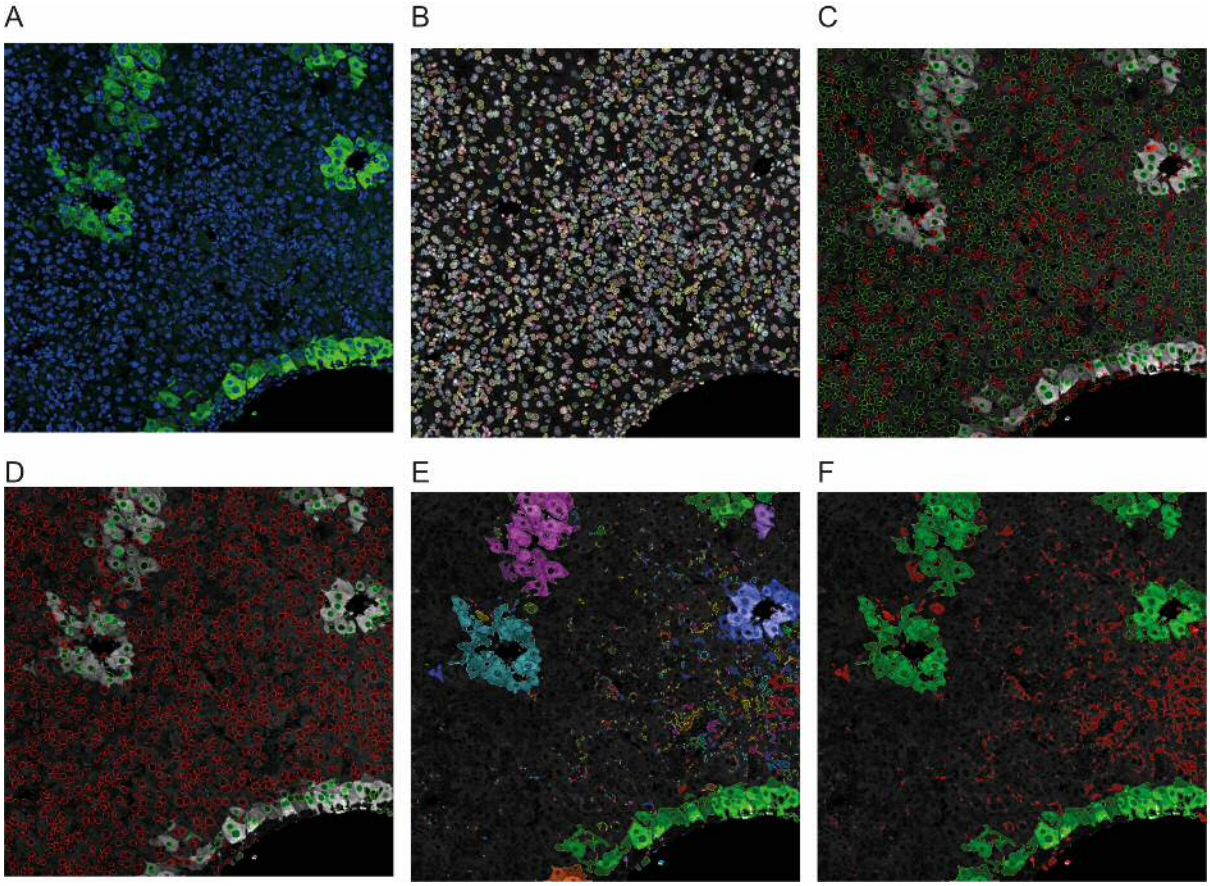

Figure2.10 GS mask analysis (A) 3-planes maximum projection GS immunostaining in put image. GS staining appears labelled in the 488 channel. Cell nuclei have been counterstained with DAPI. (B) Cells nuclei are detected in the DAPI channel using “Find nuclei method A, B or C”. (C) Hepatocytes nuclei mask partially excludes non-parenchymal and BECs nuclei based on morphology (roundness and size). (D) GS positive hepatocytes (green) are semi-automatically detected in which a filter based on 488 cytoplasmic fluorescence intensity (GS staining) has been applied using as an input image C. GS negative cells appear surrounded by a red mask. (E) The image is segmented in different areas based on 488 fluorescence intensity. (F) Area covered by GS positive hepatocytes cells is obtained by excluding auto-fluorescence (based on 488 mean intensity) and small regions (<200 µm) using as an input image from panel E.

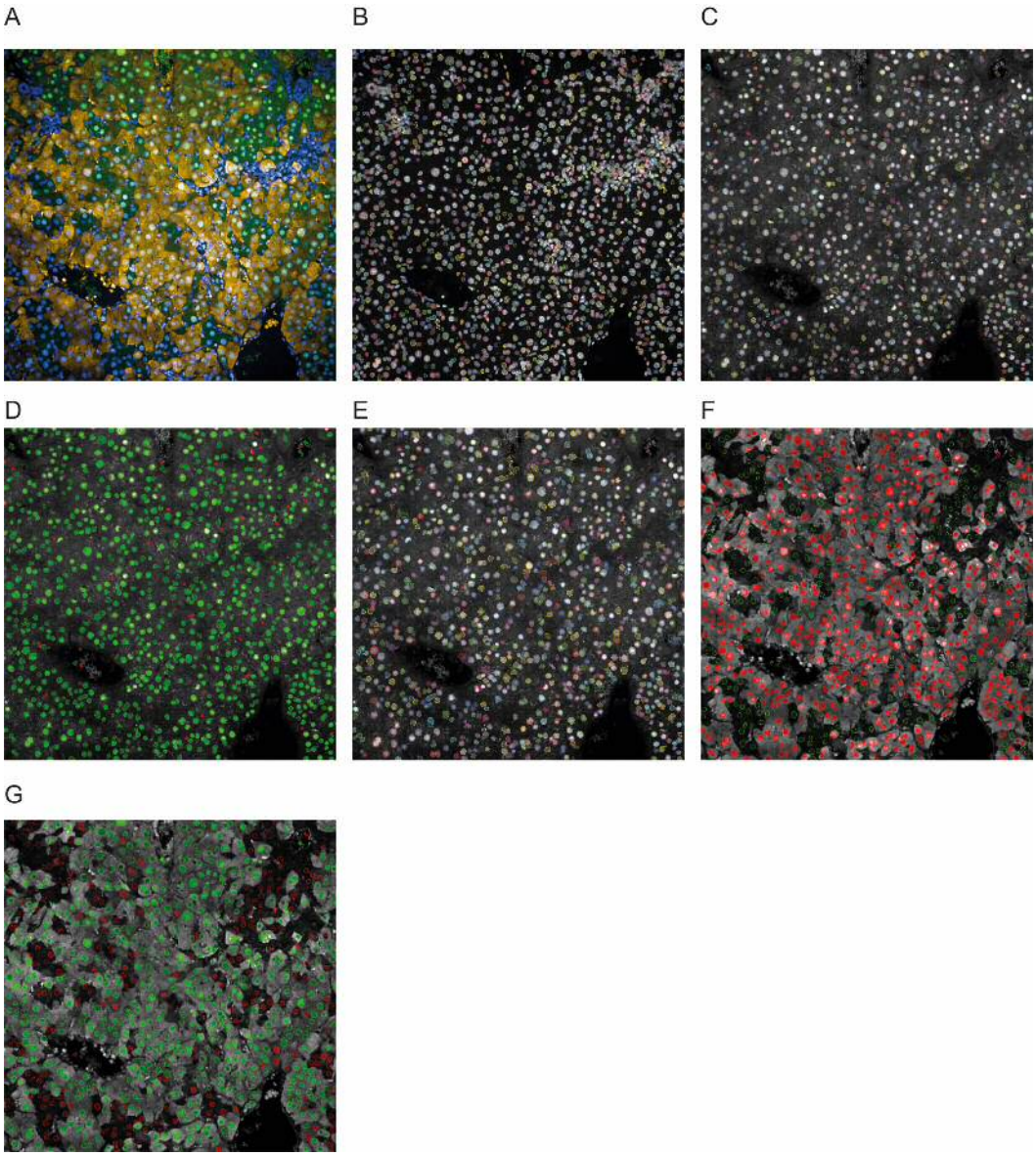

Figure2.11 (A) 3-planes maximum projection image used as input image to Harmony software. (B) Cells nuclei (all cells) are detected in the DAPI channel using "Find nuclei method A, B or M". (C) Cell nuclei of putative hepatocytes is detected in the 488 channel (corresponding to HNF4a staining) using "Find nuclei" function with method of detection A or B. (D) Hepatocytes cell nuclei mask in which a filter based on size, roundness and 488 fluorescence intensity (HNF4a staining) has been applied to remove auto-fluorescence false positives. In green, HNF4a positive nuclei considered for downstream analysis in image E, G and H. In red, objects identified by 488 nuclei mask shown in image C that do not meet the cut-off requirements. (E) The 568 (tdTom) fluorescent intensity of hepatocyte cytoplasm is calculated by drawing a thin surrounding region to all HNF4a positive nuclei obtained in image D. (F) BEC-derived mask excludes (red) pre-injury hepatocytes with high 568 (tdTom) cytoplasmic signal and counts the number of objects (green) below the established 568 intensity threshold. (G) Pre-injury hepatocytes mask excludes (red) BEC-derived hepatocytes with low 568 (tdTom) cytoplasmic signal and counts the number of objects (green) above the established 568 intensity threshold.

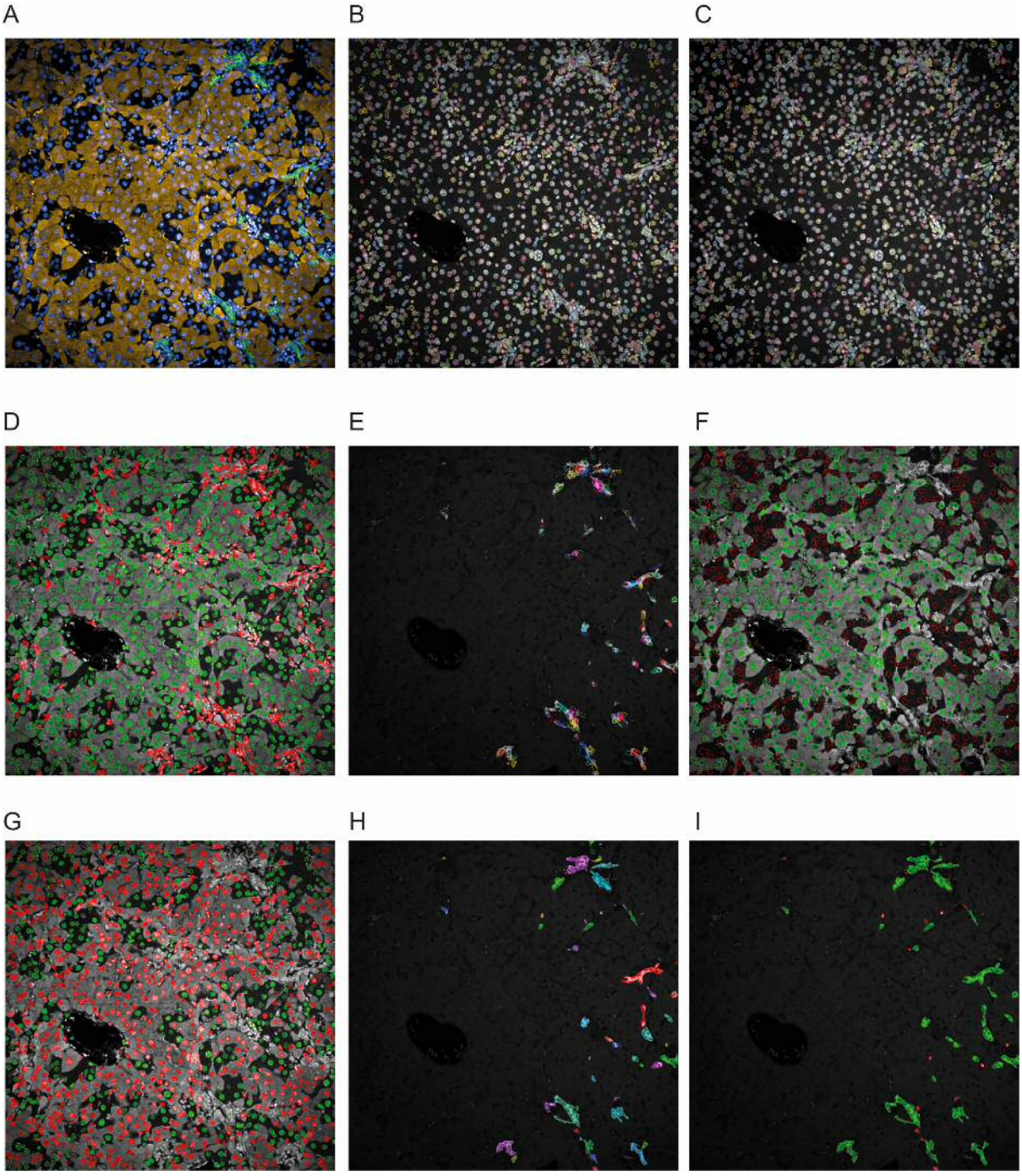

Figure2.12 (A) 3-planes maximum projection image used as input image (B) Cells nuclei are detected in the DAPI channel using “Find nuclei method C”. (C) 568 (tdTom staining) and 488 (CK19 staining) cytoplasmic fluorescent intensity is calculated in nuclei surrounding region. (D) Hepatocytes nuclei mask partially excludes non-parenchymal and BECs nuclei based on morphology (roundness and size). (E) BEC cells (CK19 positive) are highlighted based on 568 cytoplasmic intensity. (F) Mask highlighting pre-injury hepatocytes based on tdTom fluorescence. (G) Mask highlighting BEC-derived hepatocytes (tdTom negative. (H) Mask for CK19 positive cells based on 488 intensity. (I) Area covered by CK19+ cells is obtained by excluding auto-fluorescence regions.

Chapter 3. IMMOBILIZATION OF WNT/RSPO LIGANDS INTO CARBOXYLIC ACID BEADS

The primary objective of this thesis was to establish the molecular and biological tools for the generation of a liver *in vitro* system in which the local Wnt microenvironment of the hepatic CV was artificially recreated. One experimental approach set to achieve this was the covalent immobilization of the Wnt and Rspo ligands secreted by the CV onto beads.

In this chapter, I aimed to generate functionally active Wnt and Rspo beads. As the hepatic CV produces Wnt9b and Rspo3, this chapter will pay special attention to the biology resulting from the combination of these ligands. CV endothelial cells additionally produce Wnt2. However, the response to this ligand wasn't evaluated as Wnt2 was not commercially available during the completion of this project. Kate McSweeney, a BSc student summer student working under my supervision, contributed to generate the data from the LGK974 experiment presented in Figure3.2, J.

3.1 Introduction

The canonical Wnt pathway culminates with the stabilization and nuclear translocation of β-catenin, where this transcriptional coactivator drives the expression of canonical target genes in a cell context-dependent manner. In the hepatocytes, β-catenin controls the expression of metabolic genes including Glul, Cyp1a2 and Cyp2e1 [51]. The transcription of these markers is restricted to pericentral hepatocytes, reflecting that β-catenin transcriptional activity is zonated and exhibits its highest levels in the hepatocytes surrounding the hepatic CV.

Several liver resident cell types are source of Wnt ligands and Wnt pathway modulators that could potentially support the Wnt/β-catenin activation gradient in the hepatic lobule. However, to date, only Wnt signals of angiocrine origin have been shown to be essential for the establishment (Lyve1-Cre; $Wls^{fl/fl}$ and Stab2-Cre; $Wls^{fl/fl}$) and maintenance (VE-Cadherin-CreERT2; $Wls^{fl/fl}$) of Wnt-driven metabolic zonation [35,91]. Amongst all liver endothelial cells, the centrolobular location of the CV places these cells as the putative source of the Wnt/β-catenin pathway activation gradient. CV endothelial cells have been shown to express Wnt9b and Wnt2 as well as the Wnt

agonist Rspo3 [12,92,98]. It is currently unknown whether Wnt9b, Wnt2 or both ligands are required to drive activation of the canonical Wnt pathway in the hepatocytes [104].

One of the main objectives of this thesis was to develop the molecular tools for the generation of a local Wnt microenvironment that resemble the canonical Wnt niche of the hepatic central vein. In 2013, Habib and colleges covalently immobilized Wnt3a and Rspo1 onto carboxylic acid beads to dissect the biology resulting from the local exposure to these ligands [105]. As Wnt3a and Rspo1 were reported to retain the ability to activate canonical Wnt signalling when immobilized, the experimental approach set to generate an artificial central vein Wnt niche was the covalent immobilization of the Wnt and Rspo ligands secreted by the CV onto beads.

In this chapter, the ability of soluble and immobilized CV ligands to activate the Wnt/β-catenin pathway will be assessed. Wnt2 was not commercially available during the completion of this project. Thus, the first objective of this chapter will be to determine whether soluble Wnt9b and Rspo3, in the absence of Wnt2, drive canonical Wnt signalling *in vitro*. To achieve that aim, robust cell-based assays able to report canonical activation will be developed using HEK293T cells as cell system. The second objective of this chapter will be the covalent immobilization of Wnt9b and Rspo3 ligands following the Habib et al. (2013) protocol and the evaluation of the canonical Wnt activity of immobilized Wnt/Rspo ligands [105]. In addition to the CV ligands Wnt9b and Rspo3, Rspo1 and Wnt3a proteins will also be immobilized with two proposes: (1) to validate the Wnt/Rspo protein immobilization protocol of Habib et al. (2013) protocol and (2) as a contention method in the possible scenario that Wnt9b and Rspo3 beads result unable to drive the local activation of canonical Wnt signalling.

3.2 Results

3.2.1 Characterization of Wnt/Rspo soluble ligands activity

Prior to their immobilization, the ability of Wnt9b, Wnt3a, Rspo1 and Rspo3 to induce the canonical Wnt pathway was evaluated using two HEK293T cell lines expressing different versions of the TCF/LEF reporter system: a TCF-Luciferase (TCF-Luc) reporter line kindly donated by Dr Jeremy Nathans and an in-house generated TCF-eGFP reporter line (see section 3.2.1) [121]. Both these cell lines stably express a

construct in which a reporter gene (firefly luciferase or eGFP) is under the control of seven TCF/LEF binding motifs. β-catenin primarily associates with transcription factors of the TCF/LEF family to drive gene expression and, therefore, the expression of these reporter genes can be used as a proxy for Wnt pathway activation (Figure3.1). The response of the TCF-Luc to soluble Wnt and Rspo ligands will be first characterised (see section 3.2.1.1). Section 3.2.1.2 will describe the steps followed for the generation of a 'Wnt super-responder' TCF-eGFP line. The response of such TCF-eGFP cell line will be later characterized in section 3.2.1.3.

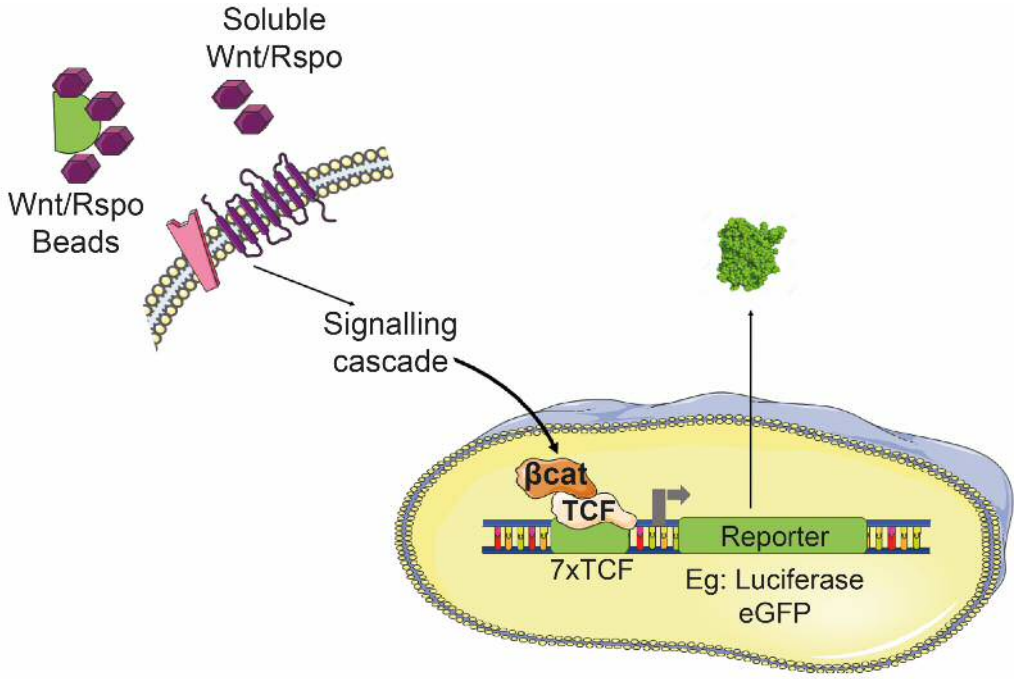

Figure3.1 TCF/LEF reporter scheme. Upon Wnt pathway activation, β-catenin translocate to the nuclei and associates with TCF/LEF family transcription factors. These transcription factors recognize and bind to the 7 TCF repeats of the construct, triggering the transcription of the reporter gene (eg. Luciferase or eGFP).
Figure3.1

3.2.1.1 Response of TCF-Luc HEK293T reporter cells to soluble Wnt/Rspo ligands

The ability of the HEK293T TCF-Luc cell line to respond Wnt pathway activation was first evaluated by exposing the cells to different concentrations of Wnt3a, a canonical

Wnt ligand that activates β-catenin transcriptional activity in different cellular contexts [128]. Wnt3a induced activation of the TCF luciferase reporter in a dose-dependent manner, confirming the validity of this cell line to report activation of the Wnt/β-catenin pathway (Figure3.2, A). However, the sensitivity of this cell line to Wnt3a was rather low as the addition of 100 ng/ml of this ligand barely triggered a 2-fold change luminescence (Figure3.2, A) [105].

Immobilization of Wnt proteins onto beads is expected to induce the TCF/LEF reporter in a less efficient manner than soluble ligands for several reasons: (1) the ability of the ligands to interact with their receptors will be limited by the area of interaction between beads and cells; (2) the ability of the immobilized ligands to activate cell surface receptors will be restricted by the efficiency of the crosslink; (3) the orientation in which Wnt proteins are presented to the receptors might not be optimal for all the immobilized molecules as the covalent crosslink occurs in a randomized manner; and (4) the beads impede the internalization of the Wnt-signalosome (see Chapter1), which in turn might prevent the activation of the pathway to its full capacity. In light of these concerns, it was felt to be desirable to develop a more sensitive Wnt assay that was able to report the presence of Wnt at lower concentrations (<100 ng /ml) as these are considered to be physiologically relevant [105].

Rspo1 has been reported to augment Wnt signalling by stabilizing Wnt receptors (Fzd and Lrp) at the cell surface (see Chapter1). Therefore, I sought to determine whether the addition of Rspo1 would increase the sensitivity of the HEK293T TCF-Luc cell line to Wnt3a ligands. To assess whether Wnt3a and Rspo1 cooperativity enhance the sensitivity of the cell line to Wnt3a activity, HEK293T TCF-Luc cells were exposed for 24h to different concentrations of Wnt3a alone or in combination with 20 ng/ml or 40 ng/ml of Rspo1. The addition of Rspo1 to the system increased the detection window to soluble Wnt as Wnt3a was detectable at concentrations as low as 20-50 ng/ml and the addition of 100 ng/ml of Wnt3a triggered a fold-change luminescence induction of ~15 and ~12 in the presence of 20 ng/ml and 40 ng/ml of Rspo1, respectively (Figure3.2, B). Wnt3a detection window of assay was maximal in the presence of 20

ng/ml of Rspo1 and, therefore, this concentration of Rspo1 will be used later to augment the sensitivity to other soluble and immobilized Wnt proteins.

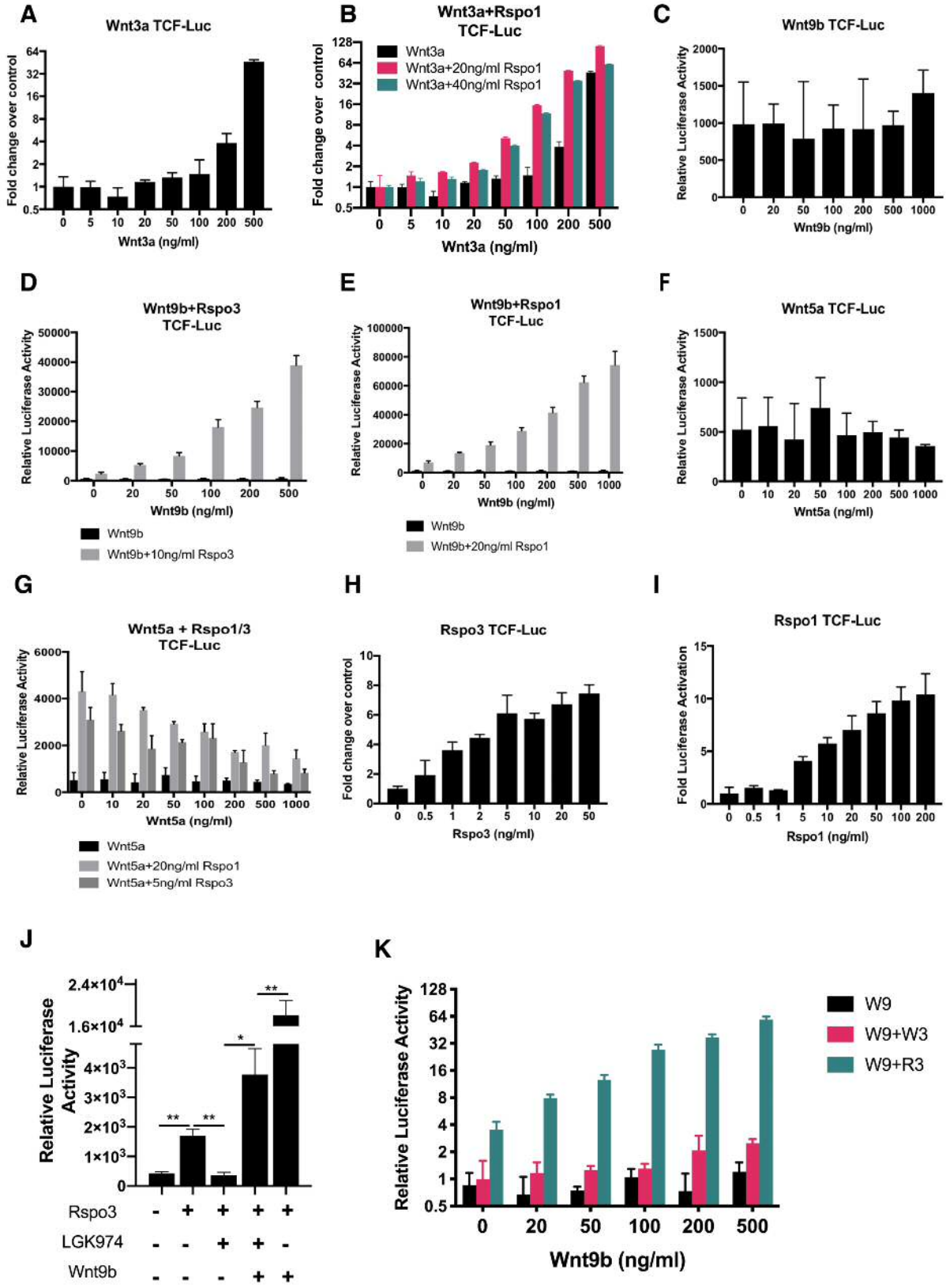

Figure3.2 24h response of HEK293TTCF-Luc reporter cells to different combinations of soluble Wnt and Rspo ligands. (A) Exposure to the canonical ligand Wnt3a triggers the induction of the TCF reporter in a dose dependent manner. (B) Wnt3a response is augmented by the presence of either Rspo1 (20 ng/ml) or Rspo3 (10 ng/ml). (C) Wnt9b by itself does not have significant effects in the basal activation levels of the TCF reporter. (D and E) Wnt9b switches to canonical behaviour and induces the TCF reporter in a dose dependent manner when Rspo3 (10 ng/ml) or Rspo1 (20 ng/ml) are present at a constant concentration. (F) Wnt5a by itself does not have significant effects in the basal activation levels of the TCF reporter. (G) Addition of Wnt5a causes a decline in the activation levels of the TCF/LEF reporter when this is induced by either Rspo1 (20 ng/ml) or Rspo3 (10 ng/ml). (H and I) Rspo3 and Rspo1 activate the TCF reporter in a dose dependent manner. (J) Blockage of endogenous Wnt secretion (exposure to 500 nM LGK974) depletes Rspo3 (10 ng/ml) mediated activation of the TCF reporter. Addition of Wnt9b (100 ng/ml) is sufficient to activate the reporter.in the presence of Rspo3. LGK974 was administrated 24h prior to Wnt9b or Rspo3 exposure and maintained during the whole length of the experiment. (K) Wnt9b synergises with Wnt3a (200ng/ml) and Rspo3 (10ng/ml) to activate the TCF reporter. All graphs show the results from three technical replicates. All experiments were repeated independently at least three times and I graphs are representative of the activation curve seen, with the exception of graph K that was only performed one time.

The activity of the central vein Wnt9b is a ligand was also evaluated in the HEK293T TCF-Luc cell line. By contrast to Wnt3a, Wnt9b did not trigger the activation of the TCF reporter at any concentration (Figure3.2, C). Wnt9b, however, did induce TCF-dependent transcription in the presence of either 10 ng/ml of Rspo3 (Figure3.2, D) or 20 ng/ml Rspo1 (Figure3.2, E). These results suggest that Wnt9b behaves as canonical Wnt ligand when Rspo proteins are present in the system.

In vivo and *in vitro* evidence suggest that Wnt9b primarily activates non-canonical Wnt signalling. To evaluate whether other non-canonical Wnt ligands switch to canonical behaviour in the presence of Rspo proteins, the response of HEK293T TCF-Luc cells to Wnt5a, a well-known non-canonical Wnt ligand, in the presence and absence of Rspo proteins was assessed [129-133]. The addition of Wnt5a alone did not have a significant effect in the basal levels of activation of the TCF-reporter (Figure3.2, F). By contrast to Wnt9b, the addition of Wnt5a actually caused a decline in the levels of Rspo1- and Rspo3-induced TCF activation levels in a dose-dependent manner (Figure3.2, G).

As Rspo1 and Rspo3 will also be immobilized onto beads (see section 3.2.2), I next evaluated the ability of the HEK293T TCF-Luc cell line to act as a quantitative readout for Rspo ligands. The addition of Rspo1 and Rspo3 activated the reporter in a dose-dependent manner in the absence of exogenous Wnt proteins, indicating that

HEK293T TCF-Luc cell line might produce Wnt ligands (Figure3.2, H and I). The ED_{50} of Rspo3 (~ 2 ng/ml) was approximately 10 times lower than the ED_{50} of Rspo1 (~ 20 ng/ml) (Figure3.2, H and I).

To assess whether Rspo3 requires the presence of endogenous Wnt ligands to induce canonical Wnt signalling, endogenous Wnt production was blocked with a porcupine inhibitor (LGK974), a compound that blocks the secretion of Wnts by interfering with the acetylation of the ligand. Exposure to 500 nM of LGK974 24h prior to the addition of Rspo3 (10 ng/ml) completely blocked the activation of the TCF reporter by this ligand, confirming Rspo3 requires the presence of Wnt proteins to activate the TCF reporter (Figure3.2, J). Rspo3 activity was rescued upon addition of exogenous Wnt9b (100 ng/ml), although the levels of activation of the reporter were 3.65±1.2 times lower than when endogenous Wnt ligands were present (Figure3.2, H). Altogether these results suggest that (1) Wnt9b is sufficient (in the presence of Rspo ligands) to induce canonical Wnt signalling and (2) Wnt9b might synergise with other Wnt ligands produced by HEK293T to drive activation of the TCF reporter.

To explore the possibility that Wnt9b might synergise with other Wnt ligands, HEK293T TCF-Luc cells were exposed to different concentrations of Wnt9b in the presence or absence of Wnt3a (200 ng/ml) and/or Rspo3 (10 ng/ml). Wnt3a was selected over other Wnt proteins for this experiment as Wnt9b and Wnt3a bind are known to bind different domains of the Lrp6 receptor and biochemical assays have shown that both proteins can be simultaneously loaded onto the Lrp6 receptor [134]. As previously reported, Wnt9b alone did not trigger the activation of the TCF reporter (Figure3.2, K). However, 500 ng/ml Wnt9b triggered ~2.5 fold-change luminescence induction when Wnt3a was present in the system, indicating that Wnt3a and Wnt9b can synergise in certain extend (Figure3.2, K). 500 ng/ml Wnt9b in combination to 10 ng/ml of Rspo3 caused a ~16 fold-change induction in the activation levels of the reporter when this was compared to the presence of Rspo3 alone, indicating that Rspo3 induces Wnt9b canonical activity more efficiently than Wnt3a Figure3.2, K).

Taken together, the responses the luciferase reporter data suggest that (1) the sensitivity of Wnt3a detection can be greatly improved when Rspo1 is present in the

system at a concentration of 20 ng/ml, (2) Wnt9b induces the TCF-Luc activity only when HEK293 cells are co-treated with either Rspo1 or Rspo3 and (3) the induction of TCF-Luc by Rspo1 and Rspo3 requires the expression of endogenous Wnt ligands and can be rescued by exogenous ligands.

3.2.1.2 Generation of a TCF-eGFP 'Wnt super-responder' HEK293T reporter line

The TCF-Luc assay requires a lysis step to release the firefly luciferase is released from the cells, providing information about the overall effect of the treatment in the pool (see section 3.2.1.1). To later evaluate the activity of the immobilized ligands at a single-cell resolution it was, however, desirable to develop a complementary reporter assay that allowed the assessment of the local rather than the global activity of the Wnt/Rspo beads. For that aim, a TCF-eGFP monoclonal HEK293T reporter line was generated in house in a process that involved (i) lentivirus-mediated delivery of the TCF-eGFP construct (p7TGC plasmid), (ii) selection of clones successfully transduced and expressing the plasmid, (iii) evaluation of the response of the pool of TCF-eGFP expressing cells to soluble Wnt3a, (iv) isolation and expansion of Wnt3a super-

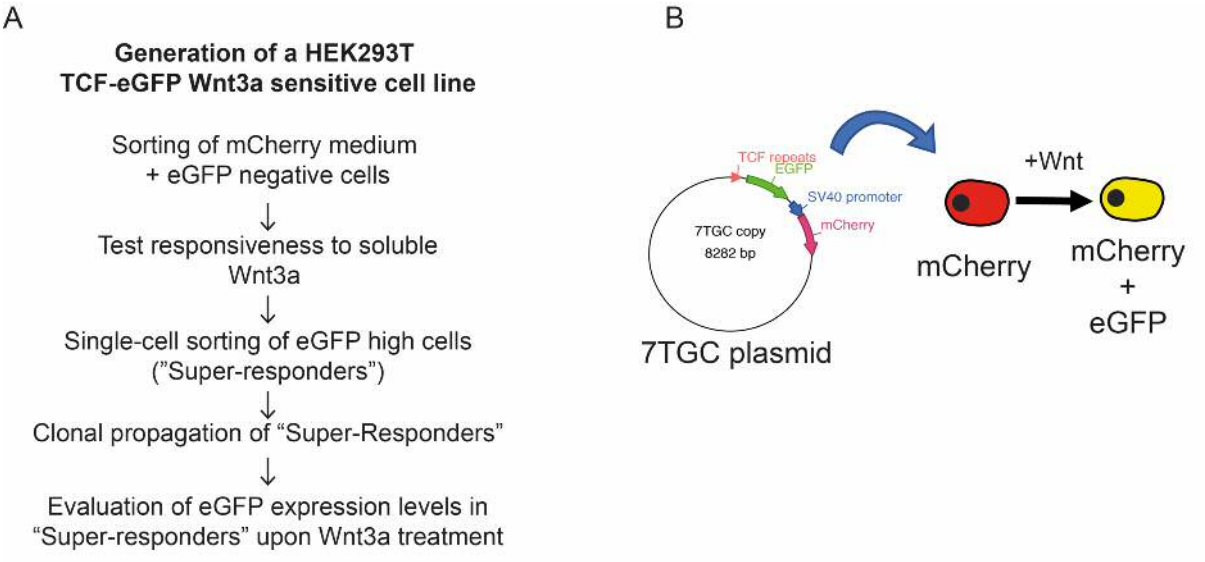

Figure3.3 Generation of a monoclonal 'Wnt super-responder' TCF-eGFP line. (A) Experimental pipeline used for the generation of Wnt3a HEK293T TCF-eGFP sensitive cell line. (B) TCF-eGFP reporter scheme. mCherry function as a selection cassette, being expressed in all succesfully transduced cells. Expression of eGFP is under the control of 7xTCF promoter repeats. Thence, eGFP expression can be used as a proxy for Wnt activation levels.

responder clones from the pool and (v) selection of the best TCF-eGFP Wnt3a super-responder clone (Figure3.3, A). In this section, the steps followed to generate a HEK293T TCF-eGFP monoclonal cell line will be described. The response of such cell line to soluble Wnt and Rspo ligands will be later described in section 3.2.1.3. P7TCG plasmid preparation and lentivirus production is described in Chapter 2, section 2.7.

The first step in the generation of the TCF-eGFP HEK293T line was the lentivirus-mediated delivery of the p7TGC plasmid. In this plasmid, eGFP is under the control of 7xTCF repeats and therefore eGFP expression might be interpreted as a proxy for canonical Wnt pathway activation levels (Figure3.3, B). To select cells that effectively express the vector and track events of silencing over time in culture, the p7TGC plasmid additionally carries a SV40-mCherry reporter cassette which labels p7GTC expressing cells with mCherry (Figure3.3, B).

Making use of the mCherry reporter, HEK293T cells successfully transfected with low TCF-eGFP background activation levels (eGFP negative) were sorted by flow cytometry and further expanded (Figure3.4). After two passages, the response of p7TCG expressing cells to soluble Wnt ligands was evaluated. For that aim, 10.000

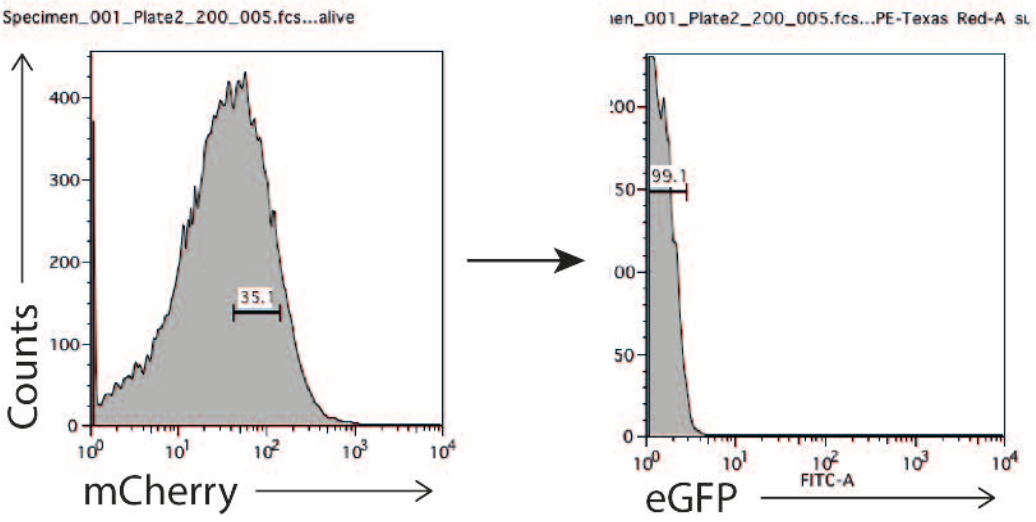

Figure3.4 Isolation of HEK293T cells successfully transduced with the TCF-eGFP reporter. Flow cytometry histograms show the gating strategy for the isolation of cells expressing the TCF-eGFP reporter that lack basal expression of eGFP.

cells/well were seeded onto 48-well plates, cultured for 2 days and exposed to different concentrations of Wnt3a in the presence or absence of 20ng/ml Rspo1. After 24h or 48h of treatment, eGFP expression levels were analysed by flow cytometry or fluorescence microscopy.

As previously reported in the TCF-Luc HEK293T cell line (see section 3.2.1.1), the addition of Wnt3a induced the activation of the TCF-eGFP HEK293T reporter in a dose-dependent manner (Figure3.5). However, only a small proportion of cells (less than 0.1% of the pool) were found to highly express eGFP when exposed to 100 ng/ml of Wnt3a (Figure3.5). Wnt3a at 100 ng/ml is a widely-used concentration for the *in vitro* study of Wnt responses with physiological relevance and therefore it was of

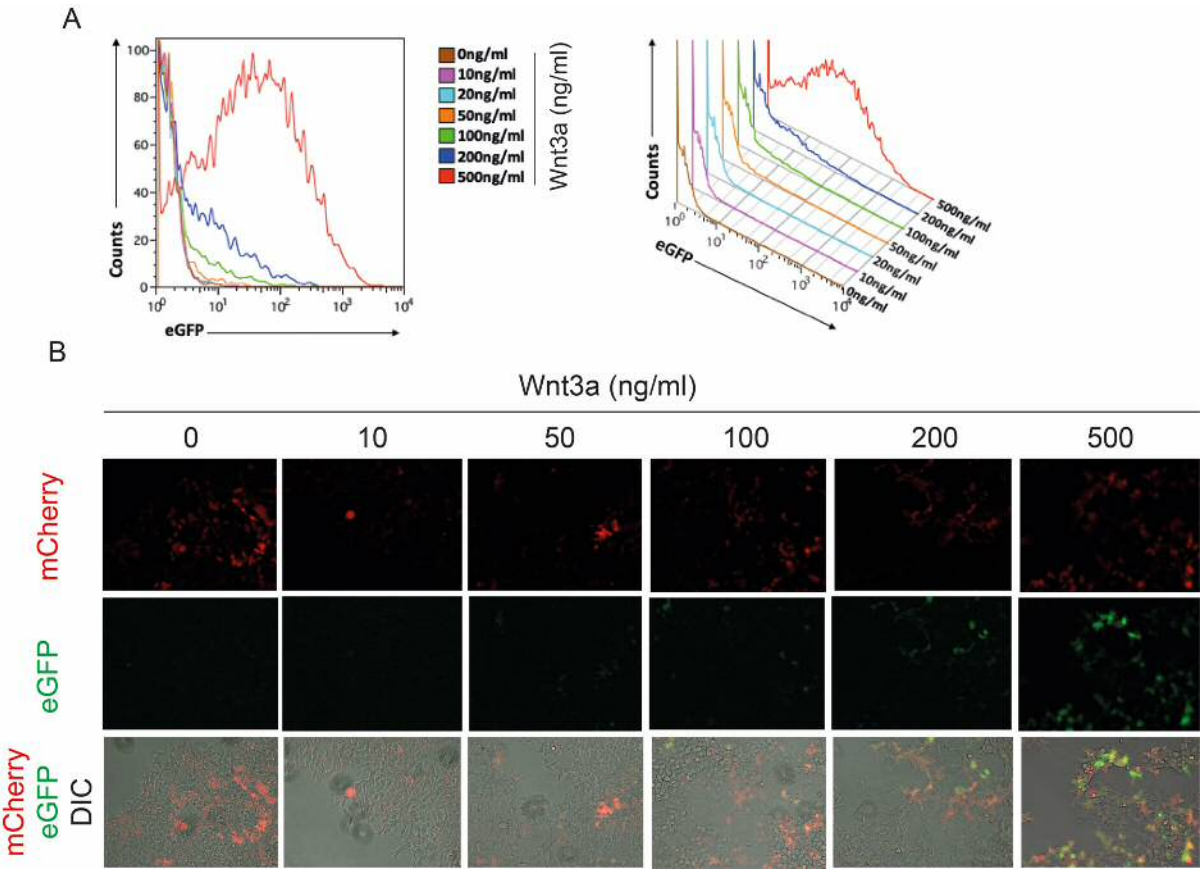

Figure3.5 Response of the pool of HEK293T TCF-eGFP cells to Wnt3a treatment (A) Flow cytometry histograms showing 24h response of HEK293T cell stably expressing the p7TGC plasmid to Wnt3a. (B) Representative fluorescence images of HEK293T stably expressing the p7TGC plasmid exposed for 48h to soluble Wnt3a.

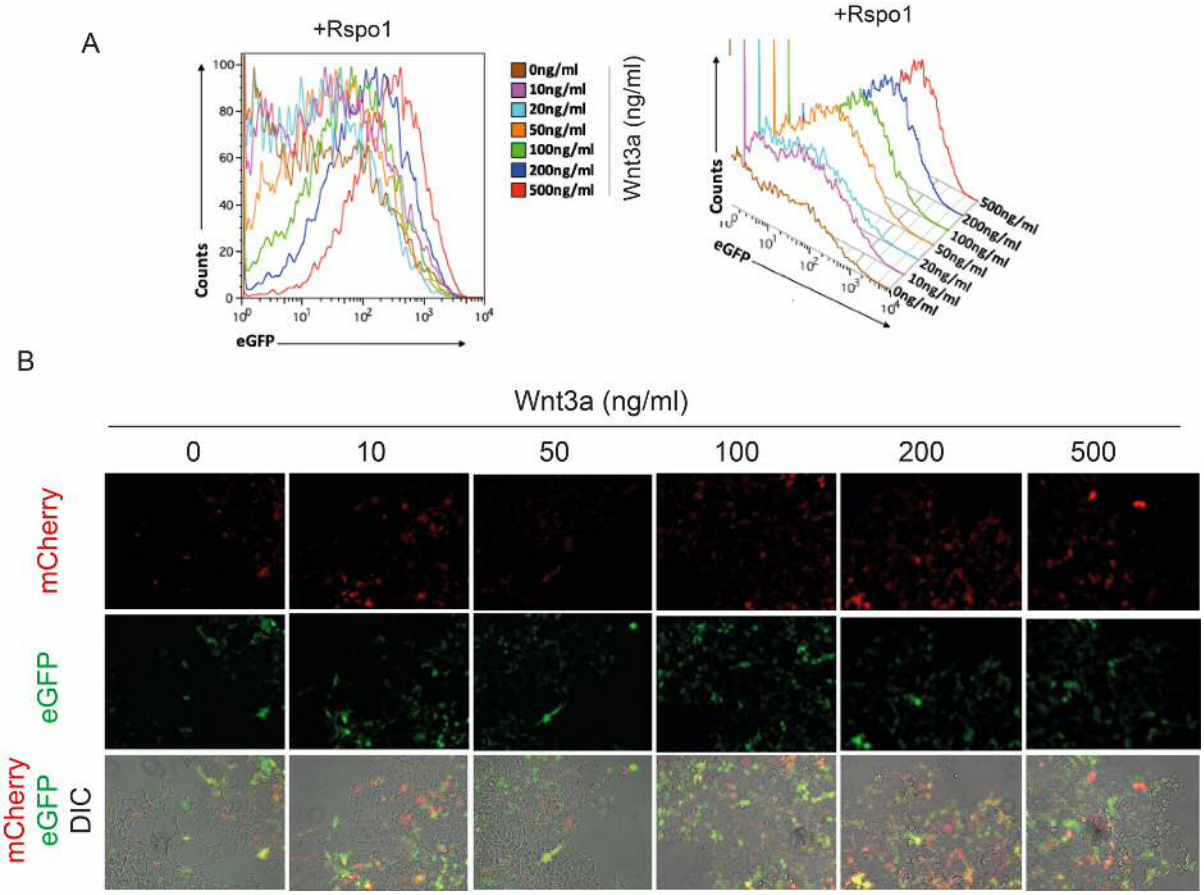

Figure3.6 Response of the pool of HEK293T TCF-eGFP cells to Wnt3a and Rspo1 co-treatment (A) Flow cytometry histograms showing 24h response of HEK293T cell stably expressing the p7TGC plasmid to Wnt3a in the presence of 20 ng/ml or Rspo1. (B) Representative fluorescence images of HEK293T stably expressing the p7TGC plasmid exposed for 48h to soluble Wnt3a in the presence of 20 ng/ml of Rspo1.

interest to increase the sensitivity of the TCF-eGFP HEK293T line to this ligand [135,136].

In section 3.2.1.1 it was described that the addition of 20 ng/ml Rspo1 to the cultures increased the window of detection to Wnt3a in the TCF-Luc cell line. To assess whether the presence of Rspo1 enhance the sensitivity of the TCF-eGFP cell line to Wnt3a activity, TCF-eGFP HEK293T cells were exposed to different concentrations of Wnt3a in the presence of 20 ng/ml of Rspo1 and the eGFP expression levels in these cells were analysed by flow cytometry or fluorescence microscopy. The TCF-eGFP reporter was highly activated by Rspo1 in the absence of Wnt3a (Figure3.6). As a result, the response to Rspo1 partially masked the dose-dependent response to Wnt3a and, therefore, this approach was unviable to enhance the detection window for Wnt3a in the TCF-eGFP HEK293T cell line (Figure3.6).

As an alternative approach to generate a TCF-eGFP HEK293T reporter line with higher sensitivity to Wnt ligands, eGFP positive cells from the pool of cells that responded to ‘low’ concentrations of Wnt3a (either 100 ng/ml or 200 ng/ml) were individually sorted and expanded (Figure3.7, A). A total of 16 clones were expanded. Due to the ability of these cells to respond to ‘low’ Wnt3a concentrations, these clonal lines were named as ‘Wnt super-responders’.

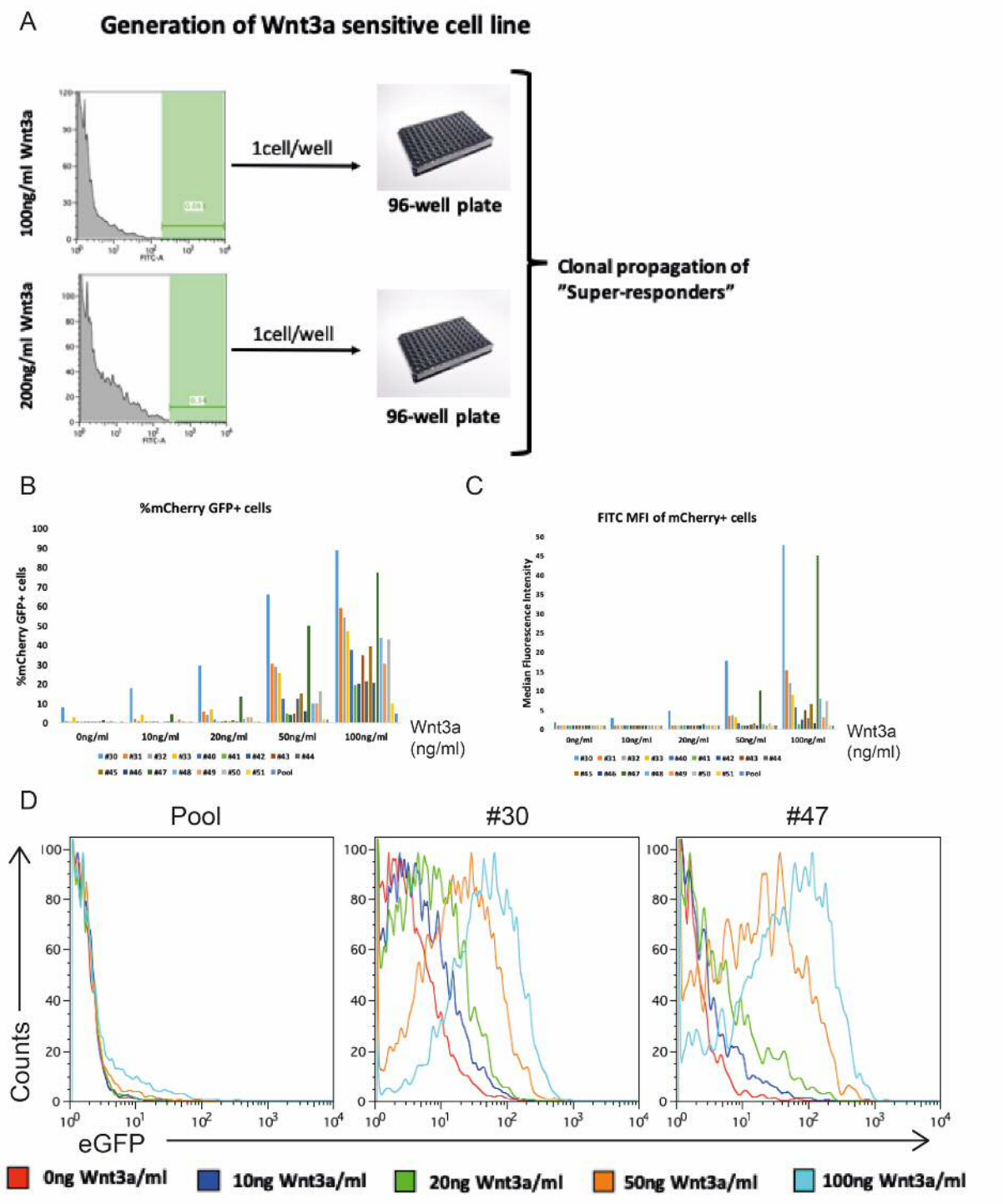

Figure3.7 The response of 16 "Wnt3a Super-responder" clones to soluble Wnt3a after 24h treatment was analysed by flow cytometry. (A) Scheme deciphering experimental strategy for the obeisance of a Wnt3a supersensitive cell line. (B) Bar graph shows number of eGFP positive cells upon 100 ng/ml Wnt3a treatment for 24h. Clones #30 and #47 stand out as the most sensitive Wnt3a Super-responders as higher proportion of cells turned eGFP positive upon treatment. Note that most of the clones exhibit an improved sensitivity to Wnt3a when compared to the TCF-eGFP pool. (C) Bar graph shows eGFP median intensity of "Wnt3a Super-responders" upon 24h exposure to 100 ng/ml of Wnt3a. Clones #30 and #47 showed the highest swift in eGFP intensity upon treatment. Most of the clones also showed enhanced responsiveness to purified Wnt3a when compared to the initial pool of successfully transduced cells. (D) Flow cytometry histogram showing responsiveness of the pool of successfully transduced 7pTGC cells, clone #30 and clone #47 to different concentrations of Wnt3a. Both clone #30 and #47 expressed high levels of eGFP upon 100 ng/ml treatment. Clone #47 showed the lowest eGFP basal expression and therefore was selected for further experiments.

To evaluate the sensitivity of the TCF-eGFP 'Wnt super-responders' cells to canonical Wnt activation, these clones were exposed to different concentrations of Wnt3a for 24h and their eGFP expression levels were assessed by flow cytometry. Out of the 16 clones, clone number #30 and #47 resulted the most sensitive to Wnt3a treatment (Figure3.7, B-D). Of note, eGFP positive cells were detectable at Wnt3a concentrations as low as 10 ng/ml in both clones #30 and #47 (Figure3.7, C). Between clone #30 and #47, clone #47 resulted the one with the highest induction / eGFP background ratio and therefore was selected as a TCF-eGFP reporter line in the experiments of this thesis (Figure3.7, D). For simplicity, clone #47 HEK293T TCF-eGFP reporter line will be further referred as TCF-eGFP reporter line.

3.2.1.3 Response of TCF-eGFP reporter cells to Wnt/Rspo soluble ligands

The TCF-eGFP line was generated to evaluate the local activity of immobilized Wnt3a, Wnt9b, Rspo1 and Rspo3 ligands. To determine whether this line was a suitable platform for that aim, the ability of soluble Wnt3a, Wnt9b, Rspo1 and Rspo3 to induce the TCF-eGFP reporter was evaluated by flow cytometry.

TCF-eGFP cells were highly sensitive to the addition of Wnt3a alone as this ligand triggered a shift in the eGFP expression levels at a concentration of 10 ng/ml, implying that immobilized Wnt3a molecules may be tested in this system in absence of Rspo1 (Figure3.8 A). Mirroring the results obtained in the TCF-Luc line, Rspo1 and Rspo3 increased the expression of eGFP in a dose-dependent manner (Figure3.8 B and C),

which suggest that the activity of Rspo1- and Rspo3- can potentially be assessed in this line in the absence of exogenous Wnt ligands. Confirming the previous observations in the TCF-Luc line, Wnt9b alone did not cause activation of the TCF-eGFP reporter at any given concentration (Figure3.8 D).

Wnt9b in combination to Rspo ligands induced activation of the TCF reporter in the TCF-Luc HEK293T cell line (see section 3.2.1). To test whether this was also the case in the TCF-eGFP line, cells were co-treated with Wnt9b in the presence of Rspo1. The exposure of the pool of TCF-eGFP HEK293T cells to 20 ng/ml of Rspo1 induced high levels of eGFP. With the aim to find a "sweet spot" in which cells were primed by Rspo1 treatment but remained eGFP negative, the activity of Wnt9b was tested in combination with lower concentrations of Rspo1 (1, 2 and 5 ng/ml). Addition of Rspo1 at 1 ng/ml and 2ng/ml caused a slight shift in eGFP levels detected although such eGFP levels were far from the saturating conditions (Figure3.8 D). At these two concentrations of Rspo1, addition of Wnt9b caused a clear dose-dependent increase in eGFP expression (Figure3.8 D). Wnt9b dose-dependent response was also noticeable in the presence of 5 ng/ml although the exposure to Rspo1 at this concentration increased the eGFP background levels of the system, partially masking Wnt9b-driven activation of the TCF-eGFP reporter (Figure3.8 D).

Taken together, these results suggest that Wnt9b requires Rspo to induce canonical Wnt signalling and that the validation of Wnt9b beads by flow cytometry might be challenging as the assay window offered by Rspo1 is quite narrow as activity of Wnt9b can only be detected clearly when Rspo1 is present at a concentration between 1 and 5 ng/ml.

3.2.2 Generation of Wnt/Rspo beads

Prior to the immobilization of the ligands following Habib et al (2013) recommendations, there are some general considerations that need to be made about the chemistry of the crosslink between peptides and beads. In the NHS/EDC two-step coupling procedure, the bond between the carboxylic acid-coated beads and the ligands occur via the free amine groups of the protein (see Chapter1, section1.14). Based on this, the number of possible crosslink sites per protein was calculated and is displayed in Table3.1.

Ligand	Putative crosslink sites
Wnt3a	15
Wnt9b	19
Rspo1	22
Rspo3	30
GFP	21

Table3.1 Table showing number of putative crosslink sites per in murine Wnt3a, Wnt9b, Rspo1 and Rspo3 proteins. Putative crosslink sites exist at the N-termini (alpha amine) and the side chain of lysine residues (epsilon amine). Wnt3a, Rspo1 and Rspo3 putative crosslink sites were obtained using the protein precursor sequences. Wnt9b putative crosslink sites were obtained using the secreted protein sequence.

The likelihood by which the protein free amines will be crosslinked will depend on the distribution and accessibility of such groups in the tertiary protein conformation and cannot be controlled by this immobilization strategy. Therefore, it's important to consider that the activity of the beads will be restricted by (1) the efficiency by which the chemical reaction of the crosslink takes place and (2) the resulting orientation of the protein in the bead, which might not be optimal for the binding to its cognate receptor and subsequent activation of the pathway.

When evaluating the capacity of the beads to activate canonical Wnt signalling, another factor to consider is that beads have a diameter of 2.8 μm, meaning that they will likely remain attached to the cell surface and, perhaps, this will prevent the formation of the Wnt signalosome (see Chapter1). The degree by which this will impact the levels of activation of the pathway is yet to be determined.

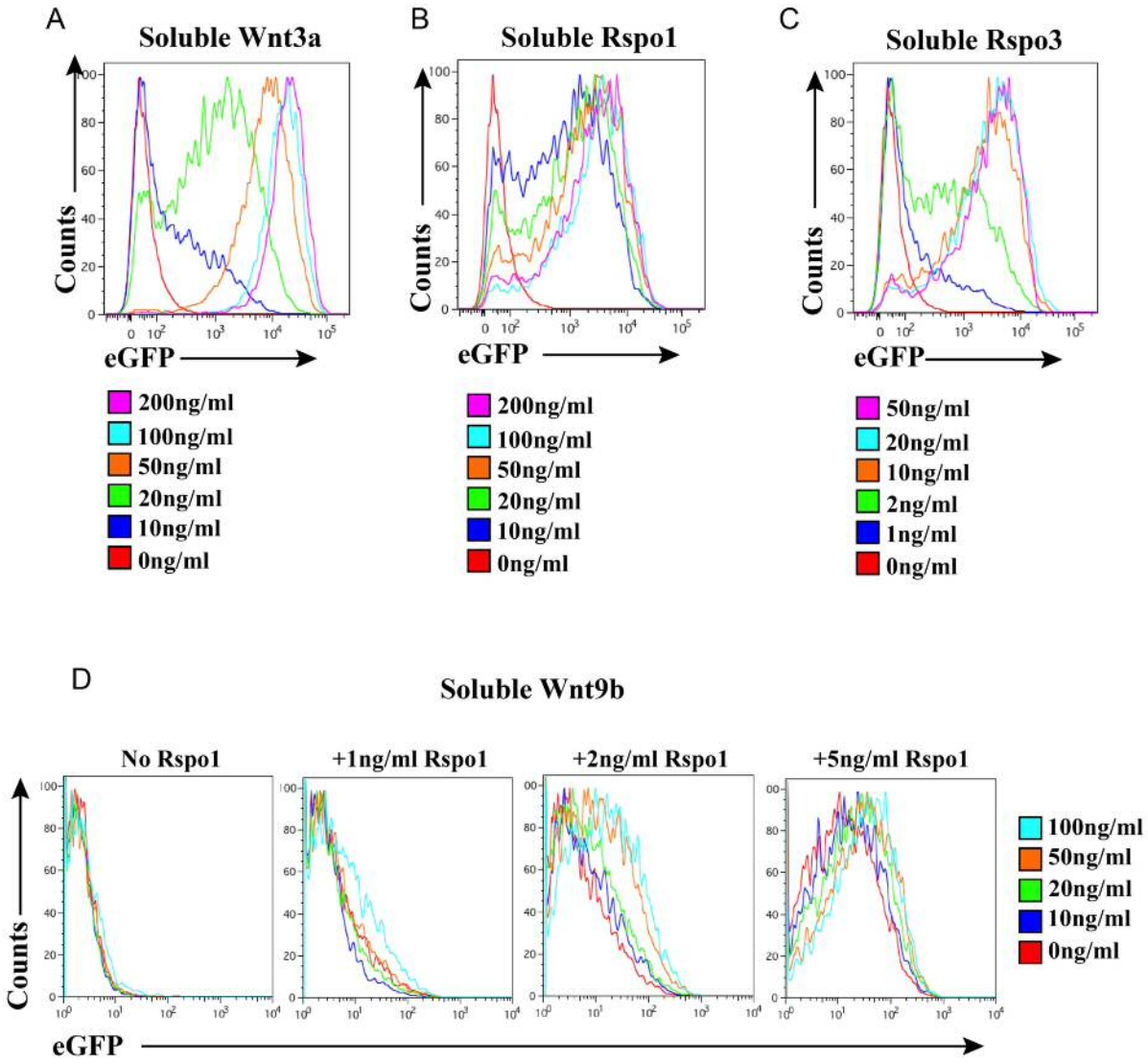

Figure3.8 Flow cytometry plots showing 24h dose response of HEK293T TCF-eGFP cells (clone #47) to soluble Rspo and Wnt ligands. (A) Addition of Wnt3a triggers the activation of the TCF-eGFP reporter in a dose dependent manner. (B and C) HEK293T TCF-eGFP cells are responsive to Rspo1 (B) and Rspo3 (C) ligands in absence of exogenous Wnt ligands. (D) In the absence of Rspo1, soluble Wnt9b does not induce eGFP expression at any given concentration. When Rspo1 is present in the system at 1 ng/ml or 2 ng/ml, Wnt9b induces the appearance of eGFP positive cells. The presence of Rspo1 at 5 ng/ml mask the effects of Wnt9b in the TCF-eGFP line.

Due to all those considerations, it will be important to validate that (1) the ligands have been successfully attached to the bead surface and (2) that the beads are biologically active.

3.2.2.1 Validation of chemical immobilization of peptides onto carboxylic acid beads

Prior to Wnt and Rspo immobilization, the successful crosslink of peptides onto carboxylic beads following the ECD/NHS crosslinking protocol was validated. For that aim, GFP was immobilized onto beads and the green fluorescence levels of the resulting beads were evaluated by fluorescence microscopy and FACS. As a control, vehicle beads that have undergo activation and 1% BSA quenching were used. In both assays, GFP beads showed higher green fluorescence intensity than vehicle beads indicating that the reagents and protocol of immobilization worked satisfactorily for this protein (Figure3.9).

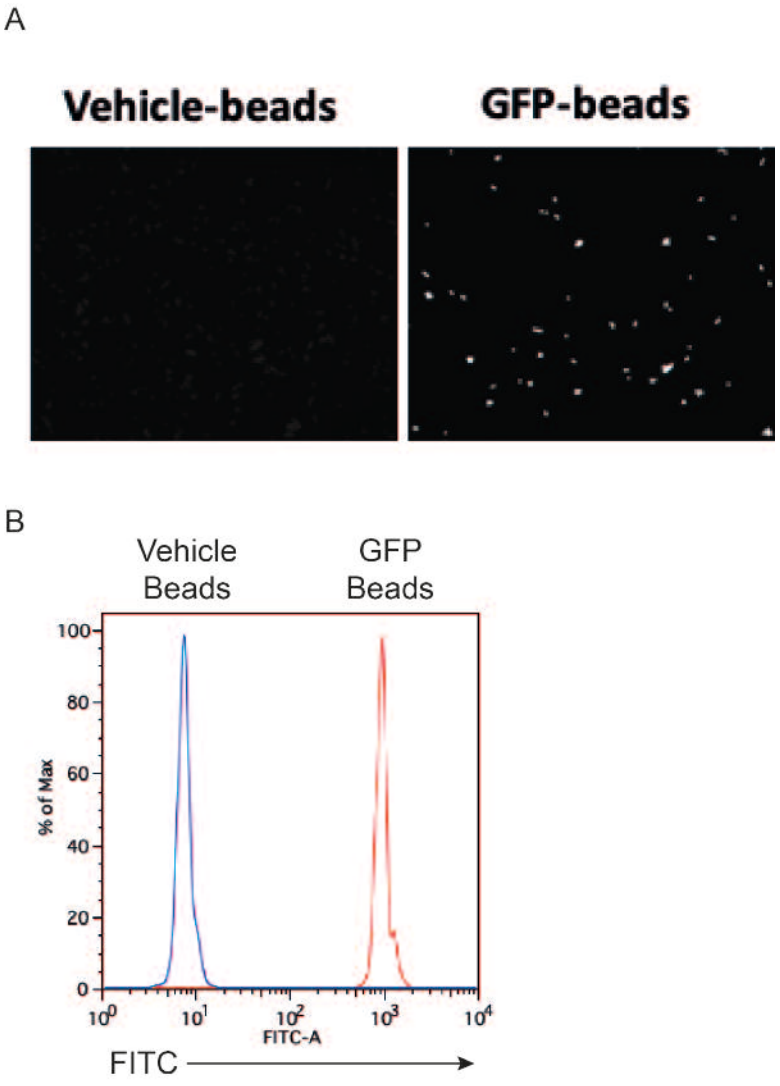

Figure3.9 Immobilization of GFP onto carboxylic acid beads (A) Representative immunofluorescence in the 488 channel images showing successful immobilization of GFP onto beads. Carboxylic acid beads activated with EDC/NHS and quenched in 0.1% BSA PBS were used as a vehicle beads. Images were taken on a Spinning Disc Olympus IX71 confocal microscope at 800ms exposure using a 488nm laser. (B) Flow cytometry histogram showing green fluorescence (FITC) intensity of vehicle (beads activated with EDC/NHS and quenched in 0.1% BSA PBS) or GFP beads.

3.2.2.2 Determination of Wnt-/Rspo- biological activity in HEK293T TCF-Luc reporter cells

To determine the canonical Wnt activity of immobilized Wnt3a, Rspo1, Rspo3 and Wnt9b onto beads using HEK293T TCF-Luc cells, TCF-Luc reporter cells were exposed to different concentrations of beads for 24h and the activity of luciferase was evaluated (Figure3.11 A). The activity of Wnt3a beads was assessed in the presence of 20 ng/ml of Rspo1, as this increased the sensitivity of the assay (see section 3.2.1.1). Wnt3a-beads induced the TCF-Luc reporter in a dose-dependent manner, confirming that immobilized Wnt3a retained the ability to activate the Wnt/β-catenin pathway (Figure3.10 B).

TCF-Luc cells were source of endogenous Wnt ligands and, therefore, the activity of Rspo1 and Rspo3 beads was evaluated in the absence of exogenous Wnt ligands (see section 3.2.1.1). Rspo1- and Rspo3- beads activated the TCF-Luc reporter in a dose-dependent manner, confirming that both Rspo1 and Rspo3 ligands were biologically active when immobilized (Figure3.10 C and D).

Finally, the activity of Wnt9b beads was evaluated in the presence of 10 ng/ml of Rspo3. Increased exposure to immobilized Wnt9b caused a gradual increase in luciferase activity, indicating that Wnt9b were also biologically active (Figure3.10 E).

Altogether, from this set of experiments it could be concluded that immobilized Wnt9b, Wnt3a, Rspo1 and Rspo3 were active and induced the TCF-Luc HEK293T reporter cells.

3.2.2.3 Determination of Wnt-/Rspo- biological activity in HEK293T TCF-eGFP reporter cells

The canonical activity of immobilized Wnt3a, Rspo1, Rspo3 and Wnt9b onto beads was also evaluated in the HEK293T TCF-eGFP cell line. For that aim, TCF-eGFP reporter cells were exposed to different concentrations of beads for 24h and subjected to flow cytometry analysis. Wnt3a-, Rspo1- and Rspo3-beads caused activation of the TCF-eGFP reporter in a dose-dependent manner, further confirming that these ligands retained the ability to induce the Wnt/β-catenin pathway when immobilized (Figure3.10, F). The activity of Wnt9b beads was not evaluated in this system as the

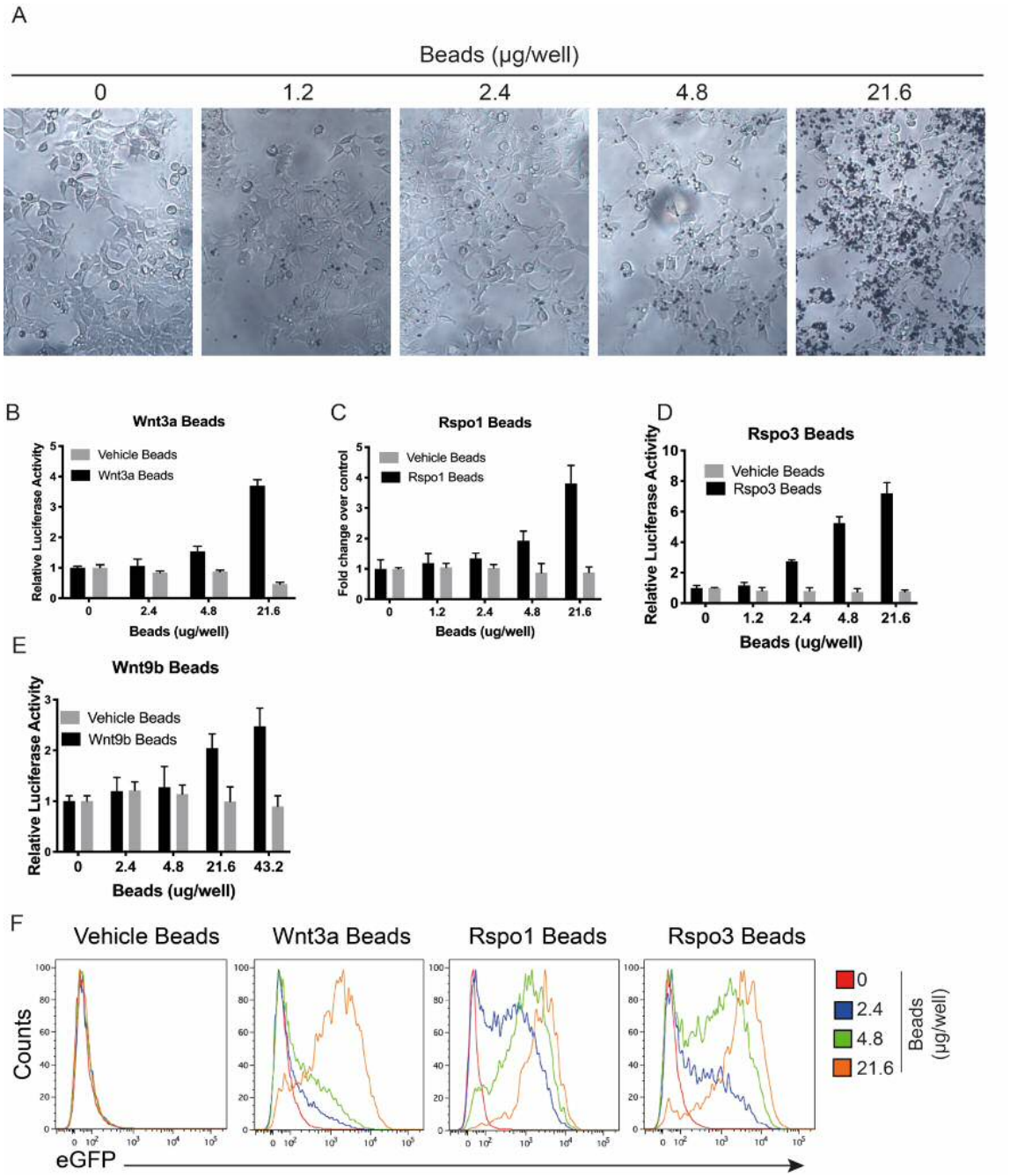

Figure3.10 (A) Representative images showing the ratio of HEK293T cell/beads at the different concentrations of beads used in the experiments of this thesis. Beads are 2.8µm and can be used as scale. (B-E) Response of HEK293T TCF-Luc reporter cells to the exposure of immobilized Wnt and Rspo ligands for 24h. Wnt3a, Rspo1, Rspo3 and Wnt9b beads but not vehicle beads triggers the activation of the TCF-Luc reporter in a dose dependent manner. Carboxylic acid beads activated with EDC/NHS and quenched in 0.1% BSA PBS were used as a vehicle beads in all the experiments. (F) Flow cytometry histograms showing eGFP fluorescence levels in HEK293T TCF-eGFP reporter cells after the exposure to Wnt/Rspo immobilized ligands. Wnt3a, Rspo1 and Rspo3 beads induce the expression of eGFP in a dose dependent manner whereas the TCF-eGFP reporter remains unaffected by the presence of vehicle beads (beads activated with EDC/NHS and quenched in 0.1% BSA PBS).

window of detection for Wnt9b activity in the TCF-eGFP line was quite narrow (see

section3.2.1.3) (Figure3.10, F).

The local activity of Wnt3a and Rspo3 beads in this cell line was also evaluated by live fluorescence microscopy. Both Wnt3a and Rspo3 induced local activation of the TCF-eGFP reporter (Figure3.11 and Figure3.12, A). However, such response was characterised by a high degree of heterogeneity as not all the cells in direct contact

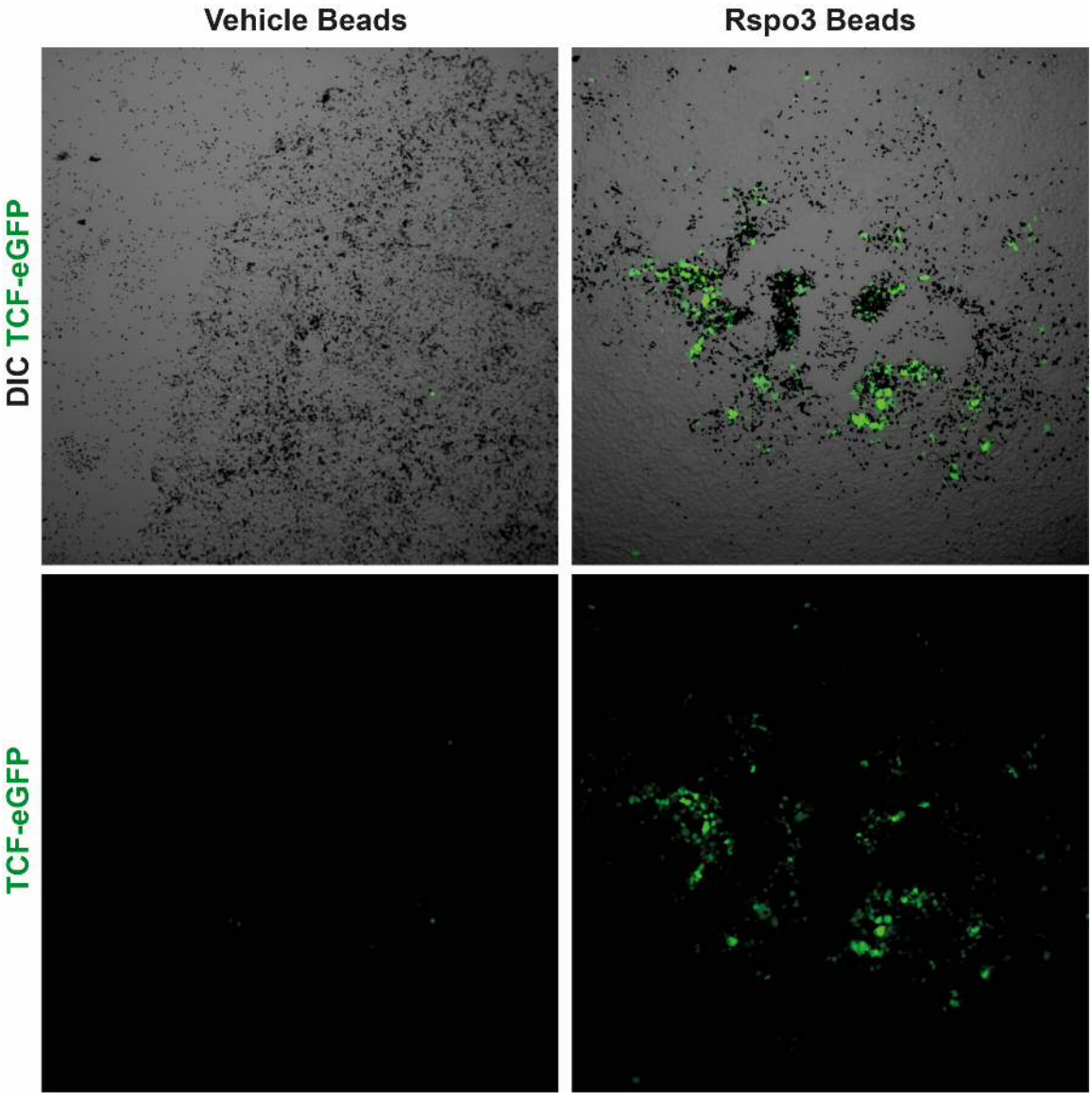

Figure3.11 Validation Rspo3 beads in TCF-eGFP HEK293T cells. Representative 10x images show the response of HEK293T TCF-Luc cells cultured in monolayers to Vehicle and Rspo3 beads in the presence of 200 ng/ml of Wnt9b. Exposure to Rspo3 beads causes a dramatic increase in eGFP expression. Image was acquired on a Spinning Disc Olympus IX71 confocal microscope. Beads of 2.8 µm can be used as scale bar.

with the beads were labelled with green fluorescence. A possible explanation for such

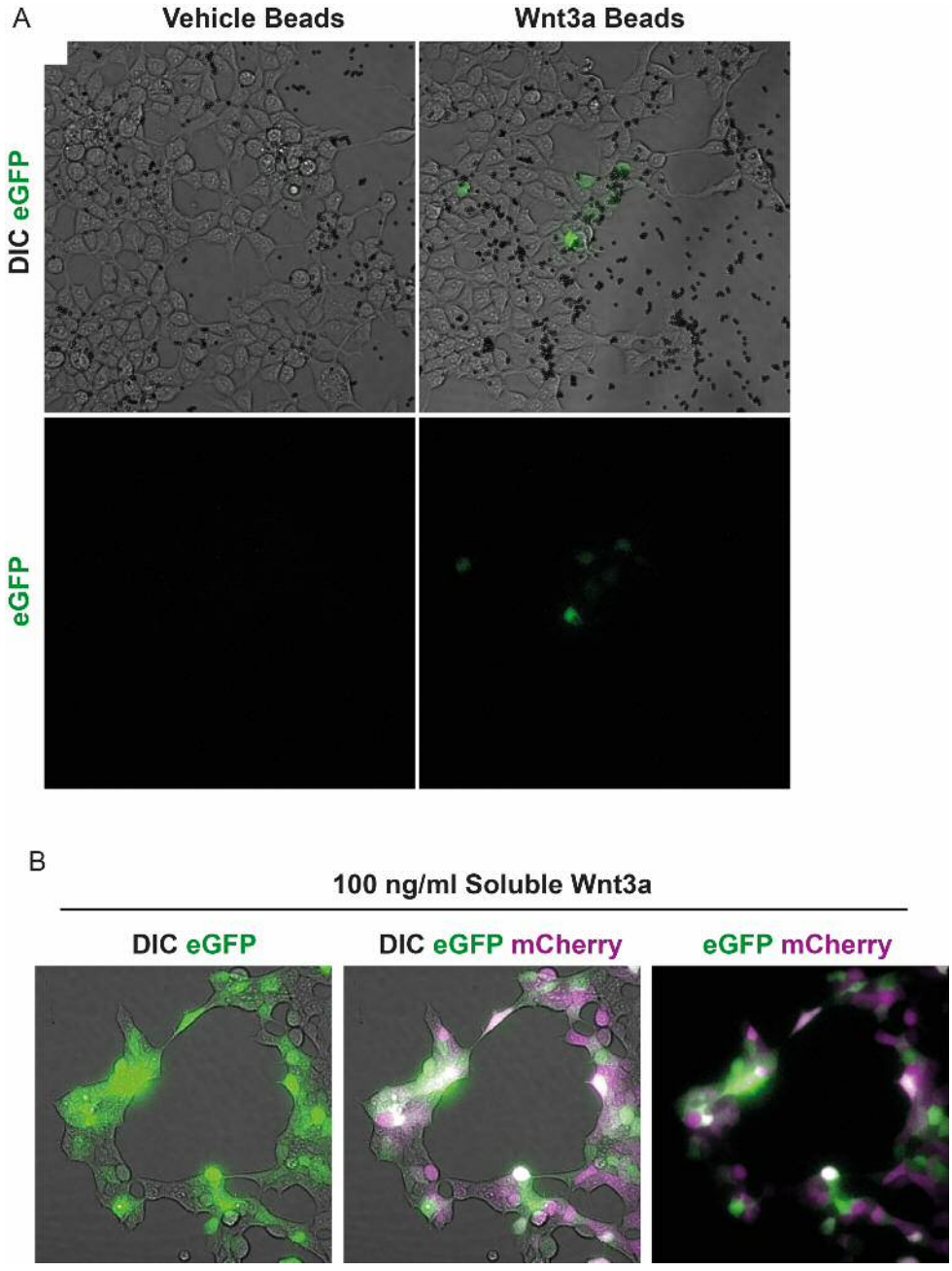

Figure3.12 Validation Wnt3a beads in TCF-eGFP HEK293T cells. (A) Representative 40x images of HEK293T TCF-Luc cells treated for 24h with vehicle or Wnt3a beads show the appearance of eGFP positive cells upon Wnt3a exposure. Note that not all the cells in contact with Wnt3a beads become eGFP positive. Beads of 2.8 µm can be used as scale bar. (B) Representative 40x images of HEK293T TCF-Luc cells treated for 24h with soluble Wnt3a (100 ng/ml) show heterogeneity in the response of the TCF-eGFP line. Level of expression of the TCF-eGFP construct correlate with mCherry expression (magenta). Note that levels of eGFP (green) do not overlap with the level of expression of the TCF-eGFP construct (magenta). (A) and (B) images were acquired on a Spinning Disc Olympus IX71 confocal microscope on the same day, with the same time of exposure and the same laser intensity. Furthermore, (A) and (B) images were subjected to the same background removal/signal enhancement and therefore fluorescence intensities are comparable.

heterogeneity is that the beads shift with respect to the cells by the time of imaging.

A second possible explanation is that such heterogeneity comes from the intrinsic ability of the cell to respond to or report Wnt activation. To evaluate whether cell intrinsic factors are a contributing element for the variegated response of the line to immobilized ligands, HEK293T TCF-eGFP cells were exposed to 100 ng/ml of soluble Wnt3a and the eGFP expression levels per cell were evaluated by live fluorescence imaging. Cells exposed to the same concentration of soluble Wnt3a exhibited differences in their eGFP expression levels (Figure3.12, B), indicating that cell intrinsic factors are a contributing element for the variegated response.

The TCF-eGFP HEK293T line was generated by the clonal expansion and therefore differences in the degree of response between cells cannot be explained by integration of the construct in different genomic regions. However, individual cells within the line could be subjected to stochastic silencing events. As previously mentioned, the p7TGC plasmid integrated in the TCF-eGFP reporter line contains a mCherry reporter cassette that allows to track silencing events upon culture. To assess whether the variegation in the cell response was related to cell-cell differences in the expression levels of the TCF-eGFP reporter, the level of expression in eGFP expressing and non-expressing cells was evaluated by live fluorescence imaging. No correlation was observed between eGFP and mCherry expression levels (Figure13, B), indicating that cell intrinsic factors other than the silencing of the TCF-eGFP vector are a contributing element for the variegated response.

Altogether, from this set of experiments it could be concluded that Wnt3a and Rspo3 beads locally activate the TCF-eGFP reporter.

3.3 Discussion

3.3.1 Comparison between TCF-Luc and TCF-eGFP HEK293T reporter cell lines

In the current chapter two different TCF/LEF HEK293T reporter cell lines were used to evaluate the canonical Wnt activity of soluble and immobilized Wnt/Rspo ligands: a TCF-Luc cell line kindly donated by Dr Jeremy Nathans (Johns Hopkins University) and a TCF-eGFP Wnt3a super responder developed in-house. In both cell lines,

exposure to a well-characterized canonical ligand, Wnt3a, activated the TCF/LEF reporter in a dose-dependent manner, indicating that in the HEK293T cell system activation of the TCF/LEF reporter can be used as a proxy of canonical Wnt activation. In Chapter 6 it will be discussed that this is not the case in all cellular contexts and/or TCF/LEF based reporters.

Both cell lines offered the possibility of measuring Wnt activation levels in a quantitative manner via the reading of luminescence levels (TCF-Luc) or by measuring eGFP levels by flow cytometry (TCF-eGFP). The TCF-Luc cell line reported global Wnt activation levels whereas the TCF-eGFP line could be used to dissect the levels of canonical Wnt signalling activation with a single-cell resolution. Cell preparation and quantitative analysis of Wnt activation levels using the TCF-Luc line is less time consuming and therefore this line was preferred for rapid characterization of the activity of putative Wnt agonist/antagonists.

One of the key observations of this chapter and that will be further discussed in Chapter 5 was that Wnt9b requires the presence of Rspo proteins to signal canonically. Both cell lines were sensitive to soluble Rspo1, Rspo3, Wnt9b and Wnt3a although the response of the TCF-eGFP line to the sole addition of Rspo proteins partially masked the response to Wnt9b. As a result, the TCF-eGFP cannot be used to accurately report the level of activity of Wnt9b.

The range of detection for the different Wnt/Rspo ligands tested was not the same in both cell lines. The TCF-eGFP line was overall more sensitive to Wnt and Rspo ligands although this was more obvious in the case of Wnt3a as this line did not require the addition of Rspo to report relatively low concentrations of this ligand. Differences in the range of detection between both lines are likely caused by differences in the integration site of the reporter. Nonetheless, strong conclusions about the exact range of detection in each of the lines must not be drawn based on the graphs presented here as they correspond to technical replicates. Despite the fact that the overall trends were preserved among biological replicates, a small variation in the curve of response to the different ligands was reported between biological replicates. Differences between biological replicates could be attributed to (1) differences in the activity of the ligands as a result of either batch-to-batch differences or due to different number of

freeze/thaw cycles of the ligands, (2) differences in the state of the cells, (3) variation introduced by the calibration of the instrument (FACS Aria II or luminometer) used for the measurement of the signal. In Table3.2 the approximate range of detection to the different ligands can be found.

	TCF-Luc reporter cells	TCF-eGFP reporter cells
Time cell preparation and quantitative analysis	~20min	~2-3h (flow cytometry) ~3-10h (fluorescence microscopy)
Wnt activity resolution at the cellular level	Pool of cells response	Single cell response
Cell population based on lentivirus integration	Monoclonal	Monoclonal
Range of response to soluble ligands (ng/ml)		
Wnt3a	20-?*	10-200
Wnt9b	20-?*	Depends on Rspo concentration
Wnt5a	20-?*	Not tested
Rspo1	5-200?	5-200
Rspo3	1-20	1-20

Table3.2 Comparative table showing the differences between TCF-eGFP and TCF-Luc HEK293T cell lines used in this project. Note that saturating concentration for Wnt3a, Wnt9b and Rspo1 was not reached for the TCF-Luc line and therefore an approximate value has been added instead. *In the presence of 20 ng/ml Rspo1. Question marks indicate that saturating concentration of the ligand was not reached.

Despite the clonal homogeneity of the TCF-eGFP cell line, cells expressed different eGFP levels when exposed to soluble Wnt3a and such heterogeneity in cell response could not solely be explained by differences in the level of expression of the reporter. Lrp6 phosphorylation, Axin2 or cytoplasmic β-catenin levels have been reported to oscillate with the cell cycle, peaking at G2/M phase [75,137,138]. Similarly, experiments performed by Ding et al. (2014) using a Venus/YFP biosensor that allowed live visualization of β-catenin interactions with TCF3 showed that interactions between these factors also fluctuates with cell cycle, peaking in S and G2 phases [139]. As components of the canonical Wnt pathway are under the control of the cell cycle, it is possible that the ability of a cell to respond to an external stimulus also change between phases. While it is not possible to determine the exact nature of the

source of the TCF-eGFP variegated Wnt response with the data presented here, it is important to consider that factors other than bead activity heterogeneity or reporter silencing may underlay differences in eGFP expression levels between cells when exposed to immobilized Wnt/Rspo ligands.

3.3.2 Biology of soluble Wnt and Rspo ligands

Data presented in the current chapter showed that Rspo3 is more potent than Rspo1, mirroring the previous observations of Kim et al. (2008) [140]. A key difference between Rspo1 and Rspo3 lies in the furin-like cysteine-rich domains (FU1 and FU2), which are responsible for the binding of the protein to their cognate receptors Rnf43/ZnrF3 and Lgr4/5/6, respectively. Studies from Lebensohn et al. (2018) showed that the FU1 domain of Rspo3 but not Rspo1 can directly engage with the E3 ubiquitin ligases ZNRF3/RNF43, which enables Rspo3 to potentiate Wnt/β-catenin signalling in the absence of Lgr4/5 and 6 receptors [141]. Consistent with a furin domain-determinant mode of signalling, Kim et al. (2008) showed that expression of Rspo3 furin domains caused higher activation of the TCF-Luc reporter than the Rspo1 furin domains when expressed in HEK293T [140]. Therefore, the reported differences between the activity of Rspo1 and Rspo3 ligands might be primarily attributed to the mode of signalling of each protein rather than to technical aspects of the protein purification process such as the isolation procedure, purity of the batch or stability of the protein in both lyophilized and soluble form.

Rspo proteins synergise with Wnt ligands by mediating the stabilization of Fzd and Lrp6 receptors [82]. In agreement with previous studies, Rspo1 and Rspo3 potentiated Wnt3a canonical signalling. Data presented in the current chapter also showed that HEK293T cells produce Wnt ligands that, in the presence of Rspo1 and Rspo3, drive activation of the Wnt/β-catenin pathway.

Wnt5a caused a decline in the levels of Rspo1- and Rspo3-induced TCF activation levels in a dose-dependent manner. These results are consistent with the literature as Wnt5a has been shown to antagonize the Wnt/β-catenin signalling pathway in many cellular contexts, including hematopoietic stem cells and cardiac progenitors [142,143]. The exact molecular mechanism by which Wnt5a opposes canonical

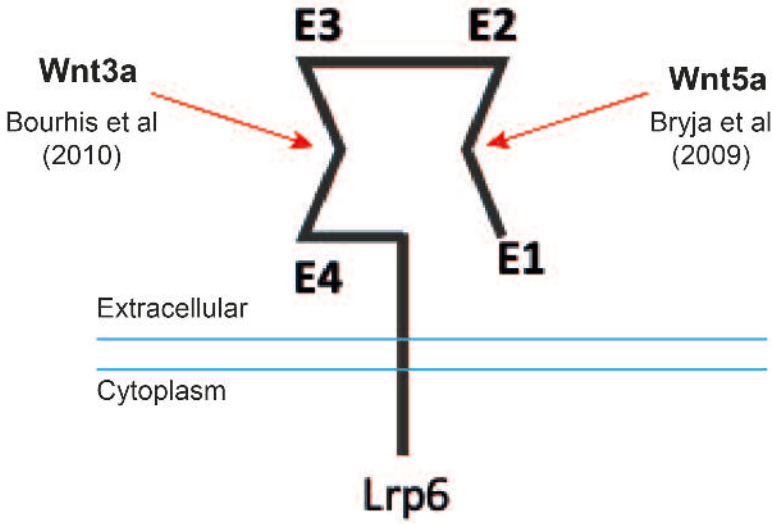

Figure3.13 Scheme representing Lrp6 structure and extracellular binding sites reported for Wnt3a and Wnt5a.

signalling remains unclear. Topol and colleagues proposed that Wnt5a controls β-catenin protein stability by modulating the mRNA expression levels of Siah2, a E3-ubiquitin ligase that was shown to promote β-catenin degradation by a GSK3-independent pathway in HEK293 cells [144]. However, Wnt5a-mediated expression of Siah2 could not be replicated years later by studies conducted by Sato et al. (2010) in both HEK293T and HeLa cells and, therefore, it has been questioned whether Wnt5a-mediated Siah2 expression is truly the underlying molecular mechanism behind the antagonistic canonical Wnt activity of Wnt5a [145] [146]. In the context of alveolar epithelial cells (A549 and MLE12 cell lines), Baarsma et al. (2017) reported that Wnt5a decreased the phosphorylation levels of Lrp6 upon Wnt3a stimulation, suggesting that inhibition of canonical signalling may occur at the receptor level [147]. Inhibition of Lrp6 phosphorylation by Wnt5a in cells treated with Wnt3a has also been reported in HeLaS3, NIH3T3, L, and C3H10T1/2 cells [145]. Experiments carried out by Bryja and colleges showed that Lrp6 physically interacts with Wnt5a [148]. Wnt5a however, bind to a different binding pocket to Wnt3a *in vitro*, implying that Wnt5a is not a direct competitor of Wnt3a (Figure3.13) [134]. Further studies involving the generation of mutants for Wnt5a binding pocket in Lrp6 receptor (region E1-E2) are required to evaluate whether Wnt5a binding to Lrp6 disrupts Wnt3a binding to Lrp6 or interferes with the engagement of the 'canonical' Fzd to the already formed Wnt3a-Lrp6 complex.

Experiments performed in this chapter failed to report Wnt9b canonical activity at any given protein concentration when this ligand was added alone to HEK293T cultures. These results are consistent with the observations of Alok et al. (2017), who also failed to detect activation of the TCF-Luc reporter in HEK293 cells cultures transfected with a plasmid containing Wnt9b coding region [149]. However, activation of the TCF-Luc reporter upon transient expression of Wnt9b plasmid in HEK293T cells and M15 cells has been reported by other research groups [150-152]. Wnt9b-driven activation of the TCF-Luc reporter in these studies was, however, very modest and therefore discrepancies between these *in vitro* studies might be explained by differences in the window of detection of Wnt9b canonical activity in the different cell-based assays. Furthermore, it should be mentioned that in this thesis the activity of Wnt9b was evaluated using the purified protein rather than overexpressing Wnt9b in the cultures. Thence, it should be also considered that steps in the purification process of Wnt9b might have slightly affected the native conformation of the protein, abrogating its already modest ability to activate the TCF-Luc reporter.

Data presented in this chapter showed that Wnt9b activated the TCF-Luc reporter at a concentration of 20 ng/ml when Rspo3 (10 ng/ml) or Rspo1 (20 ng/ml) were present in the system suggesting that, despite of the possible decrease in Wnt9b activity during the purification process (1) the ligand supplied by R&D systems retained the ability to induce of the Wnt/β-catenin pathway *in vitro* and (2) Wnt9b canonical activity is highly dependent on the presence of Rspo ligands. The possible mechanisms underpinning Wnt9b canonical behaviour in the presence of Rspo ligands will be later addressed in the discussion of Chapter 5.

Another interesting finding of the current chapter was that Wnt9b and Wnt3a proteins synergise to induce activation of the TCF-Luc reporter. Activation of the canonical branch of the Wnt signalling pathway requires the binding of Wnt ligands to a receptor

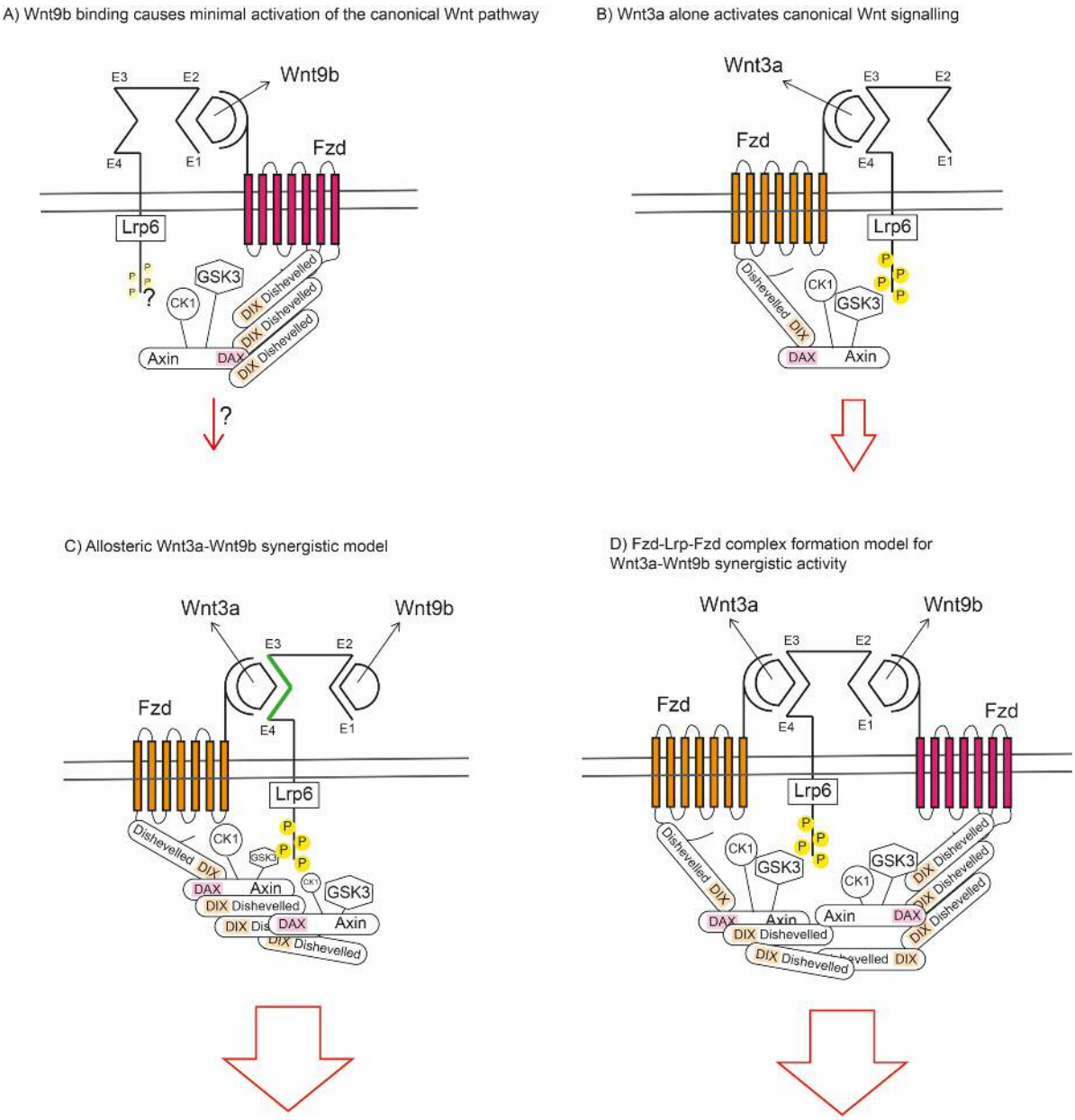

Figure3.14 Scheme representing the possible mechanisms behind Wnt3a and Wnt9b synergy. (A) Wnt9b alone is not sufficient to activate canonical Wnt signalling. A possible explanation for this might be that Wnt9b bridge the Fzd and the Lrp6 receptor in an orientation not optimal for the GSK3 and CK1 phosphorylation. (B) Wnt3a alone activates canonical Wnt signalling. (C) Allosteric Wnt3a-Wnt9b synergistic model. The binding of Wnt9b to Lrp6 potentiates Wnt3a signalling. (D) Fzd-Lrp-Fzd complex formation model. The binding of Wnt3a together with Wnt9b permits the assembly of Dsh/Axin complex more stable than Wnt3a alone. As a consequence, the signal is potentiated.

from the Fzd family and a receptor of the Lrp family (primarily Lrp5 and Lrp6) (see Chapter 1). The Lrp6 receptor contains two extracellular Wnt binding domains (E1-E2 and E3-E4) [134]. Studies conducted by Bourhis et al. (2010) showed that Wnt3a binds to E3-E4 whereas Wnt9b binds to E1-E2, and that both ligands can be simultaneously

loaded in the same Lrp6 receptor (Figure3.13) [134]. Thence, a possible explanation for these results is that Wnt9b behaves as an allosteric activator for Wnt3a canonical activity (Figure3.14, C).

Alternatively, it can be postulated that the simultaneous binding of Wnt9b and Wnt3a proteins to Lrp6 and their surrogate Fzd receptors may lead to the formation of a bigger Fzd-Lrp6-Fzd protein complex (Figure3.14, D). Gong et al. (2010) showed that a bivalent antibody targeting the E1-E2 Lrp6 domain potentiated Wnt3a-mediated activation of canonical Wnt signalling [153]. As the ability to potentiate canonical Wnt3a signalling by this antibody was lost with the monovalent recombinant one-armed version of the same antibody, Gong and colleagues concluded that dimerization of Lrp6 receptors at the level of the cell surface was the mechanism behind of the agonistic activity of the anti- E1-E2 Lrp6 domain antibody [153]. It could be therefore conceivably hypothesised that the simultaneous binding of Wnt3a and Wnt9b to a single Lrp6 receptor might enable the engagement of two Fzd receptors and subsequent formation of an Fzd-Lrp6-Fzd protein complex, which might recruit downstream effectors of the Wnt/Lrp signalling cascade more efficiently than a Fzd-Lrp6 complex (Figure3.14, D). Further work is required to evaluate whether any of these Wnt3a-Wnt9b synergistic models proposed takes place.

3.3.3 Biology of Wnt and Rspo immobilized ligands

One of the key results of the current chapter was the successful immobilization and validation of the activity of Wnt3a, Wnt9b, Rspo1 and Rspo3 beads. The fact that immobilized ligands can drive the activation of the TCF reporter partially challenges the idea that the formation and scission of the Wnt signalosome is essential for canonical Wnt signalling to occur (see Chapter1). Habib et al. (2013) reported that Wnt3a beads triggered the temporal recruitment of components of the Wnt/β-catenin pathway (β-catenin and APC) towards the bead at the level of the cell surface [105]. Thence, it is possible that, when Wnt ligands are immobilized onto 2.8 μm beads, cells bypass the requirement for the formation of the Wnt signalosome by the recruitment of Wnt/Lrp downstream components at the level of the cell surface. Alternatively, it is also possible to hypothesise that, when exposed to immobilized Wnt ligands, cells manage to cleave-off the Wnt proteins from the bead surface. Further experiments

need to evaluate the requirement or contribution of internalization events to the level of activation of Wnt pathway or clarify whether Wnt ligands are cleaved-off from the bead surface and/or whether the need of the signalosome is bypassed by the recruitment of downstream effector proteins at the level of the membrane.

3.3.4 Summary

The current chapter aimed (1) to characterise the canonical Wnt activity of the central vein ligands Wnt9b and Rspo3 and (2) to generate functional Wnt and Rspo beads able to induce canonical activation of Wnt pathway in a localized manner. Wnt9b purified protein was found to require Rspo proteins to activate canonical Wnt signalling. Conversely, Rspo3 required the presence of Wnt ligands to activate canonical Wnt signalling. Wnt3a, Wnt9b, Rspo1 and Rspo3 beads were successfully immobilized onto beads as their biological activity was validated in HEK293T cells stably expressing the TCF/LEF reporter.

Chapter 4. RESPONSE OF PRIMARY HEPATOCYTES TO CENTRAL VEIN LIGANS

Having in Chapter 3 characterised the activity of soluble and immobilized Wnt and Rspo central vein ligands using HEK293T cell lines, the next objective was to evaluate whether PH cultured in conventional 2D monolayers respond to these cues *in vitro*.

Experiments presented from Figure4.2 to 4.5 were carried out at the Beatson Institute during my visit to Dr Tom Bird's laboratory in 2018. The images presented in Figure 4.2 were acquired together with Dr Joel Johansson, a postdoc in Dr Owen Samson's laboratory, who also provided me with the antibodies and reagents for the experiment.

4.1 Introduction

The CV is source of Wnt9b and Wnt2, however, it is currently unknown whether both ligands are required to drive activation of the canonical Wnt pathway in the hepatocytes *in vivo* (see Chapter 1).

In Chapter 3 it was shown that purified Wnt9b protein, in the presence of Rspo proteins, activated canonical Wnt signalling in HEK293T cells. As HEK293T cells is a cell line derived from kidney embryonic cells, it needs to be evaluated whether Wnt9b can exert canonical activity in other cellular context including the liver.

The current chapter aims to determine whether (1) soluble and immobilized Wnt9b and Rspo3 ligands trigger activation of canonical Wnt pathway in hepatocyte cultures and (2) whether Wnt pathway activation in hepatocytes cultures induced the expression of pericentral metabolic genes. PHs cultured in conventional 2D monolayers are the gold standard for the *in vitro* evaluation of hepatocellular responses and therefore this culture system was used as a model of study this chapter.

4.2 Results

4.2.1 Characterization of 2D PHs cultures

In this chapter, the biology of the central vein ligands Wnt9b and Rspo3 in the cellular context of the hepatocytes was characterised using PHs cultured in conventional 2D monolayers as a cell system. Prior to this, I established a PH isolation and a 2D culture protocol.

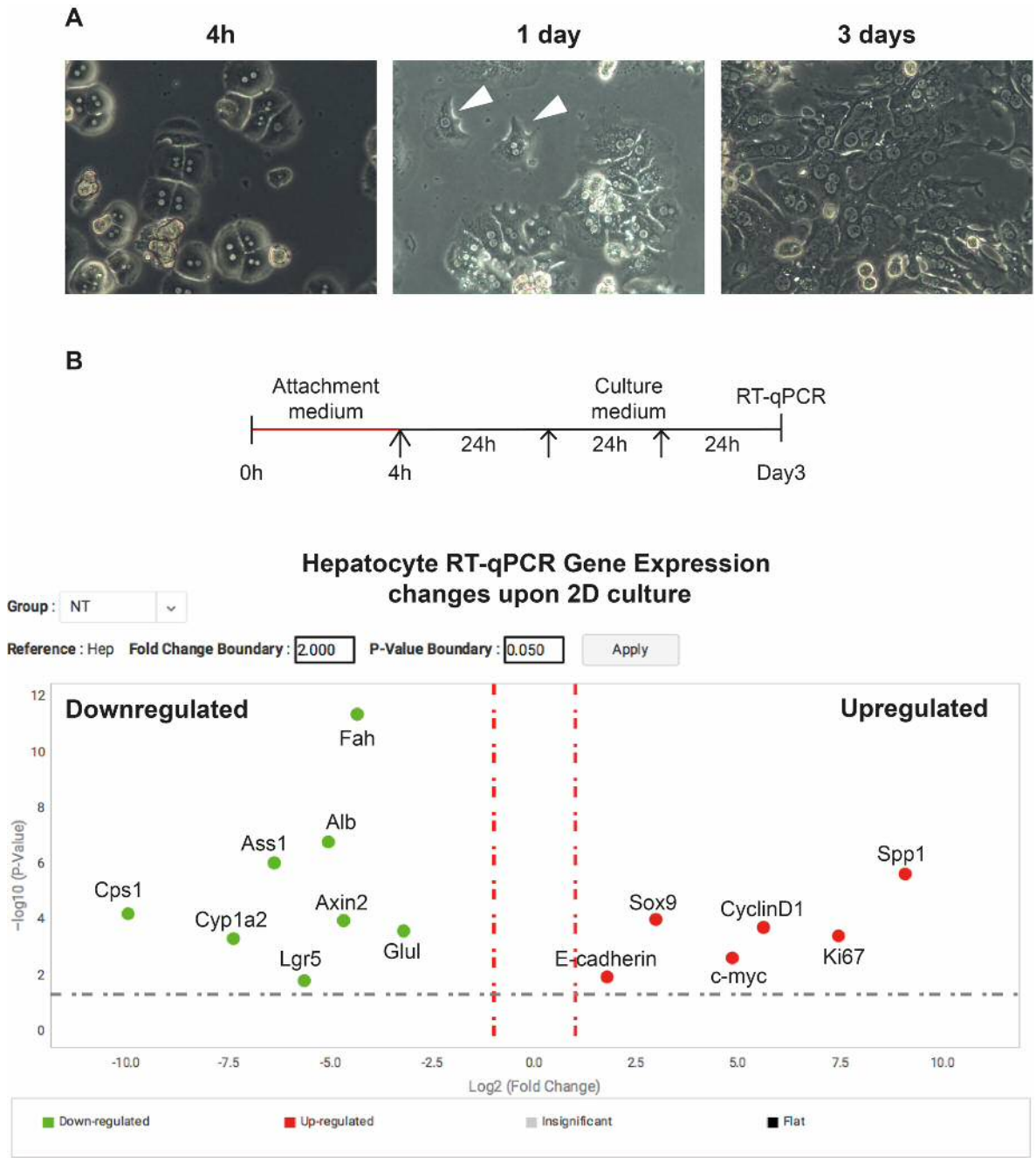

Figure4.1 (A) Representative images of PH cultured for 4h, 1day or 3days on collagen-coated plates. Arrow heads point to cells presenting a polarized morphology typical of motile cells. (B) Volcano plot shows relative gene expression levels of PH cultured for 3 days when compared with fresh isolated PH (time 0h). Genes that appear significantly downregulated and upregulated after 3days in culture appear highlighted in green and red, respectively. Top panel indicates experimental design and culture conditions and arrows indicate the time points in which the media was changed. Volcano plot and statistical analysis was performed using ThermoFisher online tool for RT-qPCR gene expression analysis. (n=4).

PHs were isolated using a standard two-step perfusion method, which involves the perfusion of the liver with (1) a solution that contains a calcium chelating agent, such as EGTA, that will clear the circulating blood and assist with the disruption of cell tight

junctions; followed by (2) a collagenase-containing solution that will digest and release the parenchymal and non-parenchymal cells that constitute the liver mass. Generally, perfusion at a constant rate of the organ would be achieved using variable speed peristaltic pumps. However, peristaltic pumps were not available in our laboratory at the time of completion of this project and therefore, I opted to develop a home-made perfusion system using aquarium pumps. Details of the perfusion system are described in Chapter 2.

Following this procedure, 10-20 million of cells with 70-99% viability were consistently isolated per mouse (data not shown). After isolation, PHs were immediately plated for 2D culture. However, PHs in suspension were found to not rapidly attach to tissue culture plates, even if they were coated with extracellular matrix (ECM) proteins such as collagen. To facilitate the adhesion of the cells to the 2D surface, the hepatocyte culture medium was supplemented with FBS and, depending on the quality of the isolation, cell attachment took between 4 to 16h. After cell adhesion, the concentration of FBS in the culture medium was reduced to 0.5 % as it has been reported FBS at a concentration higher than 1% speeds up the loss of hepatocyte markers in culture [154].

In accordance with previous studies, PHs cultured in conventional 2D monolayers lost their characteristic cuboidal morphology within 3 days of culture [110]. Cells with a 'motile' morphology started to appear after 16 to 24h of culture (Figure4.1, A). To better understand the impact that 2D culture adaptation has in the overall state of the cells, the expression of various hepatocyte genes corresponding to periportal (Cps1, Ass1, Alb and E-cadherin) and pericentral zones (Glul, Cyp1a2 and Fah) was analysed in 3-day cultured PHs and compared to fresh isolated PHs [33]. Furthermore, the expression of genes involved in cell proliferation (ki67 and CyclinD1) and survival (Sox9, c-myc and Spp1) as well as β-catenin target genes (Lgr5 and Axin2) that are upregulated in the hepatocytes in response to liver damage was additionally evaluated [12,155-158].

All the liver zonated genes assessed, with the exemption of E-cadherin, were dramatically downregulated upon 2D culture regardless of their zonal expression

pattern the liver lobule, indicating that hepatocytes overall lose expression of hepatocyte-specific functions upon 2D culture (Figure4.1, B). Lgr5 and Axin2 mRNA levels declined upon culture, indicating that the Wnt/β-catenin signalling pathway is downregulated during the 2D culture adaptation process. By contrast, the expression of ki67 and CyclinD1 was significantly upregulated, suggesting that when removed from their physiological environment and plated in 2D cells enter into a proliferative state. Finally, Sox9, c-myc and Spp1 mRNA levels were significantly increased upon 2D culture, suggesting that certain hepatocyte injury-related genes might also be activated as a response to hepatocyte-to-2D culture adaptation.

I next evaluated whether the changes in the cell architecture were accompanied by alterations to in Wnt receptors localisation, that could in turn impact Wnt ligand responsiveness. For that aim, the cellular localisation of the Wnt receptor FZD7 and the canonical Wnt co-receptor LRP6 was assessed in PHs at different culture times by IF (Figure4.2). After 4h of culture, LRP6 protein was detected in clusters near cell-cell junctions whilst it was barely detectable in the cytoplasm. LRP6 protein clusters did not co-localize with FZD7 staining. However, by 16h of culture, cytoplasmic LRP6 levels were strongly increased and LRP6 protein was detected around the nucleus and at the cell surface. Of note, LRP6 protein was not present inside the cell nuclei. At the same time point, FZD7 protein was mostly localized at the cell surface although there were significant inter-cell differences in expression. 24h after cell adhesion, cell surface protein levels of both LRP6 and FZD7 were significantly reduced. At this time point, LRP6 protein was also detected inside the nuclei.

Together, the results from this section provide further evidence of the profound structural and functional changes that hepatocytes undergo in their adaptation to 2D culture.

4.2.2 Response of 2D-cultured PHs to soluble Wnt/Rspo ligands

Data obtained in Chapter 3 suggest that Wnt9b can activate the canonical branch of Wnt pathway in kidney cell systems. To assess whether Wnt9b activates a β-catenin transcriptional response in the hepatocellular context, PHs from an Axin2CreERT2

reporter transgenic mouse model were derived and their response to the CV ligands Wnt9b and Rspo3 evaluated.

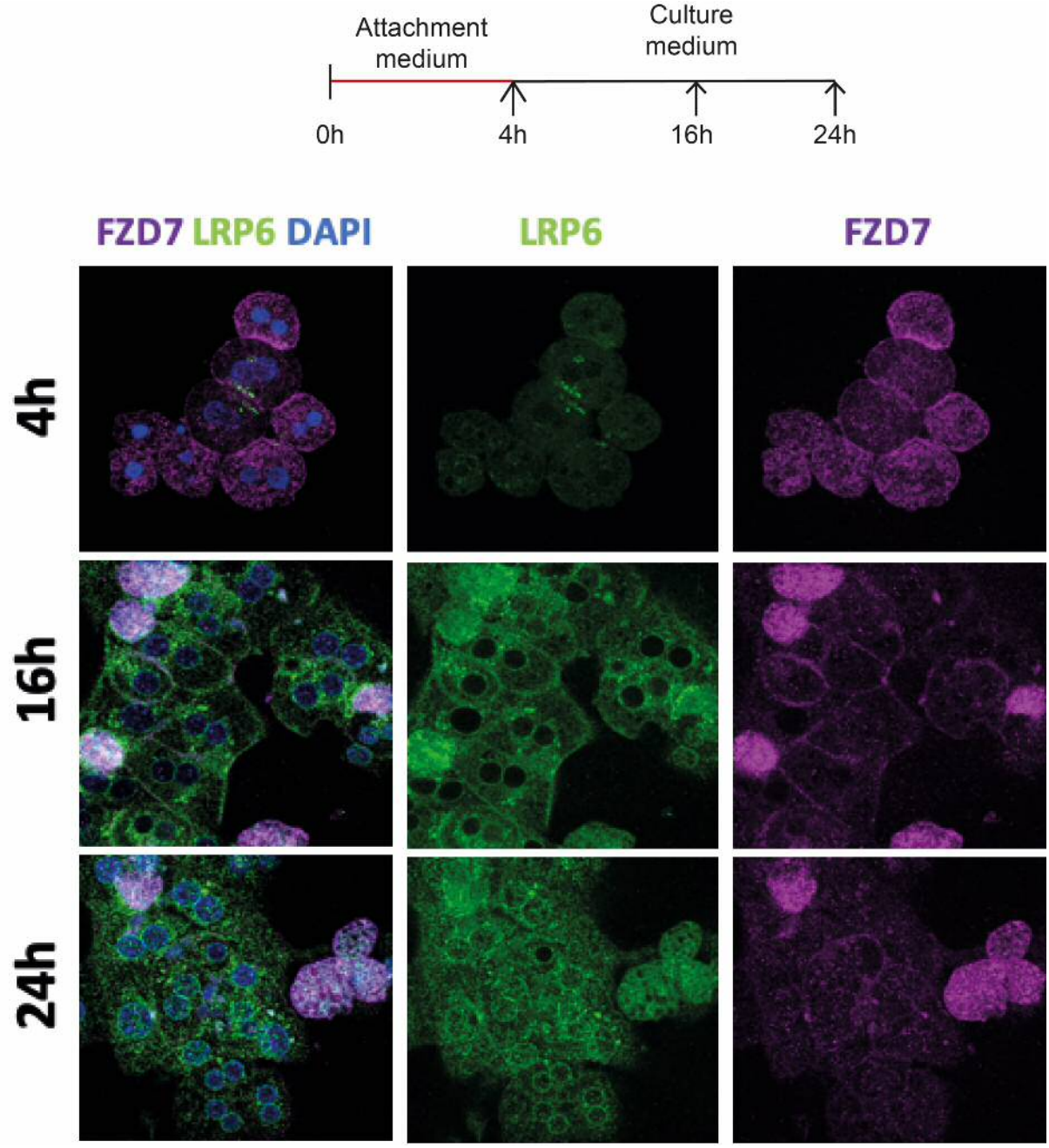

Figure4.2 Representative immunofluorescence images shows Lrp6 (green) and Fzd7* (magenta) expression in primary hepatocytes cultured for 4, 16 and 24h onto collagen-coated plates. Cell nuclei has been counterstained in with DAPI (blue). Top panel indicates experimental design and culture conditions. *Fzd7 antibody cross-react with other members of the Fzd family. Images correspond to representative images of 3 technical replicates from one biological experiment.

In the Axin2CreERT2 reporter mouse transgenic line (Axin2CreERT2 R26-LSLtdTom), the Cre recombinase has been fused to a mutated estrogen receptor (ERT2). This confers temporal control of the Cre activity as the CreERT2 protein is retained in the cytosol by heat shock proteins but shuttles to the nuclei in the presence of an estrogen analogues such as 4-hydroxy tamoxifen (4-OHT). The CreERT2 construct has also been knocked-in in the Axin2 allele, replaces, in the heterozygous state, one endogenous Axin2 allele and places CreERT2 under the transcriptional control of endogenous regulatory elements of Axin2 (Figure4.3). Axin2 is a well characterised target of β-catenin in many systems and CreERT2 expression can therefore be taken as a proxy for canonical Wnt/β-catenin activation [12]. Once in the nucleus, the CreERT2 recombinase efficiently recognizes *loxP* sites and excises the DNA segment flanked by two of these sequences. Cells derived from this mouse line also contain the two *loxP* a stop cassette (flox-Stop) inserted between a strong synthetic promoter (CAG) and a region coding for the expression of a red fluorescence protein known as tdTomato (tdTom). The CAG-flox-Stop-flox-tdTom construct has been knocked-in in a region of the genome (Rosa26 locus) that is ubiquitous expressed among tissues and that is not susceptible to genetic silencing (Figure4.3). As the flox-Stop sequence prevents that prevents the constitutive expression of tdTom, once the CreERT2 is activated, all CreERT2 expressing cells and their progeny will remain labelled by tdTom. In summary, PHs with high Wnt activation levels (Axin2 positive), together with their subsequent progeny, will be permanently labelled with tdTom upon 4-OHT administration (Figure4.3).

Using PHs derived from the Axin2CreERT2 reporter mouse model, and with a few exceptions, non-positive Axin2 cells were found after three days of culture (Figure4.4). Treatment with 100, 200 or 500 ng/ml of Wnt9b for the three days of culture did not cause an increase in the number of Axin2 positive cells (Figure4.4, B). Exposure to 50, 100 or 200 ng/ml of Rspo3 did not cause either an increase in the proportion of Axin2 positive cells in culture (Figure4.4, C). However, when cells were concomitantly treated with a combination of Rspo3 (50 ng/ml) and Wnt9b (100 or 200 ng/ml), a significant increase in the number of Axin2 positive PH was found, indicating that both ligands synergise to activate canonical signalling in PHs under these conditions (Figure4.4, D). As a positive control for Wnt activation, cells were also exposed to a

"high Wnt" medium containing 100 ng/ml Rspo1 and 5% Wnt3a CM (Figure4.4, E). Of note, nearly all the hepatocytes became Axin2 positive upon exposure to "high Wnt" medium. This was a much larger proportion when compared with the combinational treatment of Rspo3 and Wnt9b (compare Figure4.4 D and E).

Taken together, these data suggest that Wnt9b, in the presence of Rspo3, can trigger β-catenin activation in the primary hepatocytes.

4.2.3 Response of 2D-cultured PHs to immobilized Wnt/Rspo ligands

Wnt9b- and Rspo3-beads activated Wnt/β-catenin signalling in HEK293T cells, as shown by the increase in the activation levels of the TCF-Luc reporter (see Chapter 3). To assess whether immobilized Wnt9b and Rspo3 ligands activate the canonical branch of the Wnt pathway, PHs derived from the Axin2CreERT2 reporter mouse model were exposed for 2 days to Wnt9b and Rspo3 ligands in soluble and/or immobilized state and the number of Axin2 positive cells (tdTom positive) were quantified using a high-content microscope system. Vehicle (BSA-coupled) beads were used as controls.

Confirming the results from section 4.2.2, the concomitant addition of Wnt9b and Rspo3 in soluble state induced the appearance of Axin2 positive cells, being

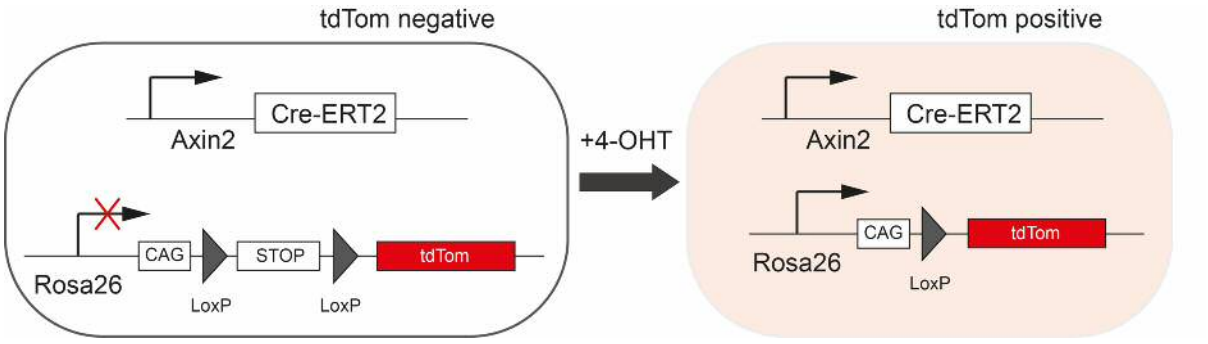

Figure4.3 Scheme representing the Axin2CreERT2 and R26-LSL-tdTomtransgenes present in the Axin2CreERT2 R26-LSL-tdTom mouse model.CreERT2 recombinase is under the control of the Axin2 promoter. Temporal activation of the Cre recombinase is obtained by the exposure to estrogen analogs (4-OHT). A gene coding for a red fluorescence protein (tdTom) is inserted in the Rosa26 locus and its constitutive expression is prevented by a stop cassette flanked by two loxP sites. When 4-OHT is administrated, the stop cassette preventing tdTom expression is exiced and the cell become permanently labelled with red fluorescence.

approximately 3 to 5 % of the total cells labelled with tdTom (Figure4.5). Similarly, cells positive for tdTom expression were also detected when Rspo3 beads were added in

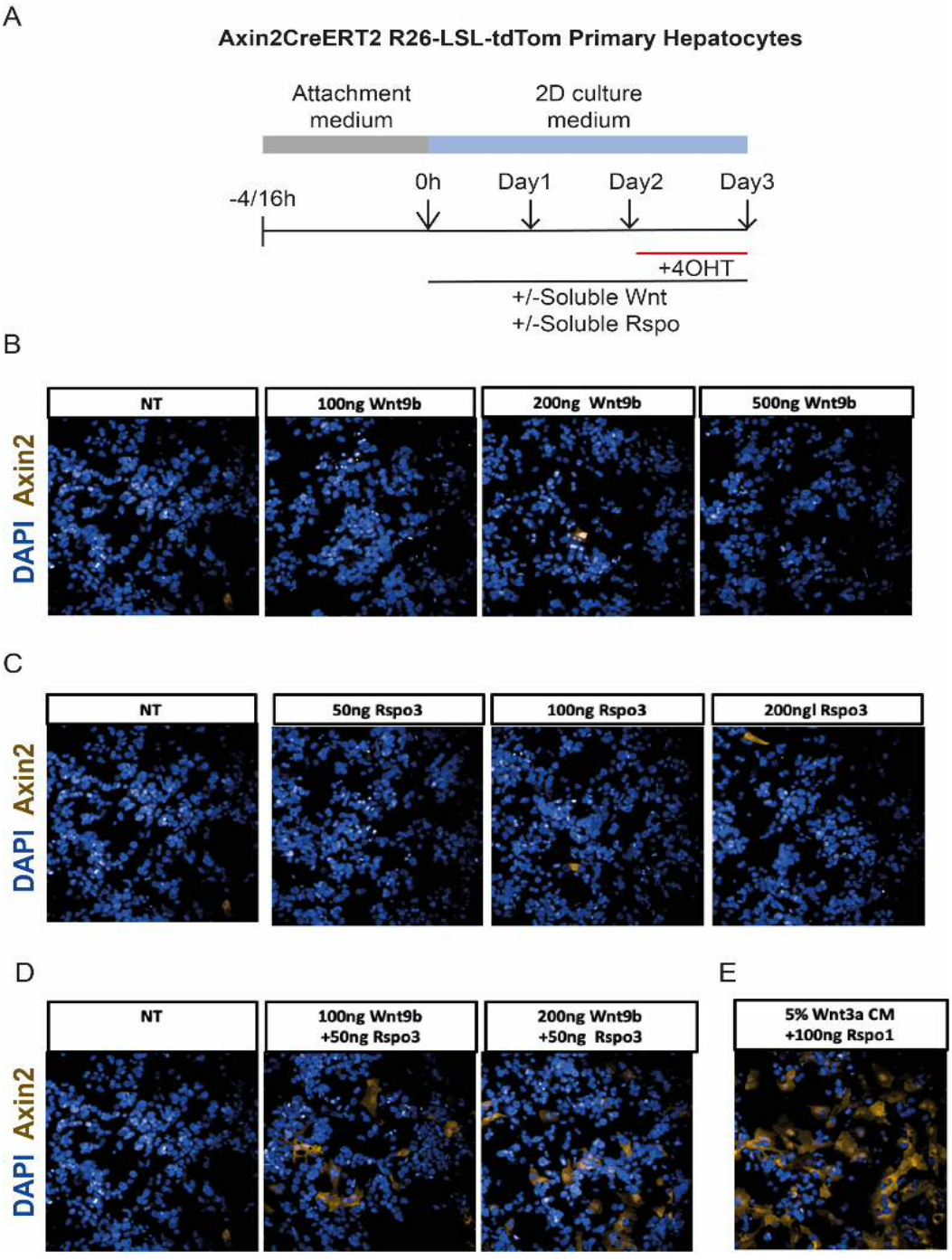

Figure4.4 Response of PH derived from an Axin2CreERT2 R26-LSL-tdTom mouse model cultured in 2D to soluble Wnt9b and Rspo3. (A) Scheme deciphering the experimental set up. Arrows indicate time points where medium was refreshed. (B-E) Axin2Cre-ERT2PH cultured onto collagen-coated plates were exposed to different concentrations of Wnt9b (B), Rspo3 (C) or a combination of both ligands (D). As a positive control for Wnt induction, PH were exposed to 5% Wnt3a conditined medium (CM) combined with 100 ng/ml Rspo1 (”high Wnt” medium conditions). Representative images of n=3 technical replicates. Note that a proportion of the hepatocytes in the image that appear labelled in blue are not longer alive. Dead cells can be distinguished by the nuclei morphology

combination with soluble Wnt9b and, in this case, 2 to 3% of the total cells were scored as Axin2 positive (Figure4.5). By contrast, Wnt9b beads in combination with soluble Rspo3 did not induce the appearance of Axin2 positive cells in culture (Figure4.5). Non-positive cells for Axin2 expression were detected upon the exposure to vehicle beads in combination with either soluble Wnt9b or Rspo3.

From this set of experiments it can be therefore concluded that (1) immobilized Rspo3 in combination with Wnt9b elicits a canonical response in PH and (2) under the current experimental settings, Wnt9b beads in combination with soluble Rspo3 do not activate β-catenin at sufficient levels to induce CreERT2 mediated recombination in PH.

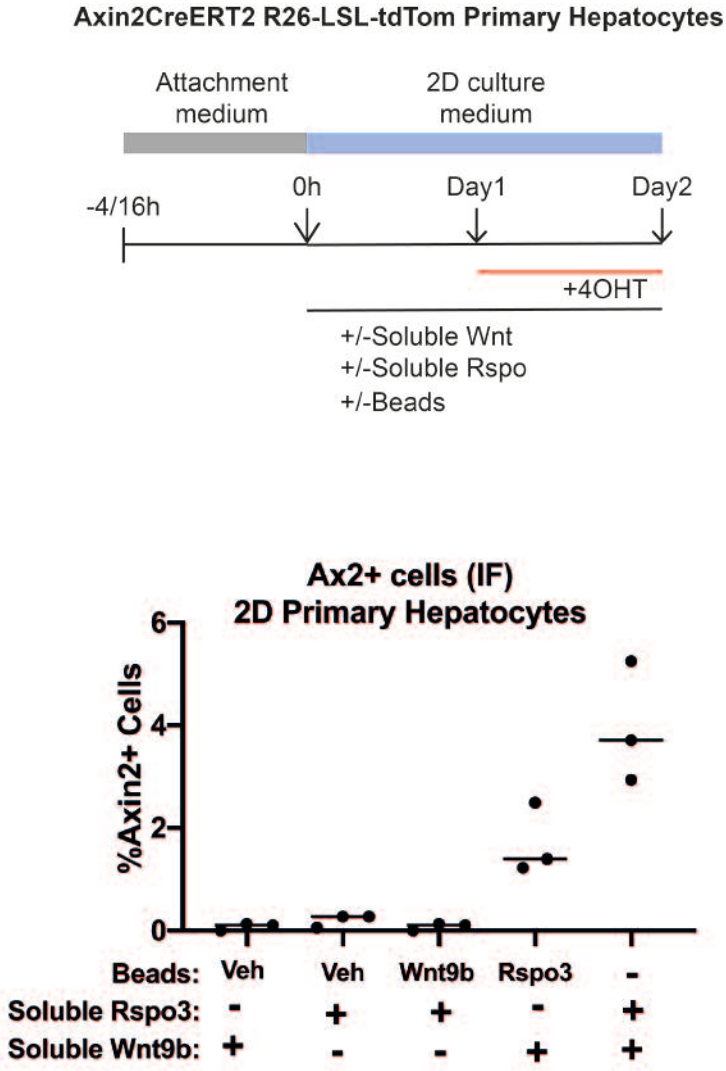

Figure4.5 Response of PH derived from an Axin2CreERT2 R26-LSL-tdTom mouse model to soluble and immobilized Wnt9b and Rspo3. Top panel indicated treatment time line and arrows indicate time points where medium was refreshed. Bottom graph shows quantifications of immunofluorescence images acquired in an Opera Phenix system at the Beatson Institute. Experiment was performed onto a 96-well plate and three technical replicates were performed per condition. The concentration of soluble Rspo3 and Wnt9b was 50 ng/ml and 100 ng/ml, respectively. Beads were added at a concentration of 21.2 ug/well. Semi-automatic quantifications were performed using Colombus software.

4.2.4 Effects of Wnt9b and Rspo3 in the expression of pericentral metabolic genes

Pericentral hepatocytes express β-catenin target genes including Axin2, Glul, Cyp1a2 and Cyp2e1 (see Chapter1). Results from section 4.2.3 show that soluble Wnt9b and Rspo3 synergise to activate the Axin2CreERT2 reporter in PHs cultured in conventional monolayers for 3 days. To determine whether hepatocyte-specific zonated genes were similarly induced, the expression of Axin2, Glul, Cyp1a2 and Cyp2e1 was compared under the same experimental conditions.

Confirming the results from the Axin2CreERT2 reporter (see section 4.2.3), a significant increase in Axin2 mRNA levels occurred upon concomitant exposure to Wnt9b and Rspo3 but not when the ligands were individually added (Figure4.6). Following a similar trend to Axin2, Wnt9b or Rspo3 alone did not induce Cyp2a1 expression but combination of both ligands caused an increase in the expression of

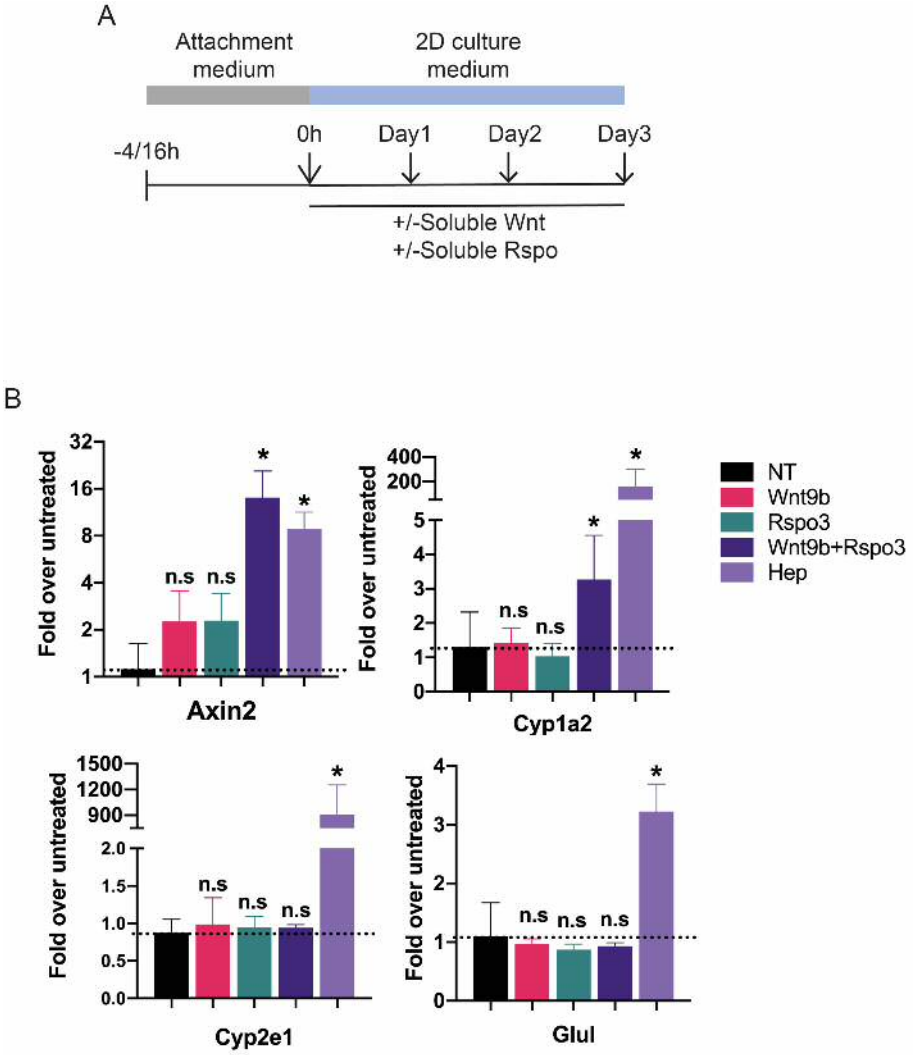

Figure4.6 Response of WT PH cultured in 2D and exposed for 3 days to soluble Wnt9b and Rspo3 ligands. (A) Scheme deciphering the experimental set up. Arrows indicate time points where medium was refreshed. (B) RT-qPCR gene expression analysis showing the levels of expression direct targets of β-catenin in hepatocytes. Wnt9b and Rspo3 were used at a concentration of 100 ng/ml and 50 ng/ml, respectively. As a reference, levels of expression in fresh isolated hepatocytes (Hep) were included. Relative significance of each treatment when compared to untreated cells (NT) has been indicated. Statistical significance was determined using Mann-Whitney t-test. (n=4 animals). p-value *< 0.06; n.s.= non-significant.

this gene (Figure4.6). By contrast, no significant increases Glul and Cyp2e1 expression were found when Wnt9b and Rspo3 were added individually or in combination (Figure4.6). Of note, the expression levels of the hepatocyte-specific target genes in the PH cultures was many fold lower than that observed in freshly isolated hepatocytes.

Taken together, these data indicate that under the current 2D culture conditions Wnt9b and Rspo3 synergise to drive the expression of some but not all the pericentral genes tested.

4.3 Discussion

4.3.1 Hepatocyte-to-2D culture adaptation

One of the main limitations of the use of PHs 2D cultures is the rapid adaptation of the hepatocytes to the *in vitro* conditions (see Chapter 1). Accordingly, data presented here showed that when removed from their physiological environment and plated in 2D, hepatocytes undergo major changes in the cell architecture and gene expression. Downregulated expression was observed from liver-specific genes involved in functions such as ammonia detoxification (Cps1 and Glul) or the metabolism of xenobiotics (Cyp1a2) and included markers of both periportal (Cps1, Ass1 and Alb) and pericentral (Cyp1a2, Glul and Fah) hepatocytes, suggesting that tissue culture adaptation affects the overall state and identity of the cells [7,33,159].

The process of hepatocyte tissue culture adaptation is commonly described as hepatocyte 'dedifferentiation'. Dedifferentiation, however, is a term that not only refers to the loss of the original cell identity but also implies the acquisition of a new global gene expression profile and/or gain of a different cell identity that can either resemble to an existing cell/tissue type found *in vivo* or be just an artificial *in vitro* construct. To identify whether hepatocytes in culture adopted a known cell signature using an unbiased approach, Godoy et al. (2016) performed global genome-wide studies in which the transcriptomes of 2D-cultured hepatocytes were compared with gene expression profiles of specific cell-type gene regulatory networks previously described by Cahan et al (2014) [160,161]. Using this approach, the authors of the study found that, upon culture, hepatocytes upregulate clusters of genes classified as regulators of inflammation and RNA processing (Myc, Klf6, Sox4 and Atf4) and cell cycle and

migration (Sox9, Smad4 and E2F) [160]. Consistent with these observations, data presented in the current chapter showed that hepatocytes cultured in monolayers for 3 days significantly increased the expression levels of Sox9, c-myc and Spp1 as well as additional genes involved in cell proliferation (ki67 and CyclinD1).

The unbiased cell identity analysis of the approach of Godoy et al. (2016) determined that although the closest cell identity type to PHs adapted to monolayer growth still was 'hepatocytes', these cells gained expression of genes associated with a 'fibroblast' signature. Godoy and colleagues argued that the gain of a 'fibroblast' signature was a reflection that the hepatocytes undergo epithelial-to-mesenchymal transition (EMT) following *in vitro* culture adaptation. Hepatocyte 2D culture adaptation has also been described as an EMT process by other authors **[45,162]**. For instance, Guo et al. (2017) reported that PHs cultured in monolayers increase the expression of mesenchymal markers such as N-cadherin, FN, Vimentin, α-SMA, Collagen1α1, Snail or Slug between day 1 and 5 of culture [45].

EMT is a tightly regulated and complex process that involves the reprogramming of epithelial cells and results in the loss of cell adhesion and acquisition of invasive and motility properties. A critical step in EMT progression is the repression of adhesion molecules such as E-cadherin [163]. Results from the current chapter showed, however, that PHs increased E-cadherin mRNA levels when cultured in monolayers for 3 days, an outcome that is contrary to the hypothesis that hepatocytes undergo EMT during 2D culture adaptation. A possible explanation for these apparent discrepancies between Guo et al. (2017) findings and mine might be that the increase in EMT markers reported by Guo and colleagues occurred when comparing hepatocytes cultured between 1 and 5 days whereas the increase in E-cadherin levels reported in the experiments presented here occurred using freshly isolated hepatocytes as a reference state [45]. Is therefore possible that in their adaptation to 2D culture conditions, hepatocytes first undergo upregulation of genes that enable their adhesion to tissue culture plates and once they are attached, an increase in EMT markers might occur between day 1 to 5 of culture. This model would fit with the observation that PHs required long time (between 4 and 16h) to initially attach to the culture plates and that cells with a polarized morphology characteristic of motile cells

were not observed until 16 to 24h post attachment. Further work needs to be carried out to establish whether hepatocyte tissue culture adaptation or certain stages of this process meet the characteristic of a true EMT process.

Another interesting observation from the 2D characterization experiments was the subcellular localization dynamics followed by LRP6 receptor protein. 16h post-attachment, LRP6 was highly expressed and, at this time, the protein was absent from cell nuclei. However, 24h post-seeding LRP6 protein was detected at high levels inside the cell nuclei. A functional role for nuclear LRP6 was recently described as LRP6 intracellular domain has been shown to be shuttled to the cell nuclei and repress transcription of the TCF/LEF-1 reporter as well as to control the splicing of mRNAs through its interaction with components of the core splicesome [164,165]. Further research is required to determine whether nuclear LRP6 is having a functional role in the process of hepatocyte-to-2D culture adaptation. A note of caution is due here since, due to the length of my visit at the Beatson, the presented images correspond to representative images from three technical replicates of a single PHs isolation. Thereby, the reproducibility of the described Lrp6 cytoplasmic-nucleo shuttling should be validated.

Taken together, results from these characterization experiments provide important insights in how hepatocytes adapt to grow in conventional 2D monolayers and highlight that this process involves a cascade of dynamic events (cell adhesion, migration, proliferation, survival, etc.). Thus, when using PHs cultured in 2D as a system of study a cautious interpretation of the results should be done as the response of the cells might be impacted by the state of adaptation they are in.

4.3.2 Response of Axin2CreERT2 PHs cultured in 2D to soluble Wnt9b and Rspo3

A combination of soluble Wnt9b and Rspo3, but not individual ligands, activated the Axin2CreERT2 reporter in PH 2D cultures. These results corroborate the previous findings of Chapter 3, where it was shown that Wnt9b requires the presence of Rspo ligands to activate canonical Wnt signalling in the context of HEK293T cells. Interestingly, Wnt9b/Rspo3-mediated activation of the Axin2CreERT2 reporter occurred only in a small proportion of hepatocytes in culture. A possible explanation

for these results is that not all the hepatocytes express the Wnt/Rspo receptors that mediate the synergy between Wnt9b and Rspo3 (Figure4.7, A). In support of this model, the expression of certain Wnt and Rspo receptors across the liver is zonated. For instance, pericentral hepatocytes are enriched for Fzd8 expression whereas Lrg5 is not only pericentrally expressed but its expression is also restricted to the hepatocytes lining the CV [14]. As upstream components of the Wnt/β-catenin cascade appear zonated, it is possible that cell-intrinsic factors will determine the ability of periportal/pericentral cells to respond to the treatment. Therefore, further research should be undertaken to investigate whether both periportal and pericentral hepatocytes are responsive to Wnt9b/Rspo3 treatment *in vitro*.

Results from this chapter also showed that nearly all the hepatocytes became Axin2 positive upon exposure to 'high Wnt' medium. These results debate the idea that only a few hepatocytes in culture can respond to Wnt activating cues and argue for a CreERT2 recombination model in which Wnt activation levels should be taken into account. The Axin2CreERT2 reporter is an On-/Off-state reporter system in which expression of tdTom only occurs in cells that produce CreERT2 at levels above certain recombination threshold (Figure4.7, B). Therefore, another possible explanation for the Wnt9b/Rspo3 variegated cell response might be that the concomitant exposure to these ligands is inducing Wnt activation at levels close to, but not exceeding, such recombination threshold, causing the activation of the reporter only in a few cells from the pool (Figure4.7, B). Following this reasoning, exposure to a 'high Wnt' medium would cause a further increase the expression of CreERT2 recombinase, exceeding the recombination threshold and causing the activation of the reporter in nearly all the cells in culture (Figure4.7, B). These considerations in the mode of activation of the Axin2CreERT2 reporter will also be important when interpreting the data from biliary-derived organoids in Chapter 5. The possible mechanisms that might underpin Wnt9b/Rspo cooperativity in regulating canonical Wnt/β-catenin signalling will be also addressed in Chapter 5.

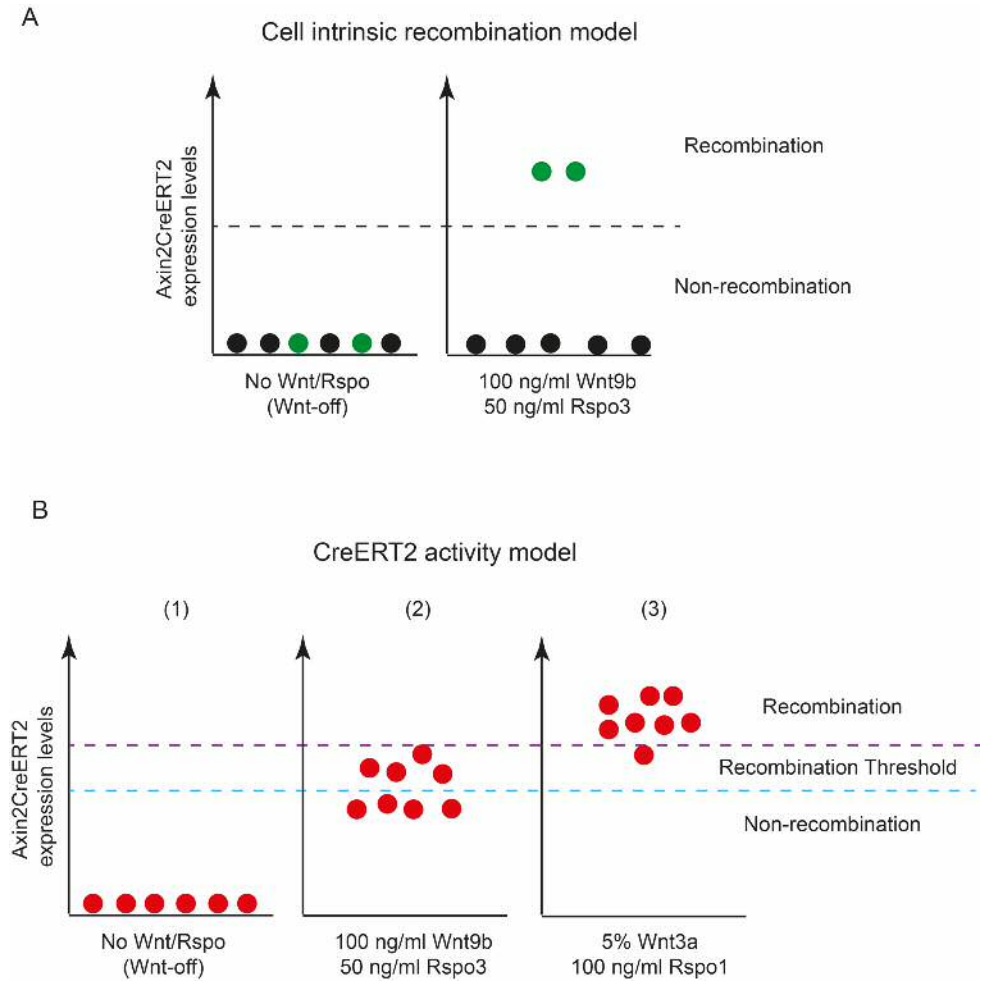

Figure4.7 Axin2CreERT2 reporter activation models. The Axin2CreERT2 reporter is an On-/Off-state reporter system in which recombination upon 4-OHT exposure only occur in cells that produce CreERT2 at levels above certain threshold. Each sphere represent a cell. The position of the sphere in the Y axis indicates the production levels of CreERT2 recombinase (Wnt activation levels) of that particular cell. (A) Cell intrinsic recombination model. Green cells contain the appropriate Wnt/Rspo receptors for Wnt9b and Rspo3 synergy to occur. Black cells do not express the appropriate upstream signalling components and therefore they are not responsive to the treatment. Cells above the dash line recombine the reporter and are permanently labelled with tdTom. (B) Wnt activation levels are reflected by the Axin2CreERT2 reporter. This model assumes all cells are responsive to the treatment ta certain extent. When CreERT2 expression levels are above the magenta dash line, enough CreERT2 protein is produced to drive recombination of the reporter upon tamoxifen induction. When CreERT2 expression levels are below the blue dash line, there is not enough CreERT2 protein available to drive the recombination of the reporter. Cells expressing CreERT2 at levels between the magenta and blue dash lines are within the recombination threshold and therefore can undergo or not recombination. Recombination within the "recombination threshold" is subjected to other cell intrinsic and extrinsic factors such as 4-OHT cell uptake or accessibility of the loxP sites in a given time. (1) In a Wnt-off state all cells do not express sufficient levels of CreERT2 recombinase for recombination to occur. (2) Wnt9b/Rspo3 treatment induce similar levels of Wnt activation in the pool of cells however only some of them reach expression levels within the recombination threshold. (3) Exposure to "high Wnt" medium (5% Wnt3a, 100 ng/ml Rspo1) causes a similar increase in Wnt activation levels in all cells. Most of the cells express CreERT2 recombinase at levels above the magenta dash line and only a few within the recombination threshold.

As mentioned earlier, exposure to Rspo3 alone did not activate the Axin2CreERT2

reporter at any concentration in PH 2D cultures. This contrast with the results presented in Chapter 3, which showed that Rspo3 was sufficient to activate the TCF-Luc and the TCF-eGFP reporter in HEK293T cells. Unlike the binary Axin2CreERT2 reporter, the TCF-eGFP is a continuous reporter system. Thus, it is possible that Rspo3, in combination with Wnt proteins endogenously produced by PH cultured in monolayers, caused the activation of the Wnt/β-catenin but not at sufficient levels to drive recombination and activation of the Axin2CreERT2 reporter.

Such an explanation does not, however, rest easily with the failure to see an Rspo3-dependent increase in Axin2 mRNA levels by RT-qPCR analysis. At least three additional alternative explanations for the discrepancies in Rspo3 activity between culture systems can be offered. First, it is possible that PHs cultured in conventional monolayers do not secrete Wnt ligands with canonical activity. Freshly isolated murine hepatocytes have been shown to express various Wnt ligands (Wnt2, Wnt4, Wnt5a, Wnt5b, Wnt9a, Wnt9b and Wnt11) of non-canonical activity [33]. Of those, at least Wnt9b in combination with Wnt4 or Wnt2 have been shown to activate Wnt/β-catenin signalling in HEK293 cells [149]. Further experiments are required to determine whether expression of Wnt ligands in hepatocytes persist upon conventional 2D culture and/or whether the combinatorial array of these activate the canonical branch of the Wnt signalling pathway.

Second, hepatocytes might not be equipped with the appropriate receptors to respond to Wnt ligands of hepatocellular source. In support of this, experiments conducted by Yang and colleagues using an Alb-Cre $Wls^{fl/fl}$ transgenic mouse model showed that Wnt proteins of hepatocellular do substantially contribute to zonation (see Chapter 1), suggesting that Wnt ligands secreted by the hepatocytes are not involved in hepatocyte-to-hepatocyte Wnt/β-catenin signalling [90].

Third, hepatocytes might loss the expression of Wnts upon 2D culture. In future investigations, it might be possible to address whether these are valid explanations.

4.3.3 RT-qPCR gene expression analysis of pericentral metabolic genes

One of the main objectives of this chapter was to assess whether Wnt pathway activation was sufficient to induce the expression of pericentral metabolic genes in PHs 2D cultures. Out of the four β-catenin pericentral genes tested (Axin2, Cyp1a2, Glul and Cyp2e1), none of them was differentially expressed upon exposure to Wnt9b or Rspo3 alone and only Axin2 and Cyp1a2 were significantly increased upon concomitant exposure to Wnt9b and Rspo3. The fact that Glul and Cyp2e1 expression levels remained unaffected upon Wnt9b and Rspo3 co-treatment might be for several reasons. For instance, it is possible that a combination of Wnt9b and Rspo3 are not sufficient to drive the expression of these genes and/or other factors besides Wnt activation are essential for the expression of these genes. Alternatively, it has also been discussed earlier that PHs cultured in conventional 2D monolayers undergo a series of tissue culture adaptations that involve the rearrangement of protein subcellular localization and changes in the overall transcriptome of the cells. Therefore, another factor to consider is that the current 2D culture conditions might not be permissive for the biological responses that resemble the *in vivo* situation. As these genes will be also included in the gene expression panel for the characterization of the Wnt response of BD and PH organoids in Chapter 5, a consideration to the possible co-regulatory mechanisms driving the expression of these genes together with and/or importance of the physiological states of the cultures to obtain a biological response that resemble the in vivo situation will be provided later in this thesis.

4.3.4 Response to immobilized Wnt9b and Rspo3

Results from Chapter 3 showed that both Wnt9b and Rspo3 beads induced canonical Wnt signalling in HEK293T cells expressing the TCF-Luc reporter. However, in the current chapter, only the Rspo3 beads were shown to activate the Axin2CreERT2 reporter in PH 2D cultures. As discussed earlier (see section 4.3.2), this inconsistency in Wnt9b-beads activity across culture systems could be attributed to the differences in the mode of activation between the Axin2CreERT2 (On/Off state reporter) and the TCF-Luc system (continuous reporter). Regardless whether this is the underlying cause, the most important implication of these results is that Wnt9b beads may not be the most optimal strategy to induce local activation of the Wnt/β-catenin pathway in hepatocyte culture systems and thereby, the use of Rspo3 beads in combination with soluble Wnt9b is recommended.

4.3.5 Summary

The current chapter aimed to characterise PH 2D cultures and determine whether Wnt9b and Rspo3 activate canonical signalling in this *in vitro* system. In agreement with previous reports, PH cultured in 2D monolayers were found to be a dynamic system of study in which cells undergo major structural and gene expression changes in a short period of time. In this *in vitro* system, a combination of soluble Wnt9b and Rspo3, but not the individual ligands, induced activation of Wnt/β-catenin signalling as shown by activation of the Axin2CreERT2 reporter in PH as well as an increase in the gene expression levels of Axin2 and Cyp1a2. Immobilized Rspo3 in combination with soluble Wnt9b triggered the activation of the Axin2CreERT2 reporter. The canonical activity of Wnt9b beads in combination with soluble Rspo3 could not be validated in this system.

In summary, the results of this chapter indicate that Wnt9b in the presence of Rspo3 ligand can exert canonical activity in cellular context of the hepatocytes and that Rspo3 beads in combination with soluble Wnt9b might be a valid strategy to induce local activation of β-catenin in hepatocyte cultures.

Chapter 5. CHARACTERIZATION OF LIVER ORGANOIDS SYSTEMS AND EVALUATION OF THEIR SUTABILITY AS MODELS FOR ZONATION

The second main objective of this thesis was to evaluate the suitability of the currently available liver organoid platforms (BD and PH organoids) as cell source to model Wnt-driven liver zonation (see Chapter1). This chapter will describe the establishment and characterization of the two-homeostatic liver organoid platforms available during the completion of this thesis and dissect their responses to Wnt activation.

Carmen Velasco Martinez and Michael Dawes, a visiting BSc student and a MRes student, respectively, working under my supervision significantly contributed to the generation of some of the data presented in this chapter and will be acknowledged where appropriate.

5.1 Introduction

As introduced in Chapter 1, organoid technology attempts to satisfy two historical needs in liver *in vitro* modelling (1) the expansion of the biological material for an indefinite period of time and (2) the maintenance of hepatocyte cell identity, polarity and function in culture.

Currently, two different strategies have been developed for the generation of liver organoids using adult biological material. BD organoids introduced by Huch and colleagues in 2013 uses HPCs derived from the liver's biliary epithelium as a cell source to initiate the system [89]. HPCs are bi-potent epithelial cells that arise in response to liver damage and have been postulated to give rise to both hepatocytes and BECs *in vivo* (see Chapter1) [89]. When cultured in 3D hydrogels, these biliary-derived cells grow in organoids that can be indefinitely expanded over the long-term and differentiated towards hepatocyte fate [89].

More recently, two protocols (Hu et al. (2018) protocol and Peng et al. (2018) protocol) from different laboratories described the generation of liver organoids using PHs as organoid initiating cell type [3,4]. Both protocols used a medium composition that allow the long-term expansion (> 6 months), therefore, overcoming a previously described limitation reported by other groups that have attempted to generate 3D PH cultures. However, only the Peng et al. (2018) provides a second 'differentiation' medium composition that was argued to bring the cells to the non-proliferative 'resting' state of the hepatocytes in the homeostatic liver (see Chapter1). For this reason, the Peng et

al. (2018) was felt to be more attractive for the aim of recapitulating homeostatic Wnt-driven zonation *in vitro* and will be later discussed in this chapter.

In the adult liver, Wnt activation drives two hepatocellular responses. In the homeostatic organ, Wnt pathway activation is restricted to pericentral hepatocytes and drives the expression of metabolic genes [166]. Upon liver damage, however, Wnt signalling orchestrates hepatocyte proliferation and regeneration of the liver parenchyma. Despite of the increasing popularity of the hepatic organoids, little is known about organoid responses to Wnt activation.

In this chapter, I aimed to determine whether liver organoids can serve as a cell platform to recapitulate Wnt-driven zonation *in vitro*. As two promising protocols were available during the completion of this project, the response of both BD and PH organoids to the central vein ligands Wnt9b and Rspo3 was evaluated. This chapter will therefore begin with a description of the characterization of both hepatic organoid systems and an evaluation of their responses to Wnt activation. In addition, data from a comparative gene expression analysis between hepatic organoids and primary tissues will be described.

5.2 Results

5.2.1 Establishment of PH organoid cultures

PH organoid cultures were established from murine PHs isolated using a two-step perfusion method (see Chapter 4, section 4.2.1) and cultured following the two-step protocol previously published by Peng et al. (2018) (Figure5.1, A) [3]. In this protocol, PH organoids are first generated and expanded in a TNFα-containing medium (PHorg expansion medium or PHorg-EM) that mimics the pro-inflammatory microenvironment of the regenerative liver and maintains the cells into a hyperproliferative state. Established PH organoids are then exposed to one of the two distinct differentiation medium formulations

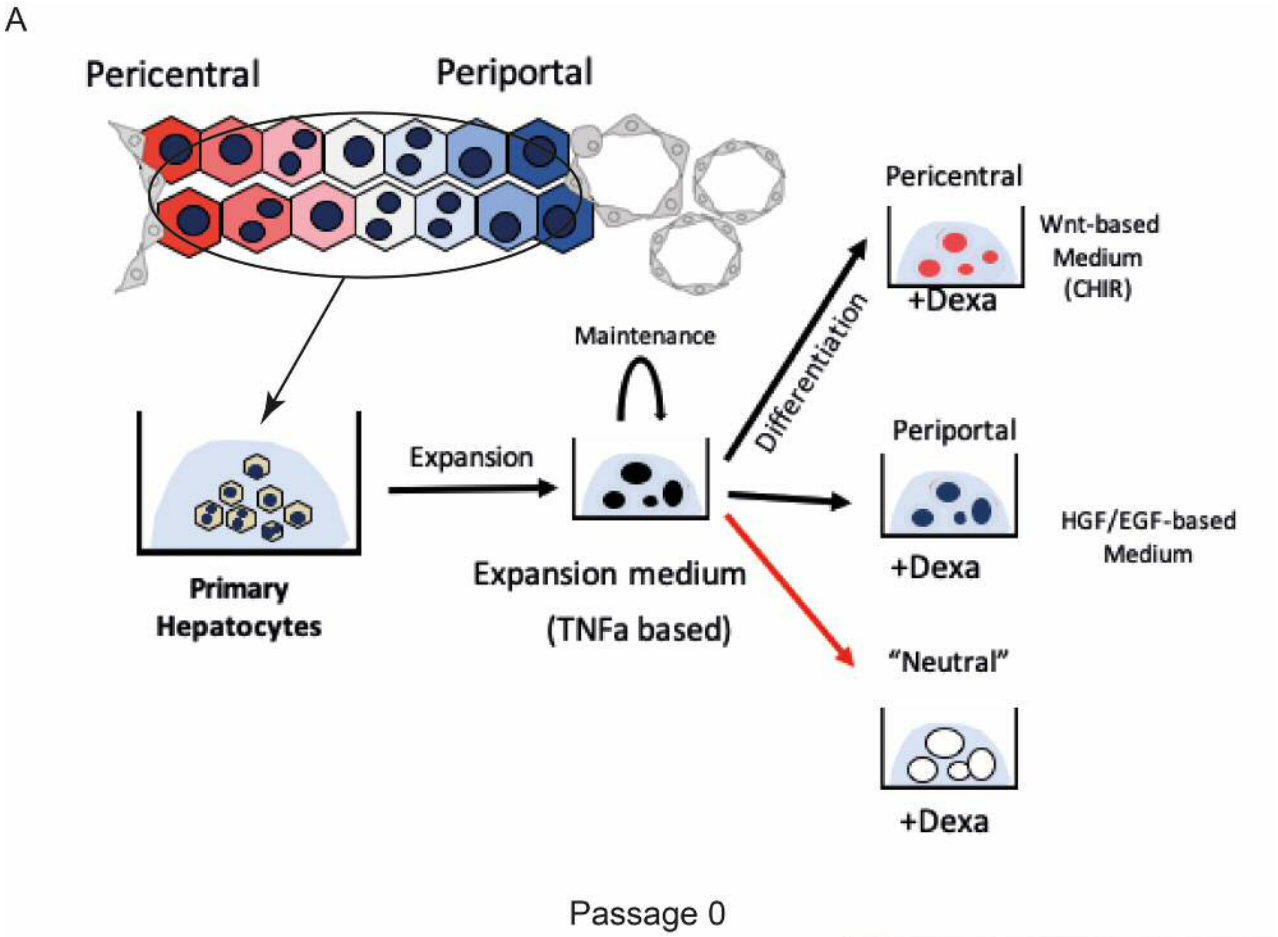
A
Pericentral
Periportal
Pericentral
Wnt-based
Medium
(CHIR)
+Dexa
Maintenance
Differentiation
Expansion
Periportal
+Dexa
HGF/EGF-based
Medium
Primary
Hepatocytes
Expansion medium
(TNFa based)
"Neutral"
+Dexa
Passage 0
B
50 µm
Day 0
50 µm
Day 3
50 µm
Day 7
100 µm
Day 13
C
Passage >2
Expansion Media
(TNFa based)
Wnt (CHIR)
Differentiation Media
EGF/HGF
Differentiation Media
Differentiation Media
(neutral)
100 µm
100 µm
100 µm

Figure5.1 (A) Scheme representing the process of establishment and culture of PH organoids. PH organoids are originated from PH cultured in Matrigel and can be expanded in culture in "expansion medium" containing TNFα. According to Peng et al (2018), upon removal of TNFα and addition of 3 μM of dexamethasone (Dexa) PH can be differentiated towards hepatocyte pericentral fate (CHIR containing medium) or periportal fate (EGF/HGF containing medium). Additionally, PH organoids in this thesis were also differentiated using a "Neutral" differentiation medium in which TNFα has been depleted and 3 μM of dexamethasone added but that does not contain either of the zonal inducers (CHIR, EGF nor HGF). (B) Representative images showing 3D culture adaptation of PH. Black arrowheads point to cell-cell junctions form between adjunct hepatocytes. White arrowhead point to cells acquiring bunch of grapes-like invasive phenotype. (C) Representative images of PH organoids adapted to 3D culture and expanded above two passages. Organoids in expansion medium show bunch of grape morphology. Four days differentiated organoids display a round and compact morphology. Scale bar 100 μm. These particular images were taken by Michael Dawes.

that promotes maturation into 'pericentral-like' or 'periportal-like' organoids. The pericentral differentiation medium is a 'Wnt-activating' medium that contains CHIR99021 (CHIR PHorg-DM), a GSK-3 inhibitor. By contrast, the periportal differentiation medium is a 'Ras-pathway activating' medium which contains EGF and HGF (EGF/HGF PHorg-DM). Both periportal and pericentral differentiation conditions differ from the expansion formulation in that they contain dexamethasone, a glucocorticoid widely used in the liver field to enhance the metabolic activity of hepatocyte cultures (Figure5.1, A) [167-169]. Furthermore, pro-inflammatory cues (TNFα) present in expansion are withdrawn in during differentiation. In addition to the pericentral and periportal differentiation conditions of Peng et al. (2018), PH organoids in this thesis were also differentiated in a third medium composition, referred as "Neutral PHorg-DM", that contained the common ingredients of both periportal and pericentral PHorg-DMs, but lacked the zonal-specific inducers (CHIR and EGF/HGF, respectively) (Figure5.1, A). A table with the detailed composition of PHorg-EM and each of the PHorg-DM used in this thesis can be found in Chapter2.

PH organoid cultures in PHorg-EM and PHorg-DM conditions were first established and characterised both morphologically and by RT-qPCR [3]. During the first three days of culture following seeding of PH in matrigel, some cells migrated to the bottom of the plate, where they attached and adopted a fibroblast-like morphology characteristic of PH 2D cultures (see Chapter2) (Appendix B, Figure1, A). PHs that remained embedded in matrigel lost their characteristic post-seeding round

morphology and aggregated with the neighbouring cells to generate small compact organoid like-structures which continued growing, likely through cell division, in the subsequent days (Figure5.1, B Day0). Some of the 3D organoid structures formed contained cells with large cytosolic inclusions (Figure5.1, B Day3). At day 13-15, cells within some the organoids acquired an 'invasive' phenotype and commenced to grow towards the matrigel, which caused the transition from a 'compact-round shape' to a 'bunch-of-grapes' organoid morphology (Figure5.1, B Day13).

After the second passage, the organoid cells lost the cytosolic inclusions and most of the PH organoids grown in PHorg-EM had acquired a 'bunch-of-grapes' morphology. On very rare occasions, PH organoids developed into a morphology that resemble duct-like structures (Appendix B, Figure1, B) (Figure5.4, C). Consistent with previous observations, PH organoids were routinely passaged at 1:2 ratio every ~2 weeks [3]. Exposure to any of the three PHorg-DM conditions tested (CHIR, EGF/HGF or Neutral), caused a notable change in morphology in which most of the organoids acquired again a compact-round morphology (Figure5.1, C). Furthermore, upon differentiation, PH organoids became optically dense and in some instances cells developed large cytosolic inclusions (Figure5.1, C).

RT-qPCR gene expression analysis revealed that PH organoid differentiation was accompanied by a gain in expression of genes associated with mature hepatocyte function (Figure5.2, B). Confirming the observations of Peng et al. (2018), PH organoids cultured in EGF/HGF PHorg-DM expressed higher levels of periportal genes (Ass1, Cyp2f2 and Alb) than organoids maintained in EM for the same length of culture (Figure5.2, B) [3]. Similarly, CHIR PHorg-DM organoids expressed, with the exception of Glul, higher mRNA levels of pericentral genes (Cyp1a2, Cyp2e1 and Fah) when compared to PHorg-EM organoids

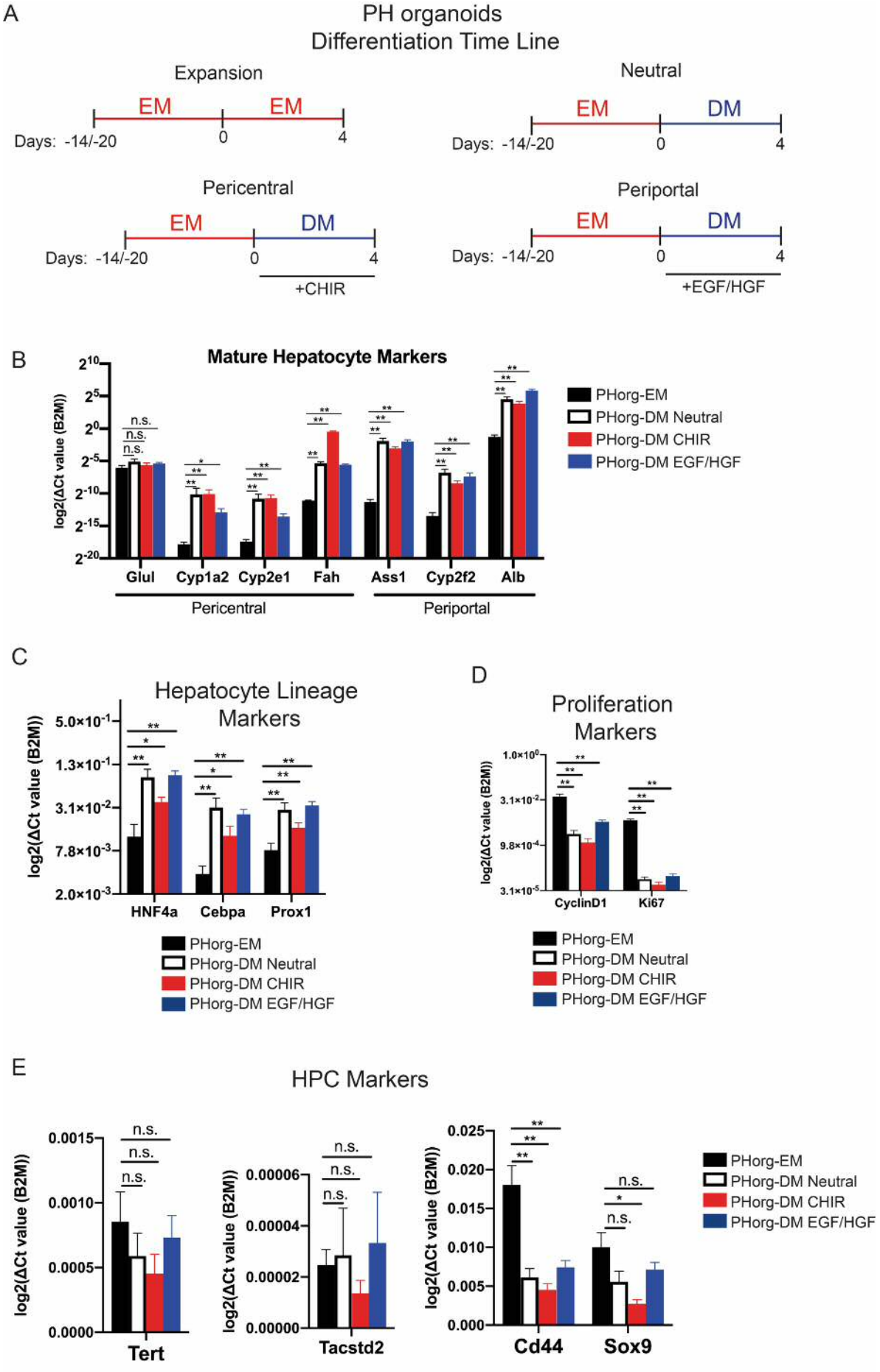
A
PH organoids
Differentiation Time Line
Expansion
EM
EM
Days: -14/-20
0
4
Neutral
EM
DM
Days: -14/-20
0
4
Pericentral
EM
DM
Days: -14/-20
0
4
+CHIR
Periportal
EM
DM
Days: -14/-20
0
4
+EGF/HGF
B
Mature Hepatocyte Markers
log2(ΔCt value (B2M))
Glul
Cyp1a2
Cyp2e1
Fah
Ass1
Cyp2f2
Alb
Pericentral
Periportal
PHorg-EM
PHorg-DM Neutral
PHorg-DM CHIR
PHorg-DM EGF/HGF
C
Hepatocyte Lineage Markers
log2(ΔCt value (B2M))
HNF4a
Cebpa
Prox1
PHorg-EM
PHorg-DM Neutral
PHorg-DM CHIR
PHorg-DM EGF/HGF
D
Proliferation Markers
log2(ΔCt value (B2M))
CyclinD1
Ki67
PHorg-EM
PHorg-DM Neutral
PHorg-DM CHIR
PHorg-DM EGF/HGF
E
HPC Markers
log2(ΔCt value (B2M))
Tert
Tacstd2
Cd44
Sox9
PHorg-EM
PHorg-DM Neutral
PHorg-DM CHIR
PHorg-DM EGF/HGF

Figure5.2 (A) PH organoids differentiation time line scheme. (B) RT-qPCR gene expression analysis of mature functional hepatocyte markers in PH organoids (n=5). (C) RT-qPCR gene expression analysis of hepatocyte lineage markers in PH organoids (n=5). (D) RT-qPCR gene expression analysis of HPCs markers in PH organoids upon differentiation. (n=5). Statistical significance was determined using Mann-Whitney t-test. p-value n.s.>0.05 ; p-value *< 0.05; p-value **< 0.01; p-value ***< 0.001; p-value ****< 0.0001. RT-qPCR experiments were run by Michael Dawes although data analysis, presentation and interpretation was performed by myself.

(Figure5.2, B). However similar periportal and pericentral gene expression induction was also achieved when organoids were cultured in Neutral PHorg-DM, suggesting that withdrawal of TNFα and the addition of dexamethasone were responsible for most of the transcriptional changes reported (Figure5.2, B). When comparing the ability of EGF/HGF and CHIR PHorg-DMs to specifically drive pericentral or periportal signatures, EGF/HGF treatment caused an overall trend of increased periportal gene expression although, out of the three periportal genes tested only Alb was induced in a statistically significant manner. Similarly, CHIR treatment, caused an overall increase in the expression of pericentral genes although only induction of Fah was statistically significant (Appendix B, Figure2).

Peng et al. (2018) PHorg-EM conditions were proposed to mimic the pro-inflammatory microenvironment of the regenerative liver [3]. During liver regeneration, hyperproliferative hepatocytes transiently downregulate the expression of hepatocyte lineage genes [170,171]. Therefore, I next questioned whether differentiation of PH organoids caused an increase in the expression of hepatocyte lineage whilst decreasing the levels of genes involved in cell proliferation. As expected, the three PHorg-DM formulations tested significantly increased the expression of the hepatocyte lineage markers Hnf4a, Cebpa and Prox1 (Figure5.2, C). Furthermore, exposure to neutral, CHIR or EGF/HGF PHorg-DMs significantly decreased the expression of the proliferation markers CyclinD1 and ki67 (Figure5.2, D).

Under certain injury conditions, regenerative hepatocytes ectopically express HPC markers. Therefore, to further characterise the PH organoid system, the gene expression of the HPCs related genes Tert, Tacstd2, Cd44 and Sox9 was evaluated. Whilst non-significant differences were found in the expression of Tert and Tacstd2 upon differentiation with any of the PHorg-DM formulations tested (Figure5.2, E), the

three PHorg-DMs caused a significant decline in the expression levels of Cd44 (Figure5.2, E). A decline in Sox9 expression was also observed in the three PHorg-DM mediums tested although this was only significant in CHIR PHorg-DM conditions (Figure5.2, E).

Taken together these results suggest that the protocol of Peng et al. (2018) for the expansion and differentiation of PH organoids was successfully implemented and that the structures observed resembled those previously published [3].

5.2.2 Establishment of BD organoid cultures

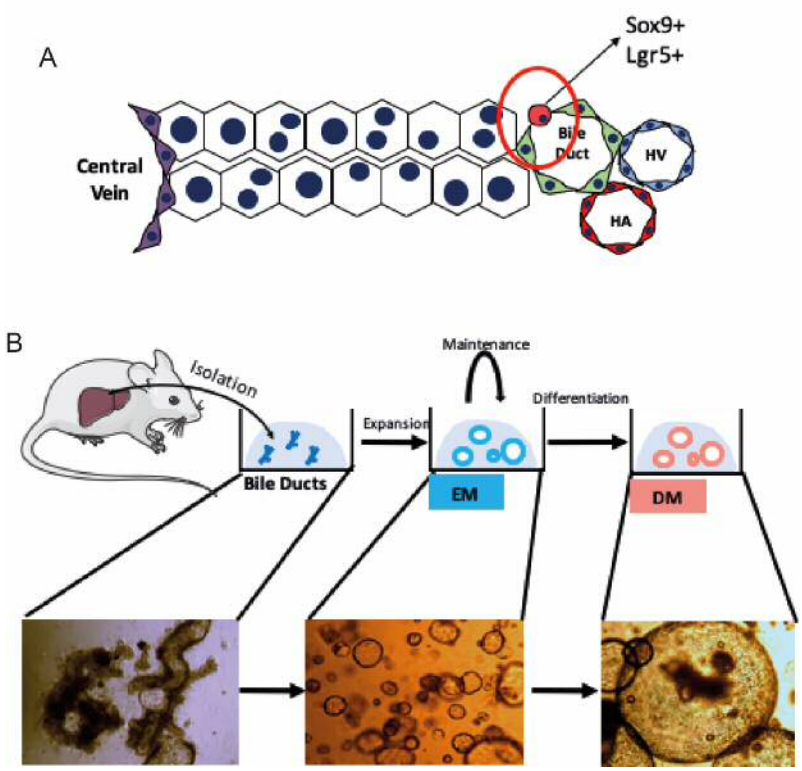

Figure5.3 (A) Scheme deciphering the structure of the mammalian lobule where the central vein (purple cells), the hepatocytes (white cells), the hepatic vein (HV, blue cells), the hepatic artery (red cells) and the cholangiocytes (green cells) have been highlighted. According to Huch et al. (2013), bile duct-resident HPSCs (red circle) are the cell of origin of bile duct-derived organoids. HPSCs are positive for the expression of Sox9 and Lgr5. (B) Scheme deciphering BD-establishment procedure with representative images of cells in each of the steps. EM, Expansion medium. DM, differentiation medium.

BD organoid cultures were established from hand-picked ductal 'tree' structures. Consistent with previous observations, BD embedded in matrigel rapidly enlarged to form cystic organoid-like structures and could be consistently passaged when cultured in in expansion medium (BDorg-EM) at a 1:5 or 1:8 by mechanical disruption (Figure5.3) [89].

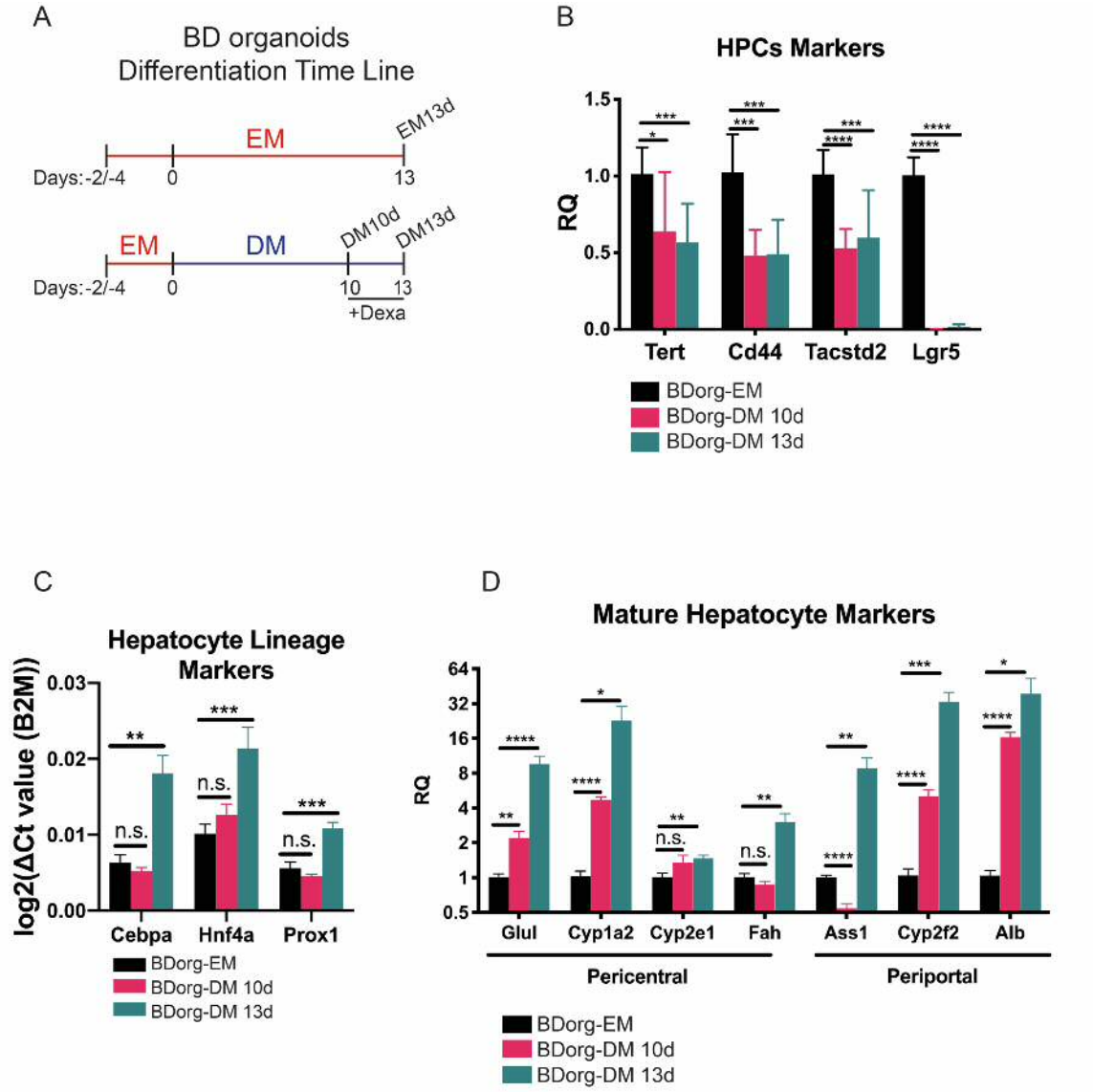

Figure5.4 (A) BD organoids differentiation time line scheme. (B) RT-qPCR gene expression analysis of HPCs markers in BD bile duct organoids upon differentiation. (n=9) (C) RT-qPCR gene expression analysis of hepatocyte lineage markers in BD organoids (n=9). (D) RT-qPCR gene expression analysis of mature functional hepatocyte markers in BD organoids (n=6). Expansion medium (EM); differentiation medium day 10 (DM 10d); differentiation medium day 13 (DM 13d). Statistical significance was determined using multiple t-test. p-value n.s.>0.05 ; p-value *< 0.05; p-value **< 0.01; p-value ***< 0.001; p-value ****< 0.0001.

In order to determine whether the BD organoids used in this thesis resembled those of Huch et al. (2013), BD organoid cultures were characterised and compared to the previously published data [89]. BDorg-EM is a Rspo1-containing medium that maintains the cells into a HPC-like state [89]. Withdrawal of Wnt-activating signals from the media together with inhibition of TGFβ and Notch pathway was shown to induce the differentiation of the BM organoids towards a hepatocyte fate [89].

Accordingly, differentiated BD organoids showed lower expression of HPCs markers (Tert, Cd44, Tacstd2 and Lgr5) and higher expression of hepatocyte lineage markers (Cebpa, Hnf4a and Prox1) than BD organoids in expansion conditions (Figure 5.4, B and C) [89]. Exposure to differentiation conditions also caused an increase in mRNA

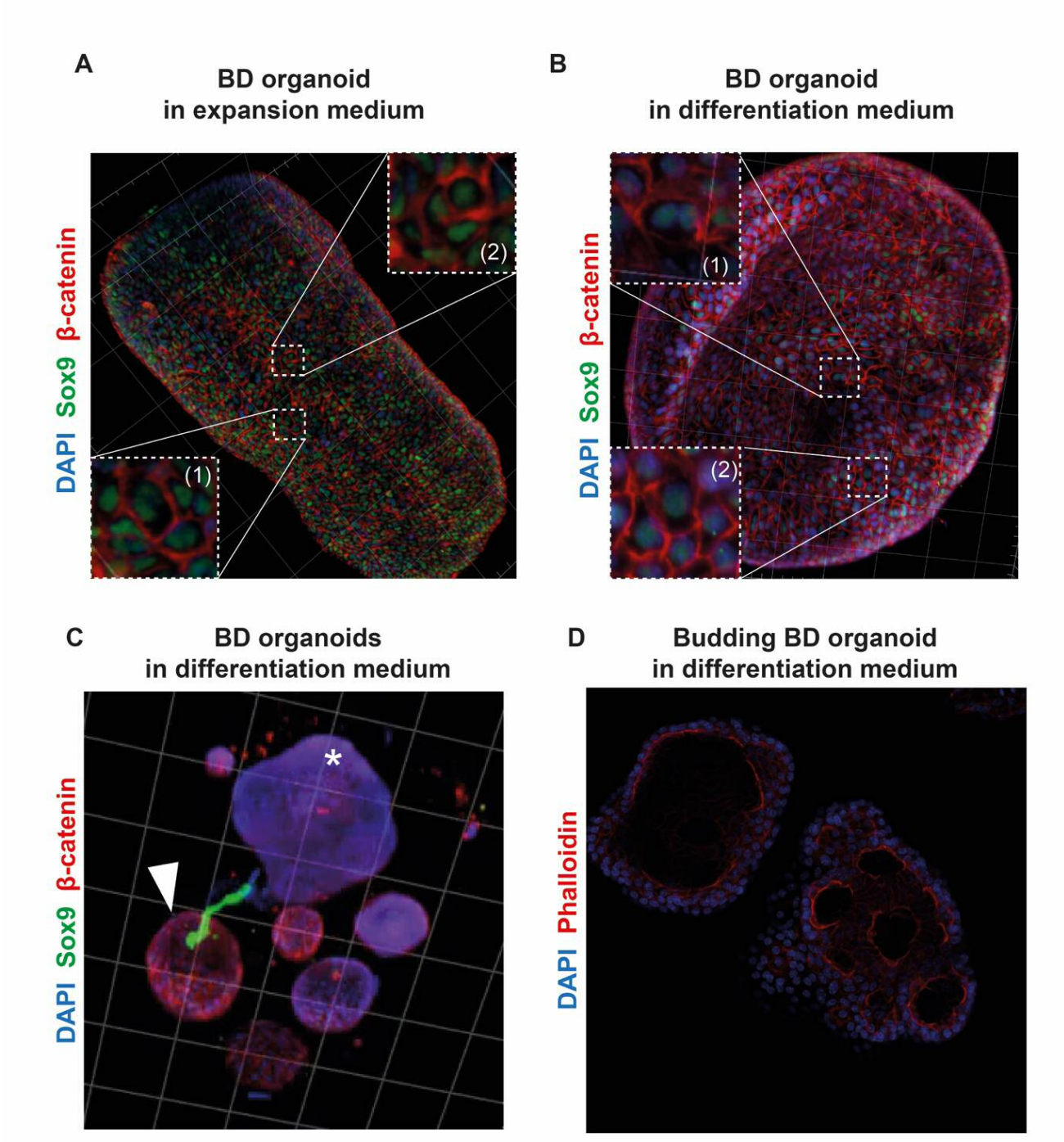

Figure5.5 (A) Light-sheet immunofluorescence image shows that BD organoids cultured in EM for 15-day harbours both (1) bi-nucleated and (2) mono-nucleated cells. β-catenin (red) staining labels cell-cell boundaries and DAPI (blue) stains cell nuclei. Green staining corresponds to Sox9, a transcription factor that is associated both with stem cell function and the ductal lineage. The sides of each of the squares of the grid correspond to 100 μm. (B) Light-sheet immunofluorescence image of a BD organoid differentiated for 13 days contain both (1) bi-nucleated and (2) mon-onucleated cells. β-catenin (red) staining labels cell-cell boundaries and DAPI (blue) stains cell nuclei. Green staining corresponds to Sox9, a transcription factor that is associated both with stem cell function and the ductal lineage. The sides of each of the squares of the grid correspond to 50 μm. (C) BD organoids differentiated for 13 days display different morphologies. Arrow head points to an example of a BD organoid presenting high-levels of membrane-bound β-catenin, enlarged cell nuclei and flat morphology. Asterisk points to an example of a budding-like BD organoid that additionally has low level of membrane-bound β-catenin and is composed by cells with small nuclei. Note that a correlation between these parameters (budding/flat phenotype, β-catenin intensity and nuclei size) was not found a priori although quantifications were not performed. Image was acquired in a commercial Z.1 Zeiss light-sheet microscope. The sides of each of the squares of the grid correspond to 100 μm. (D) Immunofluorescence confocal image shows an BD organoid that was differentiated for 13 days. In this extreme case of budding, the protrusions developed to the degree of dividing the organoid into small hollow cameras. Phalloidin (red) and DAPI (blue) counterstain the cell cytoskeleton and nuclei, respectively.

levels of various pericentral (Glul, Cyp1a2, Cyp2e1 and Fah) and periportal (Ass1, Cyp2f2 and Alb) metabolic genes characteristic of mature hepatocytes (Figure 5.4, D).

Differentiated BD organoids were previously described to contain bi-nucleated cells, a hallmark of differentiated hepatocytes. To assess whether this was the case, BD organoids were analysed by IF using DAPI to counterstain the cell nuclei and either phalloidin (cell cytoskeleton) or β-catenin staining to distinguish cell-cell boundaries. Whilst bi-nucleated cells were present in differentiated BD organoids, these were also present in organoid cultured in expansion conditions. Quantifications about the frequency in which bi-nucleated cells appear in both BDorg-EM and –DM were not performed (Figure 5.5, A and B). BD organoids in differentiation conditions were also found highly heterogeneous in terms of size and morphology (Figure 5.5, C). IF analysis revealed a large variation in β-catenin membrane levels amongst differentiated BD organoids that was not previously reported (Figure5.5, C).

As previously reported by Huch and colleagues, BD organoids cultured in both BDorg-EM and DM conditions were hollow structures composed of a single layer of cells [89]. In BDorg-DM conditions, some organoids presented budding-like protrusions and on rare occasions, such protrusions grew to the point of causing the division of the

organoid into small hollow compartments (Figure5.5, C and D). BD organoid budding was a phenomenon previously described by Huch et al. (2015) [172]. When monitoring organoid growth by DIC, BD organoid "budding" was found to be associated with the process of differentiation and became especially apparent during the last three days of culture (data not shown).

Taken together these results indicated that the protocol for expansion and differentiation of BD organoids could successfully be implemented and that the structures that had been grown resembled those previously published by Huch et al. (2013) [89].

5.2.3 Response of PH organoids to Wnt activation

Having established the culture PH organoids, the next step was to evaluate the response of this structures to Wnt9b and Rspo3. For this aim, PH organoids were generated from the Axin2CreERT2 reporter transgenic mouse model, in which Axin2 positive cells can be lineage traced upon 4-OHT exposure (see Chapter4). Using these PH organoids, Axin2 expressing cells (tdTom positive) were labelled and quantified at different times of culture when organoids were differentiated in the presence or absence of Wnt9b and Rspo3, alone or in combination. The timelines of these treatments and the 24h 4-OHT induction are shown in Figure5.6, A.

Confocal analysis revealed that at Day 1 of differentiation ~2-5% of the cells per organoid were scored as Axin2 expressing cells (tdTom positive) in all the differentiation conditions tested (Figure 5.6, B). From Day 1 to Day 4, organoids that had been differentiated in the presence of Wnt9b and Rspo3 in combination showed an increase in the percentage of tdTom positive cells per organoid when compared to PH organoids grown in Neutral conditions. By contrast, the percentage of tdTom positive cells in the rest of the PHorg-DM conditions tested decreased upon differentiation (Figure5.6, B). At Day 4 of differentiation, ~12% of the Wnt9b and Rspo3-treated organoid cells were labelled. No tdTom positive cells were detected in

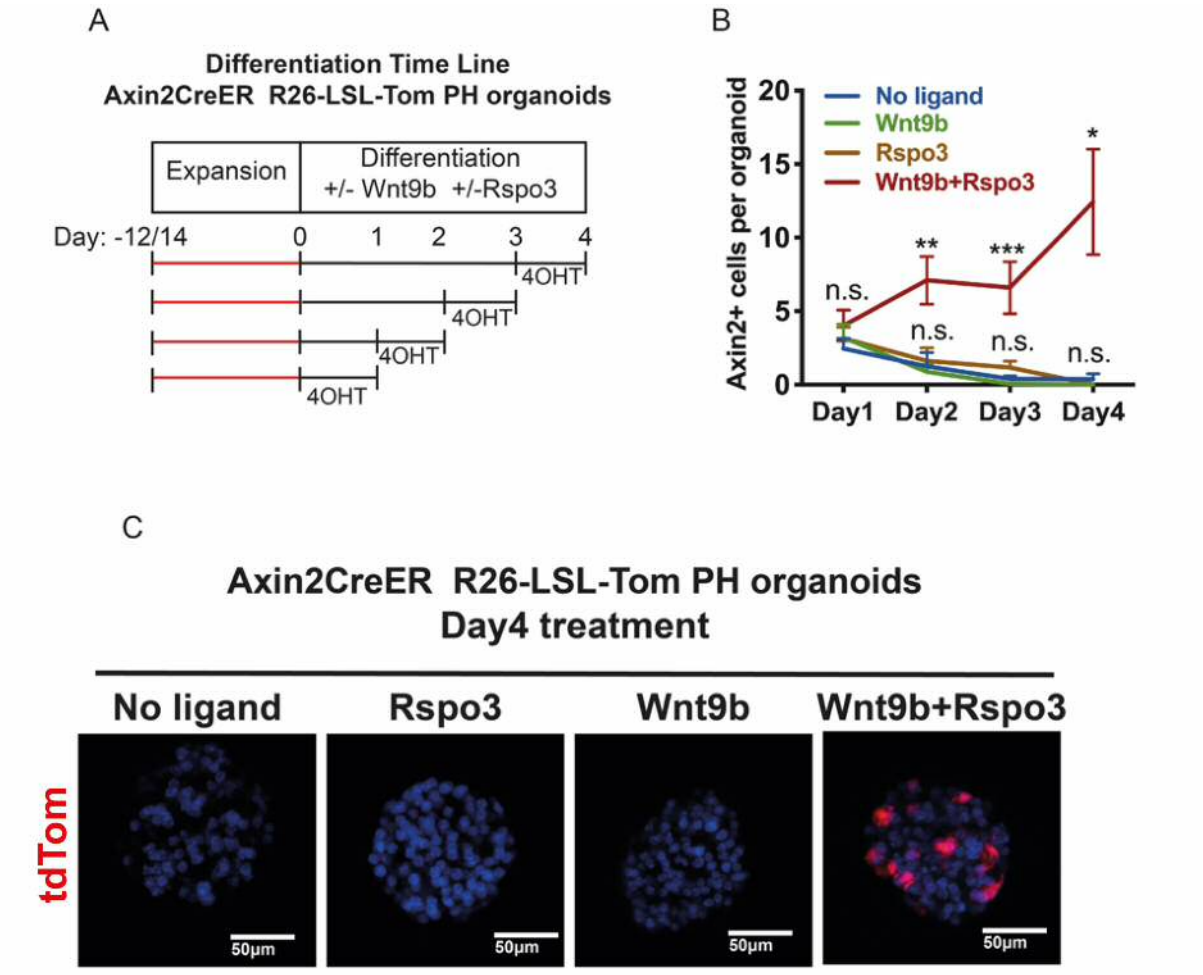

Figure5.6 (A) Axin2 lineage tracing strategy of PH organoids derived from the Axin2CreER R26-LSL-tdTom reporter mouse model. Axin2 expressing cells and their progeny are permanently labelled with red fluorescence (tdTom) upon 4OHT exposure. (B) Quantifications from Axin2 lineage tracing experiments in Axin2CreER R26-LSL-tdTom differentiated organoids shows a gradual increase in the proportion of tdTom positive cells only in Wnt9b and Rspo3 treated organoids. Statistical significance was determined using multiple t-test. p-value n.s.>0.05 ; p-value *< 0.05; p-value **< 0.01; p-value ***< 0.001; p-value ****< 0.0001 (C) Representative IF images from PH organoids differentiated for 4 days in the presence of Wnt9b/Rspo3 ligands. Organoids were exposed to 500nM 4-OHT during the last 24h of differentiation. Cell nuclei was counterstained with DAPI (blue). Axin2 expressing cells are labelled with red fluorescence (tdTom). Images show the presence of Axin2 expressing cells only in organoids concomitantly exposed to Wnt9b and Rspo3. Culture and treatment of organoids used for all experiments presented in this figure were done by Michael Dawes. Imaging and quantifications of data presented here were also performed by Michael Dawes. Experimental design and data presentation was performed by myself.

any of the other treatments, suggesting that Wnt9b and Rspo3 synergise in PH organoids to drive canonical Wnt pathway (Figure5.6, B and C).

Having validated the ability of the CV ligands Wnt9b and Rspo3 to activate canonical Wnt signalling in PH organoids, I next questioned whether the expression of pericentral metabolic genes was induced upon exposure to these ligands. For that aim, PH organoids were differentiated for 4 days in the presence/absence of Wnt9b and Rspo3 and subjected to RT-qPCR analysis. In addition, PH organoids differentiated using the original pericentral CHIR differentiation conditions of Peng et al. (2018) [3].

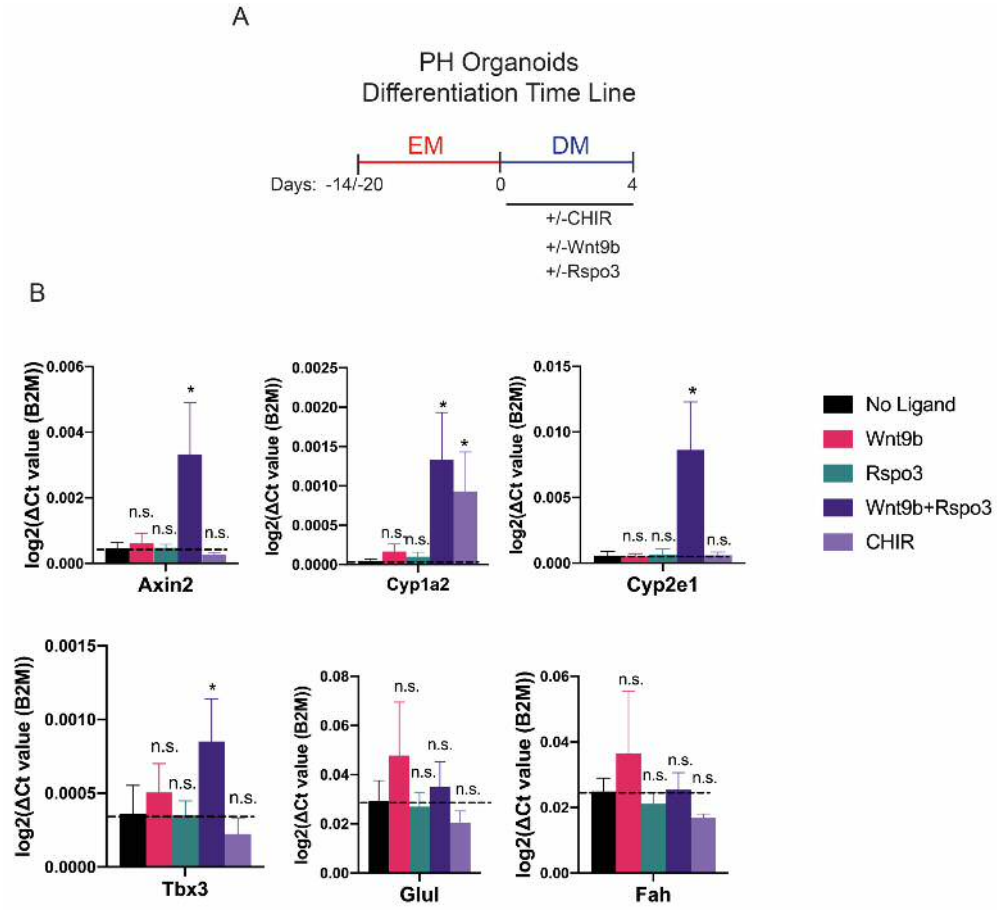

Figure5.7 (A) PH organoids differentiation time line scheme. (B) RT-qPCR gene expression analysis of pericentral metabolic genes in differentiated PH organoids (n=5). Statistical significance was determined using Mann-Whitney t-test. p-value n.s.>0.05 ; p-value *< 0.05; p-value **< 0.01; p-value ***< 0.001; p-value ****< 0.0001. RT-qPCR experiments were run by Michael Dawes although data analysis, presentation and interpretation was performed by myself.

CHIR differentiation caused a significant increase in Cyp1a2 levels but surprisingly did not increase the expression of any of the other pericentral genes tested including Axin2, a well conserved Wnt/β-catenin target gene across tissues (Figure5.7). Whilst

non-significant differences were either detected in the level of expression of Axin2, Cyp1a2, Cyp2e1 and Tbx3 when PH organoids were differentiated in the presence of Wnt9b or Rspo3 alone, a combination of Wnt9b and Rspo3 significantly increased the expression of these genes, indicating that Wnt9b and Rspo3 synergise to activate Wnt pathway targets and elicit a metabolic Wnt-driven response in PH organoids (Figure5.7). Interestingly, levels of expression of the pericentral genes, Glul and Fah remained largely unaffected when Wnt9b and Rspo3 were added alone or in combination during the differentiation process (Figure5.7).

The fact that some of the pericentral genes tested were induced upon exposure to the CV ligands Wnt9b and Rspo3 while others remained largely unaffected, prompted me to investigate whether these genes followed different expression patterns across the liver lobule. In 2017, Bahar Halpern and colleges used scRNAseq spatial

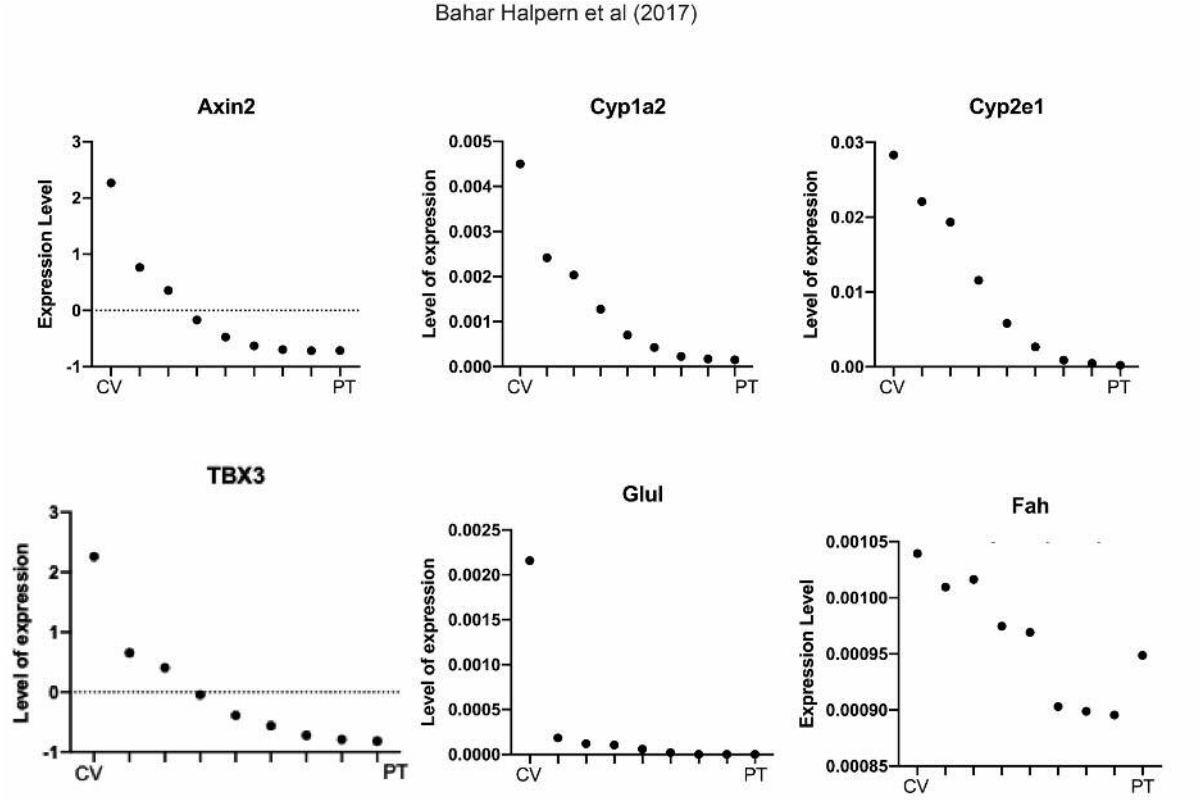

Figure5.8 Gene expression distribution of pericentral metabolic genes in the central vein (CV)- portal triad (PT) axis reveal that pericentral metabolic genes can be clustered in (1) genes that show a gradual decline in expression levels across the CV-PT axis of the liver (*Axin2, Cyp1a2, Cyp2e1* and *Tbx3*) and (2) genes that follow an expression patter other than a gradual decline (*Glul* and *Fah*). Data with hepatocyte scRNAseq transcriptomic profiles was obtained from Bahar Halpern et al (2017) {Halpern:2017fm}.

reconstruction to generate a 9-zone transcriptomic map of murine hepatocytes (see Chapter1) [33]. Using data from this study, I generated the zonal expression graphs presented in Figure5.8. This analysis confirmed that genes analysed were preferentially expressed by pericentral hepatocytes and revealed the potential clustering of the genes evaluated by RT-qPCR in two subgroups: (1) genes whose expression gradually decline across the CV-PT axis of the lobule (Axin2, Cyp1a2, Cyp2e1 and Tbx3) and (2) pericentral genes that follow an expression pattern other than a gradual decline (Glul and Fah) (Figure5.8). How these patterns might relate to differences in Wnt9b/Rspo3 treatment sensitivity will be discussed later.

Taken together, these results indicate that treatment of PH organoids with Wnt9b/Rspo3 recapitulated aspects of Wnt-driven metabolic zonation *in vitro*, but that expression of every Wnt-driven pericentral gene (most notably Glul, encoding GS) was not achieved with the current experimental conditions.

5.2.4 Response of BD organoid cultures to Wnt activation

Having successfully implemented the protocol for the expansion and differentiation of BD organoids from Huch et al. (2013) in section 5.3.2, the next step was to evaluate whether activation of Wnt pathway in BD organoids elicited a metabolic Wnt-driven response [89]. In section 5.3.3 the suitability of PH organoids as *in vitro* system to recapitulate Wnt-driven liver zonation was assessed by differentiating the organoids in the presence of Wnt9b and Rspo3. However, this approach could not be implemented in the case of BD organoids as withdrawal of Wnt-potentiating signals (Rspo1) from the medium is necessary to direct the cells towards a hepatocyte fate [173]. For that reason, to evaluate the suitability of BD organoids as *in vitro* system for modelling Wnt-driven liver zonation, BD organoids were first differentiated for 10 days in the absence of Wnt activating signals and then exposed for three days to Wnt9b and Rspo3 alone or in combination (Figure5.9).

All the treatments containing Rspo3, significantly increased Axin2 mRNA levels. However, no significant changes in the level of Glul, Cyp1a2, Cyp2e1 and Fah expression were detected with Rspo3 alone, or in combination with Wnt9b, indicating that whilst Rspo3 itself is sufficient to activate canonical Wnt signalling in BD organoids, this ligand does not elicit a pericentral metabolic program (Figure5.9).

Activation of the Wnt/β pathway in hepatocytes has been shown to antagonize the expression of periportal hepatocyte genes. Therefore, I next evaluated whether Wnt9b/Rspo3 treatment in BD organoids caused a decline in the expression of periportal genes (Ass1, Cyp2f2 and Alb). Non-significant change in the expression levels of these genes was observed upon exposure to Wnt9b and Rspo3, alone or in combination (Figure5.9).

With the exception of Axin2, none of the other periportal or pericentral genes was significantly altered upon treatment of Wnt9b and/or Rspo3 in BD organoids, suggesting that activation of Wnt pathway in these structures did not elicit a pericentral metabolic program (see Chapter4). Differentiated BD organoids are a dynamic *in vitro* system in which hepatocytes features are acquired for a period of 10 to 13 days. Thence, a possible explanation for the lack of a Wnt-induced metabolic response is that at the time of exposure to Wnt9b and Rspo3 (differentiation day 10) BD organoids did not display yet the mature hepatocyte Wnt/Rspo receptors that mediate the canonical synergy between Wnt9b and Rspo3. To explore this possibility, a BD organoid line from a Tet-O-ΔN89β-catenin mouse model was generated [120]. In the

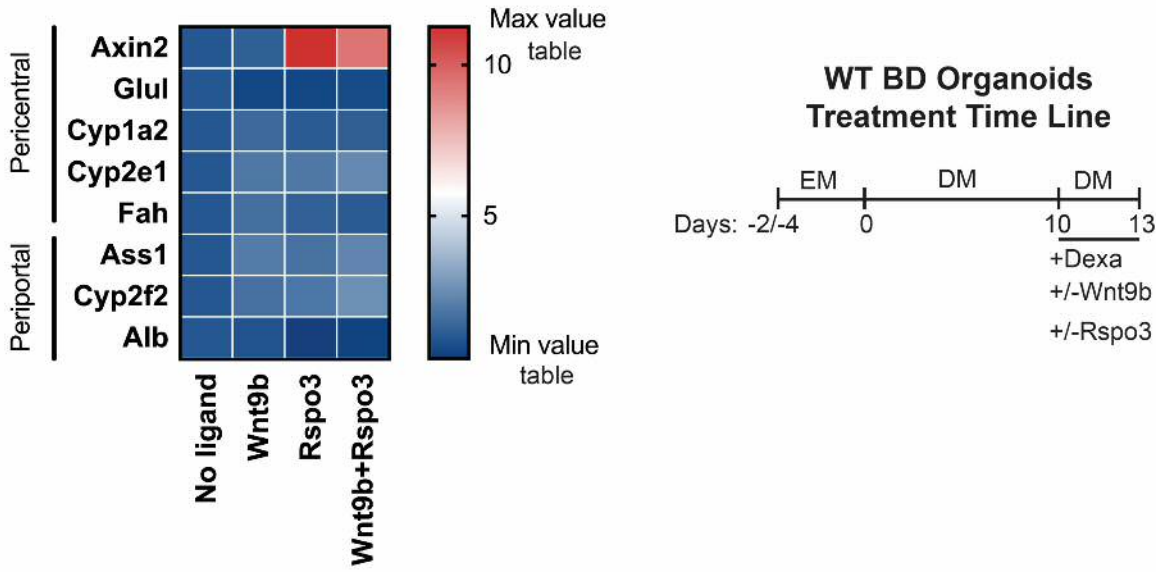

Figure5.9 Heat map showing RT-qPCR gene expression analysis of mature hepatocyte zonation markers in WT BD organoids upon exposure to Wnt9b (100 ng/ml) and or Rspo3 (50 ng/ml). All Rspo3 containing treatments trigger the expression of Axin2. (n=5)

Tet-O-ΔN89β-catenin organoid line expression of a constitutively active mutant β-catenin (ΔN89β-catenin; an N-terminal deletion of β-catenin including the destruction box) is induced upon doxycycline exposure. This allows the activation of the canonical branch of the pathway downstream of the receptors (Appendix B, Figure3, A).

The expression of the ΔN89β-catenin transgene was first confirmed to be induced in a doxycycline dose-dependent manner (Appendix B, Figure 3, B). As a robust increase the expression of ΔN89β-catenin transgene was detected following treatment for 3 days with 0.1 μg/ml doxycycline with no evidence of toxicity as shown by CellTox green and CellTiter-Glo 3D viability assays, this doxycycline concentration was subsequently used to assess the effects of β-catenin transcriptional activation in BD Tet-O-ΔN89β-catenin organoids (Appendix B, Figure 3, B to D).

Exposure of differentiated BD Tet-O-ΔN89β-catenin organoids to 0.1 μg/ml doxycycline for 3 days triggered a 100-fold increase of Axin2 mRNA levels (Figure5.10, B). Despite this robust increase in canonical Wnt signalling, none of the pericentral genes was significantly induced (Figure5.10, B). Furthermore, and with the exception of Alb that was significantly decreased, the expression of periportal genes remained also largely unaffected upon exposure to doxycycline when compared to the untreated controls (Figure5.10, B).

Canonical Wnt signalling elicits different cellular programs depending on the context, being Axin2 one of the few β-catenin target genes conserved across tissues. The fact that none of the pericentral hepatocyte-specific direct targets of β-catenin (Glul, Cyp1a2, Cyp2e1 and Fah) was induced upon robust activation of canonical Wnt signalling prompted me to investigate whether the increase in Axin2 levels in BD organoids was associated with a cellular program other than zonation.

In the regenerative liver, Wnt orchestrates hepatocyte proliferation and Wnt-activating signals (Rspo1) have been argued to maintain BD organoids in a proliferative state close to that of HPCs [89]. Thence, the expression of various proliferation and HPC markers after 3-day exposure to 0.1 μg/ml doxycycline in differentiated BD Tet-O-ΔN89β-catenin organoids was next evaluated. RT-qPCR analysis showed that various

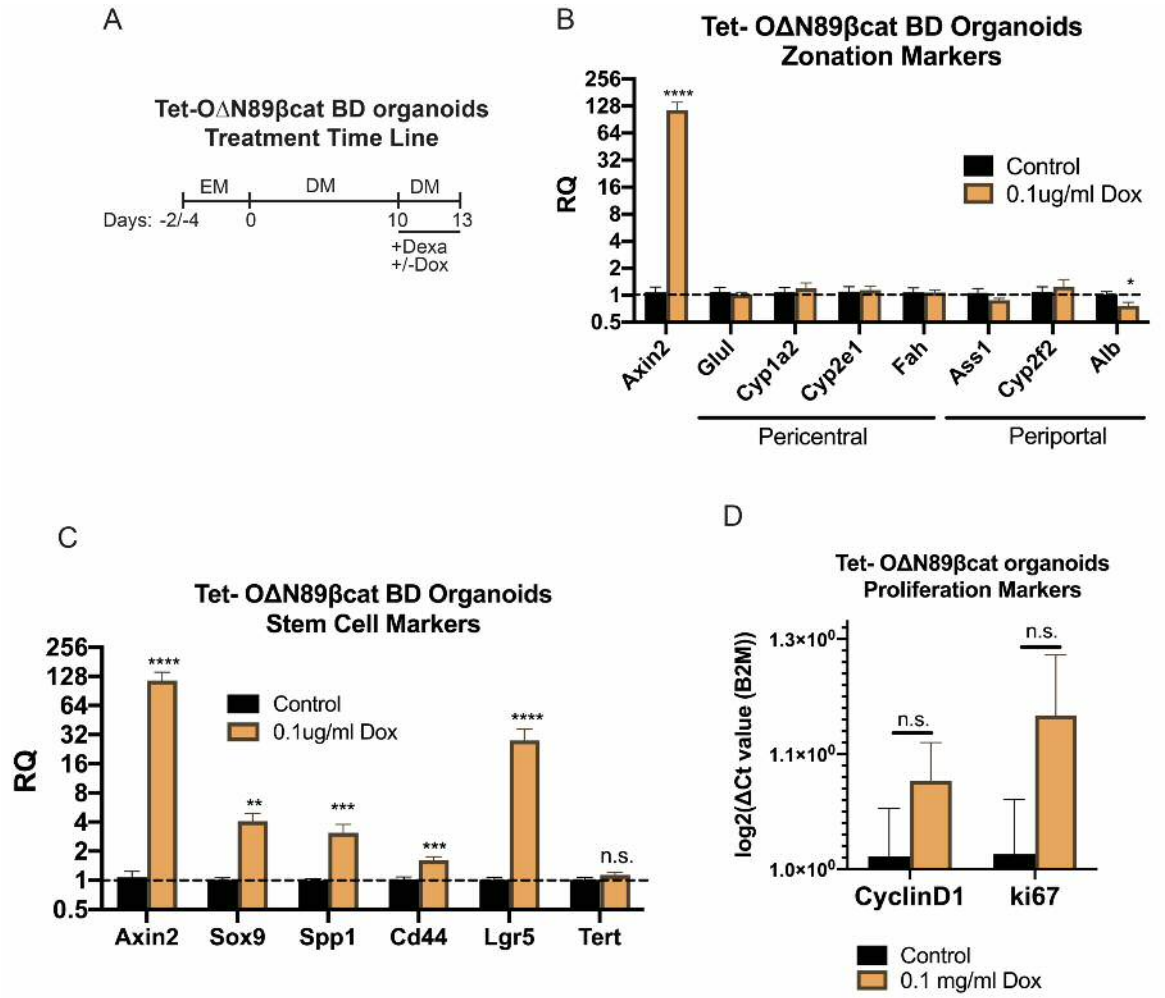

Figure5.10 (A) Treatment time line for Tet-OΔN89βcat BD organoids. Mutant activated β-catenin is expressed upon exposure to 0.1 mg/ml doxycycline (Dox) during the last three days of differentiation. (D) RT-qPCR gene expression analysis of mature hepatocyte zonation markers in OΔN89βcat BD organoids upon activation of mutant β-catenin (0.1 mg/ml Dox). (n=9). (E) RT-qPCR gene expression analysis of stem cell markers in OΔN89βcat BD organoids upon activation of mutant β-catenin (0.1 mg/ml Dox). (n=9). Statistical significance was determined using multiple t-test. p-value n.s.>0.05 ; p-value *< 0.05; p-value **< 0.01; p-value ***< 0.001; p-value ****< 0.0001. RT-qPCR experiments were run by Carmen Velasco. Data analysis, presentation and interpretation was performed by myself.

HPC (Sox9, Spp1, Cd44 and Lgr5) were induced upon β-catenin activation in differentiated BD organoids under these conditions (Figure5.10, C). Although an increasing trend in the levels of the proliferation markers cyclin D1 and ki67 was reported upon activation of the Wnt/β-catenin pathway, none of these genes were increased at significant levels upon exposure to 0.1 μg/ml doxycycline (Figure5.10, C).

In order to compare whether a HPCs and/or proliferation program was elicited upon canonical Wnt activation in other hepatocellular *in vitro* systems, a combination of Wnt9b and Rspo3 was used to activate β-catenin in PH 2D and PH organoid cultures and the expression of HPCs and proliferation markers was analysed by RT-qPCR. With the exception of *Lgr5*, none of the HPCs and proliferation markers evaluated were induced upon activation of canonical Wnt signalling in PH 2D cultures or PH organoids (Appendix B, Figure 4), suggesting that activation of the HPCs program by β-catenin is cell context-dependent and characteristic of BD differentiated organoids.

Taken together, these results indicate that BD organoids, under the current experimental conditions, cannot be used cellular platform to recapitulate Wnt-driven metabolic zonation *in vitro*.

5.2.5 Comparison of primary hepatocyte- and bile duct-derived organoids with primary tissue

To better understand the cell context that PH and BD organoids represent and why they behave differently to Wnt activation *in vitro*, differentiated PH and BD organoids were subjected to RT-qPCR gene expression analysis and compared with primary samples from the two epithelial lineages of the liver: fresh isolated PHs and primary BD trees. A panel of BECs (Hnf1b, Krt19, Krt7 and Epcam) and hepatocyte (Cebpa, Hnf4a and Prox1) lineage markers that could be used to validate the purity of the purified cell populations was first used to characterise the primary samples (Appendix B, Figure 5, A).

Upon differentiation, PH organoids increased the expression of the hepatocyte lineage markers, Cebpa, Hnf4a and Prox1 close to the levels expressed by PHs (Figure5.11, A). PH organoids both in expansion and differentiation conditions showed minimal expression of the BEC markers Krt19, Krt7 and Epcam (Figure5.11, A). The expression of the BEC lineage marker Hnf1b was however increased upon PH organoid differentiation, reaching similar levels to those present within hand-picked primary BD. These results suggest that differentiated PH organoids remain closer to

the hepatocyte lineage than the BEC lineage although the differentiation conditions might be permissive for the acquisition of certain features of BECs.

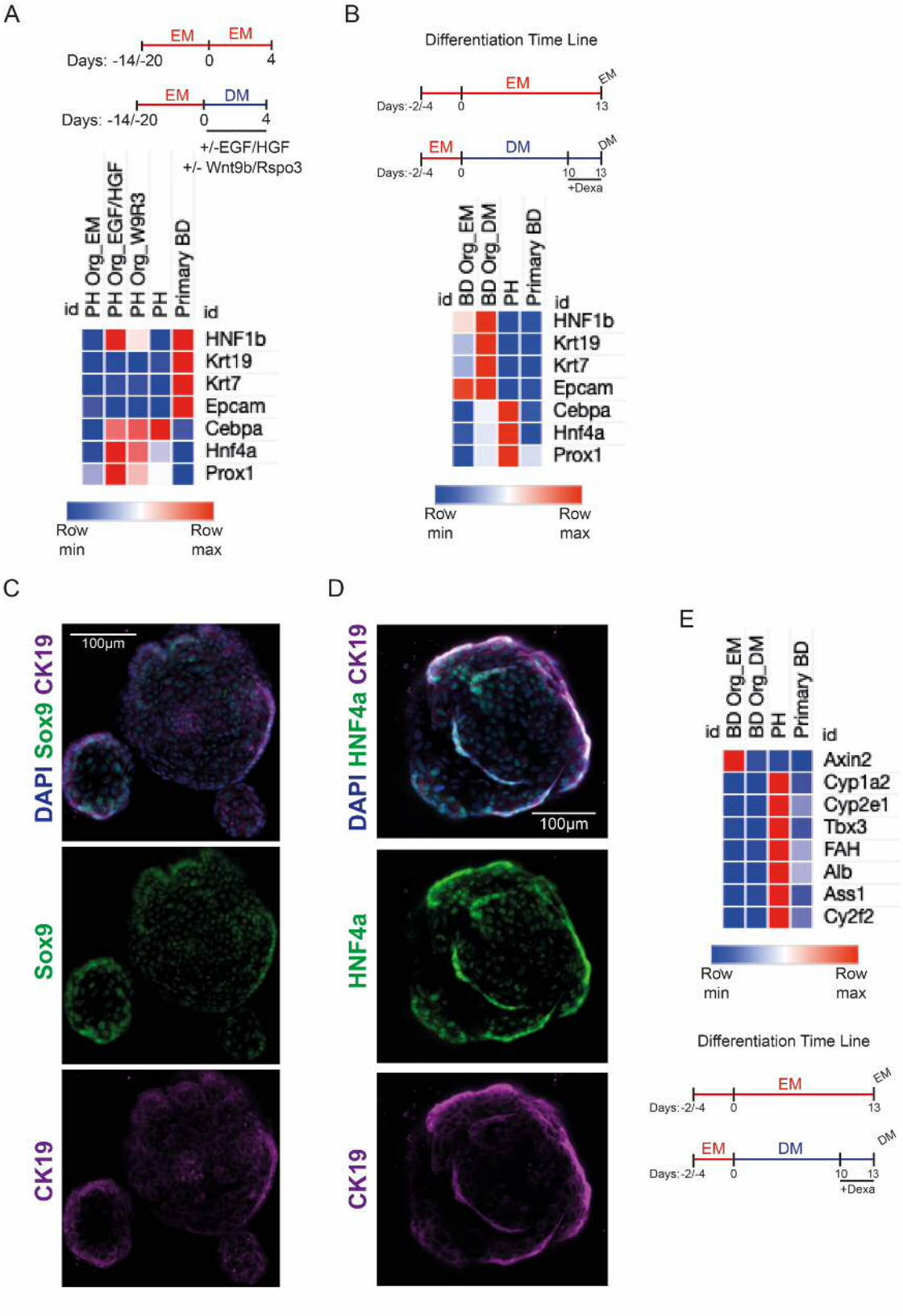

Figure5.11 (A) Heat maps showing relative RT-qPCR gene expression of BEC and hepatocyte lineage markers in primary hand-picked bile ducts (Primary BD) (n=3), primary hepatocytes (PH) (n=3) as well as in WT PH organoids in EM, EGF/HGF DM or Wnt9b/Rspo3 DM (n=5). RT-qPCR experiments performed with PH organoid samples were run by Michael Dawes. (B) Heat maps showing relative RT-qPCR gene expression of BEC and hepatocyte lineage markers in primary hand-picked bile ducts (Primary BD) (n=3), primary hepatocytes (PH) (n=3) as well as in WT BD organoids in EM or DM (B). (C) Representative IF images show that BD organoids express the bile duct markers CK19 (magenta) and Sox9 (green) at day 11 of differentiation. Cell nuclei was counterstained with DAPI (blue). (D) Representative IF images show that BD organoids express the bile duct markers CK19 (magenta) and HNF4a (green) at day 11 of differentiation. Cell nuclei was counterstained with DAPI (blue). (E) Heat maps showing relative RT-qPCR gene expression of BEC and hepatocyte lineage markers in primary hand-picked bile ducts (Primary BD) (n=3), primary hepatocytes (PH) (n=3) as well as in WT BD organoids in EM or DM.

Canonical Wnt pathway activation in differentiated BD organoids did not trigger the expression of zonation markers (see section 5.3.3.2) and therefore it was expected that their hepatocyte gene expression levels would be significantly different from homeostatic PHs. Differentiated BD organoids showed higher expression of the hepatocyte lineage markers Cebpa and Hnf4a in BDorg-DM than in BDorg-EM, although the expression of these genes did not reach the levels of PHs. Differentiated BD organoids were found to express higher levels of BECs lineage markers (Hnf1b, Krt19 and Krt7), probably reflecting that primary hand-picked primary BD preparations were contaminated with occasional hepatocytes or non-parenchymal cells other than BECs (Figure5.11, B) (Appendix B, Figure 5, B). Expression of the hepatocyte marker Hnf4a and the BEC markers Sox9 and CK19 (gene Krt19) at the protein level in differentiated BD organoids was further confirmed by IF (Figure5.11, C and D). These results suggest that, in addition to hepatocyte lineage markers, BD organoids strongly express markers of the BEC lineage.

Results from section 5.3.1 showed that BD organoids significantly increased the expression of various pericentral (Glul, Cyp1a2, Cyp2e1 and Fah) and periportal (Ass1, Cyp2f2 and Alb) metabolic genes characteristic of mature hepatocytes upon differentiation. However, data from Figure5.11 B argues that differentiated BD organoids are culture systems that remain close to the BEC lineage. Therefore, the next step was to investigate whether the reported increase in the level of expression of pericentral and periportal markers occurred on comparable levels with PHs. Data from Figure5.11 E shows that differentiated BD organoids express pericentral (Glul,

Cyp1a2, Cyp2e1 and Fah) and periportal (Ass1, Cyp2f2 and Alb) metabolic genes at comparable levels to primary BD but not PH. Altogether, these results suggest that differentiated BD organoids remain closer to the BEC lineage than the hepatocyte lineage although the current differentiation conditions might be permissive for the acquisition of hepatocyte-like features.

5.3 Discussion

5.3.1 Differentiated BD organoids as a hepatocellular model

In 2013, differentiated BD organoids presented as a possible therapeutic avenue toward regenerative therapy of the liver and a possible *in vitro* platform for drug testing. Since then, this culture system has been used to uncover potential treatments for hepatic lipidosis and research efforts have been dedicated to enable the large-scale production of these structures [118,119]. However, data presented in the current chapter debates (1) the acquisition of definitive hepatocyte identity upon differentiation of these structures and (2) the applicability of differentiated BD organoids as a hepatocellular homeostatic *in vitro* system.

The ability of BD organoids to give rise to hepatocyte-like cells was previously determined by various assays, including the increase LDL uptake and glycogen storage upon differentiation [89]. However, an increase in what a priori seem liver-specific bio-functions *in vitro* is not a definitive proof of the commitment of the cells in culture toward a hepatocyte fate. LDL is a lipoprotein that binds to hydrophobic molecules such as cholesterol and transport them throughout the blood system for the use by different cell types. As systemic LDL is mostly metabolized by hepatocytes, LDL uptake is widely used as a readout for hepatocyte maturation *in vitro*. However, uptake of LDL *in vitro* is also observed in cell lines of non-hepatocyte origin such as HEK293T or L929 cells, which are often used as cell systems to study LDL intracellular cascades [174]. Similarly, glycogen in the body is preferentially, but not exclusively, stored by hepatocytes [175]. Therefore, an increase in LDL uptake and glycogen storage upon differentiation does not necessarily indicate acquisition of a hepatocyte phenotype as it could be alternatively associated with a change in the metabolic state of cultures independent of their cell identity.

Huch et al. (2013) also reported that differentiated BD organoids show higher Cyp3a (cytochrome P450, family 3, subfamily A) activity when compared to organoids maintained in BDorg-EM [89]. As mentioned in Chapter 1, hepatocytes highly express enzymes of the cytochrome P450 superfamily, which are involved in the biotransformation and detoxification of xenobiotics. However, members of the Cyp3a subfamily are also expressed by cells other than hepatocytes, including intestinal enterocytes and BECs, and therefore, an increase in the activity of Cyp3a activity does not necessarily indicate acquisition of hepatocyte-like features [176,177]. Furthermore, it should be noted that the highest expression of Cyp-related genes in this study occurred upon dexamethasone addition. To induce BD organoid differentiation, dexamethasone was added following Huch et al. (2013) recommendations using a final concentration of 30 μM [89,172]. It should be noted that dexamethasone at a lower concentration (10 μM) is used to challenge primary hepatocytes and HepG2 cells cultured in conventional monolayers as this induces Cyp3a4 activity as a part of a pregnane X receptor (PXR)-mediated cytotoxic response [178] [109]. Therefore, it is possible that the reported increase in the expression of Cyp activity in BD organoids occurs as result of the activation of a non-hepatocyte specific cellular program to clear xenobiotics rather than to the acquisition of hepatocyte fate in culture.

BD organoids also showed increased expression of Albumin mRNA upon differentiation [89]. Albumin mRNA is detected in liver precursor cells as early as 9.5 days of embryo development and experiments performed using the Alb-Cre mouse model have shown that this allele recombines foxed sequences in both developing hepatocytes and BECs, indicating that the expression of this gene is not restricted to cells that are definitively committed to the hepatocyte lineage [179,180]. Furthermore, when comparing levels of albumin and mature hepatocyte gene expression (including Cyp1a2, Cyp2a1, Fah, Ass1 and Cyp2f2) in differentiated BD organoids and primary samples, these did not reach the levels of PH and remained below the level of expression of adult hand-picked BD. These data indicate that the expression profile of differentiated BD organoids does not resemble that of mature and terminally differentiated hepatocytes.

Bi-nucleation and polyploidization are characteristics of postnatal mature hepatocytes [181]. Huch et al. (2013) pointed to the presence of bi-nucleated cells in differentiated BD organoids as indicative of hepatocyte fate specification. However, data presented here showed that small bi-nucleated cells expressing were also present in BDorg-EM conditions prior to differentiation [89]. A potential explanation for the presence of bi-nucleated cells in BDorg-EM conditions could be that, in expansion conditions, a few proportion of cells within the organoids escaped their lineage-committed state and acquired hepatocyte features. *In vivo*, failed events of cytokinesis may result in cell bi-nucleation. Hence, the presence of bi-nucleated cells could alternatively be associated to an abnormal mitotic exit, resulting in incomplete separation of daughter cells following cell division. As the number of bi-nucleated cells in BDorg-EM and –DM conditions was not scored and, therefore, I cannot comment whether the proportion of these increase or not following differentiation. Further work is thus required to establish whether (1) the presence of bi-nucleated cells is increased upon BDorg-DM exposure and (2) the current expansion/differentiation culture conditions are interfering with cell cytokinesis.

Perhaps, a more definitive indication that the cells in culture are acquiring features of the hepatocyte lineage provided by Huch et al. (2013) is the enhanced expression of Hnf4a upon BD organoid differentiation [89]. This also accords with data presented in the current chapter, which shows that HNF4a protein was detectable by IF in differentiated BD organoids and that these 3D cultures increase the expression of hepatocyte lineage markers (*Cebpa, Hnf4a* and *Prox1*) upon differentiation. Additionally, data presented here showed differentiated BD organoids expressed higher levels of *Hnf4a* and *Cebpa* than primary hand-picked BD, further indicating the acquisition of hepatocyte-like features upon culture in BDorg-DM conditions.

Huch and colleges also showed by IF that both human and murine BD differentiated organoids contain clusters of CK19 positive cells although this was attributed to the persistence of a BEC population upon differentiation rather than the acquisition of these markers as product of the current differentiation conditions [89]. However, in this chapter it was shown that the expression of BEC lineage markers (Hnf1b, Krt7 and Krt19) in BD organoids was increased following differentiation. Furthermore, levels of Krt7 and Krt19 expression in BD organoids were significantly higher than those of

primary BD, a result that could be explained by the fact that hand-picked BD do not represent a pure population as contamination from hepatocytes and non-parenchymal cells is expected. An increase in Krt19 mRNA levels upon differentiation was also reported in human BD organoids by Huch et al. (2015) although the authors of the paper did not comment on these observations [172]. Taken together, these results suggest that the current differentiation conditions are not only permissive for the gain of hepatocyte markers but also for the increased of BEC lineage differentiation.

Huch et al. (2015) reported that the presence of CK19 and albumin protein in human BD organoids was mutually exclusive by IF and therefore the authors of this study concluded that cells in differentiated BD organoids show either features of BEC or hepatocyte lineage [89,172]. Personally, I could not find any differentiated BD organoid that contained patches of cells that clearly lacked CK19 expression. By contrast, all differentiated BD organoids screened in this study were CK19 positive and simultaneously expressed HNF4a. Nonetheless, and due to the described organoid-to-organoid heterogeneity of the cultures, the existence of a small proportion of organoids in which cells have completely lost the expression of CK19 cannot be absolutely discarded. As RT-qPCR analysis showed that both BEC and hepatocyte lineage markers increased upon differentiation, further work involving experiments with single-cell resolution will be required to determine whether gain of hepatocyte markers is indeed accompanied by a decline in the expression of BEC markers.

Hepatoblast liver progenitor cells with bi-potent properties in the foetal liver have been detected based on the dual expression of hepatocyte (Hnf4a) and BEC (Epcam, Krt19 and Sox9) lineage markers. In the adult liver, dual expression of hepatocyte and BEC markers has been observed following chronic and severe liver injury. For example, ectopic expression of HNF4a in histologically defined ducts has been described in clinical cases in which massive hepatic necrosis is associated with end-stage HCV disease [182]. Conversely, histological analysis of patients diagnosed with late-stage cirrhosis and chronic biliary obstruction reveal that chronically injured hepatocytes are positive for the expression of the BEC marker HNF3b [182] It has been hypothesised that dual expression of BEC and hepatocyte markers in chronically injured human livers is an indicator of cell plasticity in both liver epithelial cell lineages. In support of this, experiments performed in various mouse models have shown that adult BECs

and hepatocytes transdifferentiate into each others' lineages when the liver damage is prolonged and when proliferation of the one cell type is compromised [16,17,23,25,183].

IF data presented in this chapter showed that differentiated BD organoids derived from adult tissues expressed BEC (Sox9 and CK19) and hepatocyte (HNF4a) markers. Thus, it is possible that differentiated BD organoids resemble adult BECs that are undergoing BEC-to-hepatocyte transdifferentation. In support of this potential, BECs expanded as organoids and differentiated via the Huch et al. (2013) protocol were shown to transdifferentiate at low frequency into fully mature hepatocytes upon transplantation [89]. Importantly, successful engraftment of differentiated BD organoids (expressing Fah) in Fah deficient animals was achieved upon withdrawal of NTBC in the drinking water. It is therefore possible that these particular experimental conditions *in vivo* generated a microenvironment that supported BD organoid cell-to-hepatocyte transdifferentation. This possibility is discussed further in Chapter 8.

5.3.2 Response of differentiated BD organoids to Wnt activation

Data presented in this chapter showed that activation of canonical Wnt pathway in differentiated BD organoids does not elicit a metabolic Wnt-driven response. Instead, stabilization of an active form of β-catenin, drove the expression of HPC markers (Sox9, Spp1, Cd44 and Lgr5).

Wnt orchestrates hepatocellular proliferation in homeostasis and after partial hepatectomy (PHx) (see Chapter1) and therefore, an increase in HPC markers upon β-catenin stabilization could be expected if BD organoids were recapitulating the cellular context of regenerative hepatocytes [15,86,87,90]. However, and as discussed previously, data presented here suggests that differentiated BD organoids are closer to BECs than the hepatocyte lineage. Hence, the necessary following question: does Wnt pathway modulate the regeneration of the biliary epithelium?

Some evidence for a role for the Wnt pathway in BEC regeneration comes from the studies of Huch et al. (2013) in which Lgr5 was initially described as novel HPC marker [89,172]. Using a Lgr5-ires-CreERT2 mouse model carrying a R26-LSL-LacZ transgenic allele, in this study Huch and colleagues concluded that Rspo injury cues

activate quiescent bi-potent HPCs that reside in the biliary epithelium, which upon activation of the Wnt signalling pathway enter into a proliferative state to aid hepatobiliary repair [89]. Studies performed by Lin and colleagues have subsequently shown that intraperitoneal injection of Rspo1 increases the number of Lgr5 expressing BECs upon injury, attenuates liver fibrosis and accelerates the recovery of the animals after CCl_4 liver damage [184]. This data also accords with earlier observations of Okabe et al. (2016), who showed that Wls depletion from liver epithelial cells significantly reduced BEC proliferation following DDC injury [98].

These studies are, however, contrasted by the recent observations of Planas-Paz et al. (2019), who using an Alb-Cre $Lgr4^{fl/fl}$ $Lgr5^{fl/fl}$ mouse model in which Lgr4 and Lgr5 were concomitantly deleted from the biliary epithelium, have failed to identify a decrease in ki67 staining in CK19+ cells upon long-term (14 days and 6 weeks) exposure to DDC [93]. Furthermore, scRNAseq experiments from Pepe-Mooney et al. (2019) have recently revealed that Axin2 and Lgr5 mRNA transcripts were virtually absent in DDC-injured BECs, suggesting that the canonical Wnt/β-catenin pathway is not activated in BECs in response to damage [22].

Due to these discrepancies amongst studies, the reported HPC gene signature that arise upon stabilization of β-catenin in differentiated BD organoids raise a number of interesting questions concerning the biology of the canonical Wnt signalling pathway in the regeneration of the biliary epithelium and/or in BEC/hepatocyte cell plasticity. In Chapter 6, the possible biological implications of the activation of the Wnt/β-catenin signalling pathway in differentiated BD organoids will be further investigated.

5.3.3 Differentiated PH organoids as a hepatocellular model

To generate PH organoids that resemble the homeostatic hepatocellular compartment of the liver, Peng et al. (2018) developed a two-step protocol in which periportal or pericentral zonal metabolic maturation was induced in a EGF/HGF- or CHIR-containing medium, respectively, that lacked TNFα and contained dexamethasone [3]. In this study, Peng and colleges implied that CHIR PHorg-DM promoted the expression of pericentral genes whereas EGF/HGF PHorg-DM induced periportal genes, although a direct comparison between the ability of the zonal inducers CHIR

and EGF/HGF to specifically drive pericentral or periportal signature was not provided. Data presented in the current chapter showed however that most of the transcriptional changes reported upon differentiation were associated with the withdrawal of TNFα and/or addition of dexamethasone rather than being specific to the presence of the zonal inducers (CHIR and EGF/HGF). Furthermore, when comparing the gene expression levels of zonated metabolic genes between CHIR and EGF/HGF PHorg-DM conditions, only the periportal Fah and Alb were differentially expressed in a statistically significant manner. Hence, there is abundant room for the refinement of the composition of both periportal and pericentral mediums, including the replacement of CHIR with Wnt9b and Rspo3 as it will be discussed later.

Peng et al. (2018) reported that organoids grown in the absence of TNFα present intracellular lipid droplets as shown by LipidTOX staining and related the presence of such intracellular incursions with enhanced cell stress [3]. Work presented in this chapter showed that some PH organoids cultured in the presence of TNFα during the first passage also presented large cytosolic inclusions which morphologically resembled those previously described by Peng et al. (2018) [3]. Conclusions about the lipid content of such inclusions cannot, however, be drawn as the appropriated test were not run [3].

The cytosolic inclusions reported here disappeared upon cell 3D culture adaptation, being absent in most of the PH organoids after the second passage and thereby it is likely that the observed inclusions were linked to cell stress, although further experiments are required to evaluate whether this is the case.

Withdrawal of TNFα from the PH organoids cultures together with addition of dexamethasone caused dramatic morphological changes that may be associated with cell stress.

Peng et al (2018) related some of these phenotypical changes to the presence or absence of TNFα in the medium composition and proposed that activation of NF-KB signalling by TNFα was critical for the long-term maintenance of the cultures. Another factor to consider is that PH organoid differentiation is achieved by adding 3 μM of

dexamethasone. This contrast with the concentration of dexamethasone used for iPSC-to-hepatocyte differentiation (~1-10nM) or for the maintenance of PH grown in conventional 2D monolayers (~10-100 nM), as 2D collagen sandwich cultures (100 nM) as 3D spheroids (~100nM), which is 30 to 3000 times lower [113,169,185-187]. Dexamethasone at a concentration of 10 μM is widely used to induce a Cyp-mediated cytotoxic response in PHs 2D cultures [109]. Therefore, further work in which the concentration of dexamethasone is decreased and optimized would be recommended. Further studies will also be required to determine the individual contributions of dexamethasone and TNFα to the reported morphological changes. Furthermore, to develop a better picture of what morphological changes represent and their relationship with the physiological states, additional characterization and cell viability experiments will be needed.

Constitutive activation of Notch signalling in the hepatocellular compartment using a AAV8-TBG-Cre R26-LSL-NICD mouse model causes hepatocyte-to-BEC transdifferentation [188]. Such transdifferentation is accompanied by the gain in expression of biliary fate markers, including Sox9, Spp1 and Hnf1b [188]. Data presented in this chapter showed that PH organoids upregulate the expression of Hnf1b upon differentiation. It is therefore possible that the current PH organoids differentiation conditions are permissive for the commitment of the cells to the BEC lineage. Alternatively, it has been shown that Hnf1b plays a role in liver steatosis and regulates lipid metabolism in hepatocytes. Experiments performed by Long et al (2017) have shown that animals fed with high fat diet as well as db/db mice, a hyperphagic obesity mouse model that spontaneously steatosis, have increased expression of Hnf1b [189]. Interestingly, overexpression of Hnf1b in these mouse models caused a reduction in the degree of steatosis, suggesting that upregulation of Hnf1b in the hepatocytes might occur as a response to cope with the drastic increase of intracellular lipid accumulation. It has been previously discussed that upon differentiation PH organoids showed signs of cellular stress, including the presence of cytosolic inclusions that resemble the intracellular lipid droplets described by Peng et al (2018) [3]. Hence, upregulation of hnf1b in PH organoids upon differentiation could be associated with the formation of lipid droplets rather than to the acquisition of BEC identity in culture.

Finally, an array of different PH organoid morphologies in both expansion and differentiation were reported during the completion of this study. In future investigations, it would be interesting to explore whether the different PH organoid morphologies are a reflection of different organoid growth/development stages, an indication of deterioration/physiological state of the cultures or a sub-product of the spontaneous acquisition of different cellular identities in culture.

5.3.4 Response of differentiated PH organoids to Wnt activation

The current chapter showed that a combination of soluble Wnt9b and Rspo3, but not individual ligands, drives activation of the Axin2CreERT2 reporter in differentiated PH organoid cultures. The possible mechanisms that might underpin Wnt9b/Rspo cooperativity in regulating canonical Wnt/β-catenin signalling will be later addressed in section 5.3.5.

Activation of the Axin2CreERT2 reporter in PH organoids was mosaic and the number of Axin2 positive cells per organoid increased with the time of differentiation. As discussed in Chapter 4, the Axin2CreERT2 is an On-/Off-state reporter system and therefore a variegated response in this model might potentially be explained by the presence of a CreERT2 expression recombination threshold in combination with cell-intrinsic factors such as cell-to-cell differences in the level of expression of Wnt/Rspo receptors. Further work will be required to establish the cellular heterogeneity of differentiated PH organoids and whether such heterogeneity relates to the ability of each individual cell to respond to Wnt9b/Rspo3 treatment.

In addition to the increase in Axin2 expression, activation of Wnt signalling by a combination of Wnt9b and Rspo3 was accompanied by a significant increase in the level of expression of pericentral metabolic genes (Cyp1a2, Cyp2e1 and Tbx3), suggesting that these ligands elicit a metabolic Wnt-driven response in PH organoids. When analysing the patters of gene expression across the liver lobule using Bahar Halpern et al. (2017) data, I found that the pericentral genes analysed by RT-qPCR could be clustered in (1) genes that show a gradual decline in expression levels across the CV-PT axis of the liver and (2) pericentral genes that follow an expression pattern

other than a gradual decline. Interestingly, all genes significantly induced by the combination of Wnt9b and Rspo3 belonged to the category of 'CV-PT axis gradual decline', probably indicating that the distance to the central vein/diffusion of Rspo3 and Wnt9b ligands/β-catenin levels are the main determinants in the transcriptional regulation of those genes *in vivo* and *in vitro*.

By contrast, a combination of Wnt9b and Rspo3 was not sufficient to induce the expression of pericentral genes that follow a 'CV-PT expression pattern other than a gradual decline' such as *Glul* and *Fah*. In addition to Wnt signalling, other physical and biological cues derived from the circulation of the blood across the lobule have been suggested to regulate zonation. For instance, systemic glucagon represses the expression of *Glul* [48]. Pericentral hepatocytes are also exposed to lower concentration than periportal hepatocytes. Murine PH and hepatocyte-like cells derived from human ESCs cultured in hypoxic (5% O_2) conditions express significantly higher levels of pericentral *Cyp1a2* and *Glul*, respectively than their counterparts cultured in normoxic (21% O_2) conditions, suggesting that the oxygen tension is also a determinant factor in the expression of pericentral genes [109,190]. As the expression of pericentral genes *in vivo* is controlled by other factors besides Wnt, future studies which take more physicochemical and biological variables into account will need to be undertaken to fully model Wnt driven zonation *in vitro*.

Among the pericentral genes evaluated, the CV-PT expression patterns of *Glul* and the absence of response of this gene upon Wnt stimulation needs a special consideration due to its widespread use as a readout for Wnt pathway activation *in vivo*. In Chapter 3 it was shown that β-catenin and TCF4 bind to potential promoter regions of *Glul* and various reporter mouse models have shown that increased or decreased β-catenin transcriptional activity caused the expansion or retraction of *Glul* protein (GS) histologically positive tissue areas (see Chapter1). Data presented in this thesis shows however that the expression of *Glul* remains largely unaffected upon Wnt activation in both PH cultured in conventional monolayers and differentiated PH organoids. This together with the fact that in the liver lobule the expression of this gene is restricted to the layer of hepatocytes lining the central vein, suggest that either very high Wnt activation levels are required for this gene to become transcriptionally activated or, as discussed earlier, that other factors in addition to Wnt are required for

its expression. When evaluating small fluctuations of canonical Wnt activation *in vivo* or *in vitro*, it might be therefore advisable to evaluate the expression levels of other genes that become activated at a lower Wnt levels. Thence, GS staining might not be the best readout to report localized activation of canonical Wnt signalling under the current PHorg-DM culture conditions.

Another interesting finding of this chapter was that CHIR treatment did not drive the activation of the Axin2CreERT2 reporter or caused an increase in Axin2 mRNA levels in differentiated PH organoid cultures. In fact, the only pericentral gene that was significantly induced upon CHIR exposure was Cyp1a2. A recent study from Ahn et al (2019) has shown that 9 μM CHIR robustly induce (~20-fold change induction) the expression of Cyp1a2 in HepaRG cells, a well-established hepatocellular cell line derived from human liver progenitor cells, cultured in 3D. In the same study, 9 μM CHIR triggered a significant increase in Axin2 and Cyp2e1 expression, although with a much lower fold induction (~5-fold change) [191]. Thus, a potential explanation for the lack of significant induction of Axin2 and Cyp2e1 response in CHIR-treated PH organoids is that the window of assay to detect these genes was lost at the concentration of CHIR used. Furthermore, the fact that CHIR induces more efficiently Cyp1a2 than Axin2 raises the question whether induction of Cyp1a2 partially occurs in a β-catenin-independent manner. In this regard, is also worth noticing that Cyp1a2 is also a gene also implicated in the metabolism of drugs and thereby it is possible that CHIR-driven expression of Cyp1a2 occurred partially as part of a metabolic response. Further research should be undertaken to investigate whether this is the case.

Finally, increased expression in Cyp2e1, Cyp1a2 and Tbx3 mRNA levels do not necessarily mean that the whole pericentral metabolic program was elicited upon Wnt9b and Rspo3 treatment. To assess whether a combination of the central vein ligands triggers such response, RNAseq experiments in which the transcriptome landscape of the organoids in different DM conditions is analysed in more detail would be recommended. Data presented here suggest that CHIR does not robustly activate canonical Wnt signalling in PH organoids. RNAseq and β-catenin localisation

experiments would also clarify whether CHIR treatment is activating or not Wnt pathway in these structures.

In conclusion, results from the evaluation of Wnt response in PH organoids indicate that these structures might serve as *in vitro* platform to recapitulate Wnt-driven liver zonation. In Chapter 8, I will give recommendations about how Wnt/Rspo beads might be incorporated in this system to cause local activation of Wnt signalling pathway.

5.3.5 A combination of Wnt9b and Rspo3 activate canonical Wnt signalling

Upon the arrival of a Wnt stimulus, the Wnt pathway breaks into different branches (see Chapter 1). Which of these will be activated and at which intensity is determined by (1) the identity of the Wnt protein and (2) the array of the Wnt receptors available at the cell surface, which, in the case of the canonical Wnt cascade, requires at least the presence of a receptor from the Fzd family and a receptor of the Lrp family.

Work presented in this thesis showed that Wnt9b induced the Wnt/β-catenin cascade in HEK293T cells, (Chapter 3), hepatocytes cultured in monolayers (Chapter 4) and PH organoids (current chapter), thus providing evidence that Wnt9b is a Wnt protein with the 'right identity' to elicit a canonical response. The ability of Wnt9b to activate the Wnt/β-catenin cascade was, however, highly dependent on the presence of Rspo proteins. Rspo proteins are ligands that bind to Lgr4/5/6 receptors and augment Wnt signalling by inactivating the E3 ubiquitin ligases Rnf43/Znrf3 that would otherwise degrade the Wnt receptors present at the cell surface (see Chapter 1) [82]. The mode of action of Rspo proteins, therefore, provides ground for the hypothesis that Rspo ligands enable Wnt9b-mediated canonical signalling by modifying the array of receptors available at the cell surface prior to the arrival of the Wnt stimulus. Based on this hypothesis, at least three models may be provided to explain Wnt9b and Rspo3 co-cooperativity.

First, there are 10 members in the Fzd family of Wnt receptors (Fzd1-10) and it has been proposed that the panel of these that are expressed may dictate the intracellular cascade elicited by the Wnt ligand [192]. The Rspo-Znrf3/Rnf43 modules control the protein stability of FZD receptors, thus it is possible that Rspo licenses the cell for Wnt9b canonical signalling through the stabilization of the specific Fzd members

mediating such response (Figure5.12, A). This hypothesis has been previously explored by Dickinson et al (2019), who observed that Wnt9b in combination with Rspo3, but not alone, caused activation of the TCF-Luc reporter in M15 cells (a murine mesonephric cell line) [152]. M15 cells expressed Fzd1, Fzd2, Fzd3, Fzd4, Fzd5 and Fzd6 receptors [152]. Of those, ectopic expression of Fzd5 in M15 cells, augmented Wnt9b-Rspo3 canonical signalling cooperativity and therefore the authors concluded that FZD5 stabilization might be a limiting receptor for Wnt9b canonical activity [152]. Dickinson et al. (2019), however, did not assessed whether the Rspo3 treatment in M15 cells specifically increased the stability of Fzd5 nor performed Fzd5 knock-down experiments to determine whether in the absence of Fzd5 other members of the Fzd family mediate Wnt9b-canonical activity [152]. Thence, it remains possible that other members of the Fzd family besides Fzd5 contribute to Wnt9b-mediated activation of canonical Wnt signalling. According to the scRNAseq spatial reconstruction public data of Bahar Halpern et al. (2017), murine hepatocytes expressed Fzd1, Fzd4, Fzd5, Fzd6, Fzd7 and Fzd8. Of those, hepatocytes adjacent to Wnt9b-producing central vein were particularly enriched for *Fzd1* expression (Appendix B, Figure 6) [14,33]. Furthermore, *Fzd8* was restricted to pericentral hepatocytes (Appendix B, Figure 6) [14,33]. Further experiments are therefore required to establish whether Wnt9b-mediated activation of the Wnt/β-catenin in the hepatocellular compartment requires Rspo-mediated stabilization of Fzd5, Fzd1, Fzd8 or any other of the Fzd receptors expressed by murine hepatocytes.

Second, in addition to an Fzd receptor, activation of the canonical branch of the Wnt signalling cascade additionally requires a receptor from the Lrp family (primarily Lrp5 and/or Lrp6) (see Chapter 1). Rspo proteins also modulate LRP6 protein availability at the cell surface (Figure5.12, B) [193]. Dickinson et al. (2019) showed that M15 cells expressed Lrp6 but not Lrp5 [152]. Lrp6 knock-down in M15 cells impaired Wnt9b-Rspo3 canonical signalling cooperativity, an effect that could not be rescued by the ectopic expression of Lrp5 [152]. Based on these results, Dickinson and colleagues concluded that Lrp6 but not Lrp5 is required for Wnt9b-mediated activation the Wnt/β-catenin signalling cascade. Hence, it is possible that Wnt9b canonical signalling relies on Rspo-mediated stabilization of LRP6 protein levels (Figure5.12, B). Lrp6, however, is the receptor mediating the signalling for other canonical Wnt ligands. This model

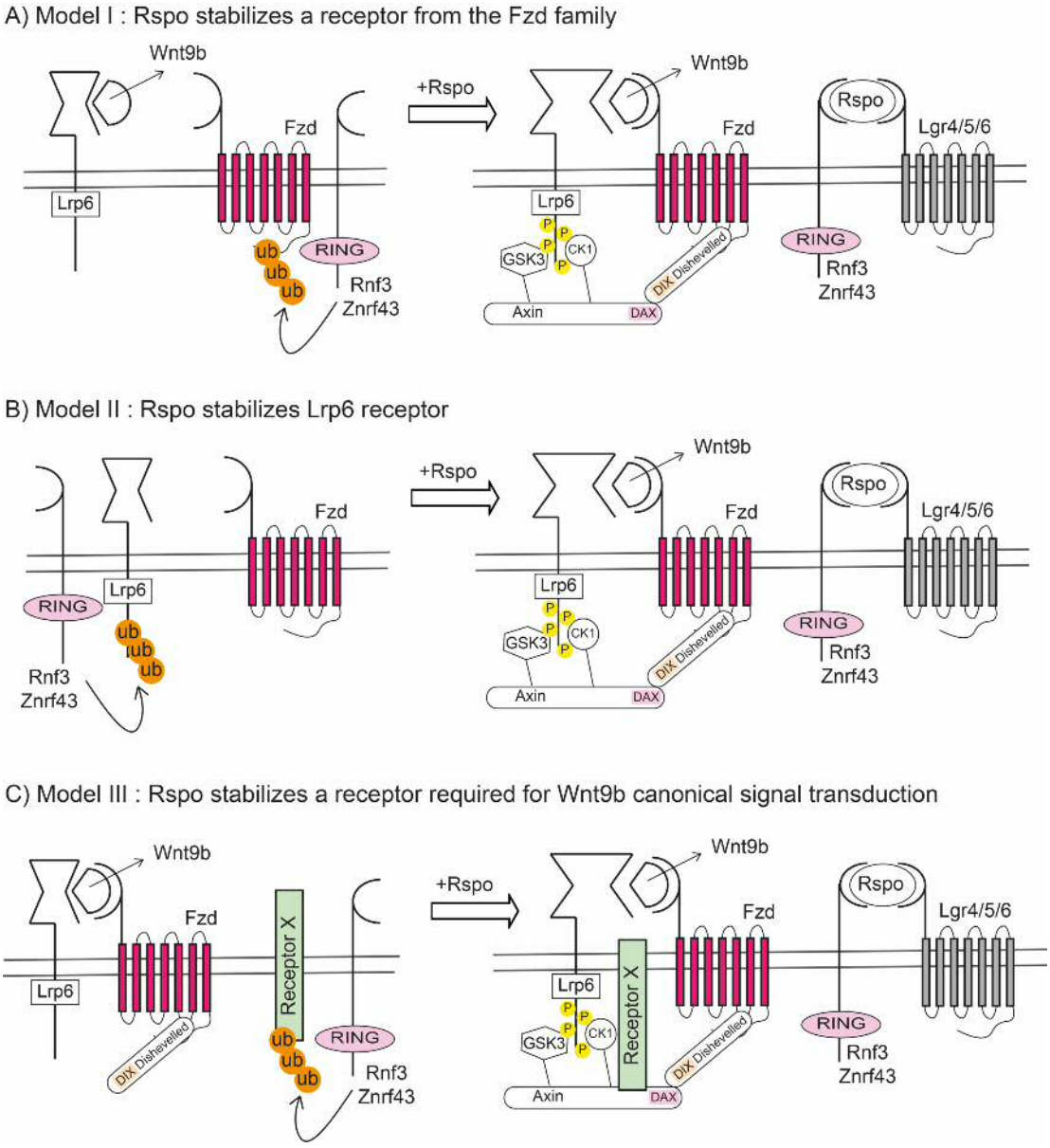

Figure5.12 Wnt9b and Rspo3 co-operation models for the activation of canonical Wnt signalling (A) Model I is based on the Rspo-mediated stabilization of Fzd receptors at the cell surface level. In the absence of Rspo proteins, the E3-ubiquitin ligases Rnf3/Znrf43 target the Fzd receptors that mediate Wnt9b canonical signalling for degradation. In the presence of Rspo ligands, Rnf3/Znrf43 proteins are sequestered in a complex formed by Rspo and Lgr4/5 or 6. This leads to the stabilization of Fzd receptors for Wnt9b, that now are able to form a complex with Wnt9b and Lrp6, leading to the initiation of Lrp-mediated signalling. (B) Model II is sustained on Rspo-mediated stabilization. Rspo proteins, in combination with Lgr4/5 or 6 receptors, sequester and inhibit the E3-ubiquitin ligases Rnf3/Znrf43 that otherwise would degrade Lrp6 receptor. This leads to the stabilization of Lrp6 protein levels at the cell surface and, therefore, to the formation of a Fzd-Wnt-Lrp6 complex competent for the induction of canonical Wnt signalling. (C) Model III is based on the assumption that the formation of a Fzd-Wnt-Lrp6 complex is not sufficient to activate the Wnt/β-catenin pathway. In this model, activation of the Wnt/β-catenin model is only achieved upon Rspo-mediated stabilization of a third hypothetical receptor (Receptor X).

would therefore not immediately explain why other canonical Wnt proteins such as

Wnt3a do not require the presence of Rspo proteins to activate the canonical branch of the pathway.

Third, Wnt7a and Wnt7b are two members of the Wnt family that, in addition to Fzd and Lrp receptors, require the co-expression of other two receptors (Reck and Gpc124) to mediate β-catenin protein stabilization [76,194-196]. Similarly, Wnt9a canonical activity in both zebrafish and HEK293 cells relied on the expression of a third receptor, Egfr, which formed a complex with Wnt9a and Fzd9b to promote Wnt/β-catenin signalling via receptor internalization and formation of the Wnt signalosome [197]. Thence, it could be conceivably hypothesised that besides an Fzd and an Lrp receptor, Wnt9b might require an additional Wnt co-receptor, the stability of which would be modulated by Rspo proteins, to mediate canonical Wnt intracellular signalling transduction (Figure5.12, C).

5.3.6 Summary

The current chapter aimed to characterise BD and PH organoids and determine whether these structures can serve as a cell platform to recapitulate Wnt-driven zonation in vitro. PH organoids were found to be structures closer to the hepatocyte (Cebpa^{high}, Hnf4a^{High} and Prox1^{High}) lineage than the BEC lineage (Krt19^{Low}, Krt7^{Low}, Epcam^{Low}, Hnf1b^{High}) whereas BD organoids were found to be structures closer to the BEC lineage (Krt19^{High}, Krt7^{High}, Epcam^{High}, Hnf1b^{High}) than the hepatocyte lineage (Cebpa^{Medium}, Hnf4a^{Medium} and Prox1^{Low}). A combination of Wnt9b and Rspo3, but not the individual ligands, induced activation of Wnt/β-catenin signalling in PH organoids, which was accompanied by an increase in the expression of the pericentral genes Cyp1a2 and Cyp2e1. By contrast, the addition of Rspo3 was sufficient to activate Wnt signalling in BD organoids and stabilization of β-catenin in differentiated BD organoids triggered the expression of HPCs related genes rather than zonation markers. The possible biological implications of the β-catenin-driven HPC signature in differentiated BD organoids will be further investigated in Chapter 6. Altogether these results indicate that PH organoids but not BD may be used as a cell platform to recapitulate Wnt-driven zonation *in vitro*

Chapter 6. CHARACTERIZATION OF THE RESPONSE OF BILE DUCT-DERIVED ORGANOIDS TO WNT ACTIVATION

One of the objectives of this thesis was to characterise the cellular responses of the current hepatic organoid systems to Wnt activation. In Chapter 5 it was described how stabilization of β-catenin in BD organoids leads to the expression of HPC genes rather than zonation markers. The current chapter further investigates the molecular mechanisms underpinning these observations with a special focus in the Wnt biology driven by Rspo1, a ligand that has been linked with liver regeneration.

Carmen Velasco Martinez also contributed to generate some gene expression data presented in this chapter. Library preparation and RNAseq experiments presented here were carried out by Dr Angela M. Marchbank and Georgina E. Smethurst, members of the Genomic Hub at Cardiff University. Dr Robert Andrews and Dr Sumukh Despande from the Data Hub (Cardiff University) partially contributed to the bioinformatic analysis of the RNAseq data presented in this chapter (see Appendix D). All contributing scientists are acknowledged where appropriated.

6.1 Introduction

The liver is composed of two epithelial cell populations: the hepatocytes and BECs. While it is well accepted that the canonical branch of the Wnt signalling pathway orchestrates hepatocyte division during liver damage, the relative importance of β-catenin in BEC regeneration is a subject of current debate.

Recent studies performed by Planas-Paz et al. (2019) and Pepe-Mooney et al. (2019) have failed to identify Axin2 or Lgr5 expression by scRNAseq in DDC-injured BECs, suggesting that BECs do not respond to Wnt/Rspo cues during biliary epithelium damage [22,93]. Accordingly, concomitant loss of Lgr4 and Lgr5 (using Lgr4/5$^{fl/fl}$:Alb-Cre) did not cause a decline in the number of proliferative BECs in DDC-injured livers [93]. Okabe et al. (2016) additionally showed that loss of the canonical Lrp5/6 receptors in the biliary epithelium (Lrp5/6$^{fl/fl}$: Alb-Cre) did not have a detrimental effect in the formation of A6-positive ductular structures in response to DDC injury regime [98].

In support for a role of the canonical branch of the Wnt signalling pathway in BEC stem cell biology and/or response to injury, using a Lgr5-ires-CreERT2:R26LacZ reporter mouse model Huch et al. (2013) showed that the Wnt/β-catenin pathway is activated

in the biliary epithelium in response to acute liver damage caused by CCl4, DDC or MCDE injury regime (see Chapter1) [89]. Experiments by Lin et al. (2017) also showed that intraperitoneal injection of Rspo1 in CCl_4 chronically damaged livers increased the number of Lgr5(+) expressing BECs that can give rise to BD organoids, further supporting that BECs respond to Rspo1 cues during injury [184] Finally, studies carried out by Apte et al. (2007) concluded that β-catenin modulates BEC proliferation as depletion of β-catenin in the biliary epithelium (β-catenin$^{fl/fl}$ Alb-Cre) caused a significant reduction in the number of A6-positive ductal structures formed in response to a DDC diet [198].

There are four members in the Rspo family (Rspo1-4) [82]. In Chapter 5 was shown that exposure of differentiated BD organoids to Rspo3 was sufficient to activate canonical Wnt signalling in these structures (see Chapter 5). The response of differentiated BD organoids to other members of the Rspo family, including Rspo1, is yet to be determined.

Differentiated BD organoids are structures that express high and low levels of BEC and hepatocyte lineage markers, respectively, and therefore, they might be recapitulating the cellular context of BECs undergoing transdifferentation to hepatocyte fate (see Chapter 5). Stabilization of β-catenin in differentiated BD organoids triggered the expression of several HPC related genes (Sox9, Spp1, Cd44 and Lgr5) (see Chapter 5), suggesting a potential role for the Wnt/β-catenin signalling pathway in the biliary epithelium regeneration and/or in BEC cell plasticity.

In this chapter, I aimed to investigate the possible biological implications of this β-catenin-driven HPC gene signature in differentiated BD organoids. As Lin et al. (2017) showed that regenerative BECs respond to environmental Rspo1 cues, the first objective was to characterise the response of differentiated BD organoids to this ligand [184]. Secondly, this chapter will explore whether the Wnt/Rspo-dependent increase of HPC-related genes could have a functional role in BEC stem cell biology using BD organoids as an *in vitro* model of study. To achieve this second aim, BD organoids derived from Wnt reporter (TCF/Lef:H2B-GFP and Axin2CreERT2) and cell cycle reporter (Fucci) mouse lines were established [199]. Finally, differentiated BD organoids will be used to address the possible effects of Wnt activation in BEC and/or

hepatocyte lineage specification. Caveats associated with the use of differentiated BD organoids as an *in vitro* system to study the biology of in vivo Wnt activation in the biliary epithelium will be discussed in Chapter 7.

6.2 Results

6.2.1 Rspo1 activation of canonical Wnt signalling in differentiated BD organoids mirrors the effects β-catenin stabilization

In Chapter 5 the activation of canonical Wnt/HPC genes in Tet-O-ΔN89β-catenin BD organoids was described. However, the activation of the canonical Wnt pathway in the Tet-O-ΔN89β-catenin line was artificial and involved the Dox-induced expression of a mutant stable form of β-catenin rather than the ligands that are expressed in vivo.

Out of the four members of the Rspo family, Rspo1 has been suggested to play a role in Lgr5(+) HPSC-driven regeneration. Hence, I explored whether exposure of differentiated BD organoids to Rspo1 caused similar transcriptional changes to that induced by stabilization of β-catenin. For that aim, the ability of Rspo1 (3 days treatment) to activate canonical Wnt signalling was first evaluated by RT-qPCR in differentiated (13 days) BD organoids derived from WT animals and then in organoids derived from the Tet-O-ΔN89β-catenin BD organoids. The effects of Rspo1 in

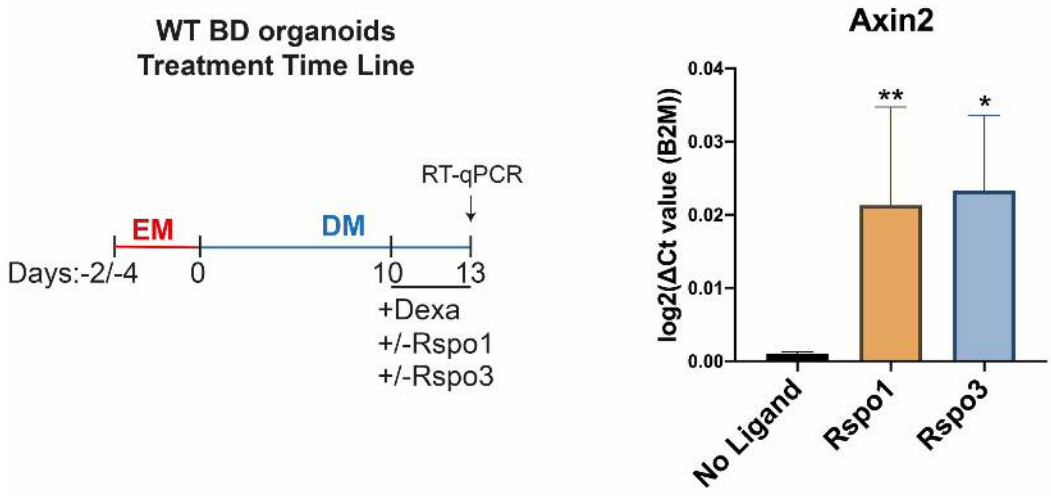

Figure6.1 RT-qPCR gene expression analysis shows that exposure to 100 ng/ml Rspo1 or 50 ng/ml of Rspo3 drives the expression of Axin2 in differentiated WT organoids. Left panel indicates organoid differentiation and treatment time line. (n=5, corresponding to organoids derived from two C57BL/6J and three WT BALB/cJ animals). Statistical significance was determined using Mann-Whitney t-test. p-value n.s.>0.05 ; p-value *< 0.05; p-value **< 0.01; p-value ***< 0.001; p-value ****< 0.0001.

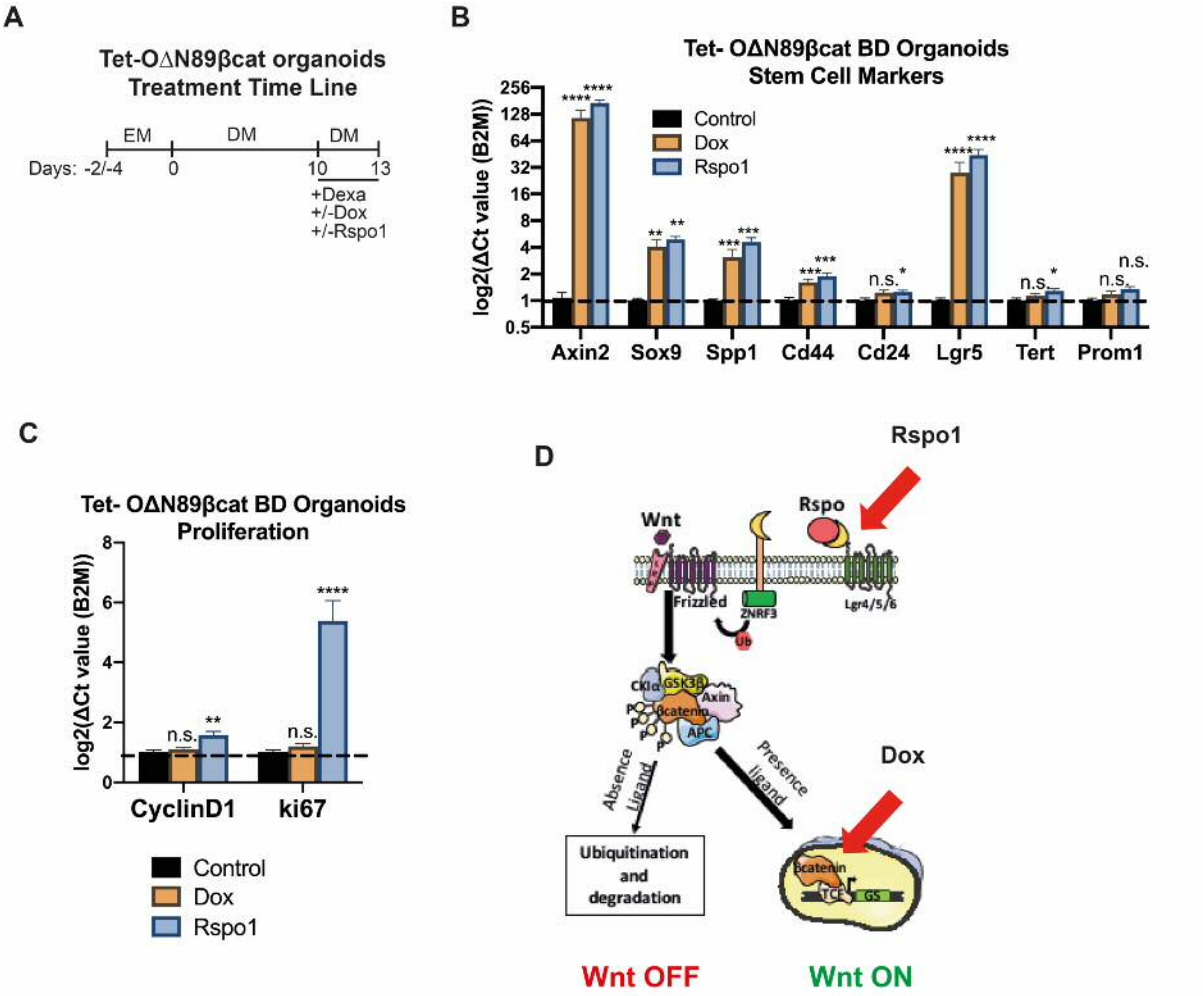

Figure6.2 Rspo1 drives the expression of HPC related genes. (A) Treatment time line for Tet-OΔN89βcat BD organoids. Wnt pathway is activated either by treatment with Rspo1 (100 ng/ml) or by stabilization of mutant activated β-catenin upon exposure to 0.1 mg/ml Dox during the last three days of differentiation. (B and C) RT-qPCR gene expression analysis of HSPCs (B) or proliferation (C) markers in OΔN89βcat BD organoids. (n=9, corresponding to organoids in 3 different passages isolated from the same animal). Statistical significance was determined using Mann-Whitney t-test. p-value n.s.>0.05 ; p-value *< 0.05; p-value **< 0.01; p-value ***< 0.001; p-value ****< 0.0001. (D) Scheme deciphering the strategy followed for Wnt pathway activation in Tet-OΔN89βcat BD organoids. Rspo1 leads to the stabilization of Wnt receptors at the level of the membrane, enhancing the activation of the pathway when Wnt ligands are present in the system. Addition of Dox in this organoid line leads to the expression of a non-degradable form of β-catenin that accumulates in the cell nuclei.

differentiated Tet-O-ΔN89β-catenin BD organoids were also compared to the transcriptional changes elicited by stabilization of β-catenin for the same length of time with Dox.

Exposure to Rspo1 (100 ng/ml) caused an increase in Axin2 mRNA in WT organoids, suggesting that it was sufficient to activate canonical Wnt signalling (Figure6.1). Similarly, Axin2 expression levels were also increased in differentiated Tet-O-ΔN89β-catenin BD organoids upon Rspo1 (100 ng/ml) or Dox (0.1 μg/ml) exposure. Treatment with Rspo1 (100 ng/ml) and Dox (0.1 μg/ml) in differentiated Tet-O-ΔN89β-catenin BD organoids triggered an increase in the expression of the HPC markers Sox9, Spp1, Cd44 and Lgr5 at comparable levels (Figure6.2, B). Rspo1 treatment additionally caused a significant increase in the level of expression of the HPC markers Cd24 and Tert and the cell cycle genes Cyclin D1 and ki67 (Figure6.2, B and C). The expression of zonated genes (pericentral and periportal) remained largely unaffected by both treatments, further suggesting that activation of the Wnt pathway in differentiated BD organoids did not induce the Wnt-driven metabolic response expected from hepatocytes (Appendix C, Figure1).

Altogether these results indicate that exposure to Rspo1 (1) is sufficient to activate the Wnt/β-catenin signalling in differentiated organoids and that (2) this leads to the expression of HPC/proliferation genes rather than zonation markers. Rspo1 will be therefore used in the rest of this chapter as Wnt-activating molecule to characterise the Wnt-driven HPC response seeing in BD organoids.

6.2.2 Rspo1-driven HPC signature in differentiated BD organoids is dependent of endogenous Wnt production

Treatment of differentiated BD organoids with Rspo1 alone caused the expression of several HPC related genes, including Axin2, Sox9, Lgr5, Cd44 and Spp1 (see section 6.2.1). Rspo proteins synergise with Wnt ligands by mediating the stabilization of Fzd and Lrp6 receptors. Thence, these results suggest that differentiated BD organoids are source of Wnt ligands with canonical activity. To assess whether endogenous Wnt ligands are required for Rspo1-driven HPC signature, Wnt production in differentiated BD organoids was blocked with LGK974 (see Chapter 3), a porcupine inhibitor that interferes with the secretion of Wnt proteins [200]. For that aim, LGK974 was added to differentiated organoids 24h prior to Rspo1 exposure and maintained upon addition of Rspo1. This set of experiments were carried out in WT organoids derived from animals with different genetic backgrounds (BALBC/cJ and C57BL/6).

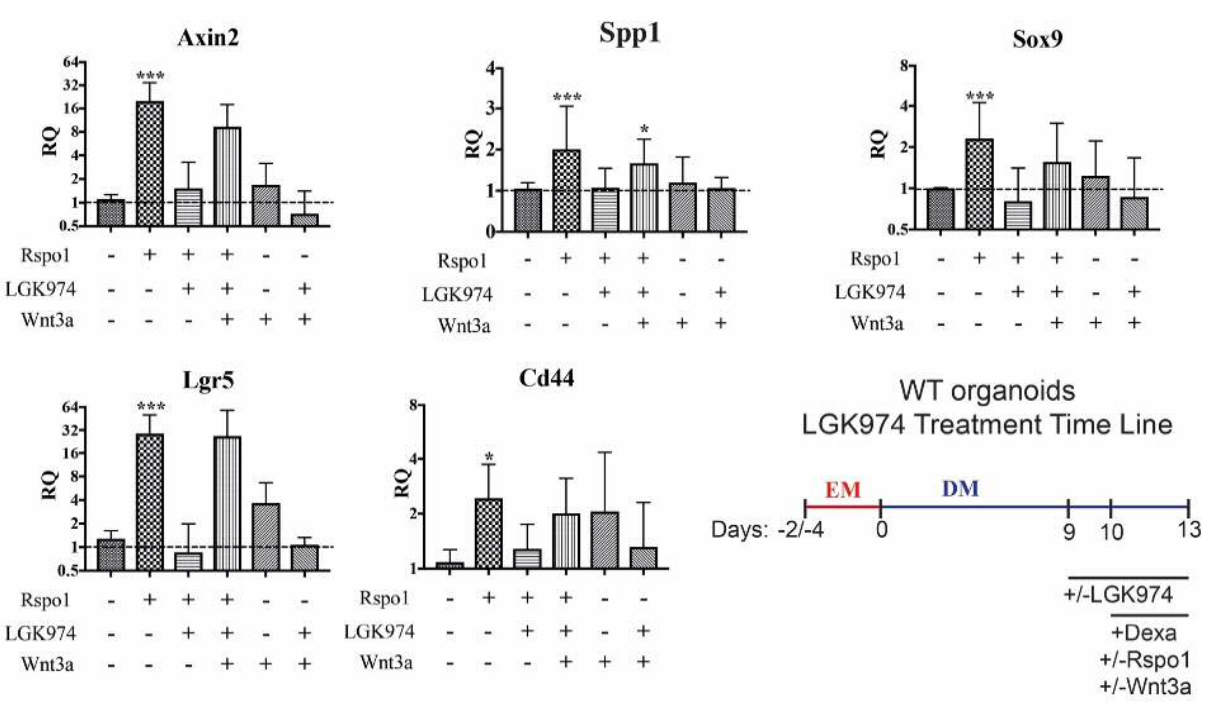

Figure6.3 LGK974 is a porcupine inhibitor that interferes with the acetylation of Wnt ligands, blocking their secretion. RT-qPCR gene expression analysis of wild type organoids shows that exposure to LGK974 (500nM) blocks Rspo1 (100ng/ml) induction of stem cell genes. LGK974 effects were partially rescued by the addition of exogenous Wnt3a (100ng/ml). As LGK974 was reconstituted in DMSO, organoids from this set of experiments that were not treated with LGK974 were exposed to the equivalent DMSO concentration. Treatment time line strategy is detailed in the left bottom of the panel. Statistics correspond to Mann-Whitney T-test. p-value * < 0.05, ** < 0.01 *** < 0.001, **** < 0.0001.

Confirming the previous findings in the Tet-O-ΔN89β-catenin organoid line, exposure to Rspo1 for 3 days induced the expression of Axin2, Sox9, Lgr5, Cd44 and Spp1 in WT organoids. The Rspo1-driven HPC signature was lost in the presence of LGK974, an effect that was attenuated by the addition of exogenous Wnt3a to the medium, suggesting that the Rspo1-driven stem cell signature required the presence of endogenous Wnt ligands (Figure6.3).

6.2.3 Establishment and characterization of Wnt reporter organoid lines

Exposure of differentiated BD organoids to Rspo1 treatment activated canonical Wnt signalling and leaded to expression of HPCs/proliferation genes (see section 6.2.1). To further characterise this response, BD organoids were derived from animals harbouring the TCF/Lef:H2B-GFP and/or the Axin2CreERT2 reporters, which are two Wnt reporters that allow the study of Wnt activation pathway with single-cell resolution.

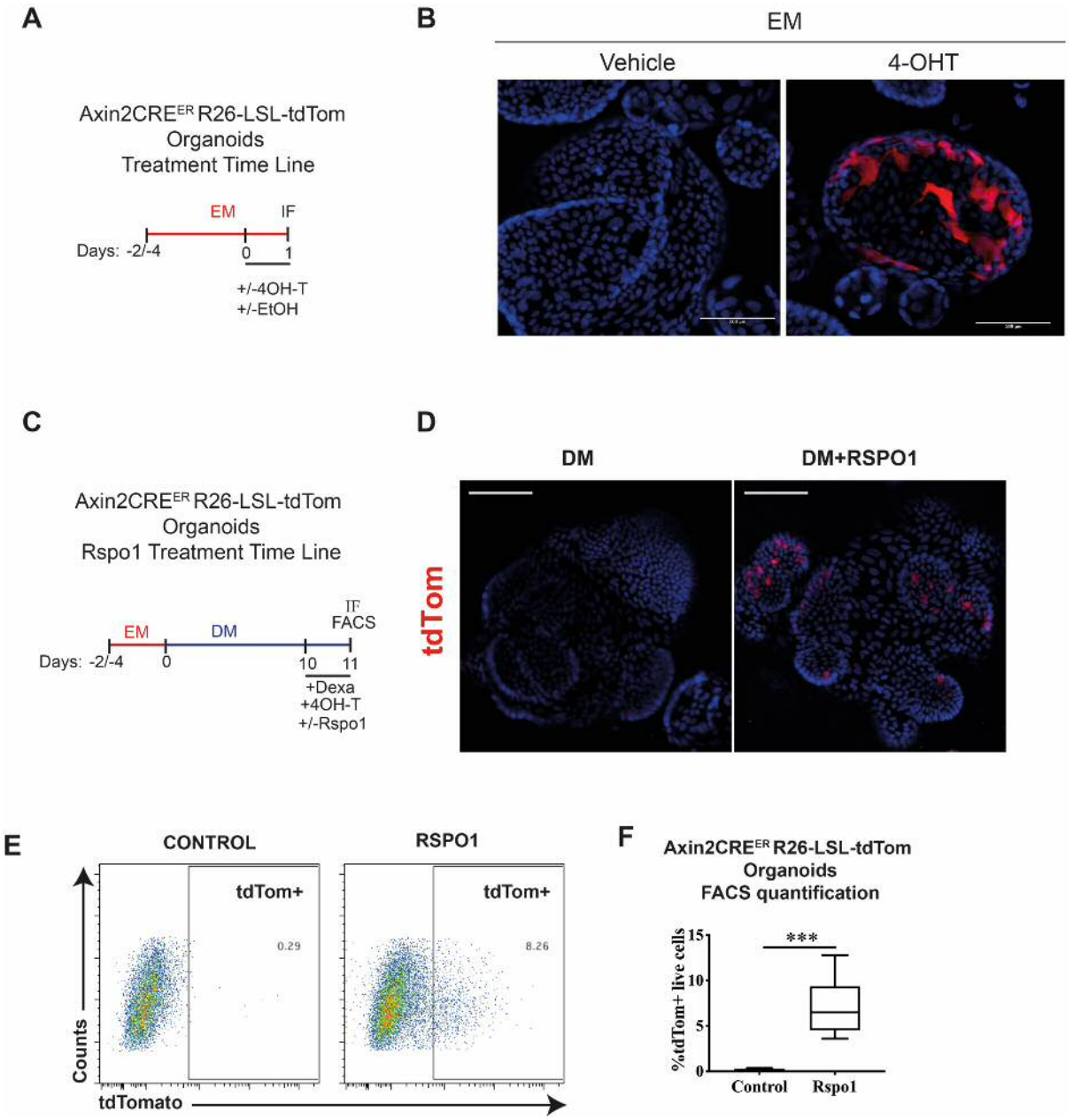

Figure6.4 Axin2CreERT2 BD organoids report the presence of Axin2 expressing cells when cultured in the presence of Wnt activating cues. (A) Treatment time line for experiment presented in panel B. (B) Representative IF images showing that Axin2 levels in BDorg-EM (EM) (see panel A) are sufficient to induce activation of the Axin2CreERT2 reporter upon 4-OHT administration. In red, endogenous tdTom labels Axin2 expressing cells. In blue, cell nuclei were labelled with DAPI. No positive cells were detected in vehicle conditions (EtOH). Scale bar 100 μm. (C) Differentiation and Rspo1 treatment time line of Axin2CreERT2 BD organoids for panels D to F. (D) Representative IF images of control and Rspo1 treated BD organoids cultured in BDorg-DM (DM) (see panel C). In red, endogenous tdTom labels Axin2 expressing cells subpopulation. Cell nuclei counterstained with DAPI (blue). Scale bar 100 μm. (E) Flow cytometry dot plots show the presence of tdTom(+) cells in BDorg-DM organoids treated with Rspo1 but not in untreated (control) conditions (see panel C for treatment time line). (F) Bar graph shows flow cytometry quantifications for the percentage of tdTom(+) cells in differentiated BD organoids (see panel C) following 24h 4-OHT Rspo1 treatment (n=7).

The TCF/Lef:H2B-GFP reporter is a continuous reporter system based on the observation that nuclear β-catenin primarily associates with transcription factors of the TCF/LEF family to drive gene expression (see Chapter1 and 3). Transgenic mice harbouring the TCF/Lef:H2B-GFP construct express H2B-eGFP fusion protein under the transcriptional control of six TCF/LEF binding motifs. H2B-eGFP expression, whose 'persistence' will be determined by the stability of the H2B-eGFP protein, serves therefore as a proxy for β-catenin transcriptional activity. By contrast, the Axin2CreERT2 reporter transgenic mouse model is an On-/Off-state reporter system where Axin2 expressing cells ('high-Wnt') can be lineage-traced as tdTom positive cells following exposure to 4-OHT (see Chapter 4).

The Axin2CreERT2 transgenic mouse model, it was first evaluated in BDorg-EM because (1) this is a high Wnt containing medium in which organoids express robustly express Axin2 and (2) characterization of the reporter can be done within 4 to 5 days. Exposure of organoids cultured in BDorg-EM to 4-OHT (500 nM) caused the appearance of tdTom positive cells, implying that BD organoid cells in these conditions express Axin2 at sufficient levels to drive activation of the reporter (Figure6.4, A).

The presence of tdTom positive cells was then evaluated in differentiated BD organoids in the presence or absence of Rspo1. For that aim, BD organoids were differentiated (11 days), exposed to 4-O-HT alone or in combination with Rspo1 (100 ng/ml) during the last 24h of differentiation and the presence of tdTom positive cells was assessed by IF and flow-cytometry. Flow cytometry gating strategy is shown in (Appendix C, Figure2). tdTom positive cells were rarely found (<0.4%) in differentiated control organoids both by flow cytometry and IF (Figure6.4, B-E). 24h concurrent exposure to Rspo1 and 4-OTH triggered the appearance of tdTom positive population that constituted 4-10% of the total cells, indicating that differentiated BD organoids only expressed Axin2 was expressed at sufficient levels to drive activation of the reporter in the presence of Rspo1 ligand (Figure6.4, B-E). tdTom positive cells in Rspo1-treated organoids were preferentially located in the organoid budding protrusions (Figure6.4, B).

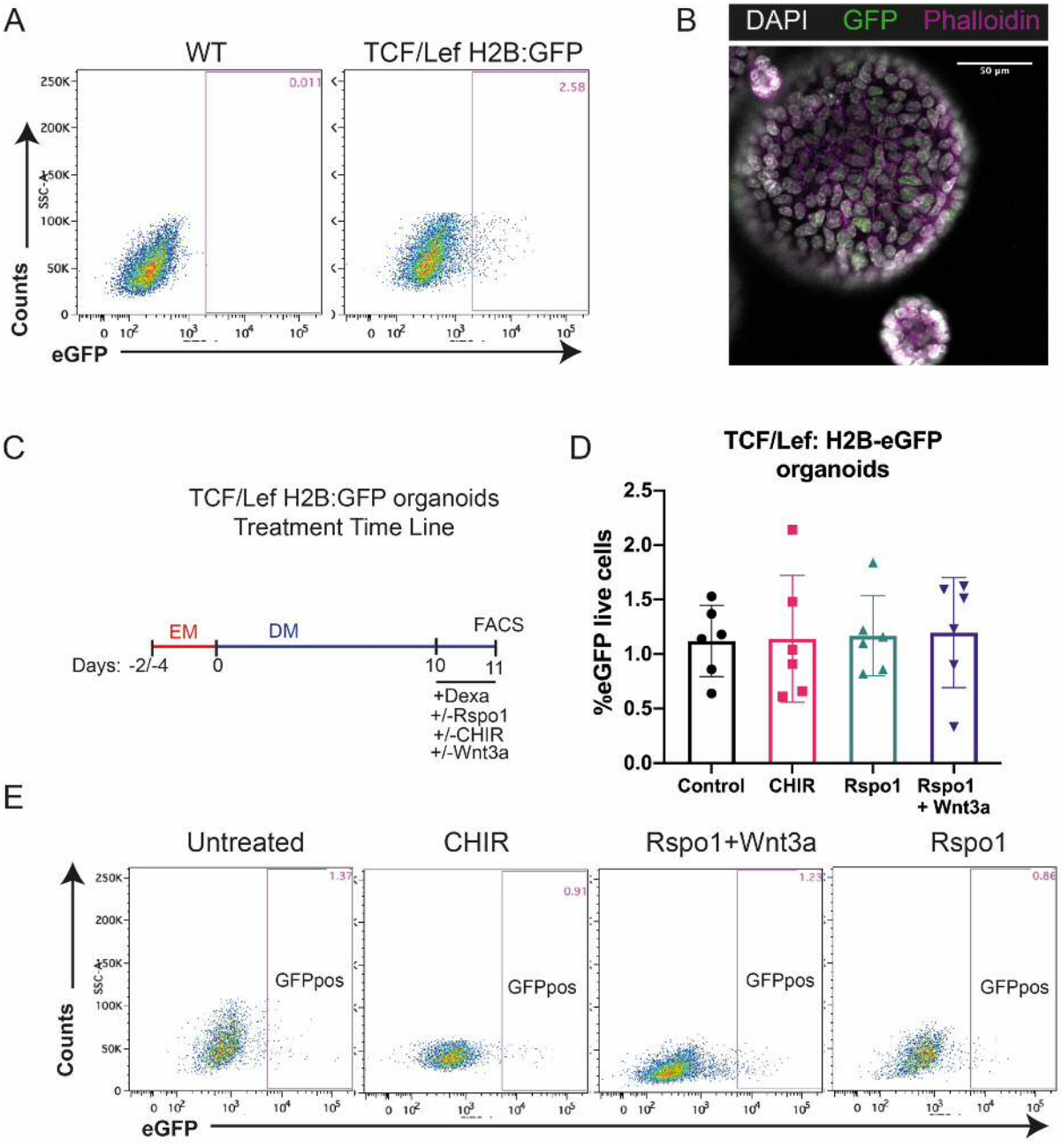

Figure6.5 Characterization of the TCF/Lef H2B:GFP organoid line. (A) Flow cytometry dot plots show the presence of GFP positive (GFPpos) cells in TCF/Lef H2B:GFP organoids cultured for 5 days in BDorg-EM. GFPpos cells were gated using WT organoids as non-fluorescence control. (B) Representative image of TCF/Lef H2B:GFP organoids cultured for 7 days in BDorg-EM shows the presence of H2B-GFP positive cell nuclei (green). Cell nuclei was counterstained with DAPI (grey), the cytoskeleton with phalloidin 647 (magenta) and endogenous GFP is shown in green. Scale bar 50 µm. (C) Experimental design used in panel D and E to evaluate the Wnt response in differentiated TCF/LEF H2B:GFP organoids by flow cytometry. (D) Bar graph show flow cytometry quantifications of TCF/LEF H2B:GFP differentiated organoids in response to Rspo1 (100 ng/ml), Wnt3a (100 ng/ml) and CHIR99021 (3 µM). (n=2 biological replicates with 3 independent technical replicates each). (E) Representative flow cytometry dot plots show that the number of GFP positive cells remained unaffected in TCF/Lef H2B:GFP differentiated organoids after 24h exposure to Wnt activating cues.

The TCF/Lef:H2B-GFP reporter organoid line was also first characterized in BDorg-

EM conditions by flow cytometry and IF. Flow cytometry analysis showed that cells expressing eGFP were detected in TCF/Lef:H2B-GFP BD organoids but not in WT organoids, indicating that a subpopulation of cells in TCF/Lef:H2B-GFP BD organoids cultured in BDorg-EM express the reporter (Figure6.5, A). IF confocal analysis of TCF/Lef:H2B-GFP BD organoids showed that eGFP signal was restricted to the cell nuclei, further confirming that the green fluorescence signal detected by flow cytometry was originated by the expression of H2B-GFP (Figure6.5, B). These results indicate that the TCF/Lef:H2B-GFP transgene is expressed in BD organoids cultured in BDorg-EM.

I next evaluated the ability of the TCF/Lef:H2B-GFP organoid line to report Wnt pathway activation in BDorg-DM conditions. For that aim, TCF/Lef:H2B-GFP organoids were differentiated (11 days) and exposed for the last 24h of differentiation to Rspo1 (100 ng/ml). Flow cytometry analysis revealed that eGFP positive cells were detectable in Rspo1-treated and untreated organoids (Figure6.5, C-E). However, non-significant differences in the proportion of eGFP positive cells were found between these two experimental conditions, indicating that the reporter was not being activated upon Wnt stimulation (Figure6.5, D and E).

A possible explanation for the lack of detection of eGFP expressing cells in differentiated BD organoids was that stimulation of Wnt signalling with 100 ng/ml of Rspo1 was not sufficient to drive activation of the reporter at detectable levels. Rspo1 and Wnt3a synergise to robustly drive the activation of the TCF/Lef reporter in HEK293T cells (see Chapter 3). Thus, I next assessed whether exposure of differentiated (11 days) TCF/Lef:H2B-GFP BD organoids to a combination Rspo1 (100 ng/ml) and Wnt3a (100 ng/ml) for 24h caused an increase in the number of eGFP expressing cells by flow cytometry. Differentiated TCF/Lef:H2B-GFP BD organoids were additionally treated for the same length of time with CHIR, a compound widely used to activate canonical Wnt signalling that drives stabilization of β-catenin through inhibition of GSK3 activity (see Chapter 1). By contrast to the results obtained with the Axin2CreERT2 organoid line, no significant changes in the proportion of cells labelled as eGFP positive were found by flow cytometry in any of the Wnt-inducing treatments tested (Figure6.5, C-E).

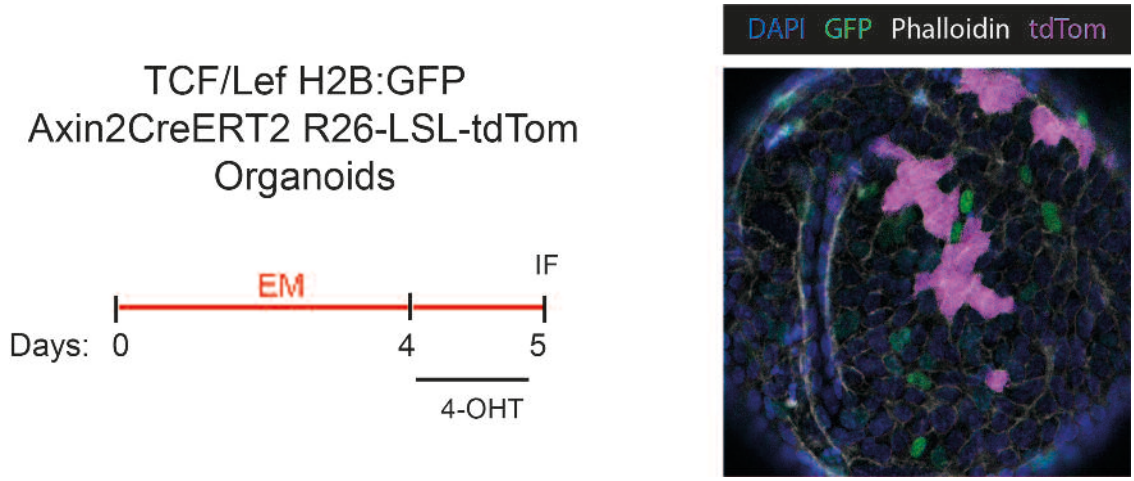

Figure6.6 Characterization of the TCF/Lef H2B:GFP Axin2CreERT2 organoid line in BDorg-EM conditions. On the left, experimental treatment time line. On the right, representative IF image of an organoid harbouring both TCF/Lef H2B:GFP and Axin2CreERT2 reporters cultured in BDorg-EM (EM) and exposed for 24h to 500nM 4-OHT. Image shows the presence of eGFP positive cells that are Axin2 negative. Endogenous tdTom labels Axin2 positive cells (magenta). GFP is shown in green. Cell nuclei and cytoskeleton was counterstained with DAPI (blue) and phalloidin (grey), respectively.

To further investigate the differences between the Axin2CreERT2 and TCF/Lef:H2B-GFP reporter results, a BD organoid line was derived from a transgenic animal harbouring both TCF/Lef:H2B-GFP and Axin2CreERT reporters and was evaluated for the presence of H2B-GFP and Axin2 (tdTom positive) expressing cells by IF. IF confocal analysis revealed that both TCF/Lef:H2B-GFP and Axin2CreERT reporters were activated in BD organoids cultured in BDorg-EM. However, the activation of the reporters did not fully overlap, which suggests that the H2B-GFP and tdTom reporters labelled different cell populations (Figure6.6).

The levels of Wnt activation at the single-cell level may fluctuate over time even when the Wnt activation stimuli is permanently present in a soluble form (see Chapter 3). One could therefore alternatively argue that it is possible that cells that recombine and simultaneously express the H2B-GFP might switch off the H2B-GFP reporter later (Figure6.7, A). This could potentially explain the presence of tdTom positive H2B-GFP negative cells in BD organoids cultured in BDorg-EM. Conversely, cells that are positive for H2B-GFP expression but negative for tdTom, might become tdTom positive later in time, giving rise to the appearance of GFP positive, tdTom negative

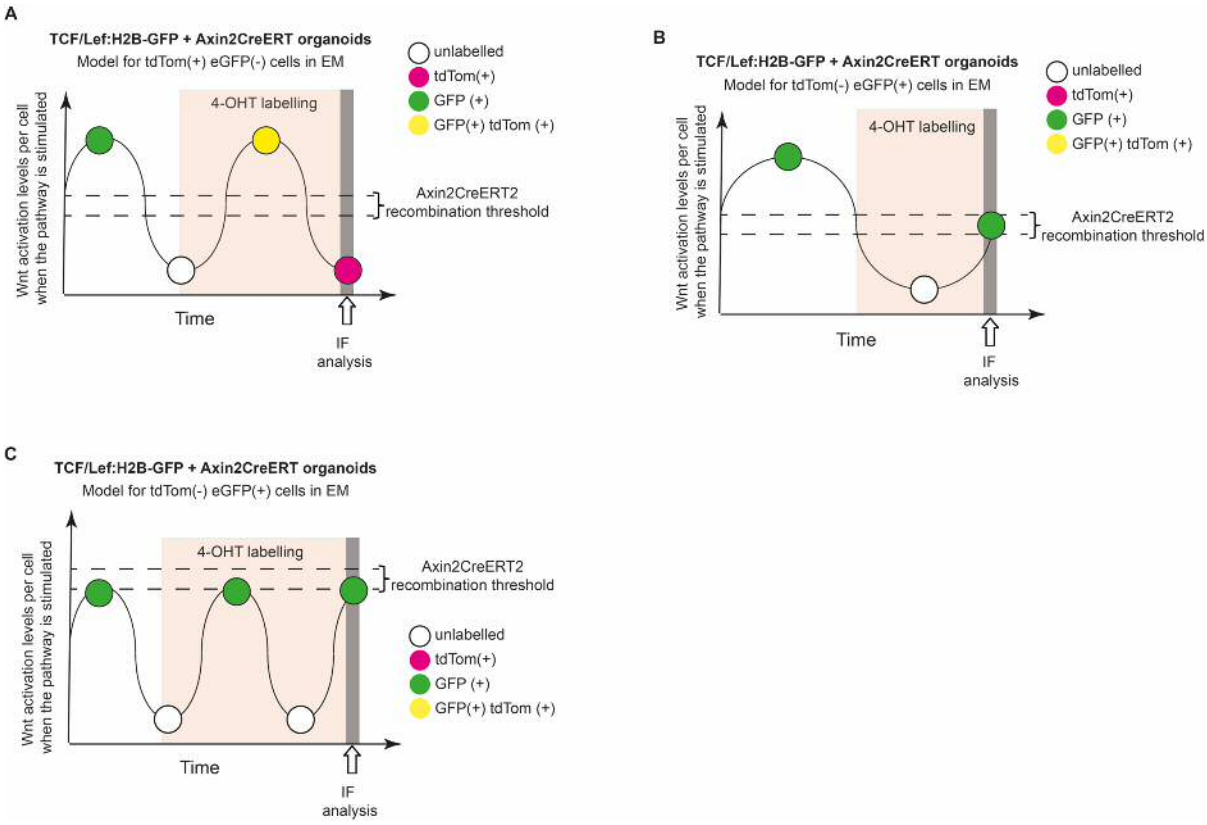

Figure 6.7 Scheme explaining possible discrepancies between the TCF H2B:GFP and the Axin2CreERT R26-LSL-tdTom Wnt reporter strategies. The TCF H2B:GFP is a continuous reporter model whereas the Axin2CreERT R26-LSL-tdTom is a binary reporter. Panel (A) gives potential explanation for the possible appearance of tdTom(+) GFP (-) cells. Panel (B and C) gives potential explanation for the possible appearance of tdTom(-) GFP (+) cells. Note that the wavelength and frequency of the Wnt activation waves presented are hypothetical. Note that the frequency and wave length of the represented Wnt activation oscillations are hypothetical and, therefore, in reality these could be higher/shorter and more/less frequent.

cells (Figure6.7, B). It is also important to consider that tdTom labelling is a binary event that only occurs when cells express Axin2 at a certain level. Thence, an additional possibility is that H2B-GFP positive cells with moderate-high Wnt activation levels remain negative for tdTom expression (Figure6.7, C). To compare both reporters regardless of their mode of activation, an experimental strategy that takes into account these considerations needs to be defined.

For BD organoids to differentiate, Rspo1 ligands are removed from the medium composition, which causes a drastic decline in Axin2 mRNA levels (Appendix C, Figure3). As BD organoid differentiation takes 13 days, I hypothesised that, despite of the differences in the mode of activation of both reporters and/or Wnt levels

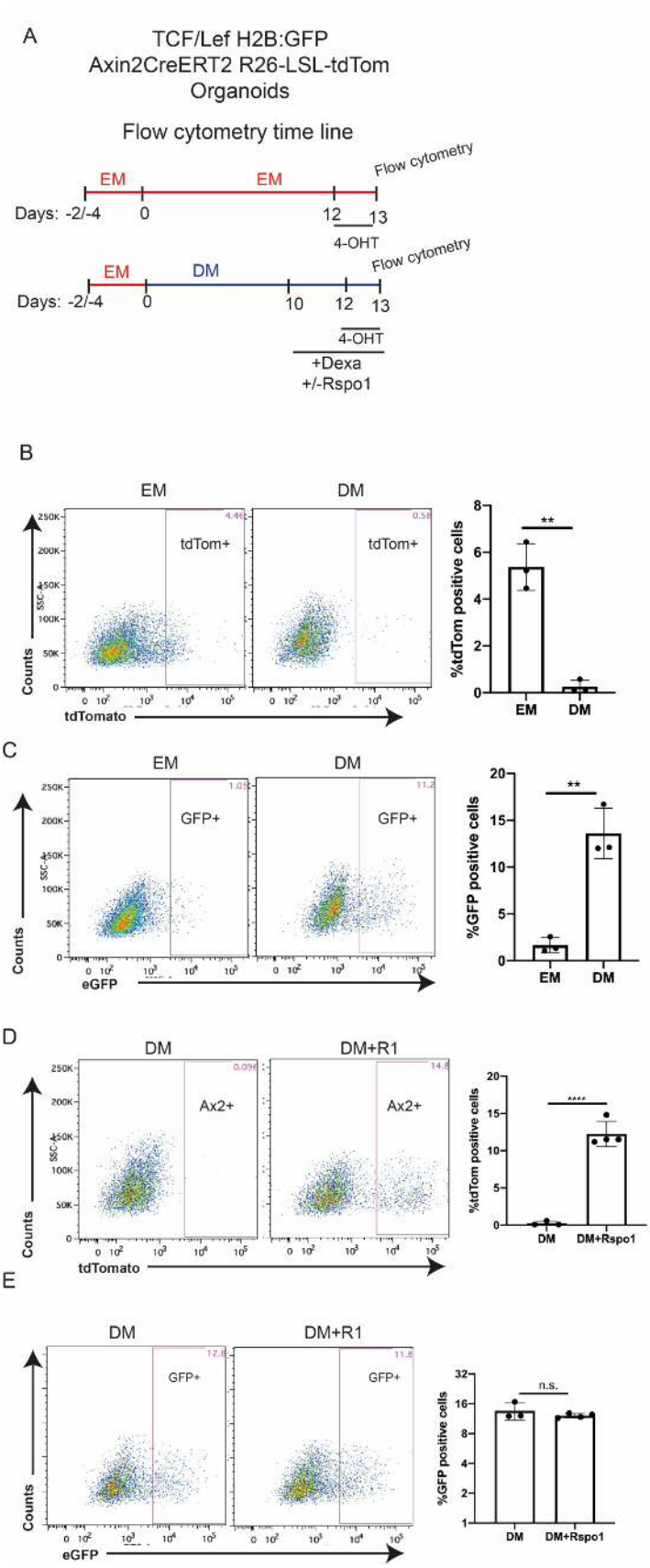

Figure6.8 Characterization of the TCF/Lef H2B:GFP Axin2CreERT2 organoid line in BDorg-DM conditions. (A) Experimental design for the study of the study of TCF/Lef H2B:GFP and Axin2CreERT2 reporters by flow cytometry. (B) Flow cytometry dot plots gated for red fluorescence show a decrease in the number of tdTom(+) cells upon differentiation. Quantifications are shown in the left panel. (n=3 technical replicates) (C) Flow cytometry dot plots show that the number of GFP positive cells is lower in expansion conditions (EM) than in differentiation conditions (DM). Bar graph shows (n=3 technical replicates) (D) The addition of Rspo1 induced the appearance of tdTom(+) cells in differentiated organoids (n=3 technical replicates). (E) Number of GFP positive cells remained largely unaffected after 3days of Rspo1 exposure. (n=3 technical replicates).

fluctuations at the single cell levels, in this time frame I should observe a decrease in the numbers of both tdTom positive and H2B-GFP expressing cells if the activation of

the reporters was dependent on Wnt activity levels. As expected, labelling of Axin2 expressing cells for 24h with 4-OHT showed that differentiated (13 days) BD organoids contained lower number of tdTom positive cells than organoids maintained in BDorg-EM for the same length of culture (Figure6.8, B). By contrast, the same organoids harbouring the TCF/Lef:H2B-GFP increased their proportion of H2B-GFP upon differentiation, indicating that activation of the TCF/Lef:H2B-GFP reporter in this system does not correlate with the Wnt activation levels of the cultures (Figure6.8, C).

Finally, using the TCF/Lef:H2B-GFP Axin2CreERT organoid line, I also examined the dynamics of activation of both reporters in differentiated BD organoids upon Rspo1 stimulation, although in this set of experiments I increased the time of exposure to Rspo1 to 3 days. Confirming the previous findings with the Axin2CreERT organoid line, labelling of Axin2 expressing cells in the TCF/Lef:H2B-GFP Axin2CreERT organoid line 24h prior to flow cytometry analysis showed that tdTom positive cells were only present in organoids exposed to Rspo1 treatment (Figure6.8, D). However, in the same organoids, significant changes in the proportion of GFP expressing cells were not detected upon 3 days of Rspo1 stimulation, further indicating that the TCF/Lef:H2B-GFP cannot be used as a proxy for Wnt activation in this system (Figure6.8, E).

Altogether, experiments from Figure6.8 provides definitive proof that the TCF/Lef:H2B-GFP and Axin2CreERT reporter behave differently upon Wnt activation in BD organoids and that among these two lines only the Axin2CreERT BD organoids might serve as reporter system to study the Wnt biology resulting from Rspo1 treatment *in vitro*.

6.2.4 Establishment and characterization of a Fucci2a cell cycle reporter organoid line

Exposure of differentiated organoids to Rspo1 increased the expression of the cell cycle genes CyclinD1 and ki67, suggesting a possible role for Rspo1 in BEC proliferation or exit of quiescence. In order to explore this possibility, I decided to establish an organoid BD line from a Fucci2a cell cycle reporter mouse mode l[199].

This animal model harbours a bicistronic reporter transgene (Fucci2a) that encodes for two fusion proteins: mVenus-hGemi and mCherry-hCtd1 [199]. mVenus-

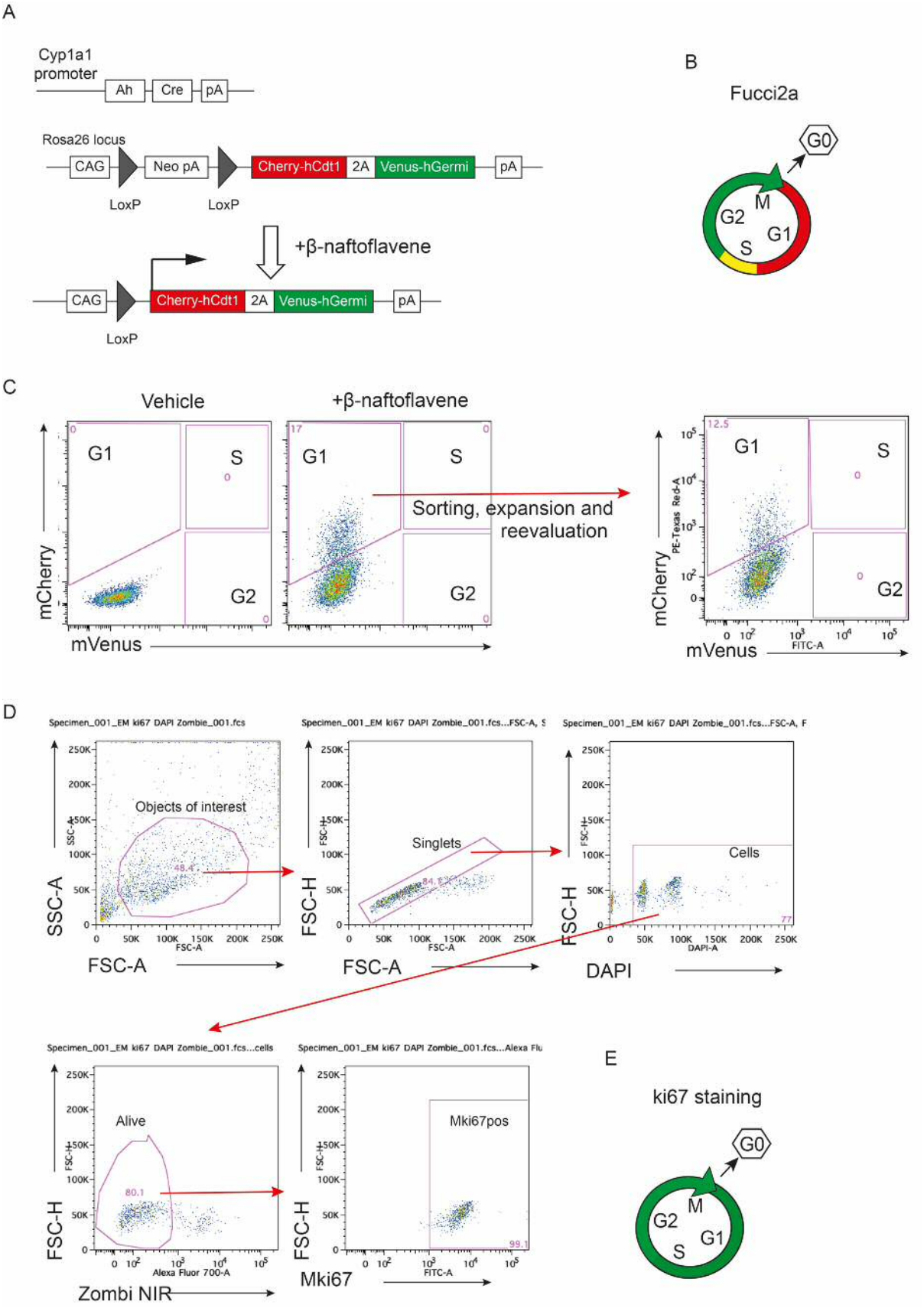

Figure6.9 Fucci2a BD organoid line characterization. (A) Scheme representing the AhCre and Fucci2a transgenes present in the Fucci2a organoid line. Cre recombinase is under the control of the Cyp1a1 promoter. Expression of Cre is induced by the exposure to lipophilic xenobiotics (β-naftoflavene). Fucci2a construct was inserted in the Rosa26 locus and its constitutive expression is prevented by a stop cassette flanked by two loxP sites. When β-naftoflavene is administrated, the stop cassette preventing Fucci2a expression is exiced and the construct is activated. (B) Activation of Fucci2a construct allows real-time visualization of cell cycle progression. Red mCherry fluorescence corresponds to cells in G1, cells in G2/M appear as Venus-green whereas yellow labels cells in S phase. Quiescent cells do not express any fluorescent protein. (C) Flow cytometry plots show the appearance of mCherry positive cells upon β-naftoflavene administration whereas no cells in S or G2/M phase were detected. Recombined mCherry positive cells were sorted, expanded and their fluorescence reevaluated by flow cytometry. No cells in S phase or G2/M were detected organoids originated from sorted mCherry positive cells. (D) Ki67 staining reveal that only a small proportion of cells (<1%) are arrested in G0.

hGemi protein arises from the fusion of the green fluorescence protein mVenus and human Geminin whereas mCherry-hCtd1 protein is created from the fusion of the red fluorescence protein mCherry and human Ctd1. Geminin and Ctd1 are proteins with antagonistic roles that are dynamically expressed during cell cycle progression. Geminin inhibits DNA replication and therefore accumulates during S/G2/M phases. By contrast, Ctd1 is absent in G1 and accumulates during G2. Hence, cells harbouring the Fucci2a construct appear labelled in green during G2/M phase and in red during G1 (Figure6.9, A and B). Cells in S phase typically appear as yellow whereas quiescent cells (G0) do not express any fluorescence. Furthermore, the mVenus-hGemi and mCherry-hCtd1 sequences in the Fucci2a transgene are linked by means of 2A self-cleaving peptides sequence. 2A-peptide mediated cleavage occurs after protein translation, this cloning strategy has been argued to produce equimolar expression of both fusion proteins.

The Fucci2a construct in this mouse model had been integrated in the Rosa26 locus (see Chapter 4) and is preceded of a stop sequence flanked by two *loxP* sites [199]. These animals also harboured an AhCre transgene in which expression of Cre recombinase is under the transcriptional control of the Cyp1a1, enabling the activation of the Fucci2a reporter upon exposure of lipophilic xenobiotics such as β-naftoflavene (β-NF) (Figure6.9, A).

Exposure of organoids in BDorg-EM (4 days) to β-NF caused the appearance of mCherry positive cells but not mVenus positive cells (Figure6.9, C). To confirm that the lack of mVenus signal was not due to defective activation of the Fucci2a construct, successfully recombined cells positive for mCherry expression were sorted, expanded in culture and their fluorescence levels re-evaluated. No mVenus positive cells were detected and only 10-15% of the cells were labelled by mCherry (G1 phase), suggesting that the system was failing to report cells in G2 phase (Figure6.9, C). Flow cytometry analysis of ki67 staining in WT BD organoids revealed that less than 1% of the cells cultured in BDorg-EM are arrested in G0, indicating that the high prevalence (85-90% of the cells) of mCherry mVenus double negative cells was not explained by the high presence of quiescent cells and further indicates that Fucci2a BD reporter organoids failed to report the presence of cells in S/G2/M phase (Figure6.9, D-E). Flow cytometry single colour staining controls are shown in Appendix C, Figure4.

Altogether these results indicate that the different cell cycles phases could not be distinguished in established Fucci2a BD organoids cultures. As a consequence, and with the exception of G1 phase labelling, the use of the Fucci2a organoid BD line does not provide any other advantage than a regular WT line. For that reason, this organoid line was not further used to characterise the effects of Rspo1 treatment in cell proliferation.

6.2.5 Functional characterization of a 'high Wnt' (tdTom positive) cell population in BD organoids

Results from the characterization of Axin2CreERT2 reporter BD organoids showed that only a small population (~4-10% of the total) of cells within the organoids express high levels of Axin2 upon Rspo1 treatment at the time of 4-OHT induction (see section 6.2.3). Exposure of differentiated organoids to Rspo1 increased the expression of various HPC and/or stem cell related genes, including *Axin2* (see section 6.2.1 and 6.2.2). I therefore hypothesised that the tdTom positive population might constitute a stem cell population within the organoid. To test this, differentiated (11 days) Axin2CreERT2 BD organoids were exposed to Rspo1, tdTom positive and negative were isolated by FACS and their ability for form secondary organoids, a proxy for stemness, was evaluated. tdTom positive cells isolated 1 day after concomitant

exposure to Rspo1 and 4-OHT showed higher organoid forming capacity than their negative counterparts (Figure6.10, A). However, when organoids were exposed for 3 days to Rspo1, tdTom positive cells gave rise to comparable number of secondary organoids to tdTom negative cells, indicating that cells resulting from short-term but

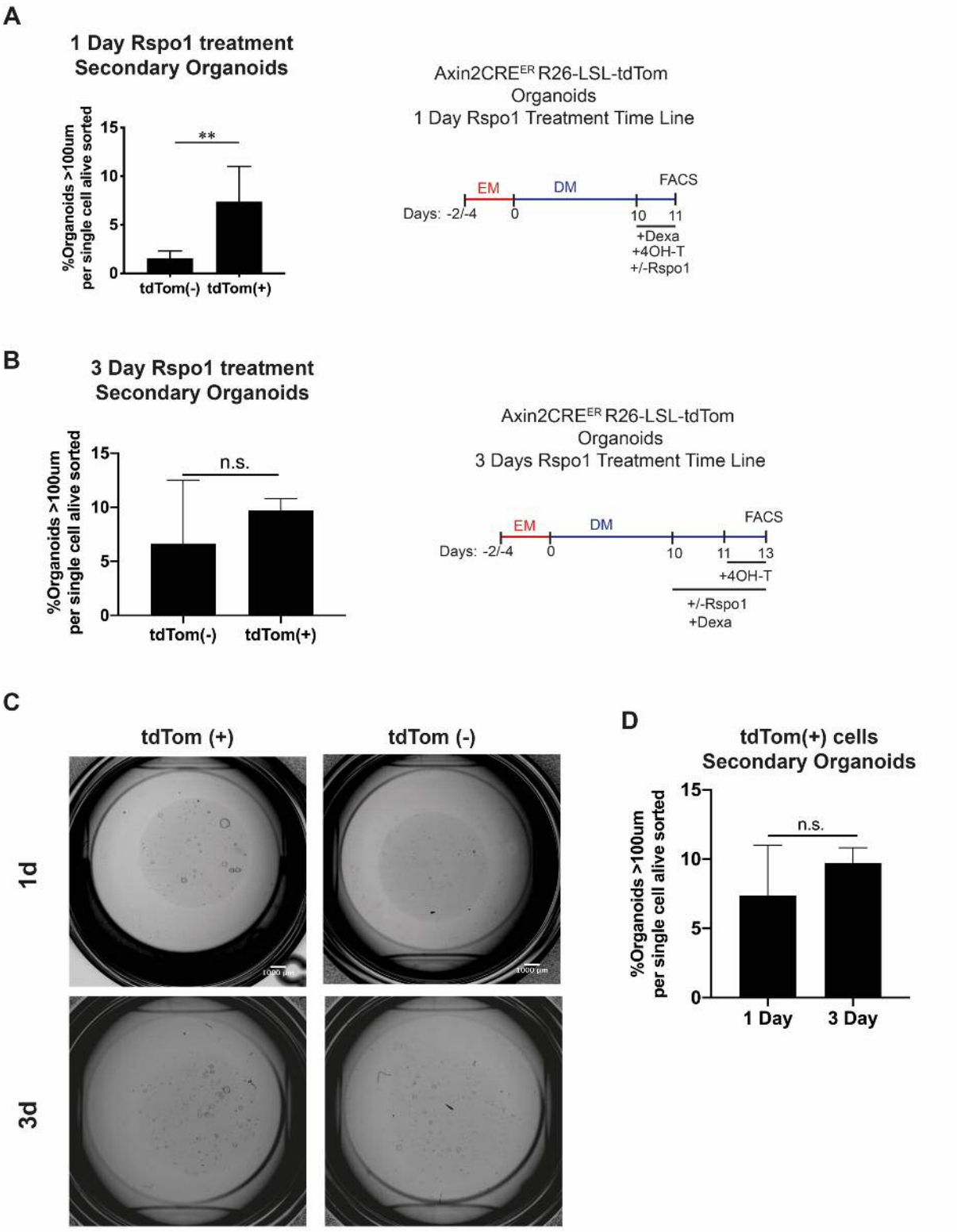

Figure6.10 Functional characterization of tdTom(+) cell population (A) Bar graph shows organoid forming capacity of tdTom(+) and tdTom(-) sorted cells from Axin2CreERT differentiated BD organoids exposed to Rspo1 for 1 day. Right panel indicates experimental design. (n= 5 independent experimental sets). (B) Organoid forming capacity quantifications of tdTom(+) (n=3) and tdTom(-) (n=2) sorted cells isolated from Axin2CreERT differentiated BD organoids exposed to Rspo1 for 3 days. Right panel indicates experimental design. (C) Representative images showing organoids formed after 7 days per 333 tdTom(+) and tdTom(-) sorted cells isolated from Axin2CreERT differentiated organoids exposed to Rspo1 for 1 or 3 days prior to isolation. (D) tdTom(+) cells isolated from organoids exposed to Rspo1 for 1 or 3 days give rise to comparable number of secondary organoids. Statistical significance was determined using t-test. p-value n.s.>0.05 ; p-value *< 0.05; p-value **< 0.01; p-value ***< 0.001; p-value ****< 0.0001.

not long-term exposure to Rspo1 have increased organoid forming ability (Figure6.10, B and C).

A defining property of stem cells is their ability to divide and self-renew for long periods. Thus, I next lineage traced tdTom positive cells after a single dose of concomitant 4-OHT and Rspo1 treatment and assessed the ability of these cells to repopulate the organoid over a period of 3 and 5 days. As the enhanced capacity of tdTom positive cells to form secondary organoids was lost upon Rspo1 long-term exposure, Rspo1 ligand was withdrawn from the medium after labelling of Axin2 expressing cells. The ratio of tdTom positive/negative cells increased over time, implying that the proliferation rate of tdTom positive cells was higher than tdTom negative cells (Figure6.11).

Altogether these results indicate that Rspo1 treatment promotes cell proliferation and stemness in BEC 3D cultures.

6.2.6 RNAseq transcriptome characterization of a 'high Wnt' (tdTom positive) cell population in BD organoids

To explore the molecular mechanisms underlying the enhanced progenitor properties of tdTom positive cells, I compared the expression profiles of tdTom positive (~4-10% of the total) and tdTom negative (~90-96% of the total) populations of BD organoids exposed for 24h to Rspo1 and 4-OHT using RNA sequencing (RNAseq) (Figure6.12). Additionally, untreated differentiated BD organoids were cultured in parallel and tdTom negative (~100% of the total) sorted cells from these organoids were also sequenced

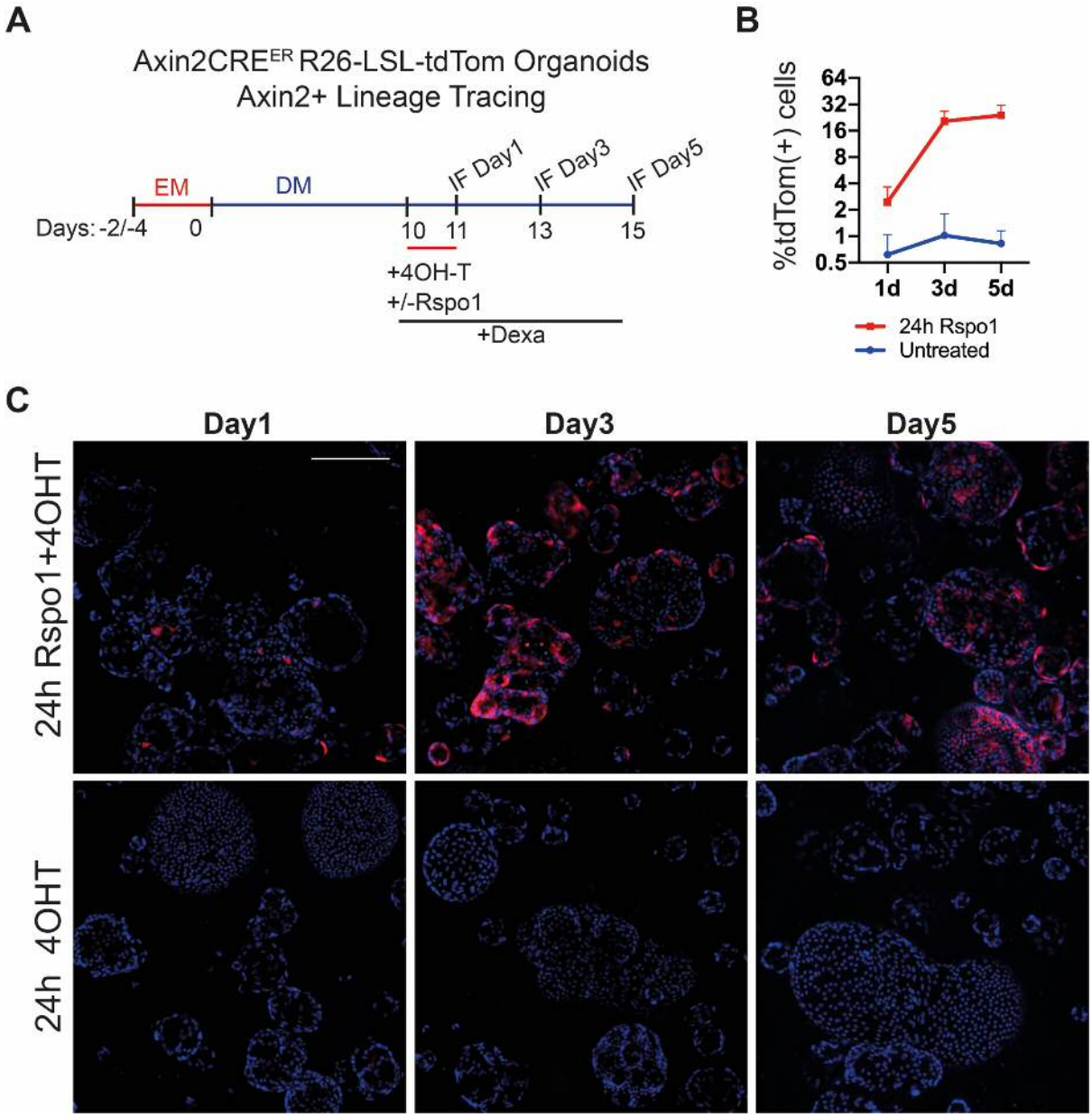

Figure6.11 Rspo1 triggers the appearance of an Axin2+ population with stem cell properties in differentiated BD organoids (A) tdTom(+) cells were lineage traced following a 24h exposure to 500nM 4-OHT and Rspo1 in Axin2CreERT2 differentiated BD organoids. Upper panel shows experimental design. Bar graph shows quantifications from the experiment (n=5, from 2 independent experiments). Representative images show a relative increase in the proportion of tdTom(+) cells (red) in culture over time. Cell nuclei is labelled by DAPI (blue). No positive cells for Axin2 expression were found in the vehicle EtOH conditions.

and included in the comparative analysis (Figure6.12). For simplicity, tdTom negative cells from untreated organoids will be further referred as “untreated” cells.

Data presented in the following sections contains the results from the differential gene expression analysis of samples from Axin2CreERT2 organoids derived from a single animal at three different passages (P5, P6 and P10), cultured and sorted at non-overlapping times (see Chapter 6 section). Differential gene expression analysis between samples was performed using DESeq2 [127]. Details regarding the determination of gene expression cut-off criterion and removal of outliers followed before running DESeq2 are in Appendix D. Appendix D additionally gathers detailed instructions about how to run DESeq2 together with the Scripts and parameters that I used for the analysis of the data presented here.

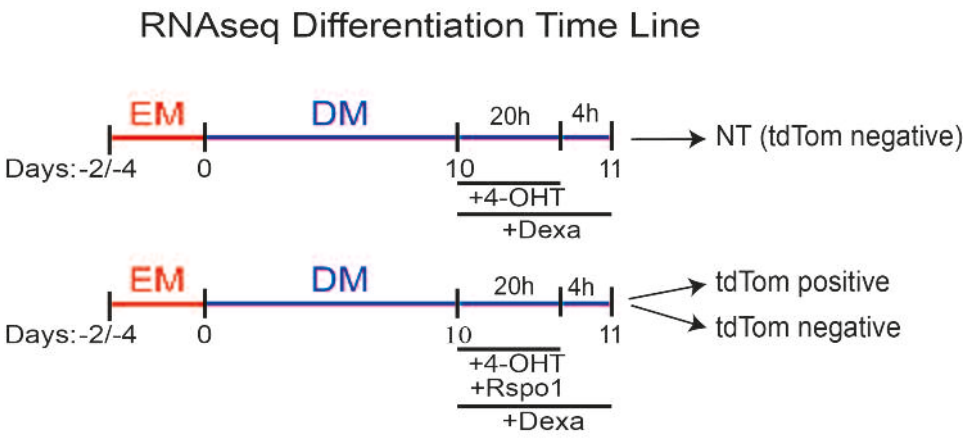

Figure6.12 RNAseq differentiation time line. BD organoids were grown in EM for 2 to 4 days and differentiated for 11 days. During the last 24 of culture differentiated BD organoids were exposed to 500 nM 4-OHT and 100 ng/mlRspo1. tdTom(+) and tdTom(-) cells were subsequently separated by FACS. tdTom(-) cells from organoids differentiated for 11 days and exposed to 500 nM 4-OHT (untreated) were also sorted. 30 μM dexamethasone was added to all the cultures during the last 24h of differentiation.

6.2.6.1 BD organoids are source of Wnt ligands and express Wnt and Rspo receptors

Data presented in the previous sections showed that Rspo1 caused an increase in the expression of HPC related genes and the appearance of a tdTom positive cell population, suggesting that these structures are equipped to sense environmental Rspo1 cues. As expected, gene expression analysis by RNAseq revealed that the Rspo receptors Lgr4 and, in lesser degree, Lgr5 were expressed in all the sequenced populations (Figure6.13). The Rspo1 co-receptors Znrf3 and Rnf43 were also expressed in the sequenced BD organoids cell populations and, of those, Rnf43 was

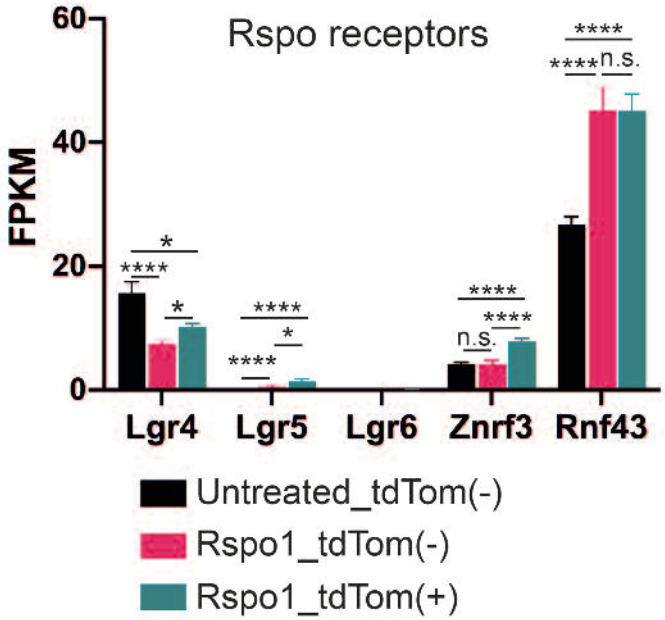

Figure6.13 Expression levels determined by RNAseq analysis of Rspo related receptors in tdTom positive, tdTom negative and untreated cells by RNAseq expressed in normalized FPKM values. (n=3)

significantly in both tdTom positive and negative populations when compared to untreated cells (Figure6.13).

Activation of the canonical Wnt signalling cascade requires at least two types of receptors: a receptor from the Fzd family and a receptor of the Lrp family (see Chapter1). BD organoids expressed various Wnt receptors of the Fzd family including Fzd1, Fzd5, Fzd6, Fzd7 and, in lesser degree, Fzd2, Fzd3, Fz4, Fzd8 and Fz9 (Figure6.14, A). Of those, Fzd5 was significantly downregulated upon Rspo1 exposure in both tdTom negative and positive cells when compared with cells from untreated organoids (Figure6.14, A). The canonical Wnt co-receptors Lrp5 and Lrp6 were additionally found expressed in differentiated BD organoid cells before and after exposure to Rspo1 (Figure6.14, B). BD organoids also expressed various Wnt co-receptors involved in the transduction of β-catenin-independent intracellular cascades (Ryk, Ptk7, Vangl1 and in lesser degree Rora, Ror1, Vangl2, Prickle1, Prickle3 and Prickle4) (Figure6.14, B).

Finally, experiments from section 6.2.2 showed that inhibition of porcupine abrogates Rspo1-driven HPC signature, suggesting that differentiated BD organoids are source of Wnt ligands. Accordingly, BD organoids were found to express several Wnts (Wnt4, Wnt7a, Wnt7b and in less amount Wnt5b and Wnt10a). RNAseq failed however to detect expression of members of the Rspo family in any of the sequenced populations (data not shown).

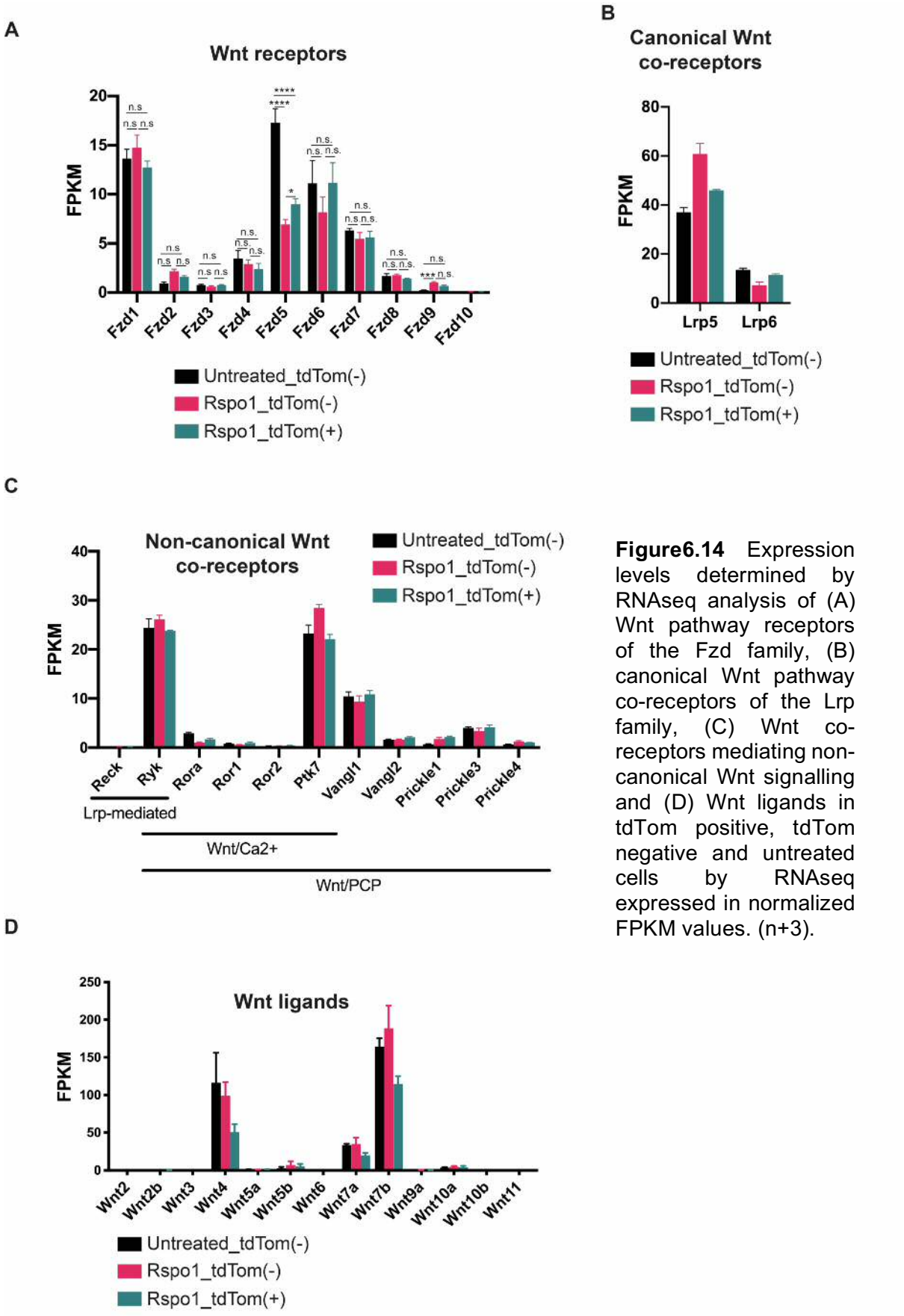

Figure6.14 Expression levels determined by RNAseq analysis of (A) Wnt pathway receptors of the Fzd family, (B) canonical Wnt pathway co-receptors of the Lrp family, (C) Wnt co-receptors mediating non-canonical Wnt signalling and (D) Wnt ligands in tdTom positive, tdTom negative and untreated cells by RNAseq expressed in normalized FPKM values. (n+3).

Altogether these results suggest that differentiated BD organoids are source of Wnt ligands and are equipped to respond to both Wnt and Rspo environmental cues.

6.2.6.2 Rspo1 treatment induces transcriptional changes in both tdTom positive and negative populations

The addition of Rspo1 to the culture induced the expression of cell cycle genes (Cdk1) and HPC related genes (Axin2, Sox9 and Lgr5) in both tdTom positive and negative populations when compared to untreated samples, suggesting that tdTom negative cells also responded to the presence of Rspo1 at certain extent. Interestingly, Rspo1 also significantly induced the expression of the pro-inflammatory cytokine Il33 as well as the Hedgehog signalling molecule Ihh (Figure6.15, A). By contrast, Bpm2 and Bmp6, two factors with liver anti-fibrotic role, were significantly decrease by Rspo1 treatment (Figure6.15, A). Gene Ontology (GO) analysis revealed that the top 500 genes introducing more variance in PC1 between tdTom negative and untreated or tdTom positive and untreated samples were enriched in GO terms related with cell division (Figure6.15, B and C).

Altogether these results indicate that tdTom negative also respond to Rspo1 at certain extent. This implies that tdTom positive and negative cells might be considered as 'high Wnt' and 'low Wnt' cell populations.

'

6.2.6.3 Transcriptome comparison between 'high Wnt' (tdTom positive) and 'low Wnt' (tdTom negative) cell populations

In total, 5333 genes were differentially expressed between tdTom positive and negative cells (padj value $\leq$0.01). The HPC-related genes Axin2, Sox9, Cd24a and Spp1 were not included among those (Figure6.16, A) (Appendix D, Figure7). Cd44 and Lgr5 were, however, found significantly upregulated in tdTom positive when compared to tdTom negative cells (Figure6.16, A). Various components of the telomere elongation machinery were also significantly upregulated in tdTom positive cells (Appendix D, Figure8). Tert itself also appeared induced in tdTom positive cells although with a padj value of 0.025 (Figure6.16, A). tdTom positive cells also showed significantly higher expression of cell cycle regulators (c-Myc and FoxM1) and genes involved in the G2/M phase of the cell cycle (ki67, Cdk1, Ccnb1, Ccnb2 and Cdc20)

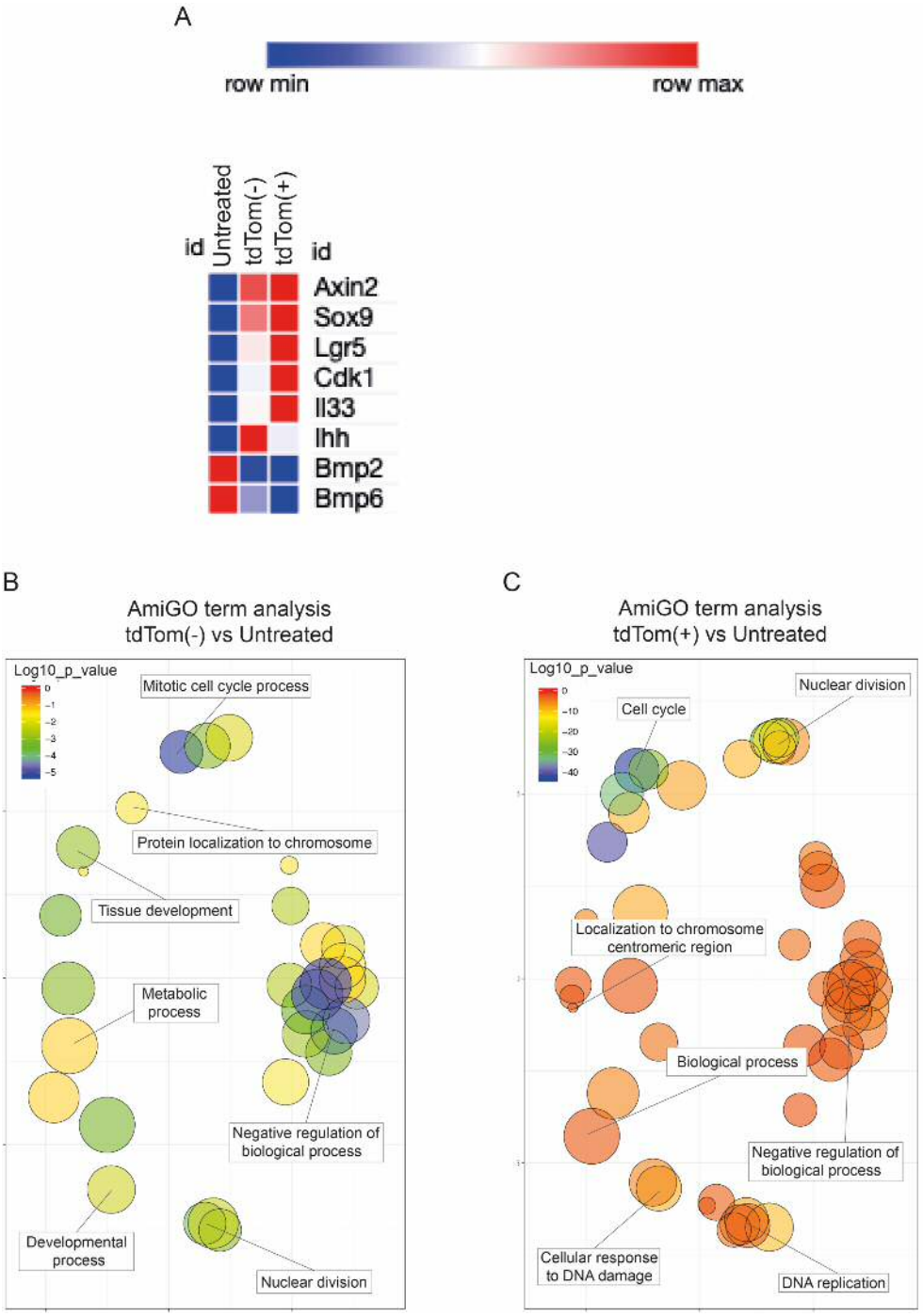

Figure 6.15 Rspo1 treatment induces transcriptional changes in both tdTom(-) and tdTom(+) populations (A) Heatmap showing genes differentially expressed between untreated and Rspo1 treated (tdTom(+) and tdTom(-)). A total of 1543 genes were differentially expressed between tdTom(+) and untreated cells with a padj < 0.01. A total of 2855 genes were differentially expressed between tdTom(-) and untreated cells with a padj < 0.01. All represented genes had a padj value < 0.01. (B) AmiGO analysis of the top 500 genes introducing more variance in PC1 between tdTom(-) and untreated samples. PCA1 explained 56% of the total variance between tdTom(-) and untreated cells. (C) GO analysis performed with amigo of the top 500 genes of tdTom(+) vs untreated pairwise PCA1 comparison. PCA1 explained 68% of the total variance between tdTom(+) and untreated cells.

(Figure6.16, B and C). Finally, the expression of genes coding for proteins of the AP-

1 complex (Fos, Fosb and Jun) were also significantly upregulated in tdTom positive

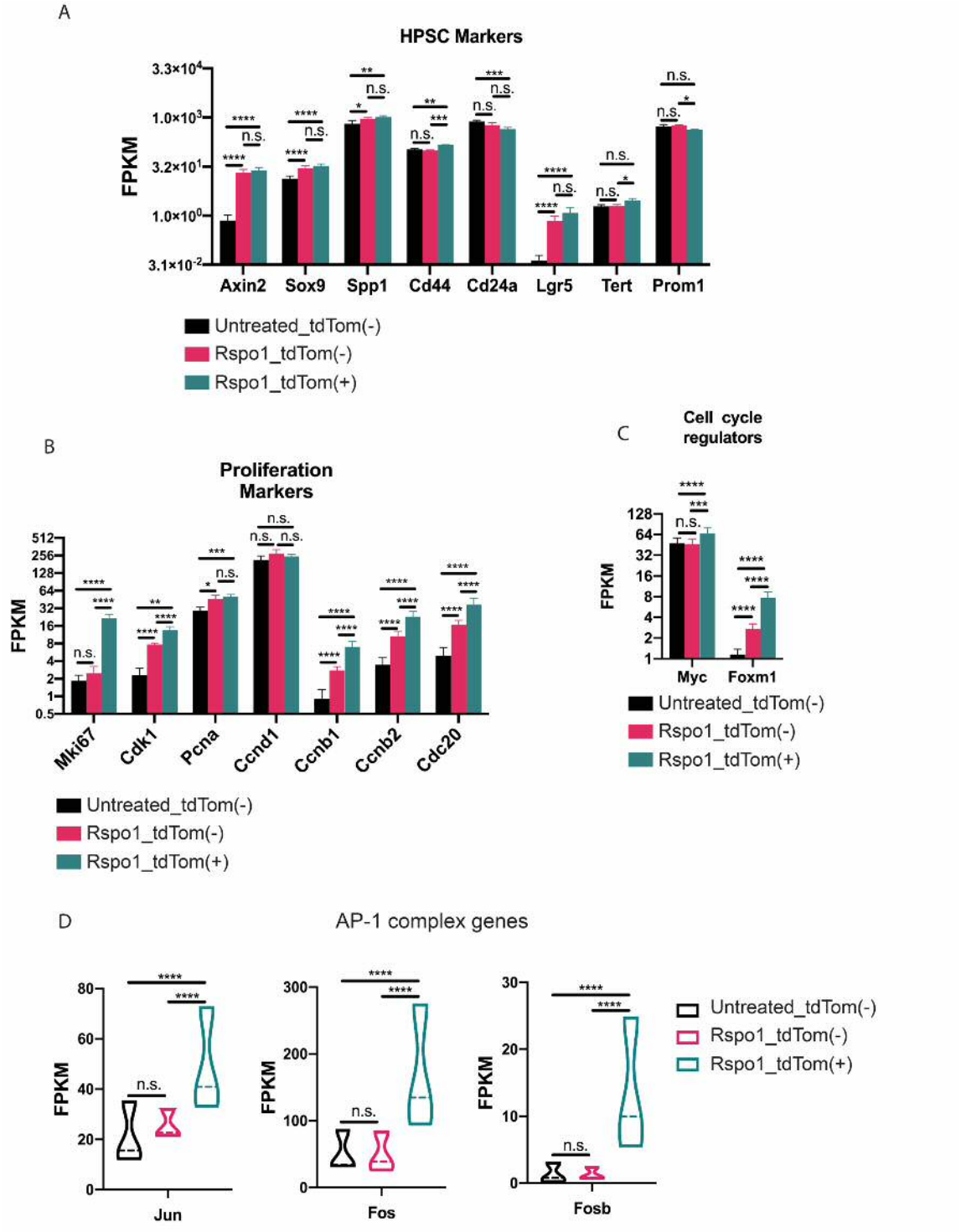

Figure 6.16 Rspo1 treatment modulates the expression of HPC markers, cell cycle regulators and members of the AP-1 complex. Expression levels determined by RNAseq analysis of (A) HPC markers, (B) proliferation genes, (C) cell cycle regulators and (D) members of the AP-1 complex in tdTom(+), tdTom(-) and untreated cells by RNAseq expressed in normalized FPKM values.

cells when compared to tdTom negative cells (Figure6.16, D).

IPA gene enrichment analysis of 2-fold change differentially expressed genes (padj value ≤0.01) between tdTom positive and negative cells (1341 genes) revealed upregulation of canonical pathways in tdTom positive cells including “Brca1 DNA damage responses”, “Cell cycle and G2/M DNA damage checkpoint”, “mitotic roles of Polo-like kinase and DNA double-strand break repair by homologous recombination” (Figure6.17, A). Furthermore, tdTom positive cells were enrich-hed in genes involved in “Wnt/Ca2+ pathway” and “Cdc42 signalling”. Top upstream regulators of such responses were *NR1H3, YY1, LDLR* and *RR1B*. IPA analysis also revealed that gene networks regulated by *ZBTB17* were significantly downregulated in tdTom positive cells.

~65% of the total variance between tdTom positive and negative populations was explained by the first component (PC1) of the analysis (Appendix D, Figure 6, C). Gene Ontology (GO) analysis with AmiGO showed that the top 500 of PC1 were enriched in GO terms such as “Cell cycle”, “Nuclear division”, “DNA repair” and “Protein localization to chromosome” (Figure6.17, B). According with an upregulation of genes involved in cell cycle progression in the tdTom positive population, Gene Set Enrichment Analysis (GSEA) using differentially expressed genes (padj value ≤0.01) between tdTom positive and negative cells (5333 genes), further showed enrichment of E2F target genes in tdTom positive cells (Figure6.17, C). Plots corresponding to the rest of the gene sets identified by GSEA are shown in Appendix D, Figure9.

Altogether, these results indicate that tdTom positive cells primarily differ from tdTom negative cells in their level of expression of genes related to cell cycle progression, G2/M transition and DNA repair.

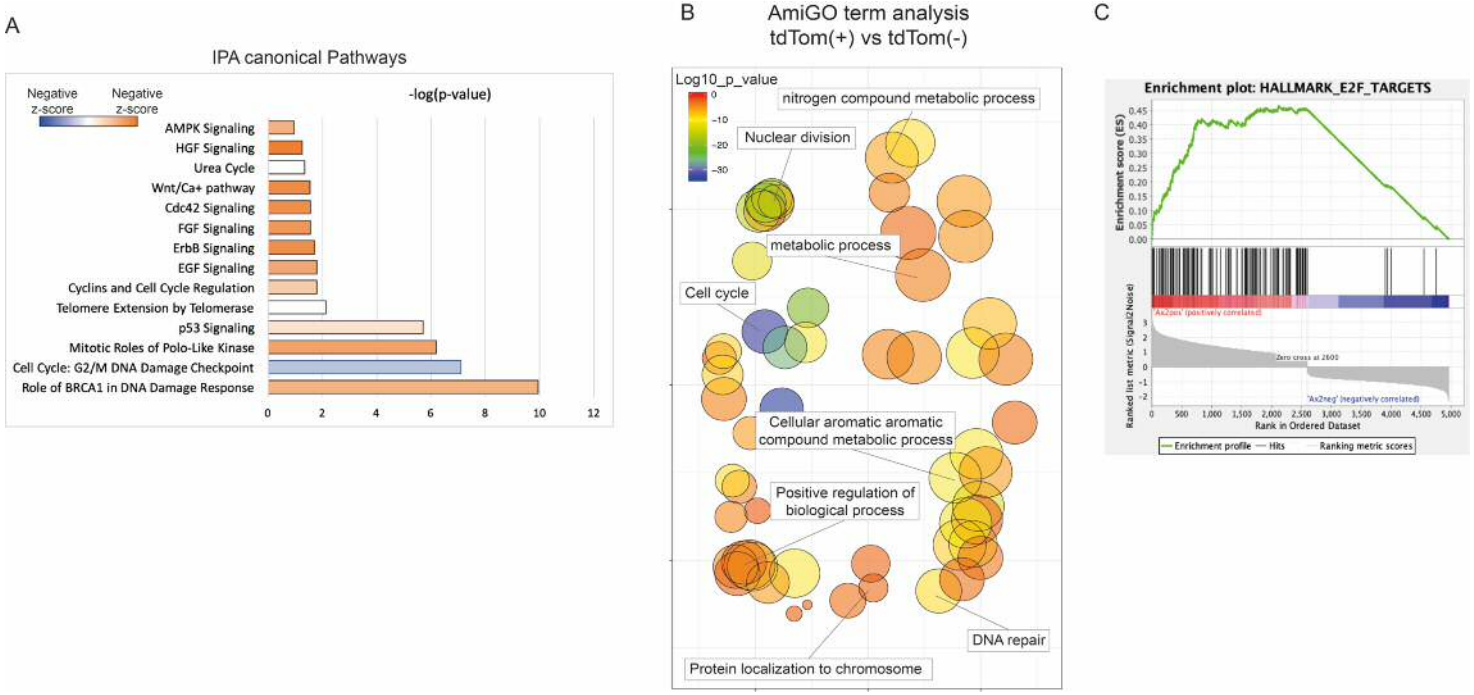

Figure 6.17 Transcriptome comparison between tdTom(+) and tdTom(-) cell populations (A) IPA canonical pathway analysis of 2-fold change differentially expressed genes (padj value ≤0.01) between tdTom(+) and tdTom(-) cells (1341 genes). (B) REVIGO scatterplot of the enriched GO terms from Rspo1-treated BD organoids RNAseq experiment. GO enrichment analysis for top most variable 500 transcripts in PC1 when comparing tdTom(+) vs tdTom(-) PC1. Analysis was performed with n=3 and excluding animal 3 from the analysis. Colours reflect the padj associated with the GO term categories while circle size reflects the number of genes relating to the term. Exemplary GO terms have been labelled. C) GSEA analysis using MSigDB C2 comprising Curated Gene Sets from online pathway databases publications in Pubmed and+ knowledge of domain experts reveal enrichment of E2F target genes in tdTom(+) cells when compared to tdTom(-) cells. Analysis was performed in genes differentially expressed genes between tdTom(+) and tdTom(-) with a padj ≤ 0.01. A total of 5333 genes where found differentially expressed. Of those 5047 had a human orthologue and therefore could be analysed using GSEA.

6.2.6.4 Hippo pathway signature genes remain largely unaffected upon Rspo1 treatment

Recent studies of Planas-Paz et al. (2019) have placed Hippo-YAP/TAZ signalling as a key mediator of the BEC hyperproliferative response seeing during DR formation following DDC treatment. I therefore next examined whether Wnt activation had an impact on YAP target gene expression considered as Hippo pathway signature genes [201]. Interestingly, Rspo1 had a differential effect in YAP-target genes. Cyr61 was significantly upregulated upon Rspo1 in both tdTom positive and negative cells. Ankrd1 appeared significantly upregulated in tdTom positive but not in tdTom negative cells when compared with untreated cells. Klf6 was significantly downregulated in both in tdTom positive and negative cells when compared to untreated cells while other YAP target genes (Ctgf, Areg, Amotl1 and Gadd45b) remained unaffected (Figure6.18).

Altogether these results suggest that, and with the exception of *Cyr61* and *Klf6*, activation of Wnt signalling in BD organoids had a minor effect in the Hippo pathway signature genes.

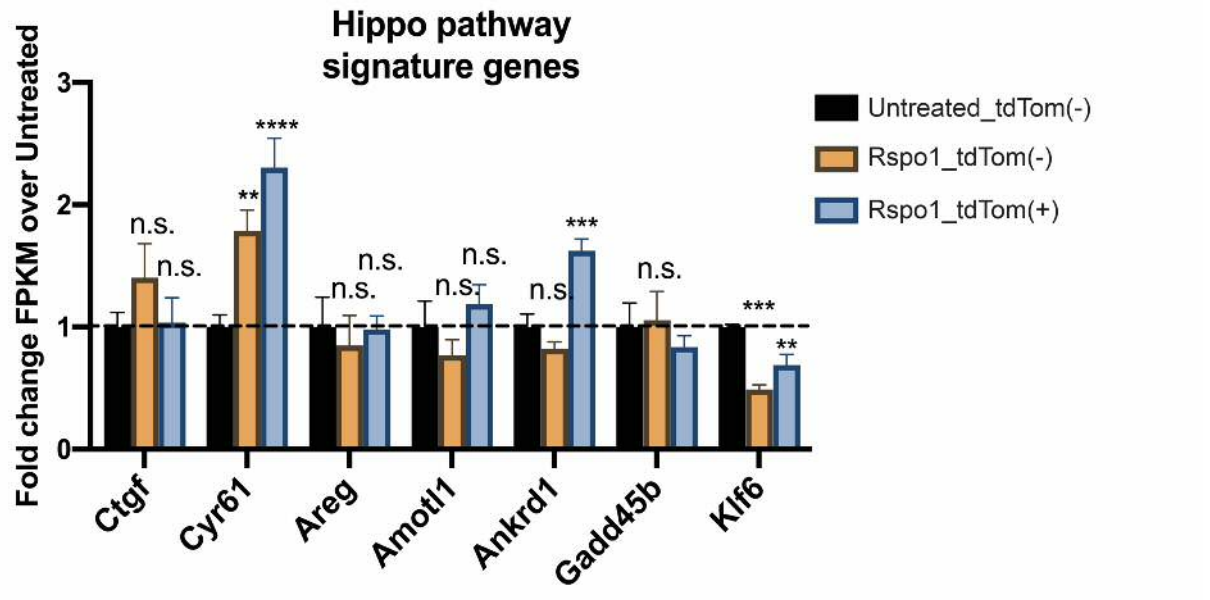

Figure 6.18 Hippo pathway signature genes remain largely unaffected upon Rspo1 treatment. RNAseq gene expression values of YAP target genes in tdTom(+), tdTom(-) and untreated cells. FPKM values were normalized over untreated cells.

6.2.6.5 Activation of Wnt pathway in differentiated BD organoids promotes escape from biliary fate

In section 6.2.1 was described that activation of the Wnt pathway in differentiated BD organoids enhanced the expression of HPC related genes, suggesting that activation of the Wnt signalling pathway in these structures promotes scape from their BEC/hepatocyte differentiated state. Thence, I next evaluated whether the expression of hepatocyte and BEC lineage markers was affected upon Rspo1 treatment. As expected, RNAseq gene expression analysis revealed an overall pattern of increase in the expression of HPC genes upon Wnt pathway stimulation (Figure6.19). By contrast, the expression levels of BEC lineage markers seem to anti-correlate with the Wnt activation levels in the sequenced cell populations. Out of the three hepatocyte lineage markers evaluated only Hnf4a showed a clear declining expression trend upon Rspo1 exposure (Figure6.19).

The decrease in the expression levels of Hnf4a, Krt19 and Epcam upon Wnt stimulation was additionally validated in the BD Tet-O-ΔN89β-catenin organoid line. For that aim, differentiated (13 days) BD Tet-O-ΔN89β-catenin organoids were

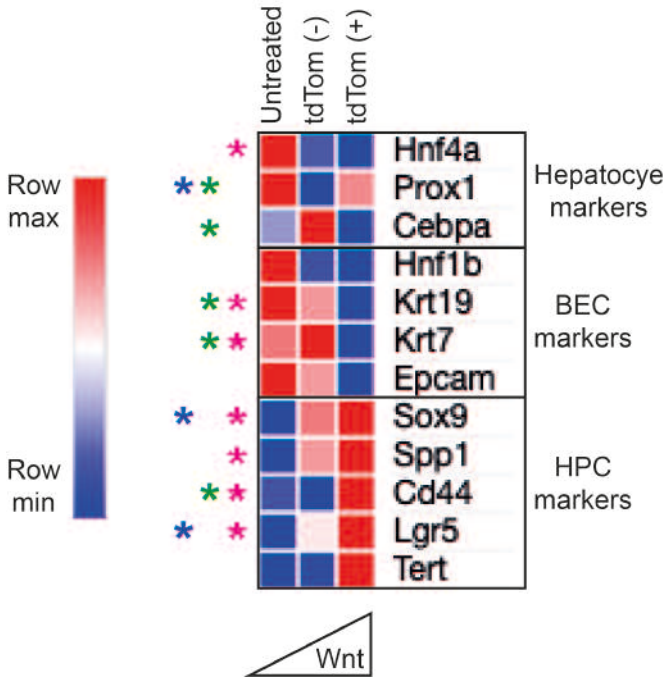

Figure6.19 RNAseq CPM gene expression values of various hepatocyte, HPC and BEC lineage markers. Blue asterisk indicates differentially expressed (padj ≤ 0.01) between untreated and tdTom(-) cells. Green asterisk indicates genes differentially expressed (padj ≤ 0.01) between tdTom(-) and tdTom(+) cells. Magenta asterisk indicates genes differentially expressed (padj ≤ 0.01) between untreated and tdTom(+) cells. The triangle at the bottom indicates the Wnt activation levels of the sequenced populations according to data presented in Figure6.15.

exposed to either Dox or Rspo1 for the last 3 days of differentiation. Activation of the Wnt signalling pathway either through β-catenin stabilization (0.1 μg/ml of Dox) or by the exposure to Rspo1 (100 ng/ml) in these cultures caused a significant decrease in the expression levels of Hnf4a and Krt19 (Figure6.20). Exposure to Rspo1 caused additionally a significant decline in the mRNA levels of Epcam.

Taken together, the results from the differentiated BD organoid platform suggest that while activation of canonical Wnt signalling promotes escape from biliary fate and, possibly, impairs hepatocyte fate specification.

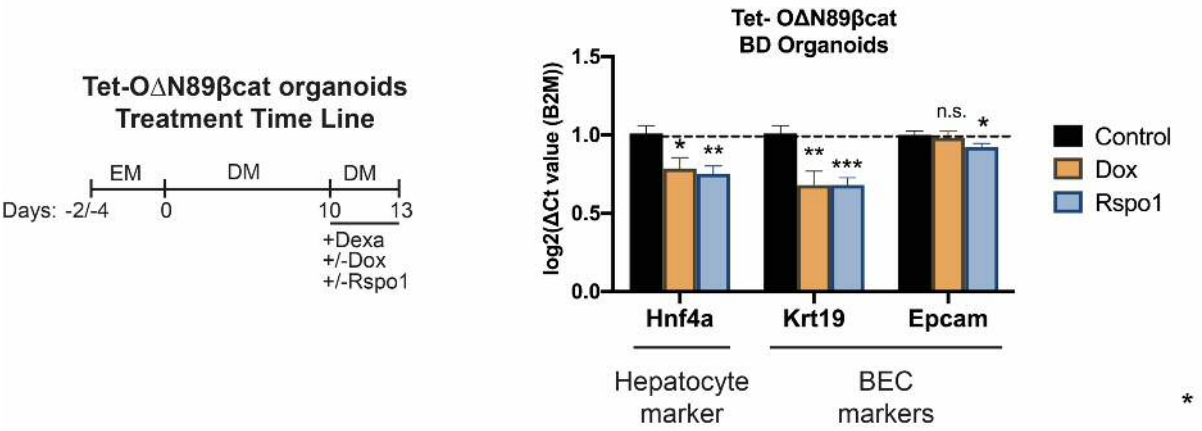

Figure6.20 On the left panel, treatment time line for Tet-OΔN89βcat BD organoids. Wnt pathway was activated either by the treatment with Rspo1 (100 ng/ml) or by stabilization of mutant activated β-catenin by the exposure to 0.1 mg/ml Dox during the last three days of differentiation. On the right panel, RT-qPCR gene expression shows a significant decline in the expression of hepatocyte (*Hnf4a*) and BEC (*Krt19* and *Epcam*) lineage markers upon Wnt activation.

6.3 Discussion

6.3.1 mVenus-hGemi expression could not be detected by flow cytometry in Fucci2a organoids

Experiments shown in the current chapter have failed to report the presence of cells positive for mVenus expression and therefore the different phases of the cell cycle could not be distinguished in established Fucci2a BD organoids cultures.

The Fucci2a mouse model is a 2A-bicistronic reporter, meaning that in this mouse model the expression of two reporter proteins is controlled by a single open reading frame (ORF) [199]. Expression of the Fucci2a transgene give rise to a single mRNA

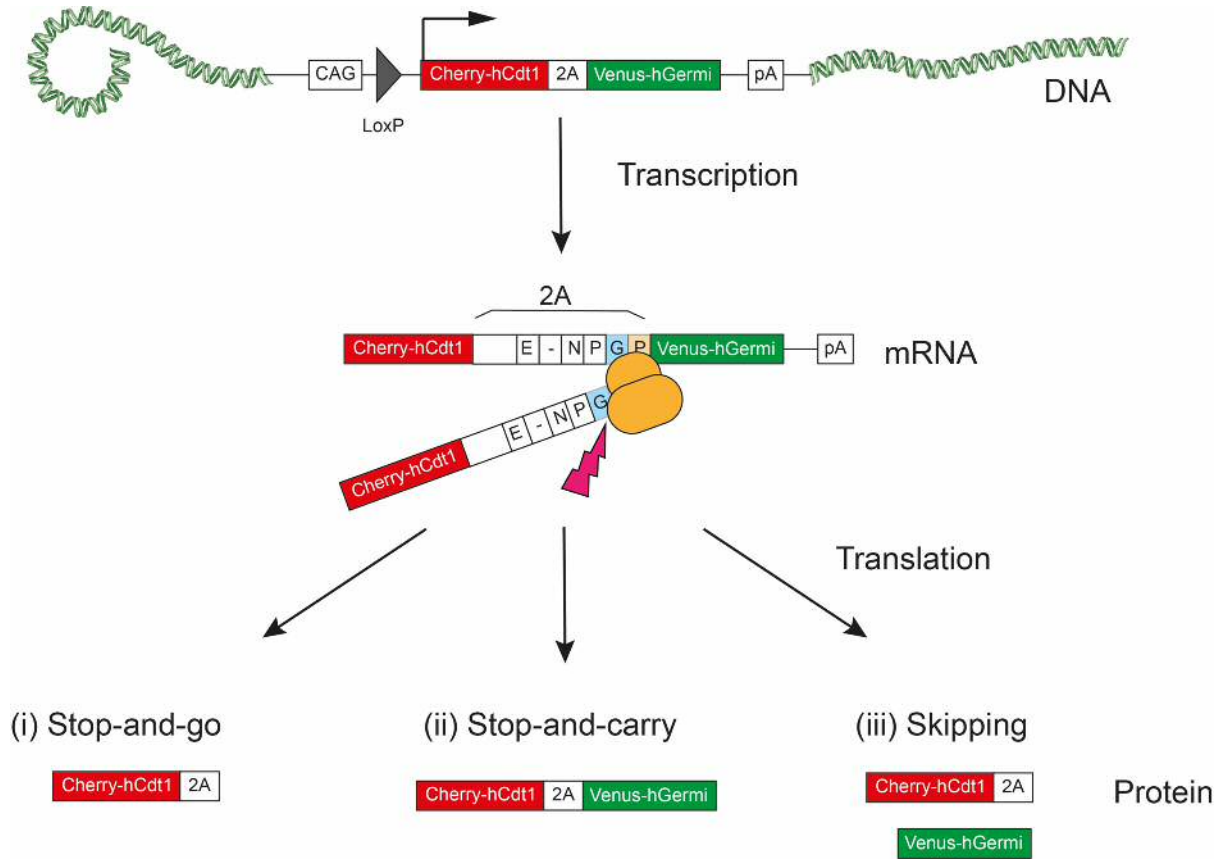

Figure 6.21 Fucci2a Ribosome Skipping. The Fucci2a construct is a bicistronic transgene where the expression for mCherry-hCdt1 and mVenus-hGemi is regulated by a single promoter (CAG). Upon transcription, a single mRNA containing both mCherry-hCdt1 and mVenus-hGemi coding sequences linked by a 2A sequence is generated. The 2A sequence causes the ribosome to stop during translation triggering three possible outcomes: (i) ribosome "stop-and-go", which would result in the sole translation of the protein preceding the 2A peptide sequence, (ii) ribosome "stop-and-carry", which would give rise to a mCherry-hCdt1/mVenus-hGemi fusion protein and (iii) ribosome "skipping", which would cause the production of both mCherry-hCdt1 and mVenus-hGemi proteins in equimolar ratio. In case of ribosome skipping, the "cleavage" occurs between the last proline and glycine of the 2A sequence.

that comprise both the coding sequence for mCherry-hCdt1 and mVenus-hGemi separated by a 2A sequence (Figure6.21). The 2A sequences are sequences of viral origin coding for a ~20aa long peptides with a conserved motif that end in proline-glycine and cause ribosome-pause during translation. This leads to the premature translation termination in absence of a stop codon and cleavage of the protein sequence at the level of the proline-glycine intersection of the 2A peptide. After the pause, the ribosome re-start the translation of the protein placed downstream of the 2A sequence. This process is known as "ribosome skipping" and as a consequence of this event, two proteins (mCherry-hCdt1 and mVenus-hGemi) that are dynamically

degraded during cell cycle progression are produced, which would cause labelling of the cells in red during G1 and in green during G2/M phase (Figure6.21).

Ribosome skipping in bicistronic transgenes is expected to produce equimolar quantities of the proteins placed upstream and downstream of the 2A sequence. However, studies performed by Liu et al. (2017) have shown that the order in which the genes are placed in polycistronic 2A systems matters during translation and it has been estimated that the expression of a gene decreases by ~70% when this is placed in the second position [202]. Non-equimolar production of the coding sequences is explained by the presence of two alternative resolution mechanisms for the pausing of the ribosome during translation: (i) ribosome "stop-and-go", an event where the ribosome fall off and the translation of the second protein is discontinued and (ii) "stop-and-carry" event, which leads to the production of a fusion protein with the 2A peptide as a linker (Figure6.21) [202,203]. As experiments shown in the current chapter have failed to report the expression of mVenus-hGemi, further studies are need to determine whether the predominant form in which the ribosome-pause induced by the 2A peptide in this system is resolved by a mechanism other than ribosome "skipping".

6.3.2 Activation of the TCF/Lef:H2B-GFP reporter may not be used as a readout for Wnt activation levels in BD organoids

The activity of the TCF/Lef:H2B-GFP reporter increased following differentiation, indicating that activation of the TCF/Lef:H2B-GFP reporter in this system does not correlate with the Wnt activation levels of the cultures. Thence, data presented in the current therefore showed that the TCF/Lef:H2B-GFP reporter may not be used to assess the Wnt activation levels on BD organoids.

These results raise two important questions regarding the TCF/Lef:H2B-GFP reporter: (1) is the TCF/Lef:H2B-GFP reporter activated in a Wnt independent manner in BD organoids and (2) why does the activity of the TCF/Lef:H2B-GFP reporter anti-correlate with the activation levels of the cultures following differentiation?

The use of TCF reporter systems as a proxy for canonical Wnt activity is based on the assumption that factors from the TCF/LEF family lack transcriptional activity in the

absence of β-catenin. However, different research groups have suggested that activation of the TCF/LEF reporter can also take place in a β-catenin-independent manner. For instance, overexpression of TCF4 and LEF1 alone is sufficient to induce activation of the TCF/LEF reporter in human chondrocytes [204]. Similarly, overexpression of TCF1 and LEF1 in HEK293 cells lead to an increase in TCF/LEF reporter activity [205] Importantly, overexpression of a mutant form of TCF1 lacking β-catenin binding domain in HEK293T also caused an increase in the activity of the TCF/LEF reporter, suggesting that TCF1-dependent activation of the reporter occurs, at least partially, independently of the presence of β-catenin [205].

In the resting liver, the TCF/Lef:H2B-GFP reporter appears highly activated in BECs despite the fact activation of canonical Wnt signalling in the biliary epithelium is virtually absent. This suggests that homeostatic BECs *in vivo* show high β-catenin-independent TCF activity. As BD organoids are structures with a cell identity close to BECs (see Chapter 5), a similar β-catenin independent mechanism for the activation of the TCF/Lef:H2B-GFP reporter is likely to take place in BD organoids.

The activation of the TCF/Lef:H2B-GFP reporter by a β-catenin independent mechanism may explain the presence of H2B-GFP positive cells in BDorg-DM conditions but does not explain itself why the number of these increase upon differentiation. To find an explanation for this phenomenon, the recycling and cell division dynamics of both GFP-labelled and non-GFP-labelled H2B might also need to be taken into consideration.

Upon division, the histones of a cell are disturbed between the newly formed daughter cells. In the case of a cell expressing high levels of H2B-GFP, this would lead to a drop in green fluorescence levels as some of the H2B-GFP histones will be substituted by non-GFP H2B histones. Thus, a chain of rapid cell divisions is expected to dilute the labelling of H2B-GFP in highly proliferative cells (Figure6.22, A). By contrast, an increase in the levels of green fluorescence is expected in slow dividing cells as

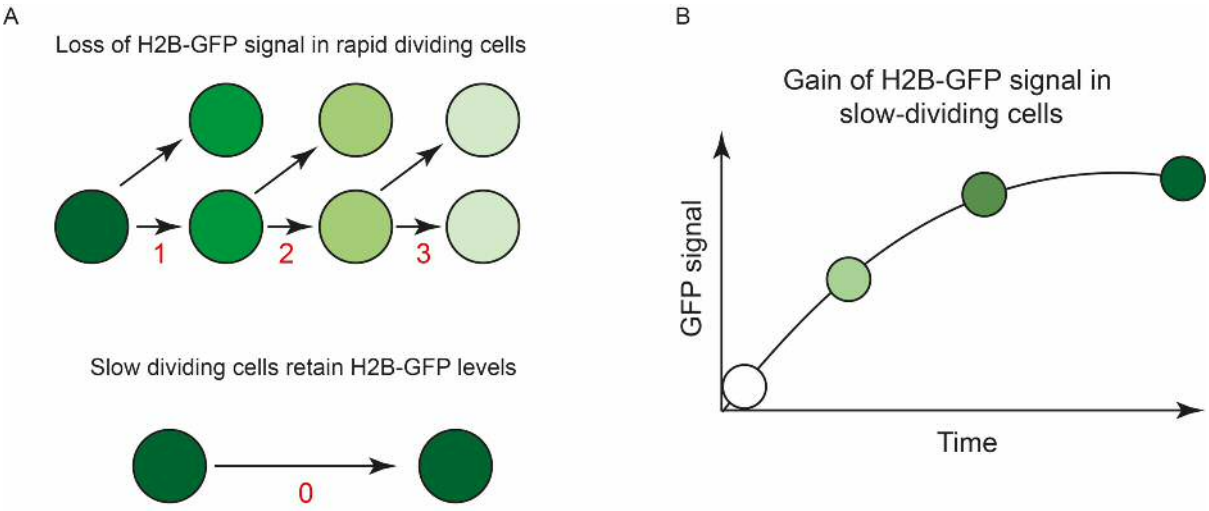

Figure 6.22 TCF H2B reporter model (A) Model for the loss of H2B-GFP signal in highly proliferative cells. Top panel represents a rapid dividing cell. Non-GFP labelled are incorporated in every cycle of division, which causes the progressive loss of H2B-GFP signal in rapid dividing cells. In the bottom panel, quiescent cells do not enter in division and therefore retain the H2B-GFP signal. Red numbers indicate the number of divisions that the parental cell have undergo. (B) Model for the gain of nuclear H2B-GFP in quiescent or slow dividing cells. Quiescent or slow dividing cells express the TCF/Lef:H2B-GFP reporter at basal levels. Upon time, non-GFP labelled H2B histones are recycled and substituted with H2B-GFP, which accumulates in the nuclei and leads to the increase overall increase in GFP fluorescence in the cell over time.

endogenous non-GFP labelled H2B be recycled and replaced by GFP-labelled H2B (Figure6.22, B).

Differentiation of BD organoids is accompanied by a decrease in the cell proliferation rate. Therefore, an increase in H2B-GFP expressing cells in BD organoids upon differentiation might be explained by the differences in the proliferation rate between cells cultured in BDorg-EM and BDorg-DM together with the assumption that the TCF/Lef:H2B-GFP reporter is expressed at low levels in a β-catenin independent manner in BD organoids.

Finally, in the TCF/Lef:H2B-GFP transgenic mouse model, the TCF/Lef:H2B-GFP construct was randomly integrated into the genome and therefore this transgene might be susceptible to silencing events upon culture, which might also be taken into account when interpretingif the presence of tdTom positive GFP negative cells.

6.3.3 Rspo1 induces the expression genes involved in G2/M transition and DNA repair in 'high Wnt' (tdTom positive) cells

Wnt pathway has been previously related to the modulation of cell proliferation in diverse cellular contexts [206]. The canonical branch of the pathway has been shown to regulate G1-to-S phase cell cycle progression as β-catenin controls the expression of genes (CyclinD1 and c-myc) required for this transition [206]. Accordingly, RNAseq data presented in the current chapter showed that BD organoid cells with high Wnt activation levels (tdTom positive) have significantly higher expression of c-myc than low Wnt cells (tdTom negative and untreated cells). Wnt signalling additionally modulate G1-to-S phase transition at the level of GSK3, as many proteins involved in the regulation of G1-to-S transition are substrates for GSK3 phosphorylation (Figure6.23).

Wnt signalling additionally controls G2-to-M cell cycle progression although this has been proposed to occur independently of β-catenin transcriptional activation. For instance, the Wnt/STOP pathway (see Chapter1) has been shown to control cell size during G2/M phase via GSK3 inhibition and protein stabilization [137] [75]. Various components of the Wnt signalling cascade (β-catenin, Axin2, Dvl, APC and GSK-3β) additionally participate in centrosome splitting at the end of G2 phase [207] [208,209]. Finally, Axin2 and APC have also been shown to localize to the mitotic spindle during mitosis and are essential for chromosome segregation [210,211].

Data presented in the current chapter indicates that Wnt activation levels in Rspo1 treated BD organoids cells correlated with the expression of genes involved in G2/M transition (Cdk1, Ccnb1, Ccnb2 and Cdc20) and G2/M checkpoints regulators. These findings are consistent with the observations of Feng et al. (2012), who using an $Axin1^{fl/fl}$ AhCre mouse model showed that activation of Wnt signalling in the hepatocellular compartment by acute loss of Axin1 caused an increase in expression of genes involved in the control of the G2/M phase of the cell cycle and, therefore, open the possibility that Wnt pathway might additionally modulate G2-to-M cell cycle progression by controlling gene expression. [212]. Further studies are required to determine whether this is the case.

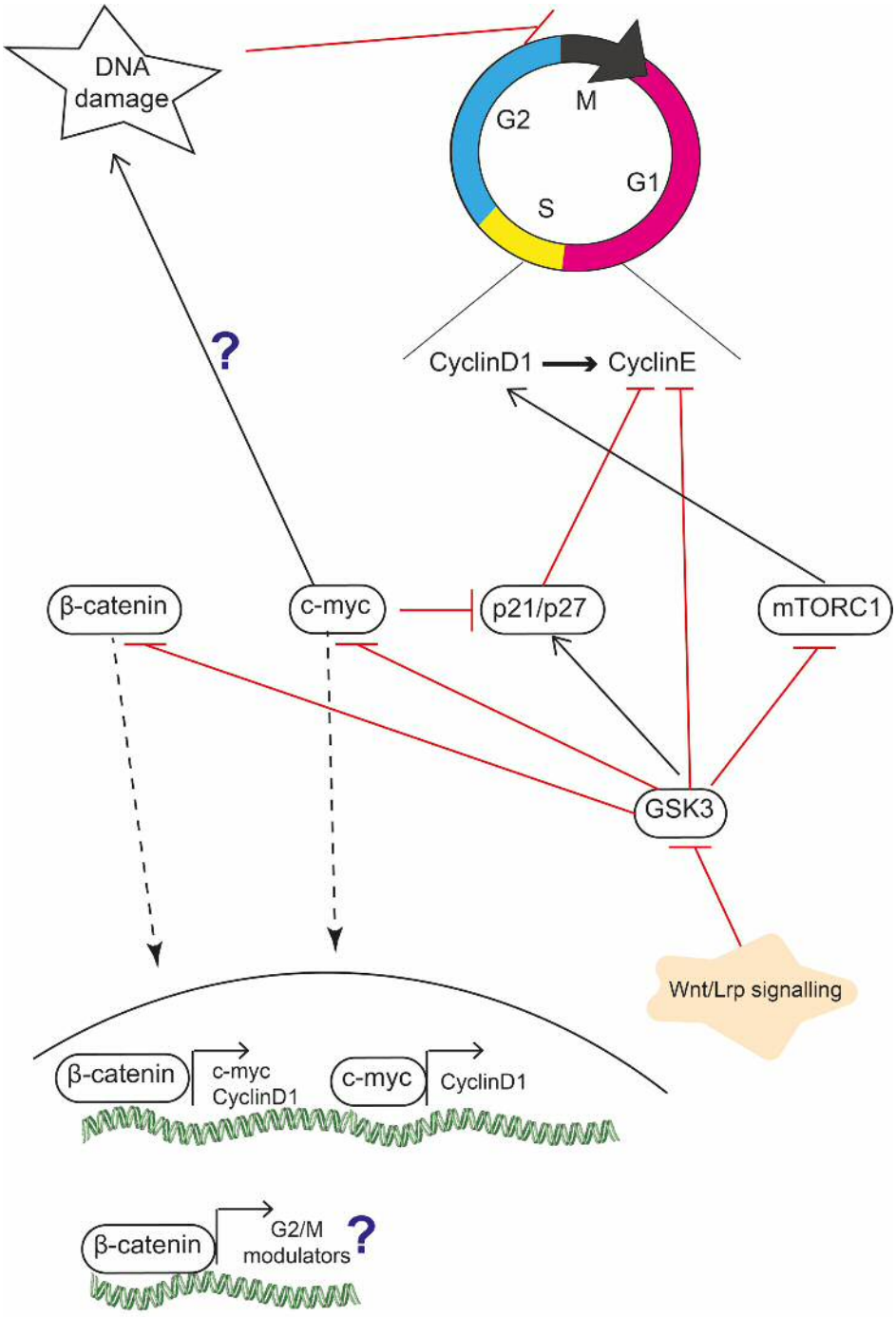

Figure 6.23 Wnt/Lrp signalling modulates G1-to-S cell cycle progression. Activation of the canonical Wnt signalling inhibits GSK3, resulting in the stabilization of β-catenin and c-myc at the protein level. Both c-myc and β-catenin drive the expression of CyclinD1, which enables activation of CyclinE and therefore, promotes G1-to-S cell cycle progression. GSK3 additionally tightly regulates the activity of mTOR and p21/p27 via phosphorylation, which also feed into G1-to-S cell cycle progression. The Wnt/Lrp signalling cascade might additionally modulate the G2-to-M cell cycle via c-myc mediated DNA damage/cell stress response and/or by controlling the expression of G2/M modulators. Figure adapted from {Acebron:2012jl}.

An alternative explanation for the enrichment of genes involved in the G2/M phase of the cell cycle is that could be that cells paused or transitioning G2/M are more sensitive to Wnt activation rather than Rspo1 treatment/Wnt activation itself is having a direct effect in the expression of these target genes. In support of this, the CDK14/PTFK1 complex phosphorylate Lrp6 Pro-Pro-Pro-Ser-Pro (PPPSP) intracellular domain during G2/M, which in turn primes Lrp6 to optimally respond to incoming Wnt cues during in G2/M [213]. Further work will be therefore required to determine whether β-catenin or other branch of Wnt signalling is indeed affecting the expression of the G2/M regulators.

Results from this chapter additionally showed that Rspo1 induced a strong DNA repair signature in tdTom positive cells when compared to tdTom negative cells. Previous studies have also related the activation of Wnt signalling with a DNA damage response. For instance, studies performed by Xu et al. (2008) showed that expression of a mutant stable form of β-catenin lacking the 87 N-terminal amino acids of the protein (ΔN87β-catenin) triggers the appearance of double-strand DNA breaks (DSBs) in thymocytes, which results in an increase of γH2AX foci [214]. Similarly, expression of Wnt-1 in human mammary epithelial cells also causes an increase in phospho H2AX, indicating that activation of Wnt signalling also induces DSBs in the context of the mammary gland [215]. BRCA1 is a protein that is recruited to DSBs following damage and associates with γH2AX to assist DNA repair [216]. One of the top canonical pathways identified by IPA was the “role of BRCA1 in DNA Damage Response”, further suggesting the possibility of Wnt pathway activation inducing the appearance of DSBs in differentiated BD organoids. To demonstrate that the molecular signatures identified by IPA in tdTom positive cells relate to the appearance of DSBs in BD organoids upon Wnt signalling stimulation, additional studies will be needed in which the proportion of tdTom positive and negative cells positive for the presence of γH2AX foci are quantified.

Rspo1 induced transcriptome changes in both tdTom positive and negative cells. When comparing tdTom positive and negative cells with untreated cells, both Rspo1-treated cell populations were enriched for GO terms related to cell proliferation such as “nuclear division” or “mitotic cell cycle process”. However, a “DNA repair”/”cellular

response to DNA damage" signature was only detected in tdTom positive cells when comparing these either with tdTom negative or untreated cells. Interestingly, tdTom positive cells expressed significantly higher levels of c-myc when compared to tdTom negative and untreated cells whereas non-significant changes in c-myc levels were detected when comparing tdTom negative cells with untreated cells. A direct mechanistic link between activation of Wnt and the appearance of DSBs DNA repair response has been suggested by the observation that overexpression of c-myc leads to DNA replication stress and DSBs in different cellular contexts [217-221]. In future investigations it might be, therefore, interesting to address whether c-myc is mediating the appearance of a Rspo1-driven DNA repair signature in the tdTom positive cell population.

Finally, an additional difference between tdTom positive and negative cells that arises from the technical approach employed for the identification of both cell populations as labelling of tdTom positive cells required the expression and activation of the Cre recombinase. Experiments performed in mouse embryo fibroblasts lacking LoxP sites have shown that activation of Cre recombinase activity can lead to the appearance of DSBs [222]. Activation of the Cre recombinase occurred 24h prior to RNAseq gene expression analysis. Thus, it is possible that transcriptional changes associated with Cre recombinase activation and putative induction of DSBs might also be captured in this analysis.

6.3.4 BD organoids are equipped to respond to Wnt activation

Data presented in the current chapter showed that BD organoids are source of various Wnt ligands (Wnt4, Wnt7a, Wnt7b and in less amount Wnt5b and Wnt10a). These ligands, in combination with Rspo1, were sufficient to activate canonical Wnt signalling in differentiated BD as shown by the increase in activity in the Axin2CreERT reporter and enhanced expression of various β-target genes by RT-qPCR, suggesting that (1) BD organoids express the receptors for Rspo1 signal transduction, (2) BD organoids express the receptors that mediate canonical Wnt signalling activation and (3) the Wnt ligands that are endogenously produced by BD organoids exert canonical Wnt activity. In the following section, it will be discussed how the different receptors and co-receptors expressed by differentiated BD organoids might relate to the ability of these

structures to respond to activation of Wnt signalling. Furthermore, a consideration to the biology of Wnt ligands expressed by differentiated BD organoids.

Rspo ligands bind to Lgr4/5/6 receptors, inactivating the E3 ubiquitin ligases Rnf43/Znrf3 that would otherwise degrade the Wnt receptors Fzd and Lrp present at the cell surface (Figure6.24). RNAseq analysis revealed that differentiated BD organoids expressed both Lgr4 and Lgr5 but not Lgr6. Lgr5 expression occurred, however, at very low levels, suggesting Lgr4 as the putative receptor mediating the response to Rspo1. Furthermore, the fact that Lgr5 was expressed at a very low levels in BD organoids might explain why recent studies from Planas-Paz et al. (2015) and Pepe-Mooney et al. (2019) have failed to identify Lgr5 expression in BECs using 10x genomics single-cell sequencing, as the depth of sequencing of this technique would likely miss genes expressed at such levels [22,93]. Differentiated BD organoids also expressed the E3 ubiquitin ligases Znrf3 and Rnf43 and of those, the expression of Rnf43 was significantly upregulated upon Rspo1 treatment, probably reflecting the presence of a feed-back negative loop to decrease Rspo1-mediated activation of the Wnt signalling pathway.

Activation of the canonical Wnt signalling cascade requires at least two types of receptors: a receptor from the Fzd family and a receptor of the Lrp family (see Chapter1) (Figure6.24). Differentiated BD organoids expressed Lrp5 and, in less amount, Lrp6 receptors (see Chapter1) (Figure6.24). Differentiated BD organoids also expressed various Wnt receptors of the Fzd family, being the most abundantly expressed Fzd1, Fzd4, Fzd5, Fzd6 and Fzd7. Of those, Fzd1, Fzd4, Fzd5 and Fzd7 have been shown to mediate activation of Wnt/β-catenin signalling (Figure6.24) [146,223-230]. Expression of these receptors is therefore consistent with the appearance of a canonical Wnt response in differentiated BD organoids. Further studies involving loss of function of Fzd1, Fzd4, Fzd5 and Fzd7 are required to evaluate the contribution of each of these receptors to Rspo1-driven activation of the canonical Wnt signalling pathway in the BD organoid *in vitro* platform.

Blockage of endogenous Wnt secretion with LGK974 abrogated Axin2 expression and depleted Rspo1-driven HPC signature, indicating Wnt7a, Wnt7b, Wnt4 or any of the other ligands expressed at low levels (Wnt10a and Wnt5b) or a combination of them

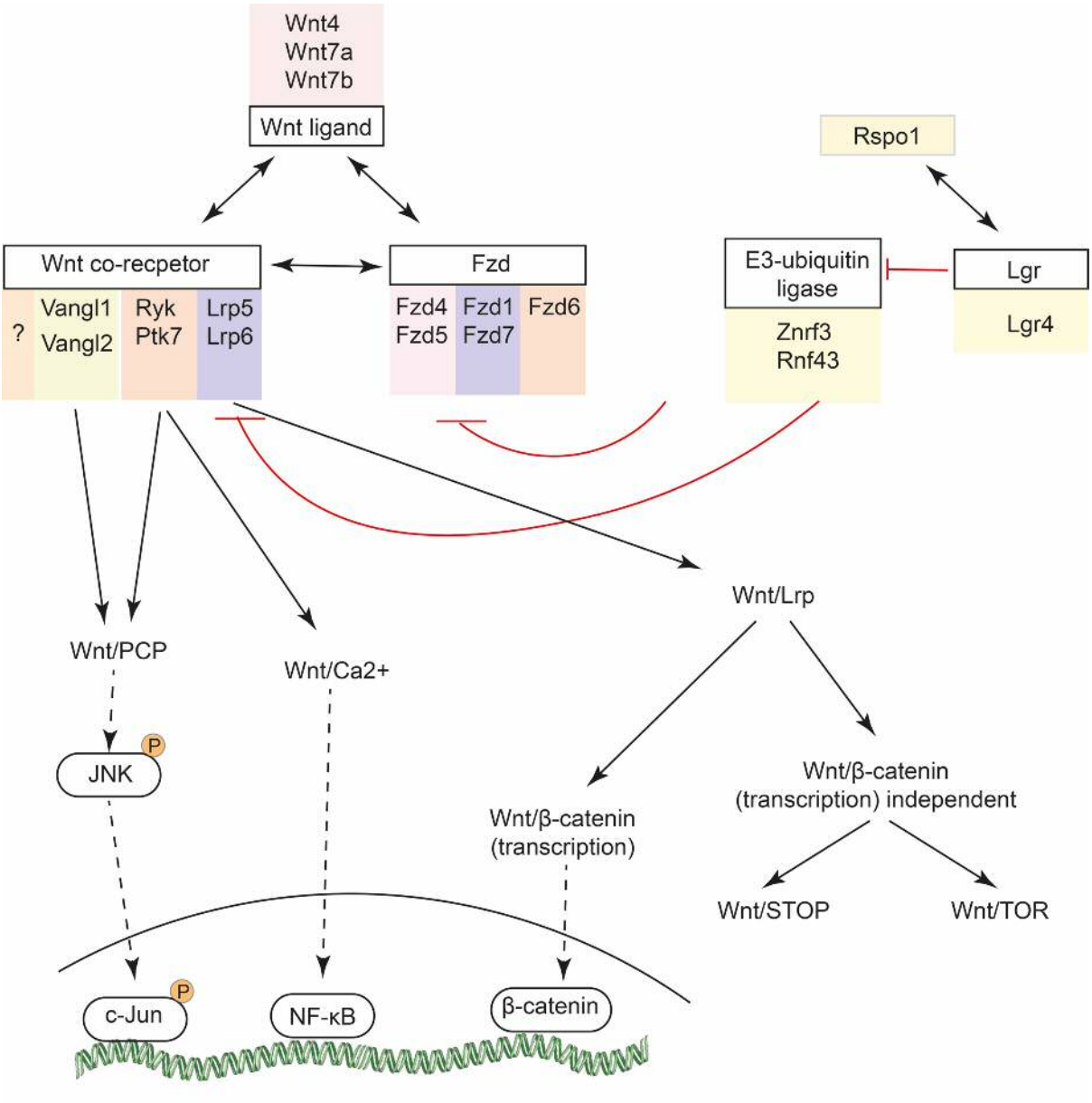

Figure 6.24 Scheme highlighting the Wnt/Rspo receptors and Wnt ligands primarily expressed by differentiated BD organoids according to the RNAseq data.

drives activation of Wnt/β-catenin signalling in differentiated BD organoids. The identity of the Wnt proteins determines which branches of the Wnt signalling pathway are activated. Hence, further experiments are required to determine whether Wnt7a, Wnt7b, Wnt4, Wnt10a or Wnt5b, or a combination of them, is responsible for the induction of canonical Wnt signalling in differentiated BD organoids.

In addition to the canonical Wnt receptors, differentiated BD organoids also expressed receptors primarily associated with Wnt Lrp-independent signalling including Ryk, Ptk7

and Vangl1 and, in lower amount Rora, Vangl2, Prickle1, Prickle3 and Prickle4. Furthermore, the Fzd receptors expressed by BD organoids have also been implicated with the signal transduction of the Wnt/Ca2+ signalling cascade (Fzd4, Fzd5 and Fzd6) as well as the Wnt/PCP pathway (Fzd1, Fzd4, Fzd5, Fzd6 and Fzd7). BD organoids primarily expressed Wnt4, Wnt7a and Wnt7b. Wnt4 is a ligand that has been historically categorised as a non-canonical Wnt protein. Wnt7a and Wnt7b are two closely related ligands that share ~77% total-aminoacid-identity and, both of them, have been shown to activate the Wnt/PCP pathway and the Wnt/Ca2+ signalling pathways [231-234].

The fact that BD organoids express ligands and receptors that mediate Lrp-independent signalling suggest that, in addition to the Wnt/β-catenin signalling, other branches of the Wnt pathway might have been activated in response to Rspo1 treatment (Figure6.24). In support of this, RNAseq analysis revealed that cells with high canonical Wnt signalling (tdTom positive cells) were also enriched for the expression of genes involved in the Wnt/Ca2+ signalling when compared to tdTom positive cells (Figure6.24). Furthermore, recent studies from Wilson et al. (2020) have shown he Wnt/PCP pathway is activated BD organoids cultured in BDorg-EM as loss of Vangl2, caused a reduction in the levels of phosphorylated-JNK$^{T183/Y185}$ and phosphorylated-c-JUN^{S73}.

Studies conducted by Wilson et al. (2020) have also showed that deletion of Vangl2 in the biliary epithelium using a Vangl2$^{fl/fl}$ Krt19-CreRT2 transgenic mouse line abrogated phosphorylated-JNK$^{T183/Y185}$ and phosphorylated-c-JUN^{S73} expression in BECs following DDC injury regime, suggesting that BECs are responsive to respond to non-canonical Wnt injury cues during liver regeneration. Loss of Vangl2 in BECs also alleviated fibrosis in DDC- and TAA-injured livers, an effect that could be mirrored by the loss of Wnt5a in myeloid cells (LysMCre, Wnt5a$^{fl/fl}$) and, therefore, the authors of this study concluded that secretion of non-canonical Wnt injury cues from myeloid origin promotes ductular scarring. Wnt5a expression following DDC injury regime was, however, not persistent throughout the treatment, suggesting that other non-canonical Wnt ligands might also contribute to tissue scaring when the damage is prolonged. BD organoids were source of various Wnt ligands with non-canonical Wnt activity (Wnt4,

Wnt7a, Wnt7b, Wnt5b and Wnt10a) that potentially activate the Wnt/PCP pathway in these structures. Among these, BECs have been shown to increase the expression of Wnt7a, Wnt7b and Wnt10a in response to DDC injury regime [22,93,98]. As the relative of contribution of Wnt ligands from BEC origin to fibrotic scaring remains largely unexplored, further research should be undertaken to investigate the role of Wnt ligands from BEC origin during regeneration of the biliary epithelium and/or ductular scarring.

Altogether, results in the current chapter showed that BD organoids express canonical and non-canonical ligands are equipped to respond to the Wnt/β-catenin, Wnt/Ca2+ and Wnt/PCP signalling cascades. The possible implications of the activation of the Wnt/β-catenin and Wnt/PCP signalling cascades in BD organoids will be discussed in the section6.3.7. when dissecting the organoid forming phenotypes of tdTom positive and negative cells.

6.3.5 **Exposure of differentiated BD organoids to Rspo1 leads to a pro-fibrotic microenvironment**

Exposure to Rspo1 induced the expression of Il33 in differentiated BD organoids. Il33 is a pro-inflammatory cytokine that promotes hepatic fibrosis through the activation and expansion of liver resident innate lymphoid cells (ILC2) and hepatic stellate cells, [235]. Rspo1 treatment additionally induced the expression of Ihh, a ligand that activates the hedgehog pathway, which also promotes fibrotic scarring by enhancing the recruitment of peripheral monocytes into the liver during damage and driving the expression of pro-fibrotic genes (Spp1, Timp1 and Col1a1) in hepatic stellate cells [236]. By contrast, Rspo1 significantly reduced the expression of Bpm2 and Bmp6, two members of the BMPs family with anti-fibrotic role in the liver [237,238]. Thence, data from the current chapter suggest that activation of the Wnt pathway in differentiated BD organoid cultures generates a microenvironment prone for fibrosis. These results are in line with the recent observations of Wilson et al. (2020), who showed that de-sensitization of Wnt signalling in the biliary epithelium through the loss Vangl2 (Vangl2$^{fl/fl}$ Krt19-CreRT2) reduced Collagen-1 deposition following liver damage [94]. Furthermore, in the same study, Wilson and colleagues showed that pharmacological inhibition of the Wnt signalling pathway with LGK974 also alleviated liver fibrosis following DDC (2 weeks) or TAA (12 weeks) injury regime, opening the

possibility of targeting the Wnt signalling pathway as a therapeutic avenue for chronic biliary pathologies [94]. Further research should be therefore undertaken to investigate whether Rspo injury cues, by modulating activation of Wnt signalling in BECs, promote a pro-fibrotic microenvironment during liver damage *in vivo*.

6.3.6 Three-day exposure to Rspo1 cancels the organoid forming advantage of 'high Wnt' (tdTom positive) cells

Experiments performed by Huch et al. (2013) using an Lgr5-LacZ mouse model showed that only a small population of BECs responded to Wnt activating cues during CCl_4 acute injury and become positive for Lgr5 expression [89]. These 'high-Wnt responders' labelled as Lgr5(+) cells presented enhanced organoid forming capacity than their negative counterparts and therefore it was hypothesised that they constitute a biliary progenitor stem cell population. Accordingly, data presented in the current chapter showed that only a small population of cells within differentiated BD organoids becomes positive for tdTom expression (a proxy for high-Wnt) upon Rspo1 exposure. tdTom positive cells induced by 24h Rspo1 treatment expressed higher Lgr5 mRNA levels and presented enhanced organoid forming capacity than their negative counterparts. Furthermore, Axin2 lineage tracing experiments additionally showed that tdTom positive cells self-renew and repopulate differentiated BD organoids faster than their negatives counterparts, further suggesting that tdTom positive cells constitute a progenitor population within the organoids.

When organoids were exposed to Rspo1 for 3days, however, tdTom positive and negative cells formed a similar number of secondary organoids. The gain of stem cell features by the tdTom positive population suggests that negative cells also respond to Rspo1 treatment upon prolonged exposure to the ligand and that cells below the Axin2CreERT2 recombination also showed enhanced stemness. As mentioned earlier, the Axin2CreERT2 reporter is an On-/Off-state reporter system. Therefore, a possible explanation for these results is that prolonged exposure to Rspo1 is triggering activation of canonical Wnt signalling in all the cells present in the organoid at levels close to the recombination threshold of the reporter. As a result, tdTom positive and negative cells would present similar Wnt activation levels independently of their recombination state (Figure6.25). Initial differences between the stemness features

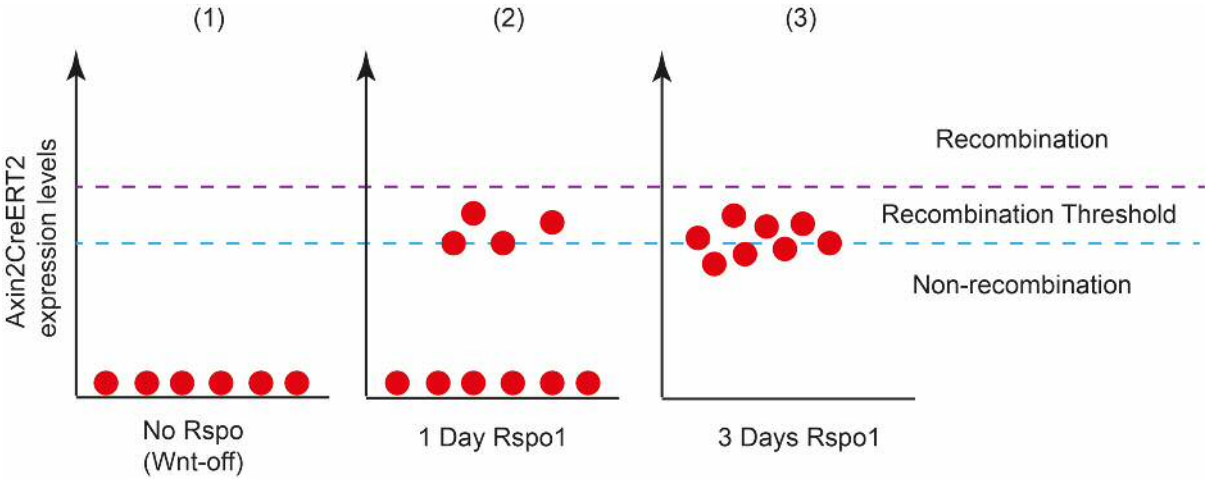

Figure 6.25 Model for the response of differentiated Axin2CreERT2 reporter BD organoids to Rspo1 exposure. Each red dot represents a cell. The position of the sphere in the Y axis indicates the production levels of CreERT2 recombinase (Wnt activation levels) of that particular cell. (1) In the absence of Rspo1, Axin2CreERT2 expression levels are below the threshold of recombination and therefore none cell results labelled with red fluorescence. (2) Upon 24h of Rspo1 exposure "quick" responders respond to the treatment and activate Wnt signalling at levels close to the recombination threshold. (3) "Slow" responders also have the capacity to respond to Rspo1 treatment although this required a prolonged exposure to the ligand. Factors such as state of differentiation, expression of Wnt/Rspo receptors, proximity to a high Wnt producing cell or phase of the cell cycle in which a particular cell is at a given time might explain differences between "quick" and "slow" responders.

between tdTom positive and negative cells can also be explained by the fact that certain cells within the organoids are primed to respond faster than others (Figure6.25).

This organoid cell response model would imply that all cells within the organoids, rather than a small population of them, are responsive to Wnt activating cues. Working under the hypothesis that Wnt triggers a regenerative program in the biliary epithelium, this would imply that all cells within the organoid may behave as progenitor cells upon sensing an injury input. These data thereby fit with the biliary epithelium stochastic regeneration model of Kamimoto et al. (2016), that proposed that inherent differences between BEC populations do not account for the regenerative potential of BECs when an injury input is perceived [18]. Furthermore, the fact that all organoid cells respond to Rspo1 upon prolonged exposure, also in the line with the latest results of Pepe-Mooney et al. (2019), who based on the observation that YAP transcriptional program is dynamically activated in BECs both in injury and homeostasis, have proposed a

biliary epithelium regenerative model in which BECs dynamically respond to environmental injury cues [22].

6.3.7 Possible molecular mechanisms behind the enhanced organoid forming capacity of 'high Wnt' (tdTom positive) cells

To prevent telomere shortening and cell cycle arrest upon several cycles of division, stem cells are equipped with telomere elongation mechanisms. IPA analysis presented in the current chapter revealed that various components of the telomere elongation machinery were significantly upregulated in tdTom positive cells. This also accords with the results from the functional assays and further supports that exposure

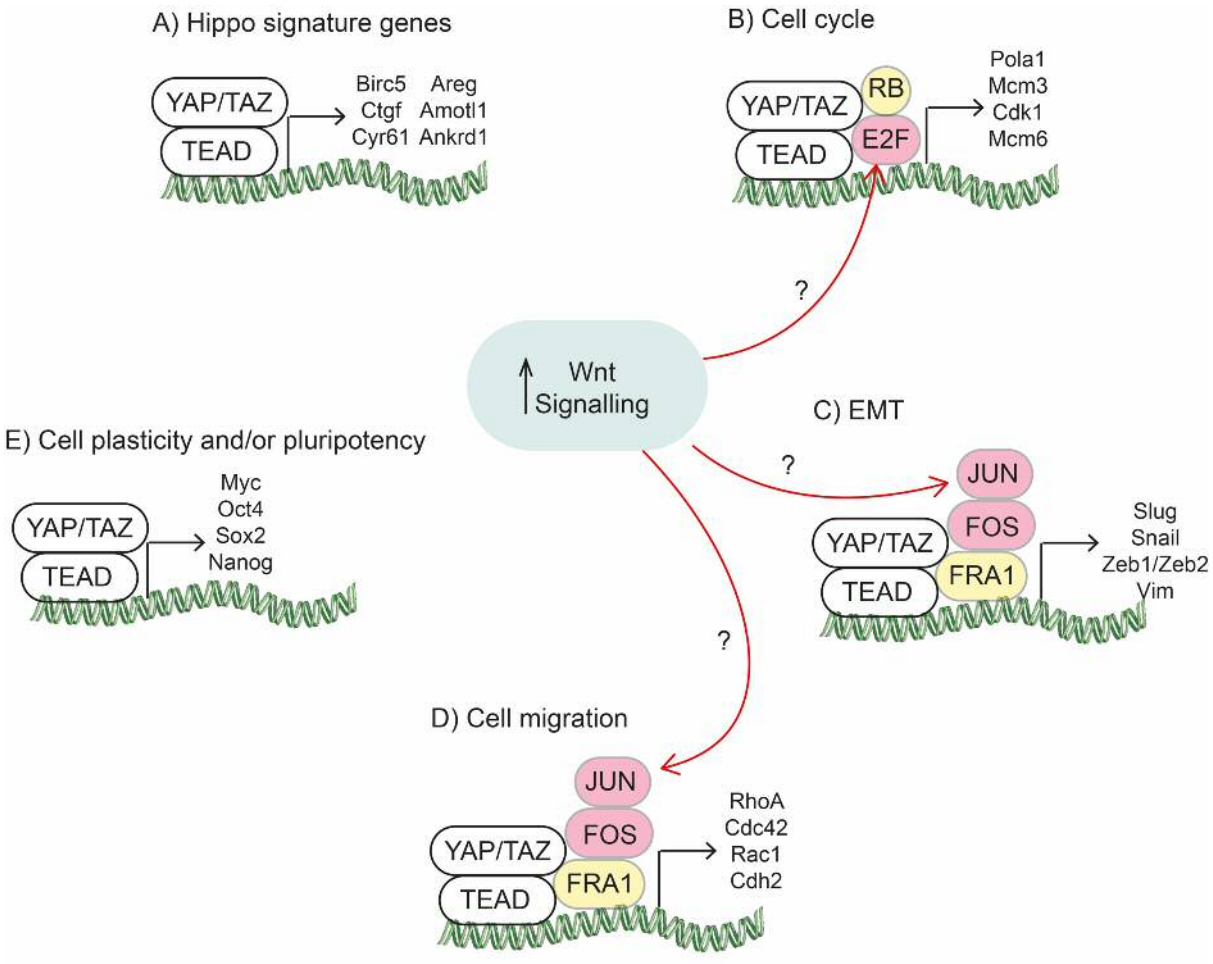

Figure 6.26 YAP signalling is highly activated in differentiated BD organoids. Thence, treatment of differentiated BD organoids with Rspo1 causes the activation of Wnt signalling in a "high YAP" cellular context. This scheme represent possible cellular responses expected from the co-operation between "high Wnt" and "high YAP" signalling in differentiated BD organoids. Figure adapted from Moya et al (2018).

to Rspo1 drives the appearance of an tdTom positive population with higher self-renewal rate and organoid forming capacity than their negative counterparts.

RNAseq analysis revealed that tdTom positive cells were enriched in cell cycle genes. However, Cyclin D1 (Ccnd1), a cell cycle gene that is under the transcriptional control of β-catenin and regulates G1-to-S phase transition, was not found differentially expressed between tdTom positive and negative cells [206]. Despite the fact that a few targets of β-catenin including Cd44 and Lgr5 were found differentially expressed between tdTom positive and negative cells, IPA analysis failed to identify Wnt/β-catenin signalling pathway as one of the pathways enriched in tdTom positive cells. Thence, based on the current RNAseq analysis, it remains unclear whether Wnt/β-catenin or another branch of the Wnt signalling pathway accounts for the Rspo1-driven cell cycle signature identified in tdTom positive.

The most abundant Wnt expressed by differentiated BD organoids was Wnt7b, a ligand that has primarily been associated with activation of the Wnt/PCP signalling pathway [76,232]. Activation of the Wnt/PCP pathway leads to the phosphorylation and activation of c-Jun N-terminal kinases (JNKs), which phosphorylates and activates Jun, Fos and Fosb (see Chapter1). Various components of the AP-1 complex (Jun, Fos and Fosb) were significantly upregulated in tdTom positive when compared to tdTom negative and untreated cells. As specific activation of the Wnt/PCP pathway will not be primarily reflected by changes in gene expression, further research involving the immunostaining of phosphor c-Jun (c-JUN^{S73}) should be undertaken to investigate whether Rspo1 activates the Wnt/PCP/JNK/c-JUN signalling pathway in differentiated BD organoids.

Recent studies from Pepe-Mooney et al. (2019) have highlighted the importance of YAP/TAZ signalling in the maintenance of the biliary epithelium homeostasis and regeneration [22]. YAP/TAZ are transcriptional co-activators that, in association with transcription factors members of the TEAD family (TEAD1-4), control the activation of diverse cellular programs including cell migration, EMT, cell cycle entry and cell plasticity and/or pluripotency (Figure6.26) [201]. For the regulation of such distinct genetic programs, YAP/TAZ/TEAD often rely on the association with other transcription factors. In combination with AP-1, YAP/TAZ/TEAD modulate the

expression of genes involved in cell migration (RhoA, Cdc42, Rac1 and Cdh2) and EMT (Slug, Snail, Zeb1/2 and Vimentin) (Figure6.26) [201]. By contrast, YAP/TAZ/TEAD complex in association with Rb/E2F drives the expression of cell cycle genes [201]. RNAseq analysis revealed that Rspo1 treatment significantly upregulated the expression of various members of the E2F family and that tdTom positive cells were enriched for the expression of E2F target genes. Furthermore, Rspo1 treatment significantly increased the expression of various members of the AP-1 complex. Thence, it would be interesting to explore whether activation of Wnt signalling in the 'high-YAP' context that represent cells of biliary fate is causing the activation the aforementioned genetic programs.

A final consideration should be paid to the fact that Axin2 was not differentially expressed between tdTom positive and negative cells. This result might be explained by the fact that the Axin2CreERT2 reporter is an On-/Off- reporter system together with the fact that the levels of Wnt activation at the single-cell level may fluctuate over time. To evaluate this hypothesis, further experiments involving labelling of tdTom positive cells at different times in combination with detection of Axin2 mRNA transcript by RNAscope should be carried out.

6.3.8 Activation of Wnt signaling in differentiated BD organoids impairs hepatocyte and BEC lineage specification

BD organoid differentiation is a dynamic process that lasts 10 to 13 days and requires the withdrawal of Rspo1 from the medium composition. Upon differentiation, BD organoids decrease the expression levels of HPC related genes (Tert, Cd44, Tacstd2 and Lgr5) while increasing the expression of BEC (Hnf1b, Krt19 and Krt7) and hepatocyte (Cebpa, Hnf4a and Prox1) lineage markers (see Chapter5). Importantly, the acquisition of BEC and, especially, hepatocyte lineage markers is more pronounced following the addition of dexamethasone to the cultures during the last three days of differentiation (see Chapter5).

Stabilization of a non-degradable form of β-catenin in BD organoids during the last three days of differentiation led to an increased expression of various immature HPC markers while causing a decrease in the expression levels of BEC (Hnf1b, Krt17 and Krt19) and hepatocyte (Hnf4a) lineage markers. Thence, a possible interpretation of

these results is that activation Wnt signalling in differentiated BD organoids keeps BD organoid cells into an HPC-like state preventing BEC/hepatocyte fate specification. In support of this, Touboul et al (2016) showed that, during human ESC differentiation into hepatocytes, activation of Wnt/β-catenin signalling is critical for the generation of proliferative bipotent hepatoblasts [239]. Conversely, Touboul and colleagues showed that treatment of these cells with a Wnt inhibitor (IWR-1) was sufficient to induce the expression of BEC (Hnf1b) and hepatocyte (Hnf4a) lineage genes, indicating that depletion of Wnt signalling is required for both hepatocyte and BEC fate progression [239].

Organoids cultured in BDorg-DM at day 10 of differentiation express high levels of Krt19 and Krt7 and, therefore, they might be closer to the cellular context of precursors committed to the BEC lineage or to more differentiated BECs rather than to hepatoblasts with fully bipotent properties. Experiments performed by Cordi et al (2016) using a Sox9-CreER/β-catenin$^{lox(\Delta Ex3)}$ mouse model showed that stabilization of β-catenin in BECs precursors during liver development (E14.5 to E18.5) impaired BEC maturation, which supports that Wnt/β-catenin pathway also controls the differentiation state of biliary precursors after commitment to the BEC lineage [240]. Interestingly, Cordi and colleagues observed that stabilization of β-catenin at ~E15.5 did not only impair BEC maturation but also caused a decrease in the already acquired differentiation markers Spp1, Hnf1b and Muc1, indicating that stabilization of β-catenin pathway at this stage of development did not only block BECs maturation but also drove partial de-differentiation of BEC progenitors to a more immature state [240]. Such de-differentiation did not cause full escape from biliary fate as cells remained negative for Hnf4a expression. Stabilization of β-catenin in differentiated BD organoids did not cause either gain in Hnf4a expression. Further studies are therefore required to determine whether activation of the Wnt signalling in differentiated BD organoids interferes with the maturation state of the BEC 3D cultures, promotes partial escape from biliary fate or a combination of both.

6.3.9 Summary

The current chapter aimed to characterise the response of differentiated BD organoids to Wnt pathway activation. 3-day stimulation of Wnt pathway with Rspo1 resulted in

increased expression of Axin2 and various HPC (Sox9, Spp1, Cd44, Lgr5 and Cd24) and proliferation (CyclinD1 and ki67) markers. Differentiated BD organoids were found to express various various Wnt ligands (primarily Wnt4, Wnt7a and Wnt7b) with potential canonical and non-canonical activity. Secretion of these ligands was necessary for the appearance of the HPC-signature induced upon 3 days Rspo1 treatment. The gain in HPC markers expression was accompanied by the loss of BEC (Hnf1b, Krt17 and Krt19) and hepatocyte (Hnf4a) lineage markers, suggesting that activation of the Wnt signalling in differentiated BD organoids interferes with the maturation state of the BEC 3D cultures and/or promotes partial escape from biliary fate.

Rspo1 (24h exposure) induced the appearance of an tdTom positive population with enhanced stem cell features in Axin2CreERT2 differentiated BD organoids. tdTom positive cells were enriched for the expression of genes involved in cell cycle progression, DNA repair and telomere elongation machinery. IPA RNAseq analysis failed to identify activation of canonical Wnt signalling as one of the pathways driving the transcriptome landscape differences between tdTom positive and negative cells, suggesting that activation of Wnt/β-catenin might not be the primary pathway driving the phenotypical differences between tdTom positive and negative populations. By contrast, RNAseq analysis revealed that tdTom positive cells were enriched for the expression of genes involved in the Wnt/Ca2+ signalling when compared to tdTom negative cells. This suggests that, in addition to the canonical signalling cascade, Rspo1 treatment activated other branches of the Wnt signalling pathway. Differentiated BD organoids expressed Wnt receptors and co-receptors of the non-canonical branches of the Wnt signalling pathway. Thence, further research should be undertaken to evaluate the potential contributions of the different branches of the Wnt pathway to the enhanced stem cell features of the tdTom positive population.

Furthermore, data from the current chapter showed that Wnt signalling modulates the expression of signalling molecules involved in ductal scarring remodelling, and as a result, treatment of differentiated BD organoid cultures with Rspo1 generated a microenvironment potentially pro-fibrotic. Further work is required to establish whether Rspo injury cues, by modulating the expression of paracrine signalling molecules in BECs, promote a pro-fibrotic microenvironment during liver damage *in vivo*.

Finally, data presented in the current chapter showed that activation of the Wnt signalling in differentiated BD organoids interferes with the maturation state of the BEC 3D cultures, suggesting that depletion of Wnt signalling in cells with HPC features is required for both hepatocyte and BEC fate progression.

Altogether, results of the current chapter using differentiated BD organoids as an *in vitro* platform suggest a potential role for Wnt signalling in BEC proliferation and/or cellular plasticity. The potential role of Wnt signalling in BEC-driven regeneration will be further evaluated in an *in vivo* setting in Chapter7. The possible caveats of using differentiated BD organoids as *in vitro* model to study BEC behaviour will be also further discussed in Chapter7.

Chapter 7. STUDY OF WNT PATHWAY DYNAMICS *IN VIVO* DURING BEC-DRIVEN REGENERATION

In Chapter 6 it was described that activation of the Wnt signalling in differentiated BD organoids interferes with the maturation state of the BEC 3D cultures, induces cell proliferation and increases the ability of these structures to forming secondary BD organoids, suggesting a role for the Wnt/β-catenin signalling pathway in biliary epithelium regeneration and/or in BEC cell plasticity. These results prompted me to contact Dr Stuart Forbes, whose laboratory has developed a series of mouse models in which BEC-to-hepatocyte transdifferentation takes place. The current chapter will further evaluate whether activation of Wnt signalling modulates BEC plasticity using diverse mouse models from the Forbes' laboratory.

Dr Alex Raven, a former PhD student at Forbes' research group, carried out the DDC β1-integrin KO liver injury animal work. Niya Aleksieva, also a former PhD student at Forbes' laboratory, performed the MCD p21 liver injury mouse model animal work, sample preparation, BEC flow-cytometry isolations and gene expression RT-qPCR analysis. Niya Aleksieva additionally performed the IF stainings of the samples presented here. Imaging of all samples, quantification and interpretation of the results were performed by myself at Cardiff University.

7.1 Introduction

Exposure of differentiated BD organoids to Rspo1 drives an HPC/cell proliferation transcriptional program (see Chapter 6, section 6.2.1). Recent studies from Planas-Paz et al. (2019) have, however, concluded that Rspo injury signals do not modulate the regenerative program of BECs following injury as loss of the Rspo receptors Lgr4 and Lgr5 from the biliary epithelium using an $Lgr4^{fl/fl}$ / $Lgr5^{fl/fl}$ Alb Cre mouse model did not decrease the number of proliferative BECs positive for ki67 expression nor affected the total number of BECs upon DDC administration, an injury regime that triggers BEC proliferation[93].

Differentiated BD organoids highly expressed BECs markers (Krt7, Krt19 and Hnf1b) and, at a lower level, markers of the hepatocyte lineage (Cebpa, Hnf4a and Prox1) (see Chapter 5). This provides ground for the hypothesis that differentiated BD organoids might resemble adult BECs that are undergoing BEC-to-hepatocyte transdifferentation (see Chapter 5, section 5.3.2). Several studies have shown that the

injury regime employed in Planas-Paz et al. (2019) studies drives BEC hyper-proliferation but not BEC-to-hepatocyte transdifferentation [16,17,23]. Hence, discrepancies between Planas-Paz et al. (2019) and the data from the differentiated BD organoid *in vitro* platform might be attributed to differences in the cellular context in which the Rspo stimulus is applied.

To date, there are three liver injury regimes in which BEC-to-hepatocyte transdifferentation takes place: (1) administration of DDC diet for over 24 weeks, (2) depletion of β1-Integrin in the hepatocellular compartment in combination with 7 days of a DDC diet and (3) overexpression of p21 in the hepatocytes in combination with 2 weeks of an MCD diet [17,23].

The relative contribution of the Wnt/β-catenin pathway in BEC-to-hepatocyte transdifferentation remains largely unexplored. Hence, the current chapter will explore the role of the Wnt signalling pathway in BEC cellular plasticity and proliferation using mouse models 2 and 3 above; the DDC/β1-Integrin KO and the MCD/p21 liver injury mouse models. First, the Wnt pathway activation dynamics during BEC-driven hepatocellular regeneration will be assessed in the MCD/p21 model. Second, the effects of pharmacological inhibition of Wnt ligand secretion for both BEC proliferation and BEC-to-hepatocyte specification will be evaluated using the DDC/β1-Integrin KO injury mouse model.

7.2 Results

7.2.1 Axin2, Lrp6 and Lgr5 are dynamically expressed during BEC-to-hepatocyte transdifferentation in the MCD p21 mouse model

To investigate whether the Wnt/β-catenin signalling pathway was activated during BEC reprogramming, the transcript levels of Axin2 and two upstream components of the Wnt signalling cascade (Lrp6 and Lgr5) were analysed in the biliary compartment during BEC-to-hepatocyte transdifferentation. Amongst the current liver injury strategies to study BEC-to-hepatocyte lineage specification, the MCD/p21 overexpression injury mouse model was chosen simply because at the time of completion of this thesis, Niya Aleksieva of the Forbes laboratory was performing flow

cytometry isolations of BECs isolated from this mouse model at different recovery

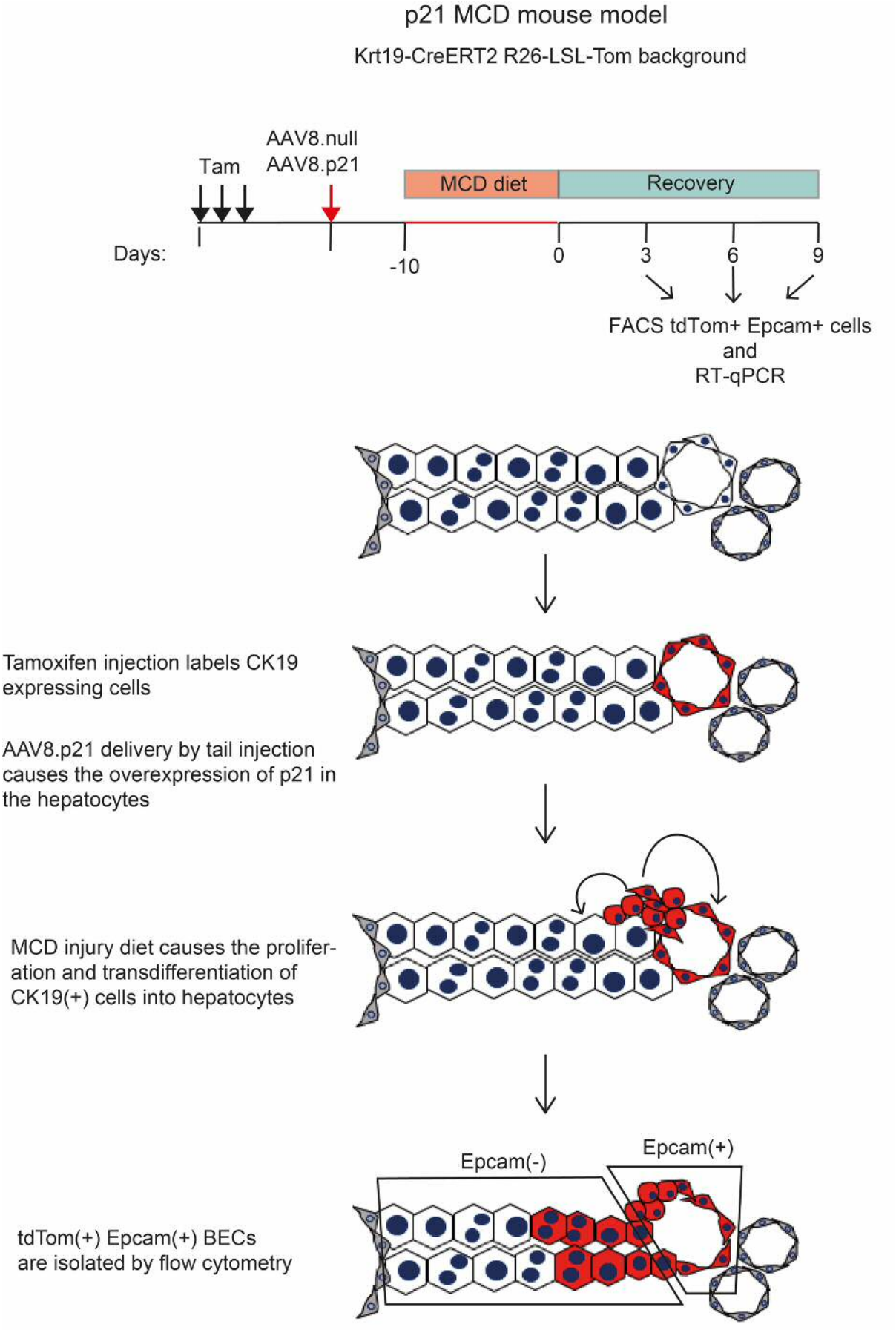

Figure7.1 Schematic representation of p21 MCD mouse model. Tamoxifen administration causes the labelling of the biliary epithelium of transgenic mice harbouring the Krt19-CreERT2 R26-LSL-tdTom is labelled with tdTom. Hepatocyte cell cycle arrest is then induced by the intravenous tail delivery of AAV8 viral particles containing p21 coding sequences. AAV8.p21 was administrated twice weekly after the first injection during the whole length of treatment. MCD injury regime induces BEC proliferation and hepatocyte damage. Following removal of the MCD injury regime, hyper-proliferative BECs with bi-potent properties give rise to both BEC and hepatocytes. Pre-injury hepatocytes (tdTom negative), BEC-derived hepatocytes (tdTom positive, Epcam negative) and BECs (tdTom positive, Epcam negative) can be distinguished and isolated by flow cytometry for downstream proposes.

times and, therefore, biological material was available.

The MCD/p21 liver injury strategy was first described by Raven et al. (2017) (see Chapter 1) [17]. This liver injury strategy consists in the overexpression of p21 in the hepatocytes by the delivery of AAV8 viral particles containing a p21 coding vector (AAV8.p21) via tail injection, followed by 10 days of MCD injury regime, which stimulate BEC-driven regeneration (Figure7.1) (see Chapter 1). Distinction between pre-injury and BEC-derived hepatocytes can be additionally achieved by carrying out this injury strategy in animals with a Krt19-CreERT2 R26-LDL-tdTom genetic background, which allows the labelling and lineage tracing of BECs with tdTom prior to injury by administrating tamoxifen intraperitoneally 2-weeks before delivering the AVV8.p21 particles (Figure7.1). In the MCD/p21 liver injury mouse model, BEC-derived hepatocytes are virtually absent during peak injury and only detectable from 3-day post MCD diet withdrawal onwards (Figure7.1). Importantly, in the absence of p21 hepatocellular expression, the biliary epithelium does not contribute to hepatocyte regeneration.

To assess the activation dynamics of Wnt/β-catenin signalling during BEC reprogramming, the transcript levels of the β-catenin target gene *Axin2* as well as the Wnt pathway receptors *Lrp6* and *Lgr5* were analysed by RT-qPCR in BEC-derived cells labelled as tdTom(+) and Epcam(+) were collected from MCD/p21 injured livers at day 3, 6 and 9 of the recovery period (Figure7.1). The gene expression of these cells was compared to tdTom(+) and Epcam(+) cells isolated from MCD-injured animals administrated with a control vector (AAV8.null) (non-transdifferentation MCD injury regime). MCD injury regimes were additionally compared to tdTom(+) Epcam(+) BECs isolated from healthy animal controls that had been injected with tamoxifen to

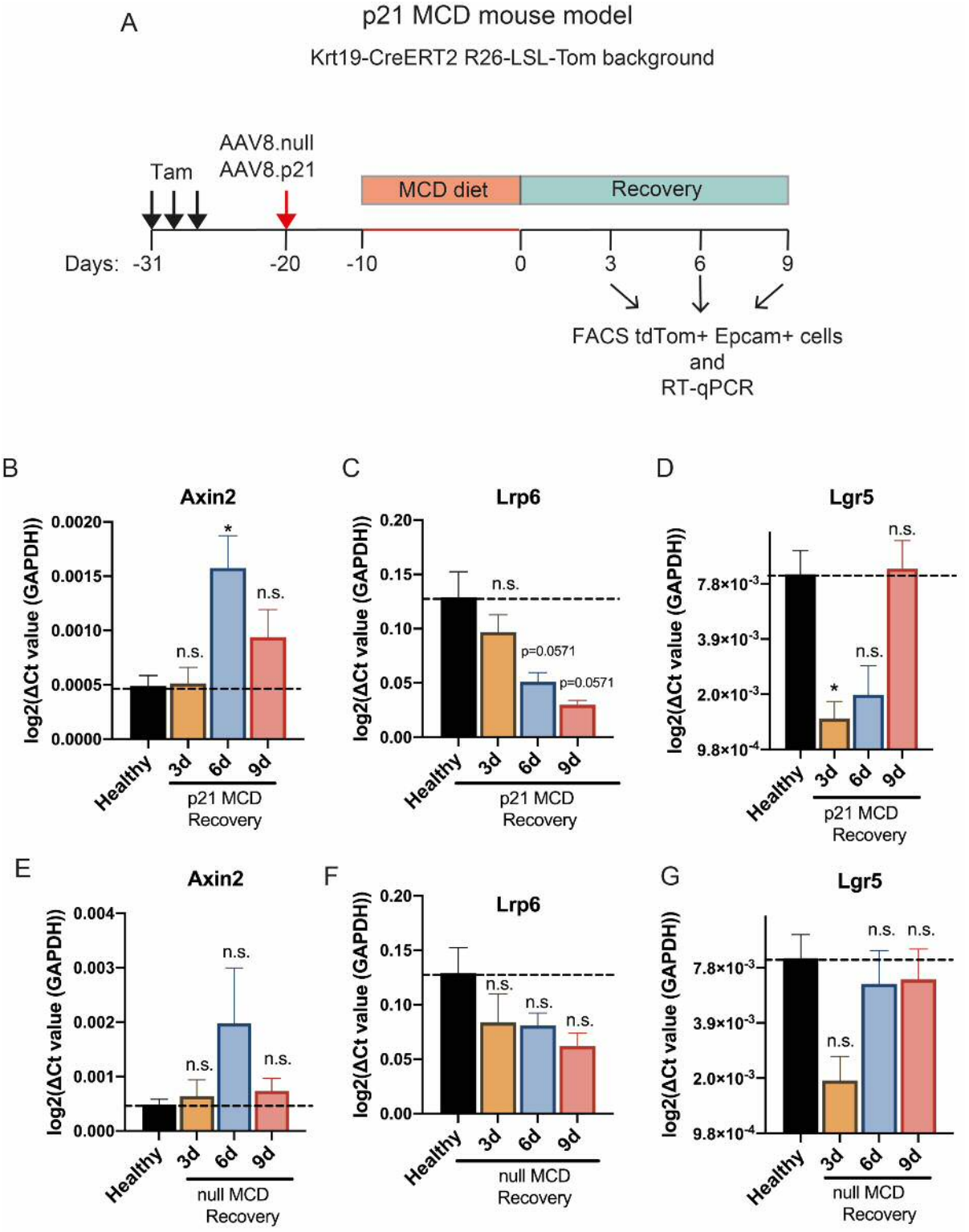

Figure7.2 (A) Top panel represents treatment time for the isolation of BECs (tdTom positive, Epcam positive cells) from the p21 MCD mouse model by flow cytometry. (B-G) RT-qPCR gene expression analysis for BEC transdifferentation (AAV8.p21, panels B to D) and non-transdifferentation (AAV8.null, panels E to G) MCD liver injury strategies for Axin2, Lrp6, and Lgr5. Gene expression was normalized over GAPDH and compared to BECs (tdTom positive, Epcam positive cells) isolated from uninjured animals (healthy controls).

label the BECs, but that had not been exposed to the MCD diet or the AAV8 viral

particles.

RT-qPCR analysis revealed that Axin2, Lrp6 and Lgr5 in both BEC transdifferentation (AAV8.p21) (Figure7.2, B to D) and non-transdifferentation (AAV8.null) (Figure7.2, E to G) MCD liver injury animals followed strikingly similar expression patterns although the fold change of induction in both injury regimes differed. In the AAV8.p21 MCD liver injury regime, Axin2 expression was significantly increased by day 6 of recovery when compared to the healthy controls, suggesting that canonical Wnt signalling is only activated in the biliary epithelium in the context of BEC-to-hepatocyte transdifferentation (Figure7.2, B). In the AAV8.p21 MCD damaged livers, the expression of Lrp6 in the biliary compartment gradually decreased upon recovery (Figure7.2, C, p-value comparing 'healthy' with 'day 6' and 'day 9' =0.0571). By contrast, *Lgr5* expression significantly declined on day 3 of recovery when compared to the healthy controls and recovered to homeostatic levels by day 9 of recovery (Figure7.2, D). Despite the similarity on the gene expression patterns from BECs isolated from AVV8.p21 and AVV8.null MCD injured livers, non-significant differences in the level of expression of Axin2, Lrp6 or Lgr5 were found at any of the recovery time points assessed in the AVV8.null MCD liver injury regime (Figure7.2, E to G).

Altogether, data from this set of experiments suggest that (1) licensing of the biliary epithelium to respond to Wnt and Rspo injury cues fluctuates during BEC reprograming and (2) the canonical Wnt pathway is dynamically activated during BEC-to-hepatocyte transdifferentation in the MCD injury regime. Furthermore, these data suggest that the expression of upstream compartments of the canonical Wnt signalling pathway as well as the activation levels of the Wnt/β-catenin cascade levels remain largely in the biliary epithelium when the regeneration of the hepatocellular compartment is fuelled by the hepatocytes.

7.2.2 Pharmacological inhibition of Wnt secretion in the β1-integrin DDC injury mouse model

Data from section 7.2.1 suggest that the Wnt/β-catenin cascade is dynamically activated in the biliary epithelium when the regeneration of the hepatocellular compartment is fuelled by BECs. This raised the question whether activation of the

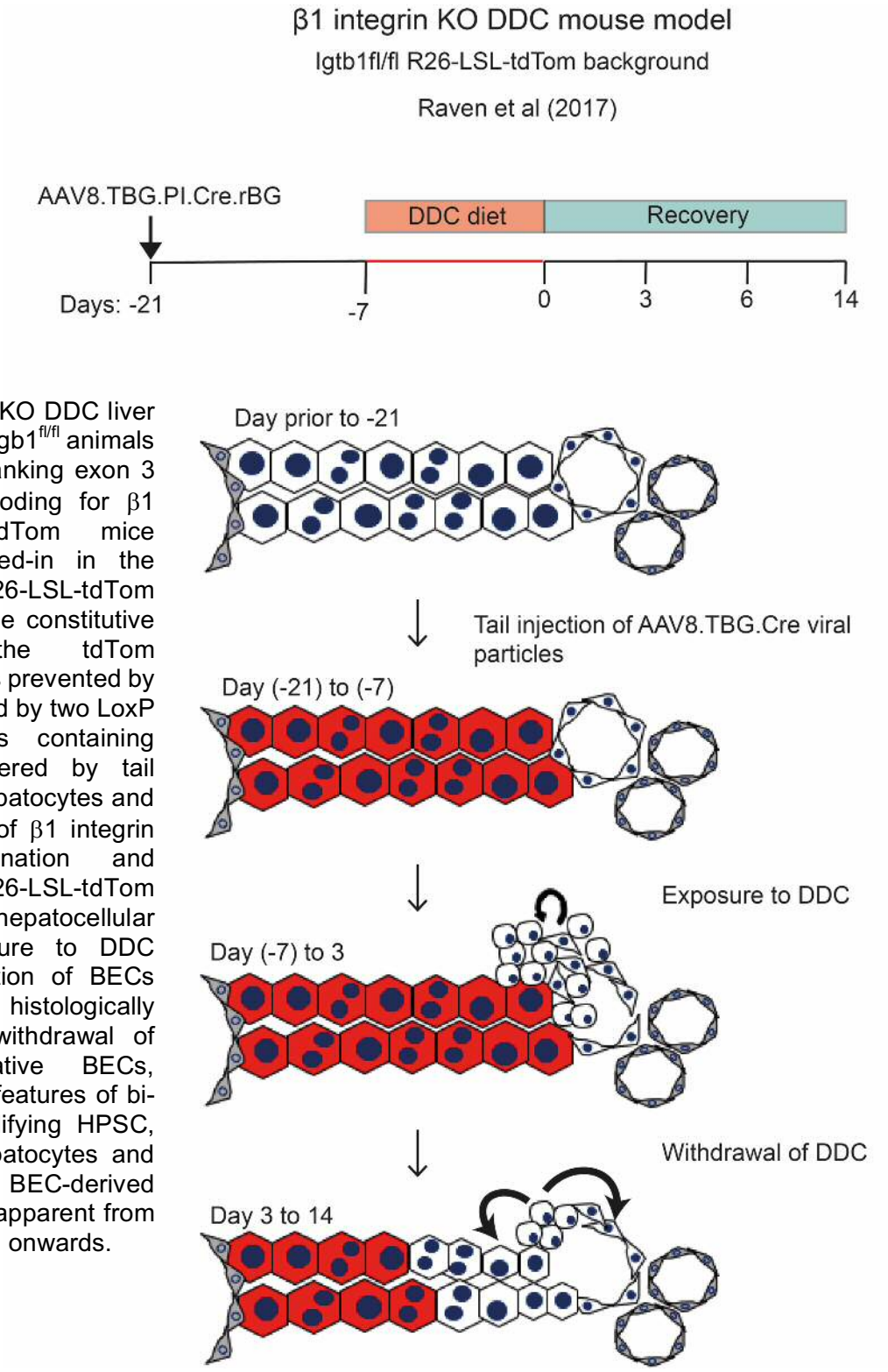

Figure7.3 β1 integrin KO DDC liver injury mouse model. Itgb1$^{fl/fl}$ animals possess loxP sites flanking exon 3 of the Itgb1 gene coding for β1 integrin. R26-LSL-tdTom mice contain have knocked-in in the Rosa26 locus the R26-LSL-tdTom transgene in which the constitutive expression of the tdTom fluorescence protein is prevented by a stop cassette flanked by two LoxP sites. Viral particles containing AAV8.TBG.Cre delivered by tail injection target the hepatocytes and cause both the loss of β1 integrin and the recombination and activation of the R26-LSL-tdTom reporter in the hepatocellular compartment. Exposure to DDC triggers the proliferation of BECs and formation of histologically defined DR. Upon withdrawal of DDC, hyperproliferative BECs, which have acquired features of bi-potent transient amplifying HPSC, give rise to both hepatocytes and homeostatic BECs. BEC-derived hepatocytes become apparent from day 3 DDC withdrawal onwards.

canonical Wnt signalling is having a functional role during BEC reprograming. Fortunately, Alex Raven carried out a series of experiments during his PhD that

involved the administration of LGK974, a compound that abrogates Wnt secretion, in the DDC/β1-Integrin KO model during BEC-to-hepatocyte transdifferentation. Samples from Raven's studies stored since his graduation were specifically analysed for the propose of this study.

The DDC/β1-Integrin KO injury strategy was also first described by Raven et al. (2017) [17]. In this model, BEC-driven regeneration is induced by a 7 days DDC treatment regime in a context where hepatocellular regeneration is impaired by conditional deletion of β1-integrin (Igtb) (see Chapter 1) (Figure7.3). Loss of β1-Integrin prior to DDC exposure is achieved by the delivery of AAV8.TBG.Cre viral particles by tail injection which leads to the selective deletion of target genes in 99.5% of hepatocytes but not of BECs (see Chapter 1) (Figure7.3) [17].

Raven's LGK974 treatment time line in DDC/β1-Integrin KO injured lives consisted on the administration of LGK974 by oral gavage, twice per day, during the 10 day 'recovery period' following DDC diet treatment. Similarly to the MCD/p21 liver injury strategy, in this liver injury strategy BEC-derived hepatocytes are virtually absent during peak injury and only detectable from 3-day post MCD diet withdrawal onwards (Figure7.3). As a control, animals were injected with an equivalent volume of DMSO (vehicle). A total of three vehicle animals (specimens 62-64) and four LGK974 animals (specimens 65-68) were analysed. The sex of the animas of each experimental cohort can be found in Table 7.1.

Animal ID	Cohort treatment	Sex
62	Vehicle	M
63	Vehicle	M
64	Vehicle	F
65	LGK974	M
66	LGK974	M
67	LGK974	F
68	LGK974	F

Table7.1 Table indicating the sex of the animals of each cohort.

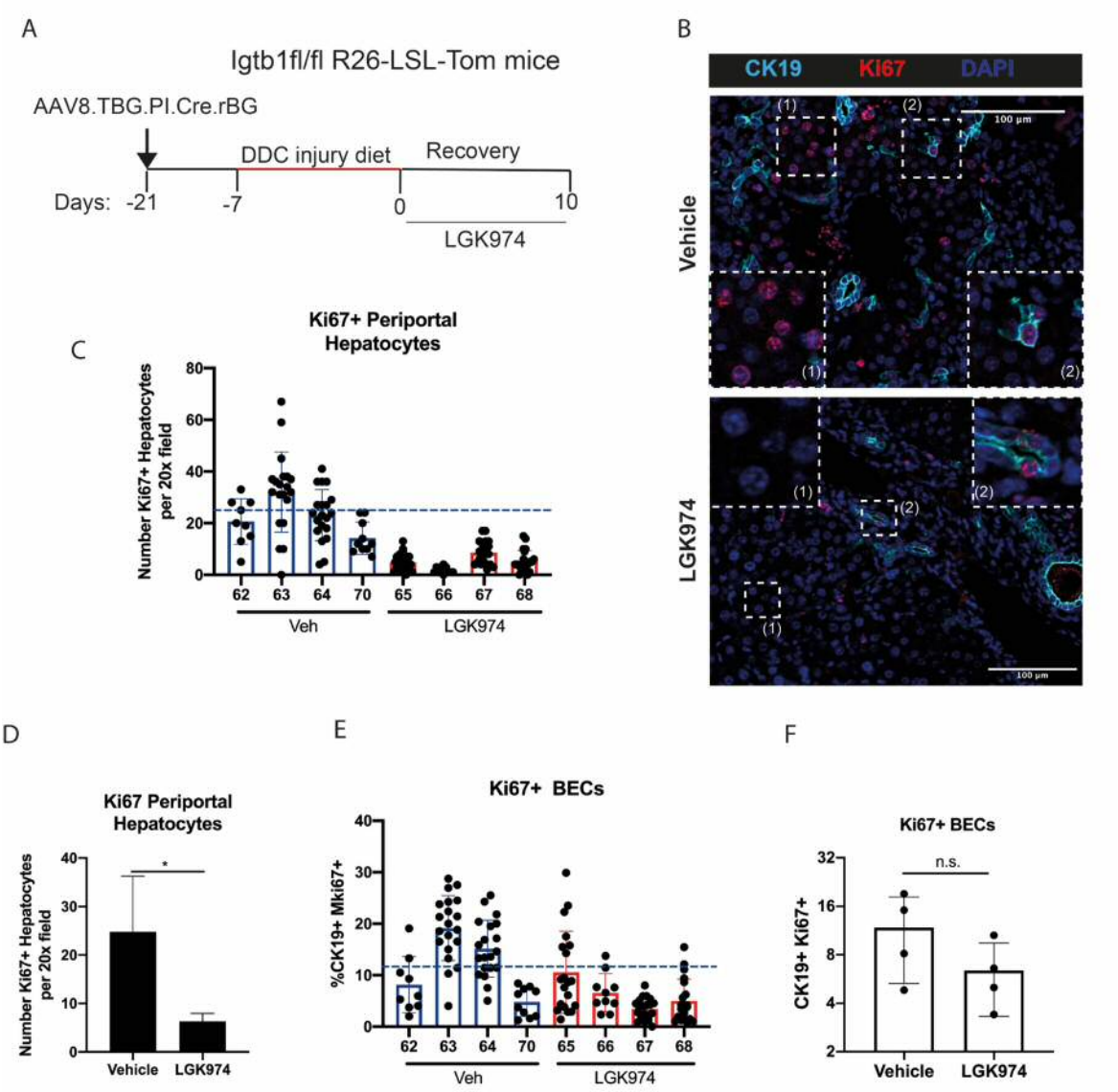

Figure7.4 (A) Scheme representing treatment time line for β1-integrin KO animals injured with DDC and recovered in the presence or absence of LGK974. (B) Immunostaining of ki67 (red) and CK19 (cyan) on β1-integrin KO animals subjected to DDC injury. Administration of LGK974 during the recovery period causes a dramatic decline in the number of periportal ki67pos hepatocytes (1). LGK974 also caused a reduction in the number of ki67pos cells BECs (2) although this occurred in a less pronounced manner. (C) ki67 IF quantifications show that the number of ki67 positive periportal hepatocytes is highly declined in all the animals subjected to LGK974 treatment. Blue dash line highlights the average of the four vehicle animals. (n=20 to 45 20x view fields per animal) (D) Bar graph shows significant decline of ki67 positive hepatocytes upon LGK974 treatment when vehicle and LGK974 animals are combined. (n=4). (E) Graph shows high variability in the number of ki67 positive BECs in vehicle and LGK974 treated animals. Blue dash line highlights the average of the four vehicle animals. (n=20 to 45 20x view fields per animal). (F) Bar graph shows quantifications of vehicle and LGK974 animals combined. (n=4).

To assess whether inhibition of Wnt pathway impaired BEC proliferation during BEC-driven liver regeneration, LGK974 treated DDC β1-Integrin KO model livers were

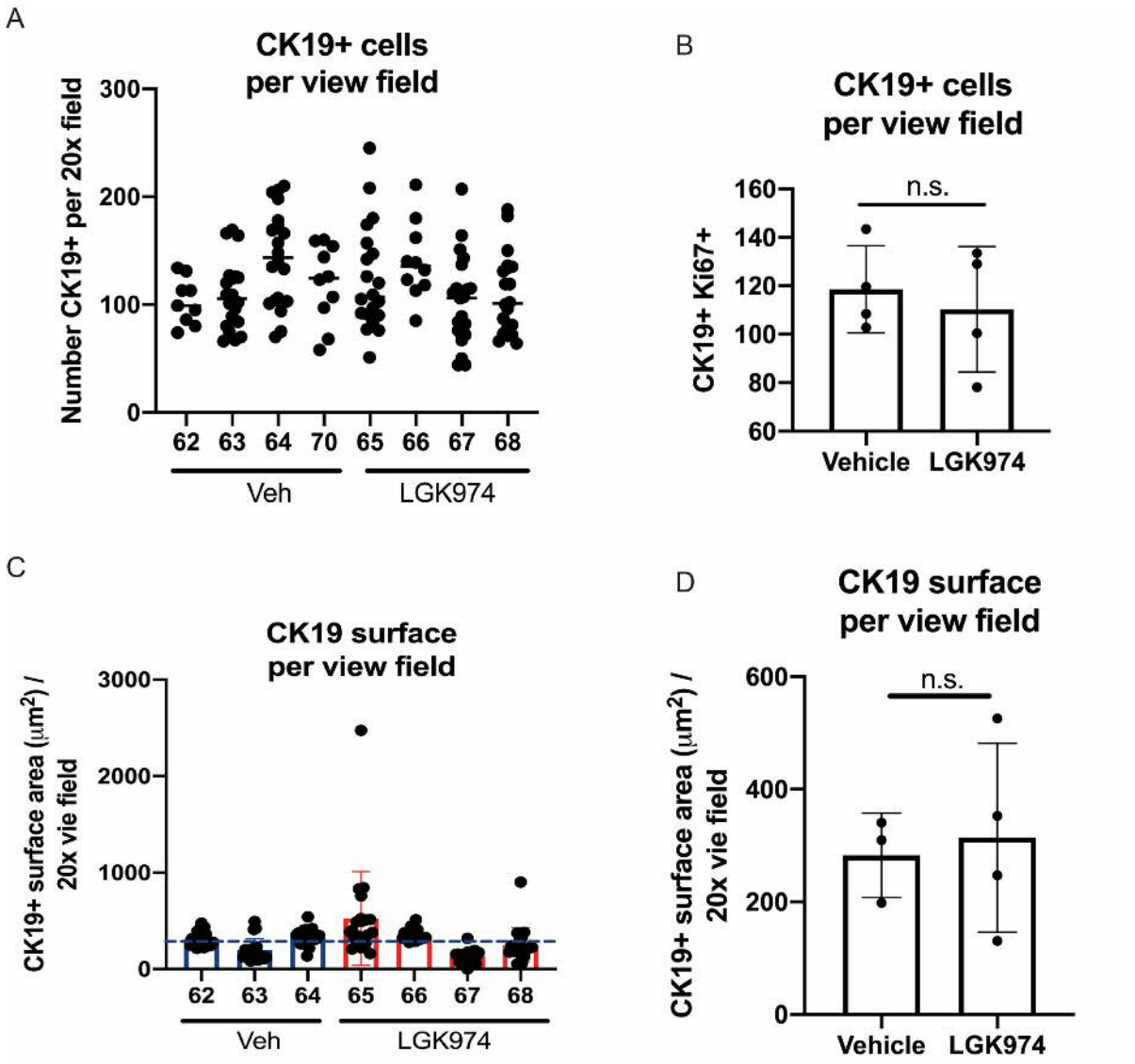

Figure7.5 (A) Manual quantifications of the number of total of BECs (CK19 positive cells) per view field show large variability in the absolute number of BECs per view field. Images were acquired in a Zeiss 710 instrument. (n=10) (B) Bar graph shows no differences in the absolute number of BECs (CK19 positive cells) between vehicle (n=3) and LGK974 (n=4) treated animals. Images were acquired in a Zeiss 710 instrument. (C) Semi-automatic quantification using Harmony software of CK19 surface area per view field. (n=20 view fields per animal). Images were acquired using an Opera Phenix instrument. Blue dash line highlights the average of the three vehicle animals. (D) Non-significant differences were found between the area covered by CK19 positive cells per 20x view field between vehicle (n=3) and LGK974 (n=4) treated animals. Images acquired in an Opera Phenix system were quantified in a semi-automatic manner using the Harmony software.

stained for CK19 and ki67. The four animals exposed to LGK974 showed a significant decline in the numbers of proliferative hepatocytes (Figure7.4, C and D). Significant differences between LGK974 and control treatments in the number of proliferative BECs stained as CK19(+) ki67(+) cells were not detected, although a lower trend was

apparent in the LGK974 treated animals (Figure7.4, E and F). In these analyses, the total numbers of CK19(+) BECs and the total surface area of CK19(+) positive per field of view was similar between LGK974 and vehicle animals (Figure7.5).

To assess whether LGK974 treatment affected the rate of BEC-to-hepatocyte transdifferentation, LGK974 and vehicle-treated DDC β1-Integrin KO injured livers were co-stained for tdTom (pre-injury hepatocytes) and HNF4a (all hepatocytes) and pre-injury hepatocytes and hepatocytes derived from a non-hepatocellular source were quantified. In the vehicle animals, ~5% of the hepatocytes were derived from non-hepatocyte origin (HNF4a(+), tdTom(-)) (Figure7.6). Animal 65 from the LGK974 treatment cohort showed a comparable BEC-to-hepatocyte transdifferentation rate to vehicle animals (~3.5%) (Figure7.6). By contrast, the LGK974 treated animals 67 and 68 showed an unusually high proportion of hepatocytes derived from non-parenchymal rate (~29% and 19%, respectively) (Figure7.6). Unfortunately, due to deficient or incomplete liver perfusion and/or problems during sample fixation, animal 66 showed high levels of auto-fluorescence, which made not possible to distinguish between tdTom positive and negative cells and therefore the number of pre-injury and newly formed hepatocytes of this animal could not be quantified. As two out of the three animals treated with LGK974 show a notoriously high proportion of BEC-derived hepatocytes, from this set of results may be concluded that inhibition of Wnt signalling during the recovery period promotes BEC-to-hepatocyte transdifferentation.

Figure7.6 (A) Scheme representing treatment time line for β1-integrin KO animals injured with DDC and recovered in the presence or absence of LGK974. (B) Images for HNF4a (magenta) and tdTom (cyan) immunostaining in β1-integrin KO DDC injured livers recovered. Hepatocytes are labelled as HNF4a positive. tdTom labels pre-injury hepatocytes whereas BEC-derived hepatocytes appear as tdTom negative. Exposure to LGK974 during the recovering period increases the proportion of BEC-derived hepatocytes/total hepatocytes in animals 67 and 68. The absolute number of hepatocytes remained largely unaffected. Images were acquired using an Opera Phenix instrument. (C) HNF4a staining quantifications show an increase in the proportion of BEC-derived hepatocytes (HNF4a positive, tdTom negative) over the total number of hepatocytes in animals 67 and 68. Blue dash line indicates the average of the 3 vehicle animals. Semi-automatic quantifications were performed using Harmony software. Animal 66 was not quantified due to the impossibility to distinguish between tdTom negative and tdTom positive cells. (n=20 view fields per animal). (D) Bar graph shows BEC-derived hepatocyte/total hepatocytes proportion quantifications of vehicle (n=3) and LGK974 (n=3) animals combined. Semi-automatic quantifications were performed using Harmony software.

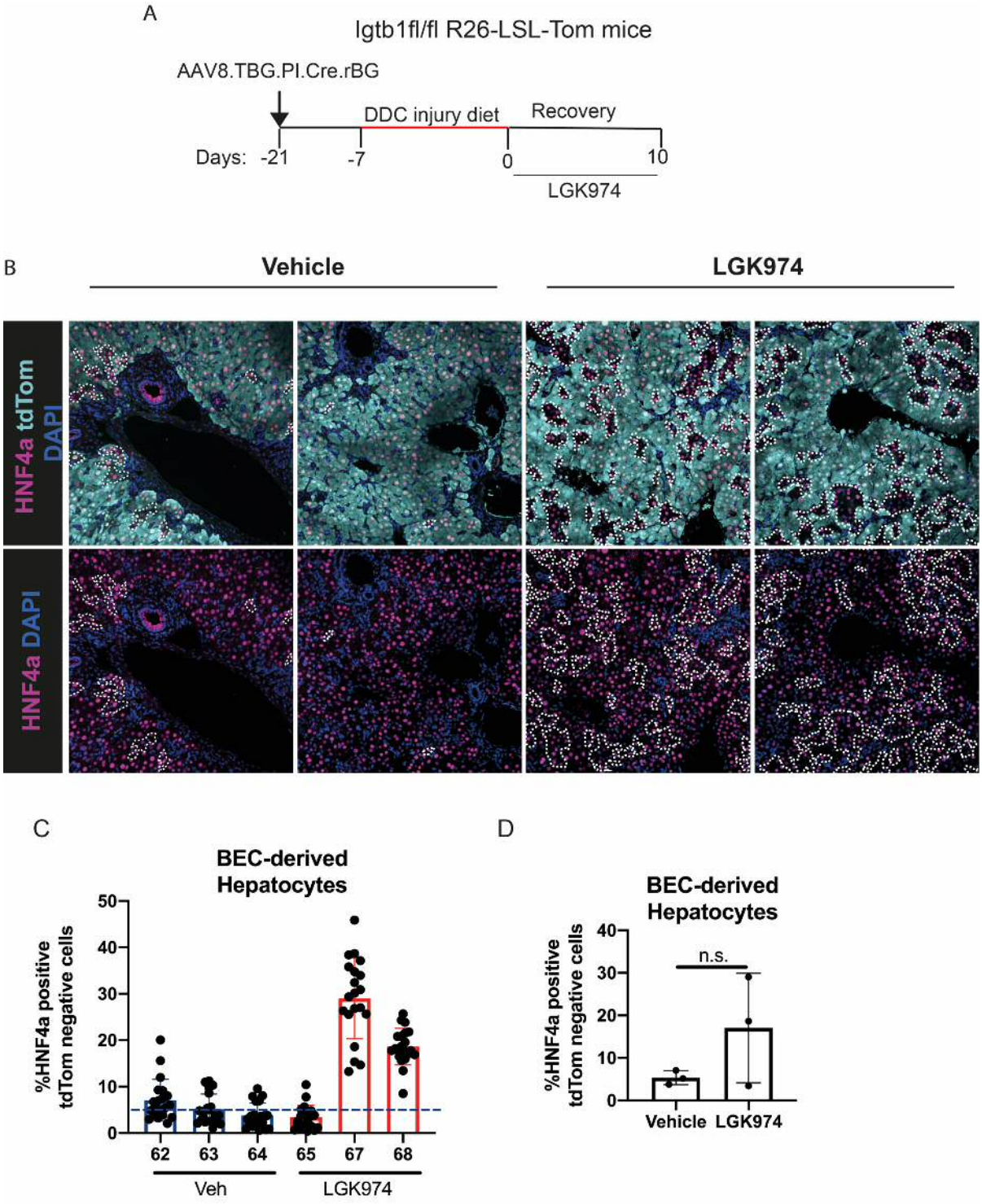

Data from HNF4a tdTom co-staining showed that the rate of BEC-to-hepatocyte transdifferentation was quite variable among animals of the LGK974 treatment cohort. To assess whether the variation in response between LGK974 treated animals was associated with differences in the level inhibition of the Wnt signalling pathway, samples were stained for the pericentral β-target gene GS. Out of the four LGK974 treated animals only animals number 66 and 67 showed significantly lower surface area per view field covered by GS positive hepatocytes as well as a decreased number

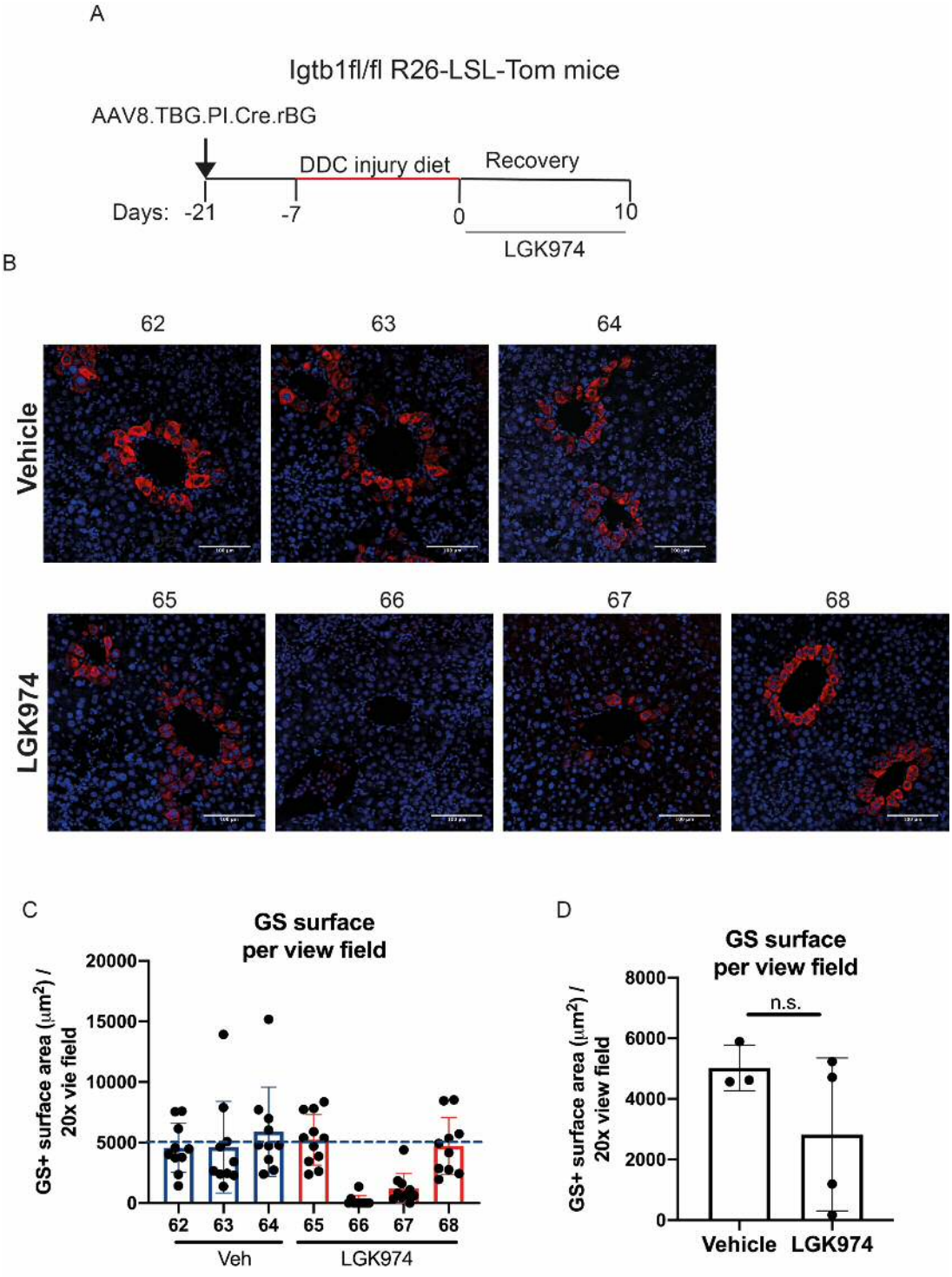

Figure7.7 (A) Schematic representation of the β1 integrin KO, DDC injury and LGK974 treatment recovery regime. (B) Representative Zeiss 710 confocal IF images showing the loss of GS positive cells (red) in the LGK974 treated animals 66 and 67. Cell nuclei has been counterstained with DAPI (blue). (C) GS surface area staining semi-automatic quantifications performed with the Harmony software shows a decline GS surface area in the LGK974 treated animals 66 and 67. Blue dash line highlights the average of the three vehicle animals (n=10 view fields per animal). (D) Bar graph shows GS staining surface area Harmony semi-automatic quantifications of Vehicle (n=3) and LGK974 animals combined (n=4).

of the hepatocytes stained as positive for GS expression at the time of sample

collection (day 10) (Figure7.7 and Appendix E, Figure1). This result contrast with the proliferation data presented in Figure7.4, B in which all the LGK974-treated animals appeared to show a decline in ki67 staining. The relevance of GS staining as a readout for Wnt signalling inhibition under these conditions will be discussed later in this chapter.

Taken together, data from this set of experiments indicate that (1) hepatocyte proliferation is modulated by Wnt signalling and (2) inhibition of Wnt pathway may enhance BEC-to-hepatocyte transdifferentation. However, the variability between animals, suggests that further analyses, such as time courses involving greater animal cohort sizes, would be required to allow clear conclusions to be drawn regarding the role of Wnt signalling in BEC proliferation and transdifferentation.

7.3 Discussion

7.3.1 Blockage of Wnt secretion affects hepatocyte proliferation during DDC injury recovery in β1-integrin deficient mice

All animals exposed to LGK974 during DDC injury recovery in β1-Integrin deficient mice showed a marked decrease in the number of hepatocytes labelled as ki67 positive, implying that hepatocyte proliferation in these injury settings was dependent on Wnt ligands present in the microenvironment. In vivo studies have shown that loss of Wls during hepatocyte, cholangiocyte (Alb-Cre; $Wls^{fl/fl}$) or Kupffer cell development (Lyz2-Cre; $Wls^{fl/fl}$) delayed hepatocyte proliferation after partial hepatectomy [90,102]. Experiments performed by Planas-Paz et al. (2019) have additionally shown that hepatocyte proliferation during recovery from DDC injury regime is dependent of Wnt signalling as concomitant loss of Lgr4/5 ($Lgr4^{fl/fl}$ $Lgr5^{fl/fl}$ Alb-Cre) resulted in a decreasing number of proliferative hepatocytes at DDC-injury day recovery 2 [93]. Therefore, the results presented in the current chapter are consistent with the literature and further support the hypothesis that hepatocyte proliferation during liver regeneration is highly dependent on Wnt injury cues.

7.3.2 Discrepancies between proliferation phenotypes driven by Wnt in BECs in vivo and *in vitro*

Exposure of differentiated BD organoids to Rspo1 caused an increase in the expression of genes involved in cell cycle progression (see Chapter 6). This observation supported the hypothesis that activation of the Wnt signalling pathway might drive BEC proliferation during liver regeneration. However, and although a lower trend was apparent in the LGK974 treated animals, significant differences between LGK974 and control treatments in the number of proliferative BECs were not detected *in vivo*. There at least four possible explanations to explain these apparent discrepancies between the *in vivo* and *in vitro* data.

First, Wnt secretion might not have been absolutely abolished during the experiment. In support of this, GS staining was not completely lost in all LKG974-treated animals, which implicates that abrogation of Wnt secretion was incomplete at least in the endothelial compartment of the liver in these animals. BECs have been additionally shown to express different members of the multidrug resistance-(MRP) associated protein family and the expression of the members MRD1, MRP1 and MRP3 have been described to be particularly high in regenerative ducts [241]. This is of special interest since the LGK974 drug disposition in the biliary epithelium could dynamically change during the experiment timeline. Incomplete inhibition of Wnt secretion could also potentially explain why a lower trend was apparent in the number of proliferative BECs was apparent in the LGK974 treated animals although this was not significant. Further experiments are required to validate that Wnt secretion was effectively abolished in the biliary epithelium during the whole length of the treatment.

Second, loss of β-catenin (β-catenin$^{fl/fl}$ Alb-Cre) or Lrp5/6 receptors (Lrp5$^{fl/fl}$ Lrp6$^{fl/fl}$ Alb-Cre) during partial hepatectomy delays but does not block hepatocyte proliferation, suggesting that the hepatocytes bypass the requirement of Wnt pathway activation during regeneration [15,90]. In the experiments presented in the current chapter, LGK974 was administrated for a total of 10 days. It is, therefore, possible that BECs also bypass the need for mitogenic Wnt cues during such length of treatment. To assess whether this is the case, future experiments involving the quantification of proliferative BECs at shorter time points of the LGK974 treatment will be required.

Third, the panel of Wnt ligands expressed are slightly different between BD organoids and injured BECs. Wnt ligands expressed by differentiated BD organoids include Wnt4, Wnt7a, Wnt7b and to a lesser degree Wnt5b and Wnt10a (see Chapter 6). However, RT-qPCR and single-cell RNAseq experiments carried out by independent research groups have only shown expression of Wnt2 in the homeostatic epithelium and Wnt7a, Wnt7b and Wnt10a in both homeostatic and DDC-injured BECs [22,93,98]. The identity of the Wnt proteins is thought to determine which branch of the Wnt signalling pathway and the cellular program that is subsequently activated. As the panel of Wnt ligands expressed between differentiated BD organoids and BECs do not fully overlap, possible discrepancies between *in vivo* and *in vitro* data could be attributed to differences in the panel of Wnt ligands expressed/available.

Fourth, Rspo1-driven proliferation signature might be an *in vitro* artefact. The RNAscope experiments of Planas-Paz et al. (2019) showed the presence of Rspo3 mRNA transcripts in sinusoidal endothelial cells adjacent to CK19 expressing BECs in DDC-injured livers [93]. However, there is no evidence that BECs enter in contact or respond to Rspo3 from this source during liver regeneration. Furthermore, it is possible that the Rspo1 concentration used *in vitro* is not physiologically relevant.

7.3.3 The canonical Wnt pathway is activated in the biliary epithelium during BEC reprograming

The expression of Axin2 in the biliary epithelium remained largely constant when regeneration was fuelled by the hepatocytes (AAV8.null MCD-injured livers). These results are therefore consistent with the recent observations of Wilson et al (2020), who recently reported that that the transcript levels of Axin2 in BECs as assessed by RNAscope were not increased following a liver injury strategy (based on DDC or TAA administration) where BEC-to-hepatocyte transdifferentation does not take place [94].

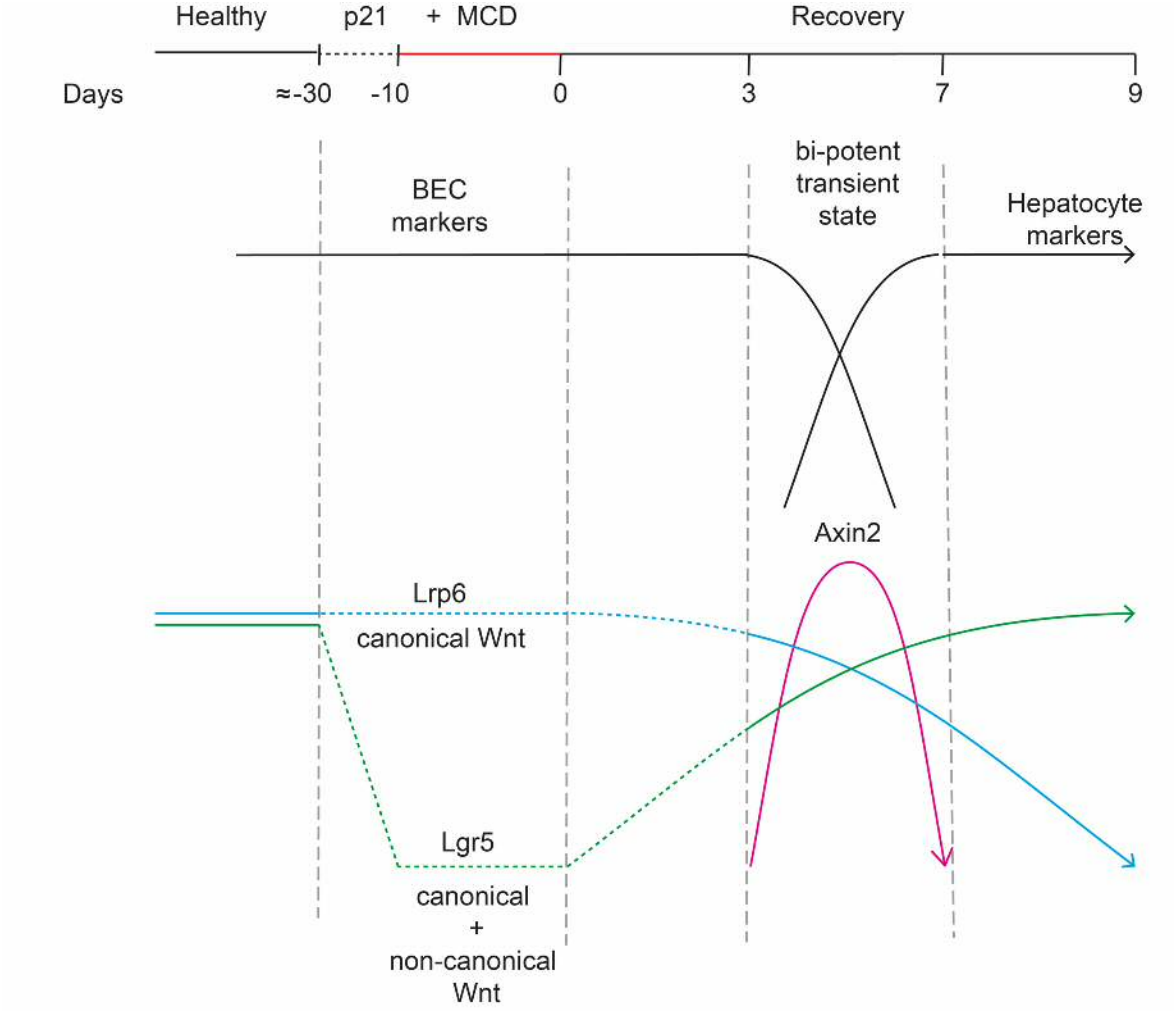

Figure7.8 Scheme integrating the dynamics of BEC-to-hepatocyte transdifferentation and the expression patterns of Axin2, Lrp6 and Lgr5 obtained by RT-qPCR analysis of BECs (tdTom positive, Epcam positive) isolated at different time points during the recovery period of the p21 MCD mouse model. In the p21 MCD injury regime, BEC-to-hepatocyte transdifferentation occurs predominantly between day 3 and day 7 of the recovery period. Lrp6 gene expression (blue line) gradually declines between day 3 and day 9. By contrast, Lgr5 gene expression (green line) gradually increases between day 3 and day 9 of the recovery period. Expression of the Wnt/β-catenin target gene Axin2 (magenta line) is significantly increased at day 6 of recovery. Sections represented with dash lines represent predicted gene expression levels.

By contrast, the Wnt/β-catenin pathway was dynamically activated in BECs isolated from AAV8.p21 MCD injured livers, suggesting that activation of canonical Wnt signalling is an event associated with BEC reprogramming.

Out of the three recovery time points analysed in AAV8.p21 MCD injured livers, Axin2 expression was only significantly upregulated in the biliary epithelium at day recovery 6 (Figure7.8). Interestingly, experiments performed by Russell et al. (2019) have

shown that BEC-to-hepatocyte transdifferentation in β-catenin KO MCD-injured livers primarily occurs between day 3 and day 7 recovery, which implies that activation of the Wnt/β-catenin in the biliary epithelium lied within the time window where the number of transitioning cells towards hepatocyte fate is expected to be maximal (Figure7.8) [24]. This observation may, therefore, support the hypothesis that activation of the Wnt signalling pathway in BECs promotes escape from their ductal-committed state and acquisition of HPC bi-potent cells features. Such hypothesis also accords with the results presented in Chapter 6, section 6.2.6.5, which showed that activation of the canonical Wnt pathway in differentiated BD organoids by exposure to Rspo1 or stabilization of a non-degradable form of β-catenin caused a significant decrease in the level of expression of BEC lineage markers while leading to an enhanced expression of various immature HPC-related genes (see discussion section 6.3.8).

Another interesting observation from data presented in the current chapter was that the reduction in the expression of the Wnt and Rspo receptors Lrp6 and Lgr5 was more pronounced in AAV8.p21 than in AAV8.null MCD-injured livers, suggesting that de-sensitization to microenvironmental Wnt/Rspo signals and/or inhibition of the canonical branch of the Wnt signalling cascade might be required for the progress of cells in an HPC-like 'bi-potent' state toward hepatocyte fate (Figure7.8). In support of this, the withdrawal of Rspo1 ligand from the BD organoid medium composition was necessary for the organoids to gain expression of Hnf4a (see Chapter 5). Similarly, studies conducted by Touboul and colleagues showed that treatment of hESC-derived 'definitive endoderm' cells with a Wnt inhibitor (IWR-1) was sufficient to induce the expression of BEC (Hnf1b) and hepatocyte (Hnf4a) lineage genes, indicating that depletion of Wnt signalling is required for both hepatocyte and BEC fate progression [239]. Finally, results from the β1-integrin KO DDC injury mouse model showed that in two out of the three LGK974-treated animals, the proportion of BEC-derived hepatocytes was dramatically increased upon pharmacological inhibition of Wnt secretion suggesting that global inhibition of Wnt secretion might promote progression from a HPC-like state towards hepatocyte fate.

The fact that pharmacological inhibition of Wnt secretion promoted BEC-to-hepatocyte transdifferentation, however, implies that depletion of environmental Wnt did not block exit from biliary fate and, therefore, questions the relative contribution of the Wnt/β-catenin pathway in the acquisition of a transient bi-potent HPC-like state. As discussed earlier (see section 7.3.2), it is possible that the abolition of Wnt secretion upon LGK974 treatment was not complete by the time in which biliary epithelium-derived cells acquired bi-potent cell properties and/or that BECs bypass the requirement of Wnt signals to acquire under the LGK974 β1-integrin KO DDC injury settings. Alternatively, it's possible that the canonical Wnt signalling pathway is not the primary driver of the escape of biliary fate and or the acquisition of the bi-potent state during BEC-driven regeneration. To determine whether the acquisition of an HPC-like bi-potent state is dependent on canonical Wnt signalling, further work involving the specific deletion of β-catenin in the biliary epithelium (β-catenin$^{fl/fl}$ R26-LSL-tdTom Krt19-CreERT2) in p21 MCD-injured livers would be required. Alternatively, experiments involving the temporal activation of Wnt/β-catenin pathway in the biliary epithelium at different stages of the recovery period using a Krt19-Cre LSL-Tet-O-ΔN89β-catenin transgenic mouse are recommended. Furthermore, as histological analysis of previous studies has shown that the injury microenvironment of DDC and MCD injury regimes is markedly different, further experiments are required in the β1-integrin KO DDC mouse model are required to confirm that the decrease in *Lgr5* and *Lrp6* expression is linked to the process of BEC-to-hepatocyte transdifferentation and not a peculiarity of the p21 MCD injury regime.

Finally, a note of caution is, however, due in the interpretations of these correlational observations as an increase in Axin2 expression could alternatively be related with the presence of cells that have acquired hepatocyte identity but retain expression of the surface biliary marker (Epcam). It has been previously discussed that hepatocytes are responsive to Wnt activating injury cues. It is, therefore, possible that upon acquisition of hepatocyte fate, cells become more responsive to environmental canonical Wnt activating cues. To evaluate whether expression of Axin2 correlates with the stage of hepatocellular differentiation of the cells, single-cell RNAseq transcriptome analysis of Epcam positive cells would be required.

7.3.4 Pharmacological inhibition of the Wnt signalling pathway enhances BEC-to-hepatocyte transdifferentation

Two out of the three LGK974-treated animals that were quantified showed a significantly higher proportion of BEC-derived hepatocytes when compared to animals from the vehicle cohort, which I have interpreted as if the levels of BEC-to-transdifferentation in LGK974-treated animals are lower than in vehicle animals. Based on this interpretation, these results suggest that global inhibition of Wnt secretion promotes BEC-to-hepatocyte transdifferentation.

The preceding discussion has coined the hypothesis that inhibition of the Wnt/β-catenin pathway in transient bi-potent cells promotes progression towards hepatocyte fate and therefore, provides an explanation for these results based on the direct effects of LGK974 on the biliary epithelium-derived cells. However, LGK974 is a compound whose inhibitory effects are not restricted to the biliary epithelium and, therefore, additional hypothesis considering the effects of depleting Wnt secretion globally in the liver need to be considered.

Studies conducted by Russel et al. (2019) reported that depletion of β-catenin in the hepatocellular compartment (β-catenin$^{fl/fl}$, tail injection of AAV8-Cre) severely impaired the regenerative capacity of the hepatocytes in response to CDE injury regime as shown by the drastic reduction of proliferative hepatocytes, enhanced steatohepatitis and elevated systemic levels of the liver injury markers ALT and AST when compared to CDE-injured WT livers [24]. Most importantly, by labelling the hepatocytes prior to injury using animals with a LSL-R26-tdTom genetic background, Russel and colleagues showed that exposure to β-catenin deficient livers showed prominent repopulation of the liver parenchyma in response to CDE diet, implying that abolition of Wnt/β-catenin signalling in the hepatocytes in combination with a liver injury agent is sufficient to drive BEC-to-hepatocyte transdifferentation [24].

In the β1-integrin KO DDC mouse model, hepatocellular proliferation was compromised by the loss of β1-integrin. The number of proliferative hepatocytes in β1-integrin KO DDC-injured livers was, however, significantly reduced in LGK974 treated animals when compared to vehicle animals, suggesting that hepatocellular regeneration in this mouse model was further impaired by the global inhibition of Wnt

secretion. Thus, it is possible to hypothesise that the increased proportion of BEC-derived hepatocytes in LGK974-treated livers in the β1-integrin KO DDC mouse model may be a consequence of the detrimental effects that the LGK974 treatment has in the hepatocytes rather than a direct effect in the biliary epithelium. Thence, further work is required to establish whether inhibition of Wnt signalling in BEC-derived HPC promotes BEC-to-hepatocyte specification. Experiments involving the evaluation of BEC-to-hepatocyte transdifferentation rate in p21 MCD injured livers upon loss of Lrp5/6 (Lrp5$^{fl/fl}$ Lrp6$^{fl/fl}$ R26-LSL-tdTom Krt19-CreERT2) or Lgr4/5 (Lgr4$^{fl/fl}$ Lgr5$^{fl/fl}$ R26-LSL-tdTom Krt19-CreERT2) receptors in the biliary compartment are recommended.

An important final note of caution is due in the enhanced BEC-to-hepatocyte transdifferentation phenotype due to the small sample size of the LGK974 cohort (3 animals). Further studies, with increased sample size and time points, would need to be undertaken to further validate these results.

7.3.5 Discrepancies between ki67, GS and BEC-to-hepatocyte transdifferentation readouts

Animal 65 showed a significantly lower number of proliferative hepatocytes than the vehicle animals, suggesting that the LGK974 treatment was effective. However, animal 65 showed a comparable BEC-to-hepatocyte transdifferentation rate to vehicle animals (~3%). BEC-to-hepatocyte transdifferentation predominantly occurs between day 3 and day 7. Thence, it is possible that if LGK974 is not properly administrated during the first 7 days of recovery drug disposition in the biliary epithelium is low during that time frame, it might no longer cause an effect in the BEC-to-hepatocyte transdifferentation rate. The lack of BEC-to-hepatocyte transdifferentation phenotype but successful inhibition of hepatocyte proliferation in animal 65 might, therefore, be explained by the inefficacy of the treatment during the first days of recovery followed by a successful inhibition of Wnt secretion.

In the hepatocytes, GS is a direct target of β-catenin and blockage of Wnt secretion with LGK974 in mice undergoing DDC injury regime has been shown to abolish GS expression in pericentral hepatocytes [94]. However, only two animals (animal 66 and 67) out of the four animals exposed to LGK974 treatment, showed a significant decline

in GS expression levels. By contrast, all LGK974-treated animals showed a significant decrease in the number of proliferative hepatocytes. Hepatocyte proliferation is highly sensitive to abolition of canonical Wnt signalling. It is possible therefore that the administrated dose of LGK974 was sufficient to inhibit hepatocyte proliferation but not GS expression in this injury context. The fact that GS expression was not completely abolished in all animals also opens the possibility that inhibition of Wnt secretion in the experiments presented in this thesis was incomplete. In future studies, it might be recommendable to increase the dose or change the administration route of LGK974.

7.3.6 Summary

The current chapter aimed to determine whether the Wnt signalling pathway orchestrated BEC-driven liver regeneration when hepatocyte proliferation was compromised. Abrogation of Wnt ligand secretion in the DDC β1-Integrin KO injured livers had minor effects the proliferation of the biliary compartment during BEC-to-hepatocyte transdifferentation. By contrast, the proliferation of the hepatocytes was highly dependent on the presence of Wnt environmental signals. The Wnt/β-catenin pathway was dynamically activated in BECs isolated from AAV8.p21 but not from AAV8.null MCD injured livers, suggesting that activation of canonical Wnt signalling is an event associated with BEC reprogramming. Licensing of the biliary epithelium to respond to canonical Wnt signals, however, decreased during BEC-to-hepatocyte transdifferentation. These data, together with the observation that pharmacological inhibition of global Wnt secretion caused a prominent BEC-to-hepatocyte transdifferentation response, support the hypothesis that while activation of the Wnt/β-catenin pathway in BECs promotes escape from their ductal-committed state, inhibition of the canonical Wnt cascade might be required for progression of transient bi-potent cells towards hepatocyte fate. Further work is required to determine whether inhibition of Wnt signalling in the biliary compartment is required for BEC-to-hepatocyte transdifferentation or whether the observed phenotype from the LGK974 experiment occurs as sub-product of the inhibition of Wnt signalling pathway in other liver cell type.

Chapter 8. CONCLUSIONS AND FUTURE PERSPECTIVES

The first objective of this thesis was to develop the molecular tools that allow the recreation of a local Wnt microenvironment *in vitro*. To this end, I have established protocols for the immobilization of Wnt3a and Rspo1 proteins as well as the CV Wnt9b and Rspo3 onto carboxylic acid beads. The biological activity of Wnt3a, Rspo1, Wnt9b and Rspo3 beads was validated in two different HEK293T Wnt reporter cell lines. The biological activity of Rspo3 beads was additionally validated in PH cultured in conventional monolayers. Finally, two important observations can be extracted from the characterization of the biological activity Wnt and Rspo ligands:

(1) Purified Wnt9b protein required the presence of Rspo ligands (Rspo1 or Rspo3) to activate canonical Wnt signaling. Based on the mode of action or Rspo proteins three models were proposed explain Wnt9b and Rspo cooperativity (see Chapter 5). Model I, Rspo stabilizes a receptor of the Fzd family that mediates Wnt9b signal transduction. Model II, Rspo stabilizes Lrp5/6. Model III, Rspo stabilized an novel unknown receptor required for Wnt9b signal transduction.

(2) The CV ligands Wnt9b and Rspo3 were sufficient to activate the canonical Wnt pathway. This observation is of special importance as suggest that the presence of these two ligands may be sufficient to artificially recreate the Wnt microenvironment of the CV *in vitro*.

The second objective of this thesis was to evaluate the suitability of the currently available liver organoid platforms (BD and PH organoids) as cell source to model Wnt-liver zonation. The characterization of the PH organoid model to the CV ligands Wnt9b and Rspo3 confirmed that these structures resemble the response of primary hepatocytes cultured in 2D, indicating that PH organoids are a suitable cellular source to model Wnt-liver zonation. By contrast, activation of Wnt pathway in BD organoids did not drive an increase in expression of pericentral metabolic genes. Importantly, further characterization of the BD organoid system revealed these structures are

closer to the BEC than to the hepatocyte lineage. This work demonstrates for the first time that differentiated BD organoids may not be used as a hepatocellular *in vitro* platform. This is of special interest as research groups in the pharma industry are currently using these cells as a hepatocellular model for drug testing.

I have further characterised the response of differentiated BD organoids to Wnt pathway activation and, particularly, to the exposure of Rspo1, a ligand that has been recently linked to liver regeneration. My work points to the role of Wnt/Rspo1 signalling in the regulation of cell cycle and possibly in the induction of a DNA damage repair response. Furthermore, exposure to Rspo1 induced the expression of various HPC-like genes and induced the appearance of a 'high Wnt' (tdTom positive) population with enhanced stem cell features and characterized by the expression of genes involved in cell cycle progression. The readouts for Wnt activation used in this thesis did not allow the activation of canonical and non-canonical Wnt signalling in the BD organoids to be distinguished and therefore, further studies will be required to evaluate the potential contributions of the different branches of the Wnt pathway to the enhanced stem cell features/ proliferative capacity of the tdTom positive population.

The preceding observations in the BD organoid platform prompted me to further investigate whether Wnt pathway has a role in BEC-driven regeneration. I interpreted the expression of Hnf4a, Cebpa and other hepatocyte markers in differentiated BD organoids as sign that these structures resemble a cellular context of BECs that are acquiring features of the hepatocyte lineage. Thus, together with members of the Forbe's laboratory, I investigated the role of Wnt pathway during BEC-to-hepatocyte transdifferentation, for which the dynamics of canonical Wnt pathway activation during BEC-to-hepatocyte transdifferentation as well as the effects of global Wnt secretion inhibition during liver recovery were studied. Global inhibition of Wnt signalling mirrored the effects of β-catenin depletion from the hepatocellular compartment described by Russell et al (2019) highlighting that hepatocellular regeneration heavily relies in environmental Wnt injury cues [24]. Intriguingly, inhibition of Wnt secretion with LGK974 had minor effects in the proliferation rate of BECs while robustly promoting BEC-to-hepatocyte transdifferentation in two out of the three animals studied. It is possible to interpret these results as evidence that inhibition of the Wnt pathway during recovery from liver injury promotes BEC-to-hepatocyte

transdifferentation, although strong conclusions should not be drawn due to the small number of animals analysed in this study.

There are still many answered questions regarding how Wnt signalling controls BEC biology during regeneration: does activation of the Wnt signalling pathway promote the acquisition of an HPC bipotent-like state? Does inhibition of the Wnt signalling pathway promotes exit from such an HPC bipotent-like state? To which extent does the canonical or the non-canonical branch of the Wnt signalling pathway coordinate BEC-driven regeneration? What is the cellular source of Wnt/Rspo regenerative ligands *in vivo*?

Ultimately this work is one of the first descriptions of the effects of therapeutically targeting the Wnt pathway in a murine severe liver damage mouse model and therefore offers insights about the possibility of molecularly intervening in this pathway as therapeutic avenue in chronic liver pathologies. Further work should be undertaken to understand the mechanisms governing BEC-hepatocyte plasticity, and in particular, the exact role of Wnt pathway in this process. This work has not persuaded the pool of hepatocytes transdifferentiating into BECs.

Modelling Wnt driven zonation *in vitro*: future perspectives

My work points out that (1) Wnt9b in the presence of Rspo3 ligand can exert canonical activity in cellular context of the hepatocytes, (2) Rspo3 beads in combination with soluble Wnt9b might be a valid strategy to induce local activation of β-catenin in hepatocyte cultures and (3) PH organoids are a suitable source to model Wnt-driven zonation *in vitro*. The next logic step would be to assess whether Rspo3 beads in combination with soluble Wnt9b induces local activation of the Wnt signalling pathway in differentiated PH organoids. For this, I suggest the extraction of differentiated PH organoids from the Matrigel and culture of these structures in a collagen or Matrigel sandwich culture platform (Figure 8.1, A). This culture strategy would be preferred over conventional 2D monolayers as, in principle, the placement of a second layer of collagen over the cells would enable the establishment of adequate cell-cell junctions and cell polarization. Rspo3 beads could be introduced in the system during the solidification of the upper layer of hydrogel. The carboxylic acid coated beads used in

this study for the immobilization of Wnt and Rspo ligands are made of iron and thereby, Rspo3 could be potentially attracted in big clusters that resemble the CV using magnets. As a proof-of-concept for this approach, I performed a series of pilot experiments using the HEK293T TCF-eGFP cell line (Figure8.1, A). Figure 8.1 B shows the successful clustering of Rspo3 beads in HEK293T collagen sandwich cultures using magnets. Figure 8.1 C shows that Rspo3 beads in combination of soluble Wnt9b induces local activation of the TCF-eGFP reporter in HEK293T collagen sandwich cultures.

Finally, bioartifical livers remain highly limited by the inability of these devices to accurately replicate the microenvironment of the liver lobule. In this thesis, I have established a set of molecular tools that may be used to recreate the local Wnt microenvironment of the hepatic CV in hepatocyte culture systems. The adaptation and controlled presentation of biological and physicochemical cues in hepatocyte culture systems may help us to better understand the regulatory mechanisms that govern hepatocyte functional specification. Such understanding is required for the development of therapies that alleviate the symptoms of liver pathological conditions where zonation is perturbed.

A

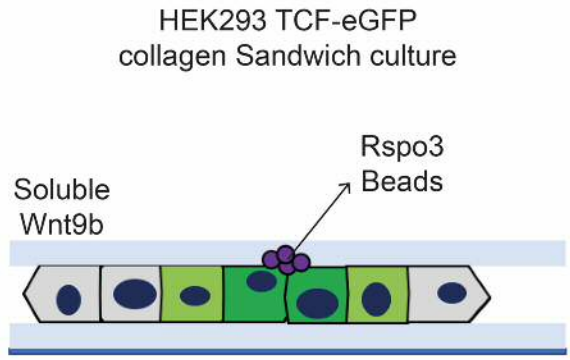

B

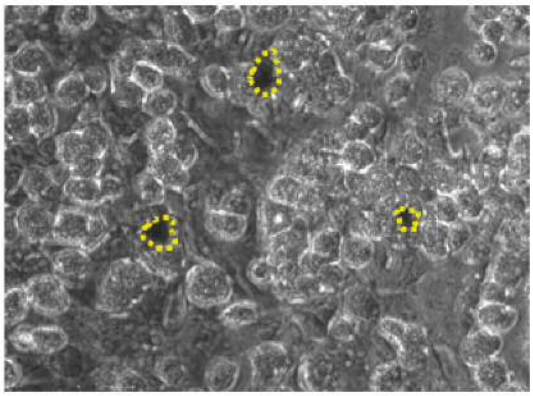

C

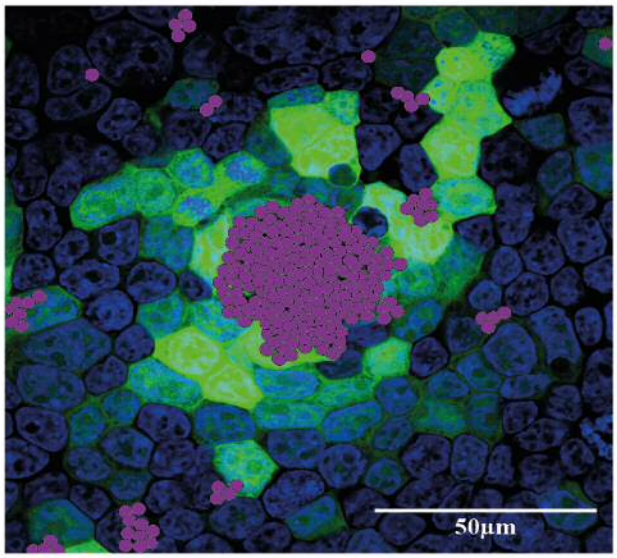

Figure 8.1 Future perspectives: recreating the CV Wnt niche *in vitro*. (A) Collagen sandwich culture strategy diagram. (B) Image shows the successful clustering of Rspo3 beads in HEK293T collagen sandwich cultures using magnets. Yellow dash line highlights the presence of bead clusters. (C) HEK293T TCF-eGFP cells cultured in a collagen sandwich platform were exposed to Rspo3 beads and soluble Wnt9b for 24h. Beads were artificially coloured in purple.

APPENDIX A

Appendix A Table1 Genotyping primers

PCR	Primer Sequences (5' to 3')	PCR Program	Expected Products
CRE	FW TGA CCG TAC ACC AAA ATT TG RV ATT GCC CCT GTT TCA CTA TC	95°C, 3min (95°C, 30s; 62°C, 30s; 72°C 1min) $_{35}$ 72°C, 10min, 4C	1000bp
GFP	FW ACAACAAGCGCTCGACCATCAC RV AGTCGATGCCCTTCAGCTCGAT	94°C, 2min (94°C, 20s; 65°C, 30s ; 72°C 1min) $_{35}$ 72°C, 2min, 4C	530bp
R26-tdTom	1 CTCTGCTGCCTCCTGGCTTCT 2 CGAGGCGGATCACAAGCAATA 3 TCAATGGGCGGGGGTCGTT	95°C, 3min (95°C, 30s; 61°C, 30s; 72°C 1min) $_{35}$ 72°C, 10min, 4C	WT 330bp Mutant 250bp

Appendix A, Table2 RT-qPCR primer list

Gene	Secuence 5-3	Source
b2m_RV	CTTTCTGGTGCTTGTCTCACTG	Anika
b2m_FW	AGCA TTTGGA TTTCAA TGTGAG	Anika
Axin2_FW	GCA GCT CAG CAA AAA GGG AAA T	Alan Clark lab
Axin2_RV	TAC ATG GGG AGC ACT GTC TCG T	Alan Clark lab
B-catenin	AGT CCT TTA TGA ATG GGA GCA A	Alan Clark lab
B-catenin	TCT GAG CCC TAG TCA TTG CAT A	Alan Clark lab
E-cadherin	CAG ATG ATG ATA CCC GGG ACA A	Alan Clark lab
E-cadherin	GGA GCC ACA TCA TTT CGA GTC A	Alan Clark lab
Axin1	CTCCAAGCAGAGGACAAAATCA	Anika
Axin1	GGATGGGTTCCCCACAGAAATA	Anika
SOX9_FV	AGTACCCGCATCTGCACAAC	Semir
SOX9_RV	ACGAAGGGTCTCTTCTCGCT	Semir
LGR5_FV	CCTACTCGAAGACTTACCCAGT	Semir
LGR5_RV	GCATTGGGGTGAATGATAGCA	Semir
c-myc_FW	CCTTTGGGCGTTGGAAACC	Anika
c-myc_RV	TCCTCGTCGCAGATGAAATAGG	Anika
Epcam_FV	TGAAAAGGCACCCGAGTTCTCC	Anika
Epcam_RV	AACCAGGACAACAATCCCCG	Anika
GAPDH_FW	CATGGCCTTCCGTGTTCCTA	
GAPDH_RV	CCTGCTTCACCACCTTCTTGAT	
Alb_FW	TGCTTTTTCCAGGGGTGTGTT	
Alb_RV	TTACTTCCTGCACTAATTTGGCA	
krt19_FW	CCTCCCGAGATTACAACCACTA	Anika
krt19_RV	AATCTTGGAGTTGTCAATGGTG	Anika
Cyp2e1_FW	CATCAACCTCGTCCCTTCCA	Eider
Cyp2e1_RV	TACAACTGTACCCTTGGGGATG	Eider
Cyp1a2_FW	AGCACTACCAAGACTTCAACA	Eider
Cyp1a2_RV	TGTCAAAGCCAGCTCCAAAGA	Eider
PROM1_FW	CCAGCCGAATGACTTCCCTC	Sonia
PROM1_RV	AGAGGGCAATCTCCTTGGAA	Sonia
FAH_FW	TCATAACAGGTCACTGCCAGG	Sonia
FAH_RV	TGTCTTGTGACTTCCGGAGC	Sonia
Ki67_FW	ACCGCTCCTTTAGGTATGAAGA	Ken
ki67_RV	CTTTGGTATCTTGACCTTCCCCATC	
GS_FW	CAGAGACCAACTTGAGGCACA	
GS_RV	CTCCATTCCAAACCAGGGGT	
CPS1_FW	ACATGGTGACCAAGATTCCTCG	PrimerBank(26324620a1)
CPS1_RV	TTCCTCAAAGGTGCGACCAAT	
Cyp2f2_FW	GGACCCAAACCTCTCCCAATC	PrimerBank(6681111a1)

Cyp2f2_RV	CCGTGAACACCGACCCATAC	
Ass1_FW	CACGGGAAAGGGGAATGACC	Eider
Ass1_RV	TCATCCATACTCCAGGGGCT	
TBP_FW	ACCGTGAATCTTGGCTGTAAAC	PrimerBank(172073170c3)
TBP_RV	GCAGCAAATCGCTTGGGATTA	
OPN_FW	AGCAAGAAACTCTTCCAAGCAA	PrimerBank(6678113a1)
OPN_RV	GTGAGATTCGTCAGATTCATCCG	
PDX1_FW	GTGGGCAGGAGGTGCTTACA	Eider
PDX1_RV	GTTCAACATCACTGCCAGCTC	

HNF4a_FW	agaggttctgtcccagcagatc	
HNF4a_RV	cgtctgtgatgttggcaatc	Guo et al (2017)
Tert_Pair2_FW	ATCTGCAGGATTCAGATGCC	Shengda Lin (2018) Nature
Tert_Pair2_RV	GCAGGAAGTGCAGGAAGAAG	Shengda Lin (2018) Nature
CD24_FW	TTCTGGCACTGCTCCTACC	Carmen Velasco
CD24_RV	GCGTTACTTGGATTTGGGGAA	Carmen Velasco
CD44_FW	CACCATTGCCTCAACTGTGC	Beyaz (2016) Nature
CD44_RV	TTGTGGGCTCCTGAGTCTGA	Beyaz (2016) Nature
AFP_FW	CTTCCCTCATCCTCCTGCTAC	Primer Bank (31982513a1)
AFP_RV	ACAAACTGGGTAAAGGTGATGG	Primer Bank (31982513a1)
TBX3_FW	AGCGGGGTACAGAGATGGTC	Primer Bank (38327622c1)
TBX3_RV	TTGGCCTTTTTATCCAGTCCAG	Primer Bank (38327622c1)
TROP2_FW	GTGGCTGAGAGTAAATGTGGG	Primer Bank (11875203a1)
TROP2_RV	TTGGTGGAATACTTGTCCGCT	Primer Bank (11875203a1)
HNF1b_FW	AGGGAGGTGGTCGATGTCA	Primer Bank (6678243a1)
HNF1b_RV	TCTGGACTGTCTGGTTGAACT	Primer Bank (6678243a1)
CK7_FW	GATGACCTCCGCAACACC	Oikawa (2008) Gastroenterology
CK7_RV	TCCAGCAGCTTGCGGTAG	
Hhex_FW	CGGACGGTGAACGACTACAC	PrimerBank (6680219a1)
Hhex_RV	CGTTGGAGAACCTCACTTGAC	PrimerBank (6680219a1)
HNF6_Pair2_FW	GGCAACGTGAGCGGTAGTTT	
HNF6_Pair2_RV	TTGCTGGGAGTTGTGAATGCT	
Cebpa_FW	aaacaacgcaacgtggaga	Seth (2014) Development
Cebpa_RV	gcggtcattgtcactggtc	
Prox1_Pair1_FW	ACAAAGCAAATGACTTTGAGGTTC	Eider
Prox1_Pair1_RV	GGATCAACATCTTTGCCCGC	

PROX1_Pair2_FW	AGAAGGGTTGACATTGGAGTGA	Primer Bank (6679483a1)
PROX1_Pair2_RV	TGCGTGTTGCACCACAGAATA	Primer Bank (6679483a1)
TBX3_Pair2_FW	gaacctacctgttcccggaaa	Seth (2014) Development
TBX3_Pair2_RV	agtgtctcgaaaacccttgc	
Lrp6_FW_P2	TTGTTGCTTTATGCAAACAGACG	Primer Bank ID: 6678718a1
Lrp6_RV_P2	GTTCGTTTAATGGCTTCTTCGC	

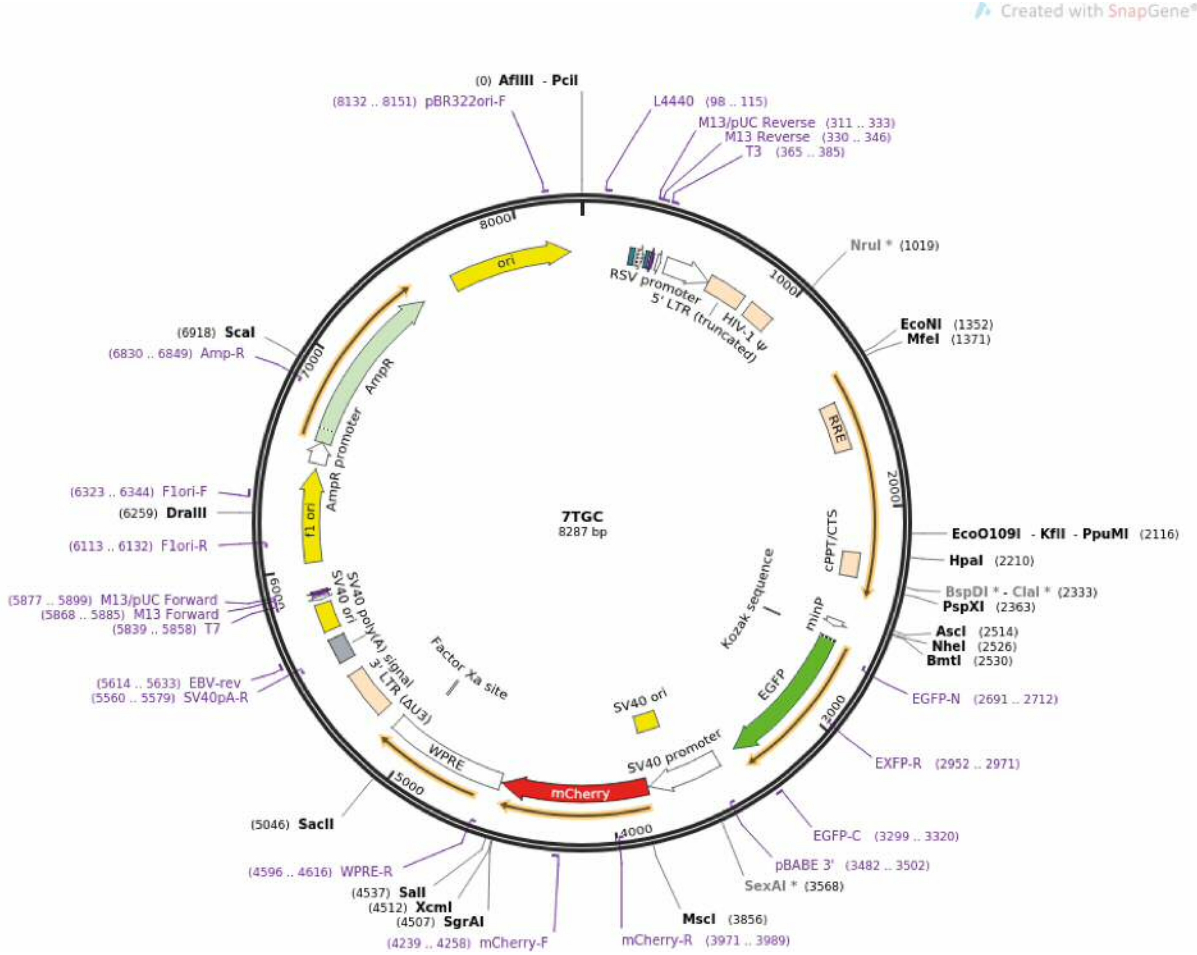

Appendix A, Figure1 p7TGC plasmid from Addgene contains the sequence coding for eGFP expression under the control of 7x TCF repeats. eGFP expression can therefore be used as a proxy for canonical Wnt activation levels. mCherry is under the control of the SV40 promoter and therefore it's expression reports successful integration and expression of the plasmid.

A)

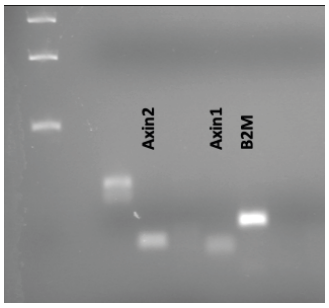

B)

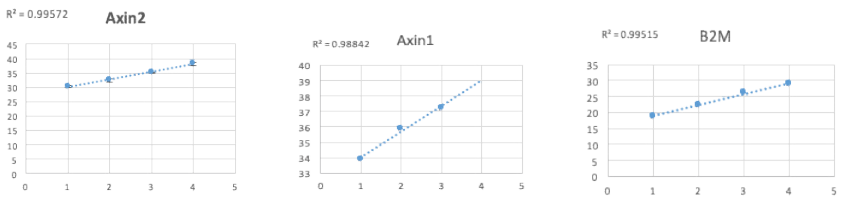

C)

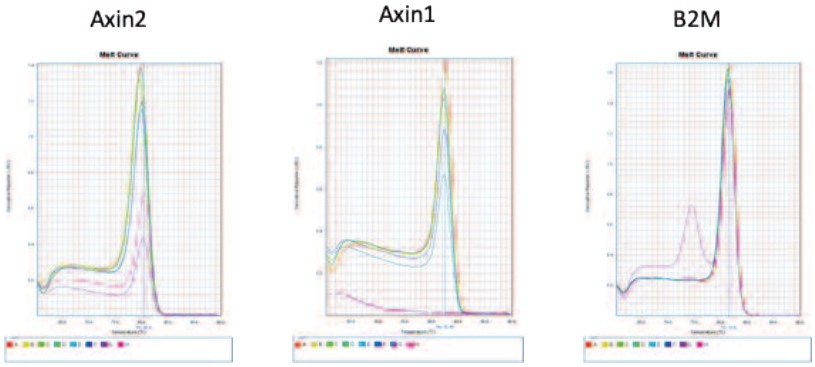

Appendix A, Figure2. Primer test results for Axin2, Axin1 and B2m primers (A) RT-qPCR amplicon bands in agarose gel (B) Linear relationship between the Ct value and the cDNA dilution number. (C) RT-qPCR melt curve.

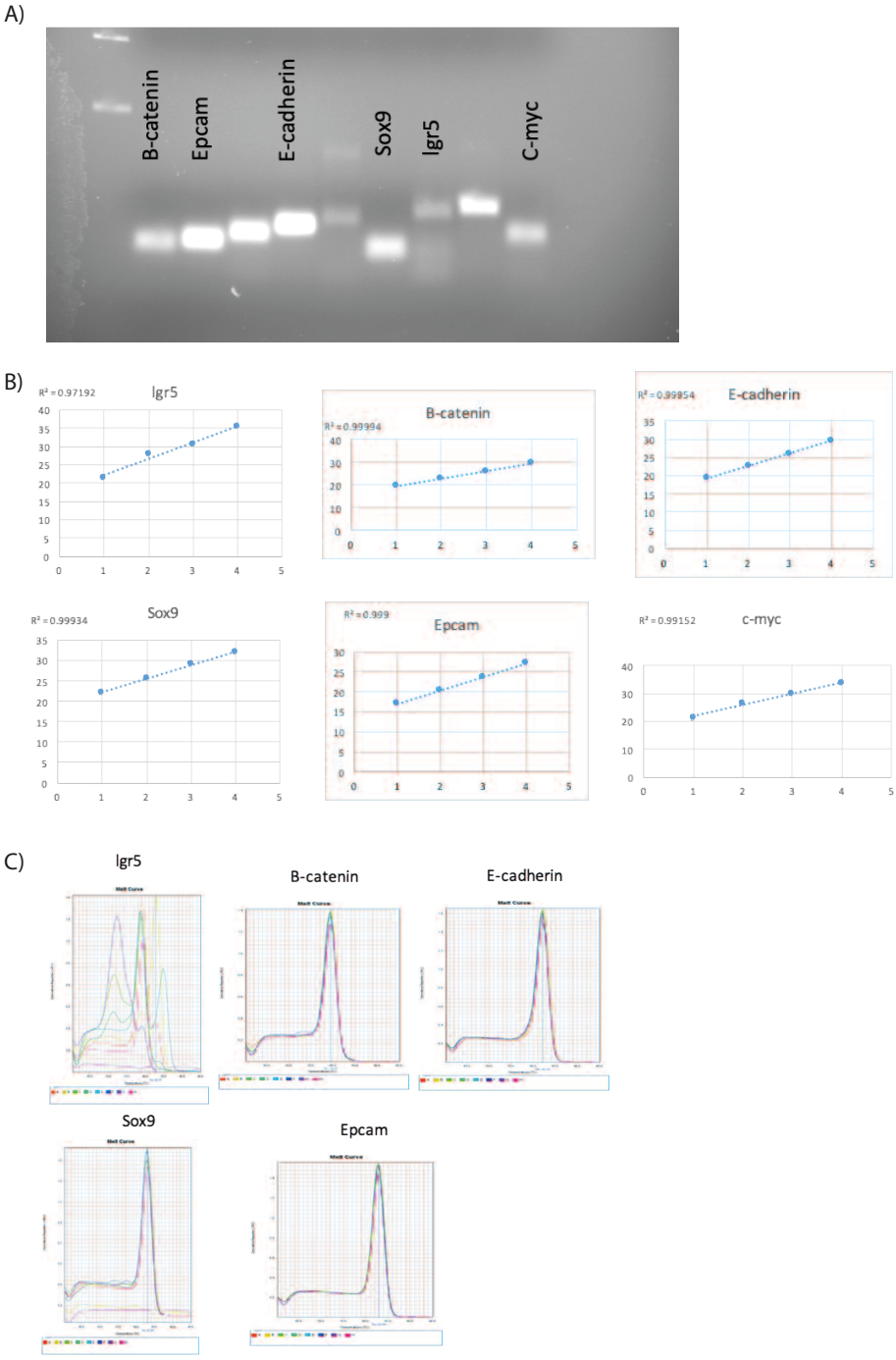

Appendix A, Figure3. Primer test results for ß-catenin, Lgr5, E-cadherin, Sox9 and Epcam primers (A) RT-qPCR amplicon bands in agarose gel (B) Linear relationship between the Ct value and the cDNA dilution number. (C) RT-qPCR melt curve.

A)

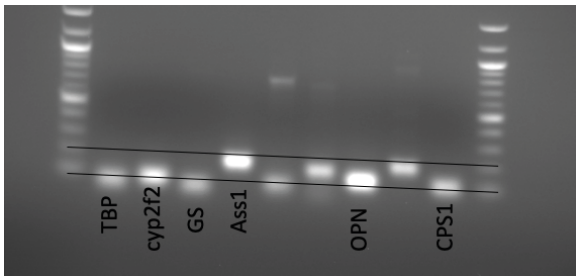

B)

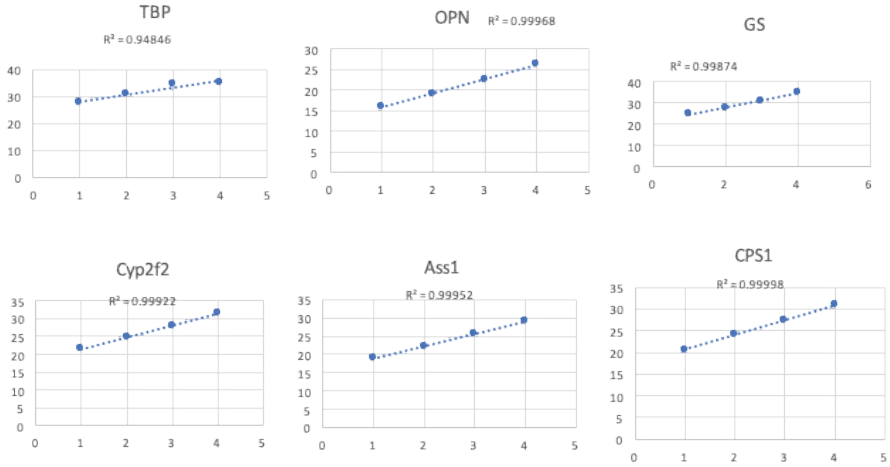

C)

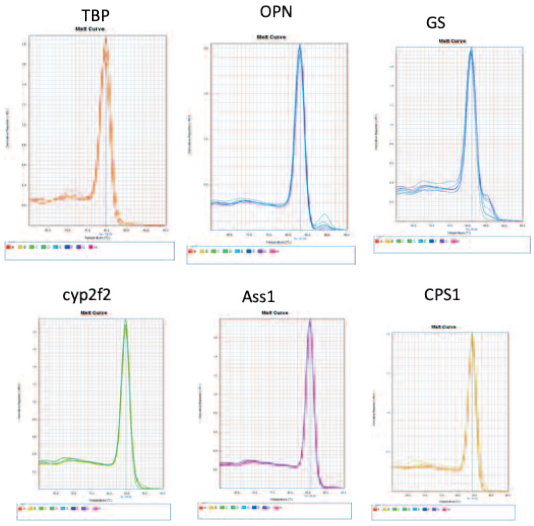

Appendix A, Figure4. Primer test results for Tbp, Spp1 (Opn), Glul (GS), Cyp2f2, Ass1 and Cps1 primers (A) RT-qPCR amplicon bands in agarose gel (B) Linear relationship between the Ct value and the cDNA dilution number. (C) RT-qPCR melt curve.

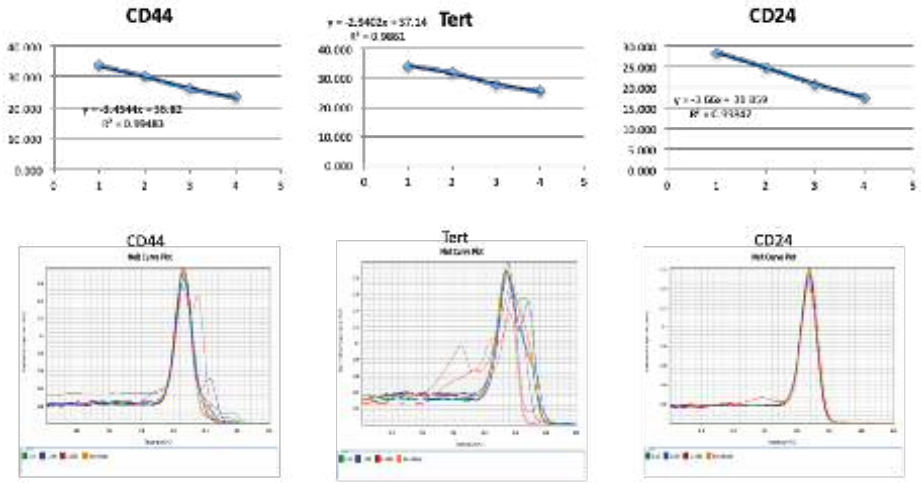

Appendix A, Figure5. Primer test results for Cd44, Tert and Cd24 primers. Top panels show linear relationships between the Ct value and the cDNA dilution number. Bottom panels show RT-qPCR melt curve.

A)

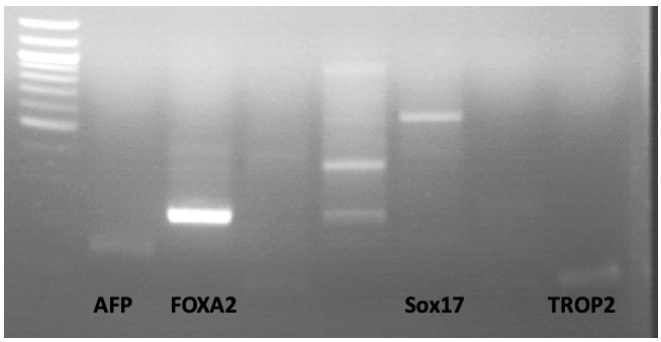

B)

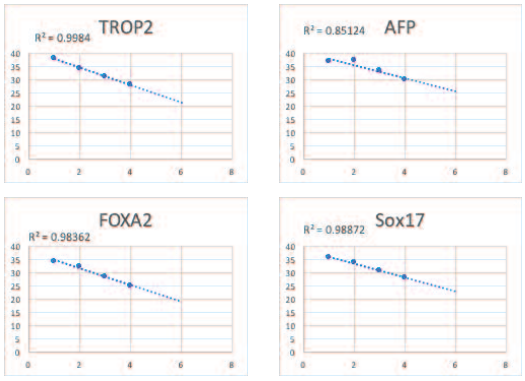

C)

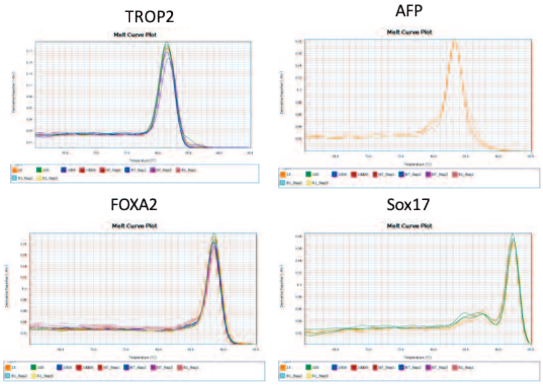

Appendix A, Figure6. Primer test results for Trop2, Afp, Foxa2 and Sox17 primers (A) RT-qPCR amplicon bands in agarose gel (B) Linear relationship between the Ct value and the cDNA dilution number. (C) RT-qPCR melt curve.

A)

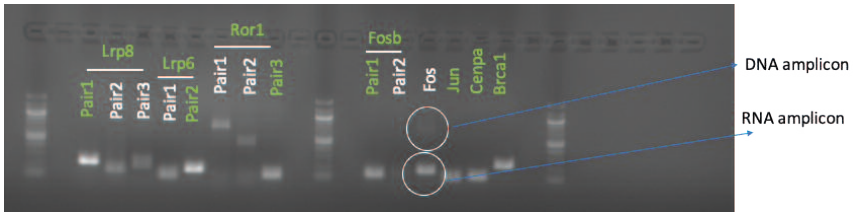

B)

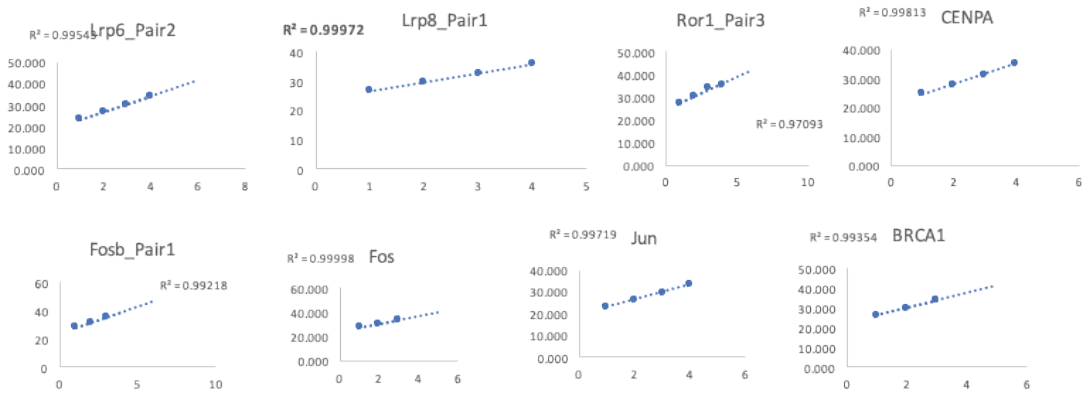

C)

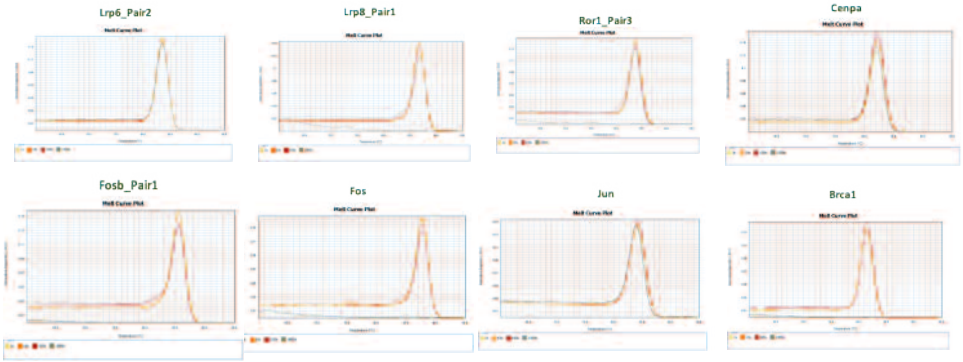

Appendix A, Figure7. Primer test results for Lrp6, Lrp8, Ror1, Cebpa, Fosb, Fos, Jun and Brca1 primers (A) RT-qPCR amplicon bands in agarose gel (B) Linear relationship between the Ct value and the cDNA dilution number. (C) RT-qPCR melt curve.

A)

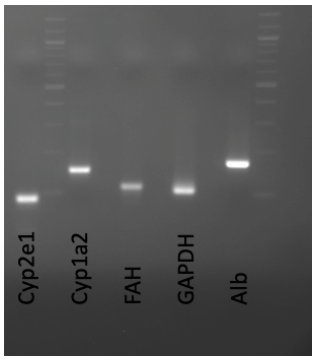

B)

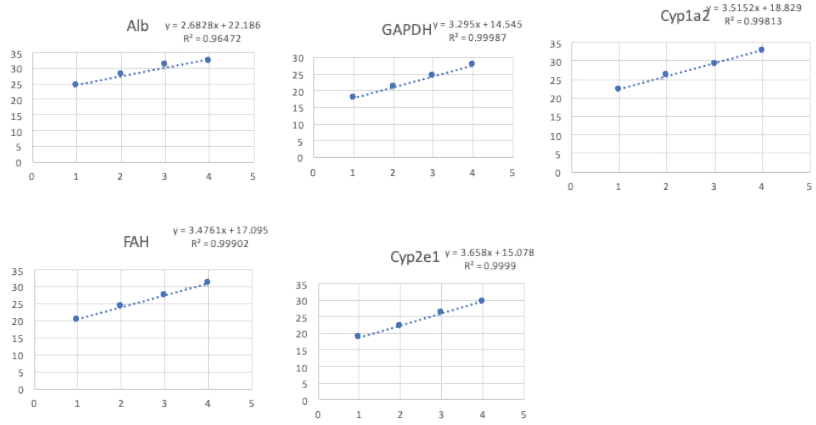

C)

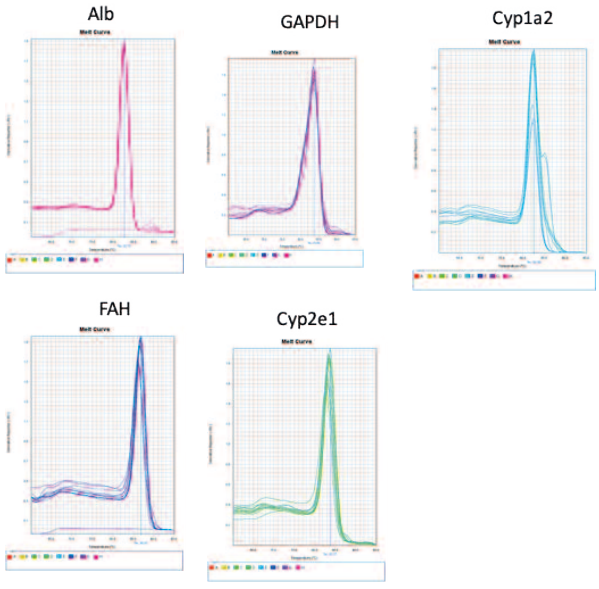

Appendix A, Figure8. Primer test results for Alb, Gapdh, Cyp1a2, Fah and Cyp2e1 primers (A) RT-qPCR amplicon bands in agarose gel (B) Linear relationship between the Ct value and the cDNA dilution number. (C) RT-qPCR melt curve.

APPENDIX B

The current appendix contains supplementary information associated with Chapter 5.

A

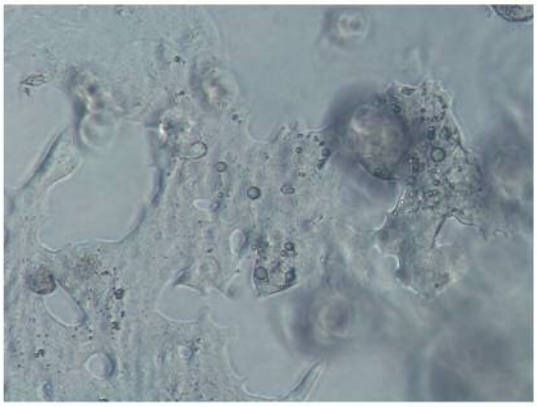

B

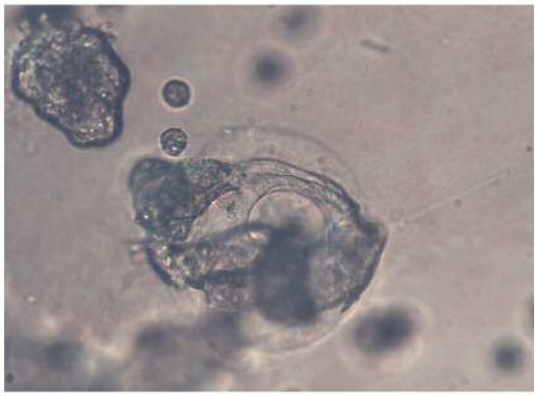

C

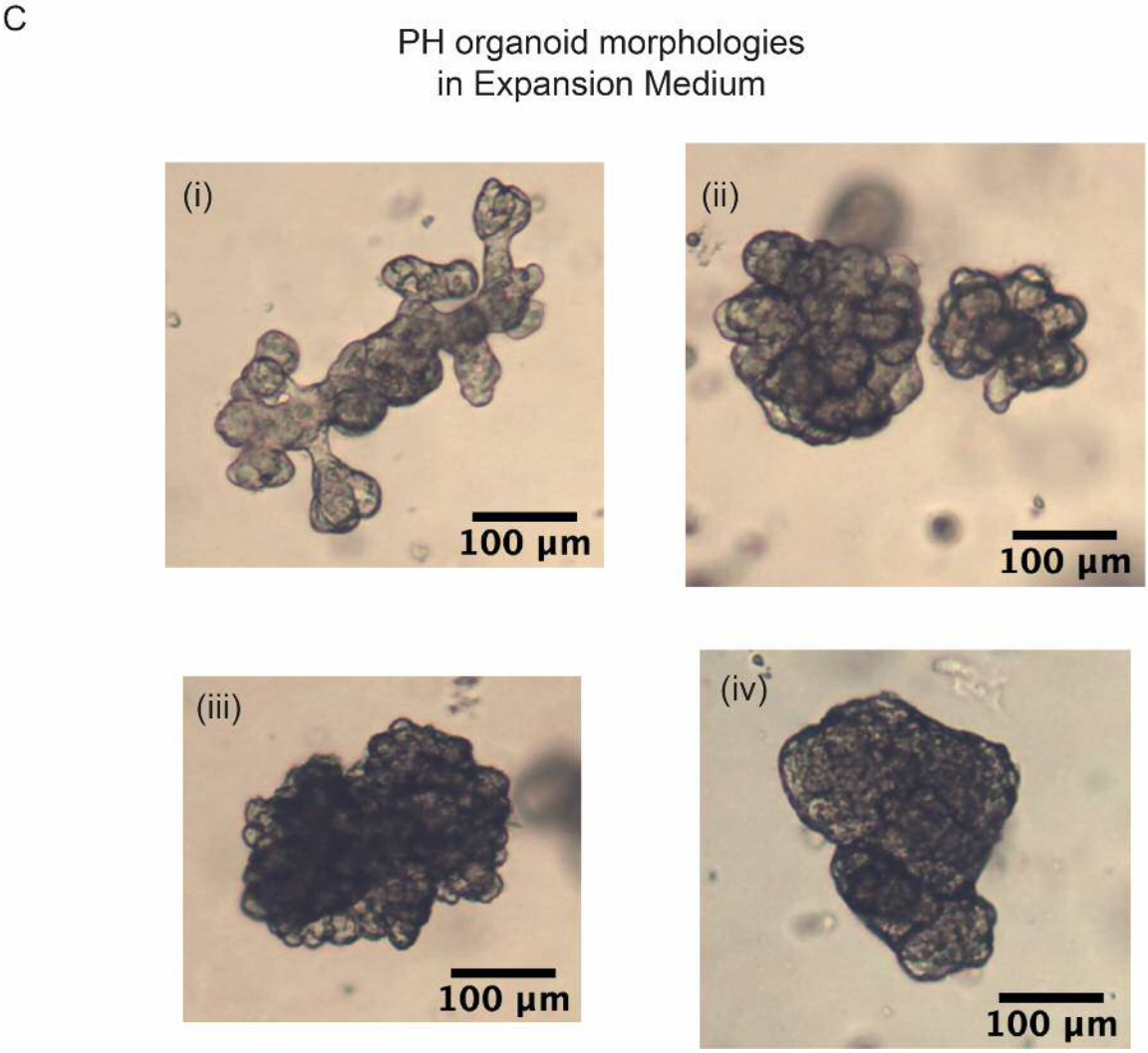

Appendix B, Figure1 PH organoids characterization (A) 10x image of PH that were seeded in Matrigel but migrated to the bottom of the plate acquiring the typical fibroblast-like morphology of PH cultured in 2D conventional monolayers. (B) 10x image of a PH organoid displaying an atypical duct-like morphology. (C) PH organoids adapted to 3D culture display a variety of morphologies. (i) Example of an organoid displaying a bunch-of-grapes morphology with “invasive” phenotype. Cells within the organoid appear to growth in cords that brunch with cells growing towards the Matrigel. (ii) Bunch of grapes-of-grapes type of organoid, displaying a non-invasive phenotype and composed of large cells. (ii) Bunch of grapes-of-grapes type of organoid, displaying a non-invasive phenotype and composed of small and tightly-packed cells. (iv) PH organoid displaying a compact “smooth” surface-type of morphology. The frequency of the presence of each morphology was variable among cultures being morphologies (i), (ii) and (iii) consistently the most frequently found.

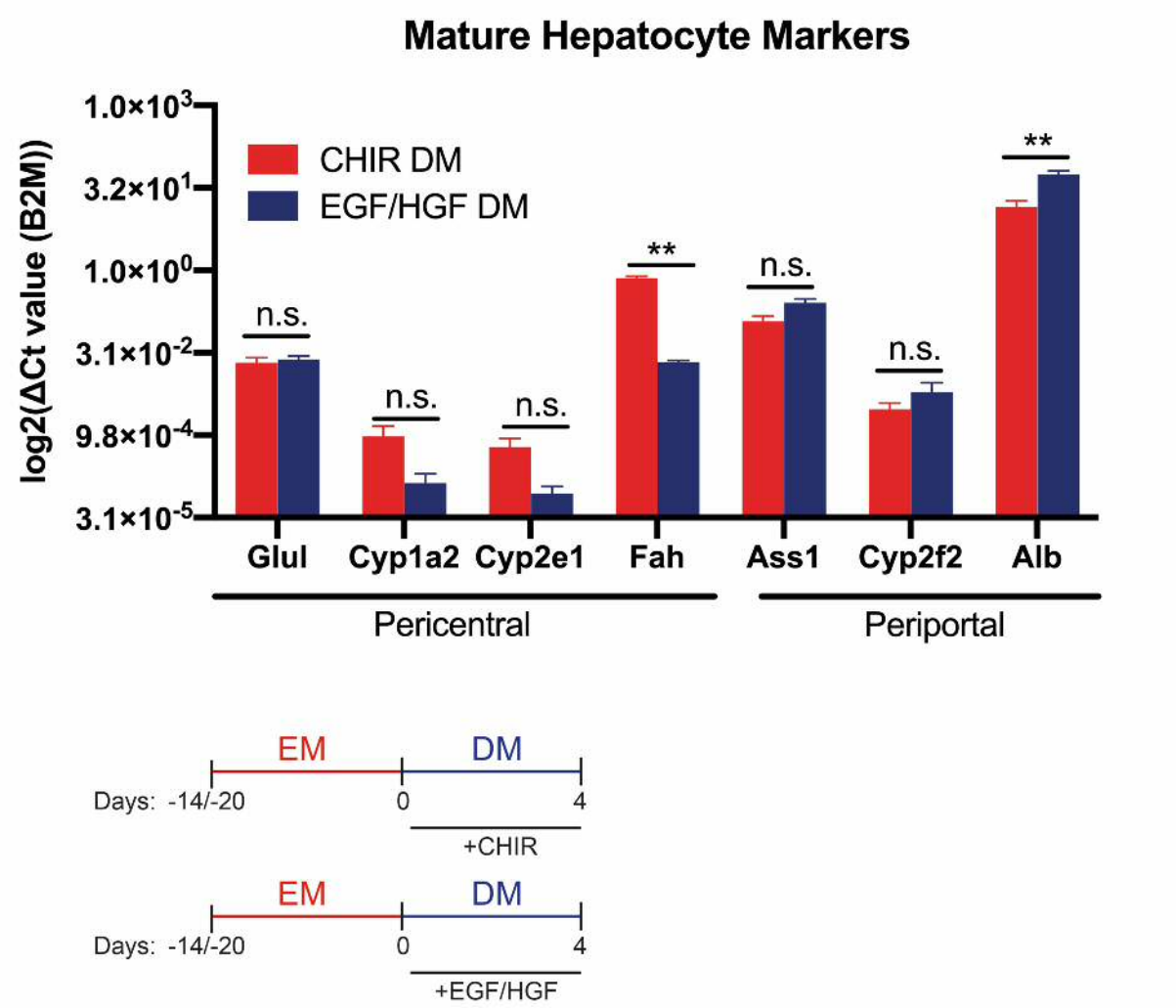

Appendix B, Figure2 (A) RT-qPCR gene expression analysis of zonated genes in PH organoids that have been differentiated for 4 days in the presence of CHIR or EGF/HGF. (n=5). (C) RT-qPCR gene expression analysis of hepatocyte lineage markers in PH organoids (n=5). (D) RT-qPCR gene expression analysis of HPCs markers in PH organoids upon differentiation. (n=5). Statistical significance was determined using Mann-Whitney t-test. p-value n.s.>0.05 ; p-value *< 0.05; p-value **< 0.01; p-value ***< 0.001; p-value ****< 0.0001. RT-qPCR experiments were run by Michael Dawes although data analysis, presentation and interpretation was performed by myself.

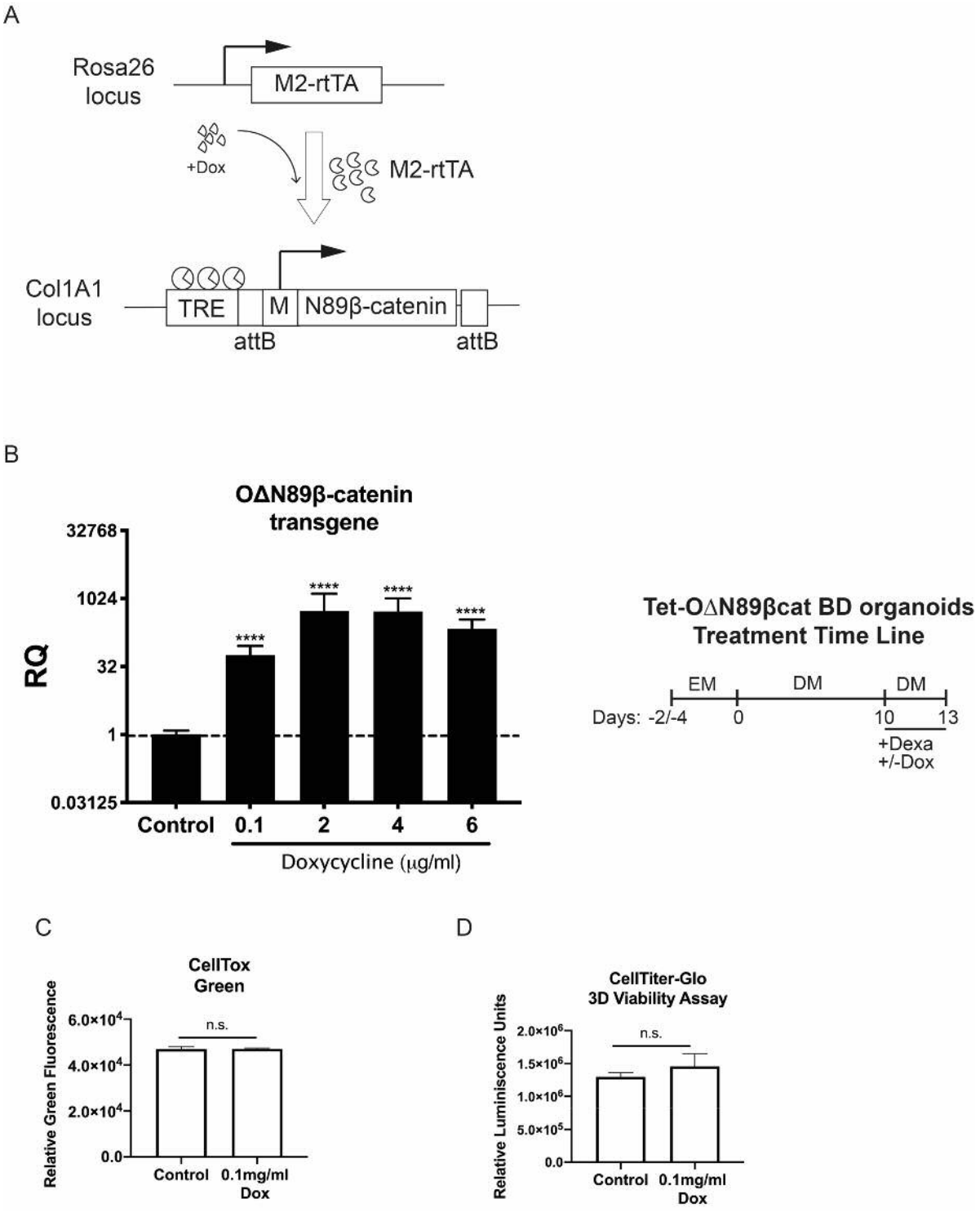

Appendix B, Figure3 (A) Schematic representation of OΔN89β-catenin and M2-rtTA transgenes present in OΔN89β-catenin organoids. Presence of doxycyclin (Dox) triggers the transcription of activated (DN89) mutant β-catenin. (B) RT-qPCR shows expression of OΔN89β-catenin upon doxycycline treatment. (C) Cell GreenTox viability assay of WT differentiated organoids shows non-significant differences in late apoptosis events in the cultures after 3days of exposure to doxycycline (n=5 technical replicates). (D) CellTiter-Glo Viability of WT differentiated organoids shows non-significant metabolic defects caused by the exposure to doxycycline after 3days of treatment (n=5 technical replicates).

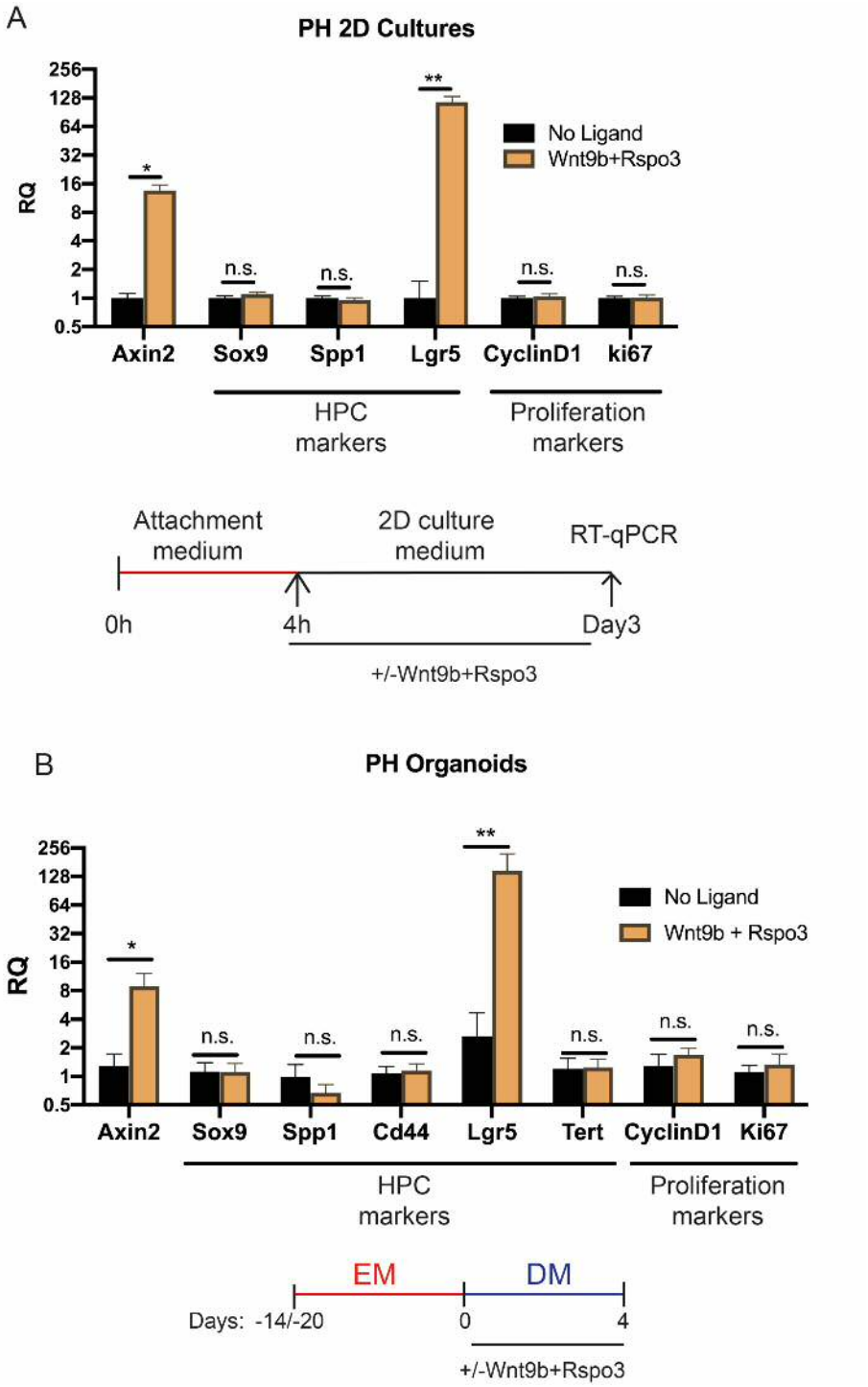

Appendix B, Figure4 (A) RT-qPCR gene expression analysis in PH conventional 2D cultures upon concomitant exposure to 50 ng/ml Rspo3 and 100 ng/ml Wnt9b (n=4). (B) RT-qPCR gene expression analysis in PH organoids upon concomitant exposure to 50 ng/ml Rspo3 and 100 ng/ml Wnt9b (n=5). RT-qPCR experiments performed with PH organoid samples were run by Michael Dawes. Data analysis, presentation and interpretation was performed by myself. Note that Lgr5 levels in untreated PH organoids (no ligand conditions) were so low that the RT-qPCR failed to assign. A Ct value in 3 of the 5 samples. These samples were included in the analysis presented by assigning them a Ct value of 40, which corresponds to the number of cycles run. Statistical significance was determined using Mann-Whitney t-test. p-value n.s.>0.05 ; p-value *< 0.05; p-value **< 0.01; p-value ***< 0.001; p-value ****< 0.0001.

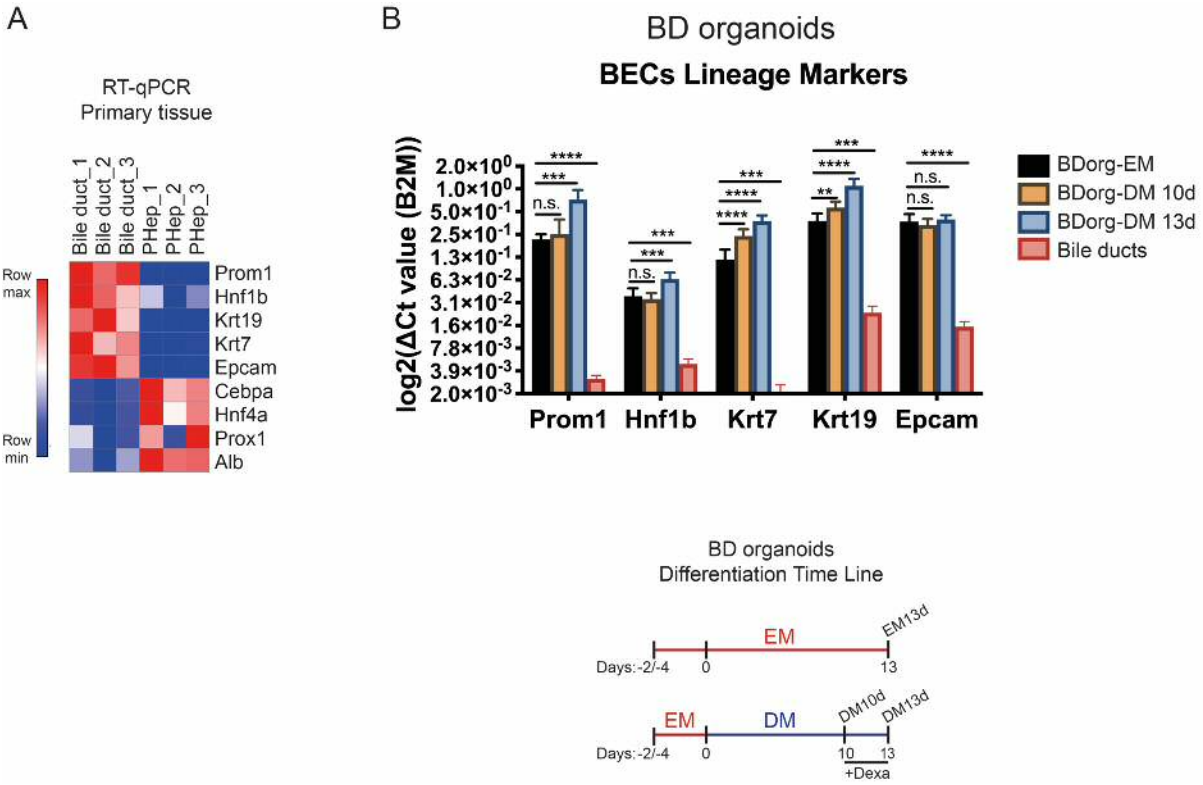

Appendix B, Figure5 (A) Heat map showing RT-qPCR relative gene expression analysis of lineage genes in primary hand-picked BD and PH (n=3 animals). (B) RT-qPCR gene expression analysis in differentiated WT BD organoids (n=5) and primary hand-picked bile ducts (n=3). Statistical significance was determined using Mann-Whitney t-test. p-value n.s.>0.05 ; p-value *< 0.05; p-value **< 0.01; p-value ***< 0.001; p-value ****< 0.0001.

APPENDIX C

The current appendix contains supplementary information associated with Chapter 6.

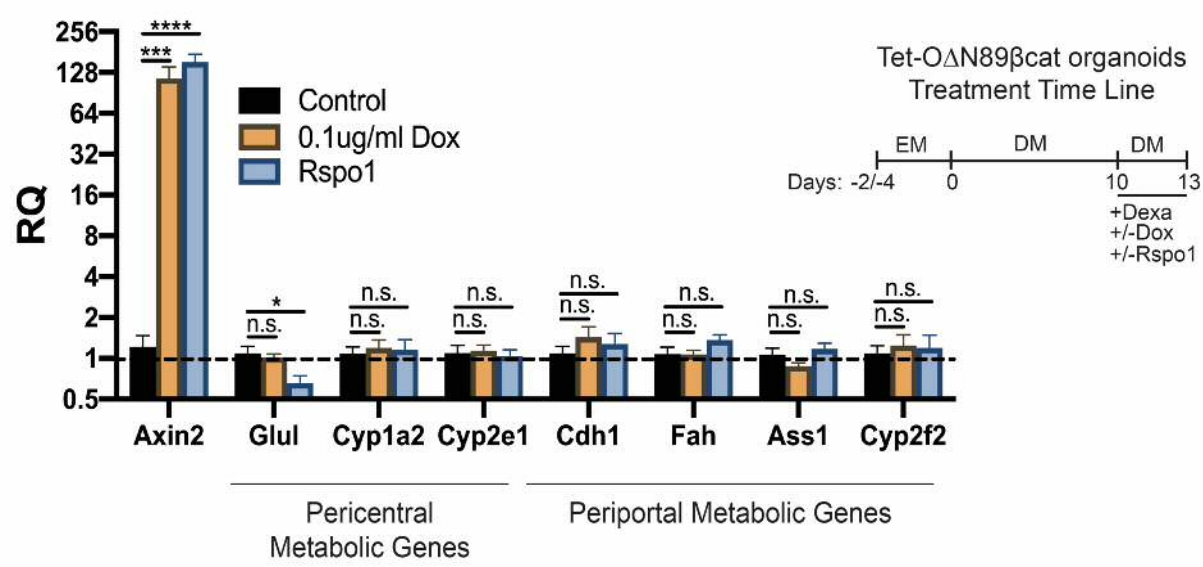

Appendix C Figure1 RT-qPCR gene expression analysis shows that mature hepatocyte zonated genes remain largely unaffected upon activation of Wnt Tet-OΔN89βcat in differentiated organoids by exposure to Rspo1 (100 ng/ml) or Dox (0.1ug/ml). (n=9, corresponding to organoids in 3 different passages isolated from the same animal). Statistical significance was determined using Mann-Whitney t-test. p-value n.s.>0.05 ; p-value *< 0.05; p-value **< 0.01; p-value ***< 0.001; p-value ****< 0.0001

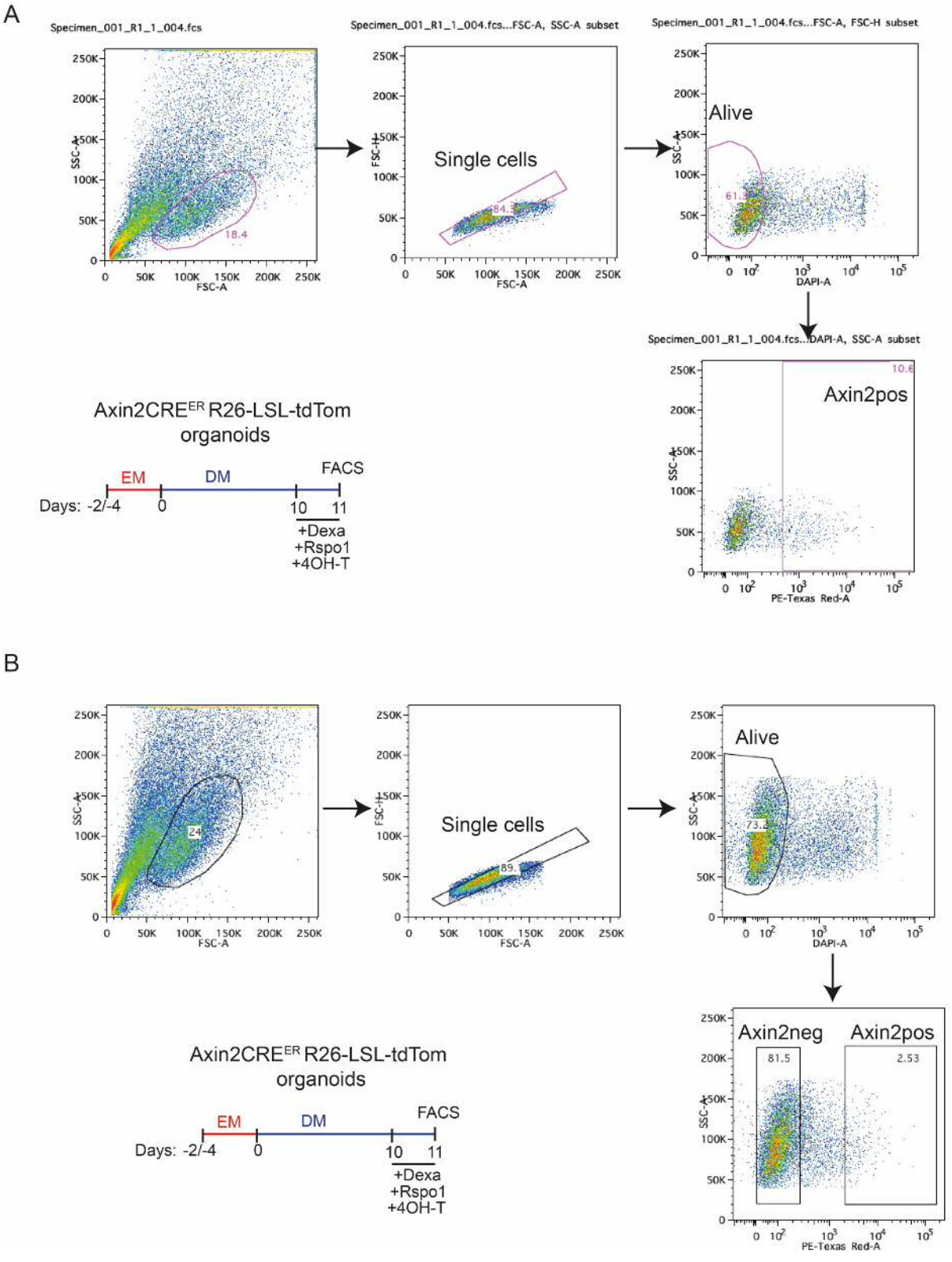

Appendix C Figure2 (A) FACS gating strategy for the quantification of the percentage of Axin2 live cells in DM organoids presented in Figure6.4, D. (B) FACS gating strategy for the isolation of tdTom positive and negative cells for RNAseq and organoid-forming capacity functional assays presented Figure6.4 and Figure6.7, respectively.

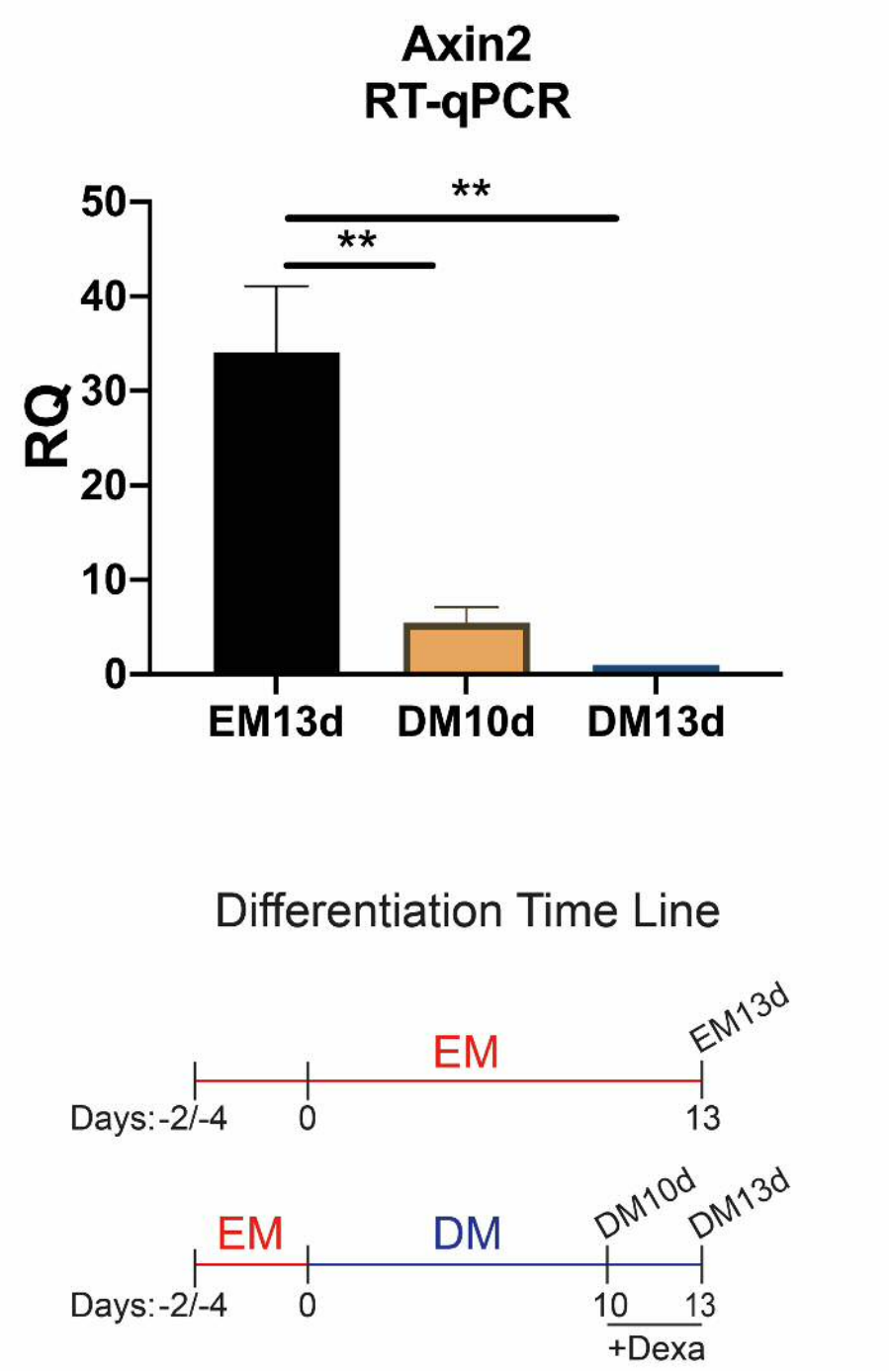

Appendix C Figure3 RT-qPCT analysis show a decline of Axin2 mRNA levels upon differentiation of WT BD organoids. Data has been normalized over gene expression levels of differentiated organoids at day 13. Bottom panel indicates differentiation time line. (n=10, corresponding to organoids from 5 different animals at different passage numbers). Statistical significance was determined using paired parametric t-test. p-value n.s.>0.05 ; p-value *< 0.05; p-value **< 0.01; p-value ***< 0.001; p-value ****< 0.0001

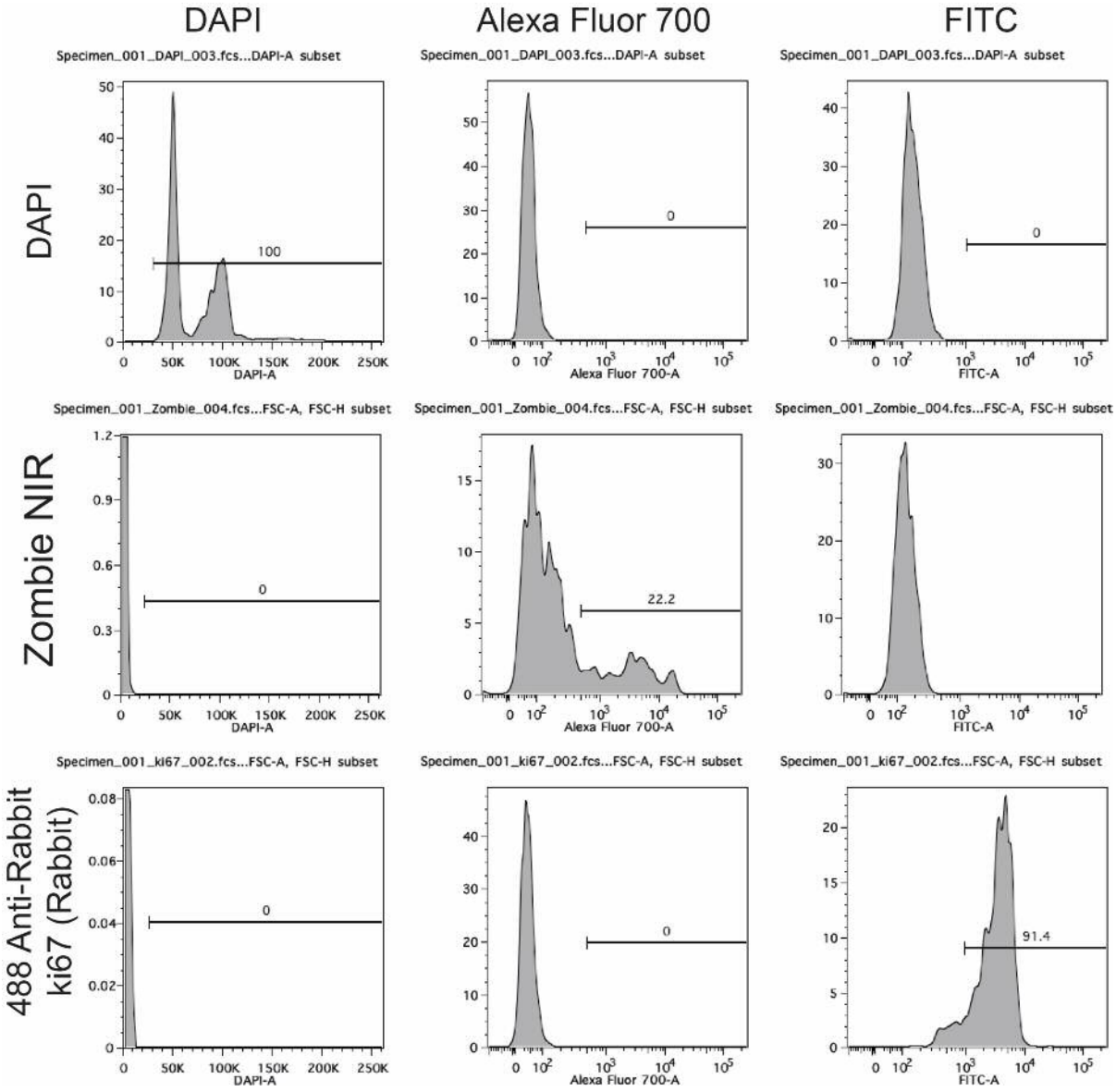

Appendix C Figure4 Single staining controls used to adjust the intensity during FACS.

APPENDIX D

To explore the molecular mechanisms underlying the enhanced stemness of tdTom positive cells, the expression profiles of tdTom positive, tdTom negative and untreated were compared (see Chapter 6, section6.2.6). Sequenced samples were from Axin2CreERT2 organoids derived from a single animal at four different passages (P5, P6, P8 and P10), cultured and sorted at non-overlapping times.

The current appendix contains information regarding the data curation process ((I) determination of gene expression cut-off criteria and (II) removal of outliers) performed prior to the gene expression differential analysis between samples with DESeq2. This appendix additionally gathers (III) detailed instructions about how to run DESeq2 together with the Scripts and parameters that I used for the analysis of the data presented in this thesis. Finally, this appendix additionally contains (IV) supporting evidence from the GSEA and IPA analysis. For better clarity, the information of this appendix has been organized into four sections.

I. Defining a pre-filtering gene expression criterion

RNAseq is a technique that allows the quantitative transcriptional profiling of a cell population without requiring previous knowledge of the sequences. In this technique, RNA is converted into cDNA. cDNA is then coupled to adapter sequences that allow the amplification and sequencing of the sample (Appendix D, Figure1). Raw data (FASTQ files) obtained from the sequencing contains both the reads for the sequences of the cDNA and the adapters and requires a set of bioinformatic processing steps prior to differential expression analysis (Appendix D, Figure2). Firstly, the adaptor sequences are removed (trimmed) and the cDNA reads are mapped back to the genome of reference. The raw read counts are then normalized based on the total RNA sequenced and expressed in counts per million (CPM) values. By probability, long gene sequences are expected to produce more reads than short gene sequences and therefore, to be able to compare the expression levels across different genes the CPM values need to be further normalized based on the gene length. This gives rise to a value known as FPKM (fragments per kilobase of exon model per million reads mapped) that reflects the normalized abundance of each gene.

After raw counts are calculated, differential gene expression analysis between samples can be performed using different bioinformatic tools. For the comparative an

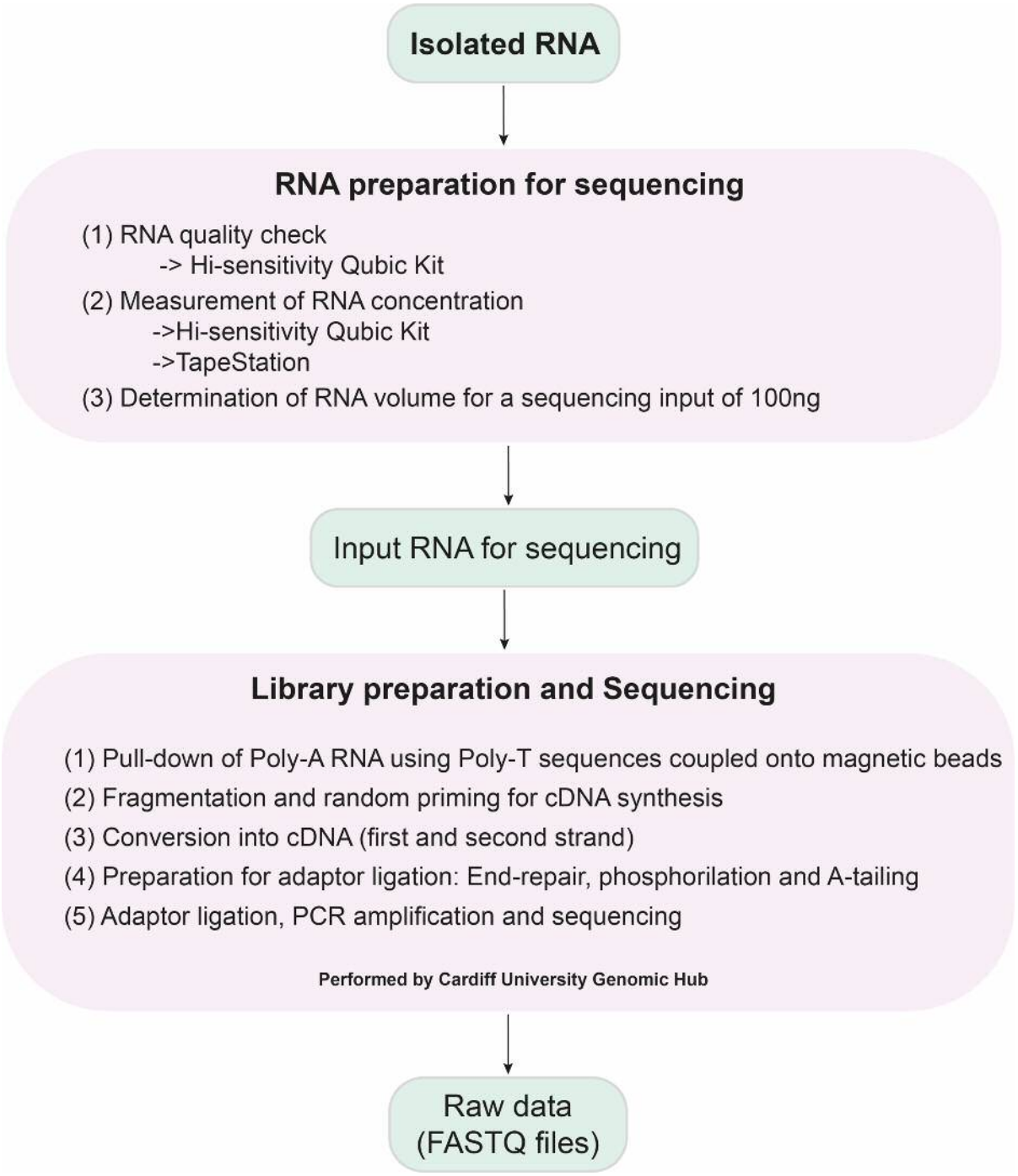

Appendix D, Figure1 RNAseq wet lab workflow. RNA is extracted from the samples and subjected to quality check (QC). RNA samples that satisfactory pass the QC are processed for cDNA library preparation and sequencing. During cDNA library preparation, mRNA from the sample is pulldown using magnetic beads coated with poly-T sequences, fragmented and converted into cDNA. Adapter sequences are subsequently ligated to each cDNA fragment. The coupling of the adapters allows the amplification and sequencing of the cDNA fragments. The resulting raw data (FASTQ files) contain information about the frequency in which cDNA fragment sequences (reads) are represented in each sample.

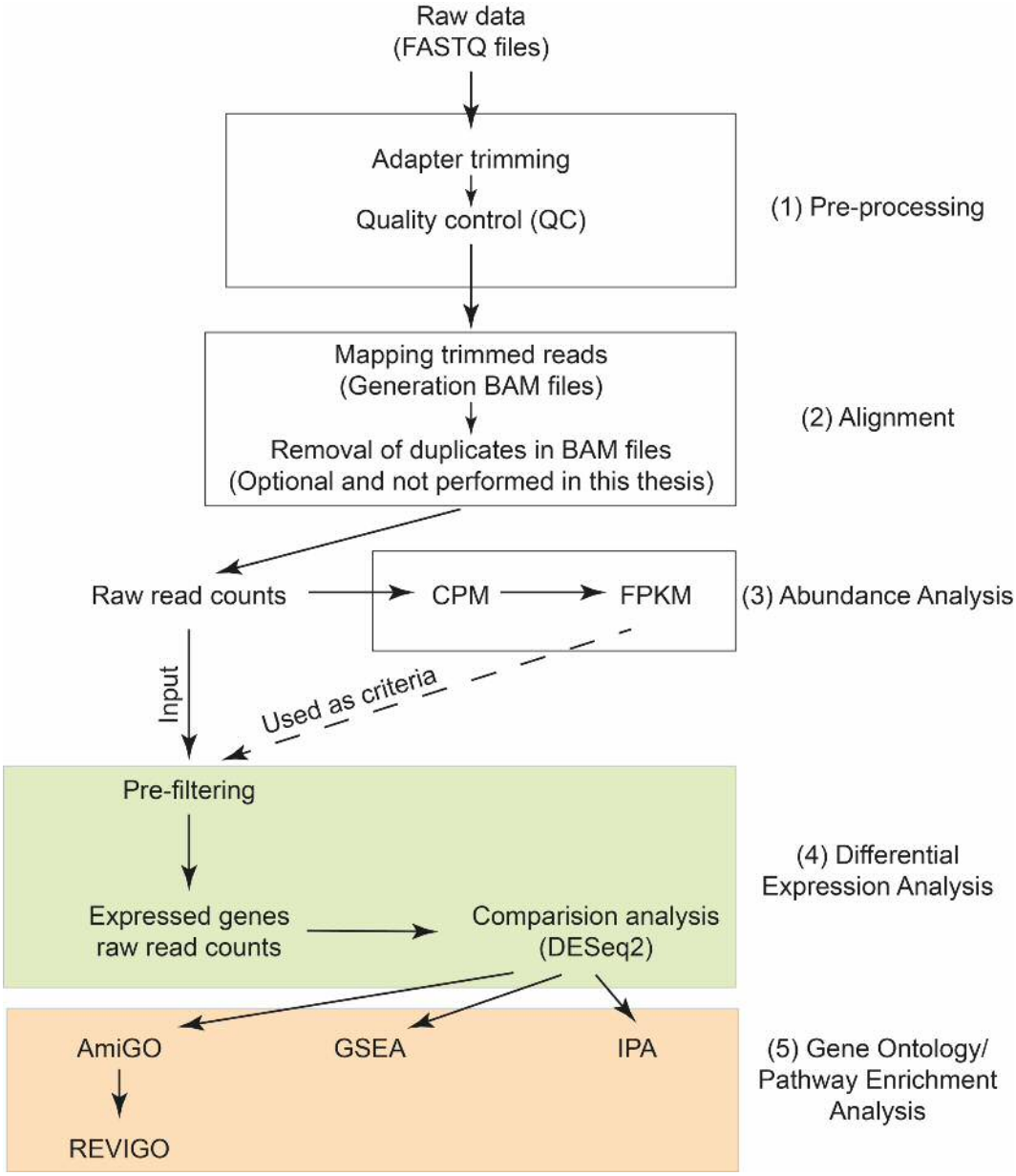

Appendix D, Figure2 RNAseq bioinformatic processing workflow. (1) The sequences from the adaptors used to sequence the samples are removed from the FASTQ files, which are subsequently subjected to QC analysis. (2) Trimmed FASTQ files are subsequently mapped to the genome of reference and raw read counts per gene calculated. (3) Raw counts are then normalized per sample based on the total amount of RNA sequenced in each of them and counts per million (CPM) calculated. Long genes have a higher probability than shorter genes to appear represented in the sequencing. For that reason, CPM values are then normalized based on the length of each gene. The resulting normalized values are expressed in fragments per kilobase per million (FKPM). (4) Differential expression analysis is run with the Bioconductor R package Deseq2. The input for Deseq2 is the raw counts of the expressed genes. This implies that raw read counts resulting from the alignment analysis should be subjected to filtering prior to feeding the Deseq2 package. FPKM and raw read count thresholds can be used as expression filtering criteria. Dr Robert Andrews and Dr Sumukh Despande carried out the pre-processing, alignment and abundance analysis. Differential expression analysis, as well as gene ontology/pathway enrichment analysis, were done by myself.

alysis presented in this thesis, I used DESeq2. DESeq2 is a method for differential

expression analysis available in R/Bioconductor package [127]. For DESeq2's statistical model to hold, the input for analysis should be the raw counts of the expressed genes, which implies that before feeding DESeq2 pipeline the non-expressed genes should be removed from the input list. Hence, to perform DESeq2 differential expression analysis of tdTom positive, tdTom negative and untreated samples, the first thing I did was to determine which genes were or were not express in my data by setting up different gene expression pre-filtering cut-offs.

To define expressed and non-expressed genes are two parameters that can be used as cut-offs: the raw counts and the FPKM values. Genes with less than 5-15 raw counts are usually considered as non-expressed. However, and as explained earlier, by probability long genes will generate more reads than short genes, therefore non-expressed long genes might not be adequately removed using this criterion. Alternatively, non-expressed genes can be removed based on FPKM values, being those with an FPKM value lower than 0.2-1 usually considered as non-expressed. Raw counts and FPKM values assigned per gene will depend on experimental factors such are the amount of RNA used as an input or the depth of the sequencing. For that reason, it is recommendable to adjust the gene expression pre-filtering cut-offs based on each RNAseq experimental data set, rather than using defined set values.

In a cell, gene expression frequency follows a normal distribution. This means that genes with extremely high or low expression levels are rarely found whereas most of the genes show a medium level of expression. Proper adjustment of gene expression thresholds can be therefore determined by whether the CPM values of the expressed genes appear represented with a frequency that follows a normal distribution. Hence, to determine in an unbiased manner which cut-offs parameters suited best my experimental data, I applied different raw counts and FPKM expression thresholds and evaluated the CPM values distribution of the resulting expressed genes. As four samples were sequenced for each of the experimental conditions (tdTom positive, tdTom negative and untreated), instead of the individual CPM, in this analysis I used the CPM average of the four replicates. Furthermore, I represented the average $\log_2$ (CPM) instead of the average CPM for visualization proposes.

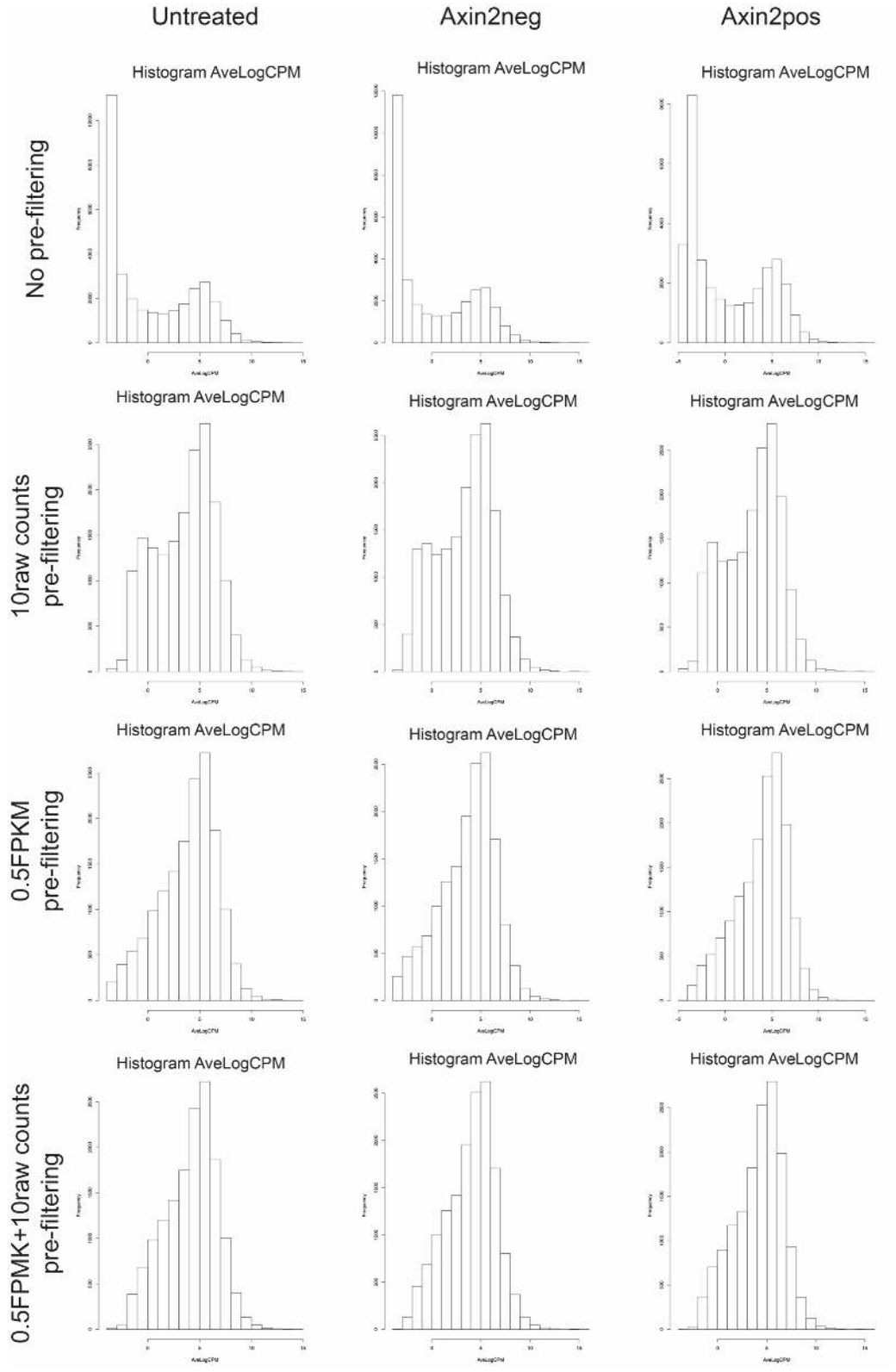

Appendix D, Figure3 Histogram showing the average log2 CPM histograms of untreated, tdTom positive (Axin2pos) and tdTom negative (Axin2neg) samples. Four replicates were sequenced and averaged for each biological group.

Appendix D, Figure3 shows that before applying any pre-filtering criteria ("No pre-

filtering"), the distribution of the average $\log_2$ (CPM) of untreated, tdTom negative and tdTom positive sequenced samples do not follow a normal distribution as genes with very low CPM values appear highly represented. Removal of genes with raw counts lower than 10 corrects this distribution although a better adjustment to a Gaussian distribution is achieved when an expression pre-filtering criterion of 0.5 FPKM alone or in combination with 10 raw counts is applied (Appendix D, Figure3). I heuristically determined that the best cut-off to define expressed genes was 0.5 FPKM and therefore, DESeq2 differential expression analysis was restricted in all samples to genes with an FPKM higher than 0.5.

II. Removal of outliers: hierarchical sample clustering and principal component analysis (PCA)

After determining and applying the gene expression pre-filtering criteria that best suited the dataset of this thesis (0.5 FPKM), I next ran DESeq2 and examined how similar was the transcriptome of tdTom positive, tdTom negative and untreated cells by calculating sample-to-sample distances and subjecting all of them to principal component analysis (PCA). Assessment of the overall similarity between samples by these two methods is an important quality control (QC) check. This type of analysis reveals how well cluster the replicates from the data set and therefore can be used for the identification of replicates from treatments with abnormal expression (outliers) and/or identification of another source of variation within the dataset.

tdTom positive, tdTom negative and untreated sequenced samples were from Axin2CreERT2 organoids derived from a single animal at four different passages (P5, P6, P8 and P10), cultured and sorted at non-overlapping times (see Chapter 6 section). Hierarchical clustering of samples is performed by calculating the correlation of gene expression (based on normalized gene expression values) for all pairwise combinations of the samples in the dataset. Results from hierarchical clustering are represented in binary colour coding heatmaps that display the samples distances where replicates from the same biological group are expected to cluster together as a block. Hierarchical clustering of the samples based on sample distances revealed that the replicates clustered by treatments, with exception of tdTom negative replicate 3, which clustered with samples from the tdTom positive group, suggesting that this sample suffered from an experimental abnormality (Appendix D, Figure4, A).

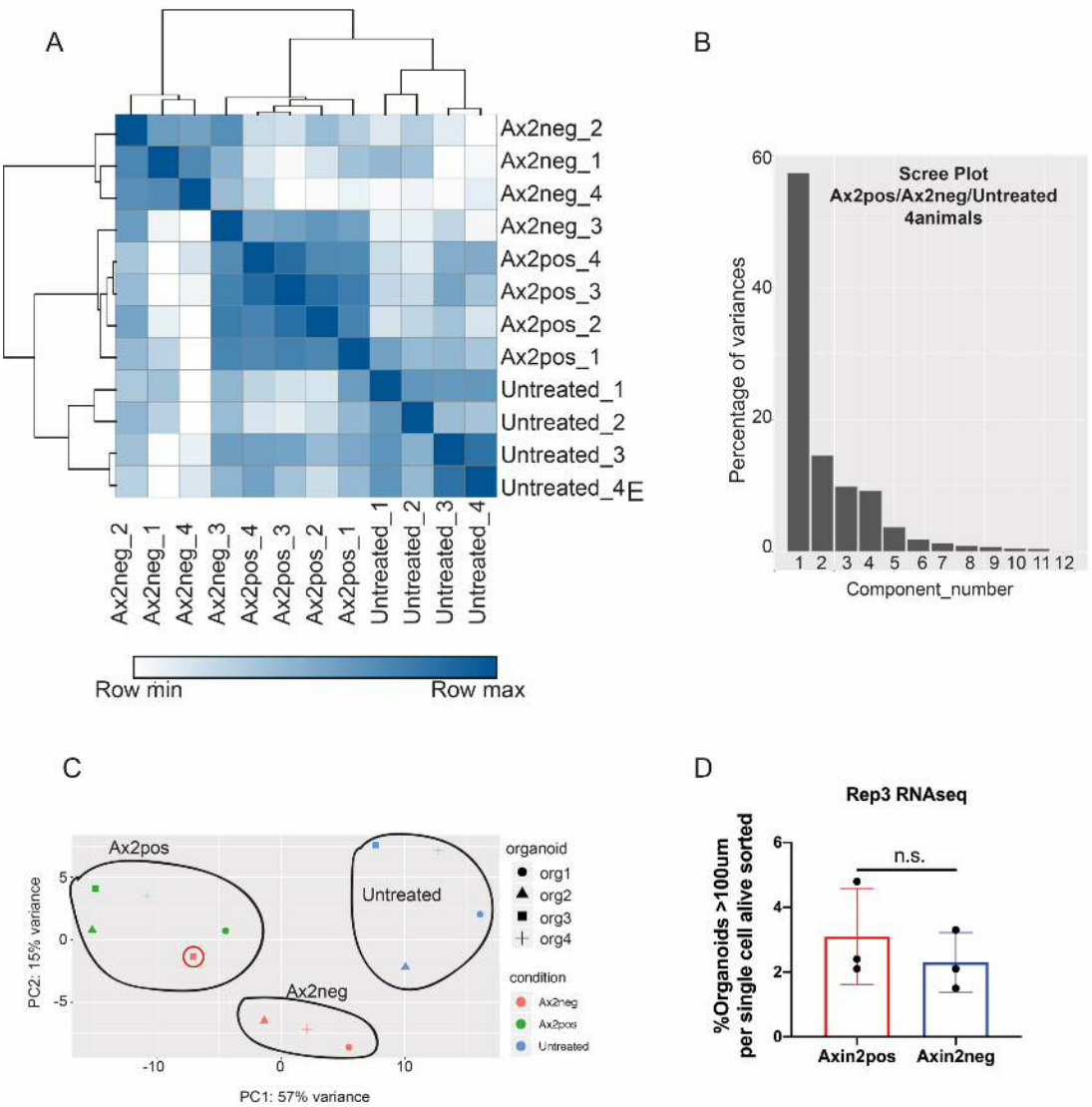

Appendix D, Figure4 Sample clustering of the four sequenced replicates using 0.5FPKM as the pre-filtering criterion. (A) Hierarchical clustering showing sample distance of the three biological replicates in a 2-dimension representation (n=4). Samples distances were calculated with R. Hierarchical clustering (one minus Pearson correlation) and sample distance representation was performed using the online bioinformatics tool Morpheus. (B) Scree plot display variance introduced by each of the eigenvectors of the PCA using the four experimental replicates as an input. The eigenvectors have been ordered based on the variation that they explain in the data set. (n=4). (C) Two-dimensional PCA plot of the first two components of the analysis for the total transcriptional landscape of tdTom positive (Axin2pos), tdTom negative (Axin2neg) and untreated cells (n=4). The red circle highlights Axin2neg sample from the experimental replicate 3, which clusters with samples from the biological group of tdTom positive (Axin2pos) cells. Black circles highlight the clustering of the biological groups. (D) The bar graph shows the organoid forming capacity of tdTom positive (Axin2pos) and tdTom negative (Axin2neg) sorted cells from RNAseq Rep3 sample derived from Axin2CreERT differentiated BD organoids exposed to Rspo1 for 1 day. (n=3 wells independently quantified). Statistical significance was determined using unpaired parametric t test. P value n.s. >0.05

The relationship between samples was also evaluated by PCA, which allow the identification of strong patterns in a complex biological dataset. In this type of analysis, the information of a multivariate dataset is reduced into a few variables called principal

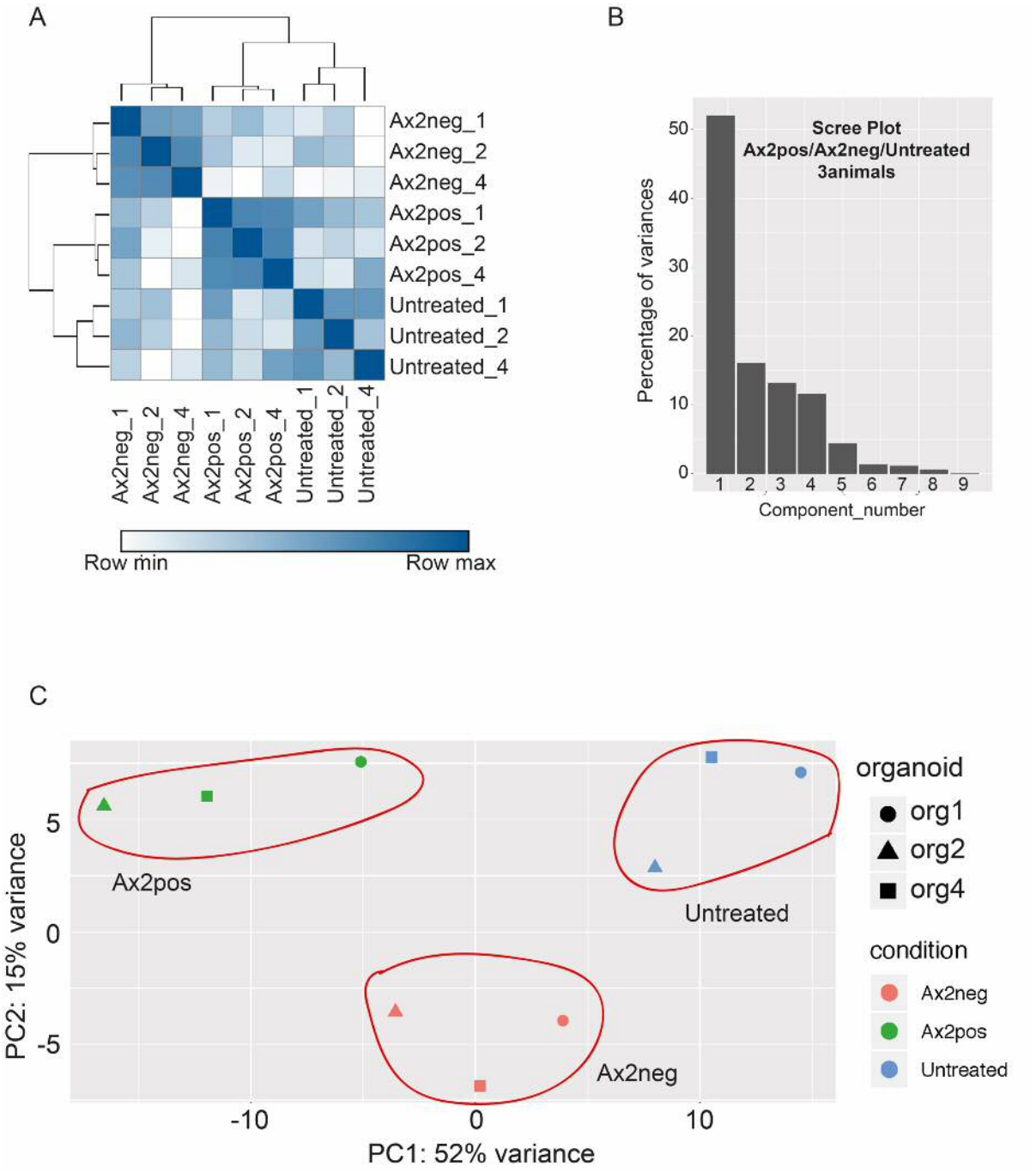

Appendix D, Figure5 Sample clustering after removal of the experimental replicate 3 using 0.5FPKM as pre-filtering criterion. (A) Heatmap showing hierarchical clustering of tdTom positive (Axin2pos), tdTom negative (Axin2neg) and untreated cells based on sample distances. Samples distances were calculated with R. Hierarchical clustering (one minus Pearson correlation) and sample distance representation was performed using the online bioinformatics tool Morpheus. (n=3). (B) Scree plot showing the eigenvalues for each of the dimensions of the PCA. (n=3) (C) Plot showing the two first dimensions of the PCA. Red circles highlight the clustering of the replicates. (n=3).

components (PCs) that capture the variance in the original samples. How much variation is introduced by each of these components (calculated eigenvalues) can be plotted and visualized in a scree plot. Most of the variation in the dataset is usually

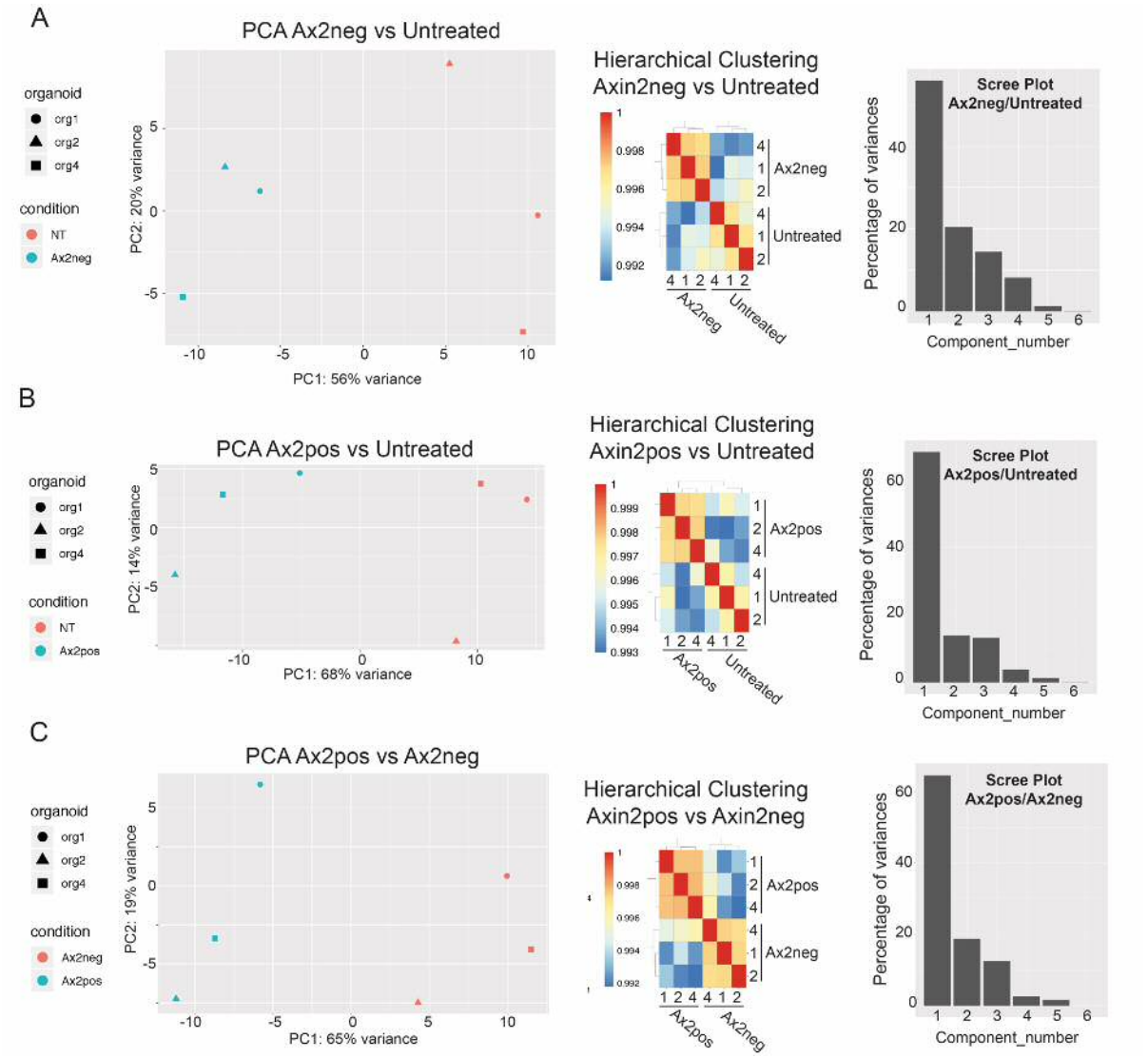

Appendix D, Figure6 Two-dimensional PCA plot of the first two components of the analysis for the total transcriptional landscape as well as hierarchical clustering showing sample distance of the biological replicates in a 2-dimension representation of (A) tdTom negative (Axin2neg) cells vs untreated cells, (B) tdTom positive (Axin2pos) cells vs untreated cells and (C) tdTom positive (Axin2pos) cells vs tdTom negative (Axin2neg) cells. (n=3).

explained by the first two of these two components (PC1 and PC2) and therefore two-dimensional representations of PC1 and PC2 are used to visualize the similarity between samples in this type of analysis.

PCA analysis revealed that ~72% of the total variance between samples could be explained by the first (PCA1) and the second (PCA2) component of the analysis (Appendix D, Figure4, B). Plotting of the first two principal components also showed that tdTom negative sample from replicate 3 preferentially clustered with tdTom

positive biological group, further indicating that the transcriptome of this sample was more similar to tdTom positive cells than to tdTom negative cells (Appendix D, Figure4, C).

The organoid-forming capacity of the sequenced tdTom positive and negative samples was assessed in parallel to the RNAseq experiment. Interestingly, tdTom negative sample from replicate 3 formed a similar proportion of organoids than tdTom positive cells isolated in the same experiment, indicating that this sample suffered from an experimental abnormality (Appendix D, Figure4, D). For that reason, tdTom negative replicate 3 sample was not included in the subsequent differential expression analysis. As statistical significance in DESeq2 was determined using a paired sample test, tdTom positive and untreated samples from replicate 3 were also removed from the downstream analysis.

After removal of replicate 3 from the RNAseq experimental set, the sample distances were re-evaluated. Hierarchical clustering of experimental replicate1, 2 and 4 showed now separation of the samples based on treatments with no exceptions (Appendix D, Figure5, A). Similarly, PCA component analysis showed clear sample clustering by treatment groups based on PCA1 and PCA2, further indicating similarity among the replicates of each biological group (Appendix D, Figure5, B and C).

PCA and hierarchical clustering showed in Appendix D, Figure5 were performed by loading the three sets of samples into the DESeq2 pipeline. However, to determine the statistical significance of differentially expressed genes between tdTom positive, tdTom negative and untreated cells, I opted to perform pairwise comparisons. Hierarchical clustering, scree and PCA plots for each of the pairwise comparisons performed show clustering of the replicates with their respective biological groups and are shown in Appendix D, Figure6.

Altogether, results from this sample-level QC analysis section show that tdTom negative replicate 3 suffered from an experimental abnormality and therefore is advisable to remove all samples from the experimental set 3 prior to differential gene expression analysis. Gene expression analysis of data presented in Chapter 6 section

was therefore generated by pairwise comparisons (Appendix D, Figure6) after removal of replicate 3 from the dataset.

III. Instructions to run DSEq2 and R Scripts

Detailed instructions about how to run DESeq2 together with the Scripts and parameters that I used for the analysis of the data presented here are as follow:

Names in green should be changed according to your data/files. Scripts are in grey. Remove # to run the lines of the script lines. To perform pairwise differentially expression analysis with DESeq2, I have followed up the Bioconductor Deseq2 guidelines that can be found: http://bioconductor.org/packages/devel/bioc/vignettes/DESeq2/inst/doc/DESeq2.html

The packages that need to be installed from Bioconductor are as follow:

```{r}
#if (!requireNamespace("BiocManager", quietly = TRUE))
  # install.packages("BiocManager")
#BiocManager::install("DESeq2")
#BiocManager::install("biomaRt")
#BiocManager::install("apeglm")
#BiocManager::install("IHW")
#BiocManager::install("pcaExplorer")
#BiocManager::install("vsn")
```

CRAN packages that need to be installed are as follow:

```{r}
#install.packages("ggplot2")
#install.packages("dplyr")
#install.packages("VennDiagram")
#install.packages("ggfortify")
#install.packages ("lfda")
```

Prior to analysis, load the installed packages:

```{r}
library(DESeq2)
library(biomaRt)
library(ggplot2)
library(dplyr)
library(VennDiagram)
library (apeglm)
```

```
library(IHW)
library(ggfortify)
library(pcaExplorer)
library(vsn)
library (lfda)
```

Set your working directory:

```{r}
setwd("~/Desktop/Deseq2 4 replicates")
```

Read in sample descriptions from the targets.txt file. Prior to this I have (1) obtained the average of the Raw counts and FPKM of each biological group and (2) filtered out the non expressed genes. In the particular dataset of this thesis a cut-off of 0.5 FPKM was employed as criterion for gene expression.

To pre-filter the data, the following lines for R can be used:

Prefiltering1 <-means1 %>% filter (fpkm.Ax2pos.average>0.5 | fpkm.Ax2neg.average>0.5 | fpkm.Untreated.average>0.5)

At least two input files are required to run DESeq2 with the following information:

- **Raw data counts table** of “expressed genes” after applying the pre-filtering criterion.
- **Identification table or ‘coldata’ table** with the samples ordered in the same manner as in the “Raw data counts” table. To perform pairwise comparison based on experimental replicates, the category “replicate” was included in this file

Additional sample information can also be also integrated into the matrix of DESeq2. This extra features table is optional:

- **Extra features table** with the name of the gene to visualize them later in the MAplot.

The following lines contain the scripts to read the aforementioned tables:

```{r}
```

```
#rawData <- read.table("Ax2pos_Ax2neg_10raw 05fpkm cutoff copy.txt",
header=TRUE, sep="\t")
#featureData <- read.table("featuredata.txt", header=TRUE, sep="\t")
#coldata <- read.table("coldata.txt", header=TRUE, sep="\t")
```

Preparation Raw Data Table for Deseq2 compatible format:

```
rownames(rawData) <- rawData$ensemblGeneID
rawData$ensemblGeneID <- NULL
```

Association of Raw data counts and identification table:

```
all(rownames (coldata)==colnames(rawData))
```

Deseq2 library loading, building Deseq2 matrix, adding extra features table and assigning the contrast condition. To perform pairwise comparison based on experimental replicates, such criterion was included in the design of the matrix.

```
library("DESeq2")
dds <- DESeqDataSetFromMatrix(countData = rawData,
                              colData = coldata,
                              design = ~ condition + replicate)
dds

featureData <- data.frame(gene=rownames(rawData))
mcols(dds) <- DataFrame(mcols(dds), featureData)
mcols(dds)
dds$condition <- relevel(dds$condition, ref = "Ax2neg")
```

Run Deseq2 with default 0.1 FDR

```
dds <- DESeq(dds)
res <- results(dds, name="condition_Ax2pos_vs_Ax2neg")
res <- results(dds, contrast=c("condition", "Ax2pos", "Ax2neg"))
res
```

######This is the part in which we can play with the FDR. Change alpha for the number you want. If you print “res” you will get the reults with the 0.1 FDR. If you print “res05” you will get the results with a FDR of 0.05.

```
res05 <- results(dds, alpha=0.05)
summary(res05)
```

In the website Bioconductor they explain you about many informative plots of your data (inclusing PCA and clustering). If you only want the results with the significance, print them using:

```
write.csv(as.data.frame(res),
  file="condition_Ax2pos_Ax2neg_01FDR.csv")
```

IV. Supporting RNAseq results figures

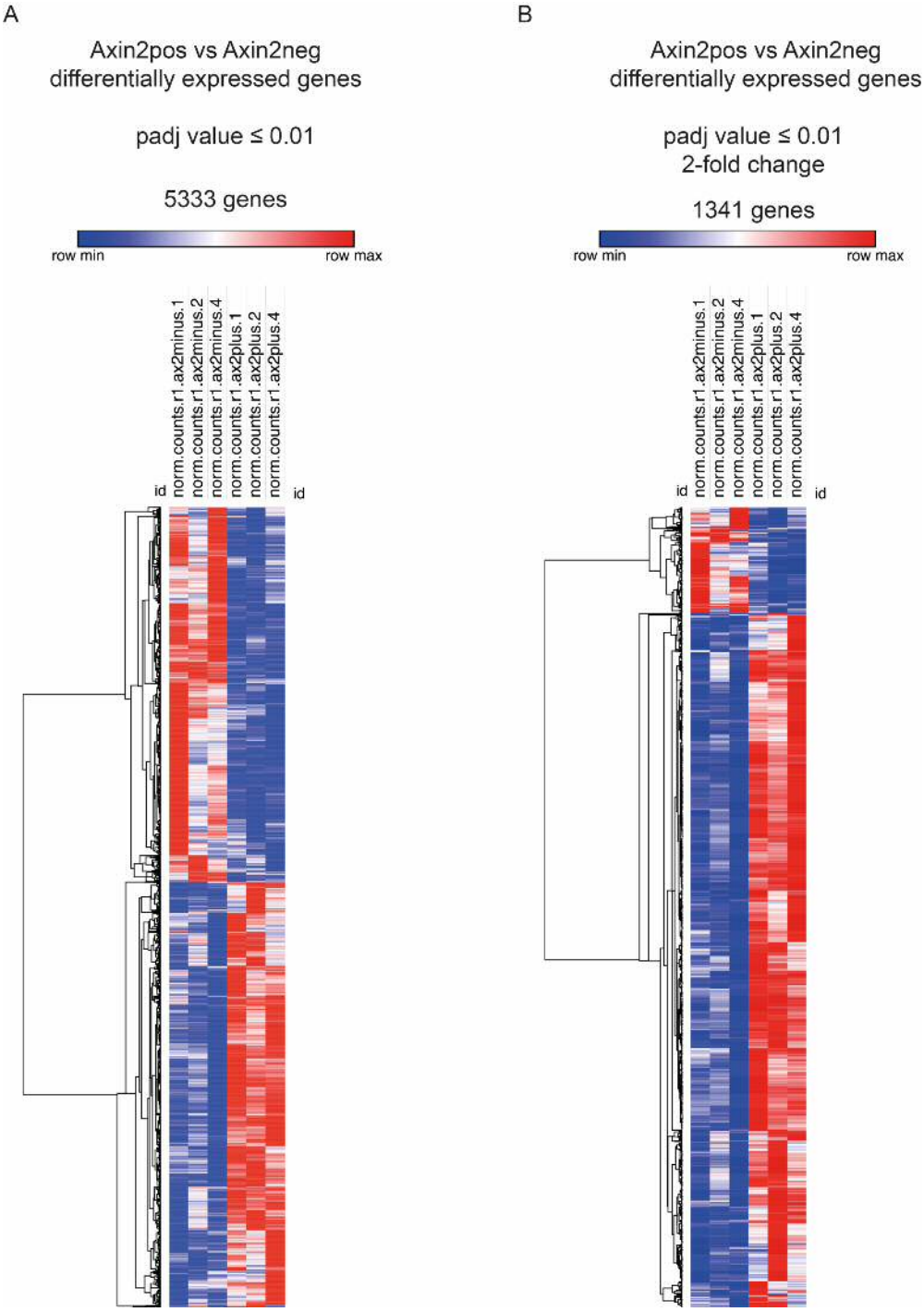

Appendix D, Figure7 Heatmaps showing the CPM of differentially expressed genes with a padj value ≤ 0.01 (A) or a padj value ≤ 0.01 ad a 2-fold change induction (B) between tdTom positive (Axin2pos) and tdTom negative (Axin2neg) cells.

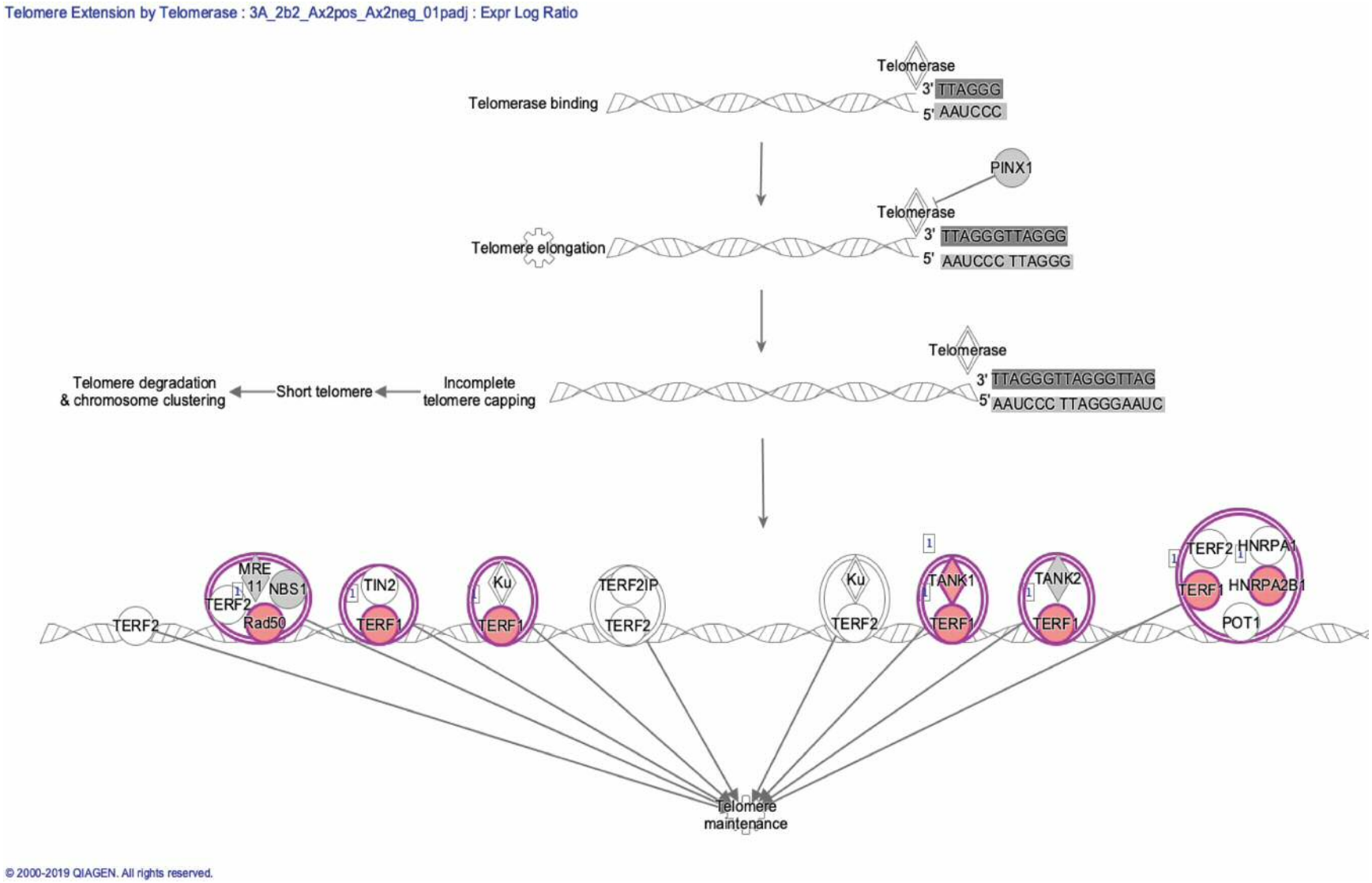

Appendix D, Figure8 IPA analysis show enrichment in the expression of genes of the telomere elongation machinery are significantly higher expressed in tdTom positive (Axin2pos) cells when compared to tdTom negative (Axin2neg) cells. Genes that are significantly upregulated (padj value ≤ 0.01 ad a 2-fold change induction) in Axin2pos cells have been highlighted in red.

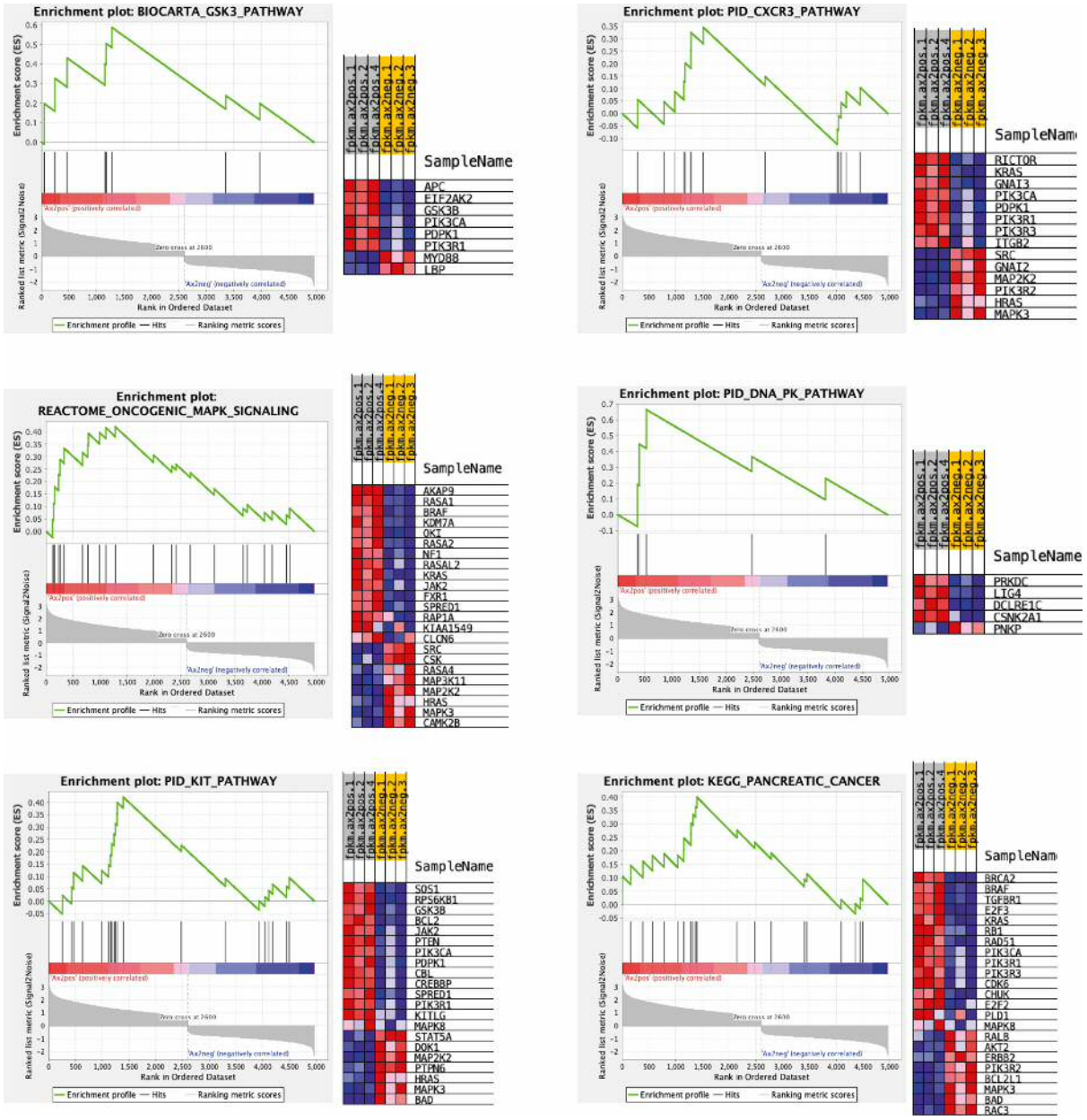

Appendix D, Figure9 GSEA analysis. GSEA analysis using MSigDB C2 comprising Curated Gene Sets from online pathway databases publications in Pubmed and knowledge of domain experts. Analysis was performed in genes differentially expressed genes between tdTom positive (Axin2pos) and tdTom negative (Axin2neg) with a padj <= 0.01. A total of 5333 genes where found differentially expressed. Of those 5047 had a human ortholog and therefore could be analysed using GSEA.

APPENDIX E

The current appendix contains supplementary information associated with Chapter 7.

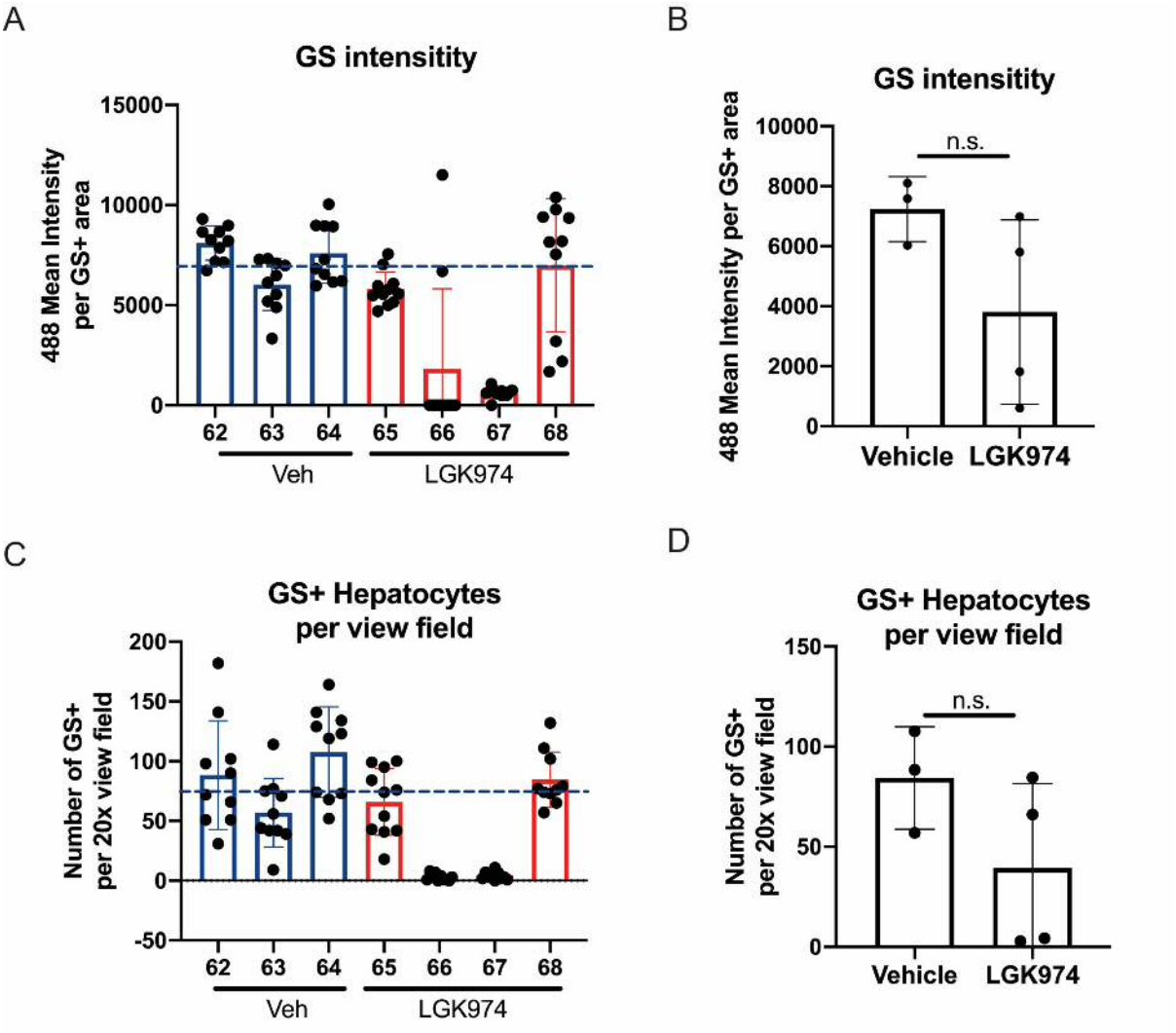

AppendixE Figure1 (A) Harmony semi-automatic quantification of GS staining intensity per GS positive area. View fields with non-GS positive areas were given a score of zero. Blue dash line highlight the average of the three vehicle animals. (n=10 view fields per animal). (B) Bar graph shows GS staining intensity per GS positive area quantifications (Harmony software) of Vehicle (n=3) and LGK974 animals combined (n=4). View fields with non-GS positive areas were given a score of zero. (C) GS staining IF quantifications (Harmony) shows a decline in the number of GS positive hepatocytes per view field in animal 66 and 67. Blue dash line highlight the average of the three vehicle animals. (n=10 view fields per animal). (D) Bar graph shows number of GS positive hepatocytes when Vehicle (n=3) and LGK974 animals combined. Quantifications were performed using the Harmony software. (n=4).

List of references

1. DiMasi JA, Grabowski HG, Hansen RW: Innovation in the pharmaceutical industry: New estimates of R&D costs. *Journal of Health Economics* 2016, 47:20–33.

2. Gómez-Lechón MJ, Tolosa L, Conde I, Donato MT: Competency of different cell models to predict human hepatotoxic drugs. *Expert Opinion on Drug Metabolism & Toxicology* 2014, 10:1553–1568.

3. Peng WC, Logan CY, Fish M, Anbarchian T, Aguisanda F, Álvarez-Varela A, Wu P, Jin Y, Zhu J, Li B, et al.: Inflammatory Cytokine TNFα Promotes the Long-Term Expansion of Primary Hepatocytes in 3D Culture. *Cell* 2018, 175:1607–1619.e15.

4. Hu H, Gehart H, Artegiani B, LÖpez-Iglesias C, Dekkers F, Basak O, van Es J, de Sousa Lopes SMC, Begthel H, Korving J, et al.: Long-Term Expansion of Functional Mouse and Human Hepatocytes as 3D Organoids. *Cell* 2018, 175:1591–1606.e19.

5. Gordillo M, Evans T, Gouon-Evans V: Orchestrating liver development. *Development* 2015, 142:2094–2108.

6. Treyer A, Müsch A: *Hepatocyte Polarity*. John Wiley & Sons, Inc; 2013.

7. Ben-Moshe S, Itzkovitz S: Spatial heterogeneity in the mammalian liver. *Nature Reviews Gastroenterology & Hepatology* 2019, doi:10.1038/s41575-019-0134-x.

8. Crawford JM, Bioulac-Sage P, Hytiroglou P: *1 - Structure, Function, and Responses to Injury*. Elsevier Ltd; 2018.

9. Michalopoulos GK, Khan Z: Liver Stem Cells: Experimental Findings and Implications for Human Liver Disease. *Gastroenterology* 2015, 149:876–882.

10. Miyajima A, Tanaka M, Itoh T: Stem/Progenitor Cells in Liver Development, Homeostasis, Regeneration, and Reprogramming. *Stem Cell* 2014, 14:561–574.

11. Michalopoulos GK: Liver Regeneration after Partial Hepatectomy. *The American Journal of Pathology* 2010, 176:2–13.

12. Wang B, Zhao L, Fish M, Logan CY, Nusse R: Self-renewing diploid Axin2+ cells fuel homeostatic renewal of the liver. *Nature* 2015, 524:180–185.

13. Lin S, Nascimento EM, Gajera CR, Chen L, Neuhöfer P, Garbuzov A, Wang S, Artandi SE: Distributed hepatocytes expressing telomerase repopulate the liver in homeostasis and injury. *Nature* 2018, 556:244–248.

14. Valle-Encinas E, Dale TC: ScienceDirect Wnt ligand and receptor patterning in the liver. *Current Opinion in Cell Biology* 2020, 62:17–25.

15. Tan X, Behari J, Cieply B, Michalopoulos GK, Monga SPS: Conditional Deletion of β-Catenin Reveals Its Role in Liver Growth and Regeneration. *Gastroenterology* 2006, 131:1561–1572.

16. Jörs S, Jeliazkova P, Ringelhan M, Thalhammer J, Dürl S, Ferrer J, Sander M, Heikenwalder M, Schmid RM, Siveke JT, et al.: Lineage fate of ductular reactions in liver injury and carcinogenesis. *J. Clin. Invest.* 2015, 125:2445–2457.

17. Raven A, Lu W-Y, Man TY, Ferreira-Gonzalez S, O'Duibhir E, Dwyer BJ, Thomson JP, Meehan RR, Bogorad R, Koteliansky V, et al.: Cholangiocytes act as facultative liver stem cells during impaired

hepatocyte regeneration. *Nature* 2017, 547:350–354.

18. Kamimoto K, Kaneko K, Kok CY-Y, Okada H, Miyajima A, Itoh T: Heterogeneity and stochastic growth regulation of biliary epithelial cells dictate dynamic epithelial tissue remodeling. *Elife* 2016, 5:656.

19. Kawaguchi Y: Sox9 and programming of liver and pancreatic progenitors. *J. Clin. Invest.* 2013, 123:1881–1886.

20. Li B, Dorrell C, Canaday PS, Pelz C, Haft A, Finegold M, Grompe M: Adult Mouse Liver Contains Two Distinct Populations of Cholangiocytes. *Stem Cell Reports* 2017, 9:478–489.

21. Sackett SD, Li Z, Hurtt R, Gao Y, Wells RG, Brondell K, Kaestner KH, Greenbaum LE: Foxl1 is a marker of bipotential hepatic progenitor cells in mice. *Hepatology* 2008, 49:920–929.

22. Pepe-Mooney BJ, Dill MT, Alemany A, Ordovas-Montanes J, Matsushita Y, Rao A, Sen A, Miyazaki M, Anakk S, Dawson PA, et al.: Single-Cell Analysis of the Liver Epithelium Reveals Dynamic Heterogeneity and an Essential Role for YAP in Homeostasis and Regeneration. *Stem Cell* 2019, 25:23–38.e8.

23. Deng X, Zhang X, Li W, Feng R-X, Li L, Yi G-R, Zhang X-N, Yin C, Yu H-Y, Zhang J-P, et al.: Chronic Liver Injury Induces Conversion of Biliary Epithelial Cells into Hepatocytes. *Stem Cell* 2018, 23:114–122.e3.

24. Russell JO, Lu W-Y, Okabe H, Abrams M, Oertel M, Poddar M, Singh S, Forbes SJ, Monga SP: Hepatocyte-Specific β-Catenin Deletion During Severe Liver Injury Provokes Cholangiocytes to Differentiate Into Hepatocytes. *Hepatology* 2019, 69:742–759.

25. Han X, Wang Y, Pu W, Huang X, Qiu L, Li Y, Yu W, Zhao H, Liu X, He L, et al.: Lineage Tracing Reveals the Bipotency of SOX9+ Hepatocytes during Liver Regeneration. *Stem Cell Reports* 2019, 12:624–638.

26. Aguilar Bravo B, Rodrigo Torres D, Ariño S, Coll M, Pose E, Blaya D, Graupera I, Perea L, Vallverdú J, Rubio Tomás T, et al.: Ductular Reaction Cells Display an Inflammatory Profile and Recruit Neutrophils in Alcoholic Hepatitis. *Hepatology* 2019, 69:2180–2195.

27. Rodrigo Torres D, Affò S, Coll M, Morales-Ibanez O, Millán C, Blaya D, Alvarez-Guaita A, Rentero C, Lozano JJ, Maestro MA, et al.: The biliary epithelium gives rise to liver progenitor cells. *Hepatology* 2014, 60:1367–1377.

28. Gouw ASH, Clouston AD, Theise ND: Ductular reactions in human liver: Diversity at the interface. *Hepatology* 2011, 54:1853–1863.

29. GEBHARDT R: Metabolic Zonation of the Liver - Regulation and Implications for Liver-Function. *Pharmacol. Ther.* 1992, 53:275–354.

30. Burke ZD, Tosh D: The Wnt/β-catenin pathway: master regulator of liver zonation? *Bioessays* 2006, 28:1072–1077.

31. Gebhardt R: Liver zonation: Novel aspects of its regulation and its impact on homeostasis. *WJG* 2014, 20:8491–15.

32. Brosch M, Kattler K, Herrmann A, Schönfels von W, Nordström K, Seehofer D, Damm G, Becker T, Zeissig S, Nehring S, et al.: Epigenomic map of human liver reveals principles of zonated morphogenic and metabolic control. *Nat Commun* 2018, 9:416–11.

33. Halpern KB, Shenhav R, Matcovitch-Natan O, Tóth B, Lemze D, Golan M, Massasa EE, Baydatch S, Landen S, Moor AE, et al.: Single-cell spatial reconstruction reveals global division of labour in the mammalian liver. *Nature* 2017, 542:352–356.

34. Ben-Moshe S, Shapira Y, Moor AE, Manco R, Veg T, Halpern KB, Itzkovitz S: Spatial sorting enables

comprehensive characterization of liver zonation. *Nature Metabolism* 2019, doi:10.1038/s42255-019-0109-9.

35. Leibing T, Géraud C, Augustin I, Boutros M, Augustin HG, Okun JG, Langhans C-D, Zierow J, Wohlfeil SA, Olsavszky V, et al.: Angiocrine Wnt signaling controls liver growth and metabolic maturation in mice. *Hepatology* 2018, 68:707–722.

36. Strauss O, Phillips A, Ruggiero K, Bartlett A, Dunbar PR: Immunofluorescence identifies distinct subsets of endothelial cells in the human liver. *Nature Publishing Group* 2017, doi:10.1038/srep44356.

37. Halpern KB, Shenhav R, Massalha H, Tóth B, Egozi A, Massasa EE, Medgalia C, David E, Giladi A, Moor AE, et al.: Paired-cell sequencing enables spatial gene expression mapping of liver endothelial cells. *Nat Biotechnol* 2018, 36:962–970.

38. Notenboom RG, Moorman AF, Lamers WH: Developmental appearance of ammonia-metabolizing enzymes in prenatal murine liver. *Microsc. Res. Tech.* 1997, 39:413–423.

39. Burke ZD, Reed KR, Yeh S-W, Meniel V, Sansom OJ, Clarke AR, Tosh D: Spatiotemporal regulation of liver development by the Wnt/β-catenin pathway. *Sci Rep* 2018, 8:275–9.

40. Ma R, Martínez-Ramírez AS, Borders TL, Gao F, Sosa-Pineda B: Metabolic and non-metabolic liver zonation is established non-synchronously and requires sinusoidal Wnts. *Elife* 2020, 9:759–24.

41. Jungermann K, Katz N: Functional specialization of different hepatocyte populations. *Physiological Reviews* 1989, 69:708–764.

42. Kietzmann T, Dimova E, Flügel D, Scharf JG: Oxygen: Modulator of Physiological and Pathophysiological Processes in the Liver. *Z Gastroenterol* 2006, 44:67–76.

43. Ferri D, Moro L, Mastrodonato M, Capuano F, Marra E, Liquori GE, Greco M: Ultrastructural zonal heterogeneity of hepatocytes and mitochondria within the hepatic acinus during liver regeneration after partial hepatectomy. *Biol. Cell* 2005, 97:277–288.

44. Allen JW: In Vitro Zonation and Toxicity in a Hepatocyte Bioreactor. *Toxicological Sciences* 2005, 84:110–119.

45. Guo R, Xu X, Lu Y, Xie X: Physiological oxygen tension reduces hepatocyte dedifferentiation in in vitro culture. *Nature Publishing Group* 2017, 7:675–9.

46. Berndt N, Holzhütter H-G: Dynamic Metabolic Zonation of the Hepatic Glucose Metabolism Is Accomplished by Sinusoidal Plasma Gradients of Nutrients and Hormones. *Front. Physiol.* 2018, 9:110–14.

47. Schleicher J, Tokarski C, Marbach E, Matz-Soja M, Zellmer S, GEBHARDT R, Schuster S: Zonation of hepatic fatty acid metabolism — The diversity of its regulation and the benefit of modeling. *BBA - Molecular and Cell Biology of Lipids* 2015, 1851:641–656.

48. Cheng X, Kim SY, Okamoto H, Xin Y, Yancopoulos GD, Murphy AJ, Gromada J: Glucagon contributes to liver zonation. *Proc Natl Acad Sci USA* 2018, 115:E4111–E4119.

49. GEBHARDT R, Jonitza D: Different proliferative responses of periportal and perivenous hepatocytes to EGF. *Biochem. Biophys. Res. Commun.* 1991, 181:1201–1207.

50. Chiang JYL: Regulation of bile acid synthesis: pathways, nuclear receptors, and mechanisms. *Journal of Hepatology* 2004, 40:539–551.

51. Gougelet A, Torre C, Veber P, Sartor C, Bachelot L, Denechaud P-D, Godard C, Moldes M, Burnol A-F,

Dubuquoy C, et al.: T-cell factor 4 and β-catenin chromatin occupancies pattern zonal liver metabolism in mice. *Hepatology* 2014, 59:2344–2357.

52. CCTS OAAM, PhD MKM, PhD RV: Drug Metabolism in the Liver. *Clinics in Liver Disease* 2017, 21:1–20.

53. Wattacheril J, Seeley EH, Angel P, Chen H, Bowen BP, Lanciault C, M Caprioli R, Abumrad N, Flynn CR: Differential Intrahepatic Phospholipid Zonation in Simple Steatosis and Nonalcoholic Steatohepatitis. *PLoS ONE* 2013, 8:e57165–11.

54. Miyaoka Y, Ebato K, Kato H, Arakawa S, Shimizu S, Miyajima A: Hypertrophy and Unconventional Cell Division of Hepatocytes Underlie Liver Regeneration. *CURBIO* 2012, 22:1166–1175.

55. Muriel P, Ramos-Tovar E, Montes-Páez G, Buendía-Montaño LD: *Chapter 40 - Experimental Models of Liver Damage Mediated by Oxidative Stress*. Elsevier Inc; 2020.

56. Best DH, Coleman WB: Treatment with 2-AAF blocks the small hepatocyte-like progenitor cell response in retrorsine-exposed rats. *Journal of Hepatology* 2007, 46:1055–1063.

57. Eagling VA, Tjia JF, Back DJ: Differential selectivity of cytochrome P450 inhibitors against probe substrates in human and rat liver microsomes. *Br J Clin Pharmacol* 1998, 45:107–114.

58. Sachar M, Anderson KE, Ma X: Protoporphyrin IX: the Good, the Bad, and the Ugly. *Journal of Pharmacology and Experimental Therapeutics* 2016, 356:267–275.

59. Clerbaux L-A, Hul NV, Gouw ASH, Manco R, Español-Suñer R, Leclercq IA: Relevance of the CDE and DDC Mouse Models to Study Ductular Reaction in Chronic Human Liver Diseases. In *Experimental Animal Models of Human Diseases - An Effective Therapeutic Strategy*. InTech; 2018:1–17.

60. Tirnitz-Parker JEE: Hepatocellular Carcinoma. *1* 2019, doi:10.15586/hepatocellularcarcinoma.2019.

61. Wu J: Utilization of animal models to investigate nonalcoholic steatohepatitis-associated hepatocellular carcinoma. *Oncotarget* 2016, 7:42762–42776.

62. Stephenson K, Kennedy L, Hargrove L, Demieville J, Thomson J, Alpini G, Francis H: Updates on Dietary Models of Nonalcoholic Fatty Liver Disease: Current Studies and Insights. *gene expr* 2018, 18:5–17.

63. Moser J, Miller I, Carter D, Spencer SL: Control of the Restriction Point by Rb and p21. *Proc. Natl. Acad. Sci. U.S.A.* 2018, 115:E8219–E8227.

64. Zhan T, Rindtorff N, Boutros M: Wnt signaling in cancer. *Nature Publishing Group* 2016, 36:1461–1473.

65. Huang H-C, Klein PS: The Frizzled family: receptors for multiple signal transduction pathways. *Genome Biol.* 2004, 5:234–7.

66. MacDonald BT, Semenov MV, Huang H, He X: Dissecting Molecular Differences between Wnt Coreceptors LRP5 and LRP6. *PLoS ONE* 2011, 6:e23537–11.

67. Brunt L, Scholpp S: The function of endocytosis in Wnt signaling. *Cellular and Molecular Life Sciences* 2017, 75:785–795.

68. Feng Q, Gao N: Keeping Wnt Signalosome in Check by Vesicular Traffic. *J. Cell. Physiol.* 2015, 230:1170–1180.

69. Niehrs C: The complex world of WNT receptor signalling. *Nat. Rev. Mol. Cell Biol.* 2012, 13:767–779.

70. Lipp P, Reither G: Protein kinase C: the “masters” of calcium and lipid. *Cold Spring Harbor Perspectives in Biology* 2011, 3:a004556–a004556.

71. Veeman MT, Axelrod JD, Moon RT: A second canon. Functions and mechanisms of beta-catenin-independent Wnt signaling. *Developmental Cell* 2003, 5:367–377.

72. Zeke A, Misheva M, Reményi A, Bogoyevitch MA: JNK Signaling: Regulation and Functions Based on Complex Protein-Protein Partnerships. *Microbiol. Mol. Biol. Rev.* 2016, 80:793–835.

73. Acebron SP, Niehrs C: Focus Review Mitotic and mitogenic Wnt signalling. *The EMBO Journal* 2012, 31:2705–2713.

74. Inoki K, Ouyang H, Zhu T, Lindvall C, Wang Y, Zhang X, Yang Q, Bennett C, Harada Y, Stankunas K, et al.: TSC2 Integrates Wnt and Energy Signals via a Coordinated Phosphorylation by AMPK and GSK3 to Regulate Cell Growth. *Cell* 2006, 126:955–968.

75. Acebron SP, Karaulanov E, Berger BS, Huang Y-L, Niehrs C: Mitotic Wnt Signaling Promotes Protein Stabilization and Regulates Cell Size. *Molecular Cell* 2014, 54:663–674.

76. Vallon M, Yuki K, Nguyen TD, Chang J, Yuan J, Siepe D, Miao Y, Essler M, Noda M, Garcia KC, et al.: A RECK-WNT7 Receptor-Ligand Interaction Enables Isoform-Specific Regulation of Wnt Bioavailability. *Cell Reports* 2018, 25:339–349.e9.

77. Arenas E: Wnt signaling in midbrain dopaminergic neuron development and regenerative medicine for Parkinson's disease. *Journal of Molecular Cell Biology* 2014, 6:42–53.

78. Ding X, Liu J, Zheng L, Song J, Li N, Hu H, Tong X, Dai F: Genome-Wide Identification and Expression Profiling of Wnt Family Genes in the Silkworm, Bombyx mori. *IJMS* 2019, 20:1221–13.

79. Yu J, Chia J, Canning CA, Jones CM, Bard FA, Virshup DM: WLS Retrograde Transport to the Endoplasmic Reticulum during Wnt Secretion. *Developmental Cell* 2014, 29:277–291.

80. Farin HF, Jordens I, Mosa MH, Basak O, Korving J, Tauriello DVF, de Punder K, Angers S, Peters PJ, Maurice MM, et al.: Visualization of a short-range Wnt gradient in the intestinal stem-cell niche. *Nature* 2016, doi:10.1038/nature16937.

81. Routledge D, Scholpp S: Mechanisms of intercellular Wnt transport. *Development* 2019, 146:dev176073–12.

82. de Lau W, Peng WC, Gros P, Clevers H: The R-spondin/Lgr5/Rnf43 module: regulator of Wnt signal strength. *Genes Dev.* 2014, 28:305–316.

83. Perugorria MJ, Olaizola P, Labiano I, Esparza-Baquer A, Marzioni M, Marin JJG, Bujanda L, Banales JM: Wnt–β-catenin signalling in liver development, health and disease. *Nature Reviews Gastroenterology & Hepatology* 2018, 16:121–136.

84. Prior N, Hindley CJ, Rost F, Meléndez E, Lau WWY, Göttgens B, Rulands S, Simons BD, Huch M: Lgr5 +stem and progenitor cells reside at the apex of a heterogeneous embryonic hepatoblast pool. *Development* 2019, 146:dev174557–14.

85. Decaens T, Godard C, de Reyniès A, Rickman DS, Tronche F, Couty J-P, Perret C, Colnot S: Stabilization of β-catenin affects mouse embryonic liver growth and hepatoblast fate. *Hepatology* 2007, 47:247–258.

86. Cadoret A, Ovejero C, Saadi-Kheddouci S, Souil E, Fabre M, Romagnolo B, Kahn A, Perret C: Hepatomegaly in transgenic mice expressing an oncogenic form of beta-catenin. *Cancer Res* 2001, 61:3245–3249.

87. Benhamouche S, Decaens T, Godard C, Chambrey R, Rickman DS, Moinard C, Vasseur-Cognet M, Kuo CJ, Kahn A, Perret C, et al.: Apc Tumor Suppressor Gene Is the “Zonation-Keeper” of Mouse Liver.

Developmental Cell 2006, 10:759–770.

88. Colnot S, Decaens T, Niwa-Kawakita M, Godard C, Hamard G, Kahn A, Giovannini M, Perret C: Liver-targeted disruption of Apc in mice activates beta-catenin signaling and leads to hepatocellular carcinomas. *Proc Natl Acad Sci USA* 2004, 101:17216–17221.

89. Huch M, Dorrell C, Boj SF, van Es JH, Li VSW, van de Wetering M, Sato T, Hamer K, Sasaki N, Finegold MJ, et al.: In vitro expansion of single Lgr5+ liver stem cells induced by Wnt-driven regeneration. *Nature* 2013, 494:247–250.

90. Yang J, Mowry LE, Nejak-Bowen KN, Okabe H, Diegel CR, Lang RA, Williams BO, Monga SP: Beta-catenin signaling in murine liver zonation and regeneration: A Wnt-Wnt situation! *Hepatology* 2014, 60:964–976.

91. Preziosi M, Okabe H, Poddar M, Singh S, Monga SP: Endothelial Wnts regulate β-catenin signaling in murine liver zonation and regeneration: A sequel to the Wnt–Wnt situation. *Hepatology Communications* 2018, 2:845–860.

92. Planas-Paz L, Orsini V, Boulter L, Calabrese D, Pikiolek M, Nigsch F, Xie Y, Roma G, Donovan A, Marti P, et al.: The RSPO–LGR4/5–ZNRF3/RNF43 module controls liver zonation and size. *Nat Cell Biol* 2016, 18:467–479.

93. Planas-Paz L, Sun T, Pikiolek M, Cochran NR, Bergling S, Orsini V, Yang Z, Sigoillot F, Jetzer J, Syed M, et al.: YAP, but Not RSPO-LGR4/5, Signaling in Biliary Epithelial Cells Promotes a Ductular Reaction in Response to Liver Injury. *Stem Cell* 2019, doi:10.1016/j.stem.2019.04.005.

94. Wilson DH, Jarman EJ, Mellin RP, Wilson ML, Waddell SH, Tsokkou P, Younger NT, Raven A, Bhalla SR, Noll ATR, et al.: Non-canonical Wnt signalling regulates scarring in biliary disease via the planar cell polarity receptors. *Nat Commun* 2020, doi:10.1038/s41467-020-14283-3.

95. Hu M, Kurobe M, Jeong YJ, Fuerer C, Ghole S, Nusse R, Sylvester KG: Wnt/β-Catenin Signaling in Murine Hepatic Transit Amplifying Progenitor Cells. *Gastroenterology* 2007, 133:1579–1591.e1.

96. Apte U, Zeng G, Thompson MD, Muller P, Micsenyi A, Cieply B, Kaestner KH, Monga SPS: β-Catenin is critical for early postnatal liver growth. *Am. J. Physiol.* 2007, 292:G1578–G1585.

97. Ji X-K, Xie Y-K, Zhong J-Q, Xu Q-G, Zeng Q-Q, Wang Y, Zhang Q-Y, Shan Y-F: GSK-3β suppresses the proliferation of rat hepatic oval cells through modulating Wnt/β-catenin signaling pathway. *Nature Publishing Group* 2015, 36:334–342.

98. Okabe H, Yang J, Sylakowski K, Yovchev M, Miyagawa Y, Nagarajan S, Chikina M, Thompson M, Oertel M, Baba H, et al.: Wnt signaling regulates hepatobiliary repair following cholestatic liver injury in mice. *Hepatology* 2016, 64:1652–1666.

99. Cadoret A, Ovejero C, Terris B, Souil E, Levy L, Lamers WH, Kitajewski J, Kahn A, Perret C: New targets of beta-catenin signaling in the liver are involved in the glutamine metabolism. *Oncogene* 2002, 21:8293–8301.

100. Ovejero C, Cavard C, Périanin A, Hakvoort T, Vermeulen J, Godard C, Fabre M, Chafey P, Suzuki K, Romagnolo B, et al.: Identification of the leukocyte cell-derived chemotaxin 2 as a direct target gene of β-catenin in the liver. *Hepatology* 2004, 40:167–176.

101. Yeh T-H, Krauland L, Singh V, Zou B, Devaraj P, Stolz DB, Franks J, Monga SPS, Sasatomi E, Behari J: Liver-specific β-catenin knockout mice have bile canalicular abnormalities, bile secretory defect, and intrahepatic cholestasis. *Hepatology* 2010, 52:1410–1419.

102. Yang J, Cusimano A, Monga JK, Preziosi ME, Pullara F, Calero G, Lang R, Yamaguchi TP, Nejak-Bowen

KN, Monga SP: WNT5A Inhibits Hepatocyte Proliferation and Concludes β-Catenin Signaling in Liver Regeneration. *The American Journal of Pathology* 2015, 185:2194–2205.

103. Mederacke I, Hsu CC, Troeger JS, Huebener P, Mu X, Dapito DH, Pradere J-P, Schwabe RF: Fate tracing reveals hepatic stellate cells as dominant contributors to liver fibrosis independent of its aetiology. *Nat Commun* 2013, 4:552–21.

104. Rocha AS, Vidal V, Mertz M, Kendall TJ, Charlet A, Okamoto H, Schedl A: The Angiocrine Factor Rspondin3 Is a Key Determinant of Liver Zonation. *Cell Reports* 2015, 13:1757–1764.

105. Habib SJ, Chen BC, Tsai FC, Anastassiadis K, Meyer T, Betzig E, Nusse R: A Localized Wnt Signal Orients Asymmetric Stem Cell Division in Vitro. *Science* 2013, 339:1445–1448.

106. Vashist SK: Comparison of 1-Ethyl-3-(3-Dimethylaminopropyl) Carbodiimide Based Strategies to Crosslink Antibodies on Amine-Functionalized Platforms for Immunodiagnostic Applications. *Diagnostics* 2012, 2:23–33.

107. Carpentier B, Gautier A, Legallais C: Artificial and bioartificial liver devices: present and future. *Gut* 2009, 58:1690–1702.

108. Bhatia SN, Underhill GH, Zaret KS, Fox IJ: Cell and tissue engineering for liver disease. *Sci. Transl. Med.* 2014, 6:245sr2–245sr2.

109. Haque A, Gheibi P, Gao Y, Foster E, Son KJ, You J, Stybayeva G, Patel D, Revzin A: Cell biology is different in small volumes: endogenous signals shape phenotype of primary hepatocytes cultured in microfluidic channels. *Nature Publishing Group* 2016, 6:447–15.

110. Bell CC, Dankers ACA, Lauschke VM, Sison-Young R, Jenkins R, Rowe C, Goldring CE, Park K, Regan SL, Walker T, et al.: Comparison of Hepatic 2D Sandwich Cultures and 3D Spheroids for Long-term Toxicity Applications: A Multicenter Study. *Toxicological Sciences* 2018, 162:655–666.

111. Guo L, Dial S, Shi L, Branham W, Liu J, Fang J-L, Green B, Deng H, Kaput J, Ning B: Similarities and differences in the expression of drug-metabolizing enzymes between human hepatic cell lines and primary human hepatocytes. *Drug Metab Dispos* 2011, 39:528–538.

112. Kvist AJ, Kanebratt KP, Walentinsson A, Palmgren H, O'Hara M, Björkbom A, Andersson LC, Ahlqvist M, Andersson TB: Critical differences in drug metabolic properties of human hepatic cellular models, including primary human hepatocytes, stem cell derived hepatocytes, and hepatoma cell lines. *Biochemical Pharmacology* 2018, doi:10.1016/j.bcp.2018.06.026.

113. Zeigerer A, Wuttke A, Marsico G, Seifert S, Kalaidzidis Y, Zerial M: Functional properties of hepatocytes in vitro are correlated with cell polarity maintenance. *Experimental Cell Research* 2017, 350:242–252.

114. Bell CC, Hendriks DFG, Moro SML, Ellis E, Walsh J, Renblom A, Fredriksson Puigvert L, Dankers ACA, Jacobs F, Snoeys J, et al.: Characterization of primary human hepatocyte spheroids as a model system for drug-induced liver injury, liver function and disease. *Sci Rep* 2016, 6:25187–13.

115. Corbett JL, Duncan SA: iPSC-Derived Hepatocytes as a Platform for Disease Modeling and Drug Discovery. *Front. Med.* 2019, 6:1–12.

116. Grompe M, Lindstedt S, Al-Dhalimy M, Kennaway NG, Papaconstantinou J, Torres-Ramos CA, Ou CN, Finegold M: Pharmacological correction of neonatal lethal hepatic dysfunction in a murine model of hereditary tyrosinaemia type I. *Nat Genet* 1995, 10:453–460.

117. Overturf K, Al-Dhalimy M, Finegold M, Grompe M: The repopulation potential of hepatocyte populations differing in size and prior mitotic expansion. *The American Journal of Pathology* 1999, 155:2135–2143.

118. Haaker MW, Kruitwagen HS, Vaandrager AB, Houweling M, Penning LC, Molenaar MR, Wolferen ME, Oosterhoff LA, Spee B, Helms JB: Identification of potential drugs for treatment of hepatic lipidosis in cats using an in vitro feline liver organoid system. *J Vet Intern Med* 2020, 34:132–138.

119. Schneeberger K, Sánchez Romero N, Ye S, van Steenbeek FG, Oosterhoff LA, Pla Palacin I, Chen C, van Wolferen ME, van Tienderen G, Lieshout R, et al.: Large-scale Production of LGR5-positive Bipotential Human Liver Stem Cells. *Hepatology* 2019, doi:10.1002/hep.31037.

120. Jardé T, Evans RJ, McQuillan KL, Parry L, Feng GJ, Alvares B, Clarke AR, Dale TC: In vivo and in vitro models for the therapeutic targeting of Wnt signaling using a Tet-OΔN89β-catenin system. *Oncogene* 2012, 32:883–893.

121. Xu Q, Wang Y, Dabdoub A, Smallwood PM, Williams J, Woods C, Kelley MW, Jiang L, Tasman W, Zhang K, et al.: Vascular development in the retina and inner ear: control by Norrin and Frizzled-4, a high-affinity ligand-receptor pair. *Cell* 2004, 116:883–895.

122. Ootani A, Li X, Sangiorgi E, Ho QT, Ueno H, Toda S, Sugihara H, Fujimoto K, Weissman IL, Capecchi MR, et al.: Sustained in vitro intestinal epithelial culture within a Wnt-dependent stem cell niche. *Nat Med* 2009, 15:701–706.

123. Shibamoto S, Higano K, Takada R, Ito F, Takeichi M, Takada S: Cytoskeletal reorganization by soluble Wnt-3a protein signalling. *Genes Cells* 1998, 3:659–670.

124. bolger AM, Lohse M, Usadel B: Trimmomatic: a flexible trimmer for Illumina sequence data. *Bioinformatics* 2014, 30:2114–2120.

125. Dobin A, Davis CA, Schlesinger F, Drenkow J, Zaleski C, Jha S, Batut P, Chaisson M, Gingeras TR: STAR: ultrafast universal RNA-seq aligner. *Bioinformatics* 2012, 29:15–21.

126. Liao Y, Smyth GK, Shi W: featureCounts: an efficient general purpose program for assigning sequence reads to genomic features. *Bioinformatics* 2014, 30:923–930.

127. Love MI, Huber W, Anders S: Moderated estimation of fold change and dispersion for RNA-seq data with DESeq2. *Genome Biol.* 2014, 15:31–21.

128. Buechling T, Boutros M: *Wnt Signaling: Signaling at and Above the Receptor Level.* Elsevier Inc; 2011.

129. Karner CM, Chirumamilla R, Aoki S, Igarashi P, Wallingford JB, Carroll TJ: Wnt9b signaling regulates planar cell polarity and kidney tubule morphogenesis. *Nat Genet* 2009, 41:793–799.

130. Park JS, Valerius MT, McMahon AP: Wnt/ -catenin signaling regulates nephron induction during mouse kidney development. *Development* 2007, 134:2533–2539.

131. Fan J, Wei Q, Liao J, Zou Y, Song D, Xiong D, Ma C, Hu X, Qu X, Chen L, et al.: Noncanonical Wnt signaling plays an important role in modulating canonical Wnt-regulated stemness, proliferation and terminal differentiation of hepatic progenitors. *Oncotarget* 2017, 8:27105–27119.

132. Baril M, Es-Saad S, Chatel-Chaix L, Fink K, Pham T, Raymond V-A, Audette K, Guenier A-S, Duchaine J, Servant M, et al.: Genome-wide RNAi Screen Reveals a New Role of a WNT/CTNNB1 Signaling Pathway as Negative Regulator of Virus-induced Innate Immune Responses. *PLoS Pathog* 2013, 9:e1003416–19.

133. Tanigawa S, Wang H, Yang Y, Sharma N, Tarasova N, Ajima R, Yamaguchi TP, Rodriguez LG, Perantoni AO: Wnt4 induces nephronic tubules in metanephric mesenchyme by a non-canonical mechanism. *Developmental Biology* 2011, 352:58–69.

134. Bourhis E, Tam C, Franke Y, Bazan JF, Ernst J, Hwang J, Costa M, Cochran AG, Hannoush RN:

Reconstitution of a frizzled8.Wnt3a.LRP6 signaling complex reveals multiple Wnt and Dkk1 binding sites on LRP6. *J. Biol. Chem.* 2010, 285:9172–9179.

135. Tanaka M, Jokubaitis V, Wood C, Wang Y, Brouard N, Pera M, Hearn M, Simmons P, Nakayama N: BMP inhibition stimulates WNT-dependent generation of chondrogenic mesoderm from embryonic stem cells. *Stem Cell Research* 2009, 3:126–141.

136. Sato T, Vries RG, Snippert HJ, van de Wetering M, Barker N, Stange DE, van Es JH, Abo A, Kujala P, Peters PJ, et al.: Single Lgr5 stem cells build crypt-villus structures in vitro without a mesenchymal niche. *Nature* 2009, 459:262–265.

137. Olmeda D, Castel S, Vilaró S, Cano A: β-Catenin Regulation during the Cell Cycle: Implications in G2/M and Apoptosis. *MBoC* 2003, 14:2844–2860.

138. Hadjihannas MV, Bernkopf DB, ckner MBU, Behrens JUR: Cell cycle control of Wnt/β-catenin signalling by conductin/axin2 through CDC20. *EMBO Rep* 2012, 13:347–354.

139. Ding Y, Su S, Tang W, Zhang X, Chen S, Zhu G, Liang J, Wei W, Guo Y, Liu L, et al.: Enrichment of the β-catenin-TCF complex at the S and G2 phases ensures cell survival and cell cycle progression. *Journal of Cell Science* 2014, 127:4833–4845.

140. Kim K-A, Wagle M, Tran K, Zhan X, Dixon MA, Liu S, Gros D, Korver W, Yonkovich S, Tomasevic N, et al.: R-Spondin family members regulate the Wnt pathway by a common mechanism. *MBoC* 2008, 19:2588–2596.

141. Lebensohn AM, Rohatgi R: R-spondins can potentiate WNT signaling without LGRs. *Elife* 2018, 7:218.

142. Nemeth MJ, Topol L, Anderson SM, Yang Y, Bodine DM: Wnt5a inhibits canonical Wnt signaling in hematopoietic stem cells and enhances repopulation. *Proc Natl Acad Sci USA* 2007, 104:15436–15441.

143. Cohen ED, Miller MF, Wang Z, Moon RT, Morrisey EE: Wnt5a and Wnt11 are essential for second heart field progenitor development. *Development* 2012, 139:1931–1940.

144. Topol L, Jiang X, Choi H, Garrett-Beal L, Carolan PJ, Yang Y: Wnt-5a inhibits the canonical Wnt pathway by promoting GSK-3–independent β-catenin degradation. *J Cell Biol* 2003, 162:899–908.

145. Sato A, Yamamoto H, Sakane H, Koyama H, Kikuchi A: Wnt5a regulates distinct signalling pathways by binding to Frizzled2. *The EMBO Journal* 2009, 29:41–54.

146. Mikels AJ, Nusse R: Purified Wnt5a Protein Activates or Inhibits β-Catenin–TCF Signaling Depending on Receptor Context. *PLoS Biol* 2006, 4:e115–13.

147. Baarsma HA, Skronska-Wasek W, Mutze K, Ciolek F, Wagner DE, John-Schuster G, Heinzelmann K, Günther A, Bracke KR, Dagouassat M, et al.: Noncanonical WNT-5A signaling impairs endogenous lung repair in COPD. *Journal of Experimental Medicine* 2016, 214:143–163.

148. Bryja V, Andersson ER, Schambony A, Esner M, Bryjová L, Biris KK, Hall AC, Kraft B, Cajanek L, Yamaguchi TP, et al.: The extracellular domain of Lrp5/6 inhibits noncanonical Wnt signaling in vivo. *MBoC* 2009, 20:924–936.

149. Alok A, Lei Z, Jagannathan NS, Kaur S, Harmston N, Rozen SG, Tucker-Kellogg L, Virshup DM: Wnt proteins synergize to activate β-catenin signaling. *Journal of Cell Science* 2017, 130:1532–1544.

150. Liu C, Widen SA, Williamson KA, Ratnapriya R, Gerth-Kahlert C, Rainger J, Alur RP, Strachan E, Manjunath SH, Balakrishnan A, et al.: A secreted WNT-ligand-binding domain of FZD5 generated by a frameshift mutation causes autosomal dominant coloboma. *Hum. Mol. Genet.* 2016, 25:1382–1391.

151. Holdsworth G, Slocombe P, Doyle C, Sweeney B, Veverka V, Le Riche K, Franklin RJ, Compson J, Brookings D, Turner J, et al.: Characterization of the interaction of sclerostin with the low density lipoprotein receptor-related protein (LRP) family of Wnt co-receptors. *J. Biol. Chem.* 2012, 287:26464–26477.

152. Dickinson KK, Hammond LC, Karner CM, Hastie ND, Carroll TJ, Goodyer P: Molecular determinants of WNT9b responsiveness in nephron progenitor cells. *PLoS ONE* 2019, 14:e0215139–16.

153. Gong Y, Bourhis E, Chiu C, Stawicki S, DeAlmeida VI, Liu BY, Phamluong K, Cao TC, Carano RAD, Ernst JA, et al.: Wnt Isoform-Specific Interactions with Coreceptor Specify Inhibition or Potentiation of Signaling by LRP6 Antibodies. *PLoS ONE* 2010, 5:e12682–17.

154. Kidambi S, Yarmush RS, Novik E, Chao P, Yarmush ML, Nahmias Y: Oxygen-mediated enhancement of primary hepatocyte metabolism, functional polarization, gene expression, and drug clearance. *Proc. Natl. Acad. Sci. U.S.A.* 2009, 106:15714–15719.

155. Zheng K, Cubero F, Nevzorova Y: c-MYC—Making Liver Sick: Role of c-MYC in Hepatic Cell Function, Homeostasis and Disease. *Genes* 2017, 8:123–20.

156. Yuan X, Li J, Coulouarn C, Lin T, Sulpice L, Bergeat D, Torre C, Liebe R, Gretz N, Ebert MPA, et al.: SOX9 expression decreases survival of patients with intrahepatic cholangiocarcinoma by conferring chemoresistance. *British Journal of Cancer* 2018, doi:10.1038/s41416-018-0338-9.

157. Font-Burgada J, Shalapour S, Ramaswamy S, Hsueh B, Rossell D, Umemura A, Taniguchi K, Nakagawa H, Valasek MA, Ye L, et al.: Hybrid Periportal Hepatocytes Regenerate the Injured Liver without Giving Rise to Cancer. *Cell* 2015, 162:766–779.

158. Patouraux S, Rousseau D, Rubio A, Bonnafous S, Lavallard VJ, Lauron J, Saint-Paul M-C, Bailly-Maitre B, Tran A, Crenesse D, et al.: Osteopontin deficiency aggravates hepatic injury induced by ischemia–reperfusion in mice. *Cell Death and Disease* 2019, doi:10.1038/cddis.2014.174.

159. Soria LR, Nitzahn M, De Angelis A, Khoja S, Attanasio S, Annunziata P, Palmer DJ, Ng P, Lipshutz GS, Brunetti Pierri N: Hepatic glutamine synthetase augmentation enhances ammonia detoxification. *Jrnl of Inher Metab Disea* 2019, 42:1128–1135.

160. Godoy P, Widera A, Schmidt-Heck W, Campos G, Meyer C, Cadenas C, Reif R, Stöber R, Hammad S, Pütter L, et al.: Gene network activity in cultivated primary hepatocytes is highly similar to diseased mammalian liver tissue. *Archives of Toxicology* 2016, 90:2513–2529.

161. Cahan P, Li H, Morris SA, Lummertz da Rocha E, Daley GQ, Collins JJ: CellNet: Network Biology Applied to Stem Cell Engineering. *Cell* 2014, 158:903–915.

162. Dooley S, Hamzavi J, Ciuclan L, Godoy P, Ilkavets I, Ehnert S, Ueberham E, Gebhardt R, Kanzler S, Geier A, et al.: Hepatocyte-Specific Smad7 Expression Attenuates TGF-β–Mediated Fibrogenesis and Protects Against Liver Damage. *Gastroenterology* 2008, 135:642–659.e46.

163. Acloque H, Thiery JP, Nieto MA: The physiology and pathology of the EMT. *EMBO Rep* 2008, 9:322–326.

164. Beagle B, Johnson GVW: Differential modulation of TCF/LEF-1 activity by the soluble LRP6-ICD. *PLoS ONE* 2010, 5:e11821.

165. Yuan T, Wang S, Hu C, Wu Y, Liang D, Li L, Liu Y, Li J, Chen Y-H: Low-density lipoprotein receptor-related protein 6 regulates alternative pre-mRNA splicing. *J Cell Mol Med* 2018, 22:4653–4663.

166. Burke ZD, Reed KR, Phesse TJ, Sansom OJ, Clarke AR, Tosh D: Liver Zonation Occurs Through a β-Catenin–Dependent, c-Myc–Independent Mechanism. *Gastroenterology* 2009, 136:2316–2324.e3.

167. Michalopoulos GK, Bowen WC, Mulè K, Stolz DB: Histological organization in hepatocyte organoid cultures. *The American Journal of Pathology* 2001, 159:1877–1887.

168. Rashid ST, Corbineau S, Hannan N, Marciniak SJ, Miranda E, Alexander G, Huang-Doran I, Griffin J, Ahrlund-Richter L, Skepper J, et al.: Modeling inherited metabolic disorders of the liver using human induced pluripotent stem cells. *J. Clin. Invest.* 2010, 120:3127–3136.

169. Michalopoulos GK, Bowen WC, Mulè K, Luo J: HGF-, EGF-, and dexamethasone-induced gene expression patterns during formation of tissue in hepatic organoid cultures. *gene expr* 2003, 11:55–75.

170. Huck I, Gunewardena S, Español-Suñer R, Willenbring H, Apte U: Hepatocyte Nuclear Factor 4 Alpha Activation Is Essential for Termination of Liver Regeneration in Mice. *Hepatology* 2019, 70:666–681.

171. Nishikawa T, Bell A, Brooks JM, Setoyama K, Melis M, Han B, Fukumitsu K, Handa K, Tian J, Kaestner KH, et al.: Resetting the transcription factor network reverses terminal chronic hepatic failure. *J. Clin. Invest.* 2015, 125:1533–1544.

172. Huch M, Gehart H, van Boxtel R, Hamer K, Blokzijl F, Verstegen MMA, Ellis E, van Wenum M, Fuchs SA, de Ligt J, et al.: Long-Term Culture of Genome-Stable Bipotent Stem Cells from Adult Human Liver. *Cell* 2015, 160:299–312.

173. Broutier L, Andersson-Rolf A, Hindley CJ, Boj SF, Clevers H, Koo B-K, Huch M: Culture and establishment of self-renewing human and mouse adult liver and pancreas 3D organoids and their genetic manipulation. *Nat Protoc* 2016, 11:1724–1743.

174. Rubina K, Talovskaya E, Cherenkov V, Ivanov D, Stambolsky D, Storozhevykh T, Pinelis V, Shevelev A, Parfyonova Y, Resink T, et al.: LDL induces intracellular signalling and cell migration via atypical LDL-binding protein T-cadherin. *Mol. Cell. Biochem.* 2005, 273:33–41.

175. Lu B, Bridges D, Yang Y, Fisher K, Cheng A, Chang L, Meng Z-X, Lin JD, Downes M, Yu RT, et al.: Metabolic crosstalk: molecular links between glycogen and lipid metabolism in obesity. *Diabetes* 2014, 63:2935–2948.

176. Khan AA, Dragt BS, Porte RJ, Groothuis GMM: Regulation of VDR expression in rat and human intestine and liver--consequences for CYP3A expression. *Toxicol In Vitro* 2010, 24:822–829.

177. Chow ECY, Maeng H-J, Liu S, Khan AA, Groothuis GMM, Pang KS: 1alpha,25-Dihydroxyvitamin D(3) triggered vitamin D receptor and farnesoid X receptor-like effects in rat intestine and liver in vivo. *Biopharm Drug Dispos* 2009, 30:457–475.

178. Pascussi JM, Drocourt L, Gerbal-Chaloin S, Fabre JM, Maurel P, Vilarem MJ: Dual effect of dexamethasone on CYP3A4 gene expression in human hepatocytes. Sequential role of glucocorticoid receptor and pregnane X receptor. *Eur. J. Biochem.* 2001, 268:6346–6358.

179. Cascio S, Zaret KS: Hepatocyte differentiation initiates during endodermal-mesenchymal interactions prior to liver formation. *Development* 1991, 113:217–225.

180. Lemaigre FP: Determining the fate of hepatic cells by lineage tracing: Facts and pitfalls. *Hepatology* 2015, 61:2100–2103.

181. Duncan AW, Dorrell C, Grompe M: Stem Cells and Liver Regeneration. *Gastroenterology* 2009, 137:466–481.

182. Limaye PB, Alarcón G, Walls AL, Nalesnik MA, Michalopoulos GK, Demetris AJ, Ochoa ER: Expression of specific hepatocyte and cholangiocyte transcription factors in human liver disease and embryonic development. *Lab Invest* 2008, 88:865–872.

183. Schaub JR, Huppert KA, Kurial SNT, Hsu BY, Cast AE, Donnelly B, Karns RA, Chen F, Rezvani M, Luu HY, et al.: De novo formation of the biliary system by TGFβ-mediated hepatocyte transdifferentiation. *Nature* 2018, 557:247–251.

184. Lin Y, Fang Z-P, Liu H-J, Wang L-J, Cheng Z, Tang N, Li T, Liu T, Han H-X, Cao G, et al.: HGF/R-spondin1 rescues liver dysfunction through the induction of Lgr5+ liver stem cells. *Nat Commun* 2017, 8:286–11.

185. Katsuda T, Kawamata M, Hagiwara K, Takahashi R-U, Yamamoto Y, Camargo FD, Ochiya T: Conversion of Terminally Committed Hepatocytes to Culturable Bipotent Progenitor Cells with Regenerative Capacity. *Stem Cell* 2017, 20:41–55.

186. Mitani S, Takayama K, Nagamoto Y, Imagawa K, Sakurai F, Tachibana M, Sumazaki R, Mizuguchi H: Human ESC/iPSC-Derived Hepatocyte-like Cells Achieve Zone-Specific Hepatic Properties by Modulation of WNT Signaling. *Molecular Therapy* 2017, 25:1420–1433.

187. Wang B, Jakus AE, Baptista PM, Soker S, Soto-Gutierrez A, Abecassis MM, Shah RN, Wertheim JA: Functional Maturation of Induced Pluripotent Stem Cell Hepatocytes in Extracellular Matrix—A Comparative Analysis of Bioartificial Liver Microenvironments. *STEM CELLS Translational Medicine* 2016, 5:1257–1267.

188. Yanger K, Zong Y, Maggs LR, Shapira SN, Maddipati R, Aiello NM, Thung SN, Wells RG, Greenbaum LE, Stanger BZ: Robust cellular reprogramming occurs spontaneously during liver regeneration. *Genes Dev.* 2013, 27:719–724.

189. Long Z, Cao M, Su S, Wu G, Meng F, Wu H, Liu J, Yu W, Atabai K, Wang X: Inhibition of hepatocyte nuclear factor 1b induces hepatic steatosis through DPP4/NOX1-mediated regulation of superoxide. *Free Radical Biology and Medicine* 2017, 113:71–83.

190. Tonon F, Giobbe GG, Zambon A, Luni C, Gagliano O, Floreani A, Grassi G, Elvassore N: In vitro metabolic zonation through oxygen gradient on a chip. *Nature Publishing Group* 2019, doi:10.1038/s41598-019-49412-6.

191. Ahn J, Ahn J-H, Yoon S, Nam YS, Son M-Y, Oh J-H: Human three-dimensional in vitro model of hepatic zonation to predict zonal hepatotoxicity. 2019, doi:10.1186/s13036-019-0148-5.

192. Huang P, Senga T, Hamaguchi M: A novel role of phospho-β-catenin in microtubule regrowth at centrosome. *Oncogene* 2007, 26:4357–4371.

193. Binnerts ME, Kim K-A, Bright JM, Patel SM, Tran K, Zhou M, Leung JM, Liu Y, Lomas WE, Dixon M, et al.: R-Spondin1 regulates Wnt signaling by inhibiting internalization of LRP6. *Proc Natl Acad Sci USA* 2007, 104:14700–14705.

194. Eubelen M, Bostaille N, Cabochette P, Gauquier A, Tebabi P, Dumitru AC, Koehler M, Gut P, Alsteens D, Stainier DYR, et al.: A molecular mechanism for Wnt ligand-specific signaling. *Science* 2018, 361:eaat1178–15.

195. Cho C, Smallwood PM, Nathans J: Reck and Gpr124 Are Essential Receptor Cofactors for Wnt7a/Wnt7b-Specific Signaling in Mammalian CNS Angiogenesis and Blood-Brain Barrier Regulation. *Neuron* 2017, 95:1056–1073.e5.

196. Posokhova E, Shukla A, Seaman S, Volate S, Hilton MB, Wu B, Morris H, Swing DA, Zhou M, Zudaire E, et al.: GPR124 Functions as a WNT7-Specific Coactivator of Canonical β-Catenin Signaling. *CellReports* 2015, 10:123–130.

197. Grainger S, Nguyen N, Richter J, Setayesh J, Lonquich B, Oon CH, Wozniak JM, Barahona R, Kamei CN, Houston J, et al.: EGFR is required for Wnt9a–Fzd9b signalling specificity in haematopoietic stem cells.

Nat Cell Biol 2019, 21:721–730.

198. Apte U, Thompson MD, Cui S, Liu B, Cieply B, Monga SPS: Wnt/β-catenin signaling mediates oval cell response in rodents. *Hepatology* 2007, 47:288–295.

199. Mort RL, Ford MJ, Sakaue-Sawano A, Lindstrom NO, Casadio A, Douglas AT, Keighren MA, Hohenstein P, Miyawaki A, Jackson IJ: Fucci2a:A bicistronic cell cycle reporter that allows Cre mediated tissue specific expression in mice. *Cell Cycle* 2014, 13:2681–2696.

200. liu J, pan S, Hsieh MH, Ng N, Sun F, Wang T, Kasibhatla S, Schuller AG, Li AG, Cheng D, et al.: Targeting Wnt-driven cancer through the inhibition of Porcupine by LGK974. *Proc. Natl. Acad. Sci. U.S.A.* 2013, 110:20224–20229.

201. Moya IM, Halder G: Hippo-YAP/TAZ signalling in organ regeneration and regenerative medicine. *Nat. Rev. Mol. Cell Biol.* 2019, 20:211–226.

202. Liu Z, Chen O, Wall JBJ, Zheng M, Zhou Y, Wang L, Ruth Vaseghi H, Qian L, Liu J: Systematic comparison of 2A peptides for cloning multi-genes in a polycistronic vector. *Nature Publishing Group* 2017, 7:663–9.

203. Wang Y, Wang F, Wang R, Zhao P, Xia Q: 2A self-cleaving peptide-based multi-gene expression system in the silkworm Bombyx mori. *Nature Publishing Group* 2015, doi:10.1038/srep16273.

204. Ma B, Zhong L, van Blitterswijk CA, Post JN, Karperien M: T Cell Factor 4 Is a Pro-catabolic and Apoptotic Factor in Human Articular Chondrocytes by Potentiating Nuclear Factor κB Signaling. *J. Biol. Chem.* 2013, 288:17552–17558.

205. Grumolato L, Liu G, Haremaki T, Mungamuri SK, Mong P, Akiri G, Lopez-Bergami P, Arita A, Anouar Y, Mlodzik M, et al.: β-Catenin-Independent Activation of TCF1/LEF1 in Human Hematopoietic Tumor Cells through Interaction with ATF2 Transcription Factors. *PLoS Genet* 2013, 9:e1003603–13.

206. Niehrs C, Acebron SP: Mitotic and mitogenic Wnt signalling. *The EMBO Journal* 2012, 31:2705–2713.

207. Bahmanyar S, Kaplan DD, Deluca JG, Giddings TH, O'Toole ET, Winey M, Salmon ED, Casey PJ, Nelson WJ, Barth AIM: beta-Catenin is a Nek2 substrate involved in centrosome separation. *Genes Dev.* 2008, 22:91–105.

208. Hadjihannas MV, ckner MBU, Behrens JUR: Conductin/axin2 and Wnt signalling regulates centrosome cohesion. *EMBO Rep* 2010, 11:317–324.

209. Fuentealba LC, Eivers E, Geissert D, Taelman V, De Robertis EM: Asymmetric mitosis: Unequal segregation of proteins destined for degradation. *Proc. Natl. Acad. Sci. U.S.A.* 2008, 105:7732–7737.

210. Fodde R, Kuipers J, Rosenberg C, Smits R, KIELMAN M, Gaspar C, Van Es JH, Breukel C, Wiegant J, Giles RH, et al.: Mutations in the APC tumour suppressor gene cause chromosomal instability. *Nat Cell Biol* 2001, 3:433–438.

211. Hadjihannas MV, Brückner M, Jerchow B, Birchmeier W, Dietmaier W, Behrens J: Aberrant Wnt/beta-catenin signaling can induce chromosomal instability in colon cancer. *Proc Natl Acad Sci USA* 2006, 103:10747–10752.

212. Feng GJ, Cotta W, Wei XQ, Poetz O, Evans R, Jardé T, Reed K, Meniel V, Williams GT, Clarke AR, et al.: Conditional Disruption of Axin1 Leads to Development of Liver Tumors in Mice. *Gastroenterology* 2012, 143:1650–1659.

213. Davidson G, Shen J, Huang Y-L, Su Y, Karaulanov E, Bartscherer K, Hassler C, Stannek P, Boutros M, Niehrs C: Cell Cycle Control of Wnt Receptor Activation. *Developmental Cell* 2009, 17:788–799.

214. Xu M, Yu Q, Subrahmanyam R, Difilippantonio MJ, Ried T, Sen JM: Beta-catenin expression results in p53-independent DNA damage and oncogene-induced senescence in prelymphomagenic thymocytes in vivo. *Molecular and Cellular Biology* 2008, 28:1713–1723.

215. Ayyanan A, Civenni G, Ciarloni L, Morel C, Mueller N, Lefort K, Mandinova A, Raffoul W, Fiche M, Dotto GP, et al.: Increased Wnt signaling triggers oncogenic conversion of human breast epithelial cells by a Notch-dependent mechanism. *Proc Natl Acad Sci USA* 2006, 103:3799–3804.

216. Scully R, Chen J, Ochs RL, Keegan K, Hoekstra M, Feunteun J, Livingston DM: Dynamic changes of BRCA1 subnuclear location and phosphorylation state are initiated by DNA damage. *Cell* 1997, 90:425–435.

217. Vafa O, Wade M, Kern S, Beeche M, Pandita TK, Hampton GM, Wahl GM: c-Myc can induce DNA damage, increase reactive oxygen species, and mitigate p53 function: a mechanism for oncogene-induced genetic instability. *Molecular Cell* 2002, 9:1031–1044.

218. Cottini F, Hideshima T, Suzuki R, Tai Y-T, Bianchini G, Richardson PG, Anderson KC, Tonon G: Synthetic Lethal Approaches Exploiting DNA Damage in Aggressive Myeloma. *Cancer Discovery* 2015, 5:972–987.

219. Karlsson A, Deb-Basu D, Cherry A, Turner S, Ford J, Felsher DW: Defective double-strand DNA break repair and chromosomal translocations by MYC overexpression. *Proc Natl Acad Sci USA* 2003, 100:9974–9979.

220. Hironaka K, Factor VM, Calvisi DF, Conner EA, Thorgeirsson SS: Dysregulation of DNA Repair Pathways in a Transforming Growth Factor α/c-myc Transgenic Mouse Model of Accelerated Hepatocarcinogenesis. *Lab Invest* 2003, 83:643–654.

221. Ray S, Atkuri KR, Deb-Basu D, Adler AS, Chang HY, Herzenberg LA, Felsher DW: MYC can induce DNA breaks in vivo and in vitro independent of reactive oxygen species. *Cancer Res* 2006, 66:6598–6605.

222. Loonstra A, Vooijs M, Beverloo HB, Allak BA, van Drunen E, Kanaar R, Berns A, Jonkers J: Growth inhibition and DNA damage induced by Cre recombinase in mammalian cells. *Proc Natl Acad Sci USA* 2001, 98:9209–9214.

223. Fredriksson R, Lagerström MC, Lundin L-G, Schiöth HB: The G-protein-coupled receptors in the human genome form five main families. Phylogenetic analysis, paralogon groups, and fingerprints. *Mol. Pharmacol.* 2003, 63:1256–1272.

224. Mardones MD, Andaur GA, Varas-Godoy M, Henriquez JF, Salech F, Behrens MI, Couve A, Inestrosa NC, Varela-Nallar L: Frizzled-1 receptor regulates adult hippocampal neurogenesis. *Molecular Brain* 2016, doi:10.1186/s13041-016-0209-3.

225. Liu T, DeCostanzo AJ, Liu X, Wang Hy, Hallagan S, Moon RT, Malbon CC: G protein signaling from activated rat frizzled-1 to the beta-catenin-Lef-Tcf pathway. *Science* 2001, 292:1718–1722.

226. Schafer ST, Han J, Pena M, Bohlen Und Halbach von O, Peters J, Gage FH: The Wnt adaptor protein ATP6AP2 regulates multiple stages of adult hippocampal neurogenesis. *J. Neurosci.* 2015, 35:4983–4998.

227. Katanaev VL, Ponzielli R, Sémériva M, Tomlinson A: Trimeric G Protein-Dependent Frizzled Signaling in Drosophila. *Cell* 2005, 120:111–122.

228. Flanagan DJ, Phesse TJ, Barker N, Schwab RHM, Amin N, Malaterre J, Stange DE, Nowell CJ, Currie SA, Saw JTS, et al.: Frizzled7 Functions as a Wnt Receptor in Intestinal Epithelial Lgr5+ Stem Cells. *Stem Cell Reports* 2015, 4:759–767.

229. He X, Semenov M, Tamai K, Zeng X: LDL receptor-related proteins 5 and 6 in Wnt/beta-catenin signaling: arrows point the way. *Development* 2004, 131:1663–1677.

230. Blumenthal A, Ehlers S, Lauber J, Buer J, Lange C, Goldmann T, Heine H, Brandt E, Reiling N: The Wingless homolog WNT5A and its receptor Frizzled-5 regulate inflammatory responses of human mononuclear cells induced by microbial stimulation. *Blood* 2006, 108:965–973.

231. Kirikoshi H, Sekihara H, Katoh M: Molecular cloning and characterization of human WNT11. *Int. J. Mol. Med.* 2001, 8:651–656.

232. Yu J, Carroll TJ, Rajagopal J, Kobayashi A, Ren Q, McMahon AP: A Wnt7b-dependent pathway regulates the orientation of epithelial cell division and establishes the cortico-medullary axis of the mammalian kidney. *Development* 2008, 136:161–171.

233. Ferrari ME, Bernis ME, McLeod F, Podpolny M, Coullery RP, Casadei IM, Salinas PC, Rosso SB: Wnt7b signalling through Frizzled-7 receptor promotes dendrite development by coactivating CaMKII and JNK. *Journal of Cell Science* 2018, 131:jcs216101–14.

234. Le Grand F, Jones AE, Seale V, Scimè A, Rudnicki MA: Wnt7a Activates the Planar Cell Polarity Pathway to Drive the Symmetric Expansion of Satellite Stem Cells. *Cell Stem Cell* 2009, 4:535–547.

235. Mchedlidze T, Waldner M, Zopf S, Walker J, Rankin AL, Schuchmann M, Voehringer D, McKenzie ANJ, Neurath MF, Pflanz S, et al.: Interleukin-33-Dependent Innate Lymphoid Cells Mediate Hepatic Fibrosis. *Immunity* 2013, 39:357–371.

236. Pereira TA, Xie G, Choi SS, Syn W-K, Voieta I, Lu J, Chan IS, Swiderska M, Amaral KB, Antunes CM, et al.: Macrophage-derived hedgehog ligands promotes fibrogenic and angiogenic responses in human schistosomiasis mansoni. *Liver Int* 2012, 33:149–161.

237. Arndt S, Wacker E, Dorn C, Koch A, Saugspier M, Thasler WE, Hartmann A, Bosserhoff AK, Hellerbrand C: Enhanced expression of BMP6 inhibits hepatic fibrosis in non-alcoholic fatty liver disease. *Gut* 2015, 64:973–981.

238. Chung Y-H, Huang Y-H, Chu T-H, Chen C-L, Lin P-R, Huang S-C, Wu D-C, Huang C-C, Hu T-H, Kao Y-H, et al.: BMP-2 restoration aids in recovery from liver fibrosis by attenuating TGF-Î²1 signaling. *Lab Invest* 2018, doi:10.1038/s41374-018-0069-9.

239. Touboul T, Chen S, To CC, Mora-Castilla S, Sabatini K, Tukey RH, Laurent LC: Stage-specific regulation of the WNT/Î²-catenin pathway enhances differentiation of hESCs into hepatocytes. 2016, doi:10.1016/j.jhep.2016.02.028.

240. Cordi S, Godard C, Saandi T, Jacquemin P, Monga SP, Colnot S, Lemaigre FP: Role of β-catenin in development of bile ducts. *Differentiation* 2016, 91:42–49.

241. Ros JE, Libbrecht L, Geuken M, Jansen PL, Roskams TA: High expression of MDR1, MRP1, and MRP3 in the hepatic progenitor cell compartment and hepatocytes in severe human liver disease. *J. Pathol.* 2003, 200:553–560.